OPTIMISING DROPLET MICROFLUIDICS FOR ANTIBIOTIC DRUG DISCOVERY

ANTONIA MOLLOY

Doctor of Philosophy

ASTON UNIVERSITY

September 2024

Optimising Droplet Microfluidics for Antibiotic Drug Discovery

Antonia Molloy
Doctor of Philosophy
Aston University
2024

Abstract

Antimicrobial resistance (AMR) represents a critical global health challenge that threatens the efficacy of modern medical procedures and our ability to treat infectious diseases. In 2019 alone, AMR was associated with more than 4.95 million deaths worldwide and by 2050, AMR could impose an additional healthcare burden of 1 trillion US dollars globally. Innovative approaches in drug discovery and development are required to improve current *in vitro* antibiotic susceptibility tests (AST). Droplet microfluidics have promising future applications in microbiology to miniaturise antibiotic screening platforms at the single-cell level. Here picodroplet technology was optimised for future droplet-based AST. Novel metal compounds were assessed for their activity against ESKAPE pathogens and mycobacterial species. Broad-spectrum activity was demonstrated, however when comparing two standard AST methods, results varied. Picodroplet technology was tested as an alternative to bulk cultures by producing monodisperse water-in-oil picodroplets of varying surfactant concentrations, culture media types, and droplet volumes. This study successfully demonstrated the generation of droplets with high monodispersity containing single or multiple MRSA bacterial cells, the maintenance of bacterial viability and proliferation within droplets, the observation of droplet shrinkage during bacterial growth, and the detection of differences in antibiotic susceptibility between the droplet and bulk cultures. Finally, dendrimer-based surfactants were assessed for their ability to prevent small molecule leakage out of the droplet bilayer to ensure antibiotics would not crosstalk between each droplet bioreactor. These optimisation investigations advances knowledge in the development of a rapid *in vitro* antibiotic susceptibility test which will reduce animal models and replicate the human infection environment for improved clinical translation.

Key Words: Droplet Microfluidics, Antibiotic Susceptibility Testing, Surfactants, Metal Antibiotics, ESKAPE Pathogens, Mycobacteria, Dendrimer.

Acknowledgements

I would like to thank Dr Jonathan Cox for giving me the opportunity to pursue this work in his laboratory and for providing collaborative prospects throughout my PhD. Thank you to Dr Ewan Ross for providing supervision of this project. For providing great thesis feedback, I thank Dr John Simms. I would also like to thank Dr Xin Li for leading our collaboration with Sphere Fluidics Ltd. Thank you for providing support, guidance, and resources throughout the project. For his unwavering support and expert knowledge, I would like to thank Dr Clive Smith. I would like to thank Dr Alaa Kadhim for her training in polymer chemistry and industrial mentorship whilst I was on placement with Sphere Fluidics. To Dr James Harrison, I thank you for introducing me to the world of microbiology, teaching me how to pour my first agar plate, and to your remarkable patience and wealth of knowledge. I would further like to thank Dr Katherine Abrahams for hosting me at the University of Birmingham and training me in all thing's lipid extraction. For her intelligent and labour intensive contribution to the susceptibility of ESKAPE pathogens of my second chapter, I would like to thank a super star named Emily Baker.

A special thanks go to my colleagues in the MB327 lab including James, Victoria, Bella, Laura, Duncan, Emily, Gemma, and Ali. Additionally, I am extremely grateful to be part of a central of doctoral training cohort filled with brilliant individuals which made the challenging moments more manageable and the successes even more rewarding.

I am profoundly grateful to my family and friends for their unconditional love and support. To my parents, Sarah-Jayne, and Thomas, thank you for always believing in me and encouraging me to pursue science. Your sacrifices have made this achievement feasible. To my partner, Lewis, your understanding and constant encouragement have made this work possible. To my sister finishing her university studies and ready to embark on a career in science, good luck!

Lastly, I would like to acknowledge the funding agencies that supported this research, including the Engineering and Physical Sciences Research Council (EP/S02347X/1), Sphere Fluidics Ltd, and Aston University.

Collaborator Acknowledgements

The work presented in Chapter 2 was conducted in conjunction with Prof. Gilles Gasser at Chimie ParisTech, PSL University. His group provided the compounds which were tested in this chapter. Only the microbiology contributions to this collaboration have been reported. Emily Baker contributed to the methodology of testing the metal-based compounds against ESKAPE pathogens.

This project was also in collaboration with Sphere Fluidics Ltd, Cambridge, who provided the picodroplet technology with an image-based closed-loop feedback mechanism.

Publications Associated with this Work

Molloy, A., Harrison, J., McGrath, J. S., Owen, Z., Smith, C., Liu, X., Li, X., & Cox, J. A. G. (2021). Microfluidics as a Novel Technique for Tuberculosis: From Diagnostics to Drug Discovery. Microorganisms, 9(11), 2330. https://doi.org/10.3390/microorganisms9112330.

Baker, E. J., **Molloy, A**., Cox, J. A. G. (2023). Drug Repurposing for the Treatment of *Mycobacterium abscessus* Infections. Infectious Microbes & Diseases, 5(3), 101. https://doi.org/10.1097/IM9.0000000000000123.

Table of Contents

List of Abbreviations

%	Percent
$	Dollars
<	Less than
>	More than
µg	Microgram
µl	Microlitre
µm	Micrometre
7H9	Middlebrook 7H9 broth
ADC	Bovine serum albumin, Dextrose, Catalase
AMR	Antimicrobial resistance
ANOVA	Analysis of variance statistical test
aq	Aqueous phase
AST	Antibiotic susceptibility test
BCG	Bacille Calmette Guerin
BMD	Broth microdilution assay
CFU/mL	Colony forming units per mililitre
CV	Coefficient of variation
DMSO	Dimethyl sulfoxide
EDA	Ethylene diamine
ESI-MS	Electrospray ionization mass spectrometry
FS	FluoSurf™
g	Gram
g/mL	Gram per millilitre
G0.5	Generation 0.5/half generation
G1	Generation 1/full generation
h	Hour
H_20	Water
HLB	Hydrophilic-lipophilic balance
IR	Infrared spectroscopy
L	Litre
M	Molar
MA	Methyl acrylate
MBC	Minimum bactericidal concentration
MCM	Minimal cholesterol media
MDR-TB	Multi-drug resistant tuberculosis
mg	Milligram

mg/mL	milligram per mililitre
MH	Mueller-Hinton broth
MIC	Minimum inhibitory concentration
mL	Millilitre
mM	Millimolar
MOA	Mechanism of action
Mw	Molecular weight
NCTC	National collection of type cultures
nm	Nanometres
NMR	Nuclear magnetic resonance
NRP	Non-replicating persistence
NTM	Non-tuberculous mycobacteria
O/W	Oil-in-water
OADC	Oleic acid, Bovine serum albumin, Dextrose, Catalase
ºC	Degrees Celsius
OD	Optical density
p	p value
PAMAM	Polyamidoamine
PBS	Phosphate buffered saline
PCR	Polymerase chain reaction
PDMS	Polydimethylsiloxane
pH	Power of hydrogen
pL	Picolitre
PS	Pico-Surf®
RIF	Rifampicin
rmp	Revolutions per minute
RRA	Resazurin reduction assay
SD	Standard deviation
TB	Tuberculosis
v/v	Volume to volume
W/O	Water-in-oil
w/v	Weight to volume
WHO	World Health Organisation
XDR-TB	Extremely drug resistant tuberculosis

Chapter 1.

Introduction: Antimicrobial Resistance and the Application of Droplet Microfluidics for Antibiotic Drug Discovery

1.1 Antimicrobial Resistance (AMR)

Antimicrobial resistance (AMR) represents a critical global health challenge that threatens the efficacy of modern medical procedures and our ability to treat infectious diseases. AMR occurs when microorganisms develop the capacity to withstand the therapeutic effects of antimicrobial drugs that were previously successful in combating infections (Ahmed et al., 2024). This phenomenon has far-reaching implications for human health worldwide. The history of AMR is closely linked to the development and use of antimicrobials. Following the groundbreaking discovery of penicillin by Alexander Fleming in 1928, the mass production and widespread use of this antibiotic led to the emergence of resistant organisms. Notably, as early as 1942, the first cases of penicillin-resistant *Staphylococcus aureus* were reported, marking the beginning of a continuous challenge in antimicrobial therapy (Ahmed et al., 2024). Several factors have exacerbated the progression of AMR. Human activities have significantly contributed to this issue, primarily through the misuse and overuse of antimicrobials, including inappropriate prescribing practices (Prestinaci et al., 2015). Concurrently, microorganisms have evolved sophisticated defence mechanisms to evade antibiotic-mediated killing (Smith et al., 2023). This dual process of human-driven selection pressure and microbial adaptation has accelerated the development and spread of AMR.

The global threat posed by AMR gained significant political recognition by 2016, leading to a concerted international response. Nations worldwide, under the umbrella of the United Nations, are committed to addressing the root causes of AMR. This commitment has resulted in the development of national action plans by 178 countries. However, despite this widespread acknowledgement and planning, insufficient funding hinders effective implementation and progress in combating AMR (The Lancet, 2024).

Recent estimates starkly illustrate the magnitude of the AMR crisis. A comprehensive report by the Antimicrobial Resistance Collaborators revealed that in 2019 alone, AMR was associated with more than 4.95 million deaths worldwide (Antimicrobial Resistance Collaborators, 2022). Figure 1.1 provides a comparative illustration of annual AMR-attributable deaths alongside other major causes of mortality, underscoring the severity of this issue. Beyond the human cost, the economic implications are equally alarming. Projections indicate that by 2050, AMR could impose an additional healthcare cost burden of US $1 trillion globally (Jonas et al., 2017). These figures highlight the urgent need for effective strategies to combat AMR.

The current trajectory of AMR presents a significant challenge, as the rate of bacterial resistance development is outpacing the introduction of novel antimicrobials to the market. This imbalance underscores the critical and urgent need for innovative approaches in drug discovery and development to address the looming crisis of AMR. Future research efforts must

focus on finding new antimicrobial agents, developing alternative therapeutic strategies, and implementing more effective stewardship programs to preserve the efficacy of existing drugs.

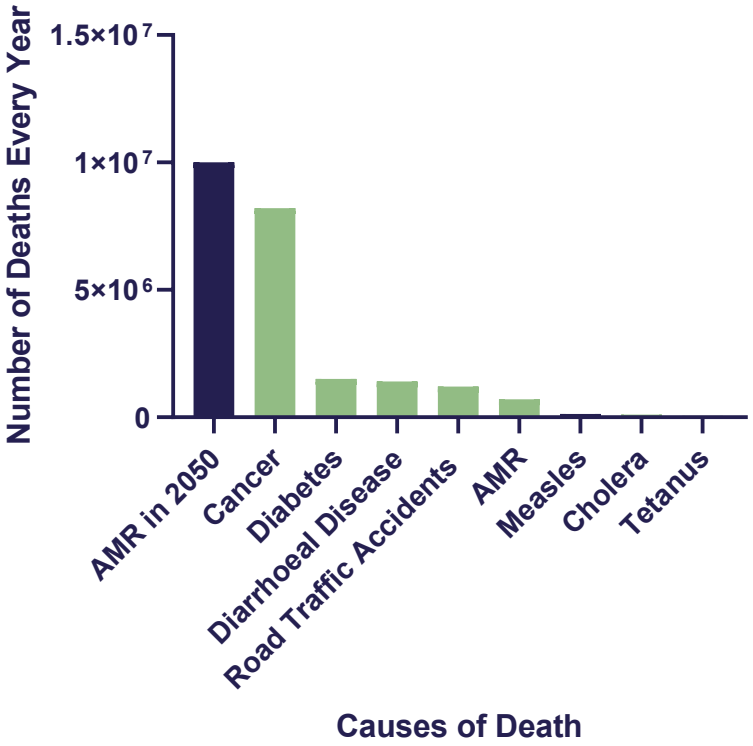

Figure 1.1 Deaths attributable to AMR every year compared to other major causes of death. Green data is the number of deaths from 2014. The blue data is predicted for 2050. Data taken from The Review on Antimicrobial Resistance, Chaired by Jim O'Neill. Created on Biorender.com.

1.1.1 Antibiotic Mechanisms of Action

Antimicrobials can exhibit a broad or narrow spectrum of effectiveness against bacteria (Saikia and Chetia, 2024). Antibiotics have distinct mechanism of actions (MOA) which can either inhibit DNA replication, inhibit protein biosynthesis, inhibit cell wall synthesis, and inhibit folic acid metabolism (Halawa et al., 2023). These mechanisms and chemical structures classify antibiotic groups. The major classes of antibiotics and their mode of action are listed in Table 1.1 and illustrated in Figure 1.2. Understanding an antimicrobial's MOA is valuable in its development, despite not being necessary for FDA approval. By understanding the MOA, clinical trials can be more successful in predicting a drug's spectrum of activity and making modifications to enhance efficacy or reduce toxicity. Various methodologies, such as biochemical and genetic approaches, are used to characterise MOAs. These include techniques like affinity chromatography, thermal proteome profiling, RNA sequencing, and comparing antibiotic signatures to better understand and optimise antimicrobial agents (Hudson and Lockless Steve, 2022).

Table 1.1. Major classes of antibiotics, their sub-class, and their mode of action. Details taken from (Saikia and Chetia, 2024).

Antibiotic Class	Sub-class	Mode of Action
β-lactams	Penicillins	Inhibit cell wall synthesis, inhibition of penicillin-binding proteins (PBPs)
	Cephalosporins	Inhibit cell wall synthesis, inhibition of PBPs
	Carbapenem	Inhibit cell wall synthesis, inhibition of PBPs
	Monobactams	Inhibit cell wall synthesis, inhibition of PBPs
	β-lactam inhibitors	Inhibit cell wall synthesis, inhibition of PBPs
Glycopeptides	-	Inhibit cell wall synthesis, inhibition of PBPs
Polymyxins	-	Target lipid A of Lipopolysaccharide in the outer membrane
Tetracyclines	-	Inhibit protein synthesis interferes with 30S ribosomal subunit
Aminoglycosides	-	Inhibit protein synthesis interferes with 30S ribosomal subunit
Macrolides	-	Inhibit protein synthesis, interferes with 50S ribosomal subunit
Chloramphenicol	-	Inhibit protein synthesis by preventing binding of tRNA to A site of 50S subunit
Oxazolidinones	-	Interfere with protein synthesis by binding to 23Sr RNA of the 50S subunit and interact with peptidyl-t-RNA
Lincosamides	-	Inhibit protein synthesis interfering 30S ribosomal subunit
Quinolones	-	Inhibit DNA topoisomerase
Fluoroquinolones	-	Inhibit DNA topoisomerase
Dihydrofolate Reductase inhibitors	-	Folic acid synthesis
Sulfonamides	-	Folic acid synthesis
Streptogramins	-	Inhibit protein synthesis interferes with the 50S ribosomal subunit
Rifamycins	-	Inhibit RNA polymerase
Others	-	DNA damage

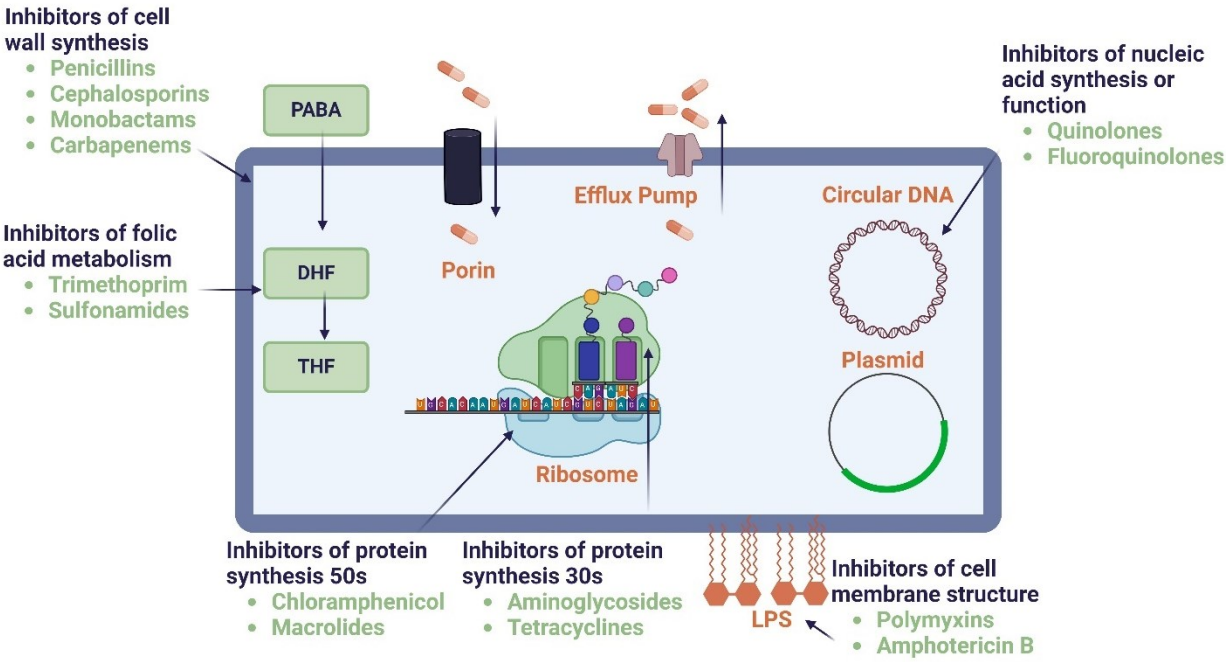

Figure 1.2. Antibiotic mechanisms of actions. Primary targets of antibiotics include efflux pumps, porin channels, ribosomes, cell wall structure, and DNA. Major classes of antibiotics are listed with each mechanism of action. Dihydrofolic acid (DHF). Lipopolysaccharide (LPS). Para-aminobenzoic acid (PABA). Tetrahydrofolic acid (THF). Created on Biorender.com.

1.1.2 Bacterial Mechanisms of Resistance

Bacteria have evolved to acquire molecular and cellular defence mechanisms against antibiotics. The major classes of antibiotics and their resistance mechanism are listed in Table 1.2. Molecular defences include target modification and protection, target repair compensation, and agent modification, binding, and degradation. Cellular defences include membranes, capsules, extracellular vesicles, efflux pumps, motility, biofilm formation, and phenotypic heterogeneity (Smith et al., 2023). Figure 1.3 illustrates the molecular and cellular mechanisms of resistance. Natural resistance mechanisms can either be intrinsic or induced (Reygaert, 2018). However, the two processes which bacteria acquire defence mechanisms are mutations and horizontal gene transfer (Smith et al., 2023). These acquired defence mechanisms appear when some strains of bacteria become resistant to the antibiotic that they were once susceptible to. Some of the efforts to inhibit, slowdown, and eliminate resistance include development of new synthetic antibiotics, finding natural products which are inhibitory, repurposing old drugs, and using drugs in combinational cocktails.

Table 1.2. Major classes of antibiotics, their sub-class, and their resistance mechanism. Details taken from (Saikia and Chetia, 2024).

Antibiotic Class	Sub-class	Mechanism of Action
β-lactams	Penicillins	Altered PBP, enzymatic degradation, decreased influx, increased efflux
	Cephalosporins	Altered PBP, enzymatic degradation, decreased influx, increased efflux
	Carbapenem	Altered PBP, enzymatic degradation, decreased influx, increased efflux
	Monobactams	Altered PBP, enzymatic degradation, decreased influx, increased efflux
	β-lactam inhibitors	Altered PBP, enzymatic degradation, decreased influx, increased efflux
Glycopeptides	-	Altered cell wall structure, target modification, acquisition of resistance genes
Polymyxins	-	Modification of phosphate group of Lipid A, multidrug efflux, reduced porin pathway, capsule formation
Tetracyclines	-	Overexpression of efflux pump, altered target, production of the proteins that bind to the active site
Aminoglycosides	-	The altered target, D-alanyl-D-alanine is changed to D-alanyl-D-lactate, aminoglycoside modifying enzymes, decreased influx, increased efflux
Macrolides	-	Altered target, overexpression of efflux pump, mutated ribosomal subunit
Chloramphenicol	-	Antibiotic inactivation, efflux pump overexpression, chloramphenicol acyl transferase
Oxazolidinones	-	Alteration of drug target, mutation leading to reduced binding of the substrate at the active site
Lincosamides	-	Active efflux and inactivation of the drug
Quinolones	-	Active efflux and mutation in topoisomerase IV or DNA gyrase
Fluoroquinolones	-	Active efflux and mutation in topoisomerase IV
Dihydrofolate Reductase (DHFR) inhibitors	-	Mutation in target
Sulfonamides	-	Mutation in dihydropteroate synthase gene
Streptogramins	-	Target modification, drug inactivation, drug efflux
Rifamycins	-	Mutation in target, enzymatic inactivation
Others	-	Decreased influx, increased efflux

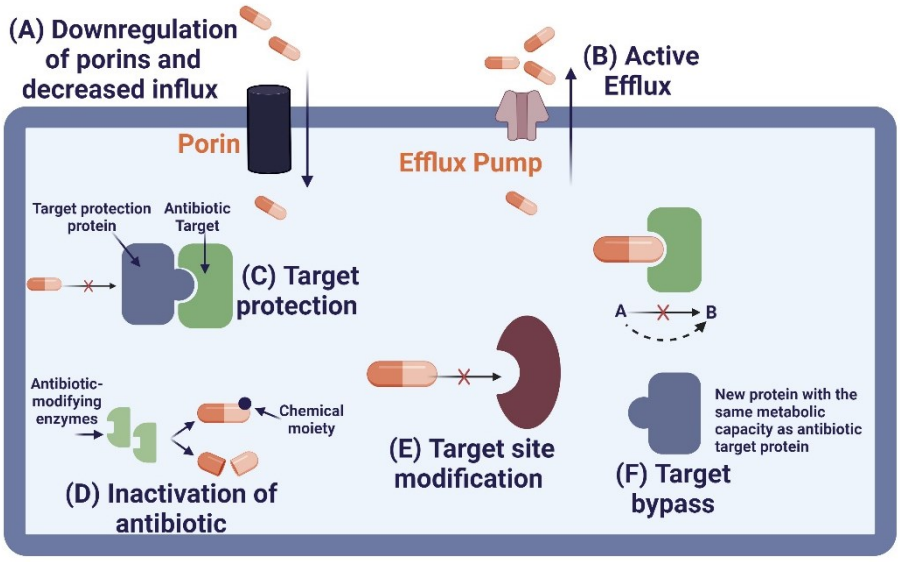

Figure 1.3. Molecular and cellular mechanisms of resistance. (A) Downregulation of porins and decreased influx. Changes to the membrane structure restrict passive transport of antibiotics into the cell. **(B)** Active Efflux. Antibiotics are transported out of cells to reduce the intercellular concentration. **(C)** Target protection. Another protein interacts with the antibiotic target, reducing the association of antibiotics to targets. **(D)** Inactivation of antibiotic. Enzymes degrade or modify the antibiotic molecule by hydrolysing the functional group. **(E)** Target site modification. The antibiotic target is altered to reduce binding of the antibiotic by mutations in the gene encoding the protein target of the antibiotic molecule or enzymatic alteration of the binding site. **(F)** Target bypass. Bacteria can produce proteins that can be used instead of the ones that the antibiotic inhibits. Adapted from (Darby et al., 2023). Created on Biorender.com.

1.1.3 ESKAPE Pathogens

The rise of antimicrobial resistance has caused a tremendous threat to human health. The World Health Organisation (WHO) has listed priority pathogens of main concern with multi-drug resistance including *Enterococcus faecium, Staphylococcus aureus, Klebsiella pneumoniae, Acinetobacter baumannii, Pseudomonas aeruginosa, and Enterobacter* spp. These pathogens are categorised as "ESKAPE" pathogens (WHO, 2024b). The ESKAPE pathogens share characteristics such as the power to flourish in the modern healthcare environment and possess resistance mechanisms which make them global infective burdens.

Bacteria are defined as Gram-positive or Gram-negative bacteria where Gram-positive bacteria have a thick peptidoglycan cell wall (20–80 nm) forming the outer shell of the cell, whereas Gram-negative bacteria have a thinner peptidoglycan cell wall (<10 nm) but also feature an additional outer membrane with various pores and appendages. These structural differences affect how the bacteria respond to external stresses like antibiotics (Mai-Prochnow et al., 2016). The group of high priority concern can be split into Gram-positive and Gram-negative organisms. Gram-positive organisms include *Enterococcus faecium* and *Staphylococcus aureus.* Whereas Gram-negative organisms include *Klebsiella pneumoniae, Acinetobacter baumannii, Pseudomonas aeruginosa, and Enterobacter* spp. (Miller and Arias, 2024).

Enterococcus faecium (E. faecium)

The commensal human gastrointestinal microbiota *Enterococcus faecium (E. faecium)* have shown resistance to vancomycin, undoubtedly through the horizontal acquisition of vancomycin-resistant genes, mainly *vanA* and *vanB* (Wei et al., 2024). Vancomycin resistant *E. faecium* is defined by the European Committee on Antimicrobial Susceptibility Testing (EUCAST) guidelines as having a minimum inhibitory concentration >4 μg ml^{-1} or according to the Clinical and Laboratory Standards Institute (CLSI) ≥32 μg ml^{-1} (Wei et al., 2024). Major clinical infections of Vancomycin-resistant *E. faecium* include bloodstream infections, infective endocarditis, intra-abdominal infections, and urinary tract infections (Miller and Arias, 2024). *E. faecium* displays resistance factors to β-Lactams, vancomycin, daptomycin, and linezolid. Antiseptics and hand hygiene are the main methods for managing transmission of *E. faecium* (Joshi et al., 2021). Up to 250,000 deaths were attributed to *E. faecium* antimicrobial resistance in 2019 (Antimicrobial Resistance Collaborators, 2022).

***Staphylococcus aureus (S. aureus*)**

S. aureus is found in the human commensal microbiota of the nasal mucosa in 20–40% of the general population (Lee et al., 2018). Methicillin-resistant *S. aureus* (MRSA) confer resistance to methicillin and, therefore, to most β-lactam antibiotics and this mutation is thought to be via horizontal gene transfer of staphylococcal cassette chromosome *mec* (SCCmec) (Lee et al., 2018). MRSA shows clinical infections of the blood, infective endocarditis, acute bacterial skin, and skin structure infections, community-acquired pneumonia, health-care-associated pneumonia/ventilator-associated pneumonia, and bone and joint infections. MRSA displays resistance factors to β-Lactams, vancomycin, daptomycin, linezolid, ceftaroline, and delafloxacin (Miller and Arias, 2024). Shockingly, MRSA caused over 100,000 deaths in 2019 (Antimicrobial Resistance Collaborators, 2022).

Klebsiella pneumoniae (K. pneumoniae)

K. pneumoniae is part of the normal human flora which spreads extensively in the mouth, skin, respiratory tract, urogenital tract, and intestine, among humans and animals (Li et al., 2023). The bacterium also can become pathogenic and shows resistance against the main antibiotic classes: carbapenems, cephalosporins, aminoglycosides, and fosfomycin, which leads to therapeutic failure (Li et al., 2023). The main medical infections of carbapenem-resistant or extended-spectrum β-lactamase-producing *K. pneumoniae* include bloodstream infections, urinary tract infections, intra-abdominal infection, community-acquired pneumonia, and healthcare-associated pneumonia/ventilator-associated pneumonia. This resistant bacterium displays resistance factors to β-Lactams, porin loss, efflux pumps, aminoglycoside modifying enzymes and 16S rRNA methyltransferases (Miller and Arias, 2024). *K. pneumoniae* was the second leading pathogen attributing to AMR deaths in 2019 (Antimicrobial Resistance Collaborators, 2022).

Acinetobacter baumannii (A. baumannii)

A. baumannii has the ability to endure on environmental surfaces and withstand disinfectants which is problematic in the healthcare setting as the bacterium tends to target patients with critical illnesses (Miller and Arias, 2024). A substantial proportion of *A. baumannii* isolates are now carbapenem-resistant (Isler et al., 2018). Carbapenem-resistant *A. baumannii* infections cause bloodstream infections, urinary tract infections, and healthcare-associated pneumonia/ventilator-associated pneumonia. Carbapenem-resistant *A. baumannii* displays resistance factors to β-Lactamases, porin loss, efflux pumps, aminoglycoside modifying enzymes and 16S rRNA methyltransferases (Miller and Arias, 2024). In 2019, *A. baumannii* resistance attributed 50,000 to 100,000 deaths (Antimicrobial Resistance Collaborators, 2022).

Pseudomonas aeruginosa (P. aeruginosa)

P. aeruginosa is associated with high morbidity and mortality in patients who are immunocompromised or have cystic fibrosis, rather than healthy individuals (Pang et al., 2019). *P. aeruginosa* displays resistance to multiple classes of antibiotics, and carbapenem-resistant *P. aeruginosa* has been well documented (De Oliveira et al., 2020). Major clinical infections of Carbapenem-resistant *Pseudomonas aeruginosa* include bloodstream infections, urinary tract infections, and healthcare-associated pneumonia/ventilator-associated pneumonia. Carbapenem-resistant *Pseudomonas aeruginosa* displays resistance factors to β-Lactamases, porin loss, efflux pumps, aminoglycoside modifying enzymes and 16S rRNA methyltransferases (Miller and Arias, 2024). Likewise, in 2019, *P. aeruginosa* resistance was one of the six leading pathogens for deaths associated with resistance (Collaborators, 2022).

Enterobacter cloacae (E. cloacae)

The *Enterobacter cloacae* complex (ECC) is split into two clusters with one associated with heterogeneity and the other associated with the healthcare environment (Miller and Arias, 2024). Dissemination of healthcare associated carbapenem-resistant *E. cloacae* has also occurred (De Oliveira et al., 2020). Carbapenem-resistant or extended-spectrum β-lactamase-producing *Enterobacter cloacae* complex show clinical infections ofthe blood, urinary tract infections, health-care-associated pneumonia/ventilator-associated pneumonia, and intra-abdominal infection. This resistant bacterium displays resistance factors to β-Lactamases, porin loss, efflux pumps, aminoglycoside modifying enzymes and 16S rRNA methyltransferases. Resistant *Enterobacter* spp*.* were responsible for 100,000 to 250,000 deaths associated with AMR (Antimicrobial Resistance Collaborators, 2022).

1.1.4 Mycobacterial Species

Another group of pathogens which are of concern are mycobacterial species. The rod-shaped bacteria from the genus *Mycobacterium* have 195 recognised species within the genus, each with distinct profiles (Armstrong Derek et al., 2023). Unlike the ESKAPE pathogens, mycobacterial species neither occupy Gram-negative or Gram-positive cell wall structures. Instead, they are defined as acid-fast bacilli which can avoid decolourisation by acids during microscopy staining procedures. This means that once the bacterium is stained, it cannot be decolorised using acids routinely used in the method. This feature enables their classification and distinction in laboratory techniques (Bayot et al., 2024). Mycobacterial cell wall composition is unique to this genus with several structural components including outer membrane lipids, mycolic acids, glycolipids, arabino-galactan, lipomannan, and phosphatidylinositol mannosides. The structural nature of mycobacterial pathogens makes them extremely hydrophobic and impenetrable which attributes in part to their multidrug resistance (Batt et al., 2020, Dulberger et al., 2020). The rod-shaped cell structures of mycobacteria are visualised in the scanning electron microscopy images in Figure 1.4. *Mycobacterium tuberculosis* and *Mycobacterium leprae* are the best well known pathogenic mycobacteria (Parish and Stoker, 1999), followed by *Mycobacterium chelonae*, *Mycobacterium fortuitum*, *Mycobacterium avium complex* and *Mycobacterium abscessus complex*, as well as many others. The mycobacteria that do not cause tuberculosis are described as nontuberculous mycobacteria (NTM)(Victoria et al., 2021).

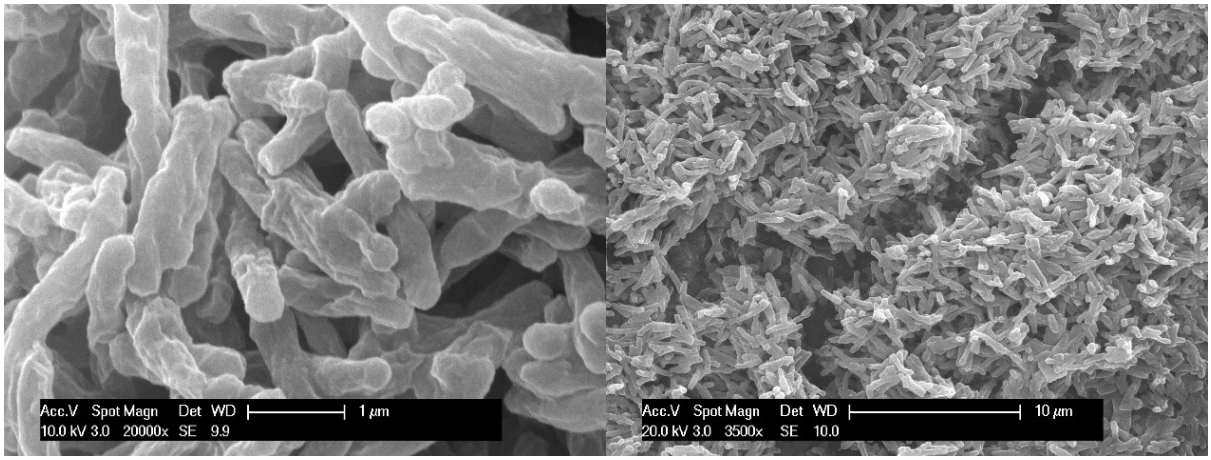

Figure 1.4. Scanning electron microscopy images of *Mycobacterium abscessus.* Images illustrate their rod-shape and clumping nature. Images taken by Antonia Molloy, 2022.

Mycobacterium tuberculosis (M. tuberculosis)

Mycobacterium tuberculosis (M. tuberculosis) is the causative agent of the human pulmonary infection tuberculosis (TB). TB is the world's leading infectious disease killer since the global COVID-19 pandemic. The World Health Organisation (WHO) estimates that 1.5 million people died from TB in 2020 (WHO, 2020). Despite most TB strains being treatable with antibiotics,

some of the key medical challenges include achieving rapid diagnostics, the rise of multi-drug resistant TB, and the poor treatment efficacy of latent TB. The current recommended treatment for drug susceptible TB takes a minimum six-month administration of isoniazid (INH), rifampicin (RIF), pyrazinamide (PZA), and ethambutol (EMB) (Lee, 2016). This first-line recommendation has failed to adapt in the last thirty-five years despite the increasing occurrence of drug resistance. Recently, a phase 3 trial provided evidence of a four-month treatment regimen with rifapentine and moxifloxacin (Dorman et al., 2021). Additionally, sufficient efforts were made to reduce the mycobacterial burden (reducing mortality and transmission), eradicate persistent mycobacterial populations, and to reduce drug resistance through various incentives such as END-TB (END-TB, 2016) and WHO End TB Strategy 2016–2035 (WHO, 2015). Research into the economic burden of TB has revealed a global cost of 983 billion US dollars from 2015–2030 if the current health status continues (Burki, 2018). There is a pressing need for innovative advancements and applications which combine multidisciplinary research for combating the looming crisis of TB.

The molecular pathology by which *M. tuberculosis* evades the host and causes disease is complex, involving a dynamic range of immune cells. The organism infects the host after the inhalation of droplet nuclei spread by aerosolization from an infected individual, which then resides in the respiratory tract (Jee, 2020). There are various types of infection that can manifest from *M. tuberculosis* in individuals—one where the infection clears, one with an active infection treated with a course of antibiotics, and one which remains in a latent form (Getahun et al., 2015). The latent form is often left untreated. Upon infection, the early innate immune system emerges with an influx of neutrophils, monocytes, macrophages, and dendritic cells of the lungs (Ernst, 2012). Through phagocytosis, bacteria are consumed by alveolar macrophages to form a phagosome and then eliminated through the formation of phagolysosomes (Pieters, 2001). However, *M. tuberculosis* can avoid this host defence response by persisting in phagosomes and inhibiting lysosome fusion (Pieters, 2001). The subsequent established intracellular infection and influx of immune cells which surround the site of infection forms a tuberculous granuloma (Ramakrishnan, 2012). The early granuloma (Figure 1.5) composes the infected macrophages in the centre, enclosed by foamy macrophages and other mononucleated cells, and surrounded by lymphocytes (Russell et al., 2009). During the maturation of the granuloma, a fibrous capsule encloses the macrophage centre and eventually forms necrotic lesions, leading to caseation (Ramakrishnan, 2012, Russell et al., 2009).

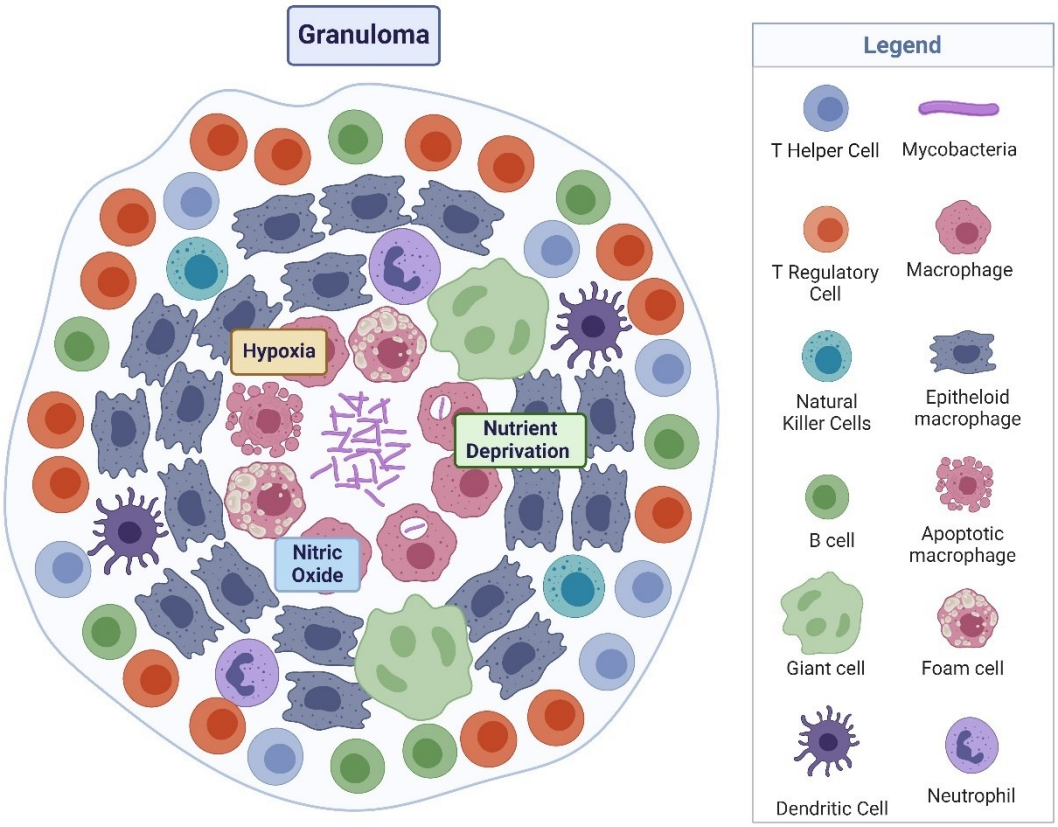

Figure 1.5. Tuberculous granuloma. Encapsulated *Mycobacterium tuberculosis* surrounded by immune cells, creating a hypoxic, nutrient-deprived, and nitric oxide environment. Image created on Biorender.com.

Here, *M. tuberculosis* can survive in a dormancy state known as non-replicating persistence (NRP). The external pressures such as hypoxia, nutrient deprivation, low pH, and high CO2 created by the hostile host environment induce this survival response of the bacteria (Martin et al., 2016). The NRP state can relapse into active disease, especially in high-risk groups such as immunodeficient individuals, persons infected with human immunodeficiency virus or undergoing organ and haematologic transplantations (Getahun et al., 2015). Houben and Dodd (2016) estimated that NRP TB infected approximately 1.7 billion people in 2014 by generating an annual risk model of infection between 1934 and 2014 (Houben and Dodd, 2016). The issue posed by the ability of NRP *M. tuberculosis* to effectively hide within the hostile environment of the granuloma is that not only does the immune system keep the bacteria trapped, it also physically restricts penetration by antimicrobials, thus protecting *M. tuberculosis* from antibiotic activity.

Early diagnosis and accurate detection of TB infection is essential for effective treatment options, especially in low-income and high-burden countries. Conventional TB diagnostics include microscopy (Ziehl–Neelsen staining), which provides 22–43% low sensitivity for a single smear (Singhal and Myneedu, 2015). Other methods include chest radiography, which

is limited in resource constraint locations (Walzl et al., 2018), and liquid/solid culturing, which requires suitable levels of biosafety (Pai et al., 2016). Diagnosis of latent infection requires a tuberculin skin test or interferon-gamma release assays. However, both of these tests do not identify individuals that will progress to active disease (Pai et al., 2016). The phenotypic evaluation of clinical isolates, by culturing *M. tuberculosis* in the laboratory in the presence of different concentrations of antimicrobials, is traditionally used to detect drug-resistant strains. The turnover time for these results is extensive, by which point the patient's health will have deteriorated (Lee et al., 2020). Improvements in molecular diagnostic testing have revolutionised detection, such as the genotypic test Cepheid GeneXpert MTB/RIF, which can give a readout in two hours of TB detection and RIF resistance (Boehme et al., 2010). The WHO supports the expansion of whole genome sequencing of TB, which still depends on culturing samples and technical methods for preparing genomic DNA for sequencing (Meehan et al., 2019). User-friendly and non-laborious detection methods, which are portable, are required to improve detection time at a lower cost. Historically, experimental modelling of TB helped scientists to discover the pathogenicity, physiology, metabolism, and the genetic make-up of the organism.

Challenges arising for researchers studying mycobacteria are the characteristics of slow growth rate, hydrophobic aggregation of cells in the absence of non-ionic surfactant when grown in culture, and the need for the containment of aerosols which brings additional safety precautions, including a biosafety level 3 (BSL-3) facility (Parish and Stoker, 1999). Additionally, the investigation of heterogenicity is difficult in bulk cultures compared with single-cell analysis (Toniolo et al., 2021). Animal models are abundant for studying TB, such as zebrafish, rabbits, guinea pigs, and mouse models (Singh and Gupta, 2018). However, the ability of each model to represent all aspects of the physiological state of the cell and tissue environment is absent (Singh and Gupta, 2018), or they entirely lack the lung immune system (Rhoades et al., 1997). However, absent is the ability of each model to represent all aspects of the physiological state of the cell and tissue environment. Extensive reviews outlined the experimental modelling of this organism in its non-replicating state (Gibson et al., 2018, Parish, 2020, Batyrshina and Schwartz, 2019). Furthermore, to date, no NRP models mimic all the physiological features of the bacteria in this condition. Therefore, novel *in vitro* experimental models of TB are imperative. Research groups often use variable types of nutrient media, inoculum starting points, and reading endpoints, making the standardisation of antimicrobial testing for *M. tuberculosis* difficult. Effort was made to standardise testing; however, protocols are still time consuming (Schön et al., 2020, Kim, 2005).

TB has shown resistance to antimicrobials, including multidrug-resistant strains resistant to RIF and INH (WHO, 2020). Alarmingly, extensive drug-resistant TB is increasing, which is resistant to RIF, INH, Fluoroquinolone, and Kanamycin (Prevention, 2006). There is an urgent

need for shorter and more effective treatment regimens, as well as the discovery of novel compounds. Biomedical engineering approaches such as applied technology have advanced the field of drug discovery and will continue to develop new research models with ever more accurate mimicry of human physiology.

***Mycobacterium bovis* BCG (*M. bovis* BCG)**

Bacillus Calmette-Guerin (BCG) is the live attenuated vaccine form of *Mycobacterium bovis* used to prevent tuberculosis from 1921 onwards (Okafor et al., 2024). *M. bovis* (BCG) is used as a model of *M. tuberculosis* in phenotypic screens of anti-TB drug discovery (Grzelak et al., 2019, Altaf et al., 2010). *M. bovis* BCG is used as a model for tuberculosis because it offers a safe, immunologically relevant, and genetically similar alternative to *M. tuberculosis*, facilitating drug discovery (Brosch et al., 2007).

Mycobacterium abscessus (M. abscessus)

Pathogens which are non-tuberculous mycobacteria (NTM) encompass fast growing mycobacteria. The *Mycobacterium* abscessus complex (MABSC) is incorporated in NTM organisms and includes opportunistic *M. abscessus* subsp*. abscessus, M. abscessus* subsp*. bolletii,* and *M. abscessus* subsp*. massiliense,* each having unique phenotypic and genotypic properties. Conflicting opinion surrounding the characterisation of these subspecies caused debate over recent years due to poor genetic sequencing techniques. (López-Roa et al., 2022, Lopeman et al., 2019).

Each subspecies of *M. abscessus* has distinct macrolide resistance profiles. The subspecies *M. abscessus* subsp*. abscessus, M. abscessus* subsp*. bolletii* are macrolide resistant and the *M. abscessus* subsp*. massiliense* strain is macrolide susceptible (Jong et al., 2022). Macrolide resistance occurs due to the presence of the gene erm(41). This gene confers the ability to produce erythromycin ribosome methylase (Erm) on most MABSC species. Erm decreases macrolide affinity to the ribosome exit tunnel by methylating the A2058 nucleotide of the 23S rRNA gene, and hence, results in weak treatment outcomes (Jong et al., 2022).

In addition to genetic variances, each subspecies has phenotypic differences in cell morphology when grown on solid agar. Smooth morphologies with a glossy appearance do not show cord formation, however, glycopeptidolipids (GPL) are present on their cell walls, which regulate bacterial hydrophobicity and, consequently, biofilm formation. Loss of GPL causes the smooth morphotype to transition irreversibly into the rough morphotype, characterised by cord formation and a waxy, textured appearance on solid agar. The rough variant is assumed more virulent as it can replicate within macrophages, induce apoptosis, and then re-release itself back into the host for re-infection (Rüger et al., 2014, Kam et al., 2022).

M. abscessus infection is associated with skin and soft tissue infections, as well as immunocompromised patients with pulmonary diseases or in cystic fibrosis patients who have an autosomal recessive disorder (Desai and Hurtado, 2018). *M. abscessus* infections can persist in patients and remain asymptomatic, akin to *M. tuberculosis* (Johansen et al., 2020). Currently, treatment of MABSC infections involves a lengthy combination of antibiotics and is associated with harmful side effects and poor success rates. Worryingly, *M. abscessus* has intrinsic drug resistance mechanisms, including an impermeable cell wall, inducible resistance genes, plasmid mediated resistance, and efflux pumps (Lopeman et al., 2019). These resistance profiles are associated with huge treatment struggles. An efficient drug development pipeline for *M. abscessus* species is required to improve treatment options and reduce resistance.

1.1.5 Drug Discovery Pipeline

The antimicrobial drug discovery pipeline is strained despite an enormous demand for new novel antibiotics. From the 1930s to the late 1950s, numerous antibiotics were discovered, classifying this period as the 'golden age' of antibiotic development. Now, many of the "low-hanging fruits" are used and development comes from semi-synthetic chemistry (Brüssow, 2024). However, the lack of economic appeal associated with antibiotics has slowed their development within the pharmaceutical industry. The profit value of antibiotics sits far below that of non-antimicrobial drug classes, such as anti-cancer compounds. Multiple pharmaceutical companies restructured and shut-down their antibiotic research and development departments, leaving small and medium-sized enterprises to fill the void (Renwick et al., 2016).

Furthermore, only 16 new antimicrobials were approved by regulatory agencies since 2017 (WHO, 2024a). The World Health Organisation published their report in 2024 on "2023 Antibacterial agents in clinical and preclinical development". The main finding concluded that only 16 out of the 128 candidates for high priority pathogens in the antimicrobial pipeline between 2017 and 2013 received market approval (WHO, 2024a). Reasoning for this poor clinical translation is causative of the problematic application of existing drug discovery tactics to the field of infectious disease, which is constantly adapting (Renwick et al., 2016). A study analysing why funding applications of antibacterial drug discovery projects submitted to two major global funders between 2016 and 2020 failed, concluded that the most common reason was due to insufficient characterisation of *in vitro* activity and/or insufficient *in vitro* testing of the hits/leads (Theuretzbacher et al., 2023). These major concerns encompass the basic research level in the drug discovery pipeline. However, studies revealed that this stage is the most underfunded (Renwick et al., 2016). This finding propagates the need to improve *in vitro* antibiotic susceptibility testing for adequate clinical progression.

1.1.6 *In vitro* Antibiotic Susceptibility Testing

Antimicrobial susceptibility testing (AST) is a critical step in discovery and characterisation of natural and synthetic antimicrobial compounds. AST combines one or more antimicrobial agents with bacteria to assess bacterial growth. Activity of an antimicrobial against bacteria is based on their minimum inhibitory concentration (MIC) which is defined as the lowest concentration of a compound which, under strictly controlled *in vitro* conditions, completely prevents visible growth of bacteria (Kowalska-Krochmal and Dudek-Wicher, 2021). Methods which are appropriate to screen and evaluate potential antimicrobial candidates are essential in the drug discovery pipeline. Several *in vitro* antimicrobial assays have been developed (as defined in Figure 1.6), providing valuable insights into the efficacy of bacterial inhibition and eradication. However, these methods do not accurately represent the physiology of the bacteria in infection environments and hence, rarely translate into clinical results (Hossain, 2024, Schumacher et al., 2018, Gajic et al., 2022). Furthermore, these screens are low throughput, laborious, and use a considerable number of plastics, leading to unsustainable practice in AST. New innovative techniques are required to improve *in vitro* AST. Microfluidics can be considered high-throughput AST platforms at the microscale level due to their ability to adjust antibiotic concentrations and environmental conditions.

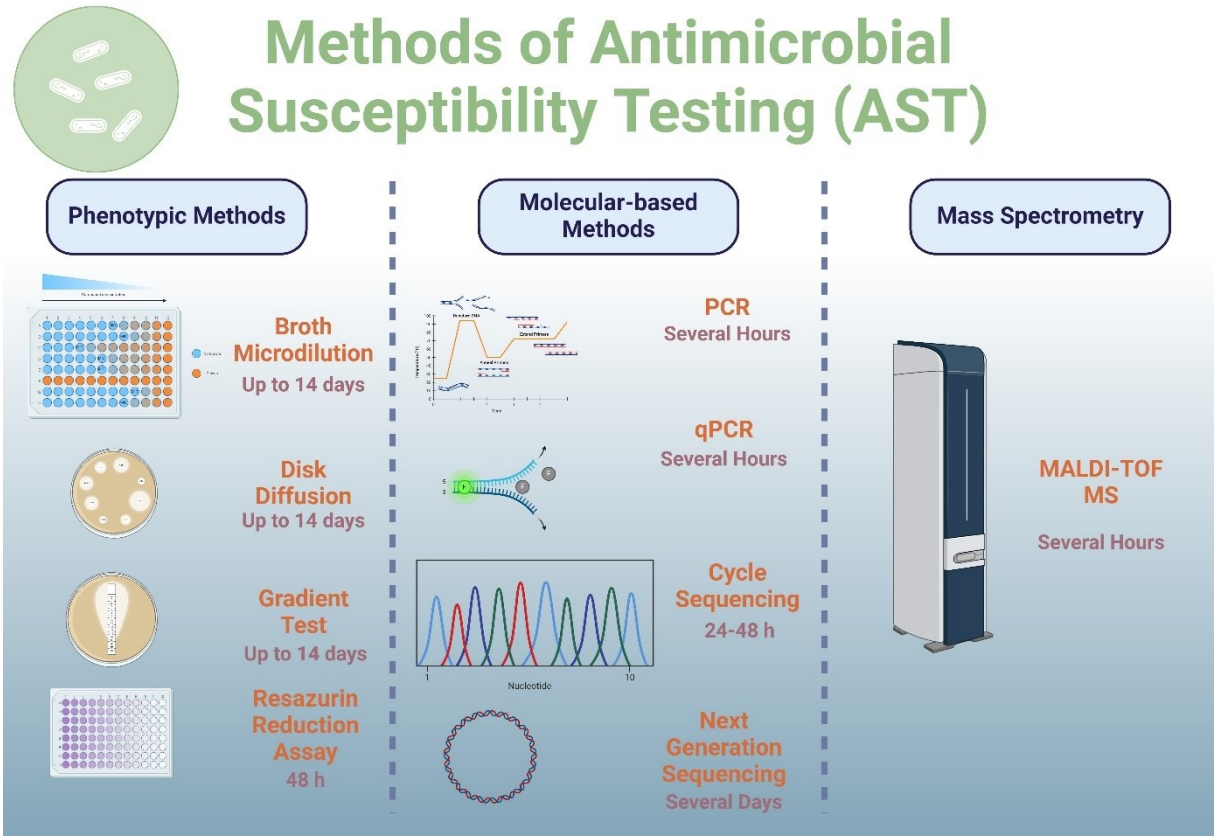

Figure 1.6. Methods of antimicrobial susceptibility testing. Assay times will depend upon bacterial growth characteristics. Created on Biorender.com.

1.2 Microfluidics

1.2.1 Technological Advancement of Microfluidics

The advancement of microbiology techniques, particularly in high-throughput phenotypic assessment, necessitates innovative and advanced technologies. Microfluidics, a rapidly evolving field at the intersection of biology, chemistry, physics, and engineering, has emerged as a promising solution. This multidisciplinary approach, leveraging advancements in micro and nanotechnology, offers wide-ranging applications in microbiology and beyond. Microfluidics is the systematic manipulation of systems featuring microscale channels, where fluid volumes ranging from nanolitres to attoliters can be precisely controlled and directed through specific geometric configurations (Whitesides, 2006). This precise control over minute fluid volumes enables various biological and chemical analysis applications. The field of microfluidics encompasses various specialised subtypes, each with unique characteristics and applications:

1. Lab/organ-on-a-chip: Mimicking complex biological systems
2. PDMS-based devices: Utilising flexible, biocompatible materials
3. Microelectromechanical systems (MEMS): Integrating mechanical and electrical components
4. Microfluidic paper electrochemical devices: Offering low-cost, disposable options
5. Centrifugal microfluidics: Harnessing centrifugal forces for fluid manipulation
6. Droplet microfluidics: Enabling precise control of discrete fluid volumes

These diverse approaches cater to various research and industrial needs (Tabeling, 2005). Microfluidic systems are particularly well-suited for microbiological applications due to their compatibility with the scale of bacteria. These platforms enable the execution of parallel biological assays under precisely controlled environmental conditions. This capability allows researchers to:

1. Conduct high-throughput screening of microbial populations
2. Study bacterial behaviour at the single-cell level
3. Analyse microbial interactions in controlled microenvironments
4. Perform rapid antimicrobial susceptibility testing

The ability to manipulate small volumes of fluid with high precision makes microfluidics invaluable in advancing our understanding of microbial systems and developing new antimicrobial strategies.

1.2.2 The Physics of Microfluidics

Different physical forces direct the behaviour of a fluid in a system. The essential behaviour of a hydrodynamic system and the dominant physical effects are typically analysed by characteristic, dimensionless numbers. These numbers compare the relative importance of competing forces, or they may be described as ratios of characteristic length, time, or energy scales. The most prominent number in microfluidics is the Reynolds number, describing the ratio of inertial forces and viscous forces (Squires and Quake, 2005):

$$(1)\ \mathbf{Re} = \boldsymbol{\rho}\mathbf{vL}/\boldsymbol{\mu}$$

with mass density (the ratio of a mass of fluid to its volume of the fluid kg/m^3) $\boldsymbol{\rho}$, velocity **v**, dynamic viscosity **μ**, and a characteristic length **L** describing the dimensions of the system. Due to the capacity of microfluidic systems and the corresponding slow flow velocities, the value of the number is typically Re<1, causing laminar flow, a regime also referred to as Stokes flow, which is a subtype of laminar flow. Mathematically, this regime is governed by the Stokes equation when Re<1 (Squires and Quake, 2005):

$$(2)\ \boldsymbol{\nabla}\mathbf{p} + \mathbf{f} = \boldsymbol{\mu}\boldsymbol{\Delta}\mathbf{v}$$

which is a linearisation of the Navier–Stokes equation, whereby the inertia term $\boldsymbol{\rho}\left(\frac{\partial v}{\partial t}\right) + \boldsymbol{v}\boldsymbol{\nabla}\boldsymbol{v}$ has been neglected. This inertia term represents the fluid version of the acceleration part $\boldsymbol{m}\frac{\boldsymbol{dv}}{\boldsymbol{dt}}$ in Newton's second law, vanishing for small Reynolds numbers. The stationary Stokes equation as shown here in Equation (2) relates the gradient of the pressure **p** to the change in velocity **v** and an external body force **f** (e.g., a gravitation or dielectrophoretic force), with **∇** and **Δ** being the Nabla and Laplace operator, respectively. Specifically, the pressure gradient and the external body force drive the fluid flow. However, for some high-throughput applications operating at high flow velocities, the assumption of small Re does not necessarily hold true as the regime of "inertia microfluidics" is entered. In this regime, the full Navier–Stokes equation, including its non-linear inertia term, must be considered.

With the absence of turbulent flow, the mixing of parallel laminar fluid flows in microfluidics only occurs by diffusion, which can be a slow process. The Péclet number (**Pe**) describes the ratio of the rates of convection and diffusion for suspended objects, and is given by (Tabeling and Chen, 2005):

$$(3)\ \boldsymbol{Pe} \equiv \frac{\boldsymbol{vw}}{\boldsymbol{D}} = \frac{\boldsymbol{diffusion\ time}}{\boldsymbol{convection\ time}}$$

where **v** and **w** are the flow velocity and microchannel width. The diffusion coefficient is given by **D** and the following Stokes–Einstein relation enables the calculation of **D** for spherical objects:

$$(4)\ \boldsymbol{D} = \frac{\boldsymbol{k}\mathbf{T}}{\boldsymbol{6\pi\mu a}}$$

In Equation (4), **k** is the Boltzmann constant, **T** is the absolute temperature, and **a** is the hydrodynamic radius of the suspended object. For micrometre-sized objects, the effect of diffusion is generally minimal and does not significantly influence overall particle trajectory. However, as object size decreases, diffusivity increases, connoting that separation efficiency will be decreased unless flow velocity is increased.

Where mixing is desired, passive mixing is introduced when designing channel geometries, such as ridges, network gradient generators, and vortex micromixers. Alternatively, active mixing can be introduced by external energy, for example, electrokinetic forces, and thermal actuation (Novotný and Foret, 2017b). Active and statistical mass transport can occur in microfluidic systems (Tabeling and Chen, 2005).

As the geometrical dimensions of a microchannel decrease, the fluidic resistance increases because of friction between the microchannel walls and the body of fluid. Generally, the surface area to volume ratio increases as the channel geometry becomes more complex, and so does the fluidic resistance $\mathbf{R}$, which can limit the fluid flow rate $\mathbf{Q}$. For pressure-driven flow, the relationship between these properties is given by:

$$(5)\ \mathbf{Q} = \frac{\Delta\mathbf{p}}{\mathbf{R}}$$

where $\Delta\mathbf{p}$ is the pressure difference along the microchannel—an increasing $\mathbf{R}$ value would cause a continuing decrease in $\mathbf{Q}$.

The three-dimensional shape of the channel governs the method required to estimate the fluidic resistance of the microchannel. In a high aspect ratio rectangular microchannel, whereby channel width or height **h** are larger than the other dimension, the fluidic resistance is given by (Beebe et al., 2002):

$$(6)\ \mathbf{R} = \frac{\mathbf{12\mu l}}{\mathbf{wh}^3}$$

where the channel length is **l**. Conversely, in a low aspect ratio rectangular microchannel (**w≈h**), the resistance is given by (Beebe et al., 2002):

$$(7)\ \mathbf{R} = \frac{\mathbf{12\mu l}}{\mathbf{wh^3}}\left[\mathbf{1} - \frac{\mathbf{h}}{\mathbf{w}}\left(\frac{\mathbf{192}}{\boldsymbol{\pi}^{\mathbf{5}}}\sum_{\mathbf{n=1,3,5}}^{\infty}\frac{\mathbf{1}}{\mathbf{n^5}}\tan\mathbf{h}\left(\frac{\mathbf{n\pi w}}{\mathbf{2h}}\right)\right)\right]^{-1}$$

The resistance in a microchannel with a circular cross-section can be calculated using:

$$(8)\ \mathbf{R} = \frac{\mathbf{8\mu l}}{\boldsymbol{\pi}\mathbf{r}^4}$$

where **r** is the radius of the circular cross-section.

1.2.3 Microfluidic Chip Materials and Fabrication

Some of the most frequently used materials in microfluidics include thermoplastics, polydimethylsiloxane (PDMS), inorganic materials such as glass or silicon, paper, and even devices made by 3D printing, a newer approach to fabrication (Nielsen et al., 2020). The most frequently used techniques for manufacturing microfluidic devices include micromachining, soft lithography, embossing, *in situ* construction, injection moulding, and laser ablation—the reader is referred to expert reviews on such methods (Tabeling and Chen, 2005, Beebe et al., 2002, Nielsen et al., 2020, Becker and Gärtner, 2008, Faustino et al., 2016).

The most suitable method of device fabrication and material selection often depends on the specific application of the device. For example, a prerequisite for microfluidic devices to be used in biological investigations is that they must, of course, be biocompatible. Further, chips to be used for biological applications should be manufactured in a clean room setting to prevent the microchannel being contaminated by dust or other matter (Tabeling and Chen, 2005). Thermoplastics and PDMS are often selected as the material of choice as they are well researched and microfluidic chip fabrication with these materials is generally a lower cost than glass or silicon (Mata et al., 2005, Martinez-Duarte, 2012, Gencturk et al., 2017). Paper microfluidics are extremely low cost and can be used to measure desired molecules quickly by visual inspection (Gong and Sinton, 2017, Xia et al., 2016, Yang et al., 2017, Li and Steckl, 2019).

Silicon micromachining was first developed for application within the field of microelectromechanical systems (MEMS) but was subsequently one of the first techniques to be used for the microfabrication of microfluidic systems (Ziaie et al., 2004). The well-understood surface modification properties of silicon, plus the material's considerable chemical resistance and ease of design, make silicon a desirable material for creating microfluidic devices for biological applications (Ziaie et al., 2004). Despite that, silicon devices are not

transparent in visible light, denoting that such devices are not well suited for fluorescence-based detection or imaging applications (Nge et al., 2013). However, making a composite device comprising transparent materials such as glass or polymers, which enclose silicon microchannels, can improve suitability for imaging and fluorescence-based activities (Nge et al., 2013).

Glass has excellent analysis performance due to its biocompatibility, optical transparency, low fluorescence background, surface stability, and chemical resistance (Nge et al., 2013). However, glass fabrication processes are generally complex, sometimes involving etching using hazardous substances such as hydrofluoric acid and/or femtosecond laser-based fabrication procedures (Italia et al., 2019), requiring intensive training and safety precautions. Furthermore, high temperature, often in combination with high pressure, is typically required during bonding. This means that dedicated equipment is often required for fabrication, and that glass devices suffer from complications in preloading reagents before assembly, which can be problematic for some biological applications (Nielsen et al., 2020).

Soft lithography is one of many techniques used to fabricate microfluidic chips, which has propelled the use of PDMS as a commonly used microfluidic device material. By contact printing, replica modelling and embossing, soft lithography can be used to create micro-patterns (Xia and Whitesides, 1998). The procedure includes making a master mould containing a design made by computer-aided design (CAD). PDMS and a crosslinking agent are poured on top of the mould and placed in a high-temperature incubator. Once hardened, it is peeled from the mould to obtain a replica of the master. Access holes are punched for inlet and outlet tubes and the PDMS is placed on a glass slide and bonded by plasma treatment (Weibel et al., 2007). This process is illustrated in Figure 1.7.

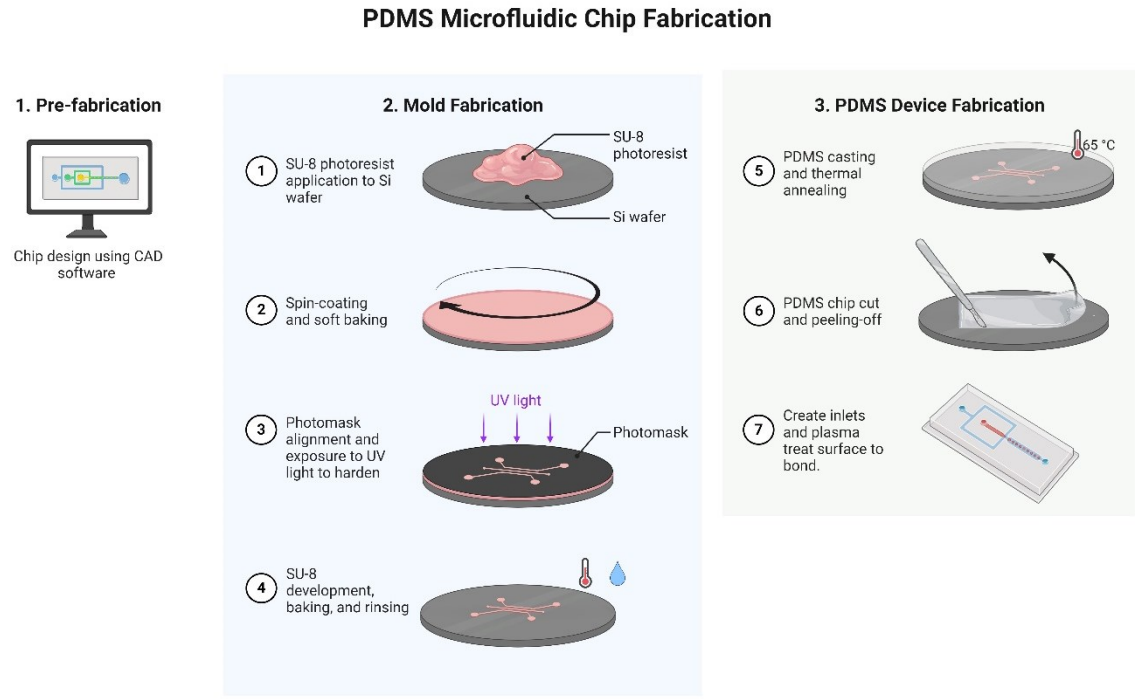

Figure 1.7. Schematic diagram of soft lithography procedure. Image created on Biorender.com.

Thermoplastics were extensively researched, refined and used for the mass production of high-quality goods, since their initial industrial uses in the 1930s (Lokensgard, 2016). Various thermoplastics exist that was used in microfluidics, including cyclo olefin (co) polymer (COC/COP), polymethyl methacrylate (PMMA), polystyrene, polytetrafluoroethylene (PTFE), and polyetheretherketone (PEEK)—an excellent review by Gencturk et al. (Gencturk et al., 2017) evaluates the physical properties of thermoplastics used in microfluidics, and the present state of the development and applications of thermoplastic microfluidic systems used in cell biology and analyses. PMMA is used as an example, which is widely used in research laboratories because it is optically transparent and can be manipulated with fabrication methods such as hot embossing, laser ablation, or precision milling (Gencturk et al., 2017). This material is useful for small-scale prototyping/production (Wu et al., 2019); however, the variability inherent in PMMA devices made by these fabrication methods often makes them unsuitable for large-scale commercial production. For example, channel smoothness can be low, and the heated sealing process can cause deformations which give variability between devices. COP/COC is generally a better material choice than PMMA due to its biocompatibility, favourable optical properties, low water uptake, low binding affinity for proteins, rigidity, strength, and stability (Piruska et al., 2005, Wright, 1989, Abdel-Wahab et al., 2017, Becker and Gärtner, 2000). Furthermore, COC's exceptional moldability makes it suitable for hot embossing microfabrication (Becker and Gärtner, 2008).

The use and prevalence of paper-based microfluidics has increased significantly in recent years due to the compatibility of such devices in point-of-care or point-of-use testing applications, plus their simplicity, fundamental low cost, biocompatibility, and hydrophilicity (Li and Steckl, 2019, Sher et al., 2017). Various medical conditions (e.g., pregnancy testing, virus assays, etc.) can be identified/evaluated using paper microfluidic systems (Li and Steckl, 2019). Fluid flow in paper devices does not require a driving external force and instead relies on capillary force to drive fluid flow, which is caused by the intermolecular force between the fluid and the porous cellulose matrix of the material (Technology, 2017). Paper-based diagnostic devices are simple to use, disposable, low cost, and environmentally friendly (Songok and Toivakka, 2016). The disposable nature of paper and paper-derived materials reduces the risk of cross contamination, and the low cost of these materials allows broader application and more frequent testing.

3D printing may solve the limitations of previous microfluidics fabrication techniques, offering lower costs and faster prototyping compared to methods like soft lithography or hot embossing (Nielsen et al., 2020). Furthermore, complex 3D structures can be manufactured without the need for a cleanroom environment. Three main 3D printing technologies exist: fused deposition modelling, PolyJet, and stereolithography. Each technology has advantages and disadvantages—the reader is directed to a specialist review to understand each of these methods (Nielsen et al., 2020).

1.3 Droplet Fluidics

Droplet microfluidics, a specialised subset of the microfluidics field, focuses on studying and manipulating multiphase flows. This technique enables generating and controlling discrete droplets with volumes ranging from nano- to femtoliters. These droplets are produced by specialised micro-nozzles in a carrier fluid, with production rates typically exceeding 10 kHz. Recent advancements have pushed these rates even higher, with some systems achieving droplet production rates exceeding 1 MHz (Vyawahare et al., 2010). This high-throughput capability, combined with precise control over droplet size and composition, makes droplet microfluidics particularly well-suited for a wide range of biological and chemical applications, especially in microbiology and antimicrobial research. The high droplet production rates achievable in droplet microfluidics systems offer the unprecedented capability to conduct millions of experiments within a single microfluidic device. This technology provides several critical advantages for microbiological research:

1. Efficient control of droplet volumes: Allowing precise manipulation of bacterial microenvironments.
2. Repeatable and reliable droplet manipulation: Ensuring experimental consistency and reproducibility.
3. High-throughput capability: Enabling rapid screening of large bacterial populations or antimicrobial compounds.
4. Single-cell analysis: Facilitating the study of individual bacterial cells and their responses to various stimuli.
5. Automation potential: Streamlining experimental processes and reducing human error.

These features make droplet microfluidics particularly valuable for studying antimicrobial resistance, where large-scale, precise experiments at the single-cell level are crucial. Droplet microfluidics has found applications across a wide range of scientific disciplines, with particular relevance to microbiology and antimicrobial research:

1. Biological assays: Including high-throughput screening of bacterial populations and antimicrobial compounds (Theberge et al., 2010).
2. Chemical analysis: Enabling precise control over reaction conditions and rapid chemical synthesis (Abou-Hassan et al., 2010).
3. Inorganic chemistry Facilitates the study of reaction kinetics and the synthesis of nanomaterials (Zheng et al., 2005).

4. Protein crystallisation: Aiding in structural biology studies, which can be crucial for understanding bacterial proteins and potential drug targets (Shim et al., 2007, Guo et al., 2012).
5. Antimicrobial susceptibility testing: Allowing rapid, high-throughput assessment of bacterial antibiotic response.

These diverse applications highlight the versatility of droplet microfluidics and its potential to accelerate research in antimicrobial resistance and drug discovery.

1.3.1 The Physics of Droplet Fluidics

For single-cell analysis applications using droplet microfluidics, liquid/liquid emulsions comprising a cell-friendly aqueous interior, and a surfactant-stabilised fluorous oil are often used. Inclusion of cells in the aqueous, dispersed phase results in the encapsulation of individual cells within the emulsion. The droplet occupancy number can be controlled by altering the concentration of cells within the dispersed phase and calculated using Poisson statistics (Collins et al., 2015). Droplet microfluidic systems allow for the convergence of two immiscible fluids, with their separation occurring solely at the interfaces (Figure 1.8), leading to the presence of interfacial tension $\boldsymbol{\gamma} i$. The term “surfactant” is a shortening of the term “surface active agent”, and describes an amphiphilic molecule, i.e., with different groups having affinities for different immiscible phases (water/oil, water/air, oil/air). In droplet microfluidics, surfactants have a basic role: to guarantee that droplets do not coalesce, which is the minimal requirement for the use of droplets as microreactors. This amphiphilic property drives surfactant molecules to the interface of the two fluids: the surface tension of the interfacial layer and interfacial tension between the two phases is decreased. The decrease in surface tension is directly influenced by the amount of molecules adsorbed at the interface, as given by the Gibbs adsorption isotherm for dilute solutions (Cabane and Hénon, 2007):

$$(\mathbf{9})\ \boldsymbol{\Gamma} = -\frac{\boldsymbol{c}}{\overline{\boldsymbol{R}}\boldsymbol{T}}\frac{\mathbf{d}\boldsymbol{\gamma}}{\mathbf{d}\boldsymbol{c}}$$

where $\boldsymbol{\Gamma}$ is the surface concentration, $\boldsymbol{c}$ the surfactant bulk concentration, $\boldsymbol{T}$ is temperature, $\overline{\boldsymbol{R}}$ the gas constant, and $\boldsymbol{\gamma}$ the surface tension.

As surfactants adsorbs to the interface, the interface rigidifies: the loss of mobility imposes a change in the boundary condition at the interface, which slows it down. The origin of the rigidification is the alleged Marangoni effect: as a drop moves, the surfactant distribution is non-uniform, with an excess at the rear of the drop (Baroud et al., 2010). The non-uniform surface concentration leads to a gradient in surface tension (the surface tension is decreased at the drop rear) which generates a stress opposed to the flow. When surface tension exists at

the interfacial layer of two phases, with surfactant added to the oil phase, the Marangoni flow counteracts film drainage to counteract phase mixing, which limits coalescence in droplet systems.

In conjunction with the interfacial tension between the two phases, complex phenomena arise that are governed by various dimensionless numbers containing the surface tension. The balance of inertial, viscous, and interfacial tension forces govern droplet formation and subsequent droplet flow. The relationship between the inertial and interfacial tension forces of the aqueous phase is quantified by the Weber number (Tabeling, 2005).

$$(\mathbf{10})\ \boldsymbol{We} = {}^{\boldsymbol{\rho L v^2}}/_{\boldsymbol{\gamma}}$$

which is often paired with the Capillary number (Tabeling, 2005):

$$(\mathbf{11})\ \boldsymbol{Ca} = {}^{\boldsymbol{\mu v}}/_{\boldsymbol{\gamma}}$$

when determining droplet formation dynamics. $\boldsymbol{Ca}$ describes the ratio of viscous to interfacial forces and plays an important role in the characterisation of two-phase flows. Meanwhile, another dimensionless number, the Ohnesorge number (Dai and Leal, 2008):

$$(\mathbf{12})\ \boldsymbol{Oh} = \sqrt{\boldsymbol{We}}/\boldsymbol{Re} = \boldsymbol{\mu}/\sqrt{\boldsymbol{\rho\gamma L}}$$

describes the relationship between the inertial, viscous, and surface tension forces on droplet microfluidic flow.

Numerous biomedical applications require materials such as solids or gels, and not liquids (Zhao and Middelberg, 2011). Solid particles made from polymeric and biological materials are used in drug delivery (Yow and Routh, 2006, Müller et al., 2000, Kawaguchi, 2000, Stolnik et al., 1995) and hydrogels (Astete and Sabliov, 2006) and are being studied for the encapsulation of cells in drug studies or for implantation. Many droplet microfluidic systems were created to generate solid particles as well as hydrogel beads using various approaches (Koh and Pishko, 2006, Steinbacher and McQuade, 2006, Seo et al., 2005). Dissolved polymers add an elastic component to the fluid that further enriches flow behaviour. The Weissenberg, Deborah, and Elasticity numbers $\boldsymbol{Wi}$, $\boldsymbol{De}$, and $\boldsymbol{El}$, describe elastic effects within microfluidic flows due to the presence of deformable materials such as polymers (Tabeling, 2005). The Weissenberg number, $\boldsymbol{Wi}$=$\tau\boldsymbol{pe}^{\cdot}$ or $\tau\boldsymbol{p}\gamma^{\cdot}$, relates the polymer relaxation time to the flow deformation time, in the form of either the inverse extension rate $\boldsymbol{e}^{\cdot}\mathbf{-1}$ or shear rate $\gamma^{\cdot}\mathbf{-1}$. When $\boldsymbol{Wi}$ is large, i.e., approaching 1, the polymer does not have sufficient time to relax and is deformed significantly.

When Wi is small, the polymer has sufficient time to relax before the flow deforms it significantly, while perturbations to equilibrium are minimal. Another relevant time scale $\tau flow$ characteristic of the flow geometry may also exist in droplet microfluidic systems. For example, a channel that contracts over a length l introduces a geometric time scale $\tau flow = l/v$ which is required for a polymer to travel through the channel. Likewise, an oscillatory flow introduces an oscillation time, where the flow time scale $\tau flow$ can be long or short compared with the polymer relaxation time τp, resulting in a dimensionless ratio known as the Deborah number $De = \tau p / \tau flow$. For both Wi and De, the equations do not directly depend on γ but are introduced due to the deformation of objects enclosed by an interface. The polymer relaxation time depends on γ, however. As the flow velocity increases, elastic effects become more influential and Wi and De increase. However, the Reynolds number Re increases too, meaning that inertial effects can also become more influential. The Elasticity number (Tabeling, 2005) $El = DeRe = \tau p \mu / \rho h^2$, where h is the shortest dimension regulating the shear rate, indicates the relative importance of elastic to inertial effects. Significantly, El is independent of flow rate and depends only on the geometry and material properties of the fluid.

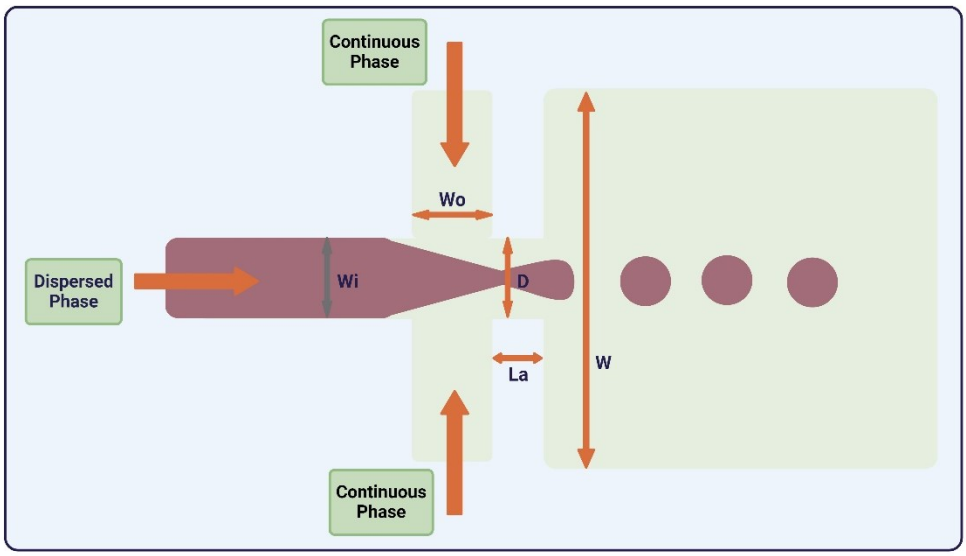

Figure 1.8. Droplet production in a flow-focusing device. The dispersed phase is squeezed by two counter-streaming flows of the carrier phase, forcing drops to form and detach. Image created on Biorender.com.

1.3.2 Droplet Chip Geometry

The most used channel geometries for microdroplet generation include the T-Junction, flow-focusing and co-flow nozzles, and step-emulsification devices (Figure 1.9), each with their own benefits and shortfalls (Sesen et al., 2017, Tran et al., 2013).

Droplets can be produced hydrodynamically within the T-junction system in the squeezing, dripping or jetting regimes, whereby **Ca squeezing** < **Ca dripping** < **Ca jetting** (Sesen et al., 2017). In the squeezing regime (Ca < 0.015), interfacial forces dominate viscous forces. Here, the droplet interface contacts both sides of the channel before breakoff. Large plugs form without the limiting effect of the viscous shear stress. Using the case of water-in-oil droplet systems as an example, constriction of the oil phase causes droplet termination/ production, i.e., when the aqueous drop fills the geometric nozzle and causes resistance by pinching the oil flow. Controlling droplet length becomes effortless in this regime due to the direct relationship between flow rate and droplet length. Further, the plugs fill the microchannel width and height, ensuring single-file flowing drops.

In the dripping regime, viscous forces are higher (i.e., due to increased flow rates) such that aqueous drop interfaces are broken before the drop is able to constrict the oil phase (Sesen et al., 2017). Droplet breakup is shear-dominated and the fluid interface is detached from the channel surface as spherical and extremely uniform drops are produced. At larger aqueous flow rates (**We** ~ 1 or greater), inertial forces begin to dominate interfacial tension forces.

At a critically high Weber number, the aqueous neck moves downstream as a wide unstable 'jet' of aqueous fluid from the nozzle (Sesen et al., 2017). A transition from dripping to jetting also occurs as oil flow rates increase. In the jetting regime (**Ca** > 0.05), flow rates are prolific, causing the aqueous phase to project into the oil phase at the drop making nozzle. Slightly downstream, droplet breakup occurs due to Rayleigh-Plateau instabilities along an elongated fluid thread, whereby the jet interface destabilises due to high viscous shear stress (i.e., in a predominantly oil filled channel), allowing formation of monodisperse droplets. The jetting regime is typically preferred for particle and fibre synthesis but has been used in picodroplet production systems.

Flow-focusing generators for liquid-liquid dispersions were first described in 2003 by Anna et al., and Drefus et al., (Anna et al., 2003, Dreyfus et al., 2003). A flow-focusing junction comprises two immiscible phases converging at a cross junction. The dispersed phase flows towards the junction in a single channel, and the continuous phase flows towards the junction in two diametrically opposed channels, each perpendicular to the dispersed phase (Figure 1.9). The dispersed phase is pinched off by the two incoming streams of the continuous phase, resulting in the generation of droplets at the drop producing nozzle. Different nozzle

dimensions influence the range of droplet volumes possible. These resulting droplets flow away from the junction through a channel opposite the incoming dispersed phase. By varying the flow rates of each phase, different sizes of droplets can be created. Flow-focusing junctions work by exploiting the hydrodynamic shear stresses induced as the dispersed phase is forced through the narrow junction by the two streams of continuous phase. Whilst more complex than T-junctions, flow-focusing junctions offer more monodispersed and controllable droplet formation.

The concept of co-flow droplet generators was introduced by Cramer et al. in 2004, where a thin capillary is used to stream the dispersed phase into a channel surrounded by the continuous phase on two sides (Quasi-2D) (Cramer et al., 2004) or all sides (3D) (Umbanhowar et al., 2000). Quasi-2D junctions are often made using traditional soft lithography techniques (McDonald et al., 2000), whilst 3D junctions are made by inserting a tapering glass capillary into a rectangular channel (Utada et al., 2007). Thereafter, the two phases flow through an orifice in the channel where they are pinched together. The physics of a co-flow generator are like that of a flow-focusing junction, although instead of having the continuous phase pinch from two sides, it pinches from all sides. As the dispersed phase streams into the sheath of the continuous phase, instabilities arise. The two phases are extruded through the narrow orifice together, and the stream of the dispersed phase collapses into droplets to minimise the surface area, and subsequently the free energy of the interface. Historically, 3D co-flow junctions were harder to fabricate than T or flow-focusing junctions. However, with recent advancements in 3D print manufacturing capabilities, it is now possible to print them (Utada et al., 2007).

In contrast to the previous droplet generation methods, which utilise hydrodynamic shear forces to create droplets within flow, step emulsification generators (Sugiura et al., 2000) (Figure 1.9) create droplets by altering the channel geometry to induce a rapid change in capillary pressure which drives the formation of droplets. The change in capillary pressure results from a step within the channel, causing a stream of dispersed phase to “fall” off a step into the continuous phase. Step emulsification has benefits over other droplet formation methods, as it can be easily and massively paralysed. Despite that, the method has some disadvantages. For example, it is more sensitive to obstructions at the nozzles, which can affect droplet monodispersity (Stolovicki et al., 2018).

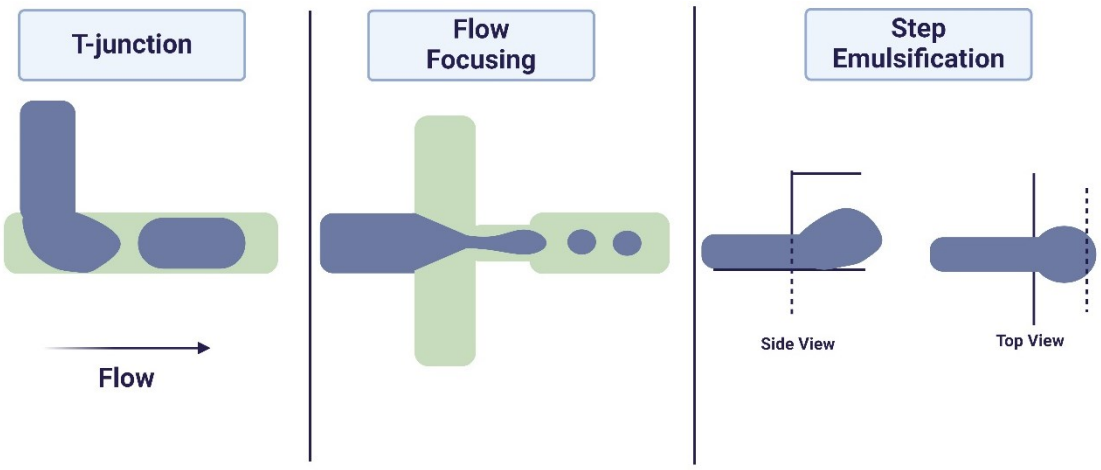

Figure 1.9. Droplet generation geometries. (A) T-junction. **(B)** Flow-focusing geometry. **(C)** Step emulsification. Image created on Biorender.com.

1.3.3 Droplet Generation

Droplets can be generated either “passively” or “actively”. Introducing a dispersed fluid into a continuous fluid leads to droplet generation in the form of either squeezing, dripping, jetting, tip-streaming, or tip-multi-breaking. In the passive method, droplet generation is controlled by either syringe pumps that supply constant flow rates or pressure regulators. The energy imputed into syringe pumps or pressure regulators enables the destabilisation of the liquid–liquid interface, whereby discrete droplet detaches from the dispersed phase occurs by converting the energy into interfacial energy (Zhu and Wang, 2017).

Using an external input of energy can also dictate droplet generation, termed “active droplet generation” application of an external force driving the creation of droplets. Numerous techniques exist for actively forming droplets, such as electrical (Link et al., 2006, Zhu and Wang, 2017), magnetic (Tan et al., 2010), centrifugal (Haeberle et al., 2007), optical (Park et al., 2011), thermal (Murshed et al., 2009), piezo-electrical (Xu and Attinger, 2008), and surface acoustic waves (Collins et al., 2013). Active generation methods often require more complex instrumentation setups and are therefore typically more expensive and less accessible. Active droplet generation designs have enabled regulation of one or more of parameters such as droplet volume (Schmid and Franke, 2013, Abate et al., 2009), generation rate (Zeng et al., 2009) and also on/off switching capabilities (Collins et al., 2013, Jin et al., 2015), e.g., making it possible to produce droplets one at a time as and when required.

1.3.4 Droplet Sensing and Manipulation

Droplet sensing is important for identification and/or manipulation of droplets, and for automation of sequential droplet activities in microfluidic Lab-on-Chip devices and/or instruments. When performing time-dependent tasks, such as manipulation of specific droplets

at a specific on-chip location, droplet sensing is crucial to ensure triggered actions have the correct timing. Further, as the number of manipulation events increases, the management, and automation of droplet manipulation activities needs precise, reliable information about the location, size, frequency, velocity, and/or content of droplets at certain locations within the system (Josephides et al., 2020). Two frequently utilised methods of sensing droplets in closed microfluidic channels are optical (Nguyen et al., 2006, Robert de Saint Vincent et al., 2012, Baret et al., 2009) and electrical (Cole and Kenis, 2009, Moiseeva et al., 2011, Niu et al., 2007) detection, for which the reader is referred to expert reviews (Niu et al., 2007, Liu and Zhu, 2020, Zhu and Fang, 2013). To sense the interior contents of droplets, techniques such as capillary electrophoresis (Niu et al., 2007), mass spectrometry (Feng et al., 2015, Oedit et al., 2015), and Raman spectroscopy (Jahn et al., 2017) were used in microfluidics, and the reader is also directed to specialised reviews (Zhu and Fang, 2013, Basova and Foret, 2015) on this topic.

The efficient manipulation of droplets (Tenje et al., 2018), i.e., to perform activities such as droplet splitting, trapping, merging, sorting, and/or to manipulate the interior droplet contents, is important in a range of research and industrial applications across various disciplines, such as biotechnology, molecular biology, and analytical chemistry. Individual droplets can be manipulated in flow via a variety of techniques, e.g., passively and hydrodynamically upon careful geometrical design, or using active forces (Novotný and Foret, 2017a). Many physical approaches from magnetic (Miltenyi et al., 1990, Mirowski et al., 2005) to electrophoretic (Yalcin et al., 2010), dielectrophoretic (Zhang et al., 2010, Yunus et al., 2013), optic (Kim et al., 2008b, Wang et al., 2005, Kim et al., 2008a), pneumatic (Lee et al., 2009) and acoustophoretic (O'Rorke et al., 2012, Geislinger and Franke, 2013, Augustsson et al., 2012) were used to manipulate droplets in a microchannel. The reader is encouraged to visit the prescribed references, where a technical understanding of some of the various methods described in the literature is advantageous. Droplet sensing and manipulation techniques are illustrated in Figure 1.10.

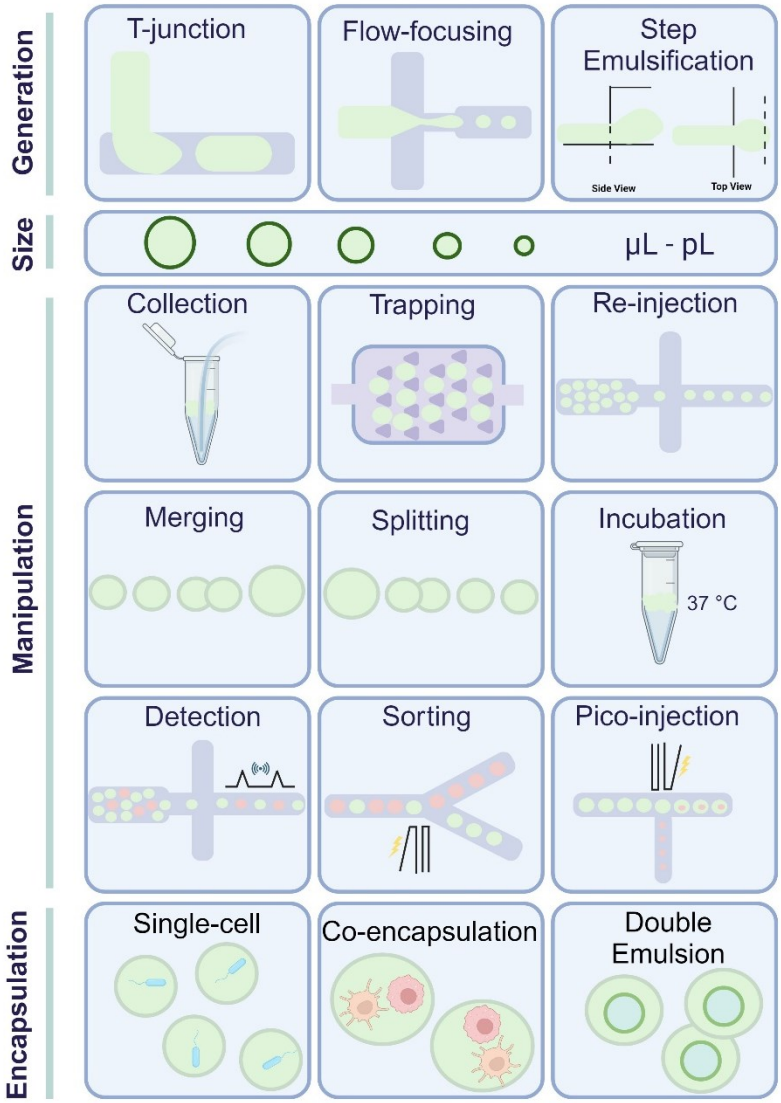

Figure 1.10. Droplet sensing and manipulation techniques. Image created on Biorender.com.

1.3.5 Droplet Applications in Microbiology

The field of applying droplet microfluidics to microbiology has been widely researched. The ability to encapsulate bacteria at the single-cell level has led to this novel application in drug discovery, microbial biotechnology, diagnostics, detection, cultivation, characterisation, omics, evolution studies, 3D models, and host-pathogen interactions (Guo et al., 2012, Hengoju et al., 2020, He et al., 2022, Kaminski et al., 2016). These applications are summarised in Figure 1.11.

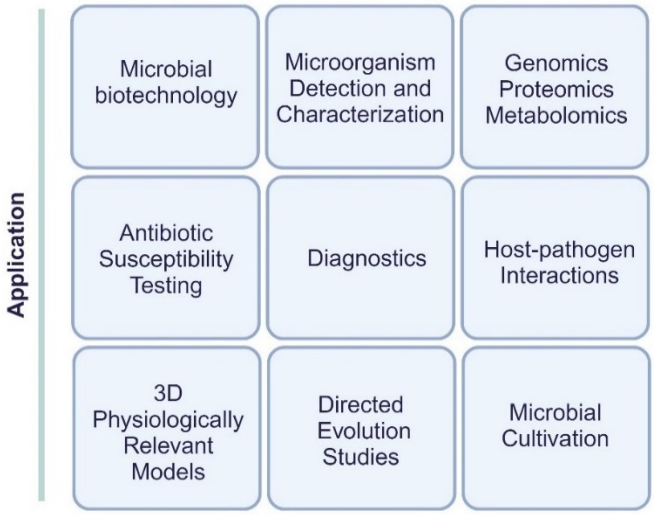

Figure 1.11. The applications of droplet fluidics in the microbiology field. Image created on Biorender.com.

Employing droplet microfluidics is a promising approach for rapid and cost-effective diagnostics for pathogens and drug-resistant strains. Using robust and reproducible fluidic models for pathogen detection offers capabilities for clinical procedures and scientific exploration. Interestingly, potential method for quantitively detecting *M. tuberculosis* in droplet microfluidics were developed by detecting cells that express the endogenous β-lactamase, BlaC—an enzyme marker naturally expressed by *M. tuberculosis*. Researchers were able to estimate the initial cell concentration by trapping a specific fluorescent probe of BlaC and samples of bacterial strains that produce BlaC in droplets through fluorescence measurement (Lyu et al., 2015). In addition, drug-resistant strains to β-lactams were fluorescently detected using a droplet-based microfluidic device and a custom 3D particle counter (Figure 1.12). The microfluidic chip comprised separate input channels for bacteria, ampicillin, and broth mixture, fluorocillin (a β-lactamase sensor), and oil to encapsulate single bacteria cells into droplets. Antibiotic-resistant clinical isolates thrived inside the droplets, detected by fluorescent microscopy (Li et al., 2020).

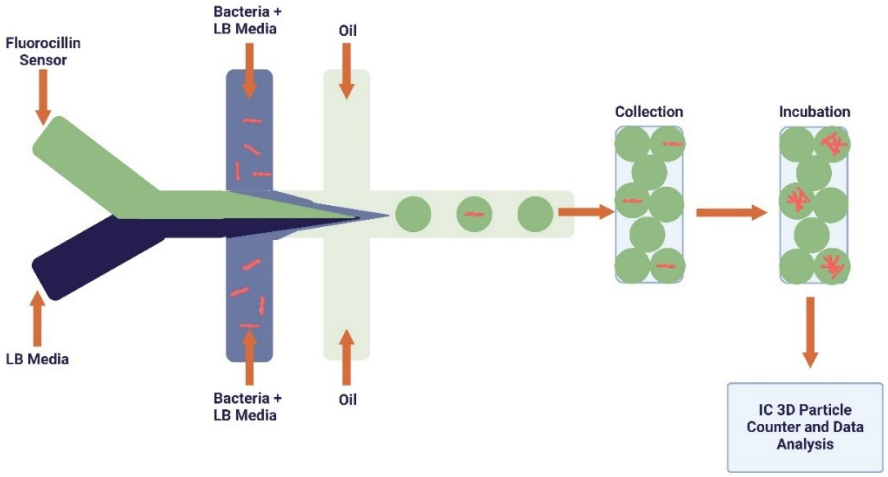

Figure 1.12. Schematic illustration of droplet system coupled to an integrated comprehensive droplet digital detection. Flow-focusing microfluidic chip geometry producing encapsulated mycobacteria in droplets. Image created on Biorender.com.

Moreover, the droplet bioreactor holds promise to create 3D models of bacterial cultural environments. Applications of engineered oxygen sensing in cultures could pave the way for controlling oxygen content when optimising new culturing models. Measuring the concentration of oxygen in picodroplets has been demonstrated. Researchers successfully measured oxygen concentration against optical density (600 nm) of *E. coli* and *Mycobacterium smegmatis* by utilising optical sensor nanoparticles. The nanoparticles had a phosphorescent indicator dye embedded in poly (styrene-blockvinylpyrrolidone) nanobeads and were easily integrated into a droplet device (Horka et al., 2016). Monitoring analytes or conditions which influence bacterial growth is important in microbiology research and could be advanced by using microfluidic “stochastic confinement” droplets.

1.3.6 Future Applications of AST in Microdroplets

One advantage of droplet microfluidics is the approach of “stochastic confinement” (Jung et al., 2018). When single-cells are confined in microdroplets of small volume, the loading is defined by Poisson statistics. When less than one bacterium is encapsulated per microdroplet, the resultant library of droplets is occupied by a single bacterium or empty. As detection time is proportional to the plug volume, then the random statistical probability of confinement amplifies the cell density and thus reduces the time required for their detection. Droplet fluidic methods were applied to antibiotic susceptibility testing of bacteria in recent years.

Using a microfluidic hybrid method, a variety of antibiotics were screened against a single bacterial sample. *E. coli* cells were encapsulated in agarose monodisperse microparticles, approximately 30 μm in diameter, using a flow-focusing microfluidic chip. Both the MIC for rifampicin and the sorting of spontaneous mutants by fluorescence-activated cell sorting (FACS) was demonstrated and characterised by DNA sequencing (Eun et al., 2011). Building

on this previous work, FACS screening of gel microdroplets has been shown, in which the bacterial pathogen *Staphylococcus aureus* is co-cultured with a recombinant host—*Saccharomyces cerevisiae* or *E. coli*, which are capable of secreting biocatalytic antibiotics and/or secondary metabolites from a metagenomic library. The gel microdroplets (25 pL) are of a size compatible with conventional FACS instruments at 3000 droplets/second, allowing the proof-of-concept selection of antibiotic-secreting yeast from a vast excess of negative controls (Scanlon et al., 2014a).

M. bovis BCG and *M. smegmatis* were encapsulated in gel microdroplets, with a mean diameter of 25 μm, along with flow cytometry as a model system to investigate the efficacy of encapsulation and the detection of clonal growth by flow cytometry (Choi et al., 2016). The characteristic slow growth of TB *bacilli*, as well as the small number found in most clinical samples, has made the direct detection of TB *bacilli* by biochemical and immunological methods difficult. Use of gel microdroplet encapsulation in combination with flow cytometry could reduce the time required to evaluate clinical samples and establish effective treatment regimens. In 2016, Keays et al. shown growth of *E. coli* in droplets and demonstrated the application of antibiotic treatments to both bacteria and drug-resistant strains of bacteria within 1 hour (Keays et al., 2016).

The flexibility of alginate hydrogel beads (65 nL, 500 μm diameter) has the advantage of being able to be shuffled back and forth between the hydrophobic and hydrophilic phase. Schmitt et al. (2019) demonstrated the co-encapsulation of a library of *Lactococcus lactis* cells producing antimicrobial lanthipeptides with approximately 150 sensor strain cells, *Micrococcus flavus*, then back to the hydrophilic phase for the activation of lanthipeptide production, and back to the hydrophobic phase for incubation and to prevent lanthipeptide crosstalk between the microdroplets (Boedicker et al., 2008). Finally, these nanolitre reactors were demulsified and stained with the fluorescent dye SYTO 9, and nanolitre reactors with no or minimal biomass, indicating the effective prevention of sensor strain growth, were isolated. Although this has yet to be conducted with other strains of bacteria, this technology holds considerable promise to screen antimicrobials against pathogenic bacteria at the single-cell level.

A label-free high-throughput method was previously reported for screening up to 1×10^9 bacteria for AMR in water-in-oil picolitre-volume droplets (picodroplets); using Poisson statistics, the occupancy per picodroplet was 100 bacteria (*E. coli* HS151) (Liu et al., 2016). From approximately 10 million picodroplets that were screened against fusidic acid, 103 droplets with drug-resistant hits were sorted. The recovered cells were grown on agar containing fusidic acid (10 μg/mL) and the mutant colonies submitted for DNA sequencing.

As evidenced by the groundbreaking research within the field of microfluidics and its use for drug discovery, undoubtedly there is an increased outlook of standardised microfluidic devices to test antimicrobials against pathogens and discover their MOA. Droplet fluidics are still rapidly evolving and will continue to grow with the success of its applications. By combining droplet fluidic technology at the picolitre scale with antibiotic drug discovery, the potential exists to develop a novel, accelerated, and highly sensitive method of antimicrobial susceptibility testing that is both high-throughput and clinically significant. Droplets allow for the compartmentalisation of single-cells from high-density cultures and the manipulation of cell environments. Thereby, droplets could prevent competition for nutrients or space among bacteria, allowing the slow-growing species to proliferate.

Future research should focus on translating these laboratory platforms into commercial applications for industry and clinical practice. Commercial products of single-cell droplet platforms were successful, such as inDrop, Drop-seq, and 10× Genomics (Suea-Ngam et al., 2019). Challenges for the commercialisation of these novel platforms include translation, user-friendliness, portability, and economic feasibility. Interdisciplinary collaboration has facilitated these advancements, usually involving biologists and engineers and their respective stakeholders. Challenges to overcome in this multidisciplinary field include the scale-up of testing and parallelisation for industry usage. Furthermore, transfer of “know-how” between designers and end users is imperative. With the miniaturisation of biological assays, more robust data points are obtainable and may need bioinformatic expertise and sophisticated computational tools.

Ultimately, to build a vibrant and innovative antimicrobial clinical pipeline to tackle AMR, droplet fluidics could advance novel compounds to lead identification and lead optimisation phases of the drug discovery pipeline.

1.4 Aims and Objectives of Thesis

This thesis aims to develop and optimise droplet microfluidic technology for enhancing antibiotic susceptibility testing (AST), focusing on leveraging picodroplet technology. This research addresses the urgent need for innovative approaches to combat antimicrobial resistance, as discussed in the earlier sections. The specific objectives of this thesis are:

1. To evaluate the susceptibility of novel metal-based compounds against high-priority pathogens using traditional antibiotic susceptibility testing methods. This will provide a baseline for comparison with droplet-based methods and identify promising compounds for further investigation.
2. Develop and optimise protocols for creating monodisperse and stable microdroplets suitable for various microbiological applications. This objective focuses on the technical aspects of droplet generation and stability, which are crucial for reliable AST assays.
3. Establish methods for encapsulating bacteria within microdroplets and validating their growth under various conditions, including antibiotic challenges. This objective aims to demonstrate the feasibility of using microdroplets as micro-bioreactors for AST.
4. To engineer droplet systems that prevent antibiotic leakage, ensuring the integrity of individual droplet environments. This is critical for accurate determination of antibiotic efficacy at the single-cell level.
5. To integrate the developments from objectives 1-4 into a comprehensive, droplet-based AST platform optimised for future antimicrobial research and clinical diagnostics applications.

By achieving these objectives, this thesis aims to contribute significantly to the field of microfluidics-based antimicrobial susceptibility testing, potentially accelerating the discovery and development of new antibiotics and improving our ability to combat antimicrobial resistance.

Chapter 2.

Broad Spectrum Antimicrobial Activity of Repurposed Metal-ion Complexes.

2.1 Introduction

The rising threat of antimicrobial resistance (AMR) has become a global health crisis. In 2019 alone, drug-resistant infections were responsible for 4.95 million deaths worldwide, with 1.27 million directly attributed to AMR (Murray et al., 2022). Disappointingly, the antimicrobial pipeline is scarce compared to other therapeutic areas, such as oncology and COVID-19 vaccines (Butler et al., 2023). These alarming trends underscores the urgent need for novel antimicrobial strategies. Our research into repurposing metal-based compounds addresses this critical gap in the antimicrobial pipeline. Developing new antibiotics is crucial for reducing the burden of AMR. This chapter investigates the potential of repurposing metal-based compounds, originally designed as anti-cancer agents, for antimicrobial applications. The objectives are to:

1. Evaluate the antimicrobial activity of 16 metal-ion complexes against ESKAPE pathogens and mycobacterial species.
2. Compare the efficacy of these repurposed compounds to existing antibiotics.
3. Identify promising candidates for further development as novel antimicrobials.

2.1.1 Drug Repurposing

Antimicrobial drug repurposing or drug repositioning/re-profiling is one novel strategy used to find novel antibiotics from current therapeutics. The advantage of drug repurposing is that it accelerates the traditional drug discovery pipeline of antibiotics by bypassing necessity toxicity testing for drugs that already have regulatory approval.

In recent years, it gained considerable attention. One published paper describes examples of repurposed drugs for combating different diseases (Zhang et al., 2020). An example of a successfully repurposed drug is cycloporin A, which is an immunosuppressant in organ transplantation, and now has displayed antibiofilm activity against *Mycobacterium tuberculosis* (Kumar et al., 2019, An et al., 2020). Additionally, there have been demonstrations of using preexisting antibiotics, commonly used for other infections, for new treatment.

Furthermore, the use of anti-cancer compounds for challenging infections has been successfully proven. In her review of drug repurposing to treat *Mycobacterium abscessus* infections, Baker *et al.* identify examples of repurposing antibiotics for other infections, as well as repurposing unconventional agents such as anticancer compounds (Baker et al., 2023). Gumbo (2020) also highlights the need to repurpose compounds for *Mycobacterium abscessus* infections, including anti-cancer compound daunorubicin (Gumbo et al., 2020). The use of anti-cancer compounds as antimicrobials is based on similarities between cancer cells and bacterial pathogens, including rapid growth, high metabolic rates, tissue dissemination, cell communication, and recruitment of the active immune system for their eradication

(Quezada et al. 2020). Research reveals that 3-Bromopyruvate (3-BP) which has been studied for its anticancer properties as it interferes with cellular metabolism (inhibiting glycolysis), disrupts metabolic processes in *S. aureus*, leading to inhibited growth and bacterial death (Visca et al., 2019).

Anti-cancer metal-based compounds have also shown promise as antimicrobials. For example, gallium nitrate used for hypercalcemia of malignancy indicates antimicrobial activity against *P. aeruginosa*, *A. baumannii,* and *M. tuberculosis (Goss et al., 2018, Tovar et al., 2020).*

2.1.2 Metal Compounds as Antimicrobials

Metal-based compounds have shown great promise in medicinal chemistry, particularly cancer treatment. The success of cisplatin, a platinum-based anticancer drug, has sparked interest in exploring other metal-containing compounds for various therapeutic applications (Frei et al., 2023). These compounds offer unique properties such as diverse coordination geometries, redox activities, and the ability to interact with biological targets in ways organic molecules cannot. Given these characteristics, metal-based compounds present an exciting opportunity for repurposing as antimicrobials, potentially offering novel mechanisms of action to combat resistant pathogens. The medicinal properties of metal-based drugs were established before their mechanism of action (Boros et al., 2020). Compounds containing metals and at least one direct metal-carbon bond are defined as organometallic compounds, and have been discovered as promising anti-cancer drug candidates (Gasser et al., 2011). Recently, metalloantibiotics, which are promising metal complexes possessing antibacterial activity, have garnered attention (Frei et al., 2023). These are characterised by complex 3D structures with chiral centres showing higher target selectivity with reduced off-target effects, as well as diverse mechanism of actions (Frei et al., 2023). In 1965, research published the inhibiting effect of platinum complexes to *E. coli* (Rosenberg et al., 1965). Since that publication, there have been numerous reports of metal-based compounds that work as antimicrobials.

As early as 1952, the antibacterial properties of ruthenium complexes were deduced (Dwyer et al., 1952). Ruthenium's antibacterial properties are attributed to their strong affinity for binding nucleic acids and proteins (Li et al., 2015). The mechanisms of action of ruthenium complexes include binding to bacterial DNA, interfering with replication and transcription processes, leading to cell death. In addition, interact with bacterial cell membranes, increasing permeability and causing cellular content leakage, which is lethal to bacteria. Some ruthenium complexes catalyse the production of reaction oxygen species ROS, which can damage essential bacterial components, such as proteins, lipids, and nucleic acids (Li et al., 2015). Previous research explored the potential of indole-containing arene-ruthenium complexes as antibiotics. The researchers synthesised a series of indole-containing arene-ruthenium complexes and tested them against a range of bacterial strains, including both Gram-positive

and Gram-negative bacteria (Nolan et al., 2022). The compounds exhibited broad-spectrum antibacterial activity and were also effective against several antibiotic-resistant bacterial strains, including MRSA (Methicillin-resistant *Staphylococcus aureus*).

Using copper as an antimicrobial has been extensively reported. Copper has been used either to coat surfaces or as nanoparticles to tackle infections (Salah et al., 2021). Examples of species killed by copper surfaces include *Salmonella enterica, Campylobacter jejuni, Mycobacterium tuberculosis, Klebsiella pneumoniae* and MRSA (Faúndez et al., 2004, Mehtar et al., 2008, Michels et al., 2009). Copper nanoparticles were previously documented to inhibit growth of *E. coli* ATCC 15224 (Raffi et al., 2010). In another example, *in vitro* studies of the inhibitory effect of copper nanoparticles were tested against *S. aureus* and *P. aeruginosa,* revealing a significant inhibitory effect (Betancourt-Galindo et al., 2014). Interestingly, when coupled to an FDA-approved drug disulfiram, the disulfiram-copper complex was toxic to *M. tuberculosis* through the mechanism of inhibiting intracellular protein functions and inducing intracellular copper stress responses (Dalecki et al., 2015).

Novel osmium complexes have also shown antimicrobial action. For example, a paper has presented that triazole-based osmium (II) complexes have significant antimicrobial activity against a range of bacterial strains, including both Gram-positive and Gram-negative bacteria (Smitten et al., 2020).

To explore repurposing metal-compounds for antimicrobials, a collaboration was undertaken by Aston University and ParisTech, PSL University, to test metal-complexes against a range of pathogenic bacteria. The set of compounds had intended to be synthesised as anti-cancerous drugs, however, did not show sufficient cytotoxicity towards mammalian cells. These were hypothesised to be susceptible to bacterial species. The table below (Table 2.1) lists the 16 compounds which were provided and tested as well as 2 control compounds and their corresponding core metals. The complexes AN3, JK-Ru5, RuBio, and RV144 were reported in the literature for their anti-cancer investigations and have been repurposed here (Notaro et al., 2020, Karges et al., 2020, Vinck et al., 2022).

In this study, we evaluate 16 metal-ion complexes, including ruthenium, copper, and osmium-based compounds, for their antimicrobial activity. We employ a comprehensive approach, using broth microdilution assays, resazurin reduction assays, and a bactericidal assay to determine minimum inhibitory concentrations (MICs) and minimum bactericidal concentrations (MBCs) against a range of ESKAPE pathogens and mycobacterial species. This multi-faceted approach allows us to assess both the growth inhibitory and killing potential of these repurposed compounds, providing a thorough evaluation of their antimicrobial efficacy.

Table 2.1. List of investigated compounds grouped into their core metal.

Ruthenium (Ru)	Copper (Cu)	Osmium (Os)	Platinum (Pt)	Non-Metal
MD7	FF175	RV239 OsBpy	Cisplatin	Meropenem
MD56	FF176			
MD72	FF177			
MD73	FF218			
KP01	FF225			
AN3				
JK-Ru5				
RuBio				
RV144				
RV158				

2.1.3 Aims and Objectives of Chapter.

The aim of this chapter is to investigate the differences in minimum inhibitory concentrations and minimal bactericidal concentrations between highly resistant bacterial species and novel metal ion-complexes. The main purpose of this study is to develop an understanding of alternative uses of failed anti-cancer metal-compounds synthesised by medicinal inorganic chemistry.

The aims of this chapter are as follows;

1. To test ESKAPE pathogens including *Enterococcus faecium* ATCC 19434, *MRSA* N315, *Klebsiella pneumoniae* H467, *Acinetobacter baumannii* NCTC 12156, *Pseudomonas aeruginosa* ATCC 19429, and *Enterobacter cloacae* ATCC 13047 against 16 metal ion-complexes and 2 control compounds.
2. To test *mycobacterium* species, including *M. abscessus* 15944 subsp. *abscessus*, DC088A subsp. *bolletii*, DC088D subsp. *massiliense* against 16 metal ion-complexes and 2 control compounds.
3. To test *M. bovis* BCG against 16 metal ion-complexes and 2 control compounds.

2.2 Methods

2.2.1 Reagents and Media Preparation

Unless stated otherwise, all consumables and reagents were purchased from either Fisher Scientific, Melford, Biosynth, or Sigma-Aldrich.

Middlebrook 7H9 Broth

2.35 g of 7H9 broth base, 450 mL of distilled water and 4 mL of 50% glycerol were added together before autoclaving (121 °C for 15 min). Once cooled, 1.25 mL of 20% filter sterile Tween® 80 is added along with 50 mL filter sterile ADC (albumin, dextrose, and catalase supplement).

ADC Supplement

5 g BSA (bovine serum albumin fraction v), 2 g dextrose, 0.85 g sodium chloride and 0.003 g catalase were added to 100 mL of distilled water. The components were dissolved before filter sterilising with a 0.22 µm sterile filter. The ADC supplement was stored at 4 °C.

Middlebrook 7H11 Agar

10.25 g of 7H11 agar base, 450 mL of distilled water (dH_20), and 5 mL of 50% glycerol were added together before autoclaving (121 °C for 15 min). Autoclaved agar was then placed in a water bath for 20 minutes to cool. Once cooled, the agar was poured into petri dishes or supplemented with OADC additive before pouring.

OADC Additive

25 mg sodium oleate, 5g BSA (bovine serum albumin fraction V), 2 g dextrose and 3 g catalase were added to 100 mL of dH_2O. Once dissolved, the solution was filter sterilised using a 0.22 µm sterile filter and stored at 4 °C. When supplementing OADC into 7H11 agar, the solution was warmed to the same temperature as the melted agar before mixing.

Brain-Heart Infusion Broth

16.65 g of Brain-Heart Infusion broth was dissolved in 450 mL of dH_2O and then autoclaved (121 °C for 15 min).

Mueller-Hinton Broth

9.45 g of Mueller-Hinton broth was dissolved in 450 mL of dH_2O and then autoclaved (121 °C for 15 min).

Mueller-Hinton Agar

17.1 g of Mueller-Hinton agar was dissolved in 450 mL of dH_2O and then autoclaved (121 °C for 15 min). Once cooled, the agar was poured into petri dishes.

Resazurin

A stock solution was made by adding 1 mg of powdered resazurin into 1 mL of dH_20. The solution was then filter sterilised using a 0.22 µm sterile filter and stored at room temperature away from sunlight.

Antibiotic Preparation

All investigative compounds were received from Prof. Gilles Gasser at the Institute of Chemistry for Life and Health Sciences at Chimie ParisTech, PSL University. Powdered compounds were weighed and dissolved in DMSO to a final concentration of 10 mM. The stock solutions in DMSO were stored at −20 °C until use. Control compounds cisplatin and meropenem were also weighed and dissolved in DMSO to a final concentration of 10 mM.

2.2.2 Bacterial Strains and Culture Conditions

Bacterial Strains

The following bacterial strains were selected for antibiotic susceptibility testing: *Enterococcus faecium* ATCC 19434, *MRSA* N315, *Klebsiella pneumoniae* H467, *Acinetobacter baumannii* NCTC 12156, *Pseudomonas aeruginosa* ATCC 19429, *Enterobacter cloacae* ATCC 13047, *M. abscessus* 15944 subsp. *abscessus*, DC088A subsp. *bolletii*, DC088D subsp. *massiliense* and *M. bovis* BCG Pasteur 1173P2.

Culture Conditions

The stocks were preserved in 50% glycerol and stored at -80°C. Glycerol stocks of bacterial species were inoculated and grown in conditions described in Table 2.2.

Table 2.2. Culture Conditions of Bacterial Species. Each species of bacteria investigated are listed with their corresponding inoculation growth condition and their growth on solid agar condition. Additional supplements to media and agar are also listed.

	Bacterial Species	Broth + Culture Condition	Agar + Colony Incubation Condition
ESKAPE pathogens	*Enterococcus faecium* ATCC 19434	20 mL Brain-Heart Infusion 24-hour static incubation 37 °C	Mueller-Hinton 24-hour static incubation 37 °C
	MRSA N315	20 mL Mueller-Hinton 24-hour shaking incubation 37 °C	Mueller-Hinton 24-hour static incubation 37 °C
	Klebsiella pneumoniae H467	20 mL Mueller-Hinton 24-hour shaking incubation 37 °C	Mueller-Hinton 24-hour static incubation 37 °C
	Acinetobacter baumannii NCTC 12156	20 mL Mueller-Hinton 24-hour shaking incubation 37 °C	Mueller-Hinton 24-hour static incubation 37 °C
	Pseudomonas aeruginosa ATCC 19429	20 mL Mueller-Hinton 24-hour shaking incubation 37 °C	Mueller-Hinton 24-hour static incubation 37 °C
	Enterobacter cloacae ATCC 13047	20 mL Mueller-Hinton 24-hour shaking incubation 37 °C	Mueller-Hinton 24-hour static incubation 37 °C
***M. abscessus* subsp**	*M. abscessus* 15944 subsp. a*bscessus*	20 mL Middlebrook 7H9 0.4% Glycerol 10% ADC 0.05% Tween80 72-hour shaking incubation 37 °C	Middlebrook 7H11 72-hour static incubation 37 °C
	M. abscessus DC088A subsp. *bolletii*	20 mL Middlebrook 7H9 0.4% Glycerol 10% ADC 0.05% Tween80 72 hours shaking incubation 37 °C	Middlebrook 7H11 72-hour static incubation 37 °C
	M. abscessus DC088D subsp. *massiliense*	20 mL Middlebrook 7H9 0.4% Glycerol 10% ADC 0.05% Tween80 72 hours shaking incubation 37 °C	Middlebrook 7H11 72-hour static incubation 37 °C
***M. bovis* BCG**	*M. bovis* BCG Pasteur 1173P2	20 mL Middlebrook 7H9 0.4% Glycerol 10% ADC 0.05% Tween80 14 -21-day shaking incubation 37 °C	Middlebrook 7H11 10% OADC 14-day static incubation 37 °C

2.2.3 Antimicrobial Susceptibility Testing

The antimicrobial activity of each metal complex against ESKAPE pathogens and mycobacteria species was assessed using a broth microdilution assay, a resazurin viability assay, and a bactericidal assay to determine the minimum inhibitory concentration (MIC) and minimum bactericidal concentration (MBC).

Broth Microdilution Assay

A master plate was prepared for each compound using a 2-fold serial dilution method. Starting with a 10 mM stock solution in DMSO, 11 serial dilutions were performed in a 96-well plate, with a final well containing only DMSO as a control. This resulted in a concentration range from 10 mM to 9.8 μM, plus a 0 mM control. Each dilution was prepared in triplicate to ensure reproducibility. The limited availability of the newly synthesised compounds only allowed for them to be tested once with one biological repeat. 5 μL of each dilution was added to a well for a total concentration of DMSO at 5% and the final concentration of serial dilutions to be 500 μM, 250 μM, 125 μM, 62.5 μM, 31.3 μM, 15.6 μM, 7.8 μM, 3.9 μM, 2 μM, 1 μM, 0.5 μM, 0.2 μM, 0.1 μM, 0.06 μM, 0.03 μM, 0.02 μM, 0.008 μM, 0.004 μM when inoculated with 95 μL of bacterial species. Several controls were included in each assay to ensure validity and aid in result interpretation:

1. DMSO-only control: To account for any potential inhibitory effects of the solvent.
2. Bacteria-only control: To establish standard growth patterns without test compounds.
3. Broth-only control: To confirm the sterility of the media and establish a baseline for optical density measurements.
4. Positive control: Meropenem, a broad-spectrum antibiotic, was used at various concentrations to validate the assay's ability to detect known antimicrobial activity.
5. Additional control: Cisplatin, an anticancer drug not known for antimicrobial activity, was used to control for non-specific effects of metal-based compounds.

The final volume of each well was 100 μL and n=3 technical replicates on each plate. Figure 2.1 below shows a visual representation of the plate map**.** All bacterial strains were inoculated into wells at optical density (OD) 570 nm= 0.1. Incubation times were optimised for each bacterial group based on their growth rates and metabolic characteristics. ESKAPE pathogens, being fast-growing organisms, were incubated for 24 hours. *M. abscessus* subspecies, known for their slower growth, required 96 hours. *M. bovis* BCG, the slowest growing organism in our panel, necessitated an extended incubation period of 336 hours (14 days) to ensure accurate assessment of growth inhibition. Optical density (570 nm) readings were taken every 24 hours for mycobacterial species and one single end point reading at 24 hours for ESKAPE pathogens using a spectrophotometric plate reader (Biotek EL808).

	1	2	3	4	5	6	7	8	9	10	11	12
A n=1	Bacteria + Drug 500 µM	Bacteria + Drug 250 µM	Bacteria + Drug 125 µM	Bacteria + Drug 62.5 µM	Bacteria + Drug 31.25 µM	Bacteria + Drug 15.625 µM	Bacteria + Drug 7.813 µM	Bacteria + Drug 3.906 µM	Bacteria + Drug 1.953 µM	Bacteria + Drug 0 µM	Bacteria Only	Broth Only
B n=2	Bacteria + Drug 500 µM	Bacteria + Drug 250 µM	Bacteria + Drug 125 µM	Bacteria + Drug 62.5 µM	Bacteria + Drug 31.25 µM	Bacteria + Drug 15.625 µM	Bacteria + Drug 7.813 µM	Bacteria + Drug 3.906 µM	Bacteria + Drug 1.953 µM	Bacteria + Drug 0 µM	Bacteria Only	Broth Only
C n=3	Bacteria + Drug 500 µM	Bacteria + Drug 250 µM	Bacteria + Drug 125 µM	Bacteria + Drug 62.5 µM	Bacteria + Drug 31.25 µM	Bacteria + Drug 15.625 µM	Bacteria + Drug 7.813 µM	Bacteria + Drug 3.906 µM	Bacteria + Drug 1.953 µM	Bacteria + Drug 0 µM	Bacteria Only	Broth Only
D Drug Only	Broth + Drug 500 µM	Broth + Drug 250 µM	Broth + Drug 125 µM	Broth + Drug 62.5 µM	Broth + Drug 31.25 µM	Broth + Drug 15.625 µM	Broth + Drug 7.813 µM	Broth + Drug 3.906 µM	Broth + Drug 1.953 µM	Broth + Drug 0 µM	Bacteria Only	Broth Only
E n=1	Bacteria + Drug 0.977 µM	Bacteria + Drug 0.488 µM	Bacteria + Drug 0.244 µM	Bacteria + Drug 0.122 µM	Bacteria + Drug 0.061 µM	Bacteria + Drug 0.031 µM	Bacteria + Drug 0.015 µM	Bacteria + Drug 0.008 µM	Bacteria + Drug 0.004 µM	Bacteria + Drug 0 µM	Bacteria Only	Broth Only
F n=2	Bacteria + Drug 0.977 µM	Bacteria + Drug 0.488 µM	Bacteria + Drug 0.244 µM	Bacteria + Drug 0.122 µM	Bacteria + Drug 0.061 µM	Bacteria + Drug 0.031 µM	Bacteria + Drug 0.015 µM	Bacteria + Drug 0.008 µM	Bacteria + Drug 0.004 µM	Bacteria + Drug 0 µM	Bacteria Only	Broth Only
G n=3	Bacteria + Drug 0.977 µM	Bacteria + Drug 0.488 µM	Bacteria + Drug 0.244 µM	Bacteria + Drug 0.122 µM	Bacteria + Drug 0.061 µM	Bacteria + Drug 0.031 µM	Bacteria + Drug 0.015 µM	Bacteria + Drug 0.008 µM	Bacteria + Drug 0.004 µM	Bacteria + Drug 0 µM	Bacteria Only	Broth Only
H Drug Only	Broth + Drug 0.977 µM	Broth + Drug 0.488 µM	Broth + Drug 0.244 µM	Broth + Drug 0.122 µM	Broth + Drug 0.061 µM	Broth + Drug 0.031 µM	Broth + Drug 0.015 µM	Broth + Drug 0.008 µM	Broth + Drug 0.004 µM	Broth + Drug 0 µM	Bacteria Only	Broth Only

Negative Control Broth Only
Positive Control Bacteria Only
DMSO Control 0 µM
Serial Dilution of Drug + Bacteria
Serial Dilution of Drug + Broth Only

Figure 2.1. Plate map of experimental compounds. The broth microdilution was prepared in a 96 well plate by adding 5 µL (w/v) of the metal-complex taken from a master plate and 95µL of either bacteria (OD = 0.1 570 nm) or broth.

Bactericidal Assay

After the last optical density reading was taken, approximately 5 µL of each well was plated out on to solid agar plates (as described in Table 2.2) using metal stampers to observe bactericidal activity. Agar plates were incubated as described in Table 2.2.

Resazurin Viability Assay

Lastly, 30 µL of 1 mg/ml resazurin dissolved in dH_20 was added to each well and incubated in darkness at room temperature for 24 hours for ESKAPE pathogens or 72 hours for mycobacteria species.

2.2.4 Data Analysis

Data Processing

All data collected were n=3 technical replicates. The broth microdilution assays were processed in Microsoft® Excel® for Microsoft 365 MSO (Version 2302 Build 16.0.16130.20806) 64-bit and then plotted and analysed using GraphPad Prism 8. Blank control values of broth only were deducted from bacteria containing wells. End point data was plotted in bar charts as the mean + SD for ESKAPE pathogens and as growth curves for all mycobacterial species.

Statistical Analysis

Data analysis was performed using GraphPad Prism 8 software. A one-way ANOVA was conducted to determine if there were any statistically significant differences between the means of the various treatment groups. Post-hoc analysis using Dunnett's multiple comparisons tests was then performed to compare each treatment concentration against the untreated control (0 μM). This allowed us to identify the lowest concentration at which a statistically significant reduction in bacterial growth occurred. Statistical significance was defined as $P \leq 0.05$, with significance levels indicated as follows: **** $P \leq 0.0001$, *** $P \leq 0.001$, ** $P \leq 0.01$, * $P \leq 0.05$, ns $P > 0.05$. MIC values were determined as the lowest concentration where no visible growth was observed and confirmed by OD measurements and resazurin colour change. The MBC was determined as the minimum concentration where no bacterial growth was visually observed on agar.

2.3 Results

Our results demonstrate varying levels of antimicrobial activity across the 16 tested metal-ion complexes against ten bacterial species. Findings are presented in the following order:

1. Overview of antimicrobial activity across all compounds and species
2. Detailed results for each bacterial species, including:
    a. ESKAPE pathogens (6 species)
    b. *Mycobacterium abscessus* subspecies (3 subspecies)
    c. *Mycobacterium bovis* BCG
3. Comparison of lead compounds across all bacterial species

This structure provides a comprehensive understanding of species-specific effects and broader trends across compounds. The lead compounds with the best antimicrobial activity were MD7 and MD56, having MICs and MBCs for almost all microorganisms tested. The complex that was least effective was KP01, exhibiting activity against only one of the microorganisms tested. The MIC was determined as the lowest concentration where bacterial growth was inhibited for the BMD assay. In the RRA experiments, the MIC values were determined based on the lowest concentration at which resazurin changes colour from pink to purple. The MBC was determined as the minimum concentration where no bacterial growth was visually observed on agar. In addition, graphs of each BMD assay are presented.

Each graph represents the growth of bacteria (measured in optical density) against various concentrations of compound as either end point data represented in bar graphs for ESKAPE pathogens or growth curves of data over time for mycobacterial species. End point data at either 24 hours, 96 hours, or 336 hours were used to perform statistical analysis using a one-way ANOVA. In all experiments, there was a significant difference between all treatments according to the one-way ANOVA. In addition, a Dunnett's multiple comparison was conducted to compare all treatments to the control of 0 μM. This analysis indicates whether a compound has a significant difference in inhibiting the growth of bacteria, albeit not displaying complete inhibition and having an MIC. The significance results from each graph represent the significance between 0 μM and the MIC of the BMD assay to summarise the data. Raw data for every statistical analysis can be requested.

2.3.1 Antimicrobial Activity of 16 Metal-ion Complexes Against *Enterococcus faecium* ATCC 19434

E. faecium was tested against the 16 metal-ion complexes and 2 control compounds. Table 2.3 lists the MIC values for the BMD assay and RRA assay, as well as the MBC values of each compound against *E. faecium*. In addition, graphs of each BMD assay are presented in Figure 2.2.

Compound AN3 had an MIC of 7.81 μM in the BMD assay as shown by the growth curve in Figure 2.2 A. The Dunnett's multiple comparison showed a significant difference in bacterial growth between 7.81 μM and 0 μM ($P<0.0001$). Interestingly, all AN3 concentrations showed significance to 0 μM except from 1.95 μM ($P=0.8029$) potentially suggesting that all concentrations still impacted the growth of *E. faecium* despite not completely inhibiting growth except for 1.95 μM. The MIC of the RRA showed a different value of 15.63 μM (Table 2.3). However, AN3 did not exhibit any bactericidal activity (>500 μM) as shown by full bacterial growth on agar plates. Discrepancies between BMD and RRA results, such as those observed for AN3 against *E. faecium* (BMD MIC: 7.81 μM, RRA MIC: 15.63 μM), may be due to differences in assay sensitivity or the compound's mode of action. The higher RRA MIC suggests that while growth is inhibited at 7.81 μM, metabolic activity may persist up to 15.63 μM. The lack of bactericidal activity (MBC >500 μM) indicates that AN3 is bacteriostatic rather than bactericidal against E. faecium at the tested concentrations.

Figure 2.2 B illustrates the growth inhibition of RV144 against *E. faecium*. The BMD MIC was 0.98 μM with a significant difference in growth ($P<0.0001$) compared to the 0 μM concentration. The lower concentration of 0.49 μM also showed significance compared to 0 μM of RV144 ($P=0.0007$) as it had an increase in growth compared to 0 μM and therefore was not impacted by RV144. The MIC of the RRA showed an identical value to the BMD assay – 0.98 μM (Table 2.3). RV144 also exhibited bactericidal activity at a concentration of 0.98 μM.

The MIC of RV158 against *E. faecium* was 0.98 and 1.95 μM for the BMD assay and the RRA, respectively (Table 2.3) The Dunnett's multiple comparison showed a significant difference in bacterial growth between 0.98 μM and 0 μM ($P<0.0001$). The lower concentration of 0.49 μM did not show any significance compared to 0 μM of RV158 ($P=0.4082$) as it was not affected by RV158. The compound also exhibited bactericidal activity to *E. faecium* as low a concentration as 1.95 μM.

MD7 also showed promising results as an antimicrobial towards *E. faecium*. The MIC of both assays displayed a value of 1.95 μM as stated in Table 2.3. Figure 2.2 D reveals the inhibition of MD7 concentrations to *E. faecium*. A significant difference ($P <0.0001$) between 1.95 μM and 0 μM was analysed using the Dunnett's multiple comparison. Intriguingly, all

concentrations of MD7 showed significance to 0 μM, suggesting that these concentrations still impacted the growth of E. faecium despite not inhibiting growth entirely. MD7 also exhibited bactericidal activity to *E. faecium* with an MBC concentration of 15.63 μM.

The other ruthenium-based compound MD72 had a poorer effect on tackling bacterial growth as shown in Table 2.3 and Figure 2.2 E. The MIC of both assays, and the MBC, displayed a value of >500 μM as specified in Table 2.3. For the BMD assay, the Dunnett's multiple comparison showed no significant difference between 0 μM and all concentrations, except for 62.5 μM. However, this concentration had an increase in bacterial growth rather than decrease and therefore validated no susceptibility to MD72.

Compound MD73 had an MIC value of 125 μM for the BMD susceptibility assay, however, showed no MIC for the RRA (>500 μM), or did not display an MBC value (MBC >500 μM). Statistical analysis showed a significant difference (P<0.0001) between 125 μM and 0 μM and all concentrations higher than 125 μM. There were no significant differences observed for concentrations below 125 μM, suggesting that these lower concentrations of MD73 had no effect on *E. faecium* growth.

Figure 2.2 G demonstrates the effect of MD56 on *E. faecium*. The MIC of both assays, as well as the MBC, displayed a value of 7.81 μM as indicated in Table 2.3. There was a significant difference between this concentration and 0 μM (P<0.0001). The lower concentration of 3.91 μM also showed significance compared to 0 μM of MD56 (P <0.0001) as it impacted the growth of bacteria, however, this was not the MIC. Concentrations below this, such as 1.95, 0.98, and 0.49 μM failed to show any differences in bacterial growth compared to the control (P= 0.9999, P=0.2098, and P= 0.9997), respectively, denoting at these concentrations, MD56 has no effect to bacterial growth.

KP01 did not display an MIC against *E. faecium*. The MIC of both assays, and the MBC, displayed a value of >500 μM as presented in Table 2.3. For the BMD assay, the Dunnett's multiple comparison showed no significant difference between 0 μM and 500 μM.

JK-Ru5 also showed promising results as an antimicrobial towards *E. faecium*. The MIC of both assays, as well as the MBC, displayed a value of 62.5 μM as indicated in Table 2.3. Figure 2.2 I presents the optical density measurements for each concentration of JK-Ru5 against *E. faecium.* There was a significant difference between 62.5 μM and 0 μM (P<0.0001). The lower concentration of 31.25 μM also showed significance compared to 0 μM of JK-Ru5 (P <0.0001) as it impacted the growth of bacteria, however, this was not the MIC. Concentrations below this, such as 15.63, 7.81, 3.91, 1.95, 0.98, and 0.49 μM did not show any differences in

bacterial growth compared to the control, connoting at these concentrations, JK-Ru5 has no effect on bacterial growth.

The complex RuBio also showed promising results at inhibiting *E. faecium*. The MIC of the BMD assay was 3.91 μM as indicated in Table 2.3. For every concentration below the MIC, growth was observed from the graph in Figure 2.2 J. From the graph and statistical analysis P<0.9963, P=0.6660, P= 0.9962 respectively. RuBio did not display a dose- dependent growth when decreasing the concentrations, meaning *E. faecium* was only affected by RuBio at a concentration of 3.91 μM and above. The MIC of the RRA showed a different value of 7.81 μM (Table 2.3). RuBio resulted in bactericidal activity (7.81 μM) as shown by no bacterial growth on agar plates.

In contrast, RV239 OsBpy had a lower value of 6.25 μM for both the MICs and MBC. This difference was due to a different dilution series in this experiment due to limited compound. Therefore, the concentrations in the assay were adjusted to mitigate this. A significant difference (P <0.0001) between 6.25 μM and 0 μM was analysed using the Dunnett's multiple comparison for the MBD method. The lower concentration of 3.13 μM also showed significance compared to 0 μM of RV239 OsBpy (P <0.0001) as it impacted the growth of bacteria, however, was not the MIC.

The MIC for the MBD assay of FF175 against *E. faecium* (Figure 2.2 L) resulted in 31.25 μM. A significant difference (P <0.0001) between 31.25 μM and 0 μM was analysed using the Dunnett's multiple comparison. Concentrations 500-15.63 μM had a statistical difference in the decrease of bacterial growth compared to 0 μM, indicating inhibitory effects. Lower concentrations of FF175 including 7.81, 3.91, 1.95, 0.98, and 0.49 μM showed no statistical difference compared to the 0 μM control, suggesting that these concentrations have no effect on bacterial growth of *E. faecium*. The MIC of the RRA showed the same MIC compared to the BMD assay – 31.25 μM (Table 2.3). FF175 also exhibited bactericidal activity at a concentration of 125 μM which is an increase in concentration compared to the MIC.

The next copper compound FF176, displayed similar results to FF175 with the same MIC in the BMD assay (31.25 μM), and a 31.25 μM MIC in the RRA experiment. The Dunnett's multiple comparison reveals a significant statistical difference for all concentrations above and including the MIC (P<0.0001). Additionally, a statistical difference (P=0.0034) is evident in the concentration below the MIC (15.63 μM). This implies that FF176 impacted the growth of bacteria at this concentration, however, did not completely inhibit growth. Furthermore, at concentrations 7.81, 3.91, and 1.95 μM, no statistical difference was obvious from the analysis and thus at these concentrations FF176 had no susceptibility to the bacteria. The unusual statistical difference of 0.98 and 0.49 μM, can be explained by an increase in growth compared

to the bacteria (P<0.0001 and P=0.0270) which conveys that's FF176 does not challenge the growth of *E. faecium* at these concentrations. FF176 also exhibited bactericidal activity at a concentration of 125 μM mirroring FF175.

FF177 compound showed poorer antimicrobial effects at inhibiting and killing *E. faecium* compared to the first two copper-based compounds. Compound FF177 had an MIC value of 125 μM for the BMD susceptibility assay, however, showed no MIC for the RRA (>500 μM), or did not display an MBC value (MBC >500 μM). Statistical analysis showed a significant difference (P=0.0012), between 125 μM and 0 μM and all concentrations higher than 125 μM (P <0.0001). There were no significant differences observed for concentrations below 125 μM, suggesting that these lower concentrations of FF177 had no effect on *E. faecium* growth.

FF218 showed fewer promising results as a copper-metal antimicrobial towards *E. faecium*. The MIC of both assays, as well as the MBC, displayed a value of >500 μM as indicated in Table 2.3. Figure 2.2 O reveals the inhibition of FF218 concentrations to *E. faecium*. Interestingly, most concentrations of FF218 showed significance to 0 μM and this may suggest that these concentrations still impacted the growth of *E. faecium* despite not completely inhibiting growth.

The last copper-based compound (FF225) investigated showed the MIC of both assays, including the MBC, a value of 7.81 μM as highlighted in Table 2.3. The Dunnett's multiple comparison showed a significant difference in bacterial growth between 7.81 μM and 0 μM (P<0.0001). No significant difference was observed for 0.49 μM and 0.98 μM of FF225 against E. faecium (P= 0.9443, P= 0.6544), indicating these lower concentrations had no impact on the growth of E. faecium. The lower concentrations of 3.91 and 1.95 μM also showed significance compared to 0 μM of FF225 (P= <0.0001) as they impacted the growth of bacteria, however, they were not the MIC.

The control cisplatin demonstrated no inhibitory activity against *E. faecium* (MIC>500) as shown in Figure 2.2 Q and Table 2.3. The results of the BMD and RRA assay conquered the same results. Moreover, no bactericidal activity was observed for cisplatin against *E. faecium* with an MBC of >500 μM.

The positive control meropenem, a clinically used carbapenem antibiotic, exhibited a MIC and MBC of 62.5 μM against *E. faecium*. Notably, 10 of our tested compounds showed lower MIC values than meropenem, with RV144 and RV158 being particularly potent (MIC: 0.98 μM). This suggests that these ruthenium-based compounds may have potential as novel antimicrobials against *E. faecium*, possibly including meropenem-resistant strains. Further testing against resistant clinical isolates would be necessary to confirm this potential.

Key findings for *E. faecium*:

- Most susceptible to ruthenium-based compounds
- Lead compounds: RV144 and RV158 (MIC: 0.98 μM)
- 13 out of 16 compounds showed antimicrobial activity
- 10 compounds outperformed the positive control (meropenem)
- 4 of the MIC values between the BMD and RRA assays differ in concentration

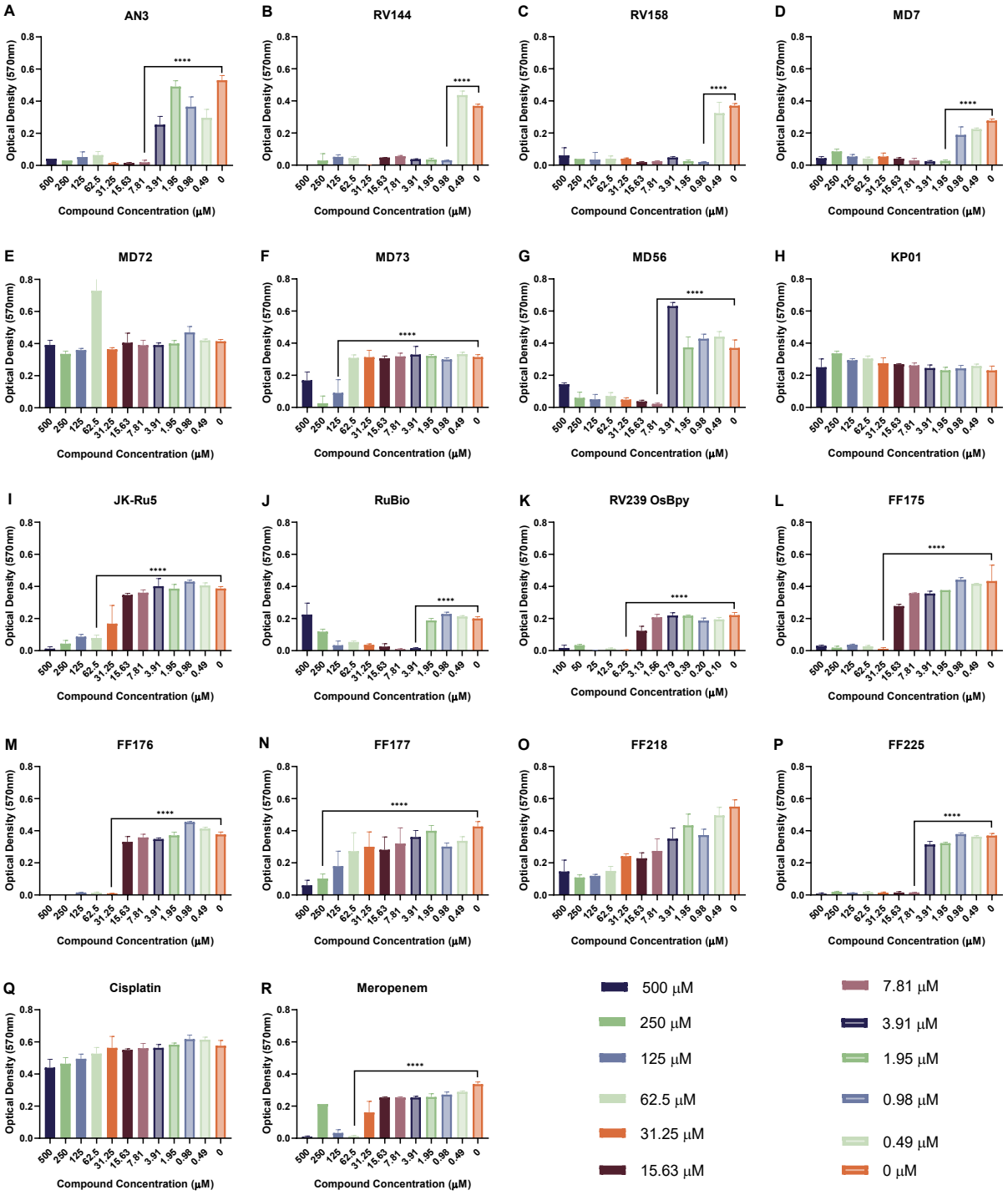

Figure 2.2. Optical density growth curves of *Enterococcus faecium* ATCC 19434*M* treated with investigative compounds. Growth curves show *E. coli* treated with **(A)** AN3, **(B)** RV144, **(C)** RV158, **(D)** MD7, **(E)** MD72, **(F)** MD73, **(G)** MD56, **(H)** KP01, **(I)** JK-Ru5, **(J)** RuBio, **(K)** RV239OsBpy, **(L)** FF175, **(M)** FF176, **(N)** FF177, **(O)** FF218, **(P)** FF225, **(Q)** Cisplatin, and **(R)** Meropenem for 24 hours. Optical density (570 nm) data are representative of n=3 technical replicates within one independent experiment. Mean values are shown, and error bars represent standard deviation. End point data, taken at 24 hours, was used for statistical analysis. P values were determined by a one-way analysis of variance (ANOVA) with Dunnett's multiple comparison, comparing all treatments to 0 μM to analyse the impact of compound concentration on the growth of *E. coli*. *P < 0.05, **P < 0.01, ***P < 0.001 and ****P < 0.0001.

Table 2.3. Summary table results of investigative compounds against *Enterococcus faecium* ATCC 19434. Data represent the minimum inhibitory concentrations (MIC) of the broth microdilutions (BMD), and resazurin reduction assay (RRA), and minimum bactericidal concentrations (MBC).

Compound	BMD MIC (μM)	RRA MIC (μM)	MBC (μM)
AN3	7.81	15.63	>500
RV144	0.98	0.98	0.98
RV158	0.98	1.95	1.95
MD7	1.95	1.95	15.63
MD72	>500	>500	>500
MD73	125	>500	>500
MD56	7.81	7.81	7.81
KP01	>500	>500	>500
JK-Ru5	62.5	62.5	62.5
RuBio	3.91	7.81	7.81
RV239OsBpy	6.25	6.25	6.25
FF175	31.25	31.25	125
FF176	31.25	31.25	125
FF177	250	>500	>500
FF218	>500	>500	>500
FF225	7.81	7.81	7.81
Cisplatin	>500	>500	>500
Meropenem	62.5	62.5	62.5

2.3.2 Antimicrobial Activity of 16 Metal-ion Complexes against MRSA N315

MRSA was tested against the 16 metal-ion complexes and 2 control compounds. Table 2.4 lists the MIC values for the BMD assay and RRA assay, as well as the MBC values of each compound against MRSA. In addition, graphs of each BMD assay are presented in Figure 2.3.

Compound AN3 had an MIC of 3.91 μM in the BMD assay as shown by the growth curve in Figure 2.3 A. The Dunnett's multiple comparison showed a significant difference in bacterial growth between 3.91 μM and 0 μM ($P<0.0001$). Remarkably, all concentrations of AN3 showed significance to 0 μM and this may suggest that these concentrations still impacted the growth of MRSA despite not completely inhibiting growth. The MIC of the RRA showed an identical value of 3.91 μM (Table 2.4). AN3 also exhibited bactericidal activity at a concentration of 15.63 μM as shown by absent growth on agar plates.

Figure 2.3 B illustrates the growth inhibition of RV144 against MRSA. The BMD MIC was 3.91 μM with a significant difference in growth ($P<0.0001$) compared to the 0 μM concentration. No significant difference was observed for 0.49 μM of RV144 against MRSA ($P=0.9996$), indicating 0.49 μM had no impact on the growth of MRSA. The MIC of the RRA showed a difference in value compared to the BMD assay – 15.63 μM (Table 2.4). RV144 also exhibited bactericidal activity at a concentration of 0.98 μM which is a decrease in concentration compared to the MIC.

The MIC of RV158 against MRSA was 1.95 and 3.91 μM for the BMD assay and the RRA, respectively μM (Table 2.4). The Dunnett's multiple comparison showed a significant difference in bacterial growth between 1.95 μM and 0 μM ($P<0.0001$). The lower concentration of 0.98 μM also showed significance compared to 0 μM of RV158 ($P=0.0012$) as it impacted the growth of bacteria, however, was not the MIC. RV144 also exhibited bactericidal activity to MRSA as low a concentration as 1.95 μM.

MD7 also showed promising results as an antimicrobial towards MRSA. The MIC of both assays, as well as the MBC, displayed a value of 1.95 μM as indicated in Table 2.4. Figure 2.3 D reveals the inhibition of MD7 concentrations to MRSA. A significant difference ($P <0.0001$) between 1.95 μM and 0 μM was analysed using the Dunnett's multiple comparison. Similarly to RV158, the lower concentration of 0.98 μM also showed significance compared to 0 μM of MD7 ($P=0.0012$) as it impacted the growth of bacteria, however, was not the MIC. All other concentrations of MD7 exhibited a significant difference in bacterial growth compared to the control, suggesting inhibiting effects.

The other ruthenium-based compound MD72 had a poorer effect on tackling bacterial growth as shown in Table 2.4 and Figure 2.3 E. Although the values of MICs between the BMD and RRA assay remained equal, there was an increase in MIC concentration to 125 μM. This higher concentration had a significant difference ($P=0.0001$) compared to 0 μM. Unfortunately, MD72 did not display any bactericidal activity for MRSA with an MBC of >500 μM.

Compound MD73 had identical MIC values of 7.81 μM for both susceptibility assays, however, did not display an MBC value (MBC >500 μM). Statistical analysis showed a significant difference ($P<0.0001$) between 7.81 μM and 0 μM and all concentrations higher than 7.81 μM. In addition, 3.91 μM showed a statistical difference ($P=0.0001$) compared to the control, indicating that it also slowed the growth of MRSA, however, did not inhibit it completely. There were no significant differences observed for concentrations below 3.91 μM, suggesting that these lower concentrations of MD73 had no effect on MRSA growth.

Figure 2.3 G demonstrates the effect of MD56 on MRSA. With an MIC as low as 1.95 μM, there was a significant difference between this concentration and 0 μM ($P=0.0001$). Concentrations below this, such as 0.98 μM and 0.49 μM did not show any differences in bacterial growth compared to the control ($P= 0.6787$ and $P= 0.9997$), respectively, meaning at these concentrations, MD56 has no effect on bacterial growth. The MIC of the RRA showed a difference in value compared to the BMD assay – 3.91 μM (Table 2.4). MD56 also exhibited bactericidal activity at a concentration of 3.91 μM as shown by absent growth on agar plates.

KP01 was the only investigative compound against MRSA, which did not display an MIC. The MIC of both assays, as well as the MBC, displayed a value of >500 μM as indicated in Table 2.4. For the BMD assay, the Dunnett's multiple comparison showed no significant difference between 0 μM and 0.49, 0.98, 1.95, 3.91, 7.81, 15.63, 31.25 μM. However, for concentrations 62.5, 125, 250, and 500 μM, there was a statistical difference compared to the control – P=0.0150, P=0.0003, P<0.0001, and P<0.0001, respectively. This signals that, although no complete inhibition is present, at high concentrations, KP01 has a reducing effect on bacterial growth towards MRSA.

JK-Ru5 also showed promising results as an antimicrobial towards MRSA. The MIC of both assays, as well as the MBC, displayed a value of 3.91 μM as indicated in Table 2.4. Figure 2.3 I presents the optical density measurements for each concentration of JK-Ru5 against MRSA. All concentrations have statistical differences compared to 0 μM (P<0.0001, P=0.0002). The OD values of 0.49 and 0.98 μM were higher than that for 0 μM, therefore, this difference was not due to growth inhibition. In contrast, the statistical difference between 1.91 μM and 0 μM is due to a decrease in bacterial growth, suggesting an impact on MRSA but not complete inhibition.

The complex RuBio showed fewer promising results at inhibiting MRSA. The MIC of both assays, as well as the MBC, displayed a value of 500 μM as indicated in Table 2.4. For every concentration except 500 μM, growth was observed from the growth graph in Figure 2.3 J. From the graph and statistical analysis (P<0.000, P=0.0004, P= 0.0193, P= 0.0287, and P=0.1585), RuBio did not display a does dependant growth when decreasing the concentrations, meaning MRSA was only affected by RuBio at a concentration of 500 μM.

Contrariwise, RV239 OsBpy had a lower value of 1.95 μM for both the MICs and MBC. A significant difference (P <0.0001) between 1.95 μM and 0 μM was analysed using the Dunnett's multiple comparison for the MBD method. The lower concentrations of 0.49 and 0.98 μM also showed significance compared to 0 μM of RV239 OsBpy (P <0.0001) as it impacted the growth of bacteria, however, it was not the MIC. All other concentrations of RV239 OsBpy exhibited a significant difference in bacterial growth compared to the control, suggesting inhibiting effects.

The MIC for the MBD assay of FF175 against MRSA (Figure 2.3 L) resulted in 7.81 μM. A significant difference (P <0.0001) between 7.81 μM and 0 μM was analysed using the Dunnett's multiple comparison. In this experiment, all concentrations showed a statistical difference compared to the control. FF175 at a concentration of 0.49 and 0.98 μM showed significant (P<0.0001), however this was in increase in bacterial growth compared to 0 μM, and therefore these lower concentrations did not affect MRSA. Conversely, 1.95 and 3.91 μM showed an inhibitory effect but did not reach an MIC with the statistical significance of P=0.0301 and

P=0.0003, respectively. The MIC of the RRA showed a difference in value compared to the BMD assay – 31.25 μM (Table 2.4). FF175 also exhibited bactericidal activity at a concentration of 31.25 μM which is an increase in concentration compared to the MIC.

The next copper compound FF176, displayed similar results to FF175 with the same MIC in the BMD assay (7.81 μM), however with an improved 15.63 μM MIC in the RRA experiment and MBC. All concentrations demonstrated statistical significance compared to 0 μM which suggests FF176 has an inhibitory effect on all concentrations ($P<0.0001$ and $P=0.0060$).

FF177 compound showed poorer antimicrobial effects at inhibiting and killing MRSA compared to the first two copper-based compounds. Both the BMD and RRA assays obtained the same MIC results of 125 μM. Concentrations 500-7.81 μM had a statistical difference in the decrease of bacterial growth compared to 0 μM, indicating inhibitory effects but not complete growth inhibition ($P<0.0001$ and $P=0.0060$). Lower concentrations of FF177 including 3.91, 1.95, 0.98, and 0.49 μM showed no statistical difference compared to the 0 μM control, suggesting that these concentrations have no effect on bacterial growth of MRSA. In addition, FF177 displayed no evidence of any bactericidal activity towards MRSA with an MBC of 500 μM.

FF218 showed promising results as a copper-metal antimicrobial towards MRSA. The MIC of both assays, as well as the MBC, displayed a value of 31.25 μM as indicated in Table 2.4. Figure 2.3 O reveals the inhibition of FF218 concentrations to MRSA. A significant difference ($P <0.0001$) between 31.25 μM and 0 μM was analysed using the Dunnett's multiple comparison. The concentrations below 31.25 μM did not show any difference in bacterial growth compared to the control. All other concentrations above 31.25 μM exhibited a significant difference in bacterial growth compared to the control, suggesting inhibiting effects.

The last copper-based compound investigated showed varied MIC and MBC results. The MIC of FF225 against MRSA was 7.81 and 15.63 μM for the BMD assay and the RRA, respectively μM (Table 2.4). The Dunnett's multiple comparison showed a significant difference in bacterial growth between 7.81 μM and 0 μM ($P<0.0001$). The lower concentrations of 0.49, 0.98, and 3.91 μM also showed significance compared to 0 μM of FF225 ($P= <0.0001$, $P<0.0001$, $P=0.0476$) as they impacted the growth of bacteria, however, were not the MIC. Peculiarly, the concentration of 1.95 μM did not show any growth difference compared to the control ($P=0.8558$), however all four of these lower concentrations had an increase in bacterial growth or the same as 0 μM, indicating these concentrations are not effected by MRSA. FF225 also exhibited bactericidal activity to MRSA, albeit at an increased concentration of 62.5 μM.

The control cisplatin demonstrated no inhibitory activity against MRSA (MIC>500) as shown in Figure 2.3 Q and Table 2.4. The results of the BMD and RRA assay conquered the same

results. Furthermore, no bactericidal activity was observed for cisplatin against MRSA with an MBC of >500 μM. The positive control meropenem exhibited an MIC of 125 μM against MRSA in both susceptibility assays and an MBC of 250 μM.

The positive control meropenem, a clinically used carbapenem antibiotic, exhibited a MIC and MBC of 250 μM against MRSA. Notably, 12 of our tested compounds showed lower MIC values than meropenem, with MD7 and RV239 OsBpy being particularly potent (MIC: 1.9 μM). This suggests that these ruthenium-based compounds may have potential as novel antimicrobials against MRSA, possibly including meropenem-resistant strains. Further testing against resistant clinical isolates would be necessary to confirm this potential.

Key findings for MRSA:

- Most susceptible Gram-positive ESKAPE pathogen tested against all investigative compounds
- Most susceptible to ruthenium-based compounds and osmium-based compounds
- Lead compounds: MD7 and RV239 OsBpy (MIC: 1.9 μM, MBC: 1.9 μM)
- 15 out of 16 compounds showed antimicrobial activity
- 12 compounds outperformed the positive control (meropenem)
- 6 of the MIC values between the BMD and RRA assays differ in concentration

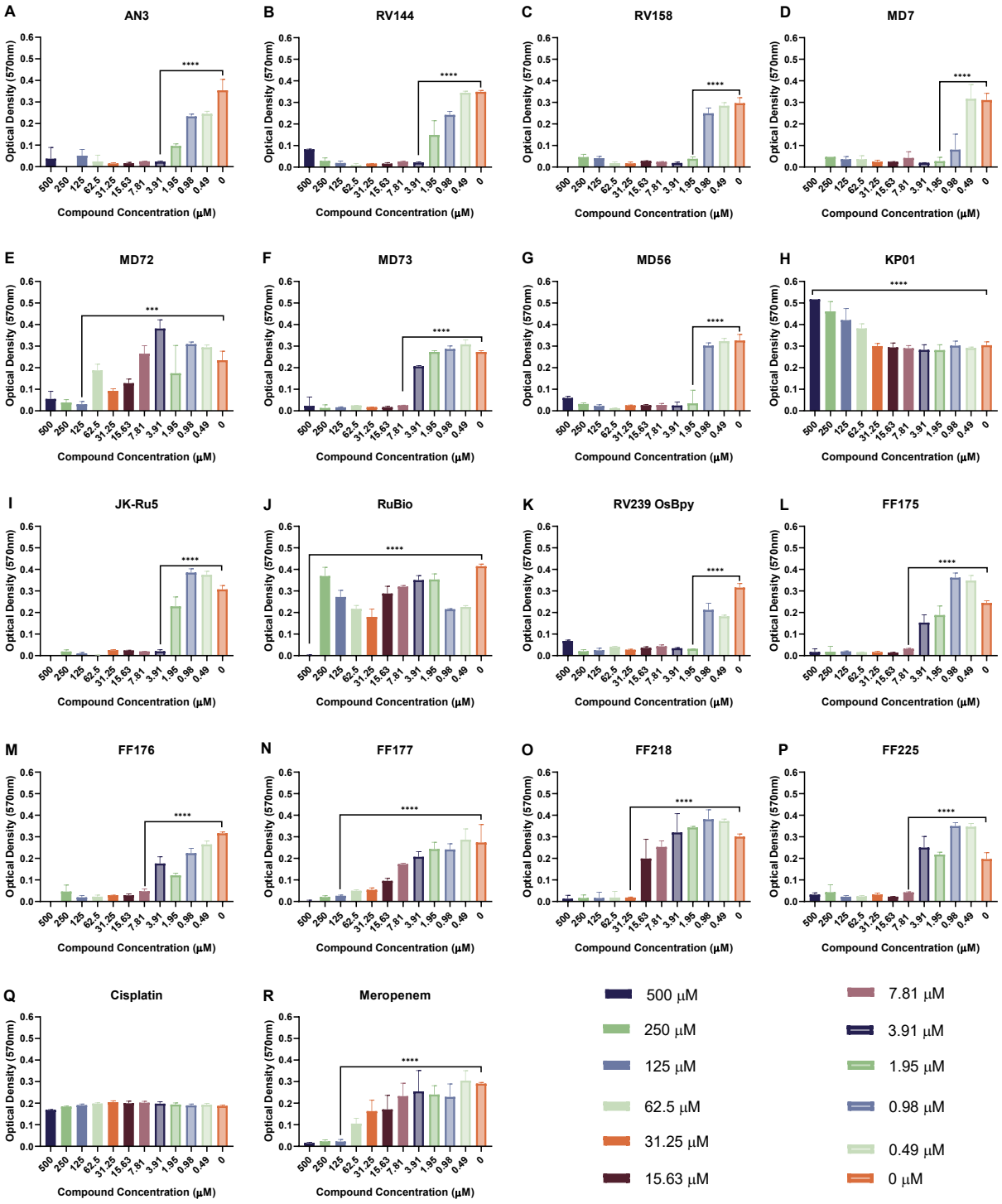

Figure 2.3. Optical density growth curves of *MRSA* N315 treated with investigative compounds. Growth curves show MRSA treated with **(A)** AN3, **(B)** RV144, **(C)** RV158, **(D)** MD7, **(E)** MD72, **(F)** MD73, **(G)** MD56, **(H)** KP01, **(I)** JK-Ru5, **(J)** RuBio, **(K)** RV239OsBpy, **(L)** FF175, **(M)** FF176, **(N)** FF177, **(O)** FF218, **(P)** FF225, **(Q)** Cisplatin, and **(R)** Meropenem for 24 hours. Optical density (570 nm) data are representative of n=3 technical replicates within one independent experiment. Mean values are shown, and error bars represent standard deviation. End point data, taken at 24 hours, was used for statistical analysis. P values were determined by a one-way analysis of variance (ANOVA) with Dunnett's multiple comparison, comparing all treatments to 0 μM to analyse the impact of compound concentration on the growth of MRSA *P < 0.05, **P < 0.01, ***P < 0.001 and ****P < 0.0001.

Table 2.4. Summary table results of investigative compounds against MRSA N315. Data represent the minimum inhibitory concentrations (MIC) of the broth microdilutions (BMD), and resazurin reduction assay (RRA), and minimum bactericidal concentrations (MBC).

Compound	BMD MIC (μM)	RRA MIC (μM)	MBC (μM)
AN3	3.91	3.91	15.63
RV144	3.91	15.63	0.98
RV158	1.95	3.91	1.95
MD7	1.95	1.95	1.95
MD72	125	125	>500
MD73	7.81	7.81	>500
MD56	1.95	3.91	3.91
KP01	>500	>500	>500
JK-Ru5	3.91	3.91	3.91
RuBio	500	500	500
RV239OsBpy	1.95	1.95	1.95
FF175	7.81	31.25	31.25
FF176	7.81	15.63	15.63
FF177	125	125	>500
FF218	31.25	31.25	31.25
FF225	7.81	15.63	62.5
Cisplatin	>500	>500	>500
Meropenem	125	125	250

2.3.3 Antimicrobial Activity of 16 Metal-ion Complexes against *Klebsiella pneumoniae* H467

Klebsiella pneumoniae (*K. pneumoniae*) was tested against the 16 metal-ion complexes and 2 control compounds. Table 2.5 lists the MIC values for the BMD assay and RRA assay, along with the MBC values of each compound against MRSA. Additionally, graphs of each BMD assay are presented in Figure 2.4. Only 5 metal-based compounds showed any inhibitory or killing activity towards *K. pneumoniae.* These compounds are MD7, MD56M KP01, and JK-Ru5, which are ruthenium based, and RV239 OsBpy, an osmium-based compound.

Figure 2.4 D illustrates the growth inhibition of MD7 against *K. pneumoniae*. The BMD MIC was 62.5 μM with a significant difference in growth ($P<0.0001$) compared to the 0 μM concentration. No significant difference was observed for 3.91, 1.95, 0.98, and 0.49 μM of MD7 against *K. pneumoniae* ($P=0.7219$, 0.7440, 0.8912, ad 0.8874), indicating these concentrations had no impact on the growth of MRSA. In contrast, 7.81, 15.63, and 31.25 μM of MD7 shows statistical significance compared to the control demonstrating a decrease in cell growth but no inhibition. The MIC of the RRA showed a difference in value compared to the BMD assay – 125 μM (Table 2.5). MD56 also exhibited bactericidal activity at a concentration of 125 μM as shown by absent growth on agar plates.

The other ruthenium-based compound which displayed susceptibility to *K. pneumoniae* was MD56 displaying the same concentrations of MD7 – 62.5, 125, and 125 μM, for the BMD assay

the RRA assay and the MBC, respectively (Table 2.5 and Figure 2.4 G). Statistical analysis concluded that concentrations as low as 15.63 µM has an inhibitory effect on *K. pneumoniae.* Surprisingly, the MIC for the BMD assay of KP01 against *K. pneumoniae* resulted in 500 µM (P, <0.0001) whereas, the RRA assay and MBC assay did not present any inhibitory concentrations (>500 µM). In contrast, the effect of JK-Ru5 against *K. pneumoniae* showed the opposite effect, whereby the MBD assay did not present an MIC (>500 µM) and the RRA had an MIC of 500 µM displayed by a colour change. In addition, JK-Ru5 depicted a bactericidal activity to *K. pneumoniae* at a concentration of 500 µM.

Lastly, RV239 OsBpy, which is an osmium-based compound, showed an MIC value of 125 µM osmium-based compound for both susceptibility assays (Table 2.5 and Figure 2.4 K). The Dunnett's multiple comparison shows no statistical difference in concentration ranging from 0.49 to 3.9 µM. In contrast, concentrations from 7.81 to 500 µM exhibited statistical differences compared to the control, suggesting RV239 OsBpy effects bacterial growth as low as 7.81 µM. RV239 OsBpy also exhibited bactericidal activity to *K. pneumoniae* at a concentration of 31.25 µM.

All other compounds including AN3, RV144, RV158, MD72, MD73, RuBio, FF175, FF176, FF177, FF218 and FF228 did not display any antimicrobial activity towards *K. pneumoniae* demonstrated by an MIC of >500 µM for both susceptibility assays and an MBC of >500 µM.

The control cisplatin demonstrated no inhibitory activity against *K. pneumoniae* (MIC>500) as shown in Figure 2.4 Q and Table 2.5. The results of the BMD and RRA assay conquered the same results. Furthermore, no bactericidal activity was observed for cisplatin against *K. pneumoniae* with an MBC of >500. The positive control meropenem exhibited an MIC of 125 µM against MRSA in both susceptibility assays as well as an MBC of 125 µM.

The positive control meropenem, a clinically used carbapenem antibiotic, exhibited a MIC and MBC of 125 µM against *K. pneumoniae*. Notably, none of the tested compounds showed lower MIC values than meropenem. This suggests that these compounds towards *K. pneumoniae* are no more efficient than the current treatment of meropenem. Further testing of other first line antibiotics against this bacterium would be necessary to find increased susceptibility of these compounds compared to clinically relevant antibiotics.

Key findings for *K. pneumoniae*:

- Most susceptible to ruthenium-based compounds
- Lead compounds: MD7 and MD56 (MIC BMD: 62.5 µM, MIC RRA: 125 µM, MBC: 125 µM for both compounds)
- 3 out of 16 compounds showed antimicrobial activity

- No compounds outperformed the positive control (meropenem)
- 4 of the MIC values between the BMD and RRA assays differ in concentration

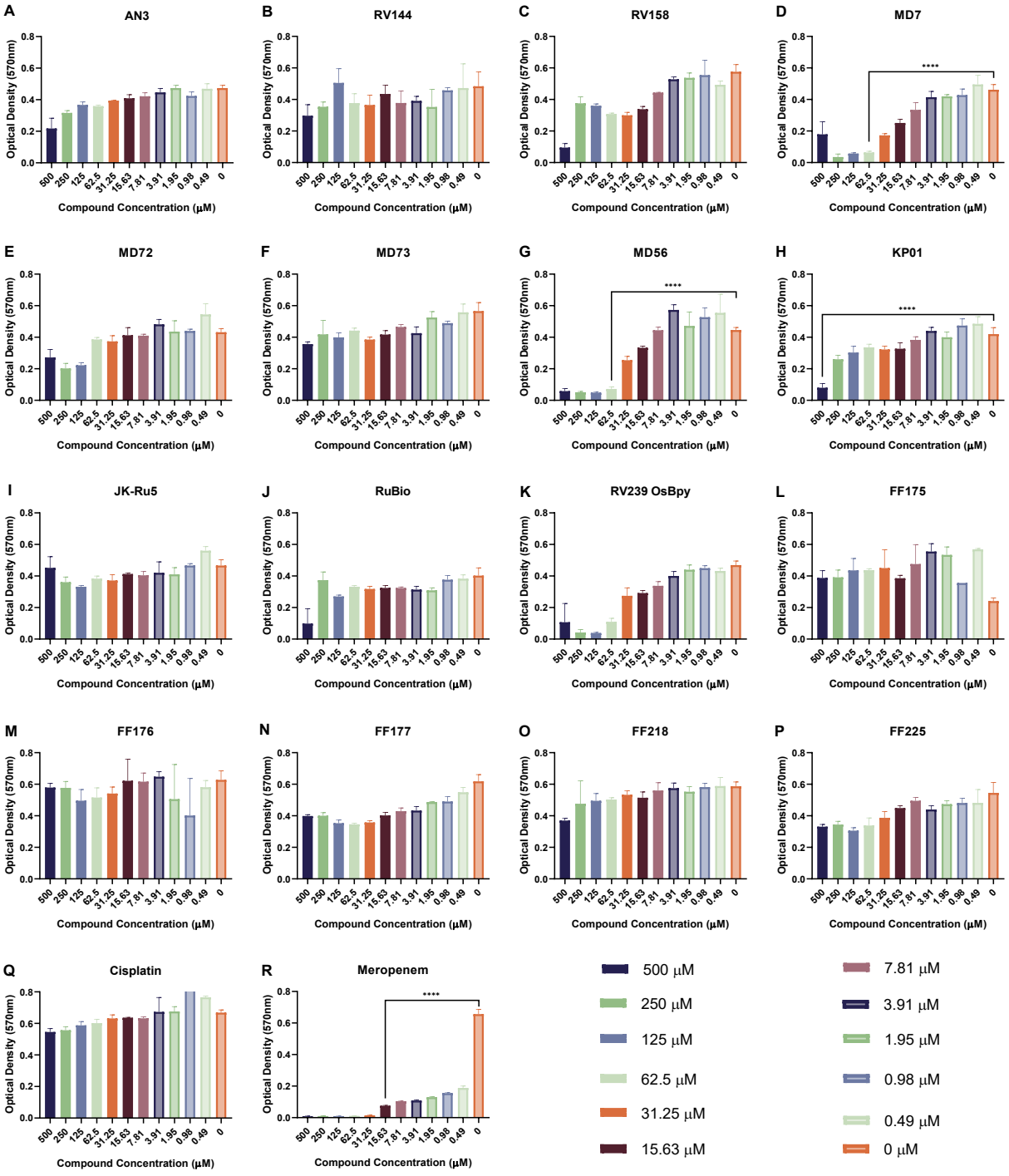

Figure 2.4. Optical density growth curves of *Klebsiella pneumoniae* H467 treated with investigative compounds. Growth curves show *K. pneumoniae* treated with **(A)** AN3, **(B)** RV144, **(C)** RV158, **(D)** MD7, **(E)** MD72, **(F)** MD73, **(G)** MD56, **(H)** KP01, **(I)** JK-Ru5, **(J)** RuBio, **(K)** RV239OsBpy, **(L)** FF175, **(M)** FF176, **(N)** FF177, **(O)** FF218, **(P)** FF225, **(Q)** Cisplatin, and **(R)** Meropenem for 24 hours. Optical density (570 nm) data are representative of n=3 technical replicates within one independent experiment. Mean values are shown, and error bars represent standard deviation. End point data, taken at 24 hours, was used for statistical analysis. P values were determined by a one-way analysis of variance (ANOVA) with Dunnett's multiple comparison, comparing all treatments to 0 μM to analyse the impact of compound concentration on the growth of *K. pneumoniae* *P < 0.05, **P < 0.01, ***P < 0.001 and ****P < 0.0001.

Table 2.5. Summary table results of investigative compounds against *Klebsiella pneumoniae* H467. Data represent the minimum inhibitory concentrations (MIC) of the broth microdilutions (BMD), and resazurin reduction assay (RRA), and minimum bactericidal concentrations (MBC).

Compound	BMD MIC (μM)	RRA MIC (μM)	MBC (μM)
AN3	>500	>500	>500
RV144	>500	>500	>500
RV158	>500	>500	>500
MD7	62.5	125	125
MD72	>500	>500	>500
MD73	>500	>500	>500
MD56	62.5	125	125
KP01	500	>500	>500
JK-Ru5	>500	500	500
RuBio	>500	>500	>500
RV239OsBpy	>500	125	125
FF175	>500	>500	>500
FF176	>500	>500	>500
FF177	>500	>500	>500
FF218	>500	>500	>500
FF225	>500	>500	>500
Cisplatin	>500	>500	>500
Meropenem	15.63	15.63	31.25

2.3.4 Antimicrobial Activity of 16 Metal-ion Complexes against *Acinetobacter baumannii* NCTC 12156

Acinetobacter baumannii (*A. baumannii*) was tested against the 16 metal-ion complexes and 2 control compounds. Table 2.6 lists the MIC values for the BMD assay and RRA assay, as well as the MBC values of each compound against MRSA. In addition, graphs of each BMD assay are presented in Figure 2.5.

Compound AN3 had an MIC of 31.25 μM in the BMD assay as shown by the growth curve in Figure 2.5 A. The Dunnett's multiple comparison showed a significant difference in bacterial growth between 31.25 μM and 0 μM ($P<0.0001$). Concentrations below 31.25 μM did not show any differences in bacterial growth compared to the control, meaning at these concentrations, AN3 has no effect on the bacterial growth of *A. baumannii*. The MIC of the RRA showed a difference in the MIC of 62.5 μM (Table 2.6). Disappointingly, AN3 did not exhibit bactericidal as shown by full bacterial growth on agar plates (>500 μM).

The MIC of RV158 against *A. baumannii* was 7.81 and 15.63 μM for the BMD assay and the RRA, respectively (Table 2.6). The Dunnett's multiple comparison showed a significant difference in bacterial growth between 7.81 μM and 0 μM ($P<0.0001$). The lower concentration of 3.91 μM also showed significance compared to 0 μM of RV158 ($P= 0.0153$) as it impacted the growth of bacteria, however, was not the MIC. RV158 also did not exhibit bactericidal activity, as shown by full bacterial growth of *A. baumannii* on agar plates (>500 μM).

MD7 also showed promising results as an antimicrobial towards *A. baumannii*. Figure 2.5 D reveals the inhibition of MD7 concentrations to *A. baumannii*. The BMD assay presents an MIC of 7.81 µM. A significant difference (P <0.0001) between 7.81 µM and 0 µM was analysed using Dunnett's multiple comparison. Concentrations below this did not show any differences in bacterial growth compared to the control, meaning at these concentrations, MD7 has no effect on bacterial growth. The MIC of the RRA showed a difference in the MIC of 62.5 µM (Table 2.6). In this instance, MD7 revealed bactericidal activity to *A. baumannii* at a concentration of 15.63 µM.

Figure 2.5 G demonstrates the effect of MD56 on *A. baumannii*. With an MIC as low as 7.81µM, there was a significant difference between this concentration and 0 µM (P=0.0001). Concentrations where significant differences were been found above the MIC include 3.91, 1.95 µM (P<0.0001 and P=0.0095). These differences are attributed to 1.95 µM having in increase in cell growth compared to the control and therefore is not affected by MD56, and 3.91 µM having a decrease in cell growth compared to the control conveying at this concentration the compound is influencing the bacteria. The MIC of the RRA also showed an identical value to the BMD assay – 7.81 µM (Table 2.6). MD56 also exhibited bactericidal activity at a concentration of 31.25 µM as shown by absent growth on agar plates.

JK-Ru5 also showed inhibitory activity towards *A. baumannii*. The MIC of both assays, as well as the MBC, displayed a value of 125 µM as indicated in Table 2.6. Figure 2.5 I presents the optical density measurements for each concentration of JK-Ru5 against *A. baumannii*. All concentrations above 125 µM have statistical differences compared to 0 µM (P=0.0054, P=0.0005, P=0.0001). The statistically different concentrations below 125 µM are due to an increase in bacterial growth compared to the control and therefore JK-Ru5 does not affect *A. baumannii* at these concentrations.

The complex RuBio showed more promising results at inhibiting *A. baumannii*. The MIC of both assays, as well as the MBC, displayed varied results. As listed in Table 2.6, the BMD assay exhibited an MIC of 7.81 µM, whereas the RRA resulted in an MIC of 15.63 µM. For every concentration below 7.81 µM, growth was observed from the graph in Figure 2.5 J. From the graph and statistical analysis (P=0.1556, P>0.9999, P= 0.9994, and P= 0.9995), RuBio did not display a does dependant growth when decreasing the concentrations, meaning *A. baumannii* was only affected by RuBio at concentrations above 7.81 µM. RuBio also exhibited bactericidal activity at a concentration of 15.63 µM as shown by absent growth on agar plates.

Figure 2.5 K demonstrates the effect of RV239 OsBpy on *A. baumannii*. With an MIC as low as 7.81µM, there was a significant difference between this concentration and 0 µM (P=0.0001). For every concentration below 7.81 µM, growth was observed from the graph in Figure 2.5 K.

From the graph and statistical analysis (P=0.863, P>0.9768, P>0.9999, and P= 0.9998), RV239 OsBpy did not display a does dependant growth when decreasing the concentrations, meaning *A. baumannii* was only affected by RV239 OsBpy at concentrations above 7.81 μM. The MIC of the RRA also showed an identical value to the BMD assay – 7.81 μM (Table 2.6). RV239 OsBpY also exhibited bactericidal activity at a concentration of 15.63 μM as shown by absent growth on agar plates.

Interestingly, copper-based compound FF225 showed an MIC for the BMD assay, but not for the RRA assay or an MBC. The BMD assay presents an MIC of 62.5 μM. A significant difference (P <0.0001) between 62.5 μM and 0 μM was analysed using Dunnett's multiple comparison. In addition, the concentration of 31.25 μM presented statistical differences, conveying this concentration also affected the growth of *A. baumannii* but not total inhibition. The RRA did not result in an MIC (>500 μM) (Table 2.6). In this instance, FF225 revealed no bactericidal activity to *A. baumannii* (>500) μM.

The control cisplatin demonstrated no inhibitory activity against *A. baumannii* (MIC>500 μM) as shown in Figure 2.5 Q and Table 2.6. The results of the BMD and RRA assay conquered the same results. Furthermore, no bactericidal activity was observed for cisplatin against *A. baumannii* with an MBC of >500 μM.

The positive control meropenem, a clinically used carbapenem antibiotic, exhibited a MIC of 7.81 μM in the BMD, a MIC of 15.63 μM in the RRA susceptibility test, and a MBC of 31.25 μM against *A. baumannii*. Notably, 5 of our tested compounds showed equal or lower MIC values than meropenem, with MD7, MD56, RuBio, and RV239 OsBpy being particularly potent (MIC: 7.81-15.53 μM). This suggests that these ruthenium and osmium-based compounds may have potential as novel antimicrobials against *A. baumannii*, possibly including meropenem-resistant strains. Further testing against resistant clinical isolates would be necessary to confirm this potential. All other compounds, including RV144, MD72, MD73, KP01, FF175, FF176, FF177, and FF218 did not display any antimicrobial activity towards *A. baumannii* demonstrated by an MIC of >500 μM for both susceptibility assays and an MBC of >500 μM.

Key findings for *A. baumannii*:

- Most susceptible to ruthenium and osmium-based compounds
- Lead compounds: MD7, MD56, RuBio, and RV239 OsBpy (MIC BMD: 7.81 μM, MIC RRA: 7.81/15.63 μM, MBC: 15.63/31.25 μM)
- 8 out of 16 compounds showed antimicrobial activity
- 5 compounds outperformed the positive control (meropenem)
- 6 of the MIC values between the BMD and RRA assays differ in concentration

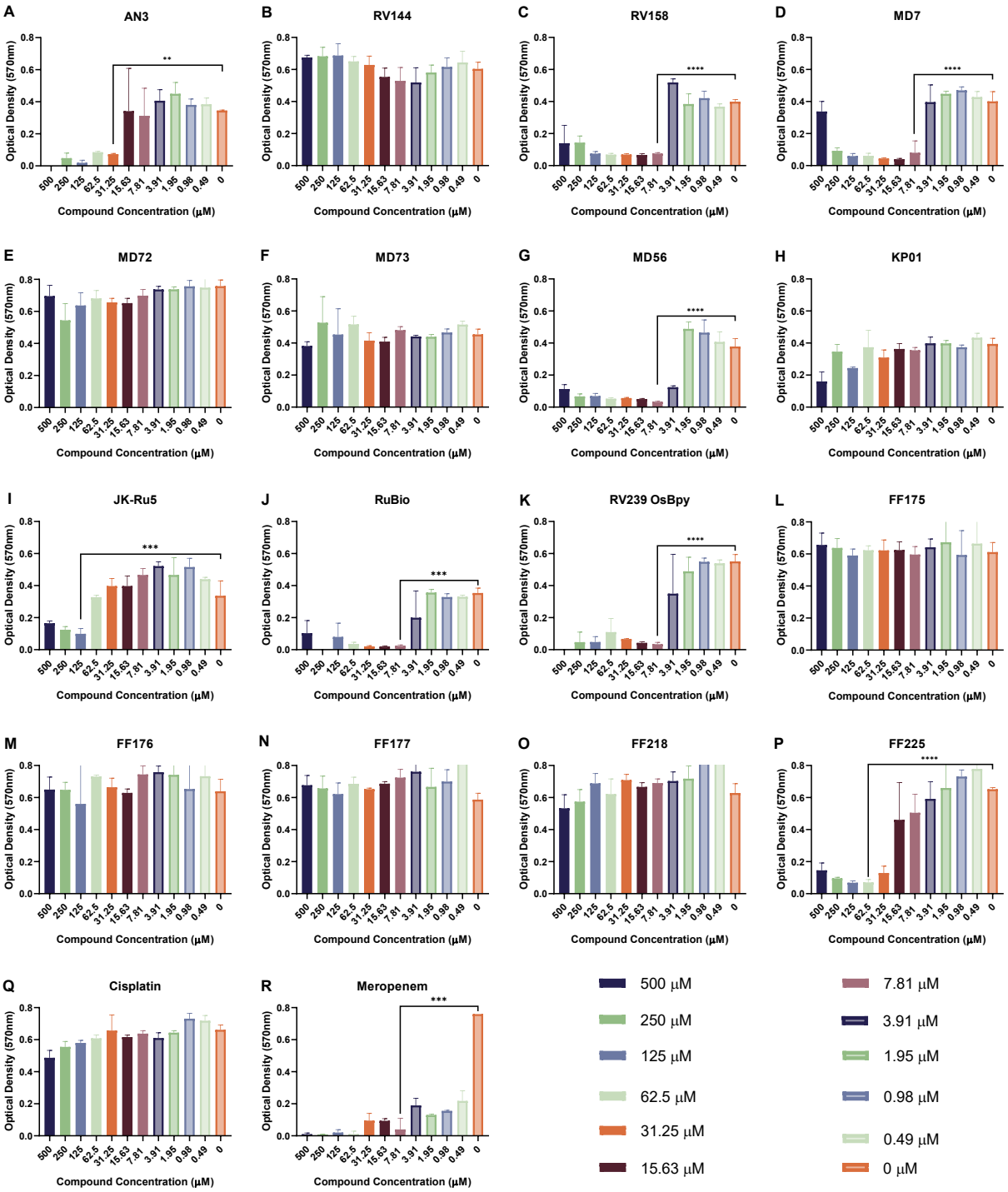

Figure 2.5. Optical density growth curves of *Acinetobacter baumannii* NCTC 12156 treated with investigative compounds. Growth curves show *A. baumannii* treated with **(A)** AN3, **(B)** RV144, **(C)** RV158, **(D)** MD7, **(E)** MD72, **(F)** MD73, **(G)** MD56, **(H)** KP01, **(I)** JK-Ru5, **(J)** RuBio, **(K)** RV239OsBpy, **(L)** FF175, **(M)** FF176, **(N)** FF177, **(O)** FF218, **(P)** FF225, **(Q)** Cisplatin, and **(R)** Meropenem for 24 hours. Optical density (570 nm) data are representative of n=3 technical replicates within one independent experiment. Mean values are shown, and error bars represent standard deviation. End point data, taken at 24 hours, was used for statistical analysis. P values were determined by a one-way analysis of variance (ANOVA) with Dunnett's multiple comparison, comparing all treatments to 0 μM to analyse the impact of compound concentration on the growth of *A. baumannii* *P < 0.05, **P < 0.01, ***P < 0.001 and ****P < 0.0001.

Table 2.6. Summary table results of investigative compounds against *Acinetobacter baumannii* NCTC 12156. Data represent the minimum inhibitory concentrations (MIC) of the broth microdilutions (BMD), and resazurin reduction assay (RRA), and minimum bactericidal concentrations (MBC).

Compound	BMD MIC (μM)	RRA MIC (μM)	MBC (μM)
AN3	31.25	62.5	>500
RV144	>500	>500	>500
RV158	7.81	15.63	>500
MD7	7.81	15.63	15.63
MD72	>500	>500	>500
MD73	>500	>500	>500
MD56	7.81	7.81	31.25
KP01	>500	>500	>500
JK-Ru5	125	125	125
RuBio	7.81	15.63	15.63
RV239OsBpy	7.81	7.81	15.63
FF175	>500	>500	>500
FF176	>500	>500	>500
FF177	>500	>500	>500
FF218	>500	>500	>500
FF225	62.5	>500	>500
Cisplatin	>500	>500	>500
Meropenem	7.81	15.63	31.25

2.3.5 Antimicrobial Activity of 16 Metal-ion Complexes against *Pseudomonas aeruginosa* ATCC 19429

Pseudomonas aeruginosa (*P. aeruginosa*) was tested against the 16 metal-ion complexes and 2 control compounds. Table 2.7 lists the MIC values for the BMD assay and RRA assay, along with the MBC values of each compound against MRSA. In addition, graphs of each BMD assay are presented in Figure 2.6. Only 4 metal-based compounds showed any inhibitory or killing activity towards *P. aeruginosa.* These compounds are MD7, MD56, and JK-Ru5, which are ruthenium based, and RV239 OsBpy, which is an osmium-based compound. The highest MIC displayed was 15.63 μM and the highest MBC was 62.5 μM.

Figure 2.6 D illustrates the growth inhibition of MD7 against *P. aeruginosa*. The BMD MIC was 62.5 μM with a significant difference in growth ($P<0.0001$) compared to the 0 μM concentration. Interestingly, all concentrations of MD7 showed significance to 0 μM except from 1.95 μM ($P=0.9998$) potentially suggesting that all concentrations still impacted the growth of *P. aeruginosa* despite not completely inhibiting growth except for 1.95 μM. The MIC of the RRA showed a difference in value compared to the BMD assay – 125 μM (Table 2.7). MD56 also exhibited bactericidal activity at a concentration of 250 μM as shown by absent growth on agar plates.

The other ruthenium-based compound which displayed susceptibility to *K. P. aeruginosa* was MD56 displaying MICs and an MBC of 15.63, 125, and 125 μM, for the BMD assay the RRA

assay and the MBC, respectively (Table 2.7 and Figure 2.6 G). Statistical analysis concluded that concentrations as low as 15.63 µM has an inhibitory effect on *P. aeruginosa* (P<0.0001)

Surprisingly, the MIC for the BMD assay of JK-Ru5 against *P. aeruginosa* resulted in 125 µM (P <0.0001) whereas, the RRA assay and MBC assay presented concentrations of 250 µM for the MIC and MBC. The Dunnett's multiple comparison shows a statistical difference at 125 µM and above concluding that JK-Ru5 did not display a dose-dependent growth when decreasing the concentrations, meaning *P. aeruginosa* was only affected by JK-Ru5 at a concentration of 125 µM and above.

Lastly, RV239 OsBpy, an osmium-based compound, showed an MIC value of 125 µM for the RRA assay but no MIC for the BMD assay (Table 2.7 and Figure 2.6 K). The Dunnett's multiple comparison shows statistical differences for varies concentrations of RV239 OsBpy, however, these are not complete inhibition differences and hence no MIC was found. RV239 OsBpy also exhibited bactericidal activity to *K. P. aeruginosa* at a concentration of 62.5 µM.

All other compounds including AN3, RV144, RV158, MD72, MD73, KP01, RuBio, FF175, FF176, FF177, FF218, and FF228 did not display any antimicrobial activity towards *K. P. aeruginosa* demonstrated by an MIC of >500 µM for both susceptibility assays and an MBC of >500 µM.

The control cisplatin demonstrated no inhibitory activity against. *P. aeruginosa* (MIC>500 µM) as shown in Figure 2.6 Q and Table 2.7. The results of the BMD and RRA assay conquered the same results. Furthermore, no bactericidal activity was observed for cisplatin against *P. aeruginosa* with an MBC of >500 µM. The positive control meropenem exhibited an MIC of 15.63 µM against MRSA in both susceptibility assays as well as an MBC of 15.63 µM.

The positive control meropenem, a clinically used carbapenem antibiotic, exhibited a MIC and MBC of 15.63 µM against *P. aeruginosa*. Notably, 1 of our tested compounds (MD56) showed an equal MIC value to meropenem (MIC: 15.63 µM). This suggests that this ruthenium-based compound may have potential as a novel antimicrobial against *P. aeruginosa*, possibly including meropenem-resistant strains. Further testing against resistant clinical isolates would be necessary to confirm this potential.

Key findings for *P. aeruginosa*:

- Most susceptible to ruthenium-based compounds
- Lead compounds: MD7 and MD56 (MIC BMD: 62.5/15.63 µM, MIC RRA: 125 µM, MBC: 250/125 µM for both compounds respectively)
- 4 out of 16 compounds showed antimicrobial activity

- 1 compound outperformed the positive control (meropenem)
- 4 of the MIC values between the BMD and RRA assays differ in concentration

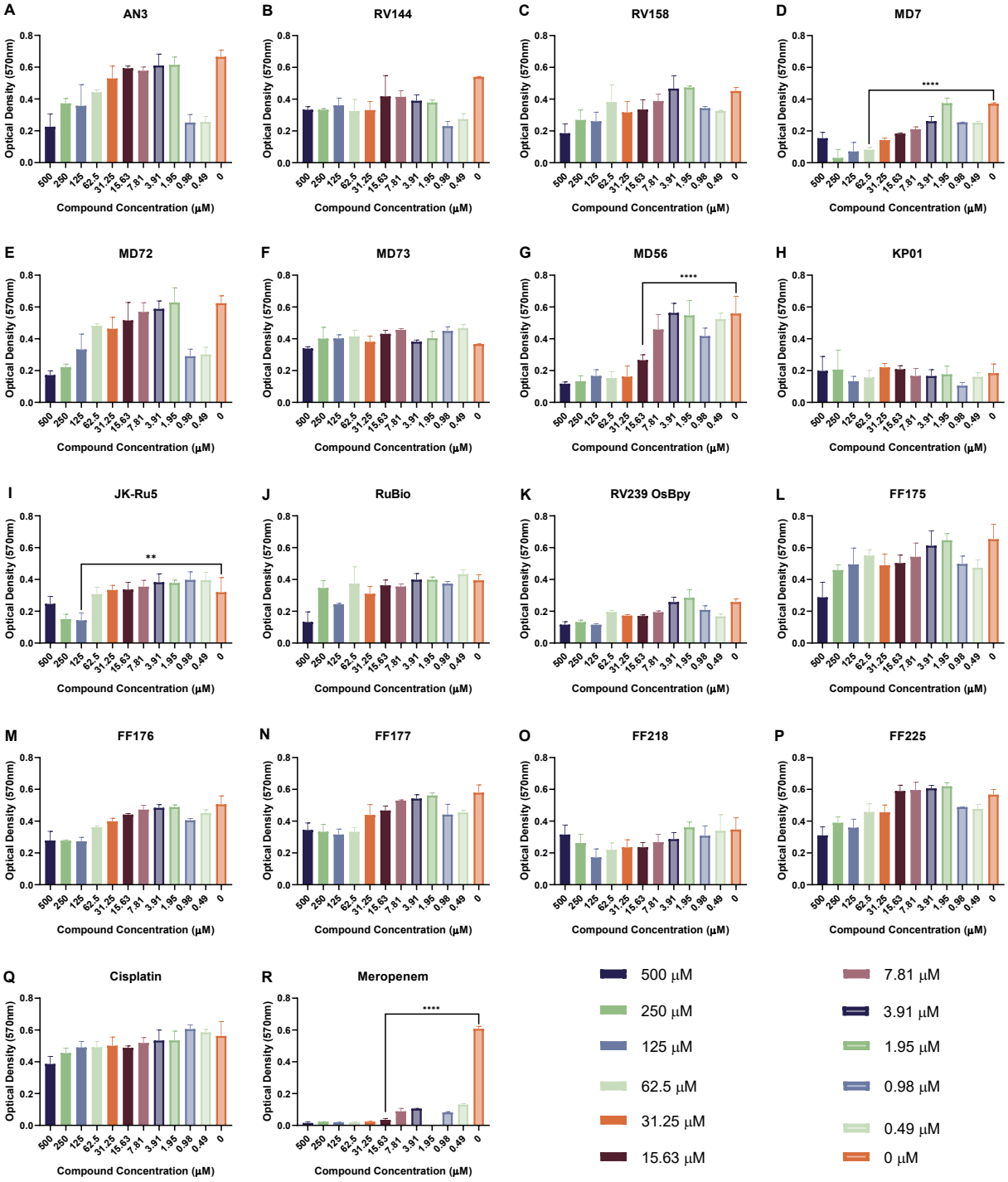

Figure 2.6. Optical density growth curves of *Pseudomonas aeruginosa* ATCC 19429 treated with investigative compounds. Growth curves show *P. aeruginosa* treated with **(A)** AN3, **(B)** RV144, **(C)** RV158, **(D)** MD7, **(E)** MD72, **(F)** MD73, **(G)** MD56, **(H)** KP01, **(I)** JK-Ru5, **(J)** RuBio, **(K)** RV239OsBpy, **(L)** FF175, **(M)** FF176, **(N)** FF177, **(O)** FF218, **(P)** FF225, **(Q)** Cisplatin, and **(R)** Meropenem for 24 hours. Optical density (570 nm) data are representative of n=3 technical replicates within one independent experiment. Mean values are shown, and error bars represent standard deviation. End point data, taken at 24 hours, was used for statistical analysis. P values were determined by a one-way analysis of variance (ANOVA) with Dunnett's multiple comparison, comparing all treatments to 0 μM to analyse the impact of compound concentration on the growth of *P. aeruginosa* *P < 0.05, **P < 0.01, ***P < 0.001 and ****P < 0.0001.

Table 2.7. Summary table results of investigative compounds against *Pseudomonas aeruginosa* ATCC 19429. Data represent the minimum inhibitory concentrations (MIC) of the broth microdilutions (BMD), and resazurin reduction assay (RRA), and minimum bactericidal concentrations (MBC).

Compound	BMD MIC (μM)	RRA MIC (μM)	MBC (μM)
AN3	>500	>500	>500
RV144	>500	>500	>500
RV158	>500	>500	>500
MD7	62.5	125	250
MD72	>500	>500	>500
MD73	>500	>500	>500
MD56	15.63	125	125
KP01	>500	>500	>500
JK-Ru5	125	250	250
RuBio	>500	>500	>500
RV239OsBpy	>500	62.5	62.5
FF175	>500	>500	>500
FF176	>500	>500	>500
FF177	>500	>500	>500
FF218	>500	>500	>500
FF225	>500	>500	>500
Cisplatin	>500	>500	>500
Meropenem	15.63	15.63	15.63

2.3.6 Antimicrobial Activity of 16 Metal-ion Complexes against *Enterobacter cloacae* ATCC 13047

Enterobacter cloacae (*E. cloacae*) was tested against the 16 metal-ion complexes and 2 control compounds. Table 2.8 lists the MIC values for the BMD assay and RRA assay, as well as the MBC values of each compound against MRSA. In addition, graphs of each BMD assay are presented in Figure 2.7. Only 4 metal-based compounds showed any inhibitory or killing activity towards *E. cloacae.* These compounds are MD7, MD56, and JK-Ru5, which are ruthenium based, and RV239 OsBpy, which is an osmium-based compound. The highest MIC displayed was 62.5 μM and the highest MBC was 125 μM.

Figure 2.7 D illustrates the growth inhibition of MD7 against *E. cloacae*. The BMD MIC was 62.5 μM with a significant difference in growth ($P<0.0001$) compared to the 0 μM concentration. Statistical analysis concluded that concentrations as low as 62.5 μM has an inhibitory effect on *E. cloacae* ($P<0.0001$). The MIC of the RRA showed a difference in value compared to the BMD assay – 250 μM (Table 2.8). MD56 also exhibited bactericidal activity at a concentration of 250 μM as shown by absent growth on agar plates.

The other ruthenium-based compound which displayed susceptibility to *K. E. cloacae* was MD56 displaying MICs and an MBC of 125, 125, and 500 μM, for the BMD assay the RRA assay and the MBC, respectively (Table 2.8 and Figure 2.7 G). All concentrations above 3.91 μM exhibited a significant difference in bacterial growth compared to the control suggesting inhibiting effects at these concentrations.

Unpredictably, the MIC for the BMD assay of JK-Ru5 against *E. cloacae* resulted in 125 μM ($P < 0.0001$) whereas, the RRA assay and MBC assay presented concentrations of 250 μM for the MIC and MBC. The Dunnett's multiple comparison shows a statistical difference at 62.5 μM and above, concluding that JK-Ru5 did not display a dose-dependent growth when decreasing the concentrations, meaning *E. cloacae* was only affected by JK-Ru5 at a concentration of 62.5 μM and above.

Lastly, RV239 OsBpy, which is an osmium-based compound showed an MIC value of 125 μM for the RRA assay but no MIC for the BMD assay (Table 2.8 and Figure 2.7 K). The Dunnett's multiple comparison shows statistical differences for various concentrations of RV239 OsBpy, above 7.81 μM ($P<0.0001$).

All other compounds including AN3, RV144, RV158, MD72, MD73, KP01, RuBio, FF175, FF176, FF177, FF218, and FF228 did not display any antimicrobial activity towards *E. cloacae* demonstrated by an MIC of >500 μM for both susceptibility assays and an MBC of >500 μM.

The control cisplatin demonstrated no inhibitory activity against*. E. cloacae* (MIC>500 μM) as shown in Figure 2.7 Q and Table 2.8. The results of the BMD and RRA assay conquered the same results. Furthermore, no bactericidal activity was observed for cisplatin against *E. cloacae* with an MBC of >500 μM. The positive control meropenem exhibited an MIC of 15.63 μM against MRSA in both susceptibility assays as well as an MBC of 15.63 μM.

The positive control meropenem, a clinically used carbapenem antibiotic, exhibited a MIC and MBC of 15.63 μM against *E. cloacae*. Notably, none of our tested compounds showed lower MIC values than meropenem. This suggests that these compounds towards *E. cloacae* are no more efficient than the current treatment of meropenem. Further testing of other first line antibiotics against this bacterium would be necessary to find increased susceptibility of these compounds compared to clinically relevant antibiotics.

Key findings for *E. cloacae*:

- Most susceptible to ruthenium-based compounds
- Lead compound: MD7 (MIC BMD: 62.5 μM, MIC RRA: 250 μM, MBC: 250 μM for both compounds)
- 4 out of 16 compounds showed antimicrobial activity
- No compounds outperformed the positive control (meropenem)
- 3 of the MIC values between the BMD and RRA assays differ in concentration

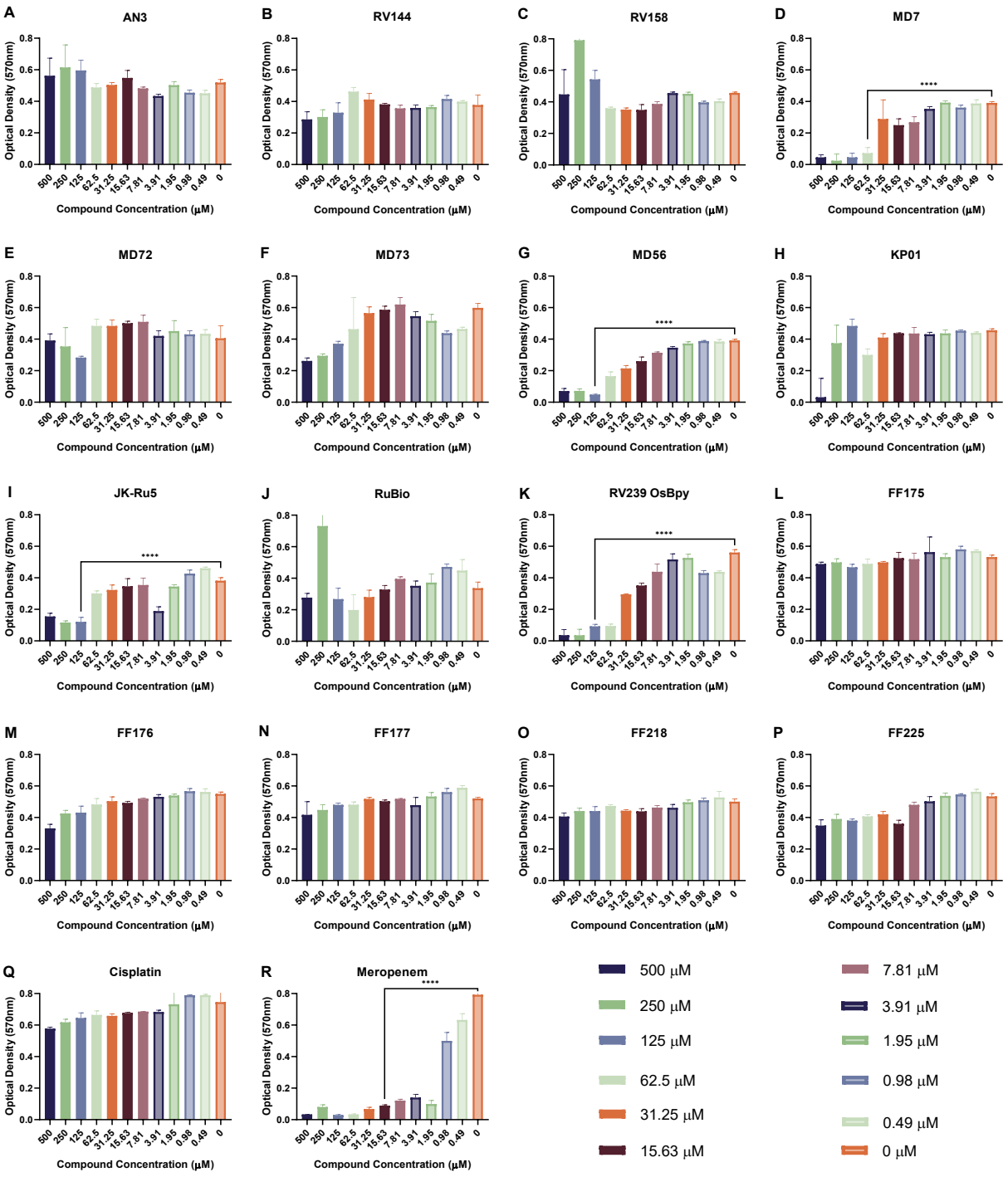

Figure 2.7. Optical density growth curves of *Enterobacter cloacae* ATCC 13047 treated with investigative compounds. Growth curves show *E. cloacae* treated with **(A)** AN3, **(B)** RV144, **(C)** RV158, **(D)** MD7, **(E)** MD72, **(F)** MD73, **(G)** MD56, **(H)** KP01, **(I)** JK-Ru5, **(J)** RuBio, **(K)** RV239OsBpy, **(L)** FF175, **(M)** FF176, **(N)** FF177, **(O)** FF218, **(P)** FF225, **(Q)** Cisplatin, and **(R)** Meropenem for 24 hours. Optical density (570 nm) data are representative of n=3 technical replicates within one independent experiment. Mean values are shown, and error bars represent standard deviation. End point data, taken at 24 hours, was used for statistical analysis. P values were determined by a one-way analysis of variance (ANOVA) with Dunnett's multiple comparison, comparing all treatments to 0 μM to analyse the impact of compound concentration on the growth of *E. cloacae* *$P < 0.05$, **$P < 0.01$, ***$P < 0.001$ and ****$P < 0.0001$.

Table 2.8. Summary table results of investigative compounds against *Enterobacter cloacae* ATCC 13047. Data represent the minimum inhibitory concentrations (MIC) of the broth microdilutions (BMD), and resazurin reduction assay (RRA), and minimum bactericidal concentrations (MBC).

Compound	BMD MIC (μM)	RRA MIC (μM)	MBC (μM)
AN3	>500	>500	>500
RV144	>500	>500	>500
RV158	>500	>500	>500
MD7	62.5	250	250
MD72	>500	>500	>500
MD73	>500	>500	>500
MD56	125	125	500
KP01	>500	>500	>500
JK-Ru5	125	250	250
RuBio	>500	>500	>500
RV239OsBpy	125	125	125
FF175	>500	>500	>500
FF176	>500	>500	>500
FF177	>500	>500	>500
FF218	>500	>500	>500
FF225	>500	>500	>500
Cisplatin	>500	>500	>500
Meropenem	15.63	31.25	31.25

2.3.7 Antimicrobial Activity of 16 Metal-ion Complexes against *M. abscessus* 15944 subsp. *abscessus*

M. abscessus subsp. *abscessus* was assessed against the 16 metal-ion complexes and 2 control compounds. Table 2.9 lists the MIC values for the BMD assay and RRA assay, as well as the MBC values of each compound against *M. abscessus* subsp. *abscessus*. In addition, graphs of each BMD assay are presented in Figure 2.7.

Compound AN3 had an MIC of 62.5 μM in the BMD assay as shown by the growth curve in Figure 2.7 A. The Dunnett's multiple comparison showed a significant difference in bacterial growth between 31.25 μM and 0 μM ($P<0.0001$). All concentrations of AN3 above the MIC showed significance to 0 μM. From the concentration ranges below 31.25 μM, no significant difference was present, as AN3 did not have an inhibitory effect at these lower concentrations. The MIC of the RRA showed an identical value of 62.5 μM (Table 2.9). Unfortunately, AN3 did not exhibit bactericidal activity at a concentration of >500 μM as shown by growth on agar plates.

Figure 2.7 B illustrates the growth inhibition of RV144 against *M. abscessus* subsp. *abscessus*. The BMD MIC was 31.25 μM with a significant difference in growth ($P<0.0001$) compared to the 0 μM concentration. No significant difference was observed for 7.81, 3.91, 1.95, 0.98, and 0.49 μM of RV144 against *M. abscessus* subsp. *abscessus* ($P=0.1218$, 0.9056, 0.7467, 0.9968, 0.9997), indicating these lower concentrations had no impact on the growth of *M. abscessus* subsp. *abscessus*. Inhibition was present as low as 15.63 μM as shown by

statistical differences, however the concentration which completely inhibited growth was 31.25 μM. The MIC of the RRA showed the same MIC compared to the BMD assay – 31.25 μM (Table 2.9). RV144 displayed no bactericidal activity (>500 μM).

The MIC of RV158 against *M. abscessus* subsp. *abscessus* was 7.81 μM for the BMD assay and the RRA (Table 2.9). The Dunnett's multiple comparison showed a significant difference in bacterial growth between 7.81 μM and 0 μM (P=0.0002). The lower concentrations of 3.91, 1.95, 0.98 and 0.49 μM showed no significance compared to 0 μM of RV158 (P=0.8148, 0.94733, 0.9783, 0.5923) as they did not impact the growth of bacteria. Again, RV158 displayed no bactericidal activity (>500 μM).

MD7 also showed promising results as an antimicrobial towards *M. abscessus* subsp. *abscessus*. The MIC of the BMD method was 15.63 μM as indicated in Table 2.9. Figure 2.7 D reveals the inhibition of MD7 concentrations to *M. abscessus* subsp. *abscessus*. A statistical difference (P=0.0426) between 15.63 μM and 0 μM was analysed using the Dunnett's multiple comparison. The MIC of the RRA showed a difference in value compared to the BMD assay – 7.81 μM (Table 2.9). MD7 had an MBC value of >500 μM conveying MD7 does not hold any bactericidal effect to MD7.

The other ruthenium-based compound MD72 had the best effect on tackling bacterial growth as shown in Table 2.9 and Figure 2.7 E. The MIC was 1.95 μM for the BMD assay and 3.91 μM for the RRA method (Table 2.9). All concentrations analysed by the one-way ANOVA demonstrated significant differences compared to the control. This indicates a dose-dependent response of MD72 to *M. abscessus* subsp. *abscessus*. Additionally, MD72 also exhibited bactericidal activity at a concentration of 15.63 μM.

Compound MD73 had different MIC values of 62.5 μM for the BMD method and 31.25 μM for the RRA method. Statistical analysis showed a significant difference (P<0.0001) between the MIC and all concentrations higher than 31.25 μM compared to 0 μM in the BMD assay, no growth occurred on agar plates from concentrations 125 μM and above, which was noted as the MBC.

Figure 2.7 G demonstrates the effect of MD56 on *M. abscessus* subsp. *abscessus*. With an MIC as low as 7.81 μM, there was a significant difference between this concentration and 0 μM (P<0.0001). The concentrations below this, such as 1.95, 0.98, and 0.49 μM did not show a difference in bacterial growth compared to the control (P=0.1832, P=0.9864, and P>0.9999), denoting at these concentrations, MD56 had no effect on bacterial growth. The MIC of the RRA showed a difference in value compared to the BMD assay – 15.63 μM (Table 2.9). MD56 also

exhibited bactericidal activity at a concentration of 31.25 μM as shown by absent growth on agar plates.
KP01 was the only compound which did not show any susceptibility to *M. abscessus* subsp. *abscessus,* including any bacteriostatic affect. The MIC of both assays, as well as the MBC, displayed a value of >500 μM as indicated in Table 2.9. However, at high concentrations (>31.25 μM), KP01 has a reducing effect on bacterial growth towards *M. abscessus* subsp. *abscessus* despite not having complete inhibition.

JK-Ru5 also showed promising results as an antimicrobial towards *M. abscessus* subsp. *abscessus*. The MIC of both assays displayed a value of 15.63 μM as indicated in Table 2.9. Figure 2.7 I presents the optical density measurements for each concentration of JK-Ru5 against *M. abscessus* subsp. *abscessus*. All concentrations have statistical differences compared to 0 μM except from lower values of <15.63 μM where the OD values were not affected by JK-Ru5. JK-Ru5 also exhibited bactericidal activity at a concentration of 62.5 μM as shown by absent growth on agar plates.

The complex RuBio showed varied results at inhibiting *M. abscessus* subsp. *abscessus*. The MIC of RuBio was 62.5 and 15.63 μM for the BMD assay and the RRA, respectively μM (Table 2.9). The Dunnett's multiple comparison showed a significant difference in bacterial growth between 62.5 μM and 0 μM (P<0.0001). In addition, all concentrations showed significance to 0 μM suggesting inhibition from low RuBio concentrations. RuBio also exhibited bactericidal activity at a concentration of 15.63 μM as shown by absent growth on agar plates.

In contrast, RV239 OsBpy had a value of 125 μM for both the MICs and MBC. A significant difference (P <0.0001) between 125 μM and 0 μM was analysed using the Dunnett's multiple comparison for the BMD method. The lower concentrations of 0.98 and 0.49 μM had no significance compared to 0 μM of RV239 OsBpy (P =0.4868 and P=0.6522) as they did not impact the growth of bacteria. However, concentrations above 1.95 μM shows statistical differences in optical density insinuating that this compound has an effect as low as 1.95. From the agar plates, RuBio exhibited bactericidal activity at a concentration of 125 μM

The MIC for the BMD assay of FF175 against *M. abscessus* subsp. *abscessus* (Figure 2.7 L) resulted in 15.63 μM. A significant difference (P <0.0001) between 15.63 μM and 0 μM was analysed using the Dunnett's multiple comparison and all other concentrations above this. The MIC of the RRA showed a higher concentration to the BMD assay – 31.25 μM (Table 2.9). FF175 also exhibited bactericidal activity at a concentration of 31.25 μM.

The next copper compound FF176, displayed related results to FF175 with a MIC in the BMD assay of 15.63 μM, however with the same concentration of 15.63 μM MIC in the RRA

experiment. All concentrations from 250 to 15.63 μM demonstrated statistical significance compared to 0 μM which suggests FF176 induces cell inhibition to *M. abscessus* subsp. *abscessus* as low a concentration as 15.63 μM. The lower values of 7.81, 3.91, 1.95, 0.98 and 0.49 μM were not affected by FF176. From the agar plates, FF176 exhibited bactericidal activity at a concentration of 125 μM.

FF177 compound showed antimicrobial effects at inhibiting and killing *M. abscessus* subsp. *abscessus*. The BMD and RRA assays obtained MIC results of 7.81 and 31.25 μM, respectively. Concentrations 250-3.91 μM had a statistical difference in the decrease of bacterial growth compared to 0 μM. Lower concentrations of FF177 including 1.95, 0.98 and 0.49 μM showed no statistical difference compared to the 0 μM control, suggesting that these concentrations have no effect on bacterial growth of *M. abscessus* subsp. *abscessus.* In addition, FF177 resulted in no bactericidal activity towards *M. abscessus* subsp. *abscessus* with an MBC of >500 μM.

FF218 showed promising results as a copper-metal antimicrobial towards *M. abscessus* subsp. *abscessus*. The MIC of both assays displayed a value of 31.25 μM as indicated in Table 2.9. Figure 2.7 O reveals the inhibition of FF218 concentrations to *M. abscessus* subsp. *abscessus*. A significant difference ($P < 0.0001$) between 15.63 μM, all higher concentrations, and 0 μM was analysed using the Dunnett's multiple comparison. FF218 displayed bactericidal activity towards *M. abscessus* subsp. *abscessus* with an MBC of 62.5 μM.

The last copper-based compound investigated showed varied MIC and MBC results. The MIC of FF225 against *M. abscessus* subsp. *abscessus* was 15.63 and 15.63 μM for the BMD assay and the RRA (Table 2.9). The Dunnett's multiple comparison showed a significant difference in bacterial growth between all concentrations >3.91 μM and 0 μM ($P<0.0001$). Unfortunately, FF225 did not display any bactericidal activity to *M. abscessus* subsp. *abscessus* at a concentration of >500 μM.

The control cisplatin demonstrated no inhibitory activity against *M. abscessus* subsp. *abscessus* (MIC>500) as shown in Figure 2.7 Q and Table 2.9. The results of the BMD and RRA assay conquered the same results. Furthermore, no bactericidal activity was observed for cisplatin against *M. abscessus* subsp. *abscessus* with an MBC of >500 μM.

The positive control meropenem, a clinically used carbapenem antibiotic, exhibited an MIC of 15.63 μM against *M. abscessus* subsp. *abscessus* in the BMD method and 15.63 in the RRA method. From the agar plates, meropenem exhibited bactericidal activity at a concentration of 31.25 μM. Notably, 10 of our tested compounds showed lower MIC values than meropenem, with MD72 being particularly potent (MIC: 1.95 μM). This suggests that these ruthenium-based

compounds may have potential as novel antimicrobials against *M. abscessus* subsp. *abscessus*, possibly including meropenem-resistant strains. Further testing against resistant clinical isolates would be necessary to confirm this potential.

Key findings for *M. abscessus* 15944 subsp. *abscessus*:

- Most susceptible to ruthenium and copper-based compounds
- Lead compounds: MD72 (MIC BMD: 1.95 μM, MIC RRA: 3.91 μM, MBC: 15.63 μM)
- 15 out of 16 compounds showed antimicrobial activity
- 10 compounds outperformed the positive control (meropenem)
- 9 of the MIC values between the BMD and RRA assays differ in concentration

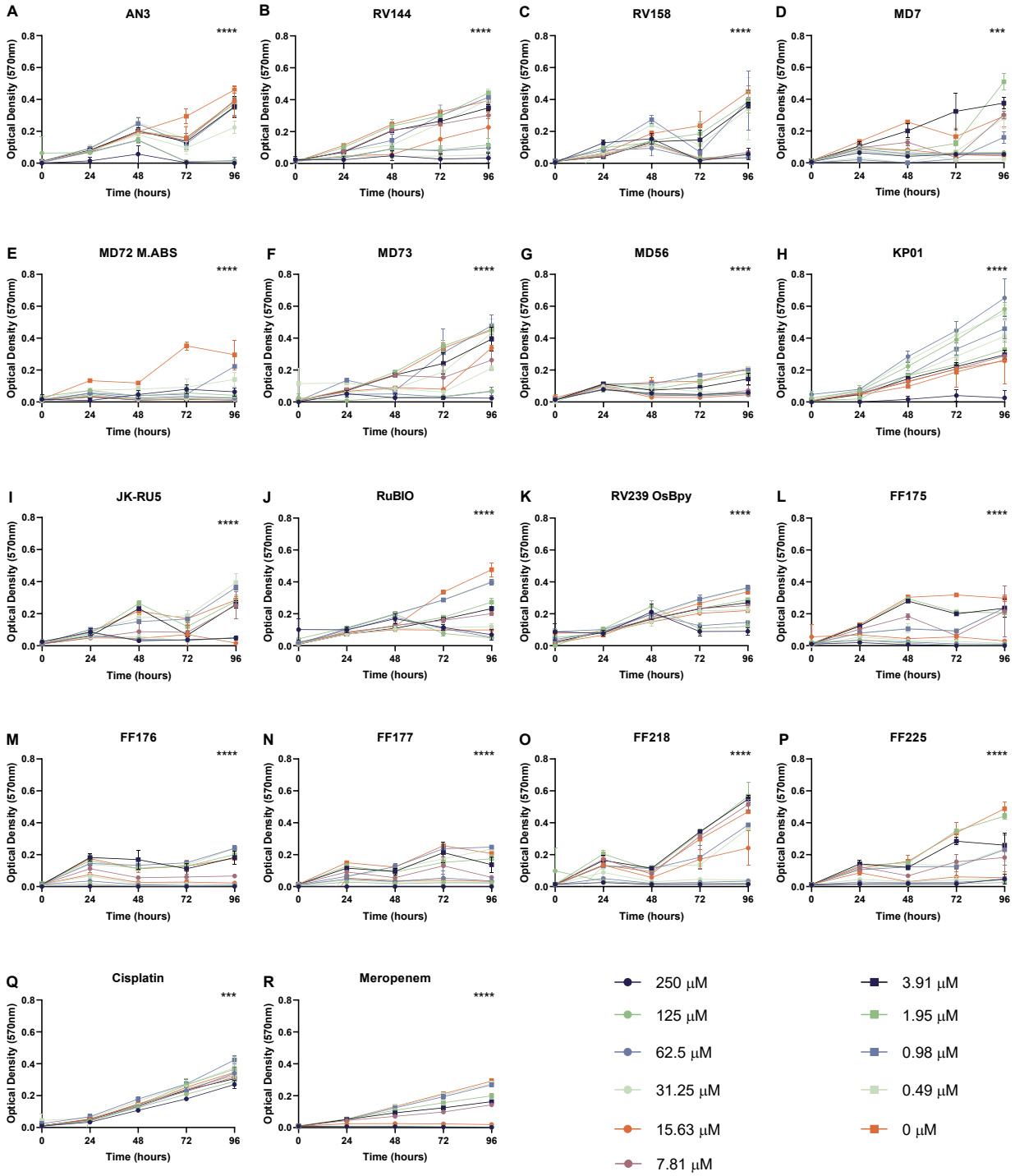

Figure 2.8. Optical density growth curves of *M. abscessus* 15944 subsp. *abscessus* treated with investigative compounds. Growth curves show *M. abscessus* 15944 subsp. *abscessus* treated with **(A)** AN3, **(B)** RV144, **(C)** RV158, **(D)** MD7, **(E)** MD72, **(F)** MD73, **(G)** MD56, **(H)** KP01, **(I)** JK-Ru5, **(J)** RuBio, **(K)** RV239OsBpy, **(L)** FF175, **(M)** FF176, **(N)** FF177, **(O)** FF218, **(P)** FF225, **(Q)** Cisplatin, and **(R)** Meropenem for 96 hours. Optical density (570 nm) data are representative of n=3 technical replicates within one independent experiment. Mean values are shown, and error bars represent standard deviation. End point data, taken at 96 hours, was used for statistical analysis. P values were determined by a one-way analysis of variance (ANOVA) with Dunnett's multiple comparison, comparing all treatments to 0 µM to analyse the impact of compound concentration on the growth of *M. abscessus* 15944 subsp. *abscessus*. *P < 0.05, **P < 0.01, ***P < 0.001 and ****P < 0.0001.

Table 2.9. Summary table results of investigative compounds against *M. abscessus* 15944 subsp. *abscessus.* Data represent the minimum inhibitory concentrations (MIC) of the broth microdilutions (BMD), and resazurin reduction assay (RRA), and minimum bactericidal concentrations (MBC).

Compound	BMD MIC (μM)	RRA MIC (μM)	MBC (μM)
AN3	62.5	62.5	>500
RV144	31.25	31.25	>500
RV158	7.81	7.81	>500
MD7	15.63	7.81	>500
MD72	1.95	3.91	15.63
MD73	62.5	31.25	125
MD56	7.81	15.63	31.25
KP01	>500	>500	>500
JK-Ru5	15.63	15.63	62.5
RuBio	62.5	15.63	15.63
RV239OsBpy	125	7.81	>500
FF175	15.63	31.25	31.25
FF176	15.63	15.63	125
FF177	7.81	31.25	>500
FF218	31.25	31.25	62.5
FF225	15.63	15.63	>500
Cisplatin	>500	>500	>500
Meropenem	15.63	15.63	31.25

2.3.8 Antimicrobial Activity of 16 Metal-ion Complexes against *M. abscessus* DC088A subsp. *bolletii*

M. abscessus subsp. *bolletii* was assessed against the 16 metal-ion complexes and 2 control compounds. Table 2.10 lists the MIC values for the BMD assay and RRA assay, as well as the MBC values of each compound against *M. abscessus* subsp. *bolletii*. In addition, graphs of each BMD assay is presented in Figure 2.9.

Compound AN3 had an MIC of 62.5 μM in the BMD assay as shown by the growth curve in Figure 2.9 A. The Dunnett's multiple comparison showed a significant difference in bacterial growth between 62.5 μM and 0 μM ($P<0.0001$). All concentrations of AN3 above the MIC and 15.63 μM showed significance to 0 μM. From the concentration ranges below 15.63 μM, no significant difference was present, as AN3 did not have an inhibitory effect at these lower concentrations. The MIC of the RRA showed a different value of 125 μM (Table 2.10). Unfortunately, AN3 did not exhibit bactericidal activity at a concentration of >500 μM as shown by growth on agar plates.

Figure 2.9 B illustrates the growth inhibition of RV144 against *M. abscessus* subsp. *bolletii*. The BMD MIC was 31.25 μM with a significant difference in growth ($P<0.0001$) compared to the 0 μM concentration. No significant difference was observed for 7.81, 3.91, 1.95, 0.98, and 0.49 μM of RV144 against *M. abscessus* subsp. *bolletii* ($P=0.0954$, 0.9994, 0.8930, 0.0873, 0.0873), indicating these lower concentrations had no impact on the growth of *M. abscessus* subsp. *bolletii*. Inhibition was present as low as 15.63 μM as shown by statistical differences,

however the concentration which completely inhibited growth was 31.25 μM. The MIC of the RRA showed the same MIC compared to the BMD assay – 31.25 μM (Table 2.10). RV144 displayed no bactericidal activity (>500 μM).

The MIC of RV158 against *M. abscessus* subsp. *bolletii* was 15.63 μM for the BMD assay and 31.25 μM for the RRA method (Table 2.10). The Dunnett's multiple comparison showed a significant difference in bacterial growth between 15.63 μM and 0 μM ($P<0.0001$). The lower concentrations below 15.63 μM showed no significance compared to 0 μM of RV158 as they did not impact the growth of bacteria. Again, RV158 displayed no bactericidal activity (>500 μM).

MD7 also showed promising results as an antimicrobial towards *M. abscessus* subsp. *bolletii*. The MIC of the BMD method was 31.25 μM as indicated in Table 2.10. Figure 2.9 D reveals the inhibition of MD7 concentrations to *M. abscessus* subsp. *bolletii*. A statistical difference ($P<0.0001$) between 31.25 μM and 0 μM was analysed using the Dunnett's multiple comparison. The MIC of the RRA showed a difference in value compared to the BMD assay – 15.63 μM (Table 2.10). MD7 had an MBC value of 125 μM conveying that it held a bactericidal effect.

The other ruthenium-based compound MD72 had the best effect on tackling bacterial growth as shown in Table 2.10 and Figure 2.9 E. The MIC was 1.95 μM for the BMD assay and 3.91 μM for the RRA method (Table 2.10). All concentrations analysed by the one-way ANOVA demonstrated significant differences compared to the control. This indicates a dose-dependent response of MD72 to *M. abscessus* subsp. *bolletii*. However, MD72 did not show bactericidal activity at a concentration of >500 μM.

Compound MD73 had different MIC values of 125 μM for the BMD method and 31.25 μM for the RRA method. Statistical analysis showed a significant difference ($P<0.0001$) between the MIC and all concentrations higher than 15.63 μM compared to 0 μM in the BMD assay. No growth occurred on agar plates from all concentrations and hence MD73 did not have a killing effect towards *M. abscessus* subsp. *bolletii.*

Figure 2.9 G demonstrates the effect of MD56 on *M. abscessus* subsp. *bolletii*. With an MIC as low as 15.63 μM, there was a significant difference between this concentration and 0 μM ($P<0.0001$). The concentrations below this, such as 7.81, 3.91, and 1.95 μM did not show a difference in bacterial growth compared to the control, meaning at these concentrations, MD56 had no effect on bacterial growth. The unusual statistical difference of 0.98 and 0.49 μM, can be explained by an increase in growth compared to the bacteria ($P<0.0001$) which conveys that's MD56 does not challenge the growth of *M. abscessus* subsp. *bolletii* at these

concentrations. The MIC of the RRA showed the same value compared to the BMD assay – 15.63 μM (Table 2.10). MD56 did not display bactericidal activity at a concentration of >500 μM as shown by absent growth on agar plates.

KP01 was the only compound which did not show any susceptibility to *M. abscessus* subsp. *bolletii* including any bacteriostatic affect. The MIC of both assays, as well as the MBC, displayed a value of >500 μM as implied in Table 2.10.

JK-Ru5 also showed promising results as an antimicrobial towards *M. abscessus* subsp. *bolletii*. The MIC of both assays displayed a value of 15.63 μM as indicated in Table 2.10. Figure 2.9 I presents the optical density measurements for each concentration of JK-Ru5 against *M. abscessus* subsp. *bolletii*. All concentrations have statistical differences compared to 0 μM except from lower values of <15.63 μM where the OD values were not affected by JK-Ru5. No MBC was present for JK-Ru5 as shown by full growth on agar plates.

The complex RuBio showed varied results at inhibiting *M. abscessus* subsp. *bolletii*. The MIC of RuBio was 62.5 and 15.63 μM for the BMD assay and the RRA, respectively μM (Table 2.10). The Dunnett's multiple comparison showed a significant difference in bacterial growth between 62.5 μM and 0 μM ($P<0.0001$). The concentrations below this, such as 31.25, 15.63, 7.81, 3.91, and 1.95 μM did not show a difference in bacterial growth compared to the control, meaning at these concentrations, MD56 had no effect on bacterial growth. The unusual statistical difference of 0.98 and 0.49 μM, can be explained by an increase in growth compared to the bacteria ($P=0.0120$, $P=0.0087$) which conveys that's RuBio does not challenge the growth of *M. abscessus* subsp. *bolletii* at these concentrations. RuBio also exhibited bactericidal activity at a concentration of 31.25 μM as shown by absent growth on agar plates.

In contrast, RV239 OsBpy had a value of 250 μM for the BMD MIC and 15.63 μM for the RRA MIC. A significant difference ($P <0.0001$) between 250 μM and 0 μM was analysed using the Dunnett's multiple comparison for the BMD method. The lower concentrations had no significance compared to 0 μM of RV239 OsBpy as they did not impact the growth of bacteria. From the agar plates, RuBio did not demonstrate bactericidal activity at a concentration of >500 μM.

The MIC for the BMD assay of FF175 against *M. abscessus* subsp. *bolletii* (Figure 2.9 L) resulted in 31.25 μM. A significant difference ($P <0.0001$) between 31.25 μM and 0 μM was analysed using the Dunnett's multiple comparison and all other concentrations above 3.91 μM. The MIC of the RRA showed the same concentration as the BMD assay – 31.25 μM (Table 2.10). FF175 also failed to show bactericidal activity at a concentration of >500 μM.

The next copper compound FF176, displayed related results to FF175 with a MIC in the BMD assay of 31.25 μM, however with the same concentration of 31.25 μM MIC in the RRA experiment. All concentrations from 250 to 3.91 μM demonstrated statistical significance compared to 0 μM which suggests FF176 induces cell inhibition to *M. abscessus* subsp. *bolletii* was as low a concentration as 3.91 μM ($P<0.0001$). FF176 also failed to show bactericidal activity at a concentration of >500 μM.

FF177 compound showed antimicrobial effects at inhibiting and killing *M. abscessus* subsp. *bolletii*. The BMD and RRA assays achieved MIC results of 15.63 and 250 μM, respectively. Concentrations 250-3.91 μM had a statistical difference in the decrease of bacterial growth compared to 0 μM. Lower concentrations of FF177 including 1.95, 0.98 and 0.49 μM showed no statistical difference compared to the 0 μM control, suggesting that these concentrations have no effect on bacterial growth of *M. abscessus* subsp. *bolletii.* In addition, FF177 resulted in no bactericidal activity towards *M. abscessus* subsp. *bolletii* with an MBC of >500 μM.

FF218 showed promising results as a copper-metal antimicrobial towards *M. abscessus* subsp. *bolletii*. The MIC of the BMD and RRA assays displayed a value of 31.25 and 62.5 μM as indicated in Table 2.10. Figure 2.9 O reveals the inhibition of FF218 concentrations to *M. abscessus* subsp. *bolletii*. A significant difference ($P <0.0001$) between 31.25 μM, all higher concentrations, and 0 μM was analysed using the Dunnett's multiple comparison. FF218 resulted in no bactericidal activity towards *M. abscessus* subsp. *bolletii* with an MBC of >500 μM.

The MIC of FF225 against *M. abscessus* subsp. *bolletii* was 31.25 and 31.25 μM for the BMD assay and the RRA (Table 2.10). The Dunnett's multiple comparison showed a significant difference in bacterial growth between all concentrations >7.81 μM and 0 μM. Unfortunately, FF225 did not display any bactericidal activity to *M. abscessus* subsp. *bolletii* at a concentration of >500 μM.

The control cisplatin demonstrated no inhibitory activity against *M. abscessus* subsp. *bolletii* (MIC>500) as shown in Figure 2.9 Q and Table 2.10. The results of the BMD and RRA assay conquered the same results. Furthermore, no bactericidal activity was observed for cisplatin against *M. abscessus* subsp. *bolletii* with an MBC of >500 μM.

The positive control meropenem, a clinically used carbapenem antibiotic, exhibited a MIC of 31.25 μM against *M. abscessus* subsp. *bolletii*. From the agar plates, meropenem did not demonstrate bactericidal activity at a concentration of >500 μM. Notably, 11 of our tested compounds showed lower MIC values than meropenem, with MD72 being particularly potent (MIC: 1.95 μM). This suggests that these ruthenium-based compounds may have potential as

novel antimicrobials against *M. abscessus* subsp. *bolletii*, possibly including meropenem-resistant strains. Further testing against resistant clinical isolates would be necessary to confirm this potential.

Key findings for *M. abscessus* subsp. *bolletii*:

- Most susceptible to ruthenium, copper, and osmium-based compounds
- Lead compounds: MD72 (MIC BMD: 1.95 μM, MIC RRA: 3.91 μM, MBC: >500)
- 15 out of 16 compounds showed antimicrobial activity
- 11 compounds outperformed the positive control (meropenem)
- 8 of the MIC values between the BMD and RRA assays differ in concentration

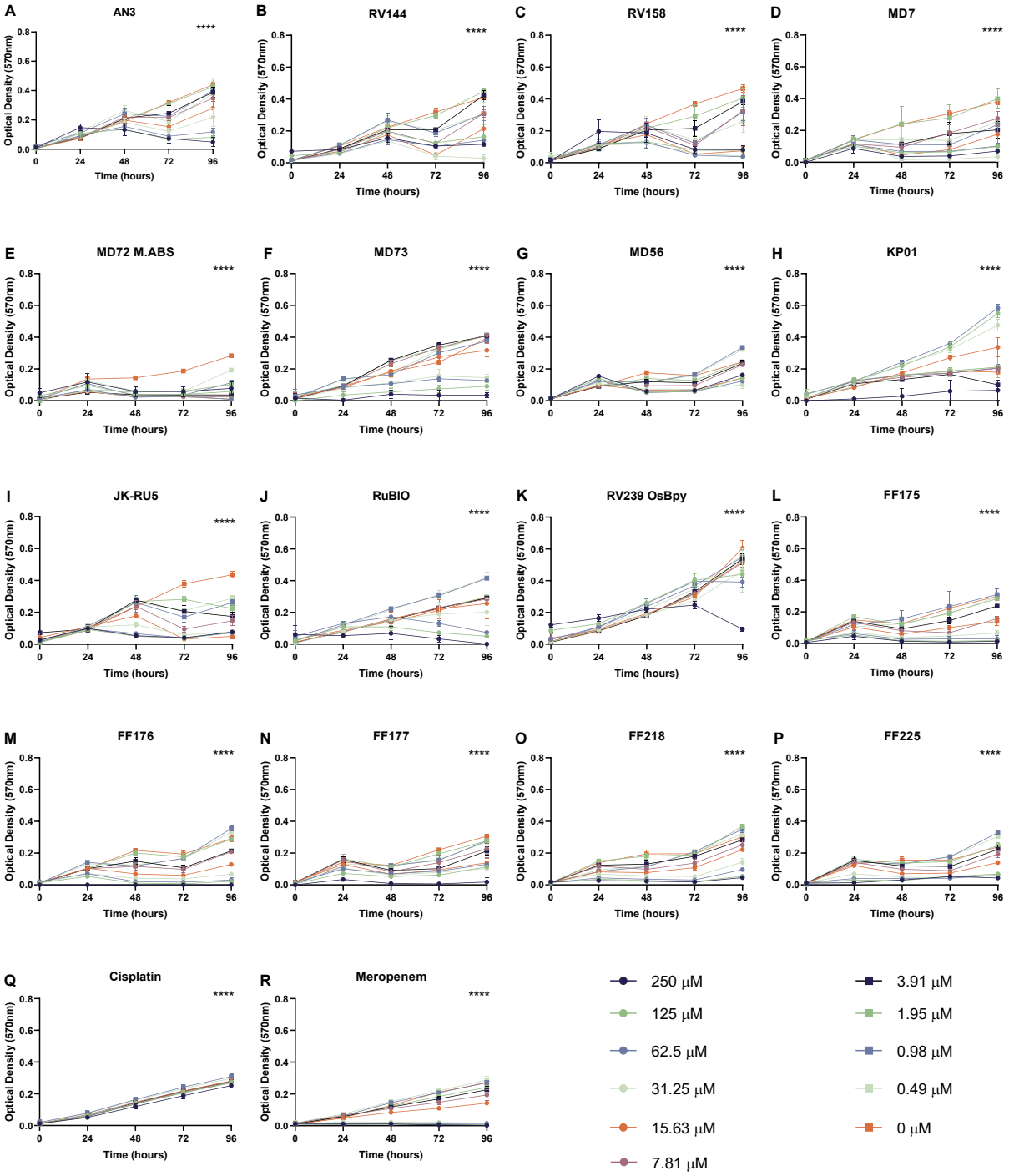

Figure 2.9. Optical density growth curves of *M. abscessus* DC088A subsp. *bolletii* treated with investigative compounds. Growth curves show *M. abscessus* DC088A subsp. *bolletii* treated with **(A)** AN3, **(B)** RV144, **(C)** RV158, **(D)** MD7, **(E)** MD72, **(F)** MD73, **(G)** MD56, **(H)** KP01, **(I)** JK-Ru5, **(J)** RuBio, **(K)** RV239OsBpy, **(L)** FF175, **(M)** FF176, **(N)** FF177, **(O)** FF218, **(P)** FF225, **(Q)** Cisplatin, and **(R)** Meropenem for 96 hours. Optical density (570 nm) data are representative of n=3 technical replicates within one independent experiment. Mean values are shown, and error bars represent standard deviation. End point data, taken at 96 hours, was used for statistical analysis. P values were determined by a one-way analysis of variance (ANOVA) with Dunnett's multiple comparison, comparing all treatments to 0 μM to analyse the impact of compound concentration on the growth of *M. abscessus* 15944 subsp. *abscessus*. *P < 0.05, **P < 0.01, ***P < 0.001 and ****P < 0.0001.

Table 2.10. Summary table results of Investigative Compounds against *M. abscessus* DC088A subsp. *bolletii*. Data represent the minimum inhibitory concentrations (MIC) of the broth microdilutions (BMD), and resazurin reduction assay (RRA), and minimum bactericidal concentrations (MBC).

Compound	BMD MIC (μM)	RRA MIC (μM)	MBC (μM)
AN3	62.5	125	>500
RV144	31.25	31.25	>500
RV158	15.63	31.25	>500
MD7	31.25	15.63	125
MD72	1.95	3.91	>500
MD73	125	31.25	>500
MD56	15.63	15.63	>500
KP01	>500	>500	>500
JK-Ru5	15.63	15.63	>500
RuBio	62.5	15.63	31.25
RV239OsBpy	250	15.63	>500
FF175	31.25	31.25	>500
FF176	31.25	31.25	>500
FF177	15.63	250	>500
FF218	31.25	62.5	>500
FF225	31.25	31.25	>500
Cisplatin	>500	>500	>500
Meropenem	31.25	31.25	>500

2.3.9 Antimicrobial Activity of 16 Metal-ion Complexes against *M. abscessus* DC088D subsp. *massiliense*

M. abscessus subsp. *massiliense* was assessed against the 16 metal-ion complexes and 2 control compounds. Table 2.11 lists the MIC values for the BMD assay and RRA assay, as well as the MBC values of each compound against *M. abscessus* subsp. *massiliense*. In addition, graphs of each BMD assay are presented in Figure 2.10.

Compound AN3 had an MIC of 62.5 μM in the BMD assay as shown by the growth curve in Figure 2.10 A. The Dunnett's multiple comparison showed a significant difference in bacterial growth between 62.5 μM and 0 μM ($P<0.0001$). All concentrations of AN3 above the MIC and 7.81 μM showed significance to 0 μM ($P=0.0029$, $P<0.0001$). From the concentration ranges below 7.81 μM, no significant difference was present, as AN3 did not have an inhibitory effect at these lower concentrations. The MIC of the RRA showed the same value of 62.5 μM (Table 2.11). Unfortunately, AN3 did not exhibit bactericidal activity at a concentration of >500 μM as shown by growth on agar plates.

Figure 2.10 B illustrates the growth inhibition of RV144 against *M. abscessus* subsp. *massiliense*. The BMD MIC was 15.63 μM with a significant difference in growth ($P=0.0001$) compared to the 0 μM concentration. No significant difference was observed for 1.95, 0.98, and 0.49 μM of RV144 against *M. abscessus* subsp. *massiliense* ($P=0.1199$, 0.0961, 0.7374), indicating these lower concentrations had no impact on the growth of *M. abscessus* subsp.

massiliense. Inhibition was present as low as 3.91 µM as shown by statistical differences, however the concentration which completely inhibited growth was 15.63 µM. The MIC of the RRA showed the same MIC compared to the BMD assay – 15.63 µM (Table 2.11). RV144 displayed bactericidal activity at a concentration of 62.5 µM.

The MIC of RV158 against *M. abscessus* subsp. *massiliense* was 7.81 µM for the BMD assay and 7.81 µM for the RRA method (Table 2.11). The Dunnett's multiple comparison showed a significant difference in bacterial growth between 7.81 µM and 0 µM ($P<0.0001$). All concentrations analysed by the one-way ANOVA demonstrated significant differences compared to the control. This indicates a dose-dependent response of RV158 to *M. abscessus* subsp. *massiliense.* Again, RV158 displayed bactericidal activity at 31.25 µM.

MD7 also showed promising results as an antimicrobial towards *M. abscessus* subsp. *massiliense*. The MIC of the BMD method was 3.91 µM as indicated in Table 2.11. Figure 2.10 D reveals the inhibition of MD7 concentrations of *M. abscessus* subsp. *massiliense*. A statistical difference ($P<0.0001$) between 3.91 µM and 0 µM was analysed using the Dunnett's multiple comparison. The MIC of the RRA showed the same value compared to the BMD assay – 3.91 µM (Table 2.11). MD7 had an MBC value of 31.25 µM conveying that it held a bactericidal effect.

The other ruthenium-based compound MD72 had the best effect on tackling bacterial growth as shown in Table 2.11 and Figure 2.10 E. The MIC was 1.95 µM for the BMD assay and 1.95 µM for the RRA method (Table 2.11). All concentrations analysed by the one-way ANOVA demonstrated significant differences compared to the control. This indicates a dose-dependent response of MD72 to *M. abscessus* subsp. *masillience*. However, MD72 did not show bactericidal activity at a concentration of >500 µM.

Compound MD73 had different MIC values of 31.25 µM for the BMD method and 31.25 µM for the RRA method. Statistical analysis showed a significant difference ($P<0.0001$) between the MIC and all concentrations higher than 15.63 µM compared to 0 µM in the BMD assay. MD73 had an MBC value of 62.5 µM conveying that it held a bactericidal effect.

Figure 2.10 G demonstrates the effect of MD56 on *M. abscessus* subsp. *masillience*. With an MIC as low as 3.91 µM, there was a significant difference between this concentration and 0 µM ($P<0.0001$). The concentrations below this, such as 1.95, 0.98, and 0.49 µM did not show a difference in bacterial growth compared to the control, signifying at these concentrations, MD56 had no effect on bacterial growth. The MIC of the RRA showed the same value compared to the BMD assay – 3.91 µM (Table 2.11). MD56 did not display bactericidal activity at a concentration of >500 µM as shown by absent growth on agar plates.

KP01 was the only compound which did not show any susceptibility to *M. abscessus* subsp. *massiliense,* including any bacteriostatic affect. The MIC of both assays, as well as the MBC, displayed a value of >500 μM as indicated in Table 2.11.

JK-Ru5 also showed promising results as an antimicrobial towards *M. abscessus* subsp. *masillience*. The MIC of both assays displayed a value of 7.81 μM as indicated in Table 2.11. Figure 2.10 I presents the optical density measurements for each concentration of JK-Ru5 against *M. abscessus* subsp. *masillience*. All concentrations have statistical differences compared to 0 μM except from lower values of <3.91 μM where the OD values were not affected by JK-Ru5. JK-Ru5 had an MBC value of 62.5 μM conveying that it held a bactericidal effect.

The complex RuBio showed varied results at inhibiting *M. abscessus* subsp. *masillience*. The MIC of RuBio was 3.91 for the BMD assay and the RRA (Table 2.11). The Dunnett's multiple comparison showed a significant difference in bacterial growth between 1.95 μM and 0 μM ($P<0.0001$). The concentrations below this, such as 0.98 and 0.49 μM did not show a difference in bacterial growth compared to the control, meaning at these concentrations, RuBio had no effect on bacterial growth. RuBio also exhibited bactericidal activity at a concentration of 7.81 μM as shown by absent growth on agar plates.

In contrast, RV239 OsBpy had a value of 3.91 μM for the BMD MIC and 3.91 μM for the RRA MIC. A significant difference ($P <0.0001$) between 3.91 μM and 0 μM was analysed using the Dunnett's multiple comparison for the BMD method. All concentrations had significance compared to 0 μM of RV239 OsBpy as they all impacted the growth of bacteria. From the agar plates, RuBio demonstrated bactericidal activity at a concentration of 3.91 μM.

The MIC for the BMD assay of FF175 against *M. abscessus* subsp. *massiliense* (Figure 2.10 L) resulted in 7.81 μM. A significant difference ($P <0.0001$) between 7.81 μM and 0 μM was analysed using the Dunnett's multiple comparison and all other concentrations above 1.95 μM. The MIC of the RRA showed a different concentration to the BMD assay – 15.63 μM (Table 2.11). FF175 also failed to show bactericidal activity at a concentration of >500 μM.

The next copper compound FF176, displayed related results to FF175 with a MIC in the BMD assay of 7.81 μM, however with the same concentration of 7.81 μM MIC in the RRA experiment. All concentrations from 250 to 1.95 μM demonstrated statistical significance compared to 0 μM which suggests FF176 induces cell inhibition to *M. abscessus* subsp. *massiliense* as low a concentration as 1.95 μM ($P= 0.0016$, $P<0.0001$). FF176 also failed to show bactericidal activity at a concentration of >500 μM.

FF177 compound showed antimicrobial effects at inhibiting and killing *M. abscessus* subsp. *masillience*. The BMD and RRA assays obtained MIC results of 7.81 and 15.63 μM respectively. All concentrations had a statistical difference in the decrease of bacterial growth compared to 0 μM. In addition, FF177 resulted in no bactericidal activity towards *M. abscessus* subsp. *massiliense* with an MBC of >500 μM.

FF218 showed promising results as a copper-metal antimicrobial towards *M. abscessus* subsp. *masillience*. The MIC of the BMD and RRA assays displayed a value of 31.25 μM as indicated in Table 2.11. Figure 2.9 O reveals the inhibition of FF218 concentrations to *M. abscessus* subsp. *masillience*. A significant difference ($P < 0.0001$) between 31.25 μM, all higher concentrations, and 0 μM was analysed using the Dunnett's multiple comparison. FF218 resulted in no bactericidal activity towards *M. abscessus* subsp. *massiliense* with an MBC of >500 μM.

The MIC of FF225 against *M. abscessus* subsp. *massiliense* was 7.81 and 15.63 μM for the BMD assay and the RRA (Table 2.11). The Dunnett's multiple comparison showed a significant difference in bacterial growth between all concentrations and 0 μM. Unfortunately, FF225 did not display any bactericidal activity to *M. abscessus* subsp. *massiliense* at a concentration of >500 μM.

The control cisplatin demonstrated no inhibitory activity against *M. abscessus* subsp. *massiliense* (MIC>500) as shown in Figure 2.9 Q and Table 2.11. The results of the BMD and RRA assay conquered the same results. Furthermore, no bactericidal activity was observed for cisplatin against *M. abscessus* subsp. *massiliense* with an MBC of >500 μM.

The positive control meropenem, a clinically used carbapenem antibiotic, exhibited a MIC of 31.25 μM against *M. abscessus* subsp. *massiliense*. From the agar plates, meropenem demonstrated bactericidal activity at a concentration of 62.5 μM. Notably, 13 of our tested compounds showed lower MIC values than meropenem, with being particularly potent (MIC: 1.95 μM). This suggests that these ruthenium-based compounds may have potential as novel antimicrobials against *M. abscessus* subsp. *massiliense*, possibly including meropenem-resistant strains. Further testing against resistant clinical isolates would be necessary to confirm this potential.

Key findings for *M. abscessus* DC088D subsp. *massiliense*:

- Most susceptible to ruthenium, copper, and osmium-based compounds
- Lead compounds: MD72 (MIC BMD: 1.95 μM, MIC RRA: 1.95 μM, MBC: >500 μM)
- 15 out of 16 compounds showed antimicrobial activity
- 13 compounds outperformed the positive control (meropenem)
- 8 of the MIC values between the BMD and RRA assays differ in concentration

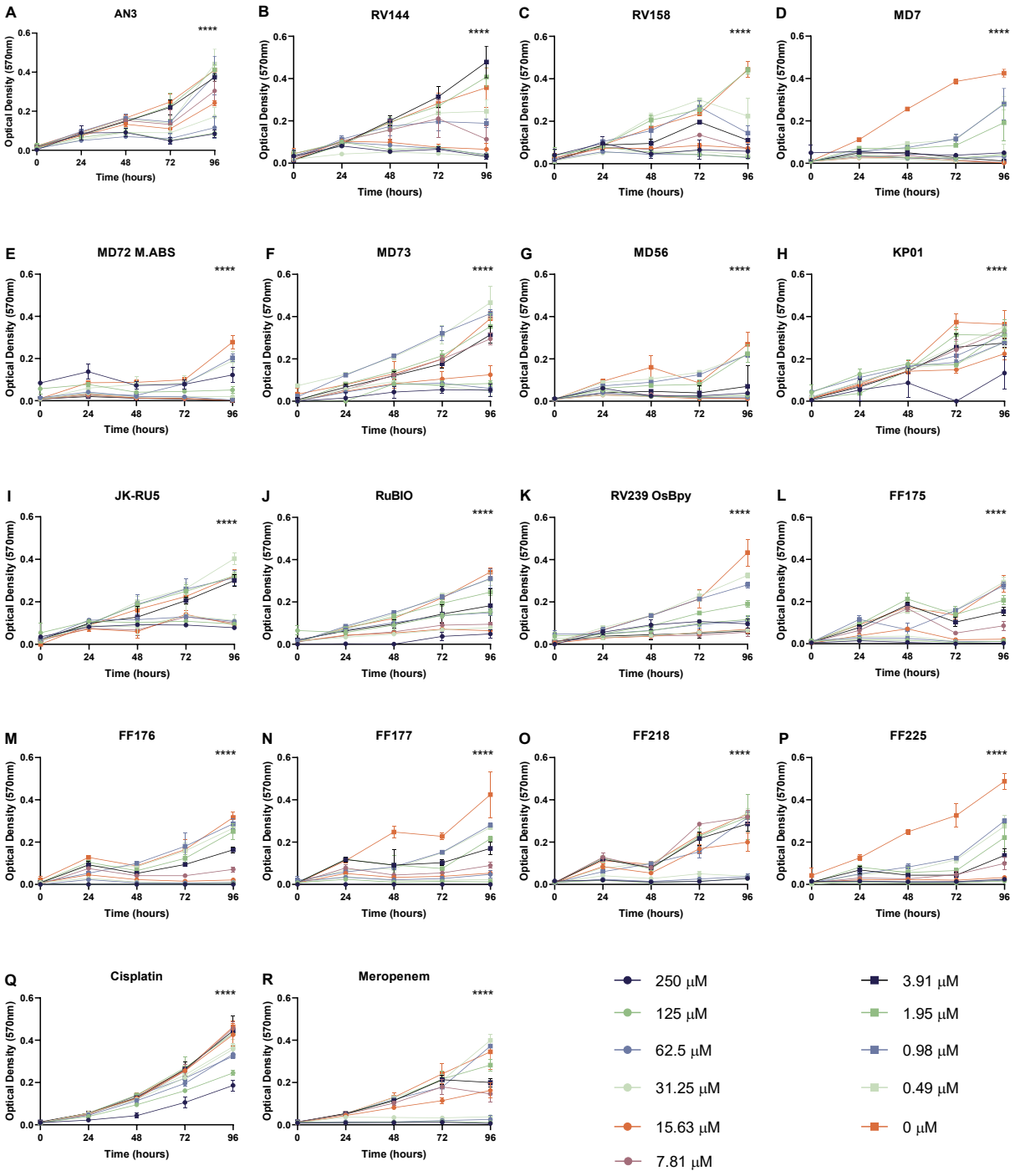

Figure 2.10. Optical density growth curves of *M. abscessus* DC088D subsp. *massiliense* treated with investigative compounds. Growth curves show *E. cloacae* treated with **(A)** AN3, **(B)** RV144, **(C)** RV158, **(D)** MD7, **(E)** MD72, **(F)** MD73, **(G)** MD56, **(H)** KP01, **(I)** JK-Ru5, **(J)** RuBio, **(K)** RV239OsBpy, **(L)** FF175, **(M)** FF176, **(N)** FF177, **(O)** FF218, **(P)** FF225, **(Q)** Cisplatin, and **(R)** Meropenem for 96 hours. Optical density (570 nm) data are representative of n=3 technical replicates within one independent experiment. Mean values are shown, and error bars represent standard deviation. End point data, taken at 96 hours, was used for statistical analysis. P values were determined by a one-way analysis of variance (ANOVA) with Dunnett's multiple comparison, comparing all treatments to 0 µM to analyse the impact of compound concentration on the growth of *M. abscessus* subsp. *massiliense* *P < 0.05, **P < 0.01, ***P < 0.001 and ****P < 0.0001.

Table 2.11. Summary table results of investigative compounds against *M. abscessus* DC088D subsp. *massiliense.* Data represent the minimum inhibitory concentrations (MIC) of the broth microdilutions (BMD), and resazurin reduction assay (RRA), and minimum bactericidal concentrations (MBC).

Compound	BMD MIC (μM)	RRA MIC (μM)	MBC (μM)
AN3	62.5	62.5	>500
RV144	15.63	15.63	62.5
RV158	7.81	7.81	31.25
MD7	3.91	3.91	31.25
MD72	1.95	1.95	>500
MD73	31.25	31.25	62.5
MD56	3.91	3.91	>500
KP01	>500	>500	>500
JK-Ru5	7.81	7.81	62.5
RuBio	3.91	3.91	7.81
RV239OsBpy	3.91	3.91	3.91
FF175	7.81	15.63	>500
FF176	7.81	15.63	>500
FF177	7.81	15.63	>500
FF218	31.25	31.25	>500
FF225	7.81	15.63	>500
Cisplatin	>500	>500	>500
Meropenem	31.25	31.25	62.5

2.3.10 Antimicrobial Activity of 16 Metal-ion Complexes against *M. bovis BCG*

M. bovis BCG was assessed against the 16 metal-ion complexes and 2 control compounds. Table 2.12 lists the MIC values for the BMD assay and RRA assay, as well as the MBC values of each compound against *M. bovis* BCG. In addition, graphs of each BMD assay are presented in Figure 2.11.

Compound AN3 had an MIC of 31.25 μM in the BMD assay as shown by the growth curve in Figure 2.11 A. The Dunnett's multiple comparison showed a significant difference in bacterial growth between 31.25 μM and 0 μM ($P<0.0001$). All concentrations of AN3 above the MIC showed significance to 0 μM. From the concentration ranges below 7.81 μM, the significant difference was due to an increase in the OD values compared to 0 μM, so this difference was not due to any inhibition of growth. The statistically significant difference between 15.63 μM and 0 μM may suggest that this concentration still impacted the growth of *M. bovis* BCG despite not completely inhibiting it. The MIC of the RRA showed an identical value of 31.25 μM (Table 2.12). AN3 also exhibited bactericidal activity at a concentration of 31.25 μM as shown by absent growth on agar plates.

Figure 2.11 B illustrates the growth inhibition of RV144 against *M. bovis* BCG. The BMD MIC was 15.63 μM with a significant difference in growth ($P<0.0001$) compared to the 0 μM concentration. No significant difference was observed for 1.95, 0.98, and 0.49 μM of RV144 against *M. bovis* BCG ($P=0.9968$, 0.2991, 0.9994), indicating these lower concentrations had

no impact on the growth of *M. bovis* BCG. Inhibition was present as low as 3.91 µM as however by statistical differences, however the concentration which completely inhibited growth was 15.63 µM. The MIC of the RRA showed a difference in value compared to the BMD assay – 7.81 µM (Table 2.12). RV144 also exhibited bactericidal activity at a concentration of 7.81 µM.

The MIC of RV158 against *M. bovis* BCG was 3.91 µM for the BMD assay and the RRA (Table 2.12). The Dunnett's multiple comparison showed a significant difference in bacterial growth between 3.91 µM and 0 µM ($P<0.0001$). The lower concentrations of 0.98 and 0.49 µM showed no significance compared to 0 µM of RV158 ($P=0.4627$, $P=0.4465$) as it did not impact the growth of bacteria. RV158 also exhibited bactericidal activity to *M. bovis* BCG as low a concentration as 3.91 µM.

MD7 also showed promising results as an antimicrobial towards *M. bovis* BCG. The MIC of the BMD method was 3.91 µM as indicated in Table 2.12. Figure 2.11 D reveals the inhibition of MD7 concentrations to *M. bovis* BCG. A significant difference ($P <0.0001$) between 3.91 µM and 0 µM was analysed using the Dunnett's multiple comparison. All concentrations of MD7 from 1.95 µM and above showed significance to 0 µM ($P <0.0001$) suggesting inhibition from as low as this concentration. The MIC of the RRA showed a difference in value compared to the BMD assay – 1.95 µM (Table 2.12). MD7 also exhibited bactericidal activity at a concentration of 1.95 µM.

The other ruthenium-based compound MD72 had a strong effect on tackling bacterial growth as shown in Table 2.12 and Figure 2.11 E. The MIC was 0.98 µM for the BMD assay and the RRA (Table 2.12). All concentrations analysed by the one-way ANOVA demonstrated significant differences compared to the control. This indicates a dose-dependent response of MD72 to *M. bovis* BCG. Additionally, MD72 also exhibited bactericidal activity at a concentration of 1.95 µM.

Compound MD73 had different MIC values of 125 µM for the BMD method and 15.63 µM for the RRA method. Statistical analysis showed a significant difference ($P<0.0001$) between the MIC and all concentrations higher than 15.63 µM compared to and 0 µM in the BMD assay, suggesting a dose-dependent drug response to MD73. No growth occurred on agar plates from concentrations 31.25 µM and above, which was noted as the MBC.

Figure 2.11 G demonstrates the effect of MD56 on *M. bovis* BCG. With an MIC as low as 3.91 µM, there was a significant difference between this concentration and 0 µM ($P<0.0001$). The concentration below this, such as 0.98 µM did not show a difference in bacterial growth compared to the control ($P= 0.7691$), meaning at this concentration, MD56 had no effect on bacterial growth. The unusual difference between 0.49 to 0 µM is due to an increase in bacterial

number and not inhibition. The MIC of the RRA showed a difference in value compared to the BMD assay – 1.95 μM (Table 2.12). MD56 also exhibited bactericidal activity at a concentration of 7.81 μM as shown by absent growth on agar plates.

KP01 showed susceptibility to *M. bovis* BCG, including a bacteriostatic effect. The MIC of both assays, as well as the MBC, displayed a value of 125 μM as indicated in Table 2.12. For the BMD assay, the Dunnett's multiple comparison showed a significant difference between 0 μM and 125 and 250μM. At high concentrations, KP01 has a reducing effect on bacterial growth towards *M. bovis* BCG ($P<0.0001$).

JK-Ru5 also showed promising results as an antimicrobial towards *M. bovis* BCG. The MIC of both assays, as well as the MBC, displayed a value of 3.91 μM as indicated in Table 2.12. Figure 2.11 I presents the optical density measurements for each concentration of JK-Ru5 against *M. bovis* BCG. All concentrations have statistical differences compared to 0 μM except from lower values of 0.49 and 0.98 μM where the OD values were not affected by JK-Ru5.

The complex RuBio showed varied results at inhibiting *M. bovis* BCG. The MIC of RuBio was 125 and 15.63 μM for the BMD assay and the RRA, respectively μM (Table 2.12). All concentrations from 15.63 μM and above showed significance to 0 μM suggesting inhibition from as low as this concentration. RuBio also exhibited bactericidal activity at a concentration of 31.25 μM as shown by absent growth on agar plates.

In contrast, RV239 OsBpy had a lower value of 3.91 μM for both the MICs and MBC. A significant difference ($P <0.0001$) between 3.91 μM and 0 μM was analysed using the Dunnett's multiple comparison for the BMD method. The lower concentrations down to 0.98 μM also showed significance compared to 0 μM of RV239 OsBpy ($P <0.0001$) as they impacted the growth of bacteria, however, were not the MIC. From the agar plates, RuBio exhibited bactericidal activity at a concentration of 7.81 μM

The MIC for the BMD assay of FF175 against *M. bovis* BCG (Figure 2.11 L) resulted in 7.81 μM. A significant difference ($P <0.0001$) between 7.81 μM and 0 μM was analysed using the Dunnett's multiple comparison and all other concentrations above this. The MIC of the RRA showed an identical value to the BMD assay – 7.81 μM (Table 2.12). FF175 also exhibited bactericidal activity at a concentration of 15.63 μM which is an increase in concentration compared to the MIC.

The next copper compound FF176, displayed related results to FF175 with a lower MIC in the BMD assay (3.91 μM), however with the same concentration of 7.81 μM MIC in the RRA experiment. All concentrations from 250 to 1.95 μM demonstrated statistical significance

compared to 0 μM which suggests FF176 induces cell inhibition to *M. bovis* BCG as low a concentration as 1.95 μM. The lower values of 0.49 and 0.98 μM were not affected by FF176 (P=0.5162 and P=0.9997). From the agar plates, FF176 exhibited bactericidal activity at a concentration of 15.63 μM

FF177 compound showed antimicrobial effects at inhibiting and killing *M. bovis* BCG**.** Both the BMD and RRA assays obtained the same MIC results of 7.81 μM. Concentrations 250-1.95 μM had a statistical difference in the decrease of bacterial growth compared to 0 μM. Lower concentrations of FF177 including 0.98 and 0.49 μM showed no statistical difference compared to the 0 μM control, suggesting that these concentrations have no effect on bacterial growth of *M. bovis* BCG (P=0.7478 and P=0.0720). In addition, FF177 displayed bactericidal activity towards *M. bovis* BCG with an MBC of 7.81 μM.

FF218 showed promising results as a copper-metal antimicrobial towards *M. bovis* BCG. The MIC of both assays displayed a value of 7.81 μM as indicated in Table 2.12. Figure 2.11 O reveals the inhibition of FF218 concentrations to *M. bovis* BCG. A significant difference (P <0.0001) between 7.81 μM, all higher concentrations, and 0 μM was analysed using the Dunnett's multiple comparison. FF218 displayed bactericidal activity towards *M. bovis* BCG with an MBC of 15.63 μM.

The last copper-based compound investigated showed varied MIC and MBC results. The MIC of FF225 against *M. bovis* BCG was 7.81 and 3.91 μM for the BMD assay and the RRA, respectively μM (Table 2.12). The Dunnett's multiple comparison showed a significant difference in bacterial growth between 7.81 μM and 0 μM (P<0.0001). FF225 also exhibited bactericidal activity to *M. bovis* BCG at a concentration of 7.81 μM.

The control cisplatin demonstrated no inhibitory activity against *M. bovis* BCG (MIC>500) as shown in Figure 2.11 Q and Table 2.12. The results of the BMD and RRA assay conquered the same results. Furthermore, no bactericidal activity was observed for cisplatin against *M. bovis* BCG with an MBC of >500 μM.

The positive control meropenem, a clinically used carbapenem antibiotic, exhibited an MIC of 7.81 μM against *M. bovis* BCG in the BMD method and 15.63 in the RRA method. From the agar plates, meropenem exhibited bactericidal activity at a concentration of 15.63 μM. Notably, 11 of our tested compounds showed lower MIC values than meropenem, with MD72 being particularly potent (MIC: 0.98 μM). This suggests that these ruthenium-based compounds may have potential as novel antimicrobials against *M. bovis* BCG, possibly including meropenem-resistant strains. Further testing against resistant clinical isolates would be necessary to confirm this potential.

Key findings for *M. bovis* BCG:

- Most susceptible to ruthenium, copper, and osmium-based compounds
- Lead compounds: MD72 (MIC BMD: 0.98 µM, MIC RRA: 0.98 µM, MBC: 1.95 µM for both compounds)
- 16 out of 16 compounds showed antimicrobial activity
- 11 compounds outperformed the positive control (meropenem)
- 8 of the MIC values between the BMD and RRA assays differ in concentration

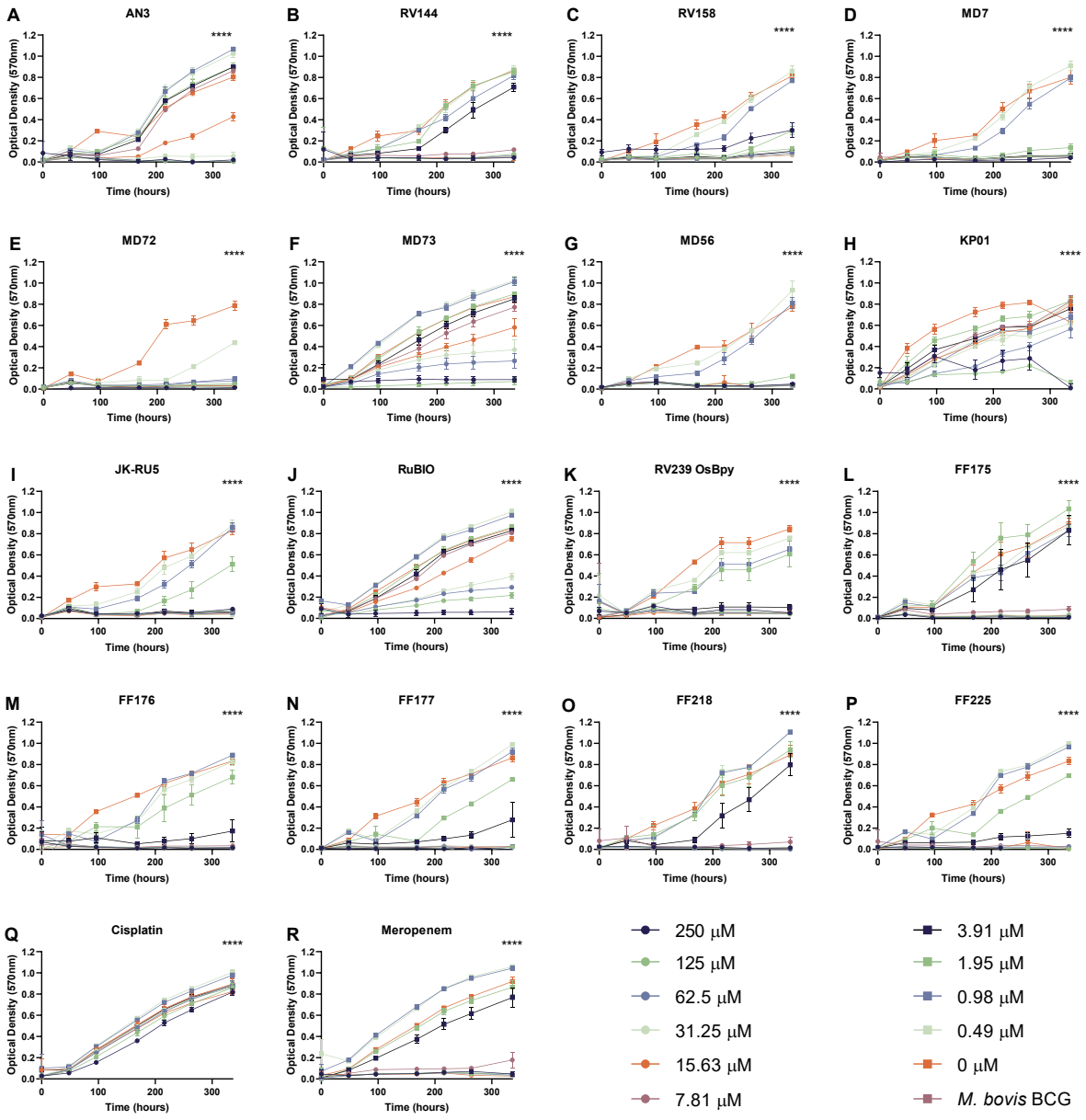

Figure 2.11. Optical density growth curves of *M. bovis* BCG Pasteur 1173P2 treated with investigative compounds. Growth curves show *M. bovis* BCG treated with **(A)** AN3, **(B)** RV144, **(C)** RV158, **(D)** MD7, **(E)** MD72, **(F)** MD73, **(G)** MD56, **(H)** KP01, **(I)** JK-Ru5, **(J)** RuBio, **(K)** RV239OsBpy, **(L)** FF175, **(M)** FF176, **(N)** FF177, **(O)** FF218, **(P)** FF225, **(Q)** Cisplatin, and **(R)** Meropenem for 336 hours. Optical density (570 nm) data are representative of n=3 technical replicates within one independent experiment. Mean values are shown, and error bars represent standard deviation. End point data, taken at 336 hours, was used for statistical analysis. P values were determined by a one-way analysis of variance (ANOVA) with Dunnett's multiple comparison, comparing all treatments to 0 µM to analyse the impact of compound concentration on the growth of *M. bovis* BCG. *P < 0.05, **P < 0.01, ***P < 0.001 and ****P < 0.0001.

Table 2.12. Summary table results of investigative compounds against *M. bovis* BCG Pasteur 1173P2. Data represent the minimum inhibitory concentrations (MIC) of the broth microdilutions (BMD), and resazurin reduction assay (RRA), and minimum bactericidal concentrations (MBC).

Compound	BMD MIC (μM)	RRA MIC (μM)	MBC (μM)
AN3	31.25	31.25	31.25
RV144	15.63	7.81	7.81
RV158	3.91	3.91	3.91
MD7	3.91	1.95	1.95
MD72	0.98	0.98	1.95
MD73	125	15.63	31.25
MD56	3.91	1.95	7.81
KP01	125	125	125
JK-Ru5	3.91	3.91	3.91
RuBio	125	15.63	31.25
RV239OsBpy	3.91	3.91	7.81
FF175	7.81	7.81	15.63
FF176	3.91	7.81	15.63
FF177	7.81	7.81	7.81
FF218	7.81	7.81	15.63
FF225	7.81	3.91	7.81
Cisplatin	>500	>500	>500
Meropenem	7.81	15.63	15.63

2.4 Discussion

This study investigated the antimicrobial potential of 16 metal ion complexes, originally designed as anti-cancer agents, against a panel of highly resistant bacterial species. Our findings reveal several promising candidates with broad-spectrum activity and potency comparable to or exceeding the clinically used antibiotic meropenem. Notably, ruthenium-based compounds MD7 and MD56 emerged as lead candidates, demonstrating efficacy against all tested pathogens, including challenging mycobacterial species. These results highlight the potential of drug repurposing in addressing the critical need for new antimicrobials to combat the growing threat of antibiotic resistance.

The main purpose of this study was to develop an understanding of alternative uses of failed anti-cancer metal-compounds synthesised by medicinal inorganic chemistry. These drugs showed promising properties, such as broad-spectrum activity across 10 pathogens and susceptibility against multi drug-resistant strains. The 16 complexes explored had variation in antimicrobial activity depending on the microorganism tested. All compounds demonstrated antimicrobial functionality. Summary heat maps are presented for the RRA MIC results (Figure 2.12) and for the MBC results (Figure 2.13) of each bacterial species challenged with each investigative compound.

The compounds with the lowest MIC concentrations were MD72 with inhibitory concentrations for *M. bovis* BCG (0.98 μM) and RV144 with inhibitory concentrations for *E. faecium* (0.98 μM). The least effective compound for broad spectrum activity was KP01, with only activity against M. *bovis* BCG. There were 4 compounds which conveyed bacteriostatic activity to all 10 microorganisms tested (MD7, MD56, JK-Ru5, and RV239 OsBpy) with a MIC value for each. The compounds with the best bactericidal activity were also MD7, MD56, JK-Ru5, and RV239 OsBpy, killing 9, 7, 9, and 8 bacterial species, respectively. The most susceptible bacterial species to all compounds was *M. bovis* BCG, with 16 compounds having MIC values and 16 compounds having MBC values. Interestingly, the copper-based compounds were better at inhibiting mycobacterial species rather than ESKAPE pathogens. When using a control of a platinum-based drug, cisplatin showed no bacteriostatic or bactericidal activity towards any pathogen tested. In addition, when using a positive control of meropenem, it was demonstrated that some of these novel compounds achieved similar or better antimicrobial activity than the approved drug, meaning these compounds could be clinically relevant. Discrepancies between the inhibitory concentrations of the BMD assay and the RRA method were evident.

In summary, it can be suggested from the evidence in this chapter that the lead compounds which showed broad spectrum activity were MD7 and MD56, which are both ruthenium-based complexes. Our findings align with and extend previous research on the antimicrobial properties of ruthenium complexes. Li, Collins, and Keene (2015) reported on the potential of

ruthenium complexes as antimicrobials, highlighting their ability to bind to nucleic acids and proteins. Our study confirms these observations and demonstrates the efficacy of ruthenium complexes against a broader range of pathogens, including challenging mycobacterial species. For instance, our lead compound MD7 showed MIC values as low as 1.95 µM against MRSA, comparable to the activity reported by Nolan et al. (2022) for their indole-containing arene-ruthenium complexes. However, our study demonstrates efficacy against mycobacteria, with MD7 showing an MIC of 3.91 µM against *M. abscessus* subsp. *massiliense*, a notoriously difficult-to-treat pathogen. It is also worth noting that Gram-negative bacteria seem to obtain a higher resistance profile to these compounds compared to Gram-positive bacteria and may be due to the additional outer membrane that Gram-negative bacteria possess.

Compound	*E. faecium*	*MRSA*	*K. pneumoniae*	*A. baumannii*	*P. aeruginosa*	*E. cloacae*	*M. abscessus* subsp. *abscessus*	*M. abscessus* subsp. *bolletii*	*M. abscessus* subsp. *massiliense*	*M. bovis* BCG
AN3	15.63	3.91	>500	62.5	>500	>500	62.5	125	62.5	31.25
RV144	0.98	15.6	>500	>500	>500	>500	31.25	31.25	15.63	7.81
RV158	1.95	3.91	>500	15.63	>500	>500	7.81	31.25	7.81	3.91
MD7	1.95	1.95	125	15.63	125	250	7.81	15.63	3.91	1.95
MD72	>500	125	>500	>500	>500	>500	3.91	3.91	1.95	0.98
MD73	>500	7.81	>500	>500	>500	>500	31.25	31.25	31.25	15.63
MD56	7.81	3.91	125	7.81	125	125	15.63	15.63	3.91	1.95
KP01	>500	>500	>500	>500	>500	>500	>500	>500	>500	125
JK-Ru5	62.5	3.91	500	125	250	250	15.63	15.63	7.81	3.91
RuBio	7.81	500	>500	15.63	>500	>500	15.63	15.63	3.91	15.63
RV239OsBpy	6.25	1.95	125	7.81	62.5	125	7.81	15.63	3.91	3.91
FF175	31.25	31.3	>500	>500	>500	>500	31.25	31.25	15.63	7.81
FF176	31.25	15.6	>500	>500	>500	>500	15.63	31.25	15.63	7.81
FF177	>500	125	>500	>500	>500	>500	31.25	250	15.63	7.81
FF218	>500	31.3	>500	>500	>500	>500	31.25	62.5	31.25	7.81
FF225	7.81	15.6	>500	>500	>500	>500	15.63	31.25	15.63	3.91
Cisplatin	>500	>500	>500	>500	>500	>500	>500	>500	>500	>500
Meropenem	62.5	125	15.63	15.63	15.63	31.25	15.63	31.25	31.25	15.63

Higher MIC

Lower MIC

Figure 2.12. Heat map Summary of MIC values for each compound against each bacterial species. Colour intensity correlates with antimicrobial activity (Green colours indicate lower MIC values and thus higher activity).

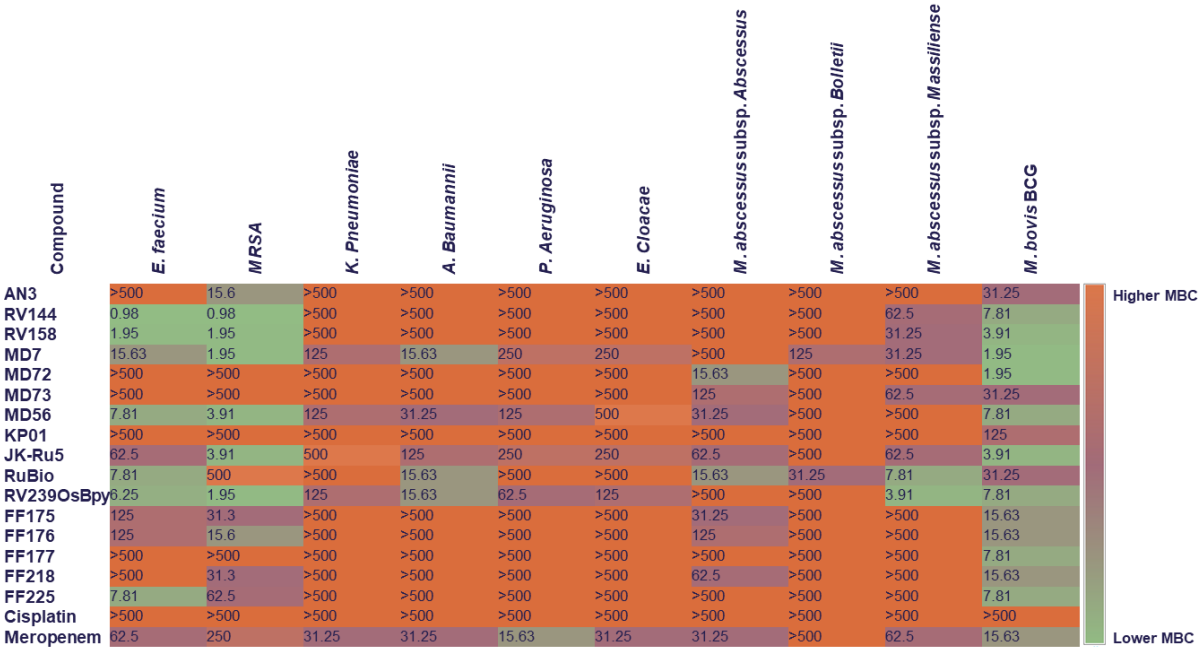

Figure 2.13. Heat map Summary of MBC values for each compound against each bacterial species. Colour intensity correlates with antimicrobial activity (Green colours indicate lower MIC values and thus higher activity).

The investigation of ruthenium metal-complexes as antimicrobials would be a fruitful area for further work. Firstly, the experiments undertaken in this chapter resulted in conclusions from 3 technical repeats as the chemicals were provided by collaborators in limited mass. Moving forward, synthesis of an abundance of these compounds would allow for biological repeats to be completed to obtain accurate *in vitro* results. Evidence suggests that ruthenium-based compounds can strongly bind to nucleic acids and proteins (Li et al., 2015). Future research should focus on elucidating the mechanisms of action of our lead compounds, particularly MD7 and MD56. This could involve:

1. Genomic and proteomic studies to identify potential cellular targets, such as specific DNA binding sites or vital metabolic enzymes.
2. Time-kill assays to determine the rate of bacterial killing and potential synergies with existing antibiotics.
3. Resistance development studies to assess the frequency of spontaneous resistance and potential cross-resistance with other antimicrobials.
4. Structure-activity relationship (SAR) studies to optimise the molecular structure for improved antimicrobial activity and reduced toxicity.
5. *In vivo* efficacy studies using relevant animal models of infection to assess these compounds' therapeutic potential and pharmacokinetic properties.

Additionally, expanding the panel of tested organisms to include clinical isolates with defined resistance mechanisms would provide valuable insights into the potential of these compounds to address specific challenges in AMR.

In conclusion, this study demonstrates the promising potential of repurposed metal-ion complexes, particularly ruthenium-based compounds, as novel antimicrobials against a diverse range of clinically relevant pathogens. Our findings contribute to the growing body of evidence supporting the antimicrobial properties of metal-based compounds and highlight a potential new avenue for addressing the urgent need for new antibiotics. The broad-spectrum activity and potency of compounds like MD7 and MD56, especially against difficult-to-treat pathogens such as M. abscessus, warrant further investigation and development. As the global threat of AMR grows, innovative approaches like drug repurposing may be crucial in bolstering our antimicrobial arsenal. This study lays the groundwork for future research that could potentially develop novel metal-based antimicrobials, offering new hope in the fight against resistant infections.

However, there are current problems with *in vitro* antibiotic susceptibility testing (ones which have been used here). While *in vitro* AST is a valuable tool for guiding antibiotic therapy, it has limitations in predicting clinical outcomes due to differences between lab conditions and the complexities of human infections.

In vitro antibiotic susceptibility testing (AST) is a widely used method to determine the effectiveness of antibiotics against specific bacteria in a controlled laboratory environment. However, there are several problems and limitations associated with this approach. It can take days to produce susceptibility results, which would either delay treatment decisions in a clinical setting or slow down the drug discovery process in an industrial setting. This is particularly problematic for rapidly progressing infections in patients or the development in new antimicrobial drug discovery to tackle AMR. Also, bacteria in the human body may exist in biofilms or other protective niches such as “persister cells”, which *in vitro* tests do not replicate. These microenvironments can affect the antibiotic’s efficacy and therefore a new model which replicate microenvironment similar to humans is needed.

While optical density (OD) measurements are widely used for assessing bacterial growth, this approach has limitations, particularly when working with mycobacteria. Due to their hydrophobic cell walls, the clumping behaviour of mycobacteria can lead to uneven distribution in culture and potentially inaccurate OD readings. This may explain our study's lower-than-expected OD values observed for mycobacterial growth. Furthermore, OD measurements cannot distinguish between live and dead cells, potentially overestimating viable cell numbers in cases where a compound may cause cell death without lysis. Future studies could

incorporate additional viability assays such as colony forming unit (CFU) counts or flow cytometry-based live/dead staining to address these limitations. While more time-consuming, these methods would provide a more accurate assessment of both growth inhibition and bactericidal activity.

In these results, the different MIC concentrations between the BMD assay and the RRA method are due to the fundamental differences in what each assay measures—bacterial growth versus metabolic activity. Antibiotics, which are bacteriostatic, inhibit bacterial growth but may not immediately kill the bacteria. In such cases, OD measurements will show inhibition of growth at a certain concentration, defining the MIC. However, the bacteria may still be metabolically active at that concentration, leading to a lower MIC in the RRA. Other factors such as the type of antibiotic, the bacterial response, the sensitivity and specificity, inoculum size, and interpretation criteria, all contribute to differences in MICs between the BMD and the RRA.

These examples of insufficient *in vitro* assays may be improved by using droplet microfluidics to create an improved *in vitro* antibiotic susceptibility assay and enhance *in vivo* correlation. Droplet fluidics would allow for high-throughput processing as well as the ability to create ‘bioreactors’ in defined environments.

Chapter 3.

Generation of Monodisperse and Stable Picodroplets using Picodroplet Technology for Bacterial Culturing.

3.1 Introduction

Creating “microbubbles” with encapsulated bacteria at the single-cell level is of interest in developing and improving antimicrobial susceptibility testing (AST). Microbubbles enhance the speed, sensitivity, and accuracy of AST by improving the interaction between bacteria and antibiotics, and facilitating faster detection of bacterial growth. Their generation with technologies like microfluidics holds great potential for the development of advanced AST platforms. The fundamental principles of generating droplets comprise emulsion dynamics, the surfactant and aqueous phase used, and the integrity of individual droplets measured by monodispersity and stability.

3.1.1 Emulsions

Emulsions have diverse applications across multiple industries. Ashaolu (2021) reviews these applications, noting their use in healthcare for drug delivery systems, in the food industry for texture modification and nutrient encapsulation, and in cosmetics as the basis for many creams and lotions. These applications share similarities with the use of emulsions in microbial studies, particularly in terms of stability and controlled release requirements (Ashaolu, 2021). An emulsion is defined as a system where two immiscible dispersed liquids form droplets (Israelachvili, 1994).

Emulsions can be categorized based on droplet size, which significantly affects their properties and applications. Anton and Vandamme (2011) distinguish between conventional macro-emulsions and nano-emulsions. Macro-emulsions comprise droplets larger than micrometres, which can be less stable over time. In contrast, nano-emulsions consist of droplets smaller than 300 nm, contributing to increased stability and improved bioavailability in many applications. For this study, we focus on micro-emulsions, which bridge the gap between macro- and nano-emulsions, offering a balance of stability and functionality suitable for microbial encapsulation (Anton and Vandamme, 2011).

There are several types of emulsions which are illustrated in Figure 3.1: oil-in-water (O/W), water-in-oil (W/O), water-in-oil-in-water ($W_1/O/W_2$), and oil-in-water-in-oil ($O_1/W/O_2$). An O/W emulsion is composed of an oil phase dispersed in an aqueous one, whereas a W/O emulsion is composed of an aqueous phase dispersed in the oil phase (Israelachvili, 1994). Other emulsions, such as $W_1/O/W_2$, and $O_1/W/O_2$, exist as well. These more complex systems as also known as double emulsions (Garti and Aserin, 2013).

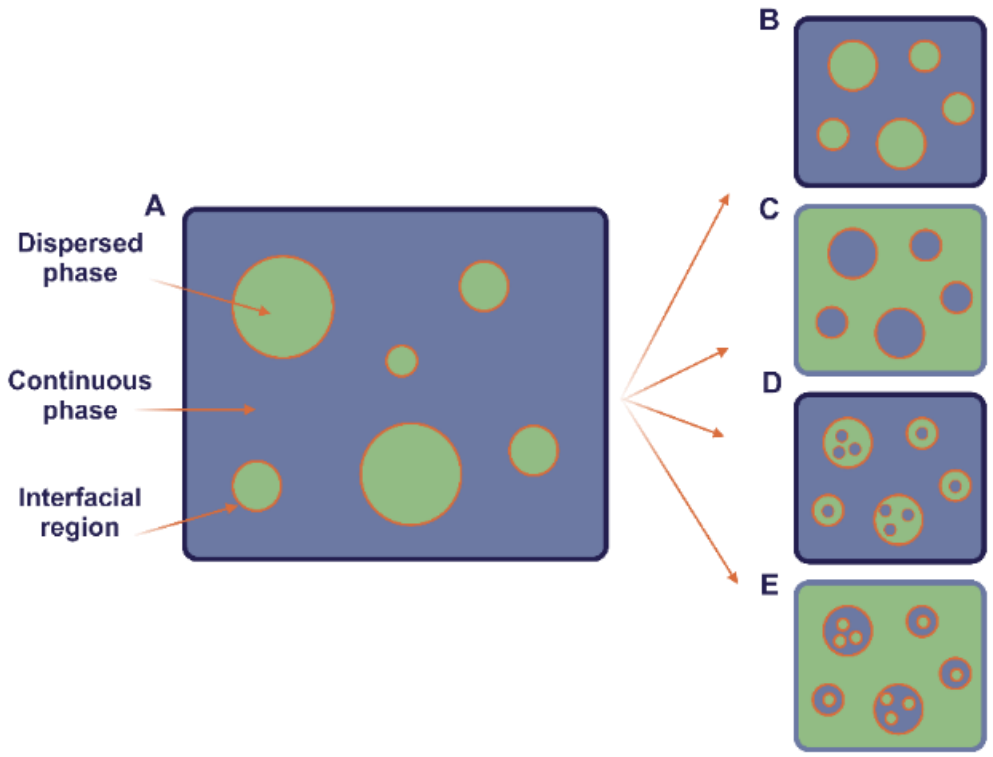

Figure 3.1. Schematic representation of emulsion types. (A) Dispersed phase and continuous phase separated by interfacial region. **(B)** Oil-in-water (O/W) emulsion. **(C)** Water-in-oil (W/O) emulsion. **(D)** Water-in-oil-in-water (W1/O/W2). **(E)** Oil-in-water-in-oil (O1/W/O2). Green and blue represent oil and water phases, respectively. Orange represents the interfacial region. Image created on Biorender.com.

When combined, water and oil are usually thermodynamically stable, which separates them in layers due to density. One of these phases may break and form into the other phase due to an increase in energy, such as mechanical force (McClements, 2007). To prepare emulsion, there are two types of methods using force – high energy and low energy methods. (Chircov and Grumezescu, 2019). Methods such as thermal/isothermal and spontaneous emulsification fall into the low energy method category. On the other hand, it is typically mechanical devices such as microfluidizers, homogenizers, and ultrasonic devises which produce smaller droplets with high energy (Chircov and Grumezescu, 2019). One high energy method can achieve producing emulsions of controlled droplet sizes – droplet microfluidics. Droplet-based microfluidics is one subcategory of emulsion production. Using this method, emulsions can be produced in a controlled manner with a surfactant-containing oil phase, an aqueous phase, and a microfluidic chip.

3.1.2 The Role of Surfactants in Stabilising Emulsions

For droplets to be stable, biocompatible surfactants are used to control the properties of the droplets. Surfactants are surface active agents which are composed of hydrophilic heads and hydrophobic tails (illustrated in Figure 3.2). The hydrophobicity of the tail enables water molecules to organise locally so the surfactant can form a micelle (Baret, 2012). An emulsion

system requires a surfactant, otherwise it would eventually homogenise into separate phases owing to minimum energy (Bibette et al., 1992). Coalescence and Ostwald ripening can occur where the film between droplets in proximity to each other can rupture or the diffusion of the aqueous phase out of small droplets and into larger ones happens, respectively. The main role of surfactants is to prevent this destabilisation (Shang et al., 2017). Not only are surfactants biocompatible, but they are favourable for creating stable droplets which endure incubation times. The micelles enclose the aqueous phase to form 'bioreactors' for biological assays. However, it is important to note that the droplets do not form a tight seal and small molecule leakage may occur out of the droplets (Courtois et al., 2009). The characteristics of the surfactants and encapsulated small molecules affect the diffusion ability and care should be taken when choosing which surfactant to use.

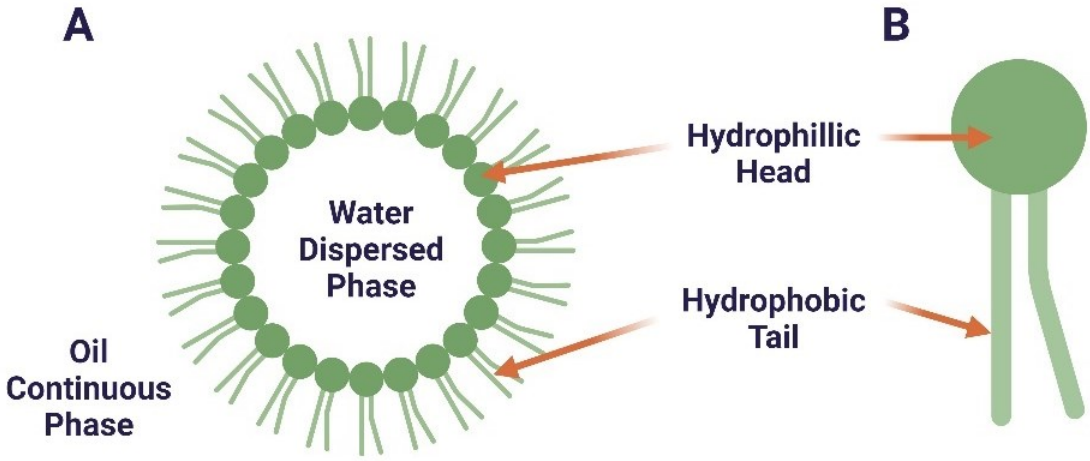

Figure 3.2. Surfactant Structure. (A) W/O micelle formed by surfactant molecules. **(B)** Surfactant molecule with polar hydrophilic (water-loving) head and non-polar hydrophobic (water-hating) tail. Image created on Biorender.com.

3.1.3 Droplet Stability

Droplets must maintain stability during biochemical assays to ensure the reliability, accuracy, and reproducibility of experiments inside droplets. Moreover, the fundamental requirement of droplet stability plays a crucial role in maintaining controlled reaction conditions within each droplet microreactor, such as the same volume of reagents and samples. Stability is important for droplet-based antibiotic susceptibility testing to guarantee bacterial species are being subjected to the same antibiotic concentrations, nutrients, and oxygen variability.

Generally, the term "droplet stability" refers to the ability of an emulsion of droplets to resist changes in its physicochemical properties over time (McClements, 2007). The preparation of emulsions that are kinetically stable over a period that is of practical use for biochemical assays requires the incorporation of substances known as stabilisers, i.e. surfactants. However, there are several aspects that need to be considered ensuring the stability of droplets, including the

type of surfactants, methods used for emulsification, size of droplet formed, and the storage conditions.

Droplets may destabilise from processes, such as sedimentation, phase inversion, flocculation, creaming, Ostwald ripening, and coalescence. These destabilisation processes can be illustrated in Figure 3.3. Sedimentation is caused by gravity where a concentrated layer of droplets has formed at the bottom of the sample because they have a higher density than the surrounding liquid (McClements, 2007). Droplets may aggregate which is known as flocculation but maintain their individual integrities. (McClements, 2007). Phase inversion results from the change of emulsion type from an O/W emulsion to a W/O emulsion, and vice versa (McClements, 2007). Creaming is caused by gravitational separation whereby droplets move upward because they have a lower density than the surrounding liquid (McClements, 2007). When a mixture of smaller and larger droplets is together in an emulsion, Ostwald ripening can occur whereby the larger particles enlarge further, and the smaller droplets disappear due to the mass transport of dispersed phase material through the continuous phase. In contrast, coalescence can occur where two or more droplets merge to form a single larger droplet. This process is irreversible and can lead to two separate layers in the sample (Mao and Miao, 2015).

Contributors to droplet destabilisation include rheology, size distribution, analyte content, and the electrical charge of the droplet surface (Hu et al., 2017). In addition, researchers published in Nature have shown that coalescence is increased with increasing temperature and that droplets coalesce less frequently when the surfactant concentration in increased (Bera et al., 2021). Visual observation, microscopy, light scattering, electrical pulse counting, and ultrasonic spectroscopy are all methods to measure the stability of droplets (Hu et al., 2017).

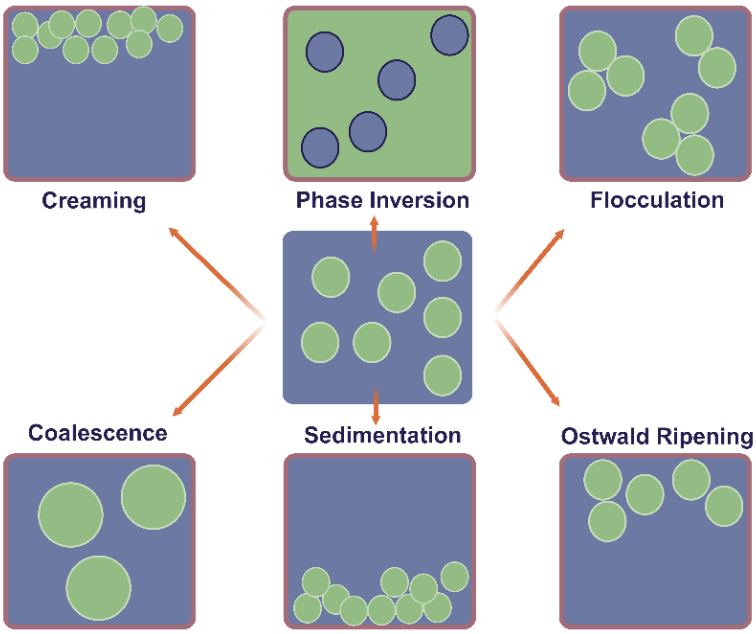

Figure 3.3. Schematic representation of droplet failure modes. Green and blue represent oil and water phases, respectively. Centred image shows stable droplets. Surrounding droplets show unstable variations of droplets. Image created on Biorender.com.

3.1.4 Droplet Monodispersity and Droplet Size Distribution

When droplet input parameters are not controlled, emulsions generated will produce "polydisperse" droplets with a wide distribution of droplet sizes. An emulsion is referred to as "monodisperse" when all the droplets in an emulsion have the same size (illustrated in Figure 3.4). Microfluidic devices enable finer control of droplet size distribution. As channel geometry, fluid viscosities, and interfacial tension do not vary within each experiment, it is the flow rate ratio which influences the generation of identical sizes. Syringe pumps which direct flow in microfluidic devices can easily control small volumes of fluids, however, fluctuations of flow-rate and pressure occur due to the mechanical oscillations of the pump motor (Zeng et al., 2015a). This dampens the control over droplet size and has slower flow rates. In contrast, pressure-driven flows allow for precise control of droplet size within seconds (Zeng et al., 2009).

Measurements of the droplet radius, diameter, or volume are used to characterise the droplet size. Methods to test droplet monodispersity can be measured by microscopy, light scattering, electrical pulse counting or ultrasonic spectrometry methods (McClements, 2007). Often, droplet size is reported as a distribution of droplet sizes or the mean/average size. The size distribution of the droplets is expressed in the form of a coefficient of variation (CV), which is defined as (1),

$$(1)\quad CV = \frac{\sigma}{ddr}$$

where σ is the standard deviation of the droplet size and ddr is the average droplet size. Droplet monodispersity in the literature is reported in the range of CV=5-10% (Jõemaa et al.,

2023). More recently, studies demonstrate variance in droplet size as low as CV=<1% (Kalantarifard et al., 2018, Kim et al., 2021).

On another note, there have been a few examples where researchers have created 'bulk' emulsions using surfactants to study bacteria. Byrnes *et al* created polydisperse droplets with encapsulated bacteria by shaking aqueous cultures and surfactant. The bulk emulsions were comparable to monodisperse droplets and showed stability for 144 hours, making the method well suited for studying slow growing bacteria (Byrnes et al., 2018). Additionally, exploration of double emulsions showed bacteria encapsulation by using a rotor-stator homogenizer (van der Ark et al., 2017). Wijk *et al* encapsulated *L. plantarum* 423 in a Pickering emulsion stabilised with hydrophobized silica particles to show bacteria viability and stability (van Wijk et al., 2014). In another application, *Lactobacillus delbrueckii* ssp. *bulgaricus* were encapsulated with artificial sesame oil emulsions and bacterial viability was tested for commercial utilisation of probiotics. The results proposed that artificial sesame oil emulsion was a potential biocapsule to encapsulate bacteria and maintain its survival under simulated gastrointestinal conditions (Hou et al., 2003). More recently, vortexing was used to co-encapsulate multiple species of bacteria and the special segregation of bacteria improved the co-cultivation of antagonistic bacteria (Dijamentiuk et al., 2023). However, despite these examples proving that bacteria can be encapsulated in emulsions, bulk emulsions are polydisperse in volume and would not be suitable for accurate antimicrobial testing. Therefore, there is a great scope for using droplet fluidics to create monodisperse and stable droplets.

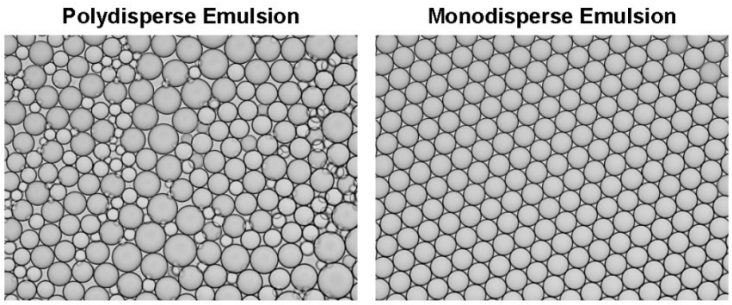

Figure 3.4. Comparison of polydisperse emulsion versus monodisperse emulsion.

3.1.5 Droplet Microfluidic Technologies

Microfluidic devices offer automation and multiplexing of biological assays, which can advance many end users, including hospitals and diagnostic centres, academic and research institutes, and pharmaceutical and biotechnology companies. In particular, the microfluidic market was valued at $22.3 billion in 2023. With an expected compound annual growth rate (CAGR) of 13%, the market is projected to reach $41.1 billion by 2028. The projected boost in the market is owed to technological advancements in the operating procedures of microfluidic components

and their extensive applications they can be marketed into (MarketsandMarkets, 2023). Despite the vast advantages of droplet microfluidics, there are major challenges in commercialising droplet microfluidic products. Firstly, multiple iterations and optimisation of different devices for similar organisms or purposes has caused a failure in standardisation (Volpatti and Yetisen, 2014).

Secondly, integration of microfluidic products into biological workflows and new applications has often been an afterthought and does not reach an end user after product development (Ortseifen et al., 2020). Research into combating multistep workflows in an automated and reproducible manner has been demonstrated by Tran et al., 2022 by using fluid handling robotics (Tran et al., 2022). Likewise, Wang's (2024) recent research reported a platform which integrates the current digital DNA amplification workflows into a one-step device (Wang et al., 2024). Together, these studies indicate that integration and standardisation of droplet methodologies can be beneficial in biological workflows.

Lastly, technical challenges include but are not limited to; formation of robust droplets, generation of droplet libraries with different sets of samples for combinational drug screening, the use of highly sensitive equipment to enable small analyte quantification, the leakage of components from the droplets, and droplet destabilisation (Holtze et al., 2017) (Payne et al., 2020). Ultimately, it can become cumbersome to perform droplet assays manually for the end user with limited technical knowledge of the multidisciplinary field of microfluidics. Efforts are required to bridge the gap in interdisciplinary collaboration between academia and industry to uphold the potential of droplet microfluidics in novel applications.

3.1.6 Sphere Fluidics Advanced Picodroplet Technology

Sphere Fluidics is a biotechnology company based in Cambridge who is collaborating with biological research scientists to shift to need-driven product development. Founded in 2010, they are expanding in single-cell analysis by engineering droplet fluidic platforms. In addition to synthesising and commercialising their biochips and droplet generating reagents, they have excelled in building automated/semi-automated platforms for research purposes. Their Cyto-Mine® automated platform enables antibody discovery and cell line development (Josephides et al., 2020). Other semi-automated platforms include Pico-mine® and Spectra-Mine® which integrate droplet sorting and mass spectrometry respectively (Kempa et al., Liu et al., 2016, Smith et al., 2013).

The company is currently engineering an updated droplet platform designed to support early-stage academic research using picodroplet technology. This droplet platform uses an image-based closed-loop feedback mechanism to advantageously find the desired picodroplet volume from scattered light and optical imaging (schematic show in Figure 3.5). More

researchers are now using closed-loop feedback control of droplet volumes to produce emulsions of high-speed (Zeng et al., 2015b, Zeng et al., 2022, Fu et al., 2017, Miller et al., 2010, Xie et al., 2020, van Elburg et al., 2021, Gyimah et al., 2022a, Jõemaa et al., 2023).

The device from the company can determine droplet frequency, determine droplet dimension, and adjust droplet dimension to desired volume in an automated manner. During droplet generation using a biochip, a continuous phase, and a discontinuous phase, the droplet frequency can be determined. The passing flow of droplets generated are illuminated in the channel and a beam splitter is used to split light into two parts – the first to a camera and a second through an aperture to a photodetector. Frequency is obtained from fluctuations in the processed signal. In addition, an image of a flow of droplets in a biochip channel can be generated with a microscope. From there, droplet physical length within the channel can be determined by assuming the droplet is a sphere, the spherical droplet volume may then be calculated using the determined radius by comparing the number of pixels against a known pixel size within the channel. For producing droplets of desired picolitre volumes, a chosen droplet volume is imputed by the end user and the feedback system will adjust the pressure of the flow of the continuous and aqueous inlets based on the determined droplet size (McGrath, 2023). This method maintains monodispersity of droplet sizes if, for instance, dust passes through the biochip and adjusts droplet size during generation. This real-time adaptation of droplet volume enables accurate control over the droplet volume when performing biological assays involving single-cell studies.

The first model of the device was reported in the literature (Crawford et al., 2017) which presented efficient monodispersed sized droplets that could be created without needing to know previous information on the fluidic properties of the system. Scientists have extended this work to include image-based closed-loop feedback control over two aqueous inlets. This development of dual aqueous droplet generation will enable libraries of droplets with defined composition ratios but same volumes to be tightly controlled (Cantwell et al., 2024). In both instances, the picodroplet technology outperformed current droplet producing techniques in terms of monodispersity in volume. The high precision of this device will allow efficient control of samples, reagents, and emulsion temperatures for biological assays. This will enable the design of an assay system with defined volumes of sample size. Optimisation is underway to make this device fully operational and applied to various applications in biomedicine.

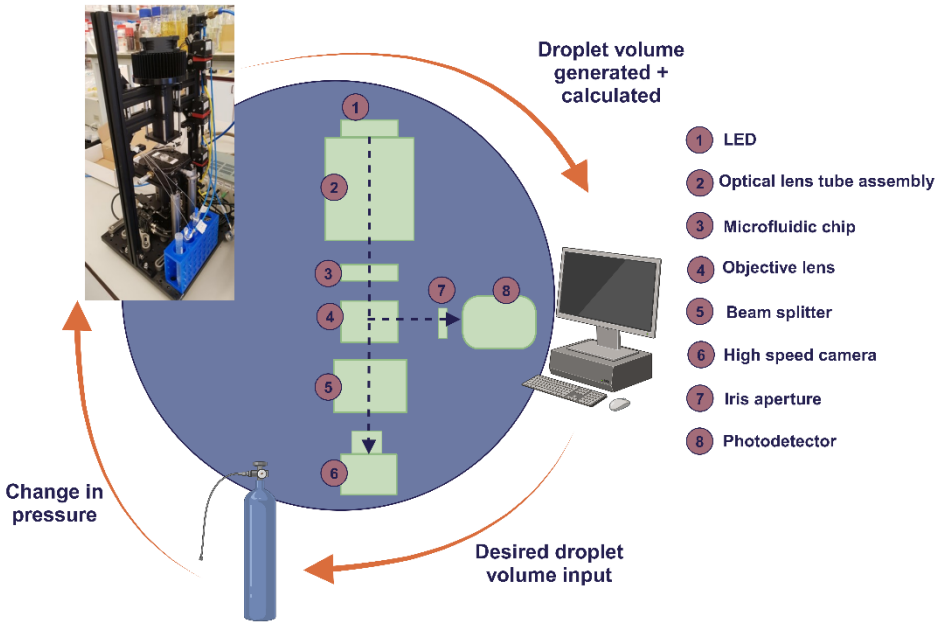

Figure 3.5. Process of determining droplet volume generated by image-based closed-loop feedback. A high-speed camera is attached to a microscope where droplets can be detected using an infra-red laser and a back-scatter detector. The camera measures the length of the droplet and from this droplet volume is calculated. The information is passed to the feedback loop to control the inlet pressures. Image created on Biorender.com.

3.1.7 Challenges in Creating Monodisperse and Stable Droplets for Microbiology Applications

Mycobacteria are hydrophobic in nature and thus provide difficulty when studying. It is therefore required to add detergents into culture media to prevent clumping of the bacteria. To culture mycobacteria, often Middlebrook 7H9 is used containing 0.05% Tween® 80. Previous studies have identified a non-replicating persistence state of mycobacteria when cultured in hypoxia and cholesterol based minimal media (Gibson et al., 2021). It is thought that the mycobacteria use cholesterol as the only carbon source and remain dormant until activated again. (Pieters, 2001). The cholesterol-based media contains 0.05% tyloxapol. As Tween® 80 and tyloxapol are detergents, it is possible that these may alter the interfacial tension of the droplets and destabilise droplets.

While droplet microfluidics has shown promise in various fields, its application in antimicrobial susceptibility testing, particularly for mycobacteria, remains challenging. The unique properties of mycobacterial culture media, including the presence of detergents like Tween® 80, may affect droplet stability. Therefore, this study aims to optimise the generation of monodisperse droplets using an image-based closed-loop feedback system, and investigate the stability of droplets formed with various bacterial culture media under different incubation conditions and surfactant concentrations.

3.1.8 Objectives and Aims of Chapter

The following chapter focuses on a method for producing monodisperse and stable w/o droplets by determining and controlling the droplet dimension during formation using picodroplet technology. Different droplet input parameters were used to test the optimal conditions required to make monodisperse and stable droplets for future microbiology applications.

The aims of this chapter are as follows;

a) To generate w/o droplets of varying desired picolitre droplet volumes by using picodroplet technology with image-based closed-loop feedback.
b) To determine the flow rate ratios of a flow of w/o microdroplets at different picolitre volumes.
c) To assess the efficiency of the picodroplet technology by producing monodisperse w/o droplets of varying surfactant concentrations, aqueous phase media types, and droplet volumes.
d) To create droplets using varying surfactant concentrations and aqueous phase media types and test their stability during collection and microbiology incubation conditions.

3.2 Methods

3.2.1 General Chemical, Reagent, and Media Preparation

All consumables and reagents were purchased from either Fisher Scientific, Melford, Biosynth, or Sigma-Aldrich, unless otherwise stated. Industrial partner Sphere Fluidics Ltd provided 5% Pico-Surf®, Pico-Glide™, and Novec™ 7500 reagents.

Pico-Surf®

For studies using 5% Pico-Surf®, the reagent was used undiluted and stored at 4 °C. The 5% Pico-Surf® was diluted to 2% and 1% using Novec™ 7500 oil.

Pico-Glide™

Pico-Glide™ was used undiluted and stored at 4 °C.

Phosphate Buffered Saline (PBS)

One tablet of PBS (Melford P32080-100T) was added to 100 mL of dH_2O to make a 1X solution. The PBS tablet was made of 137 mM sodium chloride, 2.7 mM potassium chloride, and 11.9 mM phosphate buffer. pH 7.4 at 25 °C.

Mueller-Hinton Broth

9.45 g of Mueller-Hinton broth was dissolved in 450 mL of dH_2O and then autoclaved (121 °C for 15 min).

Middlebrook 7H9 Broth

2.35 g of 7H9 broth base, 450 mL of dH_2O and 4 mL of 50% glycerol were added together before autoclaving (121 °C for 15 min). Once cooled, 1.25 mL of 20% filter sterile Tween80 is added along with 50 mL filter sterile ADC (albumin, dextrose, and catalase supplement).

ADC Supplement

5 g BSA (bovine serum albumin fraction v), 2 g dextrose, 0.85 g sodium chloride and 0.003 g catalase were added to 100 mL dH_2O. The components were dissolved before filter sterilising with a 0.22 µm sterile filter. The ADC supplement was stored at 4 °C.

Minimal Cholesterol Media

Minimal cholesterol media formation was adapted from (Gibson et al., 2021). Briefly, 2.61g of Middlebrook 7H9 media was dissolved in 500 mL of dH_2O. A magnetic stirrer bar was washed with ethanol and added. The mixture was autoclaved at 121 °C for 15 mins and then heated to 65 °C and placed on a hot magnetic stirrer plate. The cholesterol additive was added while

the media was hot and stirring. The media was the left to cool and filtered through a filtration vacuum and stored for 2 weeks at 10 °C.

Dissolved Cholesterol Additive

1 mL of tyloxapol: ethanol (50:50, v/v) mixture was made. This mixture was repeatedly vortexed and heated to 65 °C until the mixture was homogenised. 50 mg of cholesterol was then slowly dissolved in the mixture (around 5 mg at a time until dissolved). To help the dissolving process, the mixture was vortexed for 5 seconds, then immediately placed back in 65 °C. Stock solutions of dissolved cholesterol additive were made and flash frozen in liquid nitrogen and stored at -80°C.

3.2.2 PDMS Chip Fabrication

Microfluidic chips were made in-house at Aston University. Two SU-8 masters, including one with 60 x 60 µm flow-focusing channel dimensions and one with 40 x 40 µm flow-focusing channel dimensions, were provided by Sphere Fluidics Ltd. The geometries of these chips are shown in Figure 3.6. The channel of the 40 x 40 µm flow-focusing chip is shown to have blocked channels filled with dust as an example of an unsuitable chip. PDMS elastomer and curing agent (10:1) were weighed in a plastic beaker, mixed using a pasture pipette, and poured on top of the SU-8 master. The dish containing PDMS and master mould was placed in a vacuum (BACOENG) to remove all air bubbles in the PDMS and the PDMS was cured in an oven at 65 ºC for 3 hours. The device was cut around the edges with a scalpel, making sure not to damage the master, and holes were punched in the microfluidic inlets and outlets from the microfluidic side with a 1.0 mm biopsy punch. Oxygen plasma was used to enclose the channel network by bonding the cured PDMS on a glass slide. After surface activation and bonding, chips were placed in a 65 ºC oven for 5 minutes to cure. 1 mL of Pico-Glide™ solution was flowed through the channel using a syringe. The chip was left at room temperature for 45 minutes up to overnight and this step was repeated using Novec™ 7500. Compressed air was then blown in the inlets to dry the channels. To ensure the reliability of our results, several quality control measures were implemented. The PDMS chips were visually inspected for defects before each use, and new chips were fabricated after every 10 experiments to prevent degradation of channel geometry.

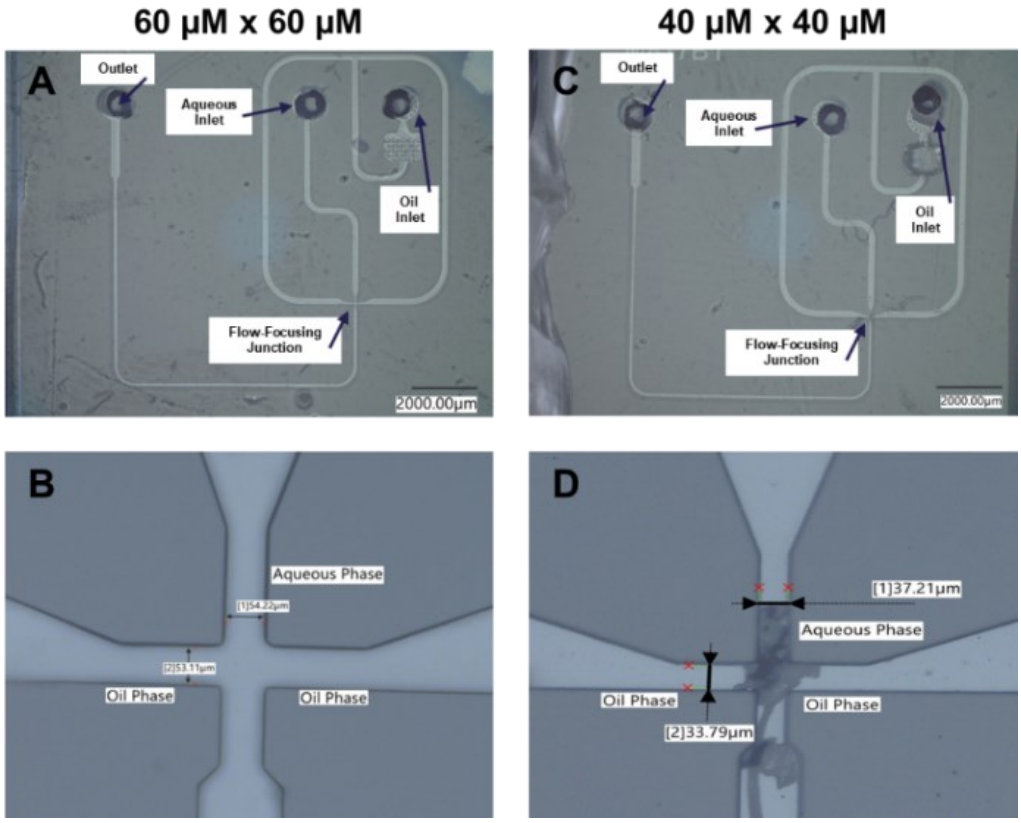

Figure 3.6. PDMS chip dimensions.

3.2.3 Picodroplet Generation Using Picodroplet Technology

Set-up

Solutions of Pico-Surf® surfactant (5%, 2% and 1%) in Novec™ 7500 was used as the oil phase. PBS, Mueller-Hinton broth, Middlebrook 7H9 broth, and minimal cholesterol media were used as the aqueous phase. The oil phase and aqueous phase (inlets) were delivered to a microchip with either a 60 µm x 60 µm flow-focusing channel or a 40 µm x 40 µm flow-focusing channel using silicon tubing with an OD (1 mm) and connected to a compressed air cylinder with regulators. LabView NXG 5 software (National Instruments, Austin, TX, USA) was opened, ready to evaluate droplet formation. The software was used to control the picodroplet generation system and for real-time analysis of droplet formation. The software was configured to capture high-speed images at 1000 frames per second and process them in real-time to measure droplet dimensions and adjust flow rates accordingly.

Picodroplet Generation

After connecting all tubing to the picodroplet technology, the pressure is turned on and the initial inlet pressures are chosen and allowed to equilibrate before starting the data acquisition of measurements. A 60 x objective is focused on the channel where droplets that have been formed are flowing to the outlet. Droplet formation was recorded by a high-speed camera. Desired droplet volumes were imputed, and the feedback-loop initiated changes in the

pressure of the inlets to adjust the droplet volumes. Droplets of sizes 60, 80, 100, 120, and 140 pL were generated using the 40 µm x 40 µm flow-focusing channel PDMS chip. Droplets of sizes 150, 200, 250, 300, 350, 400, and 450 pL were generated using the 60 µm x 60 µm flow-focusing channel PDMS chip. These volumes were selected to cover a range suitable for single-cell encapsulation of bacteria, based on typical bacterial cell sizes (1-5 µm) and the need for sufficient nutrient media around each cell (Smith Kenneth and Kirby James, 2018).For assessing the monodispersity and stability of bacterial culture media on droplet generation, 300 pL sized droplets were chosen.

Droplet Volume Calculation

The average droplet volume (pL), standard deviation (SD), coefficient of variation (CV %), flow rate ratio (aq/oil), and generation speed (droplets/second) was calculated from 25 droplets by the pixel distance along the droplet image against the pixel difference of the background. For each experimental condition, at least three independent replicates were performed on different days to account for day-to-day variability.

Picodroplet Collection and Incubation

Droplets were collected from the outlet using silicon tubing with an outer diameter of 1 mm. The tubing was connected to a 1.5 mL centrifuge tube, and droplets were collected until a visible emulsion of 1cm was collected. The tube was immediately capped after collection to minimize evaporation and contamination. Droplets of varying parameters such as droplet size, aqueous media type, and surfactant concentration was collected for long-term storage in different assay incubation conditions such as at room temperature, in the 37 ºC static incubator, in the 37 ºC shaking incubator (180 rpm), and statically in the 37 ºC anaerobic cabinet. Emulsions generated from different variable were added to PCR tubes before incubation.

3.2.4 Picodroplet Imaging and Droplet Size Quantification

10 µL of each emulsion tested was added into a chamber slide (C-chip, Neubauer Improved, NanoEnTek) and imaged at 0, 24, and 48 hours using an EVOS™ M5000 Imaging System with a 10x objective. Bright field images were taken. Droplets were considered stable if they did not homogenise into separate phases, coalesce, flocculate, or invert phases. The droplet sizes of the emulsions at each time point were assessed using ImageJ with the Hough Circle Transform Plugin. Three representative images of three different fields of view of the emulsion were measured. The Hough Circle Transform Plugin allows for circular objects to be extracted from an image and each radius to be measured, leading to a dataset containing the position and radius of every droplet detected on each image. Briefly, the perimeter of each droplet is found by Process › Find Edges. The threshold is then set, and a mask made by Image > Adjust > Threshold > Apply. Finally, the Hough Circle Transform Plugin was run by manually adjusting the minimum and maximum cutoff for the radii expected in the image. Measurements were

exported as a results table. The measurements exported are: 1) The X and Y coordinates of the centre of each droplet, 2) The radius (in pixels) of each circle, 3) The Hough score for each circle, 4) The number of circles found within that frame, 5) The actual resolution that the transform, and 6) The frame in which the circle was found. The radius (in pixels) was plotted in GraphPad Prism 8 of each droplet on each image to assess and change in droplet size over time.

3.2.5 Data Processing Statistical Analysis

Droplet monodispersity and size distribution were assessed using a function in Microsoft® Excel® for Microsoft 365 MSO (Version 2302 Microsoft Corporation, Redmond, WA, USA).The experimental results for assessing droplet monodispersity and size distribution of different variables are represented by average droplet volume (pL), standard deviation (SD), and coefficient of variation (CV%). For each experimental condition, approximately 2,500 droplets were analysed. To determine the size distribution and stability of collected and incubated droplets, the radius (in pixels) of each droplet identified on each image was plotted over the time course of the experiment. The coefficient of variation (CV%) was used to assess the change in the size variance of the droplets during incubation. The coefficient of variation (CV) was calculated as the standard deviation divided by the mean droplet size, expressed as a percentage. Droplets with a CV < 10% were considered monodisperse, based on established criteria in the field. Statistical analyses and graphing were performed using GraphPad Prism 8 (GraphPad Software, San Diego, CA, USA).

3.3 Results

3.3.1 Generation of Varied Droplet Sizes Using Different Channel Geometries

The picodroplet technology and utility of the image-based closed-loop feedback were assessed to produce monodisperse droplets with PBS as the aqueous phase and 5% Pico-Surf® as the oil phase. To evaluate the efficiency of the feedback mechanism creating droplets of desired sizes different pL sized droplets were imputed into the software and monitored. To form droplets of different volumes, the imaging feedback system changed the flow rates according to the desired droplet volume (pL). Two different PDMS chips with different dimensions were used to create a range in droplet volumes. Smaller droplets of sizes 60, 80, 100, 120, and 140 pL were generated using the 40 µm x 40 µm flow-focusing channel PDMS chip. Larger droplet sizes of 150, 200, 250, 300, 350, 400, and 450 pL were generated using the 60 µm x 60 µm flow-focusing channel PDMS chip. Image snapshots of videos were taken of the droplets being generated (Figure 3.7). Figure 3.7 shows channel images of droplets flowing through the image detection area at different volumes. As the desired droplet volume increased from 60 pL to 140 pL (Panel A) and from 150 pL to 450 pL (Panel B), a clear increase in droplet size is visible. This visual confirmation of size control demonstrates the effectiveness of the feedback system in producing droplets of various desired volumes.

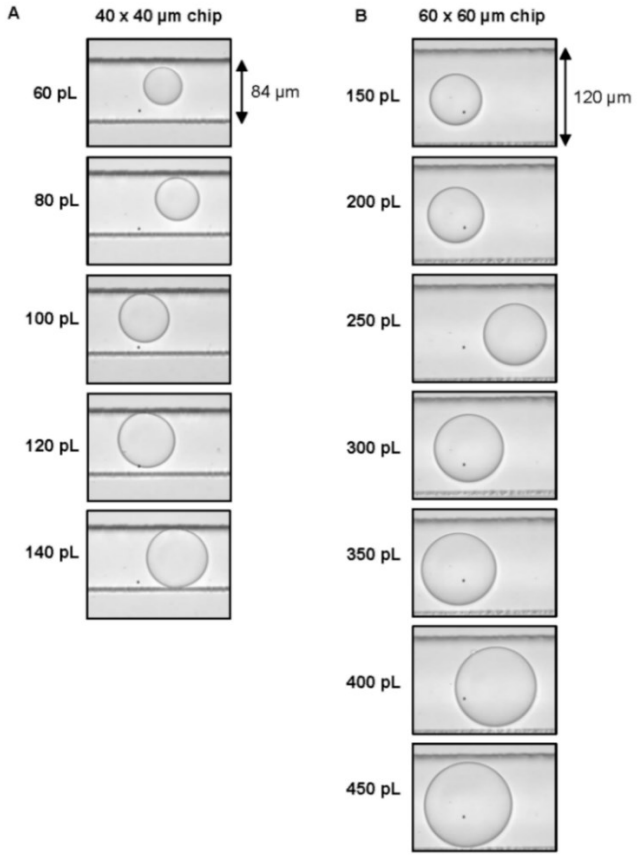

Figure 3.7. Channel image of droplets flowing through image detection area at different droplet volumes. Pico-Surf® concentration used is 5%. Droplets generated in a flow-focusing microfluidic chip **(A)** 40 x 40 µm nozzle and **(B)** 60 x 60 µm nozzle. Droplets increase in pL volume from top to bottom. Black dot is pixel background reference. Pictures are screenshots of saved videos.

3.3.2 Effect of Flow Rate Ratio on Varied Droplet Volumes

To quantify the flow rate ratio (FFR) of each droplet size generated, the pressure value of the aqueous phase was divided by the pressure value of the oil phase from the averaged data of 2,500 droplets. Using this method, the FRR of the aqueous phase and oil phase presented expected results. The FFR calculated showed that when droplet volume (pL) is increased, as does the FRR in both PDMS chip geometries (Figure 3.8). Increasing droplet volumes were plotted against FRRs and previously showed equivalent results (Loizou et al., 2018, Sartipzadeh et al., 2020). This confirmation further gleans information on the accuracy of the feedback-loop at efficiently producing desired droplet volumes through a pressurised system.

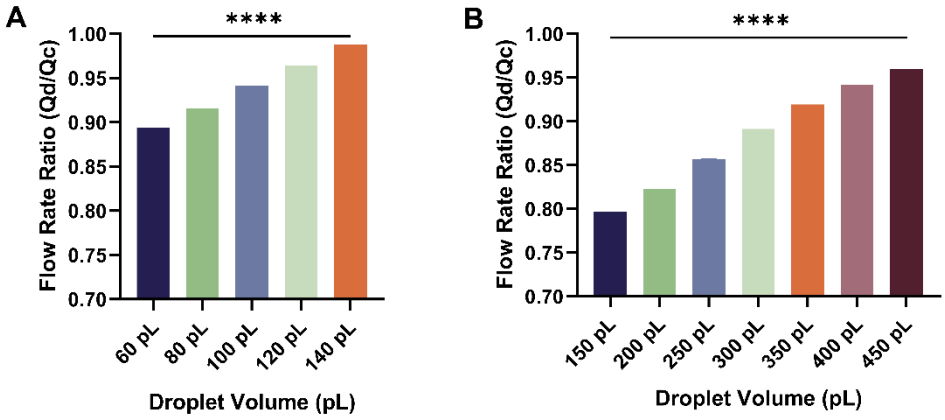

Figure 3.8. Flow rate ratios of increasing droplet size. The flow rate ratio (quotient of the dispersed phase flow rate over the continuous phase flow rate) of each droplet volume imputed by the feedback loop. **(A)** Droplets generated using the 40 x 40 µm flow-focusing junction. **(B)** Droplets generated using the 60 x 60 flow-focusing junction.

3.3.3 Monodispersity of PBS Droplets in Different Channel Geometries

The tight control of droplets generated in microfluidic devices has become pivotal, due to the multifaceted applications in biomedicine. The rationale behind the image-based closed-loop feedback is to achieve real-time control of droplet size during generation. To form droplets of different volumes and to assess the monodispersity of these droplets, the imaging feedback system was used to change flow rates according to the desired droplet volume (pL) and data were collected. Droplets containing PBS as the aqueous phase and 5 % Pico-Surf® as the oil phase were generated using the 40 µm x 40 µm flow-focusing channel for making 60, 80, 100, 120, and 140 pL droplets. The average volume (pL) and standard deviation (SD) of 25 droplets passing through the channel were calculated from the feedback software. Means and standard deviations were plotted for 100 saved time frames. Therefore, data presented below are representing droplet sizes of approximately 2,500 droplets. It is the ability of the high-speed camera to capture these data points for droplets passing through the channel. In addition to droplet size, the variance was recorded for each 25 droplets passing through the channel. Variance was examined by calculating the coefficient of variation (CV) as a percentage.

Examining these data points created droplets which are highly monodisperse. When 60 pL was input into the feedback loop, the system demonstrated high precision in droplet generation. The resulting droplets had a mean volume of 59.99 pL, with a standard deviation of 0.35 pL and a coefficient of variation (CV) of 0.59% (Figure 3.9 A). This CV value is well below the 10% threshold typically used to define monodispersity in microfluidic droplet generation, indicating excellent control over droplet size. Likewise, control of droplet generation was observed for 80 pL (Figure 3.9 B), 100 pL (Figure 3.9 C), 120 pL (Figure 3.9 D), and 140 pL (Figure 3.9 E). The mean values of droplet volumes were 0.01, 0.19, 0.13, 0.35, and 0.29 pL within range to the desired droplet size of 60, 80, 100, 120, and 140 pL, respectively. Across all experiments using the 40 µm x 40 µm flow-focusing channel, droplets demonstrated high monodispersity. Standard deviations remained below 0.7 pL, and coefficients of variation (CV) were consistently below 0.6%. These low CV values indicate exceptional uniformity in droplet size, surpassing the typical threshold of 10% CV used to define monodispersity in microfluidic systems. This high level of control over droplet size is crucial for ensuring consistent conditions in single-cell encapsulation experiments.

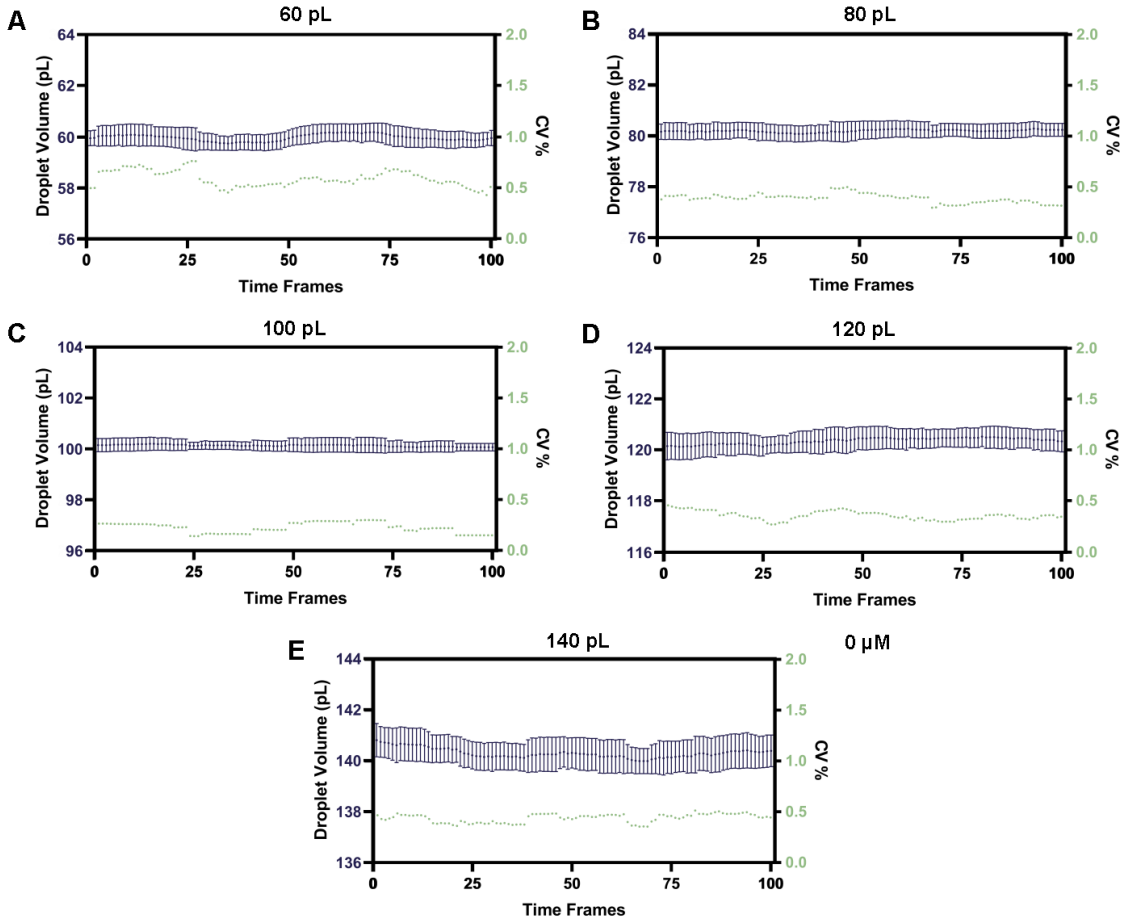

Figure 3.9. Droplet volume monodispersity of PBS containing droplets generated with 5% Pico-Surf and a 40 x 40 µm flow-focusing junction. (A) Feedback loop set at 60 pL. Mean droplet volume 59.99 pL, SD 0.35 pL, CV 0.59%. (B) Feedback loop set at 80 pL. Mean droplet volume 80.19 pL, SD 0.31 pL, CV 0.39%. (C) Feedback loop set at 100 pL. Mean droplet volume 100.13 pL, SD 0.23 pL, CV 0.23%. (D) Feedback loop set at 120 pL. Mean droplet volume 120.35 pL, SD 0.43 pL, CV 0.35%. (E) Feedback loop set at 140 pL. Mean droplet volume 140.29 pL, SD 0.61 pL, CV 0.44%. The average droplet volume (pL), standard deviation (SD) and coefficient of variation (CV %) of n=25 droplets are plotted for 100 saved frames. Each graph represents 1 of 3 repeats of 100 saved time frames.

As shown in the previous section, monodisperse droplets were efficiently produced at small volumes with the 40 μm x 40 μm flow-focusing channel. Larger droplets were next evaluated by swapping the PDMS chip to the 60 μm x 60 μm flow-focusing channel. Using the same aqueous and oil phase as before, desired droplets volumes ranging from 150-450 pL were imputed into the feedback system and variance measured. When 150 pL was imputed into the feedback loop, the flow rates of the inlets changed accordingly to generate 150 pL droplets with a mean of 149.90 pL, SD of 1.05 pL, and CV value of 0.7% (Figure 3.10 A). Similarly, control of droplet generation was observed for 200 pL (Figure 3.10 B), 250 pL (Figure 3.10 C), 300 pL (Figure 3.10 D), 350 pL (Figure 3.10 E), 400 pL (Figure 3.10 F), and 450 pL (Figure 3.10 G). The mean values of droplet volumes were 0.1, 0.07, 0.1, 0.12, 0.03, 0.33, and 0.02 pL within range to the desired droplet size of 150, 200, 250, 300, 350, 400, and 450 pL, respectively. In all experiments generating droplets with the 60 μm x 60 μm flow-focusing channel, the standard deviations were below 1.5 pL and the coefficient of variations were below 0.71 %. Again, when changing the desired droplet size into the feedback software, highly ultra-monodisperse droplets are generated. It is worth noting that when a chosen droplet size is increased, the variance in droplet size decreases from 0.70-0.24% CV.

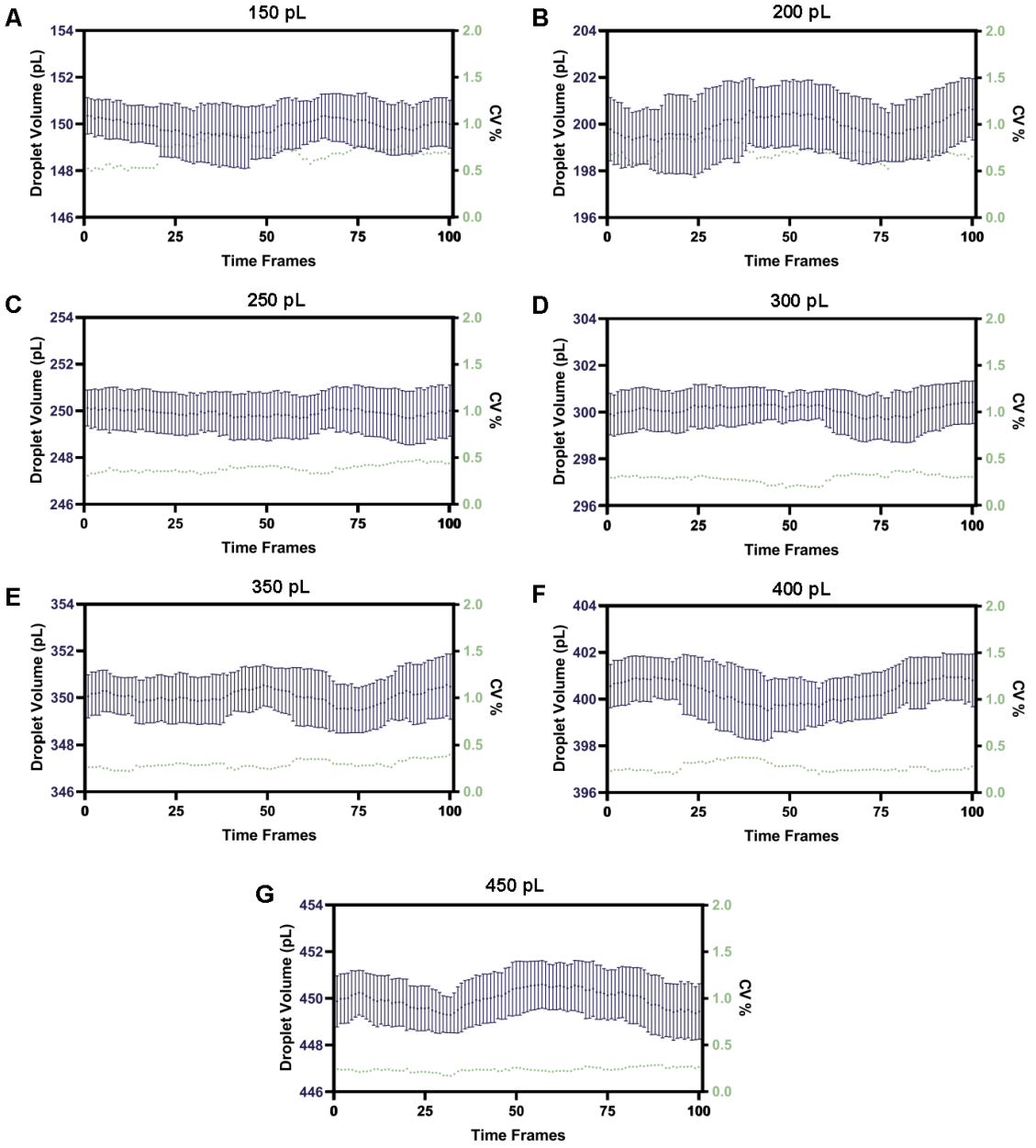

Figure 3.10. Droplet volume monodispersity of PBS containing droplets generated with 5% Pico-Surf and a 60 x 60 µm flow-focusing junction. (A) Feedback loop set at 150 pL. Mean droplet volume 149.90 pL, SD 1.05 pL, CV 0.70%. **(B)** Feedback loop set at 200 pL. Mean droplet volume 199.93 pL, SD 1.41 pL, CV 0.71%. **(C)** Feedback loop set at 250 pL. Mean droplet volume 249.90 pL, SD 0.96 pL, CV 0.39%. **(D)** Feedback loop set at 300 pL. Mean droplet volume 300.12 pL, SD 0.87 pL, CV 0.29%. **(E)** Feedback loop set at 350 pL. Mean droplet volume 350.03 pL, SD 1.03 pL, CV 0.30%. **(F)** Feedback loop set at 400 pL. Mean droplet volume 400.33 pL, SD 1.09 pL, CV 0.28%. **(G)** Feedback loop set at 450 pL. Mean droplet volume 449.98 pL, SD 1.07 pL, CV 0.24%. The average droplet volume (pL), standard deviation (SD) and coefficient of variation (CV %) of n=25 droplets are plotted for 100 saved frames. Each graph represents 1 of 3 repeats of 100 saved time frames.

3.3.4 Monodispersity and Stability of Droplets with Bacterial Culture Media

The ability to generate highly uniform structures has rendered droplet-based microfluidics as a promising tool for antibiotic susceptibility testing. As the need to generate uniform droplets in a controlled manner is the motivation for assessing antimicrobial susceptibility against bacteria in droplets, the monodispersity and stability of droplets were assessed when generating droplets with common bacterial culture media. When growing bacterial species in culture, nutrients are required to help cells proliferate in standard microbiology practices. Growth is successful with the use of culture media. Generally, most studies looking at the uniformity and stability of droplets have been conducted using only water as the aqueous phase. As the application of droplet microfluidics is expanding to the biological field, it is suitable to examine the effects of using microbiology culture media as the aqueous phase in droplet experimental designs. Culturing media for mycobacteria is of particular concern due to the hydrophobic nature of the mycobacterial cell wall, detergents such as TWEEN®80 and tyloxapol are added to culture media to disperse the bacteria. It is thought that these detergents may interfere with the surfactant and destabilise the droplets. To characterise if monodisperse droplets can be produced with microbiology culture media, 300 pL droplets were generated with 5% Pico-Surf® and either PBS as the control, Mueller-Hinton broth (MH), Middlebrook 7H9 broth (7H9), and minimal cholesterol media (MCM). The data were presented the same as before. As can be understood from the graphs in Figure 3.11, the capability to make monodisperse droplets with all culture media types was successful under these conditions. The mean values of droplet volumes for PBS, MH, 7H9, and MCM aqueous phases were 0.19, 0.14, 0.16, and 0.14 pL, respectively, within range of the desired droplet size of 300 pL. In all experiments generating droplets with 5% Pico-Surf® and bacterial culturing media, the standard deviations were below 0.98 pL and the coefficient of variations were below 0.33 %. These results suggest that diverse types of bacterial culture media are equally qualified to produce droplets of low variation and further promote the utility of the feedback software.

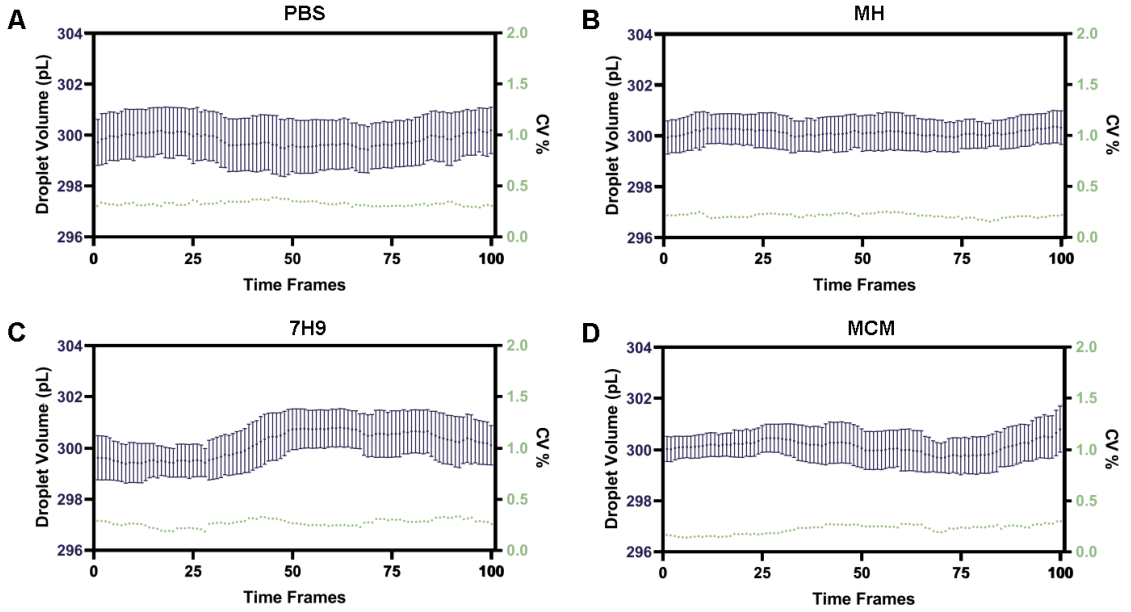

Figure 3.11. Droplet volume monodispersity of 300 pL droplets generated with 5% Pico-Surf and bacterial culture media. (A) 300 pL droplets generated with PBS as the aqueous phase. Mean droplet volume 299.81 pL, SD 0.98 pL, CV 0.33%. **(B)** 300 pL droplets generated with MH media as the aqueous phase. Mean droplet volume 300.14 pL, SD 0.64 pL, CV 0.21%. **(C)** 300 pL droplets generated with 7H9 media as the aqueous phase. Mean droplet volume 300.16 pL, SD 0.81 pL, CV 0.27%. **(D)** 300 pL droplets generated with MCM media as the aqueous phase. Mean droplet volume 300.14 pL, SD 0.67 pL, CV 0.22%. The average droplet volume (pL), standard deviation (SD) and coefficient of variation (CV %) of n=25 droplets are plotted for 100 saved frames. Each graph represents 1 of 3 repeats of 100 saved time frames.

However, when studying the physical phenomena of droplet stability during temperature incubations, the results are less promising. The optimal temperature for the growth of most bacterial pathogens is 37ºC due to the human body maintaining the same core temperature. When bacterial cultures are incubated at this temperature, they can grow and happily divide. Other optimal conditions for culturing include shaking an inoculated culture during growth. This allows enough oxygen to enter the culture flask and increases the surface-to-oxygen ratio. In some cases, bacterial species grow under anaerobic conditions. Examples of invading human pathogens which thrive under hypoxia are ones which live in human tissue, which is injured and does not have oxygen-rich blood flowing to it. When designing new drug screening assays for bacterial pathogens, it is important to design assays which can undergo various culturing conditions.

An image-based approach was chosen to analyse droplet stability. Droplets which were generated with PBS, MH, 7H9, and MCM aqueous phases were collected in centrifuge tubes as an emulsion for stability investigations. Once each sample was collected, the emulsion generated was split into four 100 µL centrifuge tubes. Each sample was either incubated aerobically at room temperature, aerobically in the static 37ºC incubator, aerobically in the shaking 37ºC incubator (180 rpm), or anaerobically in the static 37ºC incubator. Emulsions were stored in these conditions for 48 hours and imaged at time points 0, 24, and 48 hours.

The images of the emulsions in each condition over time are illustrated in Figures 3.12, 3.13, 3.14, and 3.15. Each image was quantified using image analysis software and presented with scatter plots representing each droplet radius in pixels. The mean and standard deviation of the radius (pixels) are plotted with droplets from 3 representative images. From this, variance was calculated in the form of CV to measure the stability of the emulsion over time. If the CV was<10%, droplets were concluded as monodisperse and stable.

For droplets generated with 5% Pico-Surf™, the PBS control emulsion, as expected, remained stable in all incubation conditions (Figure 3.12). Fitting the data with scatter plots, droplets remain the same size and no not coalesce when incubated over time. In each culture condition, droplets created with PBS as the aqueous phase contain low variance for each experiment with <4.5% CV. Likewise, when droplets are set up with MH broth as the aqueous phase, stability is witnessed for the full 48 hours, with the largest variance level of 5.84% CV (Figure 3.13). MH broth's stability appeared to be unaffected by the elevated temperatures.

No stability was maintained during emulsion incubation at 37ºC with 7H9 broth as the aqueous phase in contrast to the room temperature control. Droplets remained monodisperse at the first time point image, however, as the incubation time increased, droplets coalesced at 37ºC in the static, shaking, and anaerobic incubator (Figure 3.14). Interestingly, emulsions formed with Minimal Cholesterol Media (MCM) as the aqueous phase demonstrated unexpected stability. As shown in Figure 3.15, these emulsions remained stable under most conditions, except for those incubated in the anaerobic cabinet for 48 hours. This stability was surprising given the presence of cholesterol and tyloxapol in MCM, which could potentially interfere with the surfactant layer. The observed stability might be due to the specific composition of MCM, possibly creating a more favourable interface with the oil phase. However, the destabilization under anaerobic conditions after 48 hours suggests that oxygen availability may play a role in long-term emulsion stability, perhaps by affecting the surfactant's performance or the media's properties.

In summary, our results demonstrate that the picodroplet technology can successfully generate monodisperse droplets with various bacterial culture media. However, the stability of these droplets varies significantly depending on the media composition and incubation conditions. PBS and MH media consistently produced stable droplets, while 7H9 media showed poor stability at 37°C. These findings highlight the importance of optimizing droplet composition for specific bacterial culture conditions, particularly for challenging organisms like mycobacteria.

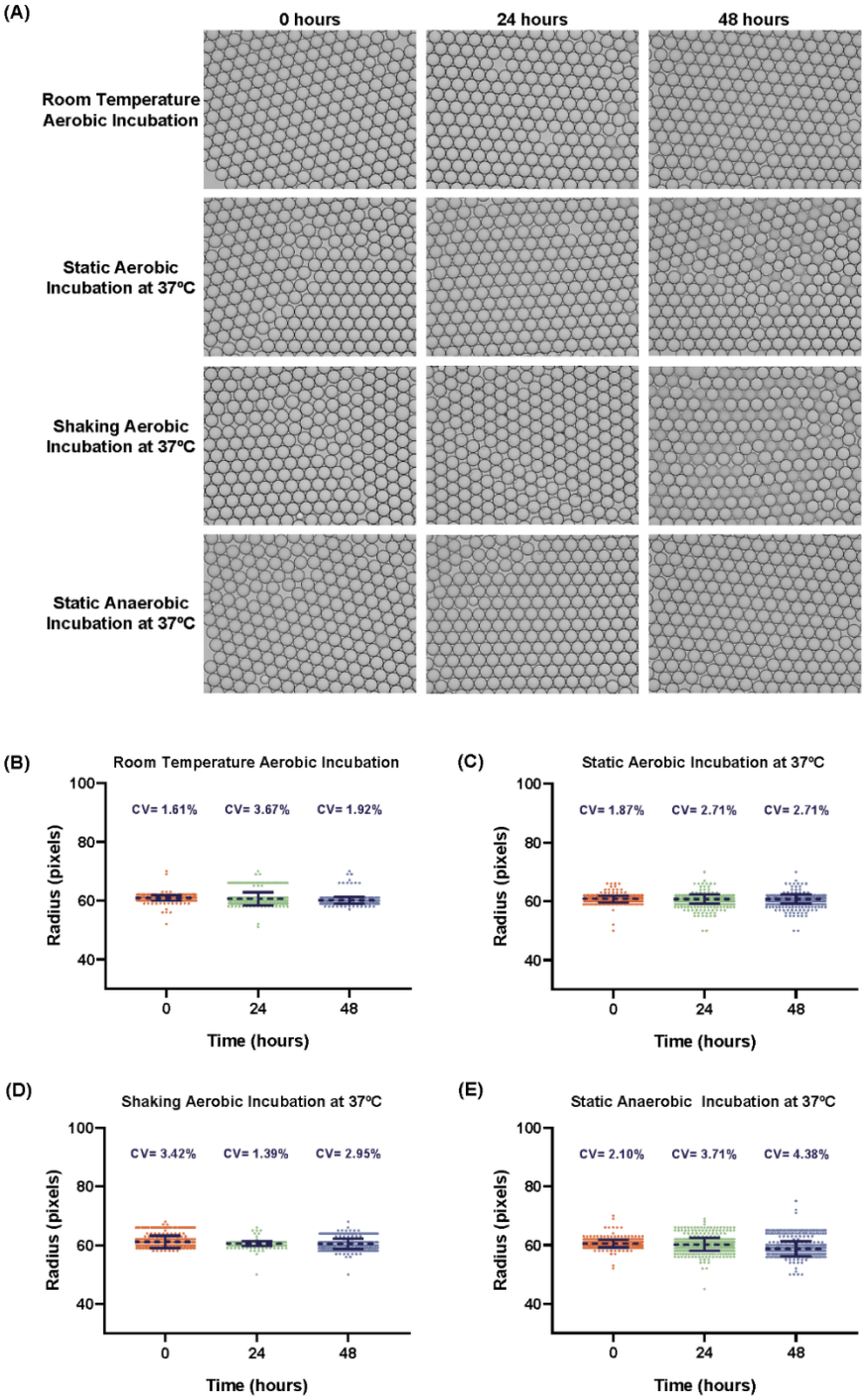

Figure 3.12. Droplet stability over 48 hours for droplets generated with 5% PS and PBS. Each scatter plot illustrates the variance in droplet size over time of an emulsion in different incubation conditions. **(A)** Images of droplets in different incubation conditions at 0, 24, and 48 hours. **(B)** Droplets incubated at room temperature aerobically for 48 hours. Mean= 61 pixels, SD= 1 pixels, CV= 1.61%, n= 658 droplets at 0 hours. Mean = 61 pixels, SD= 2 pixels, CV= 3.67%, n= 666 droplets at 24 hours. Mean = 60 pixels, SD= 1 pixels, CV= 1.92%, n= 660 droplets at 48 hours. **(C)** Droplets incubated at 37ºC in the static incubator aerobically for 48 hours. Mean = 61 pixels, SD= 1 pixels, CV= 1.87%, n= 630 droplets at 0 hours. Mean = 61 pixels, SD= 2 pixels, CV= 2.71%, n= 613 droplets at 24 hours. Mean = 61 pixels, SD= 2 pixels, CV= 2.71%, n= 613 droplets at 48 hours. **(D)** Droplets incubated at 37ºC in the shaking incubator aerobically for 48 hours. Mean = 61 pixels, SD= 2 pixels, CV= 3.41%, n= 624 droplets at 0 hours. Mean = 61 pixels, SD= 1 pixels, CV= 1.391%, n= 649 droplets at 24 hours. Mean = 60 pixels, SD= 2 pixels, CV= 2.95%, n= 637 droplets at 48 hours. **(E)** Droplets incubated at 37ºC in the static incubator anaerobically for 48 hours. Mean = 60 pixels, SD= 1 pixels, CV= 2.10%, n= 645 droplets at 0 hours. Mean = 60 pixels, SD= 2 pixels, CV= 3.7%, n= 682 droplets at 24 hours. Mean = 59 pixels, SD= 3 pixels, CV= 4.38%, n= 682 droplets at 48 hours. Data for each time point is from three representative images of different fields of view of the emulsion. Each data point represents the radius (pixels) of an individual droplet in an image. Dotted line is the mean and error bars show the standard deviation of droplet size.

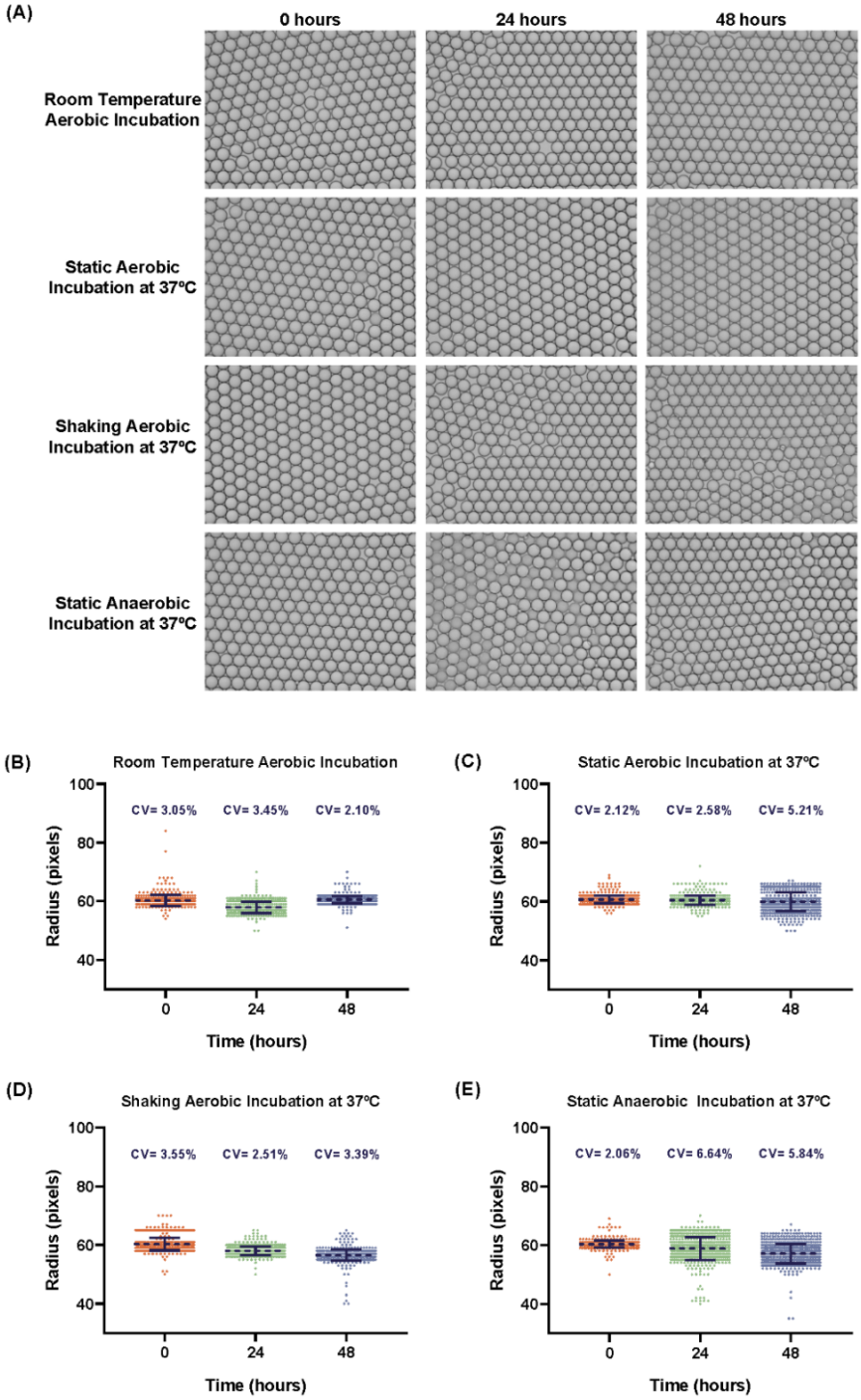

Figure 3.13. Droplet stability over 48 hours for droplets generated with 5% PS and MH media. Each scatter plot illustrates the variance in droplet size over time of an emulsion in different incubation conditions. **(A)** Images of droplets in different incubation conditions at 0, 24, and 48 hours. **(B)** Droplets incubated at room temperature aerobically for 48 hours. Mean = 60 pixels, SD= 2 pixels, CV= 3.04%, n= 621 droplets at 0 hours. Mean = 58 pixels, SD= 2 pixels, CV= 3.45%, n= 693 droplets at 24 hours. Mean = 61 pixels, SD= 1 pixels, CV= 2.1%, n= 642 droplets at 48 hours. **(C)** Droplets incubated at 37ºC in the static incubator aerobically for 48 hours. Mean = 61 pixels, SD= 1 pixels, CV= 2.12%, n= 629 droplets at 0 hours. Mean = 60 pixels, SD= 2 pixels, CV= 2.58%, n= 638 droplets at 24 hours. Mean = 60 pixels, SD= 3 pixels, CV= 5.2%, n= 658 droplets at 48 hours. **(D)** Droplets incubated at 37ºC in the shaking incubator aerobically for 48 hours. Mean = 60 pixels, SD= 2 pixels, CV= 3.55%, n= 672 droplets at 0 hours. Mean = 58 pixels, SD= 1 pixels, CV= 2.51%, n= 693 droplets at 24 hours. Mean = 57 pixels, SD= 2 pixels, CV= 3.39%, n= 726 droplets at 48 hours. **(E)** Droplets incubated at 37ºC in the static incubator anaerobically for 48 hours. Mean = 60 pixels, SD= 1 pixels, CV= 2.06%, n= 663 droplets at 0 hours. Mean = 59 pixels, SD= 4 pixels, CV= 6.64%, n= 680 droplets at 24 hours. Mean = 57 pixels, SD= 3 pixels, CV= 5.84%, n= 709 droplets at 48 hours. Data for each time point is from three representative images of different fields of view of the emulsion. Each data point represents the radius (pixels) of an individual droplet in an image. Dotted line is the mean and error bars show the standard deviation of droplet size.

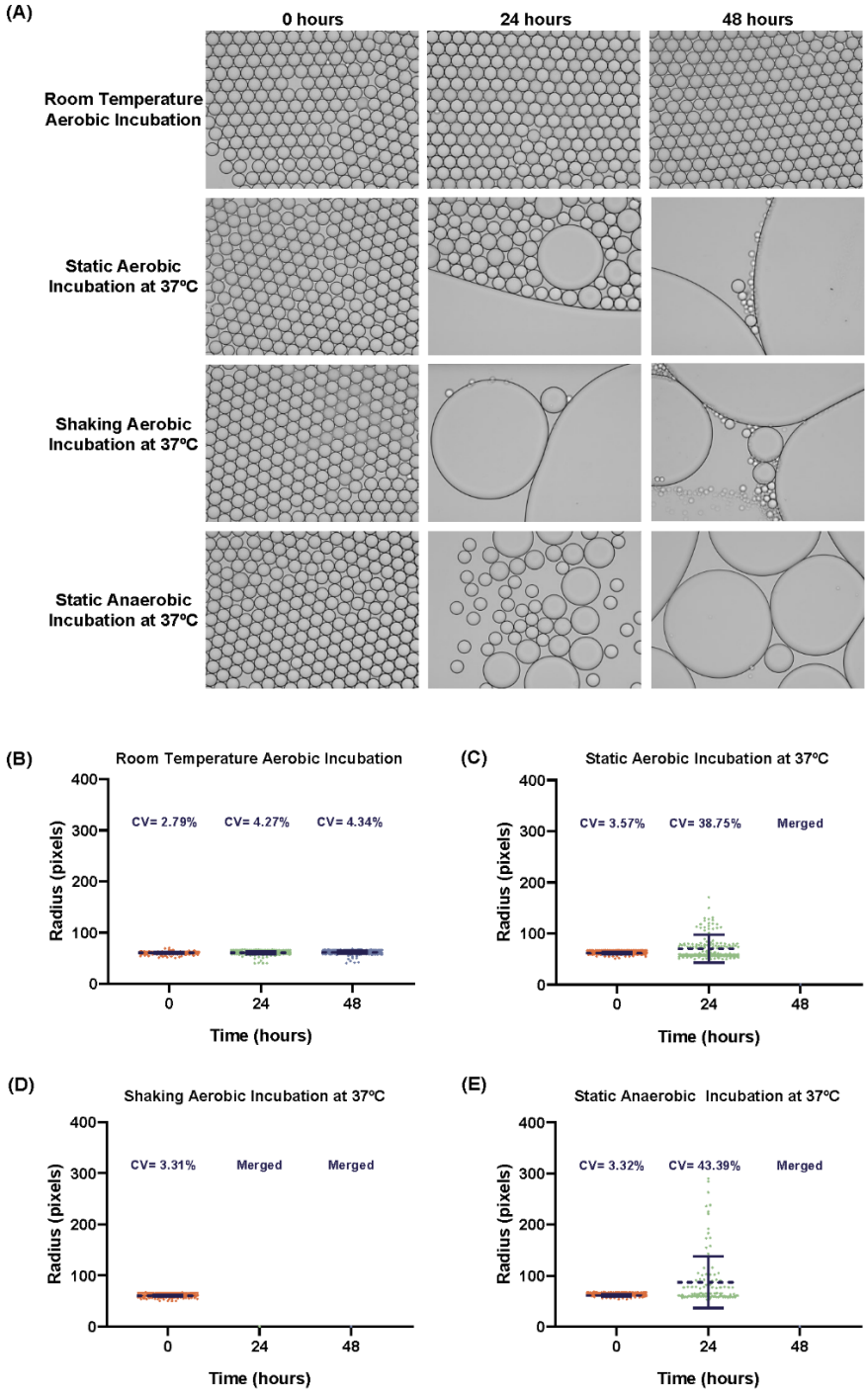

Figure 3.14. Droplet stability over 48 hours for droplets generated with 5% PS and 7H9 media. Each scatter plot illustrates the variance in droplet size over time of an emulsion in different incubation conditions. **(A)** Images of droplets in different incubation conditions at 0, 24, and 48 hours. **(B)** Droplets incubated at room temperature aerobically for 48 hours. Mean = 60 pixels, SD= 2 pixels, CV= 2.79%, n= 624 droplets at 0 hours. Mean = 61 pixels, SD= 3 pixels, CV= 4.27%, n= 650 droplets at 24 hours. Mean = 61 pixels, SD= 3 pixels, CV= 4.34%, n= 607 droplets at 48 hours. **(C)** Droplets incubated at 37ºC in the static incubator aerobically for 48 hours. Mean = 61 pixels, SD= 2 pixels, CV= 3.57%, n= 623 droplets at 0 hours. Mean = 70 pixels, SD= 27 pixels, CV= 38.75%, n= 193 droplets at 24 hours. Droplets at 48 hours had merged completely. **(D)** Droplets incubated at 37ºC in the shaking incubator aerobically for 48 hours. Mean = 60 pixels, SD= 2 pixels, CV= 3.31%, n= 638 droplets at 0 hours. Droplets had completely merged at 24 and 48 hours. **(E)** Droplets incubated at 37ºC in the static incubator anaerobically for 48 hours. Mean = 62 pixels, SD= 2 pixels, CV= 3.32%, n= 641 droplets at 0 hours. Mean = 87 pixels, SD= 38 pixels, CV= 43.39%, n= 119 droplets at 24 hours. Droplets at 48 hours had merged completely. Data for each time point is from three representative images of different fields of view of the emulsion. Each data point represents the radius (pixels) of an individual droplet in an image. Dotted line is the mean and error bars show the standard deviation of droplet size.

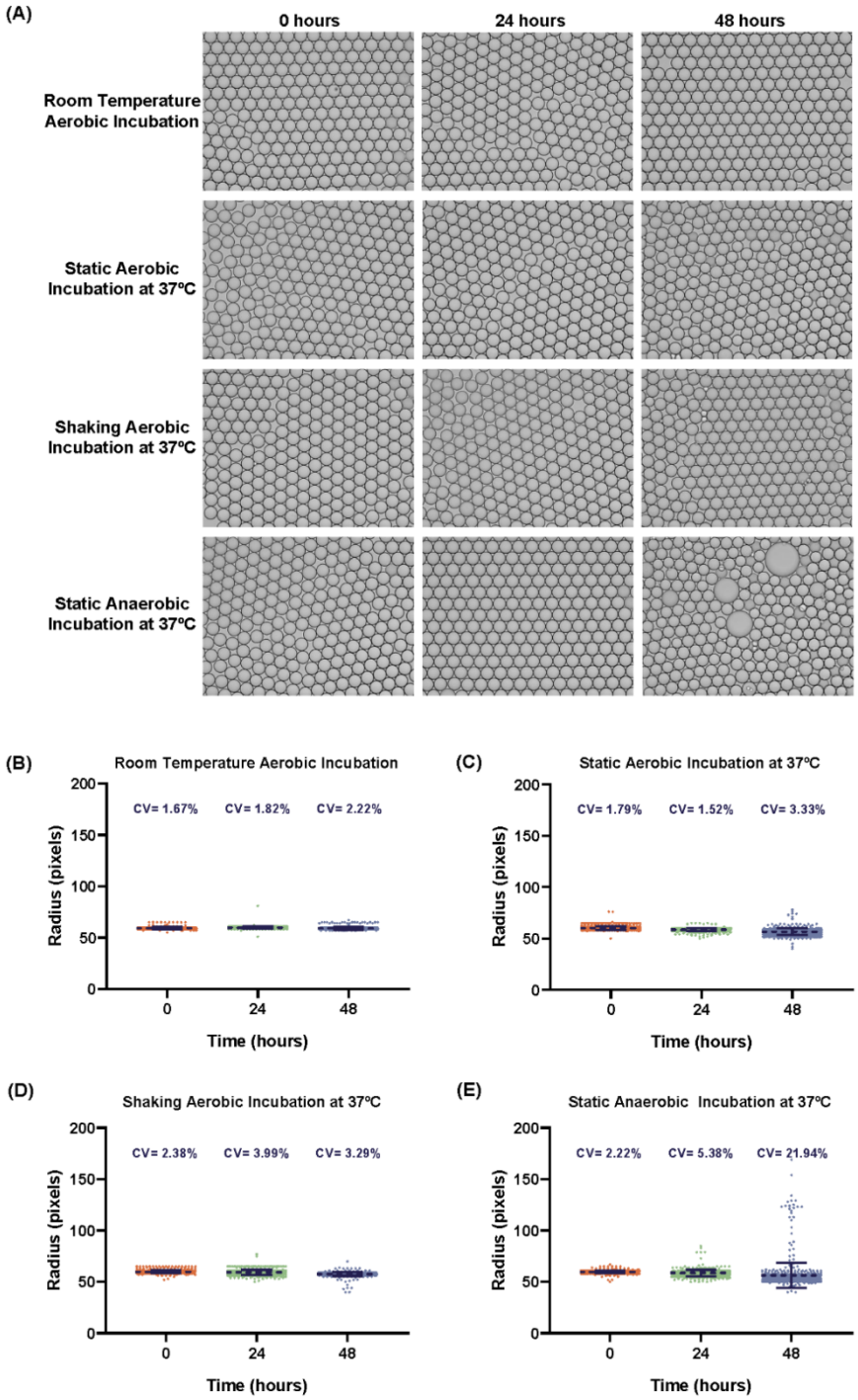

Figure 3.15. Droplet stability over 48 hours for droplets generated with 5% PS and MCM media. Each scatter plot illustrates the variance in droplet size over time of an emulsion in different incubation conditions. **(A)** Images of droplets in different incubation conditions at 0, 24, and 48 hours. **(B)** Droplets incubated at room temperature aerobically for 48 hours. Mean = 59 pixels, SD= 1 pixels, CV= 1.67%, n= 657 droplets at 0 hours. Mean = 60 pixels, SD= 1 pixels, CV= 1.82%, n= 658 droplets at 24 hours. Mean = 59 pixels, SD= 1 pixels, CV= 2.22%, n= 679 droplets at 48 hours. **(C)** Droplets incubated at 37ºC in the static incubator aerobically for 48 hours. Mean = 60 pixels, SD= 2 pixels, CV= 2.98%, n= 648 droplets at 0 hours. Mean = 59 pixels, SD= 2 pixels, CV= 2.57%, n= 632 droplets at 24 hours. Mean = 57 pixels, SD= 3 pixels, CV= 5.87%, n= 707 droplets at 48 hours. **(D)** Droplets incubated at 37ºC in the shaking incubator aerobically for 48 hours. Mean = 60 pixels, SD= 1 pixels, CV= 2.38%, n= 617 droplets at 0 hours. Mean = 59 pixels, SD= 2 pixels, CV= 3.99%, n= 665 droplets at 24 hours. Mean = 57 pixels, SD= 2 pixels, CV= 3.29%, n= 709 droplets at 48 hours. **(E)** Droplets incubated at 37ºC in the static incubator anaerobically for 48 hours. Mean = 60 pixels, SD= 1 pixels, CV= 2.22%, n= 634 droplets at 0 hours. Mean = 59 pixels, SD= 3 pixels, CV= 5.38%, n= 671 droplets at 24 hours. Mean = 56 pixels, SD= 12 pixels, CV= 21.95%, n= 754 droplets at 48 hours. Data for each time point is from three representative images of different fields of view of the emulsion. Each data point represents the radius (pixels) of an individual droplet in an image. Dotted line is the mean and error bars show the standard deviation of droplet size.

3.3.5 Effect of Surfactant Concentration on Droplet Stability

The concentration of surfactant can influence droplet stability and monodispersity. To assess surfactant concentration and to test if decreasing the surfactant concentration can help stability with droplets generated with mycobacterial culture media, stability experiments were set up the same as before but with 2% Pico-Surf® as the oil phase. Initially, the picodroplet technology was used to generate 300 pL droplets with 2% Pico-Surf® and distinct types of culture media. Convincing evidence that 2% Pico-Surf® could make monodisperse droplets with all culture media types is presented in Figure 3.16. The mean values of droplet volumes for PBS, 7H9, and MCM aqueous phases were 0.46, 0.49, and 0.41 pL respectively within range of the desired droplet size of 300 pL. In all experiments generating droplets with 2% Pico-Surf® and bacterial culturing media, the standard deviations were below 1.07 pL and the coefficient of variations were below 0.36 %. These results suggest that mycobacterial culture media as well as PBS are still qualified to produce droplets of low variation when the surfactant concentration is reduced to 2%. Conversely, although generating droplets qualified for monodispersity, when incubated in culturing conditions, stability was poor for droplets created with mycobacterial culture media. As previously demonstrated, droplets generated with 7H9 broth remained monodisperse at the first time point image. However, as the incubation time increased, droplets coalesced at 37ºC in the static, shaking, and anaerobic incubator (Figure 3.18). The only samples which presented destabilisation for PBS (Figure 3.17) or MCM (Figure 3.19) containing droplets with 2% Pico-Surf® were anaerobic conditions at 48 hours and 24 and 48 hours, respectively.

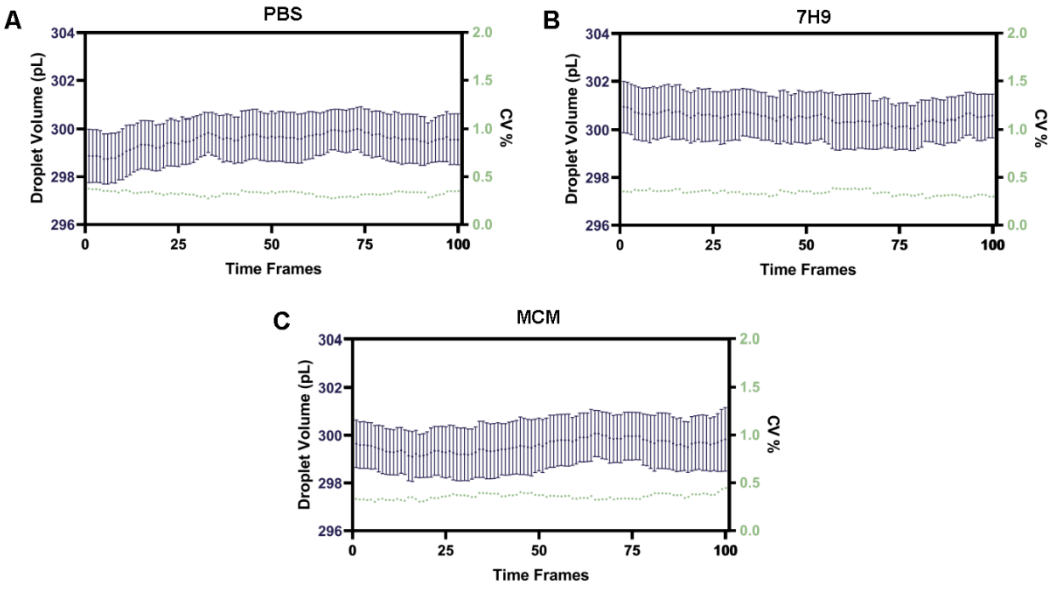

Figure 3.16. Droplet volume monodispersity of 300 pL droplets generated with 2% Pico-Surf™ and mycobacteria culture media. (A) 300 pL droplets generated with PBS as the aqueous phase. Mean droplet volume 299.54 pL, SD 0.98 pL, CV 0.33%. **(B)** 300 pL droplets generated with 7H9 media as the aqueous phase. Mean droplet volume 300.49 pL, SD 1.02 pL, CV 0.34%. **(C)** 300 pL droplets generated with cholesterol media as the aqueous phase. Mean droplet volume 299.59 pL, SD 1.07 pL, CV 0.36%. The average droplet volume (pL), standard deviation (SD) and coefficient of variation (CV %) of n=25 droplets are plotted for 100 saved frames. Each graph represents 1 of 3 repeats of 100 saved time frames.

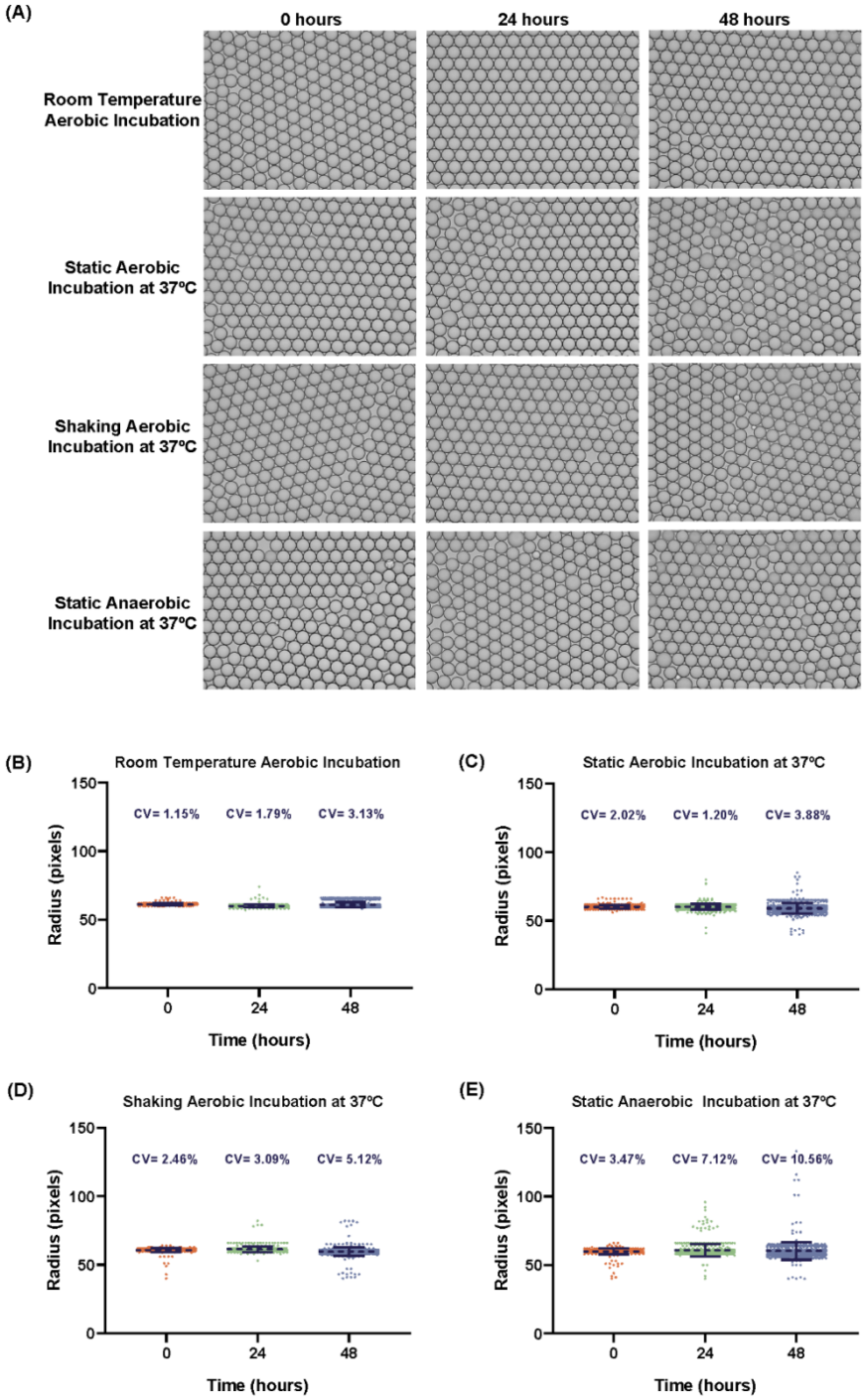

Figure 3.17. Droplet stability over 48 hours for droplets generated with 2% PS and PBS media. Each scatter plot illustrates the variance in droplet size over time of an emulsion in different incubation conditions. **(A)** Images of droplets in different incubation conditions at 0, 24, and 48 hours. **(B)** Droplets incubated at room temperature aerobically for 48 hours. Mean = 61 pixels, SD= 1 pixels, CV= 1.15%, n= 648 droplets at 0 hours. Mean = 60 pixels, SD= 1 pixels, CV= 1.79%, n= 662 droplets at 24 hours. Mean = 61 pixels, SD= 2 pixels, CV= 3.13%, n= 632 droplets at 48 hours. **(C)** Droplets incubated at 37ºC in the static incubator aerobically for 48 hours. Mean = 60 pixels, SD= 1 pixels, CV= 2.02%, n= 641 droplets at 0 hours. Mean = 60 pixels, SD= 2 pixels, CV= 3.32%, n= 645 droplets at 24 hours. Mean = 59 pixels, SD= 4 pixels, CV= 6.56%, n= 664 droplets at 48 hours. **(D)** Droplets incubated at 37ºC in the shaking incubator aerobically for 48 hours. Mean = 61 pixels, SD= 1 pixels, CV= 2.46%, n= 644 droplets at 0 hours. Mean = 61 pixels, SD= 2 pixels, CV= 3.09%, n= 636 droplets at 24 hours. Mean = 60 pixels, SD= 3 pixels, CV= 5.12%, n= 870 droplets at 48 hours. **(E)** Droplets incubated at 37ºC in the static incubator anaerobically for 48 hours. Mean = 60 pixels, SD= 2 pixels, CV= 3.47%, n= 641 droplets at 0 hours. Mean = 61 pixels, SD= 4 pixels, CV= 7.12%, n= 643 droplets at 24 hours. Mean = 60 pixels, SD= 6 pixels, CV= 10.58%, n= 656 droplets at 48 hours. Data for each time point is from three representative images of different fields of view of the emulsion. Each data point represents the radius (pixels) of an individual droplet in an image. Dotted line is the mean and error bars show the standard deviation of droplet size.

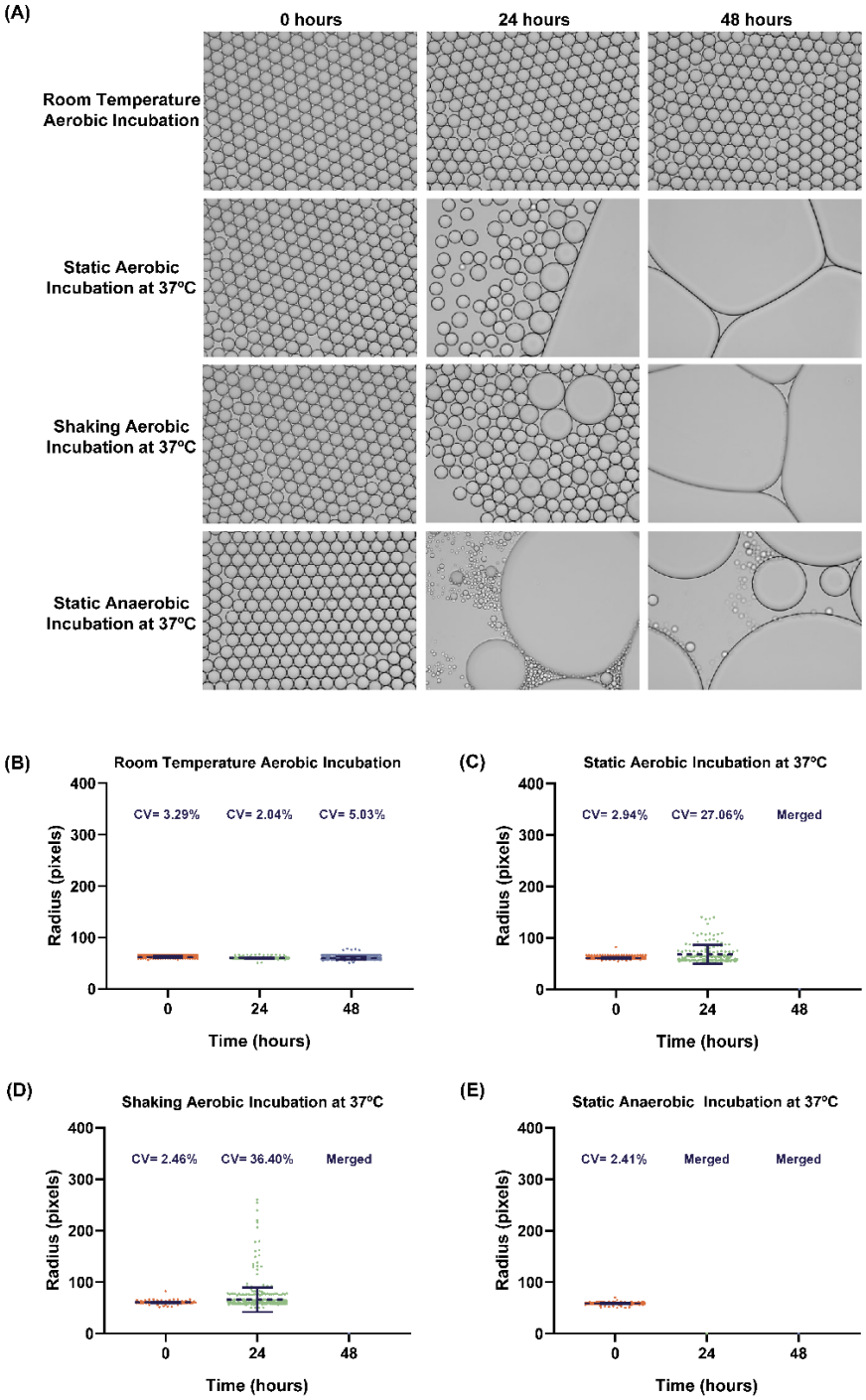

Figure 3.18. Droplet stability over 48 hours for droplets generated with 2% PS and 7H9 media. Each scatter plot illustrates the variance in droplet size over time of an emulsion in different incubation conditions. **(A)** Images of droplets in different incubation conditions at 0, 24, and 48 hours. **(B)** Droplets incubated at room temperature aerobically for 48 hours. Mean = 62 pixels, SD= 2 pixels, CV= 3.29%, n= 644 droplets at 0 hours. Mean = 60 pixels, SD= 1 pixels, CV= 2.04%, n= 656 droplets at 24 hours. Mean = 60 pixels, SD= 3 pixels, CV= 5.03%, n= 642 droplets at 48 hours. **(C)** Droplets incubated at 37ºC in the static incubator aerobically for 48 hours. Mean = 61 pixels, SD= 2 pixels, CV= 2.94%, n= 639 droplets at 0 hours. Mean = 68 pixels, SD= 18 pixels, CV= 27.06%, n= 172 droplets at 24 hours. Droplets at 48 hours had merged completely. **(D)** Droplets incubated at 37ºC in the shaking incubator aerobically for 48 hours. Mean = 60 pixels, SD= 1 pixels, CV= 2.46%, n= 636 droplets at 0 hours. Mean = 66 pixels, SD= 24 pixels, CV= 36.41%, n= 503 droplets at 24 hours. Droplets at 48 hours had merged completely. **(E)** Droplets incubated at 37ºC in the static incubator anaerobically for 48 hours. Mean = 59 pixels, SD= 1 pixels, CV= 2.41%, n= 645 droplets at 0 hours. Droplets at 24 and 48 hours had merged completely. Data for each time point is from three representative images of different fields of view of the emulsion. Each data point represents the radius (pixels) of an individual droplet in an image. Dotted line is the mean and error bars show the standard deviation of droplet size.

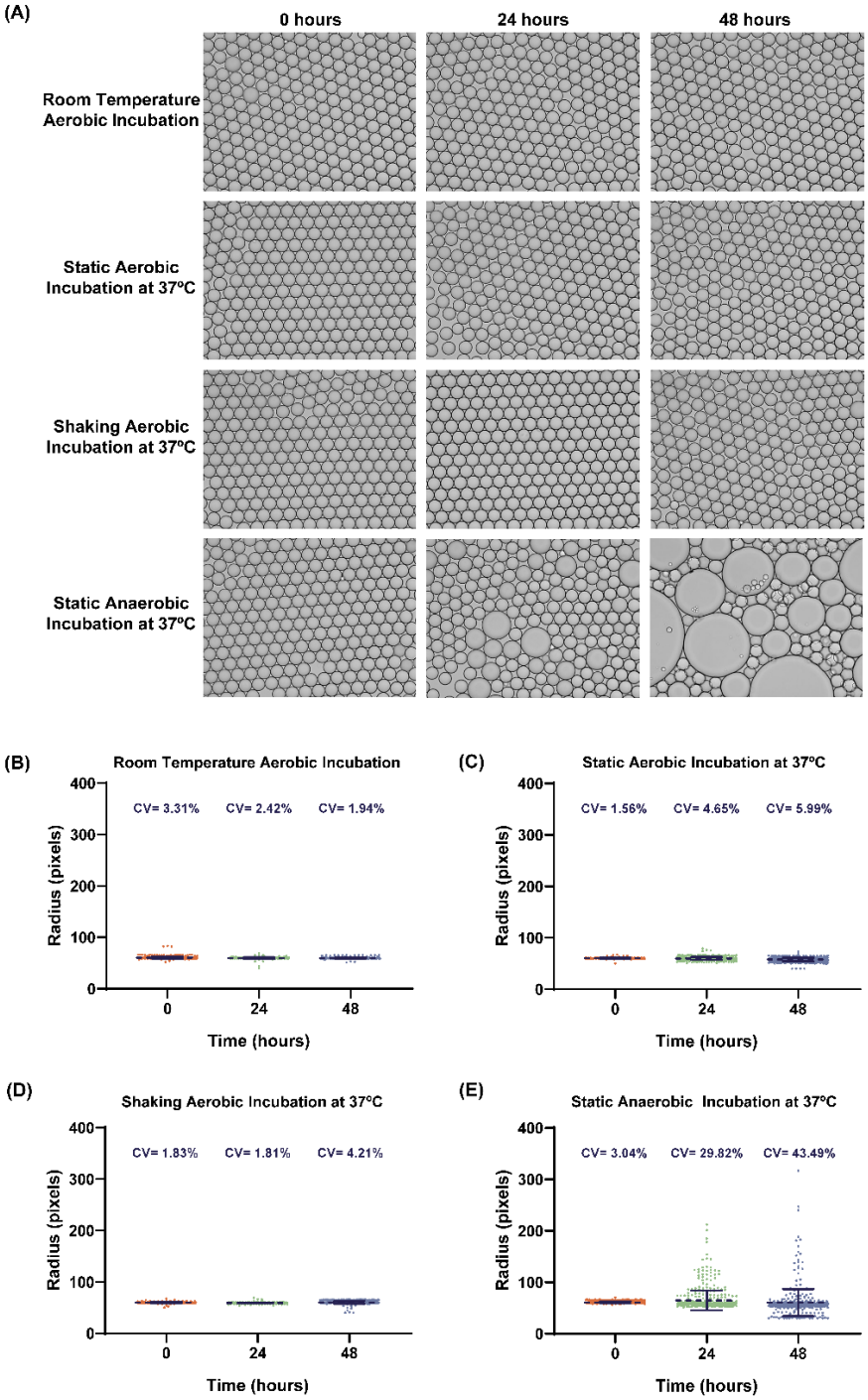

Figure 3.19. Droplet stability over 48 hours for droplets generated with 2% PS and MCM media. Each scatter plot illustrates the variance in droplet size over time of an emulsion in different incubation conditions. **(A)** Images of droplets in different incubation conditions at 0, 24, and 48 hours. **(B)** Droplets incubated at room temperature aerobically for 48 hours. Mean = 60 pixels, SD= 2 pixels, CV= 3.31%, n= 657 droplets at 0 hours. Mean = 60 pixels, SD= 1 pixels, CV= 2.42%, n= 641 droplets at 24 hours. Mean = 60 pixels, SD= 1 pixels, CV= 1.94%, n= 656 droplets at 48 hours. **(C)** Droplets incubated at 37ºC in the static incubator aerobically for 48 hours. Mean = 60 pixels, SD= 1 pixels, CV= 1.56%, n= 664 droplets at 0 hours. Mean = 60 pixels, SD= 3 pixels, CV= 4.65%, n= 651 droplets at 24 hours. Mean = 58 pixels, SD= 3 pixels, CV= 5.99%, n= 673 droplets at 48 hours. **(D)** Droplets incubated at 37ºC in the shaking incubator aerobically for 48 hours. Mean = 60 pixels, SD= 1 pixels, CV= 1.83%, n= 643 droplets at 0 hours. Mean = 59 pixels, SD= 1 pixels, CV= 2.51%, n= 665 droplets at 24 hours. Mean = 60 pixels, SD= 3 pixels, CV= 4.21%, n= 648 droplets at 48 hours. **(E)** Droplets incubated at 37ºC in the static incubator anaerobically for 48 hours. Mean = 61 pixels, SD= 2 pixels, CV= 3.04%, n= 635 droplets at 0 hours. Mean = 64 pixels, SD= 19 pixels, CV= 29.82%, n= 538 droplets at 24 hours. Mean = 61 pixels, SD= 26 pixels, CV= 43.49%, n= 452 droplets at 48 hours. Data for each time point is from three representative images of different fields of view of the emulsion. Each data point represents the radius (pixels) of an individual droplet in an image. Dotted line is the mean and error bars show the standard deviation of droplet size.

The monodispersity and stability were then assessed for droplets generated with 1% Pico-Surf® and bacterial culture media. Figure 3.20 provides the experimental data on the use of the feedback loop at producing 300 pL droplets with PBS (Figure 3.20 A), 7H9, (Figure 3.20 B), and MCM (Figure 3.20 C) as the aqueous phase with this surfactant concentration. The mean values of droplet volumes for PBS, 7H9, and MCM aqueous phases were 1.09, 0.08, and 0.12 pL respectively within range to the desired droplet size of 300 pL (Figure 3.20). In all experiments generating droplets with 1% Pico-Surf® and bacterial culturing media, the standard deviations were below 1.05 pL and the coefficient of variations were below 0.35%. These results suggest that mycobacterial culture media as well as PBS are still qualified to produce droplets of low variation when the surfactant concentration is reduced to 1%. In contrast, the decrease in surfactant concentration appeared to make stability of droplets with 7H9 and MCM medias worse when incubated. For droplets generated with the control sample PBS, stable droplets can be visualised for the full time of the assay and in each incubation condition (Figure 3.21). The most surprising aspect of the data is that droplets generated with 7H9 media and 1% Pico-Surf® suffered from destabilisation from the first time point image (0 hours). Figure 3.22 displays images of polydisperse droplets at 0 hours in all incubation conditions and then increased coalescence for droplets incubated in the static, shaking, and anaerobic incubator.

The quantifiable image-based method was pursued to verify the variance in droplet sizes at each time point and all samples had a coefficient of variance value >10%, confirming stable droplets were unattainable with 7H9 and 1% surfactant. Interestingly, only in an anaerobic condition after 48 hours did MCM containing droplets show any sign of destabilisation which was concluded from CV = 27.67% (Figure 3.23).

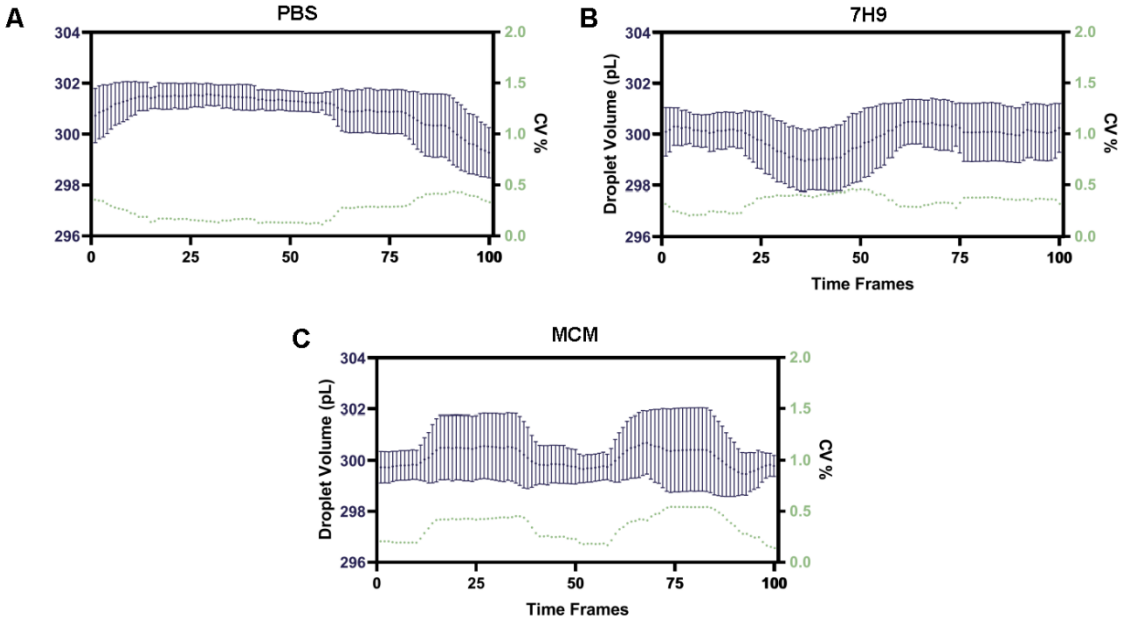

Figure 3.20. Droplet volume monodispersity of 300 pL droplets generated with 1% Pico-Surf and mycobacteria culture media. (A) 300 pL droplets generated with PBS as the aqueous phase. Mean droplet volume 301.01 pL, SD 0.72 pL, CV 0.24%. **(B)** 300 pL droplets generated with 7H9 media as the aqueous phase. Mean droplet volume 299.92 pL, SD 1.04 pL, CV 0.35%. **(C)** 300 pL droplets generated with cholesterol media as the aqueous phase. Mean droplet volume 300.12 pL, SD 1.05 pL, CV 0.35%. The average droplet volume (pL), standard deviation (SD) and coefficient of variation (CV %) of n=25 droplets are plotted for 100 saved frames. Each graph represents 1 of 3 repeats of 100 saved time frames.

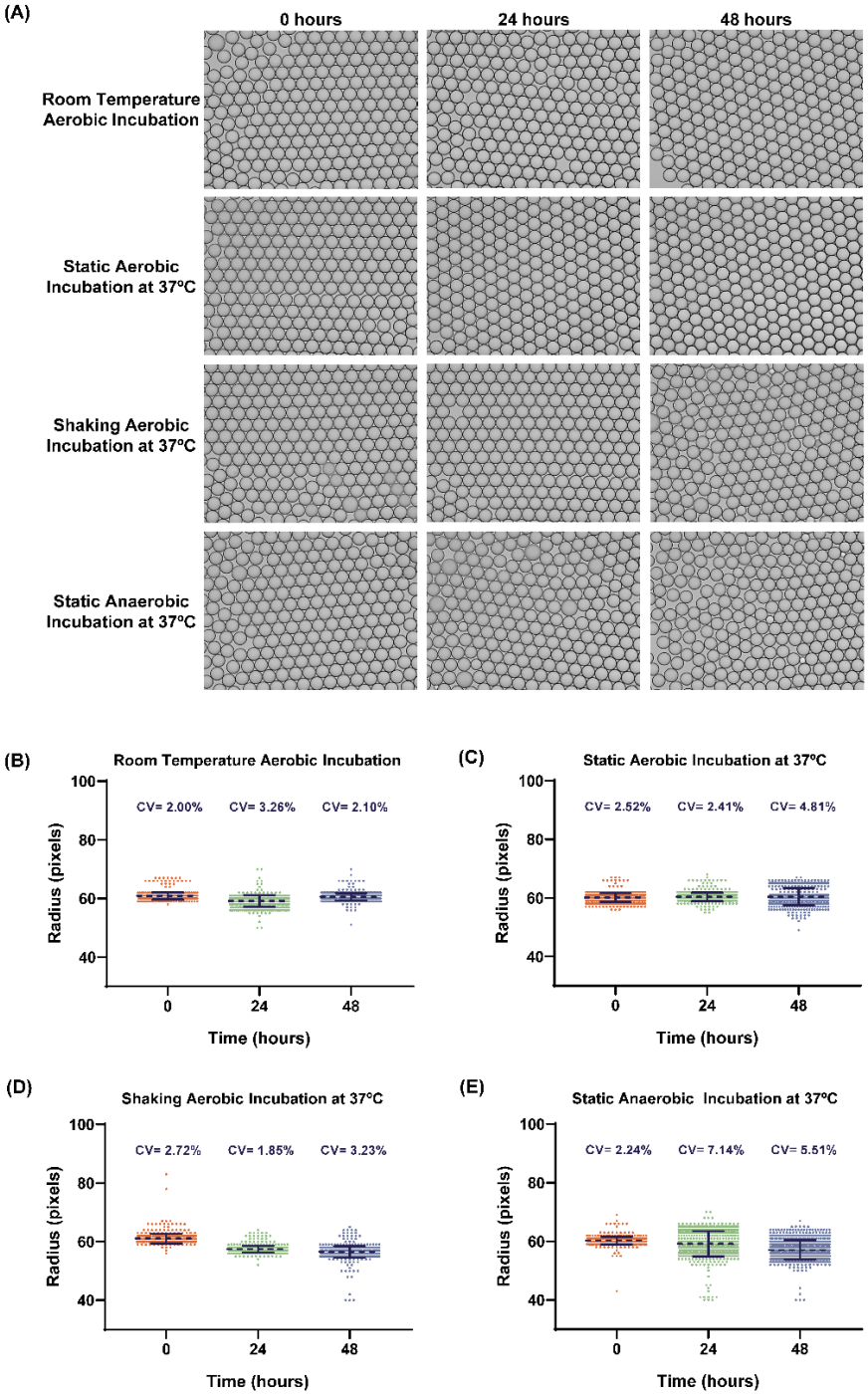

Figure 3.21. Droplet stability over 48 hours for droplets generated with 1% PS and PBS media. Each scatter plot illustrates the variance in droplet size over time of an emulsion in different incubation conditions. **(A)** Images of droplets in different incubation conditions at 0, 24, and 48 hours. **(B)** Droplets incubated at room temperature aerobically for 48 hours. Mean = 61 pixels, SD= 1 pixels, CV= 2.00%, n= 639 droplets at 0 hours. Mean = 61 pixels, SD= 2 pixels, CV= 3.26%, n= 673 droplets at 24 hours. Mean = 61 pixels, SD= 1 pixels, CV= 2.10%, n= 642 droplets at 48 hours. **(C)** Droplets incubated at 37ºC in the static incubator aerobically for 48 hours. Mean = 60 pixels, SD= 2 pixels, CV= 2.52%, n= 647 droplets at 0 hours. Mean = 60 pixels, SD= 1 pixels, CV= 2.41%, n= 639 droplets at 24 hours. Mean = 61 pixels, SD= 3 pixels, CV= 4.81%, n= 503 droplets at 48 hours. **(D)** Droplets incubated at 37ºC in the shaking incubator aerobically for 48 hours. Mean = 61 pixels, SD= 2 pixels, CV= 2.72%, n= 613 droplets at 0 hours. Mean = 61 pixels, SD= 1 pixels, CV= 1.85%, n= 690 droplets at 24 hours. Mean = 61 pixels, SD= 2 pixels, CV= 3.23%, n= 729 droplets at 48 hours. **(E)** Droplets incubated at 37ºC in the static incubator anaerobically for 48 hours. Mean = 60 pixels, SD= 1 pixels, CV= 2.24%, n= 662 droplets at 0 hours. Mean = 60 pixels, SD= 4 pixels, CV= 7.14%, n= 692 droplets at 24 hours. Mean = 60 pixels, SD= 3 pixels, CV= 5.51%, n= 729 droplets at 48 hours. Data for each time point is from three representative images of different fields of view of the emulsion. Each data point represents the radius (pixels) of an individual droplet in an image. Dotted line is the mean and error bars show the standard deviation of droplet size.

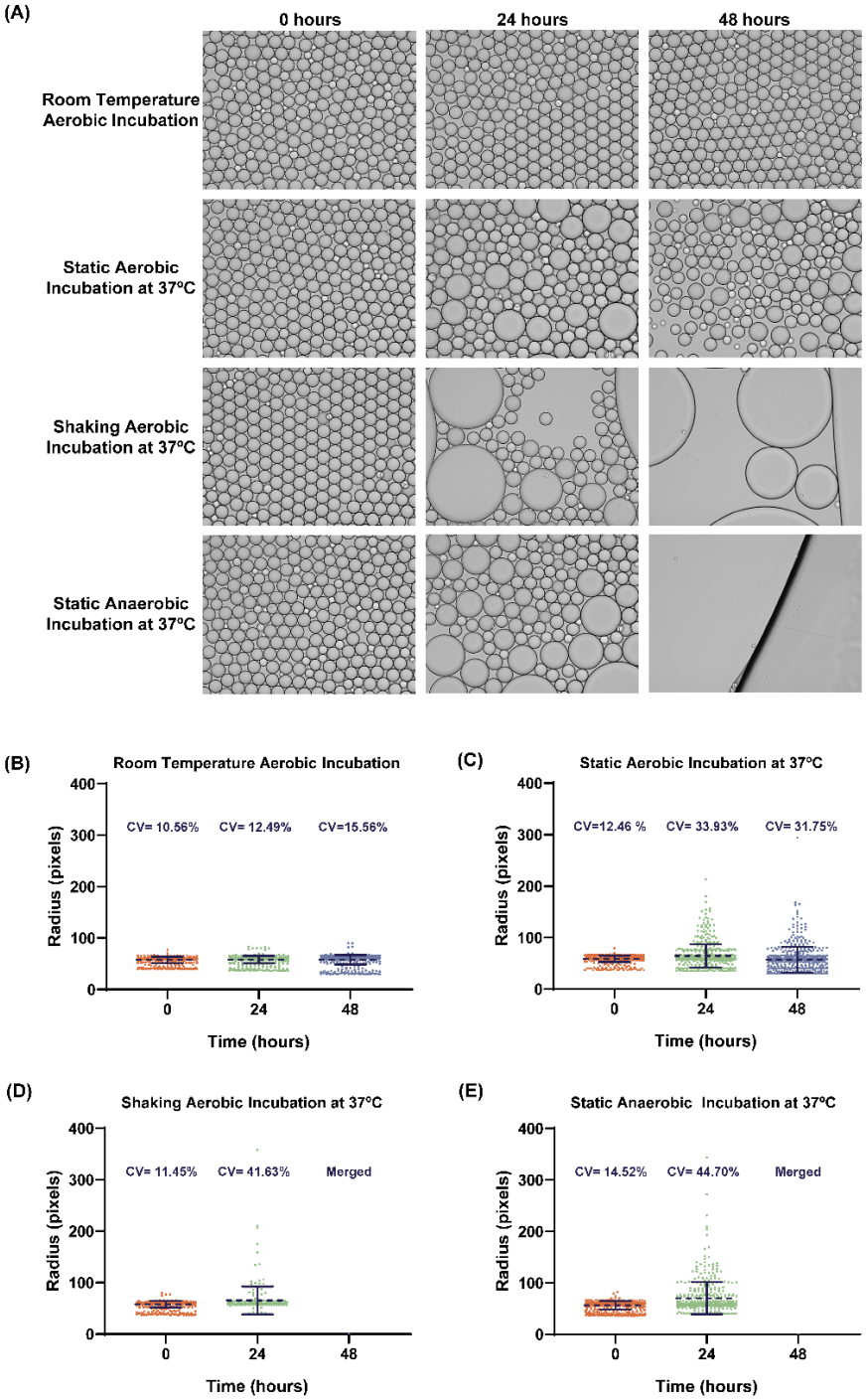

Figure 3.22. Droplet stability over 48 hours for droplets generated with 1% PS and 7H9 media. Each scatter plot illustrates the variance in droplet size over time of an emulsion in different incubation conditions. **(A)** Images of droplets in different incubation conditions at 0, 24, and 48 hours. **(B)** Droplets incubated at room temperature aerobically for 48 hours. Mean = 58 pixels, SD= 6 pixels, CV= 10.56%, n= 645 droplets at 0 hours. Mean = 58 pixels, SD= 7 pixels, CV= 12.49%, n= 681 droplets at 24 hours. Mean = 58 pixels, SD= 9 pixels, CV= 15.67%, n= 685 droplets at 48 hours. **(C)** Droplets incubated at 37ºC in the static incubator aerobically for 48 hours. Mean = 59 pixels, SD= 7 pixels, CV= 12.46%, n= 645 droplets at 0 hours. Mean = 66 pixels, SD= 22 pixels, CV= 33.93%, n= 681 droplets at 24 hours. Mean = 63 pixels, SD= 20 pixels, CV= 31.75%, n= 685 droplets at 48 hours. **(D)** Droplets incubated at 37ºC in the shaking incubator aerobically for 48 hours. Mean = 58 pixels, SD= 7 pixels, CV= 11.45%, n= 682 droplets at 0 hours. Mean = 65 pixels, SD= 27 pixels, CV= 41.63%, n= 245 droplets at 24 hours. Droplets at 48 hours had merged completely. **(E)** Droplets incubated at 37ºC in the static incubator anaerobically for 48 hours. Mean = 56 pixels, SD= 8 pixels, CV= 14.52%, n= 720 droplets at 0 hours. Mean = 70 pixels, SD= 31 pixels, CV= 44.70%, n= 433 droplets at 24 hours. Droplets at 48 hours had merged completely. Data for each time point is from three representative images of different fields of view of the emulsion. Each data point represents the radius (pixels) of an individual droplet in an image. Dotted line is the mean and error bars show the standard deviation of droplet size.

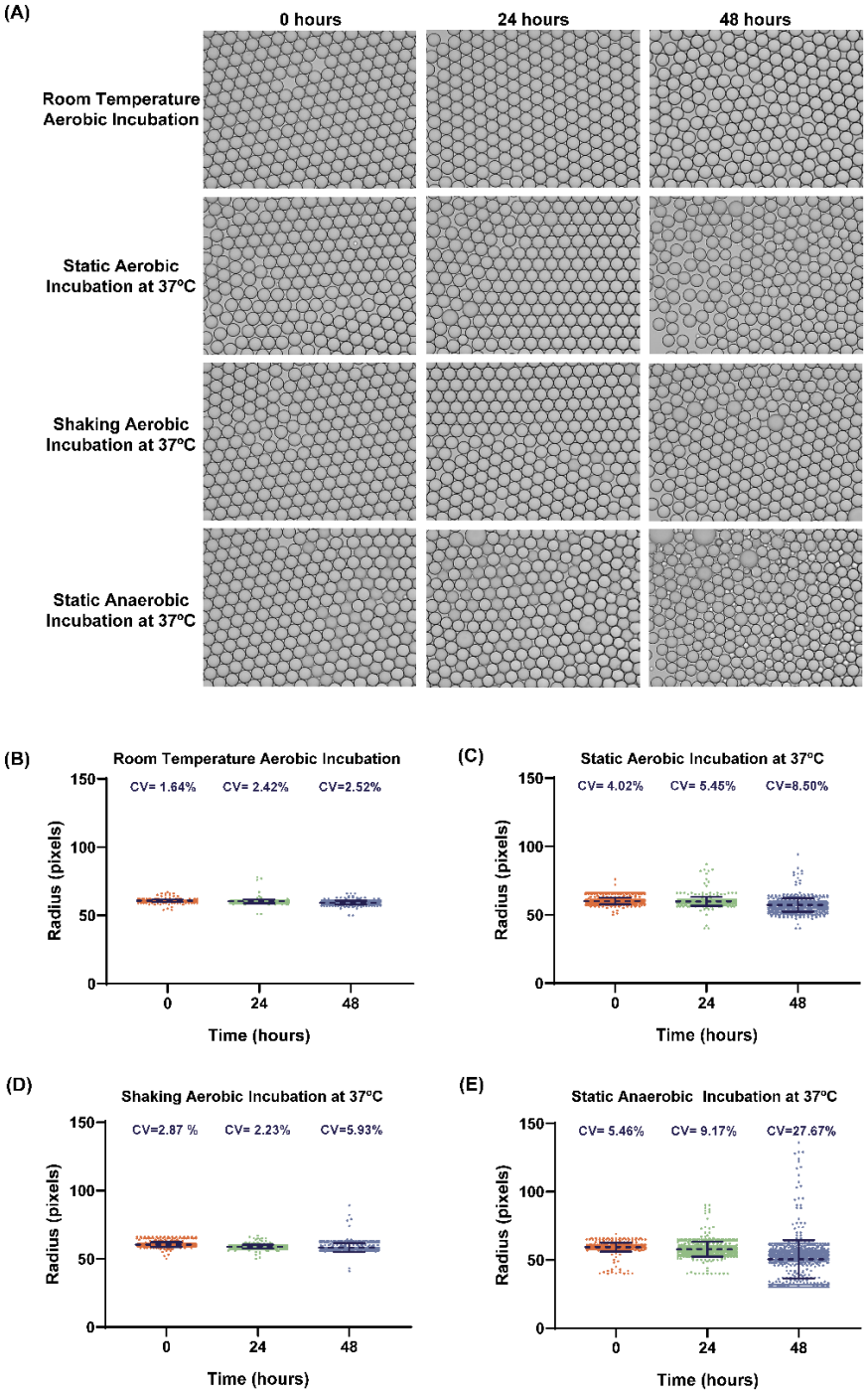

Figure 3.23. Droplet stability over 48 hours for droplets generated with 1% PS and MCM media. Each scatter plot illustrates the variance in droplet size over time of an emulsion in different incubation conditions. **(A)** Images of droplets in different incubation conditions at 0, 24, and 48 hours. **(B)** Droplets incubated at room temperature aerobically for 48 hours. Mean = 61 pixels, SD= 1 pixels, CV= 1.64%, n= 648 droplets at 0 hours. Mean = 60 pixels, SD= 1 pixels, CV= 2.42%, n= 644 droplets at 24 hours. Mean = 59 pixels, SD= 1.49 pixels, CV= 2.52%, n= 630 droplets at 48 hours. **(C)** Droplets incubated at 37ºC in the static incubator aerobically for 48 hours. Mean = 60 pixels, SD= 2 pixels, CV= 4.02%, n= 643 droplets at 0 hours. Mean = 60 pixels, SD= 3 pixels, CV= 5.45%, n= 652 droplets at 24 hours. Mean = 57 pixels, SD= 5 pixels, CV= 8.50%, n= 655 droplets at 48 hours. **(D)** Droplets incubated at 37ºC in the shaking incubator aerobically for 48 hours. Mean = 60 pixels, SD= 2 pixels, CV= 2.87%, n= 626 droplets at 0 hours. Mean = 58 pixels, SD= 1 pixels, CV= 2.23%, n= 659 droplets at 24 hours. Mean = 58 pixels, SD= 3 pixels, CV= 5.93%, n= 658 droplets at 48 hours. **(E)** Droplets incubated at 37ºC in the static incubator anaerobically for 48 hours. Mean = 59 pixels, SD= 3 pixels, CV= 5.46%, n= 671 droplets at 0 hours. Mean = 58 pixels, SD= 4 pixels, CV= 9.17%, n= 678 droplets at 24 hours. Mean = 51 pixels, SD= 14 pixels, CV= 27.67%, n= 821 droplets at 48 hours. Data for each time point is from three representative images of different fields of view of the emulsion. Each data point represents the radius (pixels) of an individual droplet in an image. Dotted line is the mean and error bars show the standard deviation of droplet size.

3.4 Discussion

This study demonstrated the successful generation of monodisperse picolitre droplets using an image-based closed-loop feedback system, achieving coefficients of variation below 0.7% across various droplet sizes. However, the stability of these droplets varied significantly when using different bacterial culture media, particularly for mycobacterial growth conditions. These findings highlight both the potential and the challenges of using droplet microfluidics for antimicrobial susceptibility testing. For single bacterial cells to be encapsulated with discrete concentrations of antibiotics in individual droplets, droplets must be monodisperse in size and maintain their stability during bacterial incubation. The main challenge for generating droplets is ensuring each droplet generated is equal in volume and monitoring this in real-time is complex when droplets are produced at high generation speeds. This is particularly difficult when the flow of immiscible liquids are disrupted due to dust presenting within the channels of the microfluidic chip, the inlet pressures changing, or an increase in hydrodynamic resistance of the main channel. Importantly, a universal methodology for microbiologists to generate high monodisperse droplets in a high throughput manner with ease of use does not exist. In addition, when assessing droplet monodispersity and stability of droplets, most studies in the field have focused on water as the aqueous phase and have not investigated common microbiology culture media. As variables such as viscosity, surface tension, chemical composition, particle content, pH, ionic strength, and temperature influence droplet stabilisation, it is important to test whether standard media used for microbiology culturing will be suitable for a droplet-based assay.

This chapter aimed to optimise parameters used to form monodisperse and stable droplets with bacteria culture media, striving to develop a drug screening assay of mycobacteria and other pathogens in picodroplets.

In this chapter, Sphere Fluidics picodroplet technology was utilised to create droplets of desired volumes with low variance using an image-based closed-loop feedback mechanism. W/O droplets were generated with flow-focusing PDMS chips of varied dimensions and the accuracy of the feedback mechanism was assessed on different droplet volumes by calculating the mean droplet size created, the standard deviation, the coefficient of variation, and the flow rate ratio. In addition, a quantitative image-based approach was used to assess the stability of droplets of varying surfactant concentrations and aqueous phase media types during collection and microbiology incubation conditions.

When desired droplet volumes in picolitres were imputed into the feedback system, the pressures of the inlet channels changed accordingly. Droplets containing PBS and 5% Pico-Surf® surfactant were efficiently generated using two different flow-focusing junctions of

different channel dimensions. A flow-focusing geometry was used as it generates droplets at a higher rate than T-junction geometries. However, T-junctions are favourable for making monodisperse droplets with accurate control. Nevertheless, as the feedback system counteracted external fluctuations that originate from the imperfections of the flow source, ultra-monodisperse droplets could be achieved with accuracy and high-speed. The high-speed camera enabled data to rapidly generate of fast-flowing droplets. For the experiments presented in this chapter, the highest generation rate reached approximately 579 droplets per second. When moving from one desired droplet size to another, the time for droplets to stabilise was minimal compared to syringe-based devices.

The observed linear relationship between droplet volume and flow rate ratio not only confirms the accuracy of our system but also provides a predictable model for droplet generation. This predictability is crucial for designing experiments with specific droplet sizes, allowing researchers to tailor droplet volumes to particular bacterial species or antibiotic concentrations. Such precise control over droplet size has been a challenge in previous microfluidic systems and represents a significant advancement in the field.

Droplets made could achieve standard deviations of below 2 pL and variance level between 0.2-0.7% CV. This finding of low droplet variance and high throughput is consistent with that of Kalantarifard (2022) and Kim et al (2021) who generated droplets <0.5% CV (Kalantarifard et al., 2022, Kim et al., 2021). It can be assumed that there is no difference in accuracy in developing droplets with either different channel dimensions or droplet sizes. This extends the possibility of designing unique experiments for specific applications.

Compared to previous research that used closed-loop feedback with T-junction geometries (Zeng et al., 2015b, Zeng et al., 2022, Fu et al., 2017), the method presented in this chapter utilised a flow-focusing geometry for precise control of droplet production as well as high generation speeds. For studies that have also used closed-loop feedback with flow-focusing geometries show control of droplet diameter ranges from 40-400 μM (Miller et al., 2010), 14-24 μM (Xie et al., 2020), 30-60 μM (Gyimah et al., 2022b), and 50-200 μM (Jõemaa et al., 2023). This study also demonstrates controlled droplet sizes using a closed-loop feedback system and a flow-focusing geometry within the ranges of 48-95 μM (60-450 pL) confirming enhanced practicability and robustness for various applications. However, the previous literature does not investigate the monodispersity and stability of picolitre droplets created with microbiological culture media or incubation conditions.

The image-based closed-loop feedback control software which constantly monitors the instantaneous error and regulates the droplet volume based on the feedback signal could be favourable for developing a droplet-based antimicrobial susceptibility assay and offers

potential to generate millions of ‘bioreactors’ acting as individual experiments generated in parallel at high-throughput.

The second part of the chapter was to assess if droplet generating characteristics such as a pressure pump, a flow-focusing PDMS chip, Pico-Surf™ surfactant, and common bacterial culture media were adequate for producing monodisperse and stable droplets. To summarise all data sets examining the stability of emulsions generated, each time point of each droplet variable assessed was split into low variance (<10% CV) and high variance (>10% CV) of droplet size and illustrated in a heat map (Figure 3.24). Samples that were labelled high variance were depicted as unstable due to their polydispersity or mergence. The Figure summarises that from all aqueous types used, mycobacterial culture media, particularly 7H9, and less importantly MCM, were poor at maintaining droplet stability in incubation conditions overtime. Whereas droplets made from PBS and MH media maintained monodispersity and stability. In most cases, the room temperature incubation control remained stable throughout the experiment, as expected. When comparing the variation in droplet size between droplets which were incubated statically and shaking, there was no difference in stability. On the other hand, stability is further affected in anaerobic conditions more than aerobic and in elevated temperatures compared to room temperatures. When increasing the surfactant concentration, there was a decrease in sample types, which were stable.

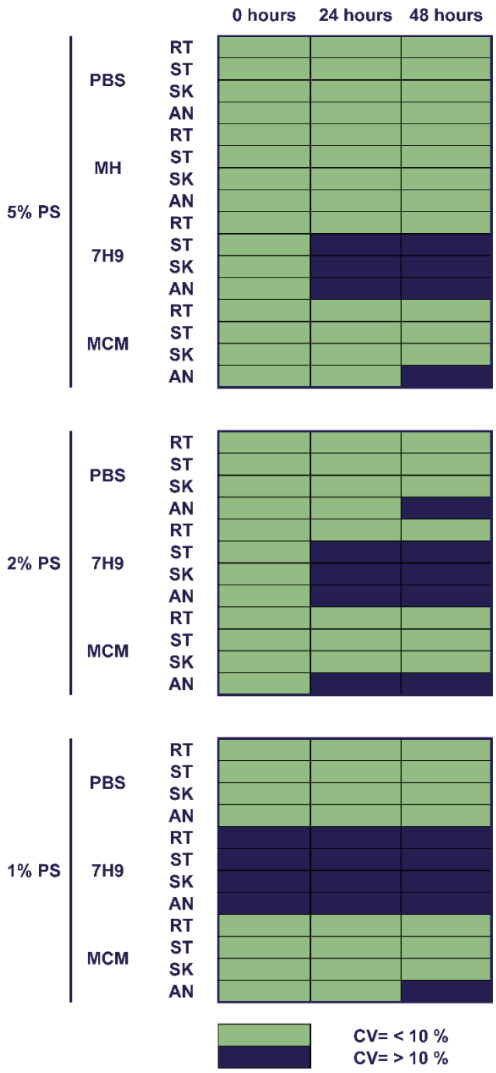

Figure 3.24. Summary heat map of stable droplets under different conditions. Stable droplets are labelled green which have low variance (CV=<10%). Unstable droplets are labelled blue which have high variance due to coalescence (CV=>10%). RT = room temperature aerobic incubation. ST = static aerobic incubation at 37ºC. SK = shaking aerobic incubation at 37ºC. AN = static anaerobic incubation at 37ºC.

A key limitation of this study was the variation in droplet formation frequency across experiments. While this did not affect our ability to generate monodisperse droplets, it introduces a potential confounding variable when comparing results across different experimental conditions. Droplet formation frequency can impact the time droplets spend in the microfluidic channels, potentially affecting their stability or the encapsulation of bacteria. Future studies should aim to standardize this parameter or systematically investigate its effects on droplet characteristics and bacterial growth.

In addition, when generating droplets, jetting was not assessed. The implications of jetting may cause disruption in single-cell encapsulation and therefore may be less accurate. Also, assessing jetting helps in diagnosing and correcting issues with channel geometry to ensure smooth operation of the microfluidic device and the correct pressure balance. An additional uncontrolled factor is that the velocity of the aqueous phase was not considered. This may

cause problems when using special media types for culturing bacteria. Also, when capturing an image of each droplet generated, this is in a 2-dimensional format rather than in 3D. 3D imaging would allow for studying the dynamic behaviour of droplets as they move through microchannels, including interactions with other droplets, cells, surfaces, or channel boundaries. More importantly, the complex set-up of the methodology may not be suitable for inexperienced users in microfluidics. For the development of a droplet-AST, future work is required to automate the process of microbiology applications for the end user.

A final note on the future direction of this work is the consideration of exploring the ability of a different surfactant with structural differences to maintain each droplet integrity using culture media. It is not suitable enough to increase the concentration of surfactant, as this introduces low microbial cytotoxicity for microbial culture. A balance between high droplet stability using higher surfactant concentrations and biocompatibility needs to be investigated.

Also, when assessing stability, droplets were incubated in an emulsion, which is known to be less stable than droplets separated without touching one another. To address the stability issues observed with certain media types, future studies could explore novel PDMS chip designs that incorporate individual droplet trapping mechanisms. Such designs could minimize droplet-droplet interactions, potentially enhancing long-term stability. Additionally, these trapped droplets could be monitored individually over time, allowing for more detailed studies of bacterial growth and antibiotic effects at the single-cell level. This approach could significantly enhance the capabilities of droplet-based antimicrobial susceptibility testing, particularly for slow-growing organisms like mycobacteria.

In addition, all experiments conducted above that were incubated were at 37 ºC. As some bacteria can proliferate at 30 ºC, perhaps testing at this temperature could increase stability. Furthermore, additional bacterial media types are required to be tested as the aqueous phase in droplets, such as more viscous sputum media for modelling mycobacteria infections in cystic fibrosis.

In conclusion, these findings suggest that while the current picodroplet generation system is suitable for culturing bacteria in minimal media, such as those used for MRSA, significant challenges remain for its application to mycobacteria. The poor stability of droplets containing mycobacterial culture media, particularly 7H9 broth, indicates that further optimisation of surfactant composition or concentration may be necessary. This highlights the need for media-specific tailoring of droplet formulations in microfluidic systems. Future research should focus on developing surfactant mixtures that can stabilize droplets containing the detergents necessary for mycobacterial growth, potentially opening new avenues for high-throughput drug susceptibility testing in these challenging organisms.

Chapter 4.

Encapsulation of MRSA in Picodroplets at the Single-cell and Multi-cell Level and Determination of Antibiotic Susceptibility.

4.1 Introduction

4.1.1 Overview of Droplet Microfluidics in Microbiology

Encapsulating bacteria in droplet microfluidics is a transformative technique that allows individual bacterial cells to be isolated within tiny, picolitre-sized droplets. These droplets function as miniature bioreactors, enabling the study of bacterial behaviour at the single-cell level in a high-throughput manner. This method is particularly useful in microbiology for studying cellular heterogeneity, metabolic activity, drug resistance, and many other applications.

4.1.2 Poisson Distribution and Single-cell Encapsulation

Droplet microfluidics is an emerging technology that allows manipulation of fluids at the microscale. One key application is single-cell encapsulation, which involves trapping or isolating individual cells within tiny compartments or droplets. This technique enables researchers to study cellular behaviour at unprecedented resolution. The concentration of cells must be carefully controlled to achieve the desired encapsulation efficiency (maximising single-cell droplets while minimising empty or multi-cell droplets). However, this might be unachievable since cells are randomly distributed in their carrier solution. It was shown that cell encapsulation follows the Poisson formula in this case. When bacterial cells are randomly distributed in cell culture media, Poisson statistics determine the quantity of cells per encapsulated droplet volume. The Poisson distribution is given by;

$$p(k, \lambda) = \lambda k e - \lambda k!$$

where the number of particles is defined as k and the number of cells per droplet volume is defined as λ. From this, the desired volume of droplet and cell culture concentration can be calculated to obtain single-cell encapsulation (Collins et al., 2015). Therefore, the average number of cells per droplet will rise with increasing cellular concentrations. This ensures the parameter of starting concentration in biological assays is equal. In essence, Poisson distribution helps in predicting and controlling the cell loading in droplets during single-cell encapsulation, which is key to the success of various single-cell experiments.

4.1.3 Bacterial Behaviour in Droplets

4.1.3.1 The Effect of Bacteria on the Stability of Emulsions

While single-cell encapsulation offers numerous advantages for studying bacterial behaviour, it also presents challenges. One such challenge is maintaining emulsion stability when encapsulating bacteria in droplets. The stability of emulsions can be compromised due to bacterial characteristics such as their surface-active properties and metabolic activity.

Understanding these effects is crucial for developing reliable droplet-based assays for bacterial studies. A study in 2022 demonstrated that droplet stability improved with the presence of bacteria, which was due to dead cells having a higher affinity towards the interface. Interestingly, this study showed that the stability of droplets is species dependent, with *E. coli* providing better stability as compared to *Lactobacillus paracasei* (Mohd Isa et al., 2022). Ly et al. demonstrated that this may be due to the surface charge on the bacterial cell wall (Ly et al., 2006). In contrast, a study has shown the opposite effect of bacteria destabilising emulsions. *E. coli* cells promoted droplet flocculation and coalescence, albeit, these droplets were oil-in-water, not water-in-oil droplets (Li et al., 2001). Previous studies have highlighted the potential of using bacteria for emulsion stabilisation, with bacterial surface properties playing a crucial role in the stabilisation process (Dorobantu et al., 2004, Wongkongkatep et al., 2012, Firoozmand and Rousseau, 2016). Intriguingly, another effect which bacteria has on emulsions reported droplet shrinkage as *E. coli* and *Pseudomonas fluorescens* proliferated inside droplets (Geersens et al., 2022). Understanding the effect of bacteria on droplet stability is crucial for the design and optimisation of microfluidic systems. This knowledge has far-reaching implications in various fields, including:

1. Single-cell analysis: Enabling high-throughput studies of bacterial heterogeneity and behaviour at the individual cell level.
2. Biochemical assays: Developing more sensitive and accurate tests for bacterial detection and characterization.
3. Drug testing: Facilitating rapid screening of antimicrobial compounds against pathogenic bacteria.
4. Synthetic biology: Creating controlled microenvironments for engineered bacterial communities.

By ensuring consistent droplet behaviour, researchers can develop more reliable and powerful tools for addressing pressing challenges in microbiology and biotechnology.

4.1.3.2 Inoculum Effect

Inoculum effect is an issue with assessing MIC values in AST. The inoculum effect (IE) refers to the phenomenon where the effectiveness of an antibiotic is reduced when a higher number of bacteria (a higher bacterial inoculum) is present. This means that at higher bacterial concentrations, higher doses of an antibiotic may be required to achieve the same level of bacterial killing that would be effective at lower bacterial concentrations (Brook, 1989, Diaz-Tang et al., 2022, Smith Kenneth and Kirby James, 2018). The Clinical and Laboratory Standards Institute (CLSI) has stated that a standardised inoculum density of 5×10^5 CFU ml^{-1} with an allowable range of 2×10^5 to 8×10^5 CFU ml^{-1} is appropriate for BMD assays (CLSI, 2015). Microfluidics is a possible solution to the IE. The IE does not affect AST in individual

microcompartments where the concentration of bacteria is at the single-cell level and thus AST at the microscale could be less prone to errors from IE than traditional bulk AST (Postek and Garstecki, 2022).

The IE was previously studied in droplet-based microfluidics. The study by Huang et al. (2015) examines how population-wide antibiotic titration with streptomycin (Strep) impacts bacterial survival, focusing on the IE. This analysis found that at an intermediate Strep concentration (4 μg/ml), bacterial droplets with high initial cell densities survive, while those with low densities do not, demonstrating IE. This occurs due to the accumulation of ribosomes and the heat shock response (HSR) induced by Strep, which is crucial for IE. Antibiotics that did not induce HSR did not show IE (Huang et al., 2015). The paper on "Microfluidic screening of antibiotic susceptibility at a single-cell level" investigates how the antibiotic cefotaxime affects *E. coli* at different cell densities, focusing on the IE. The study uses droplet microfluidics to monitor *E. coli* responses to cefotaxime at the single-cell level, revealing that higher bacterial densities can withstand the antibiotic better than lower densities. This demonstrates the IE, where the effectiveness of cefotaxime decreases as the initial bacterial population increases, highlighting the importance of considering cell density in antibiotic treatments (Postek et al., 2018). An additional research paper studying the inoculum effect in droplets from Scheler et al. allows precise quantification of how population size (of *E. coli*) impacts the antibiotic concentration needed to inhibit growth, providing insights into the relationship between heteroresistance and the IE (Scheler et al., 2020). In addition, research into the inoculum effect using droplet microfluidics as a methodology has tested a β-lactamase-producing *E. coli* DH5α against a β-lactam antibiotic ampicillin (Ding et al., 2023). Furthermore, droplet microfluidics provides a valuable platform for exploring how single-cells, like “leader” cells, influence the lag phase and inoculum effect in bacterial populations as shown by a study investigating a single "leader" cell in a *Pseudomonas fluorescens* population and showed it can trigger the end of the lag phase and initiate rapid growth for the entire population (Ardré et al., 2022).

Although droplet fluidics holds an excellent methodology for assessing inoculum effect of antibiotics on bacteria, an opinion by Postek and Garstecki suggesting a negative effect of single-cell MIC data cannot be ignored. The authors emphasise the importance of carefully considering compartment size and statistical analysis when interpreting single-cell MIC data in microfluidics. They also accentuate the need for defining clear criteria for measuring single-cell MIC that align with CLSI standards. This is due to two possible reasons. First, different compartment sizes will have a different ratio of antibiotic molecules to the number of bacterial cells and thus affect the MIC. Second, due to the small scale, the inoculum differences are larger in droplets between each droplet (100% between 1 or 2 cells encapsulated), whereas, in a bulk culture, there are inoculum differences between 100 and 101 cells for example (1%) (Postek and Garstecki, 2022).

4.1.3.3 Quorum sensing

In addition to the IE in droplets, quorum sensing (QS) was witnessed. Quorum sensing is a process where bacteria regulate gene expression based on changes in cell-population density. Bacteria release chemical signal molecules known as autoinducers, which accumulate as the population grows. When the concentration of autoinducers reaches a certain threshold, it triggers changes in gene expression. Both Gram-positive and Gram-negative bacteria employ quorum sensing systems to control various physiological functions, such as symbiosis, virulence, competence, conjugation, antibiotic production, motility, sporulation, and biofilm formation (Miller and Bassler, 2001). Research has demonstrated that confining single *Pseudomonas aeruginosa* bacterial cells in small droplet volumes can induce high-density quorum sensing behaviours and highlight the variability in growth and response among cells in these confined conditions (Boedicker et al., 2009). Previously, it was demonstrated that confining individual Staphylococcus aureus bacteria in droplets impacts their quorum sensing behaviour. This confinement triggers the activation of virulence and metabolic pathways necessary for survival (Carnes et al., 2010). In another impressive study, authors trapped two different droplets together in a trapping device and studied the sensing abilities by the process of diffusion between one droplet containing a signalling molecule and another containing a quorum sensing bacterium. The study reveals how quorum sensing signals are exchanged and perceived between cells in the double droplet setup. This set-up allows for the observation of quorum sensing dynamics that occur in a more controlled and measurable environment compared to bulk studies (Bai et al., 2013). Examinations into how microfluidics-generated double emulsions can be used to create programmable microenvironments for studying quorum sensing revealed that variations in the microenvironment, such as different concentrations of signalling molecules or nutrients, significantly affect quorum sensing behaviours. For instance, higher concentrations of signalling molecules can enhance the quorum sensing response (Zhang et al., 2013). Droplet microfluidic confinement can be used to study quorum sensing at a single-cell level, providing insights into how spatial constraints influence bacterial communication and behaviour. This has implications for understanding bacterial infection dynamics and developing targeted treatments.

4.1.3.4 Biofilm Formation

Other cell behaviours, such as biofilms, are studied in droplets. These studies involve monitoring the development of bacterial biofilms within the droplets over time, using imaging techniques and other assays to assess biofilm formation and characteristics. Biofilms are complex communities of microorganisms that adhere to surfaces and embed within a self-produced matrix of extracellular polymeric substances (EPS). This matrix, which includes proteins, polysaccharides, and nucleic acids, helps the microorganisms stick together and on surfaces, protecting them from environmental factors like antibiotics and immune responses (Zhao et al., 2023). An investigation by Scheler et al. noted that their confocal images of

droplets encapsulated with bacteria showed clusters of high-intensity pixels inside those droplets which they interpreted as bacterial clumps. They hypothesised the droplet assay captured the early stages of biofilm formation (Scheler et al., 2020). In one study, *B. subtilis* was used as a model to study biofilm formation and described that the bacteria first swam alone, aggregated in 12 hours around the droplet edges, and then finally sporulated in 48 or 72 hours (Chang et al., 2015). Researchers also highlight how they can improve the ability to control and study biofilm formation compared to static or less controlled environments by encapsulating *Pseudomonas aeruginosa* bacteria in droplets and placing them on a substrate to monitor antibiotic susceptibility (Jin et al., 2018). A prominent example of how bacterial cells interact with the oil droplet bilayer was published, showing a droplet platform which allows researchers to observe the initial stages of biofilm formation on oil droplets, providing insights into how microbes attach, colonise, and develop biofilms in the presence of oil. This is important for understanding how biofilms might contribute to the degradation or persistence of oil in the environment (White et al., 2019). These examples of how biofilms can be studied in droplets can provide insight into how growing bacterial communities interact with their mechanical environment, show resistance to antibiotics through-biofilm generating mechanisms, or *in vitro* infection modelling.

4.1.4 Techniques to Enumerate Bacteria in Droplets

Since microfluidic droplet assays are being developed for microbiology use, there have been many custom platforms developed to enumerate bacteria in droplets. Techniques are being used to detect, count, or sort “positive” and “negative” droplets in droplet-based assays. For example, fluorescent detection of droplets was utilised to indicate bacterial viability and growth (Harmon et al., 2020, Postek et al., 2018, Scheler et al., 2020, Zang et al., 2013). In one example, droplets with growing bacteria were sorted using a fluorescence resonance energy transfer (FRET)-based RNA probe (Ota et al., 2019). A reliable, albeit labourious method to quantify viable bacteria in droplets is to break droplets open and enumerate bacteria by CFU counting of the recovered sample (Liu et al., 2016). Some studies have used droplet sorting to separate positive and negative droplets (Zang et al., 2013) and others have bar-coded coloured-coded droplets for analysis (Cui et al., 2022, Jeong et al., 2021). Furthermore, the droplet volume was used as a measurement of bacteria metabolic activity (Geersens et al., 2022, Boitard et al., 2012). Optofluidic detection was witnessed by integrating micro-lenses and embedding optical fibre to a droplet platform to detect absorbance, fluorescence, and bacterial susceptibility.

Image analysis software has advanced to detect droplet boundaries and their cell contents inside. Sanka et al. compared the different free image analysis software tools for high-throughput droplet detection (Sanka et al., 2021). The author also contributed to creating a pipeline called “EasyFlow”, which combines a data processing tool with image-analysis

software to analyse droplet images (Sanka et al., 2023). Imaging software “CellProfiler” has showed excellent abilities to detect droplets in an image, quantify fluorescent viable bacteria, and analyse an image with multi-coloured droplets containing different chemical compositions (Bartkova et al., 2020). An impressive algorithm developed by researchers named “FluoroCellTrack” was able to quantify cellular responses to drugs, track droplets, and quantify intracellular fluorescence (Vaithiyanathan et al., 2019). To conclude, the analysis of bacteria inside droplets usually comprises analysis software coupled to specific droplet platforms and can include image-based, fluorescence, optical, and bar-coding detection.

4.1.5 Staphylococcus aureus and MRSA

This chapter aims to develop and optimise a methodology for encapsulating methicillin-resistant *Staphylococcus aureus* (MRSA) in picolitre droplets using advanced picodroplet technology. By systematically varying droplet input parameters, the optimal conditions for bacterial proliferation within these microenvironments were sought after. This work lays the foundation for future applications in rapid antibiotic susceptibility testing, potentially revolutionising our approach to combating antibiotic-resistant pathogens.

Staphylococcus aureus (S. aureus) is an opportunistic, Gram-positive, aerobic, coccus bacterium (Vitko and Richardson, 2013). *S. aureus* is found in the environment, normal human flora, on skin, mucous membranes, and it is calculated that 15% of the population persistently carry *S. aureus* in the anterior nares (Taylor and Unakal, 2024). The pathogen can cause a wide variety of serious clinical manifestations, including pneumonia, osteomyelitis, endocarditis, skin and soft tissue infections, and septicaemia (Vitko and Richardson, 2013). Antibiotics used to treat *S. aureus* infections include vancomycin, trimethoprim/sulfamethoxazole, tetracyclines, and clindamycin (Siddiqui and Koirala, 2024). However, *S. aureus* is capable of becoming resistant to all of these classes of antibiotics, which are clinically available (Vestergaard et al., 2019). Strains which are resistant to multiple antibiotics are defined as methicillin-resistant *S. aureus* (MRSA) (Elward et al., 2009). The *mecA* gene is responsible for MRSA resistance. The gene encodes a penicillin-binding protein, which confers resistance to methicillin and all current β-lactam drugs (Elward et al., 2009). With the huge presence of this resistance, intravenous vancomycin is used in hospital setting to treat MRSA infections, however, the development of vancomycin-resistant *S. aureus* has now occurred (Fait et al., 2024). MRSA is categorised as a high priority “ESKAPE” pathogen by the World Health Organisation (WHO, 2024b). The World Health Organisation also emphasises that new anti-infective drugs to prevent and treat MRSA infection are urgently required (WHO, 2017). This pathogen is listed as one of the top pathogens attributed to 50 % of the AMR fatal burden as stated by The Global Burden of Disease study (Murray et al., 2022).

On the one hand, breakthroughs in antibiotic drug discovery for MRSA have recently been advanced using deep learning to identify a new structural class of antibiotics, offering both a novel solution to antibiotic resistance and a powerful method for future drug discovery efforts. Researchers discovered novel structural classes of antibiotics, which were experimentally validated to be effective against *S. aureus*, including drug-resistant MRSA (Wong et al., 2024). Additionally, research has recently led to the conclusion that polyamine derivatives are impressive drug candidates against MRSA (Douglas et al., 2022). Comparatively, MRSA has shown heteroresistance (Deresinski, 2009) and biofilm formation (Cascioferro et al., 2021) and thus, standard susceptibility tests may lead to an underestimation of resistance and inappropriate antibiotic therapy. Also, traditional *in vitro* susceptibility tests for MRSA can take 24–48 hours to produce results, which delay the initiation of appropriate therapy or slow down the drug discovery process (Vitko and Richardson, 2013). Overall, while *in vitro* susceptibility tests are essential tools for guiding MRSA treatment or drug discovery, these challenges highlight the need for ongoing improvements in testing methodologies and interpretation to ensure accurate and clinically relevant results. One methodology which could solve these problems is droplet microfluidics to encapsulate MRSA at the single cell level and model infection.

4.1.6 *Staphylococcus aureus* and MRSA Detection, and AST in Emulsion Droplets

A growing body of literature has investigated *Staphylococcus aureus* in microdroplets. Various studies have assessed the diagnostic potential of *s. aureus* in emulsion droplets from automated point-of-care testing with direct patient samples (Schulz et al., 2020) to epidemiological surveillance using droplet-PCR (Lu et al., 2013). For instance, Luo et al., 2017 used droplet-PCR to directly identify MRSA from nasal swabs of patients by encapsulating the bacteria at the single-cell level, temperature-controlling release of genomic DNA, and amplification and detection of genetic markers (Luo et al., 2017). Other researchers who used droplet-based PCR methods to detect *S. aureus* have shown success in reliable detection of *S. aureus* to inform treatment decisions or epidemiological surveillance of bacterial infections (Ma et al., 2019, Schulz et al., 2020, Suea-Ngam et al., 2019). Interestingly, a study has shown that *S. aureus* when co-cultured with *E. coli* could be detected using a Gram assay inside droplets after 20 hours of culture (Wang et al., 2023).

In addition to detecting *S. aureus* in droplets, antibiotic susceptibility was demonstrated in these microreactors. Boedicker (2008) encapsulated a drug-resistant strain of *S. aureus* and measured the MIC of the antibiotic cefoxitin as well as distinguished between sensitive and resistant strains of *S. aureus* in infected samples of human blood plasma (Boedicker et al., 2008). High-throughput AST for MRSA using a droplet microarray based on hydrophilic-superhydrophobic patterning was shown by scientists which screened a library of over 2000 compounds (Lei et al., 2022). A unique paper introduces the use of an ultrahigh-throughput

microfluidic droplet platform to profile the antimicrobial activity of the entire oral microbial community of the Siberian bear. The researchers successfully isolated *Bacillus* strains that demonstrated antimicrobial activity against *S. aureus*. Through genome mining, they identified the antibiotic amicoumacin A as the key agent responsible for inhibiting *S. aureus* growth (Terekhov et al., 2018). Other AST in droplets demonstrated a result within 3-8 hours when encapsulating *S. aureus* in droplets and testing against broad-spectrum drugs (Yi et al., 2019). An assay using resazurin to monitor the growth of bacteria in 2 nL droplets demonstrated susceptibility within 5 hours using a four-chamber gravity-driven step emulsification device (Kao et al., 2020). A device called the Microwell-SERS system displayed AST activities which integrate surface-enhanced Raman scattering (SERS) technology, providing results within 2 hours (Huang et al., 2020). In another example, the time for detection was dramatically reduced to 15-30 minutes for clinically relevant bacteria known to cause urinary tract infection including *S. aureus* by using an imagine-based approach with four integrated microdroplet arrays for parallel studies (Kang et al., 2019). An alternative approach of AST in droplets is to utilise hydrogels. Researchers created hydrogel droplets which were 25 pL in volume and screened a metagenomic library for secreted antibiotics that kill *S. aureus* (Scanlon et al., 2014b). Collectively, these studies outline an increasing utility for droplet fluidics to provide rapid AST to *S. aureus.*

4.1.7 Objectives and Aims of Chapter

The following chapter focuses on a methodology for encapsulating MRSA in picolitre droplets using picodroplet technology. Different droplet input parameters were used to test the optimal conditions required for bacterial proliferation in droplets for future antibiotic susceptibility applications.

The aims of this chapter are as follows;

1. Encapsulate MRSA at the single-cell and multi-cell level and evaluate the encapsulation efficiency, monodispersity of droplets generated, the stability of droplets, and the survival of MRSA in the droplets during incubation.
2. To compare proliferation rates of different starting inoculum CFU/ mL in picodroplets and compare this to bulk cultures.
3. To analyse antibiotic susceptibility to MRSA in droplets in comparison to a bulk culture.

4.2 Methods

4.2.1 General Chemical, Reagent, and Media Preparation

All consumables and reagents were purchased from either Fisher Scientific, Melford, Biosynth, or Sigma-Aldrich, unless otherwise stated. Industrial partner Sphere Fluidics Ltd provided 5% Pico-Surf®, Pico-Glide™, Pico-Break™ and Novec™ 7500 reagents.

Pico-Surf®

For studies using 5% Pico-Surf®, the reagent was used undiluted and stored at 4 °C.

Pico-Glide™

Pico-Glide™ was used undiluted and stored at 4 °C.

Pico-Break™

Pico-Break™ was used undiluted and stored at 4 °C.

Phosphate Buffered Saline (PBS)

One tablet of PBS (Melford P32080-100T) was added to 100 mL of dH_2O to make a 1X solution. The PBS tablet was made of 137 mM sodium chloride, 2.7 mM potassium chloride, and 11.9 mM phosphate buffer. pH 7.4 at 25 °C.

Antibiotic Preparation

Investigative compounds, including doxycycline and MD56, were weighed and dissolved in DMSO to a final concentration of 10 mM. The stock solutions in DMSO were stored at −20 °C until use.

Mueller-Hinton Broth

9.45 g of Mueller-Hinton broth was dissolved in 450 mL of dH_2O and then autoclaved (121 °C for 15 min).

Mueller-Hinton Agar

17.1 g of Mueller-Hinton agar was dissolved in 450 mL of dH_2O and then autoclaved (121 °C for 15 min). Once cooled, the agar was poured into petri dishes.

4.2.2 Bacterial Strain and Culture Conditions

10 mL of Mueller-Hinton Broth was inoculated with MRSA N315 from a frozen glycerol stock and was grown for 24 hours in an orbital incubator at 37 °C.

4.2.3 CFU/mL vs Optical Density (570nm) Standard Curve

An overnight culture of MRSA N315 was grown, as described in section 2.2.11, into a mid-log phase. Optical density (570 nm) was measured using a spectrophotometric plate reader (Biotek EL808) and Mueller-Hinton broth was used as the blank. Cultures were adjusted to 0.05, 0.1, 0.2, 0.3, 0.4, 0.5, and 0.6 OD (570 nm) by re-suspending cells into 1 mL centrifuge tubes with Mueller-Hinton broth. Each OD sample was serially diluted in 1/10 to give dilutions of 10^{-1}, 10^{-2}, 10^{-3}, 10^{-4}, 10^{-5}, 10^{-6}, 10^{-7}, 10^{-8}. To determine the number of colony forming units (CFU) in each OD sample, the Miles and Misra technique was applied. Briefly, 20 µL of each dilution was dropped onto solid Mueller-Hinton agar. Once each spot dried, the agar was inverted and incubated at 37 °C for 24 hours. Each sample was observed for growth. Confluent growth, or many merged colonies over the area of the drop, indicated high concentrations of cells. Colonies were counted in the dilution containing between 2-20 colonies. To calculate the number of CFU/ mL from the original optical density sample, the average number of colonies for a dilution was multiplied by 50 and then multiplied by the dilution factor. Each CFU/ mL value was plotted against the corresponding OD. From this, a standard curve was generated using a linear regression model to relate these units so that optical density could be used to approximate bacterial cell density. Data collected were 3 technical replicates and 3 biological replicates.

4.2.4 PDMS Chip Fabrication

Microfluidic chips were made in-house at Aston University as described in section 3.2.10.

4.2.5 Picodroplet Generation Using Picodroplet Technology

MRSA Aqueous Phase Preparation

To prepare bacteria for encapsulation, an overnight culture of MRSA N315 was grown in Mueller-Hinton broth at 37°C with shaking at 180 rpm. The culture was then diluted in fresh Mueller-Hinton broth to optical densities (OD570) of 0.025, 0.05, 0.1, 0.3, or 0.6. These OD values corresponded to cell concentrations of 2.42×10^7, 4.85×10^7, 9.70×10^7, 2.91×10^8, or 5.82×10^8 CFU/mL, respectively, based on the standard curve generated in section 4.3.1. The diluted cultures were kept on ice until droplet generation to minimize further growth.

Set-up

Pico-Surf® surfactant (5%) was used as the oil phase. Mueller-Hinton broth containing MRSA N315 cells was used as the aqueous phase with either different concentration of cells or different concentrations of antibiotics. For antibiotic susceptibility studies, either doxycycline or MD56 was dissolved in DMSO and added to each culture at 5% to give final concentrations between 500-62.5 µM for doxycycline and 31.25-0.98 µM for MD56. The oil phase and aqueous phase (inlets) were delivered to a microchip with either a 60 µm x 60 µm flow-focusing

channel or a 40 µm x 40 µm flow-focusing channel using silicon tubing with an OD (1 mm) and connected to a compressed air cylinder with regulators. LabView NXG 5 software was opened, ready to evaluate droplet formation.

Picodroplet Generation

After connecting all tubing to the picodroplet technology, the pressure is turned on and the initial inlet pressures are chosen and allowed to equilibrate before starting the data acquisition of measurements. A 60 x objective is focused on the channel where droplets that have been formed are flowing to the outlet. Droplet formation was recorded by a high-speed camera. Desired droplet volumes were imputed, and the feedback-loop initiated changes in the pressure of the inlets to adjust the droplet volumes. Droplets of sizes 60 and 300 pL were generated using the 40 µm x 40 µm and 60 µm x 60 µm flow-focusing channel PDMS chip, respectively. The average droplet volume (pL), standard deviation (SD), coefficient of variation (CV%), flow rate ratio (aq/oil), and generation speed (droplets/second) was calculated from 25 droplets by the pixel distance along the droplet image against the pixel difference of the background.

Picodroplet Collection and Incubation

Droplets were collected from the outlet by silicon tubing with an OD (1 mm) into a 1.5 mL centrifuge tube. Centrifuge tubes were pierced with small holes and covered with Breath-Easy® gas permeable membrane to facilitate gas exchange. Droplets of varying parameters, such as droplet size, MRSA N315 cell concentration, and antibiotic concentration were collected for incubation in the 37 ºC shaking incubator (180 rpm).

Picodroplet Imaging and Droplet Size Quantification

10 µL of each emulsion tested was added into a chamber slide (C-chip, Neubauer Improved, NanoEnTek) and imaged at different time points using an EVOS™ M5000 Imaging System with a 10x and 20x objective. Bright field images were taken. The 20x objective was used to assess bacterial encapsulation and growth in picodroplets, and the 10x objective was used to assess droplet stability during incubation. Droplets were considered stable if they did not homogenise into separate phases, coalesce, flocculate, or invert phases. The droplet sizes of the emulsions at each time point were assessed using ImageJ with the Hough Circle Transform Plugin. Three representative images of three different fields of view of the emulsion were measured. The Hough Circle Transform Plugin allows for circular objects to be extracted from an image and each radius to be measured, leading to a dataset containing the position and radius of every droplet detected on each image. Briefly, the perimeter of each droplet is found by Process > Find Edges. The threshold is then set, and a mask made by Image > Adjust > Threshold > Apply. Finally, the Hough Circle Transform Plugin was run by manually adjusting the minimum and maximum cutoff for the radii expected in the image. Measurements were

exported as a results table. The measurements exported are: 1) the X and Y coordinates of the centre of each droplet, 2) the radius (in pixels) of each circle, 3) the Hough score for each circle, 4) the number of circles found within that frame, 5) the actual resolution that they transform, and 6) the frame in which the circle was found. The radius (in pixels) was plotted in GraphPad Prism 8 of each droplet on each image to assess and change in droplet size over time.

4.2.6 Enumeration of CFU/ mL in Droplets Compared to Bulk Culture

To determine the bacterial number in picodroplets after each time point, 40 µL of the emulsion was added into a 100 µL centrifuge tube by pipetting slowly, followed by adding 40 µL of Pico-Break™ that was warmed to room temperature. The emulsion was gently vortexed and centrifuged for 10 seconds. The oil phase was removed and the aqueous phase containing bacteria was pipetted out and recovered. CFU was determined by doing serial dilutions of the cell suspension recovered from the picodroplet emulsion in PBS, followed by the previously described Miles and Misra technique. To calculate the number of CFU/ mL from the original optical droplet sample, the average number of colonies for a dilution was multiplied by 50 and then multiplied by the dilution factor.

4.2.7 Minimum Inhibitory Concentration (MIC) and Minimum Bactericidal Concentration (MBC) of MD56 against MRSA N315 in 100 µL Bulk Culture.

The antimicrobial activity of MD56 against MRSA N315 in bulk culture was assessed using a broth microdilution method to determine the minimum inhibitory concentration (MIC). A master plate was designed with a serial dilution of MD56 in DMSO ranging from 10 mM to 0 mM. 5 µL of each dilution was added to a well for a total concentration of DMSO at 5% and the final concentration of serial dilutions to be 500 µM, 250 µM, 125 µM, 62.5 µM, 31.3 µM, 15.6 µM, 7.8 µM, 3.9 µM, 2 µM, 1 µM, 0.5 µM, 0.2 µM, 0.1 µM, 0.06 µM, 0.03 µM, 0.02 µM, 0.008 µM, 0.004 µM when inoculated with 95 µL of MRSA N315. Controls included DMSO only, bacterial only, and media only. The final volume of each well was 100 µL and n=3 technical replicates on each plate. MRSA N315 was inoculated into wells at optical density (OD) 570 nm= 0.1. 96-well plates were incubated at 37 °C for a total of 24 hours, with orbital shaking at 180 rpm. Optical density (570 nm) readings were taken after 24 hours using a spectrophotometric plate reader (Biotek EL808). After the optical density reading was taken, 5 µL of each well was plated out on to solid agar plates using metal stampers to observe bactericidal activity. Agar plates were incubated at 37 °C for 24 hours. The MBC was determined as the minimum concentration where no bacterial growth was visually observed. Last, 30 µL of 1 mg/ml resazurin dissolved in de-ionised water was added to each well and incubated at room temperature for 24 hours. The MIC was determined as the lowest concentration where bacterial growth was inhibited, indicated by optical density and a blue coloured well. All data collected were n=3 technical replicates. The broth microdilution assays were processed in Microsoft® Excel® for Microsoft

365 MSO (Version 2302 Build 16.0.16130.20806) 64-bit and then plotted and analysed using GraphPad Prism 8. Blank control values of media only were deducted from bacteria containing wells. The endpoint data at 24 hours were then analysed using a one-way ANOVA.

4.2.8 Statistical Analysis

Poisson Statistic Calculations

To study cells at the single and multi-cell layer, the occupancy of the number of bacteria in each droplet was statistically determined using the Poisson distribution given by,

$$p(k,\lambda) = \frac{\lambda^{\kappa} e^{-\lambda}}{k!}$$

where k is the number of particles in a droplet and λ is the average number of cells per droplet volume. For experiments in this chapter, the droplet volume chosen was 60 pL or 300 pL and the starting cell concentration was 2.42x10^7, 4.85 x10^7, 9.70 x10^7, 2.91 x10^8, or 5.82 x10^8. Where the number of cells encapsulated is between 0-20 cells, experiments were defined as "single-cell level" studies and where the number of cells encapsulated is between 20-230 cells, experiments were defined as "multi-cell level" studies.

Colony Forming Unit Calculation

Bacterial growth was quantified by log10 transformation of CFU/mL data. As appropriate, statistical comparisons between groups were performed using one-way or two-way ANOVA with Tukey's post-hoc test. All statistical analyses used GraphPad Prism (version 8.0, GraphPad Software). A p-value < 0.05 was considered statistically significant. All experiments were performed in triplicate unless otherwise stated. For each susceptibility experiment conducted, the MIC was determined as the lowest concentration where bacterial growth was inhibited, indicated by a negative change in log CFU/ mL.

Droplet Monodispersity and Size Distribution

Droplet monodispersity and size distribution were assessed using a function in Microsoft® Excel® for Microsoft 365 MSO (Version 2302 Build 16.0.16130.20806) 64-bit and then plotted and analysed using GraphPad Prism 8. The experimental results for assessing droplet monodispersity and size distribution of different variables are represented by average droplet volume (pL), standard deviation (SD), and coefficient of variation (CV%). For each experimental condition, approximately 2,500 droplets were analysed. To determine the size distribution and stability of collected and incubated droplets, the radius (in pixels) of each droplet identified on each image was plotted over the time course of the experiment. The coefficient of variation (CV%) was used to assess the change in the size variance of the droplets during incubation.

4.3 Results

4.3.1 Standardisation Curve for MRSA CFU/mL Versus Optical Density (OD570)

From the previous chapter, it was concluded that MH media does not affect the monodispersity or stability of droplets generated with 5% Pico-Surf® during incubation. Therefore, MRSA, which can be cultured in MH media, was chosen to investigate droplet-based bacterial studies in this chapter. Growth curves provide valuable information on bacterial growth kinetics and cell physiology. The number of CFU/ mL of a bulk culture is an excellent way of quantifying bacterial growth. However, to obtain this measurement, growth relies on incubation for analysis. On the other hand, optical density provides an instant approximation of bacterial count, which is measured by a spectrophotometer by measuring the absorbance of light particles passing through a culture. Optical density increases as the bacterial culture grows. To generate droplets with desired cell concentrations, the starting bacterial concentration of the aqueous phase must be determined in CFU/ mL and adjusted if needed. To approximate the number of CFU/ mL in an inoculated culture of MRSA, a standard curve was generated using a linear regression to correlate optical density to CFU/ mL. In this experiment, optical density samples of 0.05, 0.1, 0.2, 0.3, 0.4, 0.5 and 0.6 (570 nm) were serially diluted and CFU/ mL was determined in each sample by using the Miles and Misra technique. The decision to plot only up to an optical density of 0.6 OD was based on the fact that higher optical densities lead to less accurate correlations to CFU/mL due to changes in cell shape and extracellular products in the media, which impact the optical density reading. Figure 4.1 shows the standard curve and correlation model (y=969771689*X) of the linear regression. This equation was then used for all future experiments, encapsulating MRSA in droplets by measuring optical density of an inoculated culture and adjusting the concentration with MH broth to a desired CFU/ mL. This technique assisted single-cell or multi-cell encapsulation.

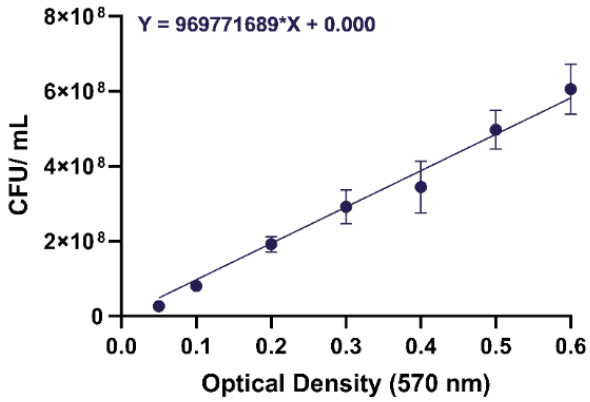

Figure 4.1. Standard curve for MRSA CFU/mL versus optical density (570nm) in Mueller Hinton broth. Linear regression obtained by Miles and Misra counting was used to generate a standard curve of the approximation of CFU/mL of a batch culture to its correlated optical density (Y = 969771689*X + 0.000). The relationship is plotted between CFU/mL and 7 optical density ranges 0.05, 0.1, 0.2, 0.3, 0.4, 0.5, and 0.6. Y value is CFU/mL and X value is OD570 nm. R^2=0.99. Data are presented as mean values of triplicate biological repeats and triplicate technical repeats (n=9) with error bars representing the standard error of the mean (SEM).

4.3.2 Controlled Single-cell MRSA Encapsulation and Quantification of Viability in 60pL Droplets.

To validate single-cell encapsulation of bacteria in monodisperse droplets using picodroplet technology, MRSA was encapsulated inside droplets using 5% Pico-Surf® as the surfactant. MRSA was compartmentalised into droplets using the picodroplet technology and then collected for incubation before being assessed for viability over time. The process followed the Poisson distribution whereby if 60 pL droplets were generated with a starting concentration of $2.42x10^7$ CFU/ mL (OD=0.025) MRSA cells, then the probability of droplets containing 1 cell was 33.96% and the probability of droplets that were empty was 23.35% as depicted in Figure 4.2. By using these two parameters of droplet size and starting cell concentration, the value of λ is 1.45 (the average number of bacteria per droplet). Therefore, following Poisson statistics, the range of number of cells encapsulated using the two parameters is between 0 and 8 cells, which is defined here as “single-cell” studies. For the remaining studies in this chapter, “single-cell” encapsulation is referred to as - the number of cells encapsulated per droplets is between 0 and 20. In contrast, “multi-cell” studies can be referred to as the number of cells encapsulated is between >20 per droplet.

A

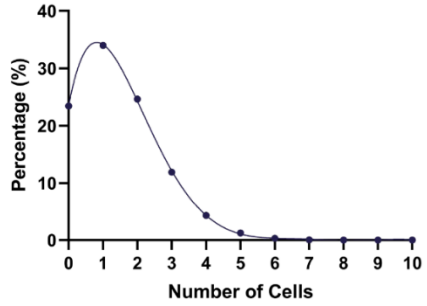

B

CFU/ mL	2.42E+07
λ	1.45
% of Empty Droplets	23.35%
% of Droplets Containing 1 Cell	33.96%
% of Droplets Containing 2 Cells	24.70%
% of Droplets Containing 2+ Cells	17.99%
Monoclonality	44.31%
Range of Number of Cells Encapsulated	0-8

Figure 4.2. Number distribution of MRSA CFU/mL encapsulated in 60 pL droplets with starting cell concentration 2.42E+07. (A) Modelling cell number distribution in picodroplets based on Poisson statistics with 60pL droplets and 2.42x107 CFU/ mL starting concentration. **(B)** Table of probability statistics with 60pL droplets and 2.42x107 CFU/ mL starting concentration.

To evaluate successful single-cell encapsulation of MRSA using the picodroplet technology, two samples of emulsions were generated; MRSA containing droplets and control droplets contains MH media only. Monodispersity of droplets generated by the image-based closed-loop feedback technology was assessed and proved that despite encapsulation of bacteria into the droplets, droplets can be generated with equal volumes (Figure 4.3 A). Droplets containing MRSA and MH media as the aqueous phases and 5% Pico-Surf® as the oil phase was generated using the 40 µm x 40 µm flow-focusing channel for making 60 pL droplets. MRSA containing droplets had a mean volume of 60.33 pL, a SD of 0.35 pL, and a CV of 0.57% (Figure 4.3 A), calculated consistently with the previous chapter. Likewise, control of droplet generation was observed for 60 pL droplets containing MH media only with a mean volume of 60.26 pL, a SD of 0.33 pL, and a CV of 0.55% (Figure 4.3 B).

Images were taken of droplets containing MRSA and empty control droplets incubated for 0, 2, 4, and 6 hours to observe bacterial count (Figure 4.3 C) as well as the stability of droplets (Figure 4.3 D). A single bacterial cell can be observed at 0 hours (Figure 4.3 C). During incubation, an individual droplet can be seen to increase in bacterial cells compared to the media only control (Figure 4.3 C). In addition, the effect of bacteria on the stability of droplets was tested by assessing droplet size over time. The images in Figure 4.4 illustrate that majority of droplets remain stable during incubation, however, from time point 0-hour smaller droplets are visible for both samples suggesting instability during generation. This is unsurprising, as smaller droplets tend to have lower stability.

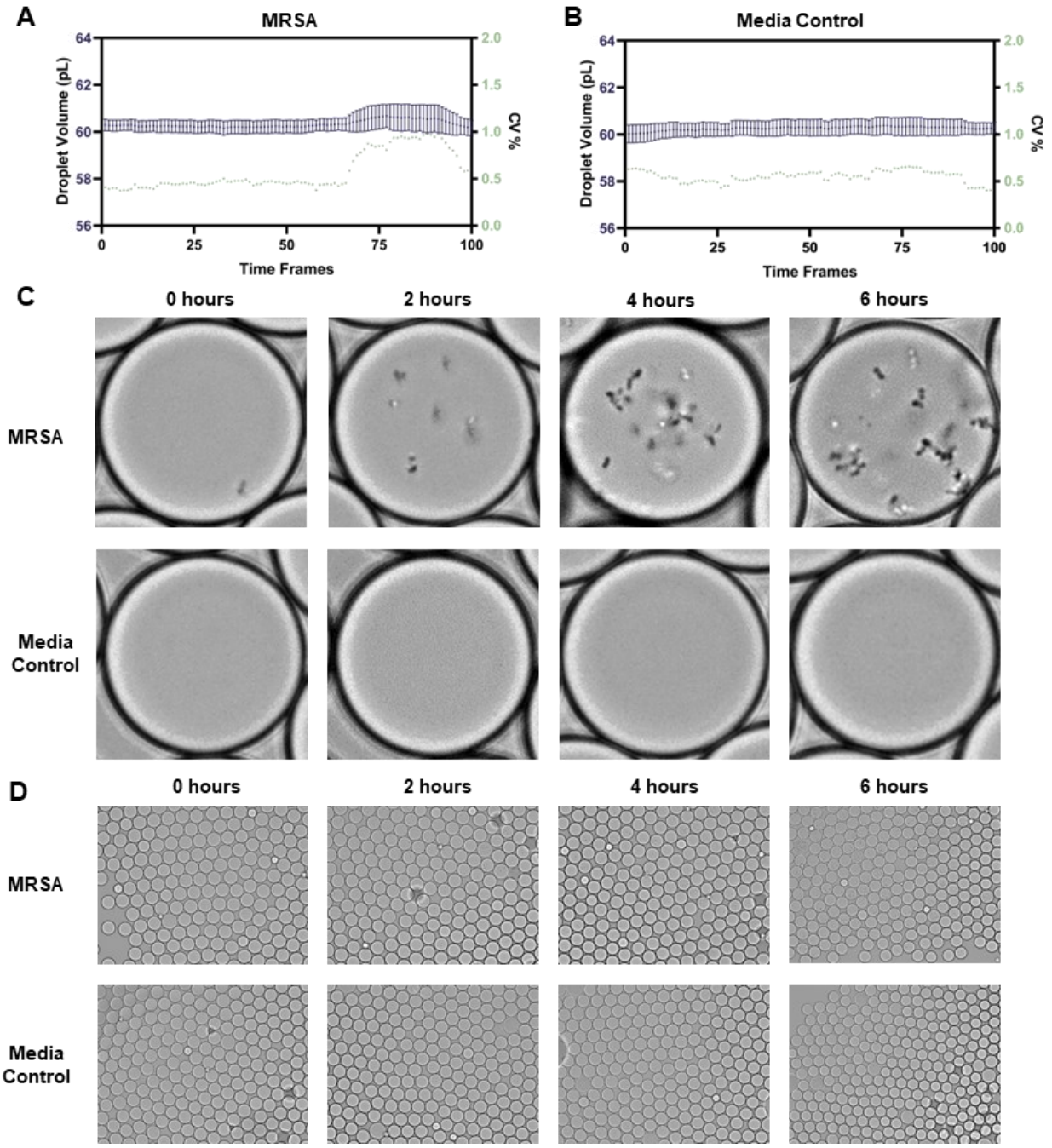

Figure 4.3. Monodispersity and droplet images of 60 pL droplets encapsulated with MRSA at a starting concentration of 2.42x10^{7}. Image-based feedback loop set at 60 pL. **(A)** Monodispersity of droplets generated with MRSA. Mean droplet volume 60.33 pL, SD 0.35 pL, CV 0.57%, FRR 0.89, and droplet generation speed 159/s. **(B)** Monodispersity of droplets generated with MH media control. Mean droplet volume 60.26 pL, SD 0.33 pL, CV 0.55%, FRR 0.90, and droplet generation speed 167/s. The average droplet volume (pL), standard deviation (SD), coefficient of variation (CV%) and flow rate ratio (FRR) of n=25 droplets are plotted for 100 saved frames. Each graph represents 1 of 3 repeats of 100 saved time frames. **(C)** Droplet images of encapsulated MRSA at 0, 2, 4, and 6 hours compared to the control. **(D)** Images of droplet stability at 0, 2, 4, and 6 hours compared to the control. Images represent n=3 technical replicates of 3 fields of view.

To quantify the size of droplets over time, image analysis software was used as the same as before to detect the radius of each droplet. Droplet radius (pixels) was plotted in scatter diagrams for the two samples. Figure 4.4 A concludes that droplets remain stable for the full six hours of the experiment depicted by CV values below 10%. There was no noticeable difference between droplets containing MRSA and empty droplets (Figure 4.4 B).

Previous research showed that picodroplets can be used as bioreactors for bacterial proliferation. To ensure bacterial viability inside these potential antibiotic susceptibility bioreactors, CFU/ mL counts were used to determine survival in such small volumes. At each time point, droplets were collected, and each sample was separated into its oil phase and aqueous phase using Pico-Break™ reagents. The separation of phases allows the aqueous phase containing MRSA cells to be quantified by CFU/ mL plating. What is evident in Figure 4.4 C is the continued survival of MRSA inside droplets during incubation compared with empty control droplets shown by a significant difference. For the sample containing no bacteria, strong evidence suggests that this flow of methodology does not contaminate the samples, as shown by the negative growth. Closer inspection of the data revealed that MRSA proliferated significantly in droplets over 6 hours (P=0.0009), with bacterial counts increasing from 9.1 log CFU/mL to 9.6 log CFU/mL. This 0.5 log increase represents approximately 3.16-fold growth, suggesting that cells underwent 1-2 divisions during this period, which is consistent with the known doubling time of MRSA in optimal conditions. Interestingly, the CFU counts of MRSA in 60 pL droplets showed a slight decrease between 4 and 6 hours of incubation (Figure 4.4C). This observation contrasts with the continuous growth typically seen in bulk cultures and suggests that factors specific to the droplet microenvironment may be influencing bacterial growth dynamics. This might be due to variables such as available nutrient content or oxygen availability. The full results from the 2-way ANOVA are presented in appendix 4.1.

In summary, these results inform that MRSA can be encapsulated at the single-cell level in w/o picodroplets which are highly monodisperse generated with picodroplet technology and are able to survive inside incubating droplets over the course of a few hours, presenting no contamination. Noteworthy, is that the results from this experiment convey that 5% Pico-Surf® would be effective at maintaining droplet stability with droplets containing MH media as the aqueous phase. In addition, the ability to quantify cell counts inside droplets was made possible by the successful method of breaking the droplets open and CFU/ mL plating.

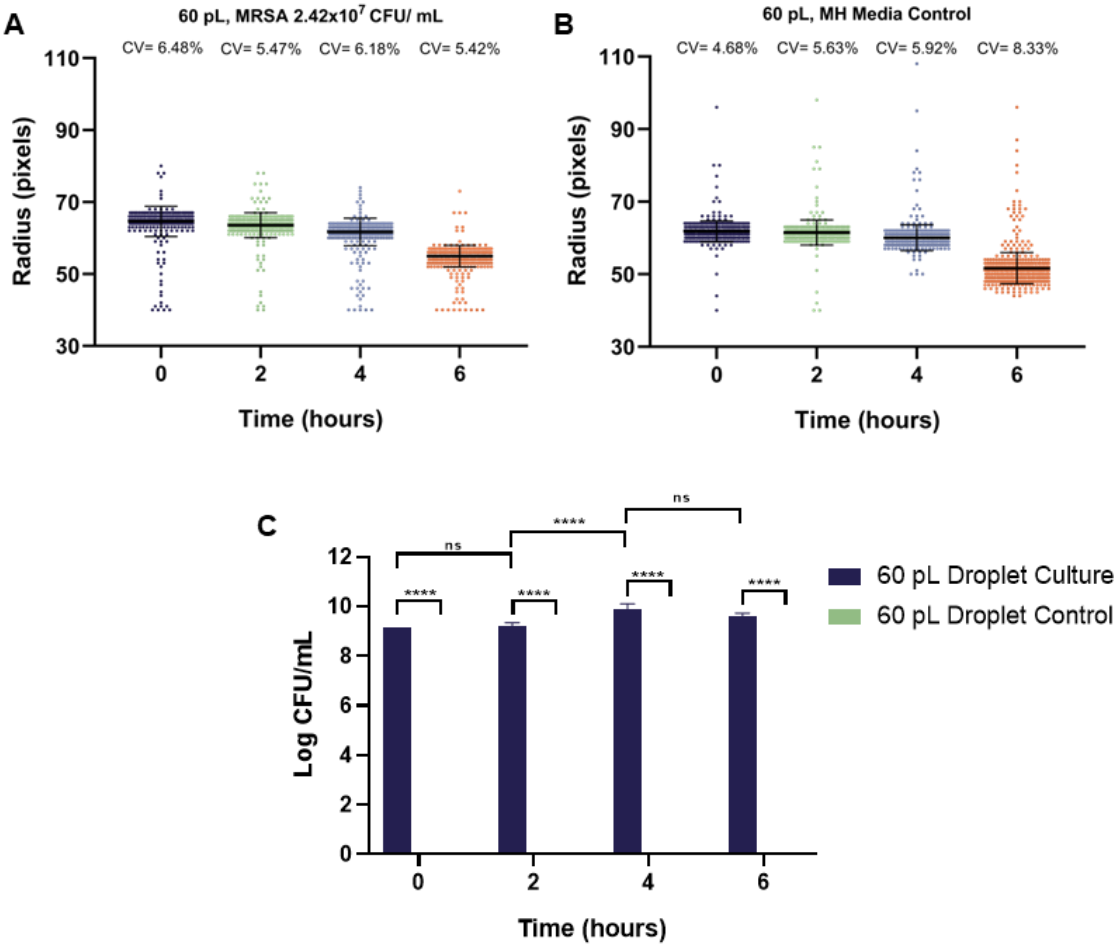

Figure 4.4. Droplet stability and bacterial survival in 60 pL droplets encapsulated with MRSA at a starting concentration of 2.42x10^7. Scatter plots show variance in droplet size at 0, 2, 4, and 6 hours of droplets encapsulated with MRSA **(A)** compared to MH media only **(B)**. Mean = 65 pixels, SD= 4 pixels, CV= 6.48%, n= 520 droplets at 0 hours, mean = 64 pixels, SD= 3 pixels, CV= 5.47%, n= 547 droplets at 2 hours, mean = 62 pixels, SD= 4 pixels, CV= 6.18%, n= 576 droplets at 4 hours, mean = 55 pixels, SD= 3 pixels, CV= 5.42%, n= 648 droplets at 6 hours for droplets encapsulated with MRSA. Mean = 62 pixels, SD= 3 pixels, CV= 4.68%, n= 555 droplets at 0 hours, mean = 62 pixels, SD= 3 pixels, CV= 5.63%, n= 541 droplets at 2 hours, mean = 60 pixels, SD= 4 pixels, CV= 5.92%, n= 615 droplets at 4 hours, mean = 52 pixels, SD= 4 pixels, CV= 8.33%, n= 781 droplets at 6 hours for droplets encapsulated with MH media only. Data for each time point is n=3 from three representative images of different fields of view of the emulsion. Each data point represents the radius (pixels) of an individual droplet in an image. Black line is the mean, and error bars show the standard deviation of droplet size. **(C)** Recovered CFU/ mL of encapsulated MRSA in 60 pL at 0, 2, 4, and 6 hours compared to media control. CFU data represent n=3 technical replicates within one independent experiment. *P* values were determined by a two-way analysis of variance (ANOVA) with Tukey's multiple comparison tests to analyse the effect of culture condition and time on bacterial growth. **P* < 0.05, ***P* < 0.01, ****P* < 0.001 and *****P* < 0.0001.

4.3.3 Controlled Single-cell MRSA Encapsulation and Quantification of Viability in 300 pL Droplets.

To compare the difference of MRSA single-cell encapsulation on survival and proliferation between smaller and larger droplets sizes, the same experiment mentioned above was repeated with the droplet volume adjusted to 300 pL by the closed-loop feedback. The effect of droplet size on single-cell encapsulation was then studied. When adjusting the droplet volume, the probability of a certain number of encapsulated cells per droplet is changed according to the Poisson distribution (Figure 4.5). When the starting cell concentration of MRSA is $2.42x10^7$ CFU/ mL and the droplet size is 300 pL, the number of empty droplets is reduced to 0.07% and the probability that each droplet contains 1 cell is 0.50%. Using these parameters, the monoclonality is reduced to 0.50% and the range of the number of cells encapsulated in each droplet is between 0-19 as depicted in Figure 4.5 B. Here, this experiment is still at the "single-cell" level. Droplet encapsulation, monodispersity, stability, and bacterial proliferation were assessed in the same way as before using 300 pL as the bioreactor size.

A

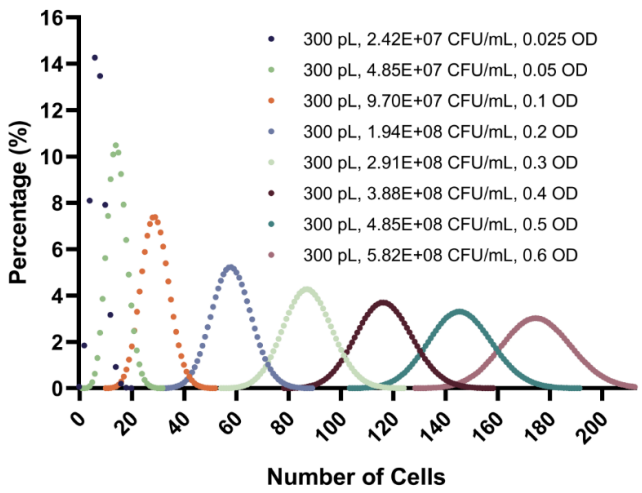

B

CFU/ mL	2.42E+07	4.85E+07	9.70E+07	1.94E+08	2.91E+08	3.88E+08	4.85E+08	5.82E+08
λ	7.27	14.55	29.09	58.18	87.28	116.37	145.47	174.56
% of Empty Droplets	0.07%	0%	0%	0%	0%	0%	0%	0%
% of Droplets Containing 1 Cell	0.50%	0%	0%	0%	0%	0%	0%	0%
% of Droplets Containing 2 Cells	1.84%	0.01%	0%	0%	0%	0%	0%	0%
% of Droplets Containing 2+ Cells	97.59%	99.99%	100%	100%	100%	100%	100%	100%
Monoclonality	0.50%	0%	0%	0%	0%	0%	0%	0%
Range of Number of Cells Encapsulated	0-19	2-31	11-51	32-88	54-123	79-157	104-190	129-223

Figure 4.5. Number distribution of MRSA CFU/mL in 300 pL droplets. (A) Modelling cell number distribution in picodroplets based on Poisson statistics with 300pL droplets and increasing CFU/ mL starting concentration. **(B)** Table of probability statistics with 300pL droplets and increasing CFU/ mL starting concentration.

Droplets containing MRSA and MH media as the aqueous phases and 5% Pico-Surf® as the oil phase were generated using the 60 µm x 60 µm flow-focusing channel for making 300 pL droplets. MRSA containing droplets had a mean volume of 299.57 pL, a SD of 1.39 pL, and a CV of 0.47% (Figure 4.6 A) calculated in a similar manner as the previous chapter. Likewise, control of droplet generation was observed for 300 pL droplets containing MH media only with a mean volume of 299.95 pL, a SD of 0.91 pL, and a CV of 0.30% (Figure 4.6 B). These quantifications concluded that 5% Pico-Surf® and the picodroplet technology were able to create monodisperse 300 pL droplets containing MRSA.

Images were taken of 300 pL droplets containing MRSA and empty control droplets incubated for 0, 2, 4, and 6 hours to observe bacterial count (Figure 4.6 C) as well as stability of droplets (Figure 4.6 D). Few bacterial cells can be observed at 0 hours (Figure 4.6 C). During incubation, an individual droplet can be seen to increase in bacterial cells compared to the media only control (Figure 4.6 C). In addition, the effect of bacteria on the stability of droplets was tested by assessing droplet size over time. From the images in Figure 4.6 D, the illustration reveals that droplets remain stable during incubation.

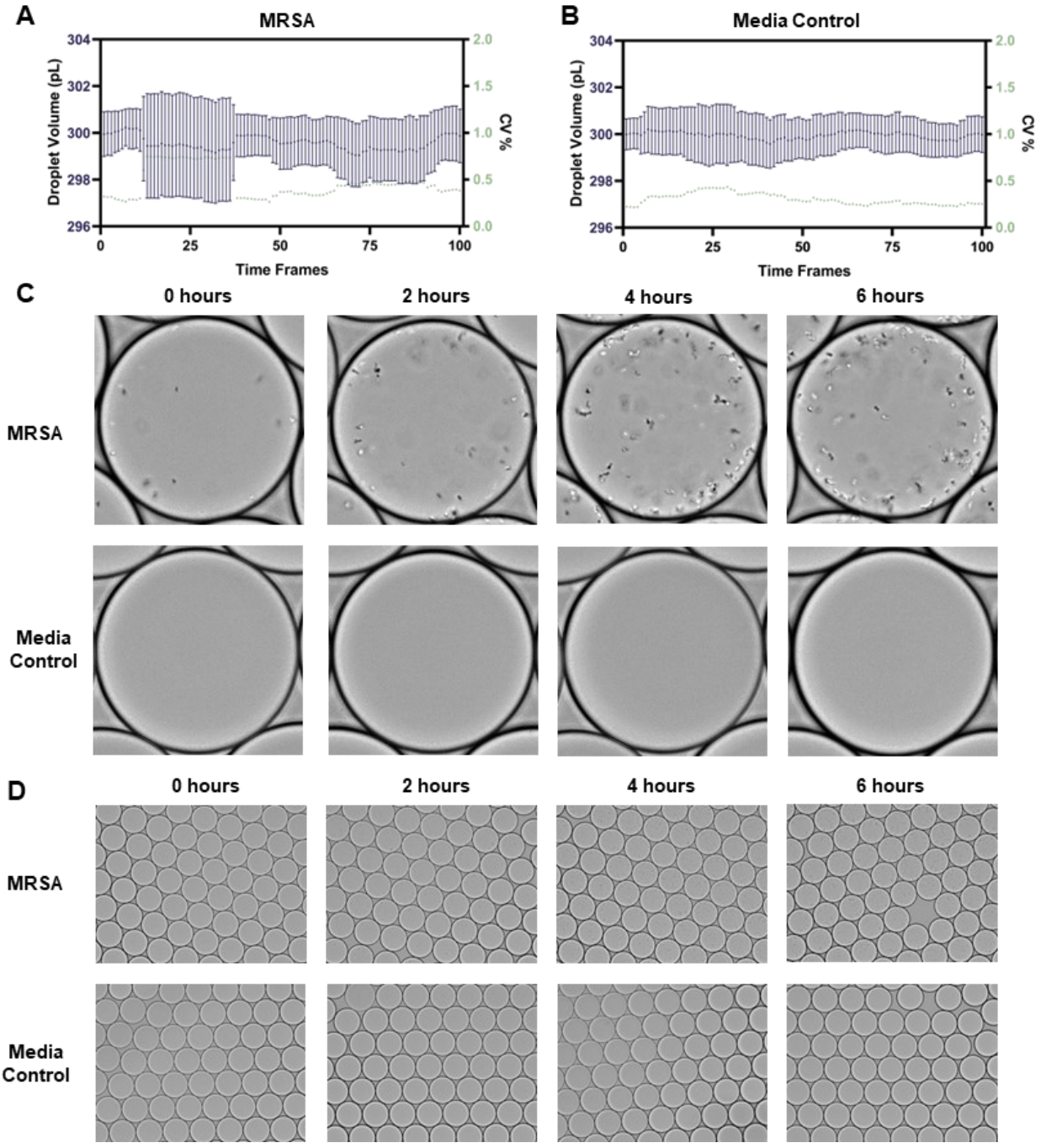

Figure 4.6. Monodispersity and droplet images of 300 pL droplets encapsulated with MRSA at a starting concentration of 2.42x10^{7}. Image-based feedback loop set at 300 pL. **(A)** Monodispersity of droplets generated with MRSA. Mean droplet volume 299.57 pL, SD 1.39 pL, CV 0.47%, FRR 0.88, and droplet generation speed 445/s. **(B)** Monodispersity of droplets generated with MH media control. Mean droplet volume 299.95 pL, SD 0.91 pL, CV 0.30%, FRR 0.88, and droplet generation speed 423/s. The average droplet volume (pL), standard deviation (SD), coefficient of variation (CV%) and flow rate ratio (FRR) of n=25 droplets are plotted for 100 saved frames. Each graph represents 1 of 3 repeats of 100 saved time frames. **(C)** Droplet images of encapsulated MRSA at 0, 2, 4, and 6 hours compared to the control. **(D)** Images of droplet stability at 0, 2, 4, and 6 hours compared to the control. Images represent n=3 technical replicates of 3 fields of view.

To quantify the size of droplets over time, image analysis software was used as the same as before to detect the radius of each droplet. Figure 4.7 A can conclude that droplets remain stable for the full 6 hours of the experiment depicted by CV values below 10%. There was no noticeable difference between droplets containing MRSA and empty droplets (Figure 4.7 B). Again, to ensure bacterial viability inside the 300 pL droplets, CFU/ mL counts were used to determine survival. Results display survival of MRSA inside 300 pL droplets during incubation compared with empty control droplets shown by a significant difference ($P < 0.0001$). In addition, the data showed that droplets containing MRSA had a significant difference ($P < 0.0001$) in proliferation from 6.6 log CFU/ mL to 7.9 log CFU/ mL within the number of cell divisions possible in 6 hours (Figure 4.7 C). Unlike the 60 pL droplets, the 300 pL droplets appeared to facilitate a larger proliferation rate, possibly due to the increased space and nutrients as depicted by a significant different in CFU/ mL between 4 and 6 hours ($P < 0.0001$). The full results from the 2-way ANOVA are presented in appendix 4.2.

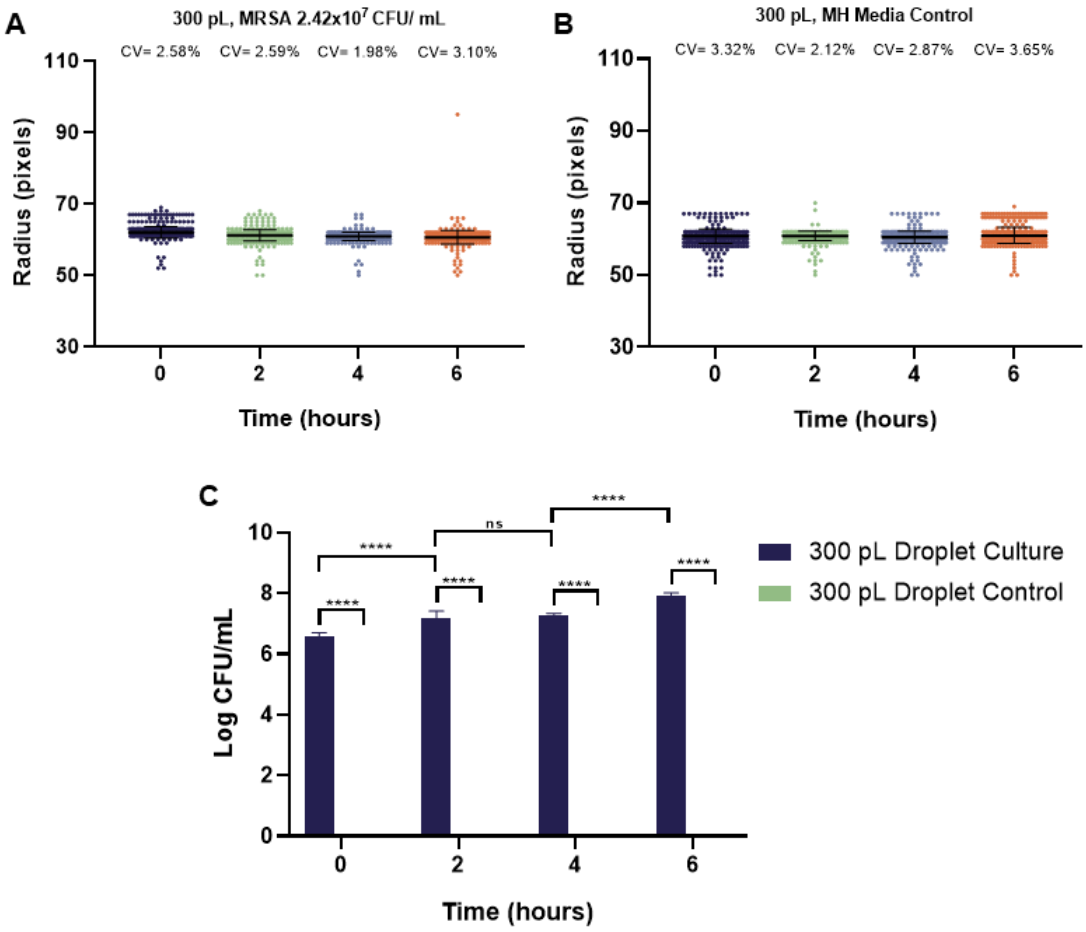

Figure 4.7. Droplet stability and bacterial survival in 300 pL droplets encapsulated with MRSA at a starting concentration of 2.42x10^7. Scatter plots show variance in droplet size at 0, 2, 4, and 6 hours of droplets encapsulated with MRSA **(A)** compared to MH media only **(B)**. Mean = 62 pixels, SD= 2 pixels, CV= 2.68%, n= 633 droplets at 0 hours, mean = 61 pixels, SD= 2 pixels, CV= 2.59%, n= 613 droplets at 2 hours, mean = 61 pixels, SD= 1 pixels, CV= 1.98%, n= 643 droplets at 4 hours, mean = 61 pixels, SD= 2 pixels, CV= 3.10%, n= 650 droplets at 6 hours for droplets encapsulated with MRSA. Mean = 61 pixels, SD= 2 pixels, CV= 3.32%, n= 629 droplets at 0 hours, mean = 61 pixels, SD= 1 pixels, CV= 2.12%, n= 631 droplets at 2 hours, mean = 61 pixels, SD= 2 pixels, CV= 2.87%, n= 641 droplets at 4 hours, mean = 61 pixels, SD= 2 pixels, CV= 3.65%, n= 647 droplets at 6 hours for droplets encapsulated with MH media only. Data for each time point is n=3 from three representative images of different fields of view of the emulsion. Each data point represents the radius (pixels) of an individual droplet in an image. Black line is the mean, and error bars show the standard deviation of droplet size. **(C)** Recovered CFU/ mL of encapsulated MRSA in 60 pL at 0, 2, 4, and 6 hours compared to media control. CFU data represents n=3 technical replicates within one independent experiment. *P* values were determined by a two-way analysis of variance (ANOVA) with Tukey's multiple comparison tests to analyse the effect of culture condition and time on bacterial growth. **P* < 0.05, ***P* < 0.01, ****P* < 0.001 and *****P* < 0.0001.

4.3.4 Controlled Multi-cell MRSA Encapsulation and Quantification of Viability in 300 pL Droplets.

Having examined single-cell encapsulation, next the picodroplet technology was utilised to evaluate encapsulation, monodispersity, stability, and bacterial proliferation inside droplets at the multi-cell level. The 300 pL volume on the feedback loop was maintained, however, the starting inoculum was changed to 5.82×10^8 CFU/ mL to change the possibility of 1 cell being encapsuled in each droplet. An explanation is shown in Figure 4.5 of the Poisson statistic calculation of using these two parameters of droplet size and starting cell concentration. The number of empty droplets are reduced to 0% and the probability that each droplet contains 1 cell is 0%. By utilising these parameters, the monoclonality is also reduced to 0%, and the range of the number of cells encapsulated in each droplet is depicted in Figure 4.5B, with values ranging from 129 to 223.

As mentioned before, to generate 300 pL droplets containing MRSA and MH media as the aqueous phases, 5% Pico-Surf® and the 60 µm x 60 µm flow-focusing channel were used. Multi-cell encapsulation of MRSA containing droplets had a mean volume of 300.65 pL, a SD of 0.849 pL, and a CV of 0.28% (Figure 4.8 A) calculated identically in the previous chapter. Equally, control of droplet generation was observed for 300 pL droplets containing MH media only with a mean volume of 300.04 pL, a SD of 0.71 pL, and a CV of 0.24% (Figure 4.8 B). These quantifications concluded that 5% Pico-Surf® and the picodroplet technology were able to create monodisperse 300 pL droplets containing MRSA at the multi-cell level. Contrary to the hypothesis, increasing cell starting concentration did not block the flow-focusing junction of the PDMS chip, as droplets were generated with ultra-high monodispersity.

Images were also taken of 300 pL droplets containing MRSA and empty control droplets incubated for 0, 2, 4, and 6 hours to observe bacterial count (Figure 4.8 C) as well as the stability of droplets (Figure 4.8 D). The droplets at time point 0 hours are observed to have multiple cells compared with the two previous experiments (Figure 4.8 C) but still appear to increase in bacterial cells compared to the media only control (Figure 4.8 C). In addition, the effect of bacteria on the stability of droplets was tested by assessing droplet size over time. The images in Figure 4.8 D demonstrate the enduring stability of droplets during incubation. The most salient result to emerge from the data is that droplets containing MRSA appear to be reducing in size during the incubation.

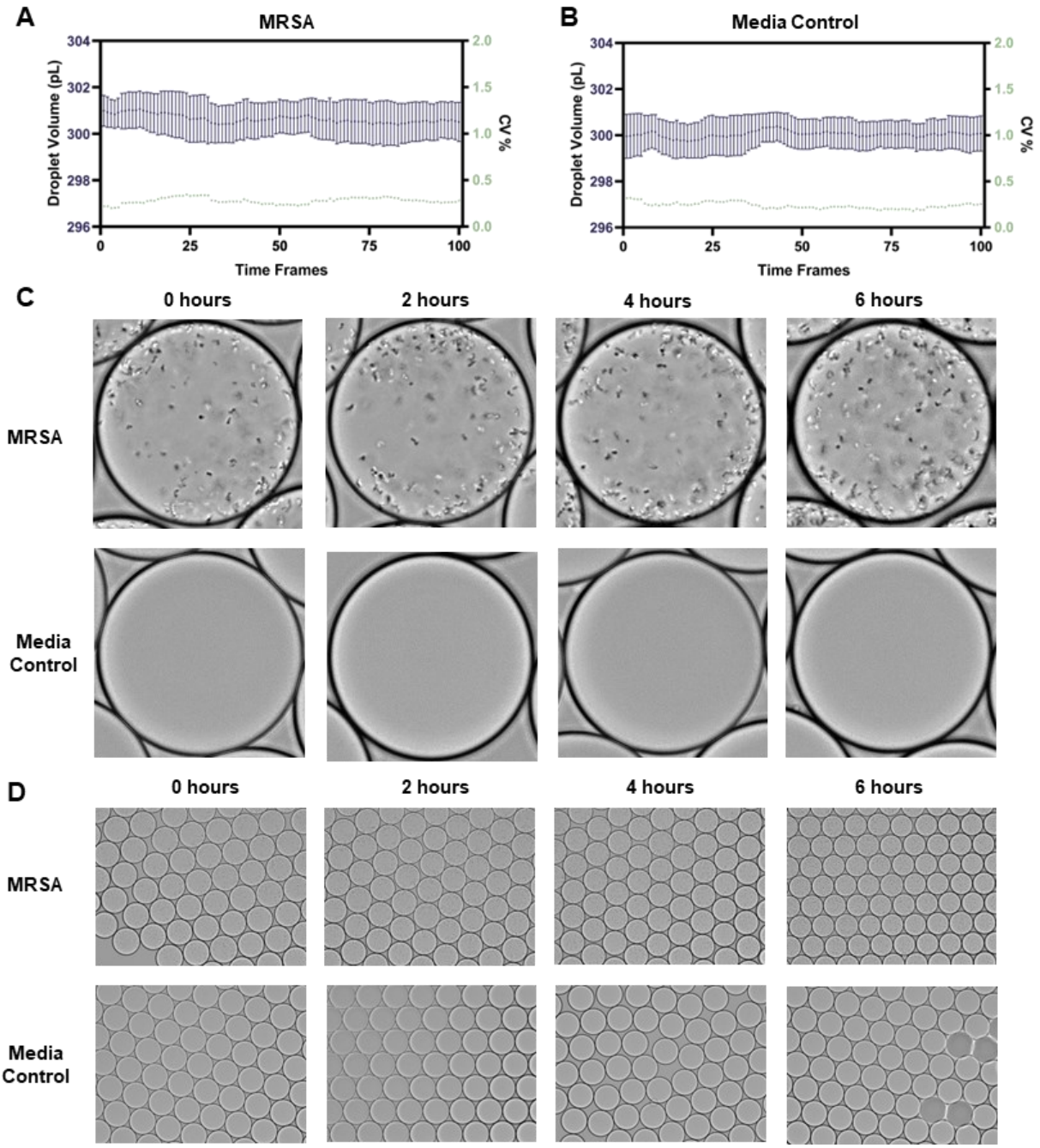

Figure 4.8. Monodispersity and droplet images of 300 pL droplets encapsulated with MRSA at a starting concentration of 5.82x10^{8}. Image-based feedback loop set at 300 pL. **(A)** Monodispersity of droplets generated with MRSA. Mean droplet volume 300.65 pL, SD 0.84 pL, CV 0.28%, FRR 0.89, and droplet generation speed 367/s. **(B)** Monodispersity of droplets generated with MH media control. Mean droplet volume 300.04 pL, SD 0.71 pL, CV 0.24%, FRR 0.92, and droplet generation speed 448/s. The average droplet volume (pL), standard deviation (SD), coefficient of variation (CV%) and flow rate ratio (FRR) of n=25 droplets are plotted for 100 saved frames. Each graph represents 1 of 3 repeats of 100 saved time frames. **(C)** Droplet images of encapsulated MRSA at 0, 2, 4, and 6 hours compared to the control which were shaken at 37°C. **(D)** Images of droplet stability at 0, 2, 4, and 6 hours compared to the control. Images represent n=3 technical replicates of 3 fields of view.

To quantify the size of droplets over time, image analysis software was used as the same as before to detect the radius of each droplet. Figure 4.9 A suggests that droplets maintain stability with CV values below 10% for the entire six-hour duration of the experiment. However, there was a noticeable difference between droplets containing MRSA and empty droplets with a decrease in radius of droplets containing MRSA (Figure 4.9 B). The shrinkage in droplet size may be due to the increase in the inoculum size of the droplet. With the initial presence of more cells and subsequent increased cell divisions during incubation in the 300 pL culture, nutrient uptake likely increased, causing droplets to shrink through the process of osmosis.

CFU counting was also assessed to examine the effect of an increased starting cell concentration on the proliferation of MRSA in droplets (Figure 4.9 C). Results display viability of MRSA inside 300 pL droplets during incubation compared with empty control droplets shown by a significant difference ($P < 0.0001$). In addition, the data showed that droplets containing MRSA had a significant difference ($P=0.0083$) in proliferation from 7.9 log CFU/ mL to 8.4 log CFU/ mL within the number of cell divisions possible in 6 hours. Unlike droplets encapsulated with $2.42x10^7$ CFU/ mL cells, a starting inoculum of $5.82x10^8$ CFU/ mL saw a decrease in log CFU/ mL between 4 and 6 hours which could indicate that an increased inoculum size correlates with a decrease in nutrient availability and droplet shrinkage. The full results from the 2-way ANOVA are presented in appendix 4.3.

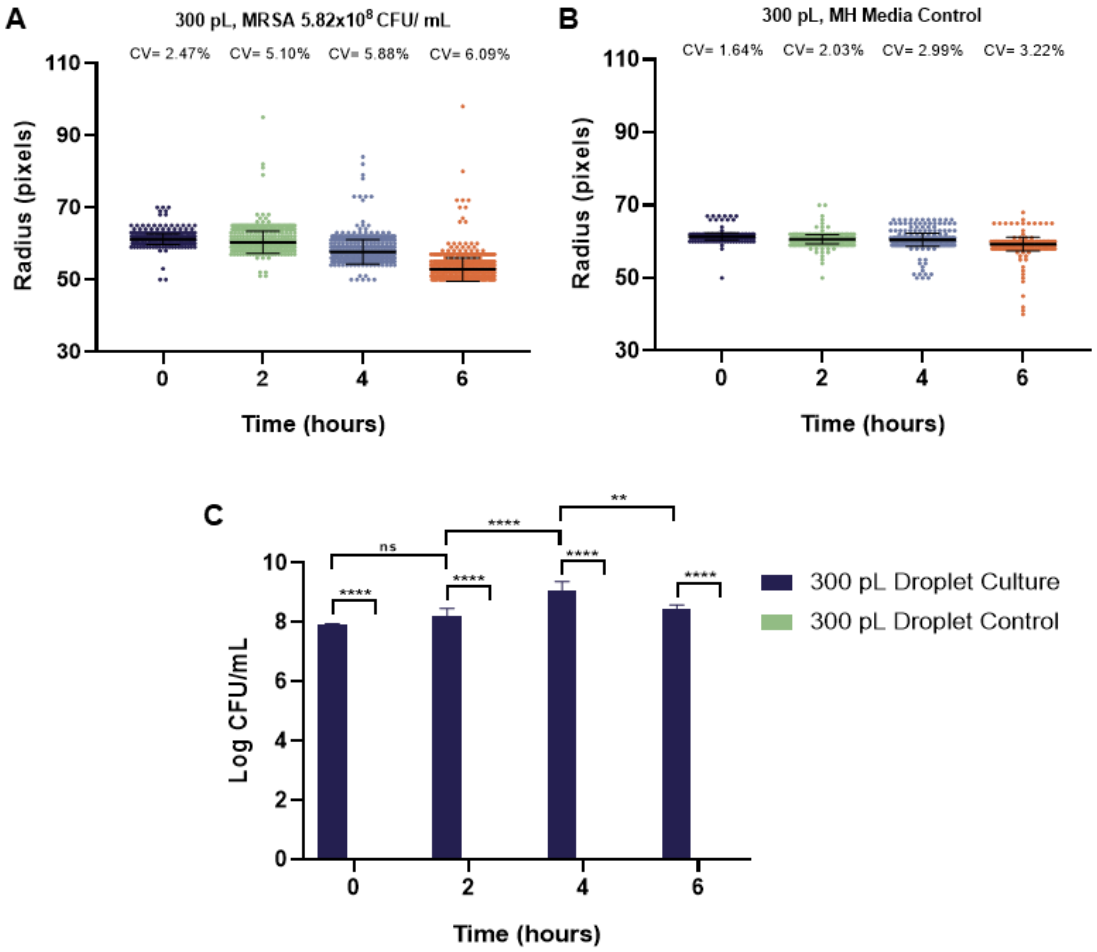

Figure 4.9. Droplet stability and bacterial survival in 300 pL droplets encapsulated with MRSA at a starting concentration of 5.82x10^8. Scatter plots show variance in droplet size at 0, 2, 4, and 6 hours of droplets encapsulated with MRSA **(A)** compared to MH media only **(B)**. Mean = 61 pixels, SD= 2 pixels, CV= 2.47%, n= 641 droplets at 0 hours, mean = 60 pixels, SD= 3 pixels, CV= 5.10%, n= 656 droplets at 2 hours, mean = 58 pixels, SD= 3 pixels, CV= 5.88%, n= 617 droplets at 4 hours, mean = 53 pixels, SD= 3 pixels, CV= 6.09%, n= 792 droplets at 6 hours for droplets encapsulated with MRSA. Mean = 61 pixels, SD= 1 pixels, CV= 1.63%, n= 630 droplets at 0 hours, mean = 61 pixels, SD= 1 pixels, CV= 2.03%, n= 630 droplets at 2 hours, mean = 60 pixels, SD= 2 pixels, CV= 2.99%, n= 614 droplets at 4 hours, mean = 59 pixels, SD= 2 pixels, CV= 3.22%, n= 668 droplets at 6 hours for droplets encapsulated with MH media only. Data for each time point is n=3 from three representative images of different fields of view of the emulsion. Each data point represents the radius (pixels) of an individual droplet in an image. Black line is the mean, and error bars show the standard deviation of droplet size. **(C)** Recovered CFU/ mL of encapsulated MRSA in 60 pL at 0, 2, 4, and 6 hours compared to media control. CFU data represent n=3 technical replicates within one independent experiment. *P* values were determined by a two-way analysis of variance (ANOVA) with Tukey's multiple comparisons tests to analyse the effect of culture condition and time on bacterial growth. **P* < 0.05, ***P* < 0.01, ****P* < 0.001 and *****P* < 0.0001.

4.3.5 The Effect of Increasing the Starting Droplet Inoculum on MRSA Proliferation in Droplets and the Stability of Droplets.

Having inspected bacterial proliferation for up to 6 hours in droplets, next the inoculum effect was examined in further detail and compared to a 3 mL bulk culture for up to 24 hours. The microenvironment in droplets might differ from the environment in traditional bulk cultures and thus a basic understanding of the growth behaviour in droplets needs to be established for future droplet-based antibiotic susceptibility screening.

To investigate if changing the starting inoculum size effects 300 pL droplet generation, using the same aqueous and oil phase as before, 300 pL was imputed into the feedback system and monodispersity was measured of different aqueous samples including 2.42 $x10^7$, 4.85 $x10^7$, 9.70 $x10^7$, 2.91 $x10^8$, 5.82 $x10^8$ CFU/ mL and MH media only control. The table in Figure 4.5 lists the probabilities of the number of cells encapsulated per droplet for each inoculum.

When 300 pL was imputed into the feedback loop, the flow rates of the inlets changed accordingly to generate 300 pL droplets. Droplets encapsulated with 2.42 $x10^7$ CFU/ mL generated a mean droplet size of 300.69 pL, a SD of 0.52 pL, and a CV of 0.17% (Figure 4.10 A) Similarly, control of droplet generation was observed for 4.85 $x10^7$ CFU/ mL, (Figure 4.10 B), 9.70 $x10^7$ CFU/ mL (Figure 4.10 C), 2.91 $x10^8$ CFU/ mL (Figure 4.10 D), 5.82 $x10^8$ CFU/ mL (Figure 4.10 E), and MH media only control (Figure 4.10 F). The mean values of droplet volumes were 0.84, 0.17, 0.56, 0.07, and 0.24 pL aligned with the desired droplet size of 300 pL, corresponding to cell starting concentrations of 4.85 x107, 9.70 x107, 2.91 x108, 5.82 x108, and MH media only control. In addition, respectively, to these cell concentrations, the average standard deviation for droplet generation was 0.52, 0.73, 1.11, 1.0, 0.87, 0.75 pL. In all experiments generating droplets with the 60 µm x 60 µm flow-focusing channel, the coefficient of variations were below 0.91%. When changing the aqueous phase of different MRSA concentrations, highly ultra-monodisperse droplets were successfully generated.

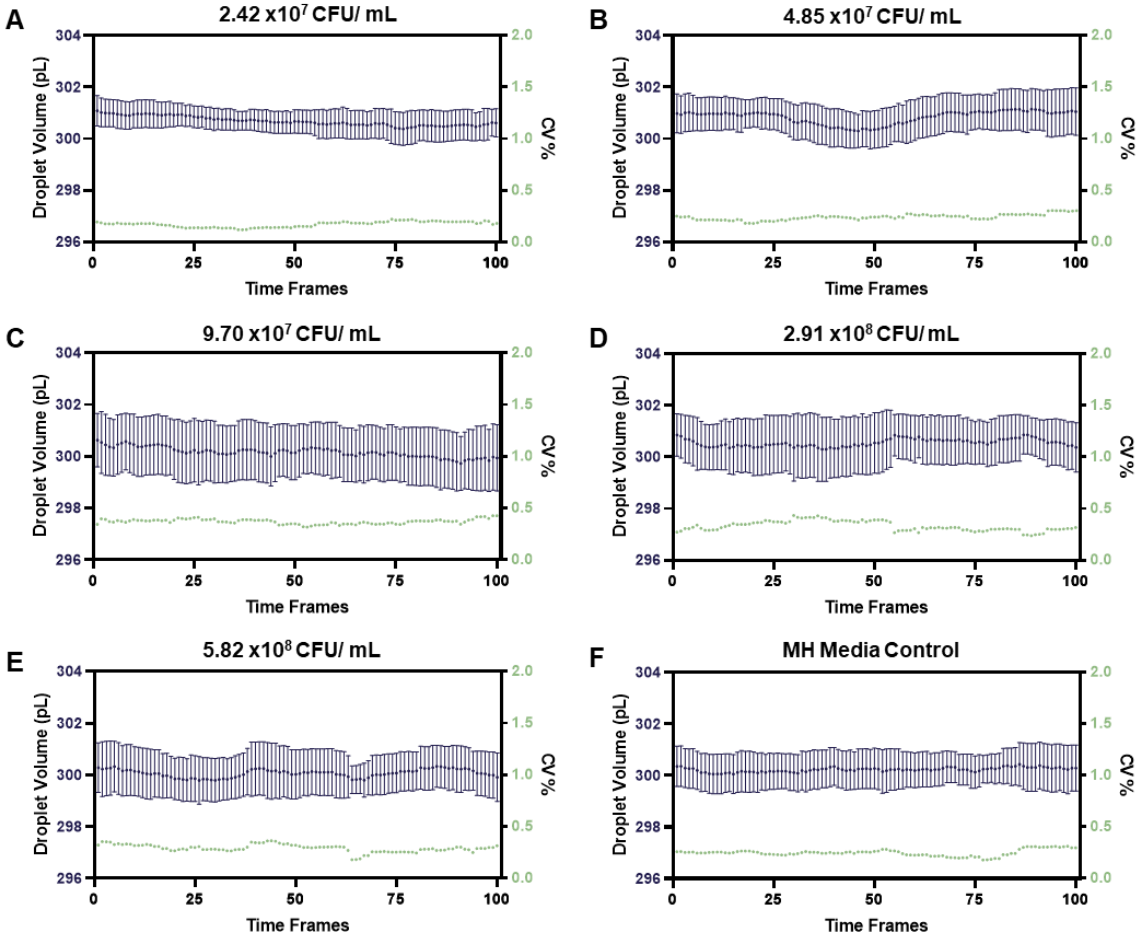

Figure 4.10. Monodispersity of 300 pL generated droplets encapsulated with different starting CFU/mL concentrations of MRSA. Image-based feedback loop set at 300 pL. **(A)** Starting inoculum 2.42 x10^7 CFU/ mL. Mean droplet volume 300.69 pL, SD 0.52 pL, CV 0.17%, FRR 0.92, and droplet generation speed 476/s. **(B)** Starting inoculum 4.85 x10^7 CFU/ mL. Mean droplet volume 300.84 pL, SD 0.73 pL, CV 0.24%, FRR 0.92, and droplet generation speed 423/s. **(C)** Starting inoculum 9.70 x10^7 CFU/ mL. Mean droplet volume 300.17 pL, SD 1.11 pL, CV 0.37%, FRR 0.01, and droplet generation speed 457/s. **(D)** Starting inoculum 2.91 x10^8 CFU /mL. Mean droplet volume 300.56 pL, SD 1.0 pL, CV 0.33%, FRR 0.93, and droplet generation speed 498/s. **(E)** Starting inoculum 5.82 x10^8 CFU /mL. Mean droplet volume 300.07 pL, SD 0.87 pL, CV 0.29%, FRR 0.89, and droplet generation speed 286/s. **(F)** MH media control. Mean droplet volume 300.24 pL, SD 0.75 pL, CV 0.29%, FRR 0.91, and droplet generation speed 187/s. The average droplet volume (pL), standard deviation (SD), coefficient of variation (CV%) and flow rate ratio (FRR) of n=25 droplets are plotted for 100 saved frames. Each graph represents 1 of 3 repeats of 100 saved time frames.

In addition to generating droplets encapsulating different samples of MRSA concentration, 3 mL bulk cultures were set up of the different inoculum concentrations and examined for proliferation. Samples of encapsulated droplets and bulk control cultures were taken at 0 hours and 24 hours. Images of encapsulated droplets were taken at time point 0 hours and after 24 hours of incubation. Figure 4.11 presents the comparison of droplets before and after MRSA incubation for each sample. At 0 hours, there is an obvious increase in cell number as the inoculum is increased from single-cells to multiple cells. Images of droplets at 24 hours appear to show a gradual decrease in proliferation from the low to high inoculum. To quantify this, CFU/ mL was counted as previously described in section x for both droplet samples and control samples.

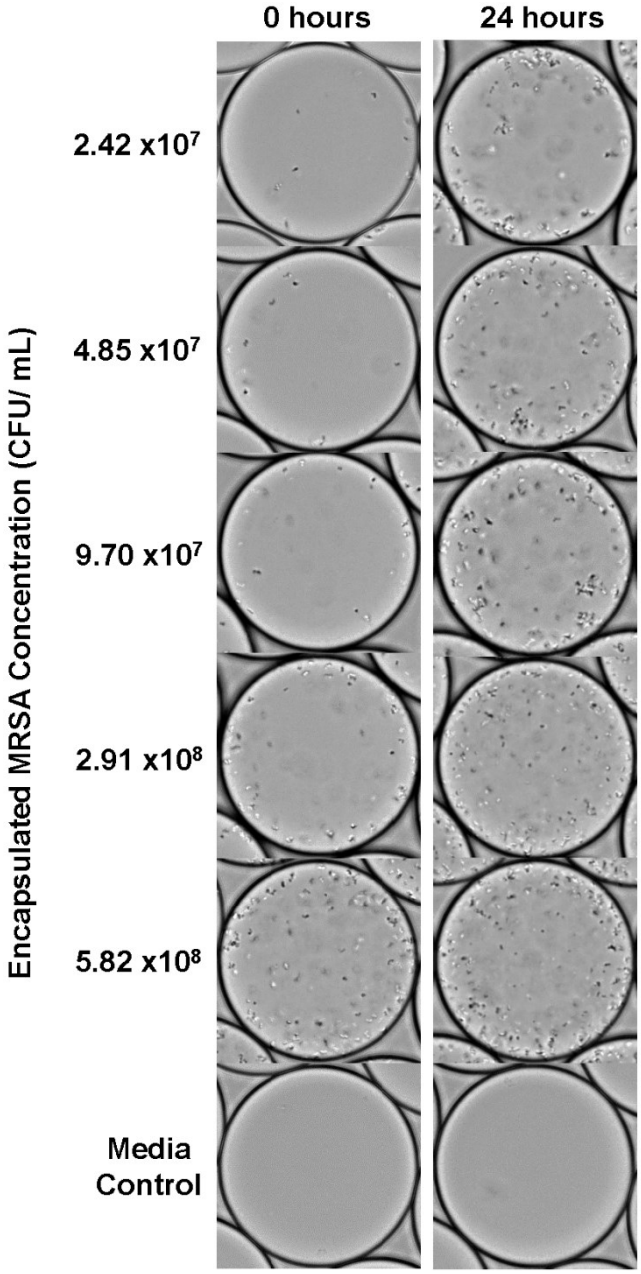

Figure 4.11. Image of MRSA proliferation inside 300pL droplets containing different starting encapsulated MRSA concentration (CFU/ mL) concentrations.

A change in log CFU/ mL was plotted for each inoculum concentration for both droplet and bulk culture samples (Figure 4.12). A positive log CFU/mL change is observed for all samples, indicating bacterial growth. However, the magnitude of growth decreases with the increase in the initial encapsulation concentration of MRSA. This suggests that while higher initial concentrations do not prevent survival, they may impact proliferation rates, possibly due to faster depletion of nutrients or accumulation of waste products. In addition, there is a notable difference between a change in log CFU/ mL between droplet cultures and 3 mL bulk cultures. Several factors could explain this observation. First, the two different cultures may be creating a different physiological environment for the bacteria and therefore experiencing different growth curve dynamics. Second, perhaps the 3 mL culture is providing more space and nutrient

availability for bacterial division. Last, the differences in bioreactors could alter the oxygen concentration the bacteria receives, which could cause a significant difference in proliferation. It is apparent from this data that MRSA can survive and proliferate in picolitre bioreactors for up to 24 hours using a range of inoculum concentrations. It is worth noting that the control samples of MH media only did not display any CFU/ mL for the duration of the experiment, again indicating that this methodology of encapsulation prevents any contamination to the samples. The full results from the 2-way ANOVA are presented in appendix 4.6.

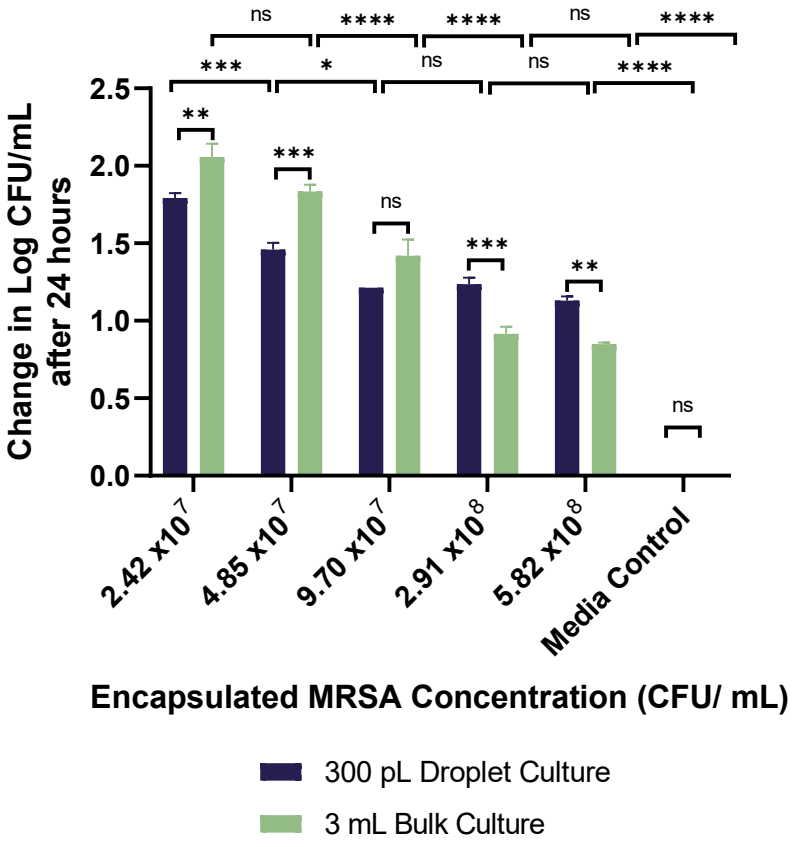

Figure 4.12. Change in MRSA Log CFU/mL after 24 hours of 300 pL droplets encapsulated with different starting CFU/mL concentration compared to 3 mL bulk culture. The bar graph shows the change in log CFU/mL of MRSA encapsulated with different inoculum concentrations in a droplet culture (Blue) and in a bulk culture (Green). Data represents n=3 technical replicates and n=3 biological replicates. Each bar represents the mean change in CFU/ mL and error bars represent the standard deviation of 9 replicates. P values were determined by a two-way analysis of variance (ANOVA) with Tukey's multiple comparison, comparing all treatments to analyse the impact of inoculum concentration on the growth of MRSA in a droplet and bulk culture. *P < 0.05, **P < 0.01, ***P < 0.001 and ****P < 0.0001.

The radius of each droplet in each sample was monitored between the time point to ensure that droplets remain stable during the experiment and to investigate if increasing the inoculum has any effect on droplet size. Figures in appendix 4.4 and appendix 4.5 illustrate the droplets monitored at 0 hours and 24 hours with a 10x and 20x objective respectively. Figure 4.13 quantifies droplet stability of 300 pL droplets encapsulated with different starting MRSA CFU/mL concentrations. At the beginning of the experiments, all samples produced monodisperse droplets with CV values below 10%. However, after 24 hours, each sample, including the media, only control displayed variation in droplet size with CV values above 10% variance.

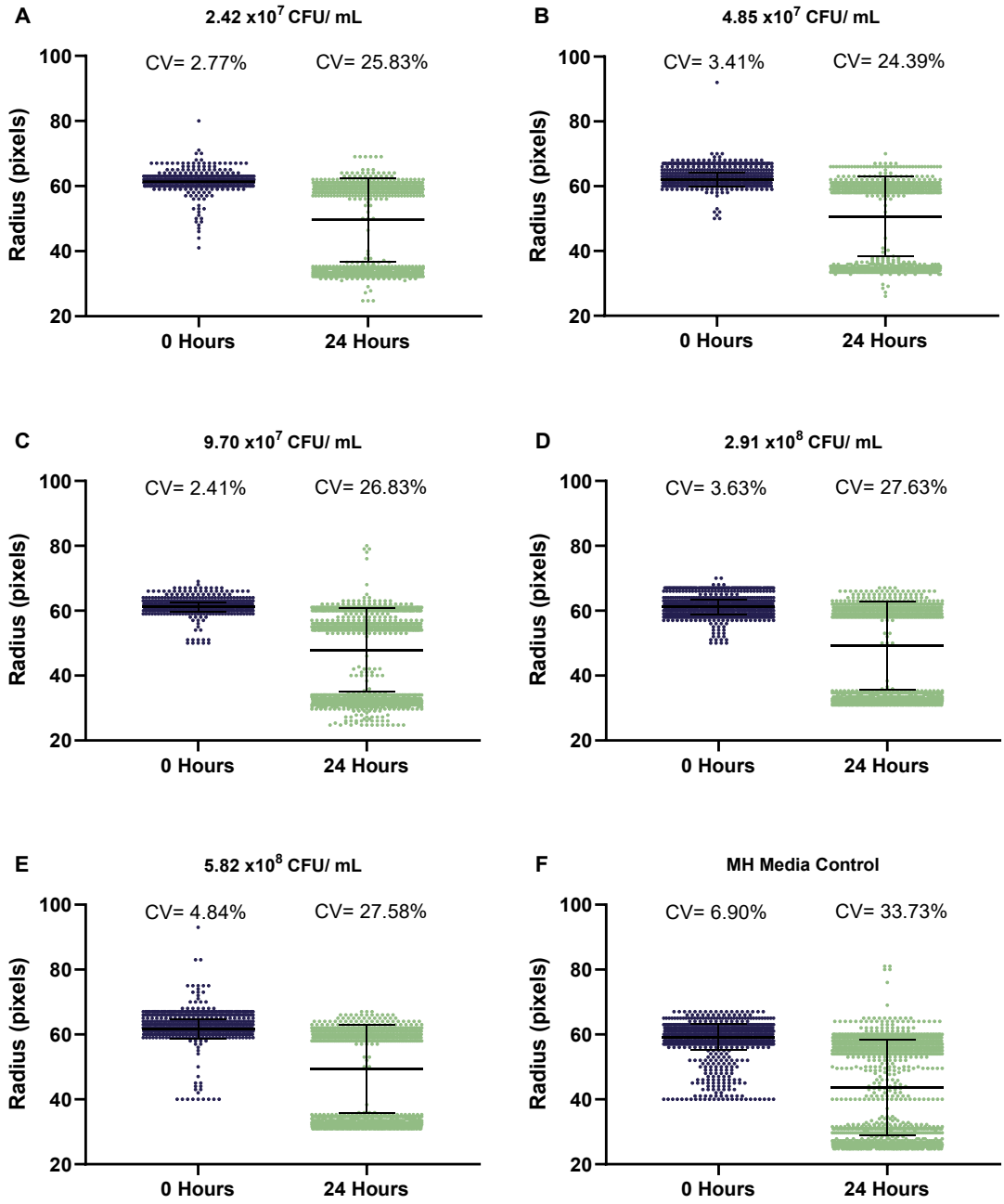

Figure 4.13. Droplet stability of 300 pL droplets encapsulated with different starting MRSA CFU/mL concentrations. Each scatter plot illustrates the variance in droplet size at 0 and 24 hours of an emulsion incubated containing different inoculum concentrations of MRSA. **(A)** Starting inoculum 2.42 x10^7 CFU/mL. Mean = 61 pixels, SD= 2 pixels, CV= 2.77%, n= 1873 droplets at 0 hours. Mean = 50 pixels, SD= 13 pixels, CV= 25.83%, n= 2095 droplets at 24 hours. **(B)** Starting inoculum 4.85 x10^7 CFU/mL. Mean = 62 pixels, SD= 2 pixels, CV= 3.41%, n= 1806 droplets at 0 hours. Mean = 51 pixels, SD= 12 pixels, CV= 24.39%, n= 2041 droplets at 24 hours. **(C)** Starting inoculum 9.70 x10^7 CFU/mL. Mean = 61 pixels, SD= 1 pixels, CV= 2.41%, n= 1758 droplets at 0 hours. Mean = 48 pixels, SD= 13 pixels, CV= 26.83%, n= 2231 droplets at 24 hours. **(D)** Starting inoculum 2.91 x10^8 CFU/mL. Mean = 61 pixels, SD= 2 pixels, CV= 3.63%, n= 1886 droplets at 0 hours. Mean = 49 pixels, SD= 14 pixels, CV= 27.63%, n= 2124 droplets at 24 hours. **(E)** Starting inoculum 5.82 x10^8 CFU/mL. Mean= 62pixels, SD= 3 pixels, CV= 4.84%, n= 1864 droplets at 0 hours. Mean = 49 pixels, SD= 14 pixels, CV= 27.58%, n= 2126 droplets at 24 hours. **(F)** Starting inoculum MH Media Control. Mean = 59 pixels, SD= 4 pixels, CV= 6.90%, n=1956 droplets at 0 hours. Mean = 44 pixels, SD= 15 pixels, CV= 33.73%, n= 2562 droplets at 24 hours. Data for each time point is n=9 from three representative images of different fields of view of the emulsion of three experiments. Each data point represents the radius (pixels) of an individual droplet in an image. Black line is the mean, and error bars show the standard deviation of droplet size.

4.3.6 The Effect of Challenging MRSA with Doxycycline in Droplets

Having inspected bacterial proliferation for different inoculum concentrations, next the effect of antibiotic challenge was examined and compared to a 3 mL bulk culture for up to 24 hours. The microenvironment in droplets might differ in antibiotic susceptibility from traditional bulk cultures and thus a basic understanding of the inhibition behaviour in droplets needed to be established for future droplet-based antibiotic susceptibility screening.

To investigate if increasing concentrations of antibiotic effects the growth of bacteria in droplets, doxycycline was added into samples of aqueous phases at concentrations of 500, 250, 125, 62.5, 31.25 and 0 μM. Doxycycline is a tetracycline antibiotic, and it has a molecular target to the 30s ribosomal subunit, halting bacterial replication by preventing the addition of new amino acids to the growing peptide chain (Chopra and Roberts, 2001). Doxycycline is used as antibiotic therapy to treat MRSA and hence this relevance was the reason it was investigated in droplets (Siddiqui and Koirala, 2024). Two emulsions were also generated as controls, including MRSA only and media only. Droplets of 300 pL were imputed into the feedback system and monodispersity was measured for different aqueous samples, including different concentrations of doxycycline.

When 300 pL was imputed into the feedback loop, the flow rates of the inlets changed accordingly to generate 300 pL droplets. Droplets encapsulated with 500 μM of doxycycline generated a mean droplet size of 300.25 pL, a SD of 1.17 pL, and a CV of 0.39% (Figure 4.14 A) Similarly, control of droplet generation was observed for 250 μM of doxycycline, (Figure 4.14 B), 125 μM of doxycycline (Figure 4.14 C), 62.5 μM of doxycycline (Figure 4.14 D), 0 μM of doxycycline (Figure 4.14 E), and MH media only control (Figure 4.14 F). The mean values of droplet volumes were 0.76, 0.31, 0.17,0.37, 0.26, and 0.36 pL within range to the desired droplet size of 300 pL, respectively, to 500, 250, 125, 62.5, 31.25 and 0 μM of doxycycline, and MRSA and MH media only control. Additionally, respective to these antibiotic concentrations, the average standard deviation for droplet generation was 0.95, 1.04, 1.24, 1.01, 1.14, 0.82, and 1.32 pL. In all experiments generating droplets with the 60 μm x 60 μm flow-focusing channel, the coefficient of variations were below 0.42%. When changing the aqueous phase of different doxycycline concentrations, highly ultra-monodisperse droplets were successfully generated.

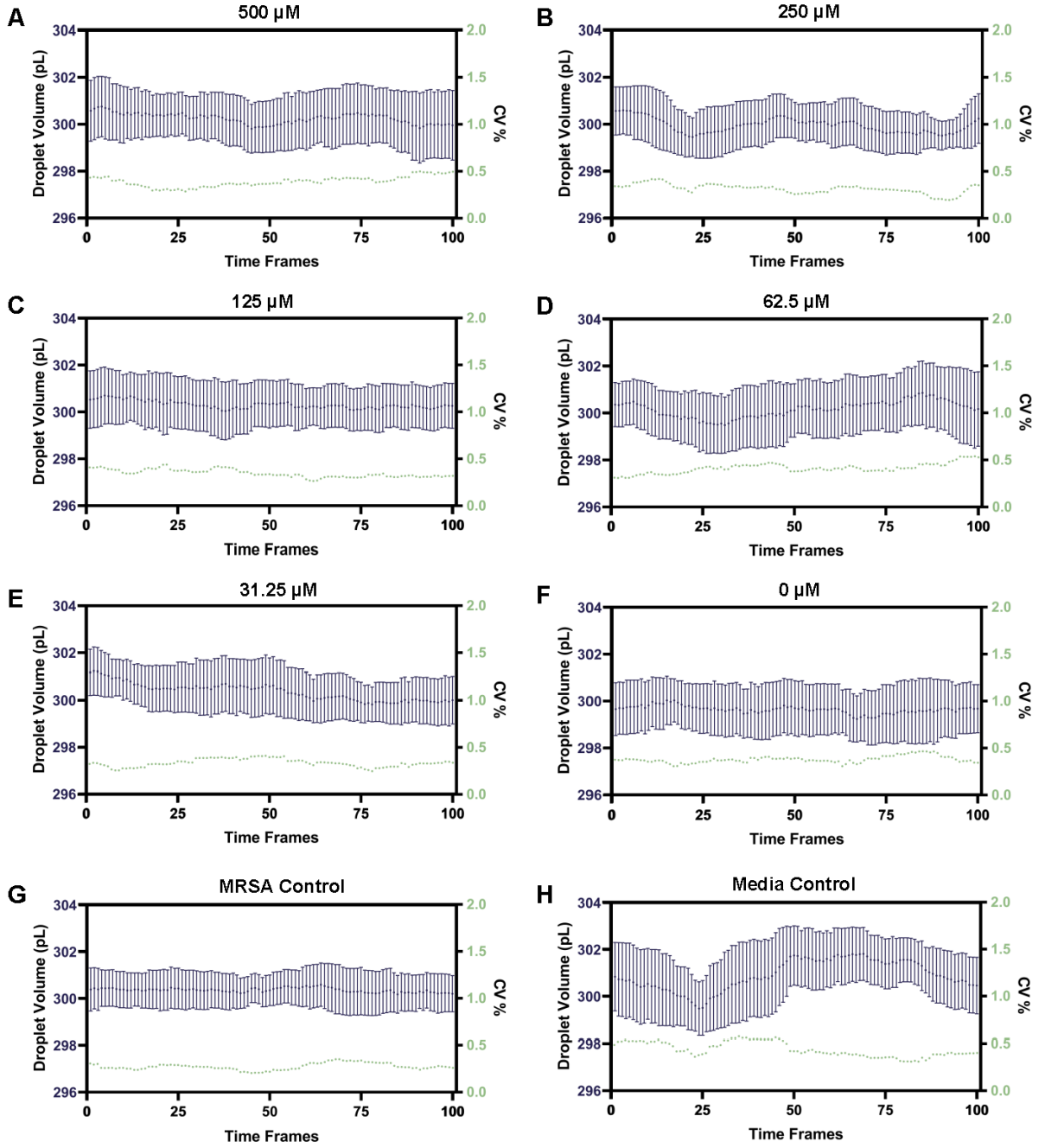

Figure 4.14. Monodispersity of 300 pL generated droplets encapsulated with MRSA and doxycycline. Image-based feedback loop set at 300 pL. **(A)** 500 µM of doxycycline encapsulated. Mean droplet volume 300.25 pL, SD 1.17 pL, CV 0.39%, FRR 0.97, and droplet generation speed 615/s. **(B)** 250 µM of doxycycline encapsulated. Mean droplet volume 299.24 pL, SD 0.95 pL, CV 0.32%, FRR 0.97, and droplet generation speed 549/s. **(C)** 125 µM of doxycycline encapsulated. Mean droplet volume 300.31 pL, SD 1.04 pL, CV 0.35%, FRR 0.96, and droplet generation speed 619/s. **(D)** 62.5 µM of doxycycline encapsulated. Mean droplet volume 300.17 pL, SD 1.24 pL, CV 0.41%, FRR 0.96, and droplet generation speed 473/s. **(E)** 31.25 µM of doxycycline encapsulated. Mean droplet volume 300.37 pL, SD 1.01 pL, CV 0.34%, FRR 0.21, and droplet generation speed 128/s. **(F)** 0 µM of doxycycline encapsulated. Mean droplet volume 299.64 pL, SD 1.14 pL, CV 0.38%, FRR 0.96, and droplet generation speed 496/s. **(G)** MRSA only droplet control. Mean droplet volume 300.36 pL, SD 0.82 pL, CV 0.27%, FRR 0.90, and droplet generation speed 157/s. **(H)** Media only droplet control. Mean droplet volume 300.91 pL, SD 1.32 pL, CV 0.44%, FRR 0.96, and droplet generation speed 601/s. The average droplet volume (pL), standard deviation (SD), coefficient of variation (CV%) and flow rate ratio (FRR) of n=25 droplets are plotted for 100 saved frames. Each graph represents 1 of 3 repeats of 100 saved time frames.

In addition to generating droplets encapsulating different samples of doxycycline concentrations, 3 mL bulk cultures were set up of the different concentrations and examined for proliferation. Samples of encapsulated droplets and bulk control cultures were taken at 0 hours and 24 hours. Images of encapsulated droplets were taken at time point 0 hours and after 24 hours of incubation. Figure 4.15 presents the comparison of droplets before and after MRSA incubation for each sample. At 0 hours, there does not appear be an observable difference in cell number between droplets generated with different doxycycline concentrations. However, after 24 hours, it might look as if concentrations of below and including 125 μM have an increase in cell number, shown by an increase in dark specs on the image. In contrast, the control of media only does not appear to contain any bacterial cells and therefore, again, proves that contamination is not present in this assay.

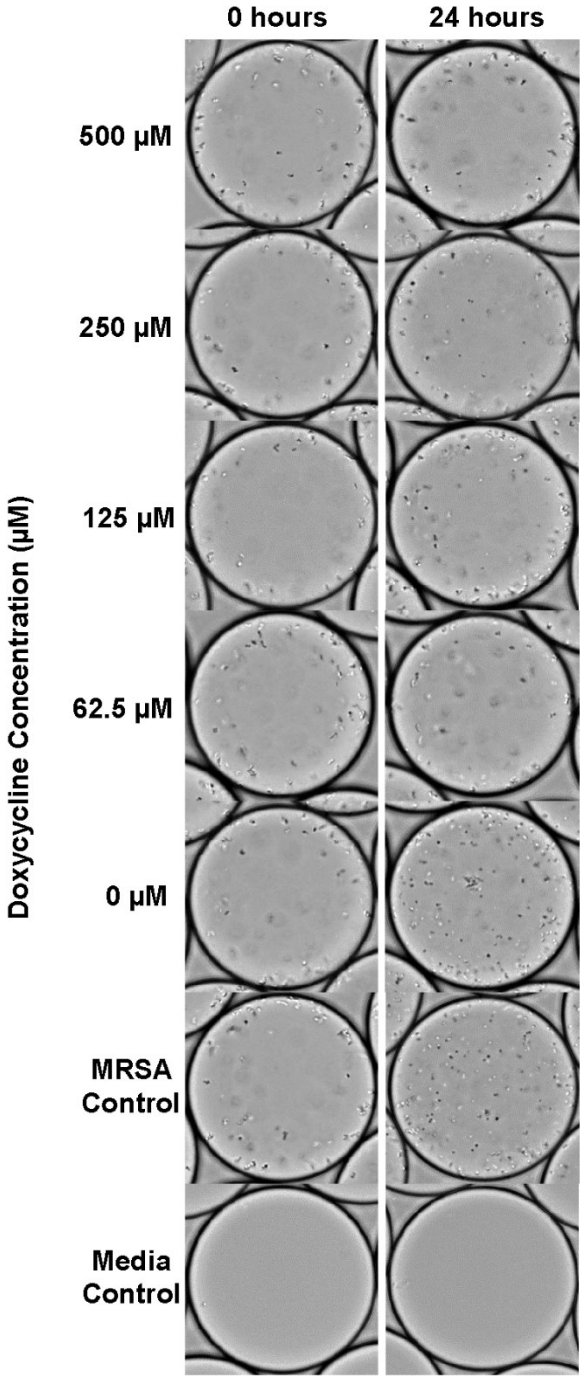

Figure 4.15. Image of MRSA proliferation inside 300pL droplets containing different doxycycline concentrations.

To quantify this, CFU/ mL was counted as previously described in section x for both droplet samples and control samples (Figure 4.16). A change in log CFU/ mL was plotted for each doxycycline concentration of both droplet and bulk culture samples. The graph reveals a discrepancy between the MIC of the droplet culture and the MIC of the bulk culture. The MIC of the droplet culture is 250 µM as shown as the lowest concentration at which the bacteria has no increase in growth. This is emphasised by the orange dot in the diagram. On the other hand, the MIC of the bulk culture is 125 µM as indicated by the absent growth at this concentration. In addition, there is a notable difference between a change in log CFU/ mL between droplet cultures and 3 mL bulk cultures. It is worth noting, the control samples of MH media only did not display any CFU/ mL for the duration of the experiment, again indicating that this methodology of encapsulation prevent any contamination to the samples. The full results from the 2-way ANOVA are presented in appendix 4.9.

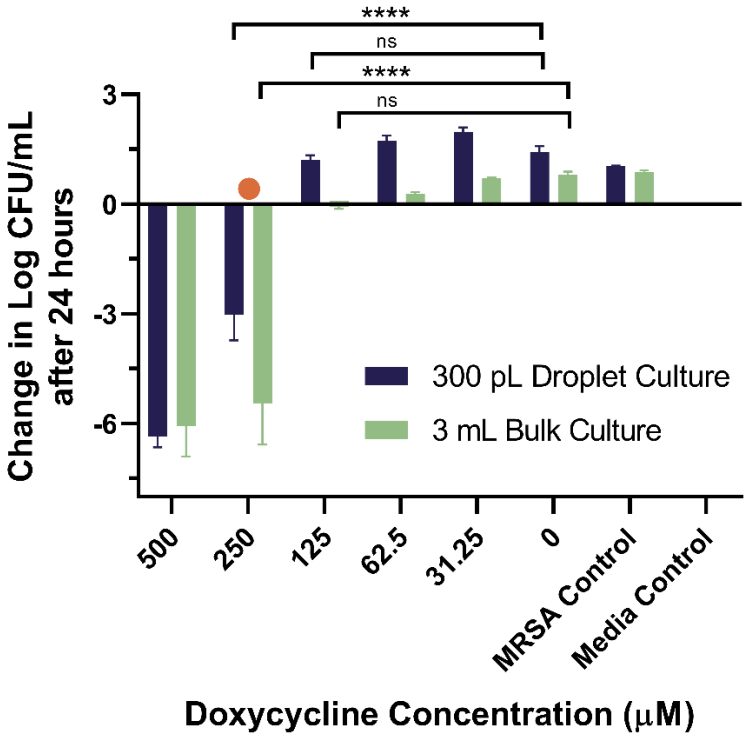

Figure 4.16. Change in MRSA Log CFU/mL after 24 hours of doxycycline challenge in 300 pL droplet culture compared to 3 mL bulk culture. The bar graph shows the change in log CFU/mL of MRSA treated with different doxycycline concentrations in a droplet culture (Blue) and in a bulk culture (Green). Data represents n=3 technical replicates and n=3 biological replicates. Each bar represents the mean change in CFU/ mL and error bars represent the standard deviation of 9 replicates. The orange dot represents the MIC of the droplet assay. P values were determined by a two-way analysis of variance (ANOVA) with Tukey's multiple comparison, comparing all treatments to analyse the impact of compound concentration on the growth of MRSA in a droplet and bulk culture. *P < 0.05, **P < 0.01, ***P < 0.001 and ****P < 0.0001.

The radius of each droplet in each sample was monitored between the time points to ensure that droplets remain stable during the experiment and to investigate if increasing the doxycycline concentration has any effect on droplet size. Figures in appendix 4.7 and appendix 4.8 illustrate the droplets monitored at 0 hours and 24 hours with a 10x and 20x objective. Figure 4.17 quantifies droplet stability of 300 pL droplets encapsulated with different starting doxycycline concentrations. Again, there is a noticeable decrease in radius with droplets containing bacteria. Surprisingly, the droplet stability results vary and do not follow a pattern. All droplet samples containing different concentrations of doxycycline remain stable and monodisperse except samples inoculated with 250 (Figure 4.17 B) and 62.25 (Figure 4.17 D) μM of doxycycline.

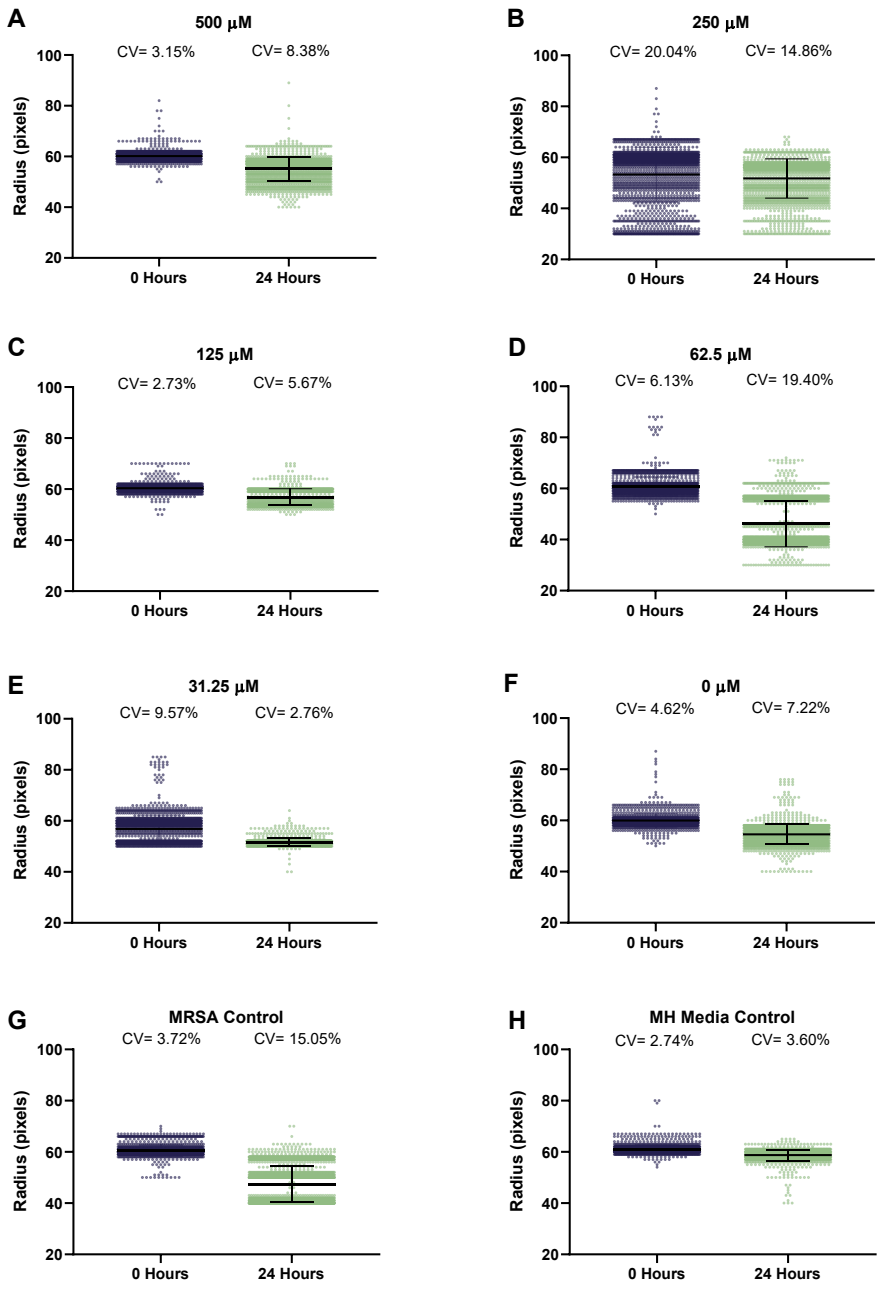

Figure 4.17. Droplet stability of 300 pL droplets encapsulated with different starting doxycycline CFU/mL concentrations. Each scatter plot illustrates the variance in droplet size at 0 and 24 hours of an emulsion incubated containing different doxycycline concentrations and MRSA. **(A)** 500 µM. Mean = 60 pixels, SD= 2 pixels, CV= 3.15%, n= 1880 droplets at 0 hours. Mean = 55 pixels, SD= 5 pixels, CV= 8.38%, n= 2274 droplets at 24 hours. **(B)** 250 µM. Mean = 53 pixels, SD=11 pixels, CV= 20.04%, n= 2454 droplets at 0 hours. Mean = 52 pixels, SD= 7.69 pixels, CV= 14.86%, n= 2570 droplets at 24 hours. **(C)** 125 µM. Mean = 60 pixels, SD= 2 pixels, CV= 2.73%, n= 1875 droplets at 0 hours. Mean = 57 pixels, SD= 3 pixels, CV= 5.67%, n= 1379 droplets at 24 hours. **(D)** 62.5 µM. Mean = 61 pixels, SD= 4 pixels, CV= 6.14%, n= 1878 droplets at 0 hours. Mean = 46 pixels, SD= 9 pixels, CV= 19.40%, n= 2055 droplets at 24 hours. **(E)** 31.25 µM. Mean= 57 pixels, SD= 5 pixels, CV= 9.57%, n= 2071 droplets at 0 hours. Mean = 52 pixels, SD= 1 pixels, CV= 2.76%, n= 1621 droplets at 24 hours. **(F)** 0 µM. Mean = 60 pixels, SD= 3 pixels, CV= 4.62%, n=1929 droplets at 0 hours. Mean = 55 pixels, SD= 4 pixels, CV= 7.22%, n= 2237 droplets at 24 hours. **(G)** MRSA only control Mean = 61 pixels, SD= 3 pixels, CV= 3.72%, n=1923 droplets at 0 hours. Mean = 47 pixels, SD= 7 pixels, CV= 15.05%, n= 3051 droplets at 24 hours. **(H)** MH media control. Mean = 61 pixels, SD= 2 pixels, CV= 2.74%, n=1896 droplets at 0 hours. Mean = 59 pixels, SD= 2 pixels, CV= 3.60%, n= 2015 droplets at 24 hours. Data for each time point is n=9 from three representative images of different fields of view of the emulsion of the three experiments. Each data point represents the radius (pixels) of an individual droplet in an image. Black line is the mean, and error bars show the standard deviation of droplet size.

4.3.7 The Effect of Challenging MRSA with Novel Metal Complex MD56 in Droplets

Having inspected the effect of a front line antibiotic inside droplets, next, a new novel compound was tested. The ruthenium metal compound MD56, which showed susceptibility to MRSA in the first research chapter of this thesis (section 2.3.2) was used to encapsulate inside droplets. The previous results from chapter 2 (Figure 2.3 J) used a bulk comparison of MIC as limited compound was available. MD56 exhibited an MIC of 1.95 μM against MRSA in the broth microdilution assay.

To investigate if increasing concentrations of antibiotic effects, the growth of bacteria in droplets, MD56 was added into the aqueous phase at concentrations of 31.25, 15.63, 7.81, 3.91, 1.95, 0.98 and 0 μM. Two emulsions were also generated as controls, including MRSA only and media only. Droplets of 300 pL were imputed into the feedback system and monodispersity was measured for different aqueous samples, including different concentrations of MD56.

When 300 pL was imputed into the feedback loop, the flow rates of the inlets changed accordingly to generate 300 pL droplets. Droplets encapsulated with 31.25 μM of MD56 generated a mean droplet size of 300.33 pL, a SD of 2.06 pL, and a CV of 0.69% (Figure 4.18 A) Similarly, control of droplet generation was observed for 15.63 μM of MD56, (Figure 4.18 B), 7.81 μM of MD56 (Figure 4.18 C), 3.91 μM of MD56 (Figure 4.18 D), 1.96 μM of MD56 (Figure 4.18 E), 0.98 μM of MD56 (Figure 4.18 F), MRSA only droplets (Figure x 4.18 F), and MH media control droplets (Figure 4.18 I).

The mean values of droplet volumes were 0.33, 0.05, 0.40, 0.49, 0.05, 0.32, 0.34, 0.80, and 0.39 pL aligned with the desired droplet size of 300 pL within the range to 31.25, 15.63, 7.81, 3.91, 1.95, 0.98, and 0 μM of MD56, MRSA only and MH media only control. In addition, respectively, to these antibiotic concentrations, the average standard deviation for droplet generation were 2.06, 1.46, 1.34, 1.37, 1.12, 1.54, 1.18, 1.19, and 1.0 pL. In all experiments generating droplets with the 60 μm x 60 μm flow-focusing channel, the coefficient of variations were below 0.69%. When changing the aqueous phase of different MD56 concentrations, highly ultra-monodisperse droplets were successfully generated.

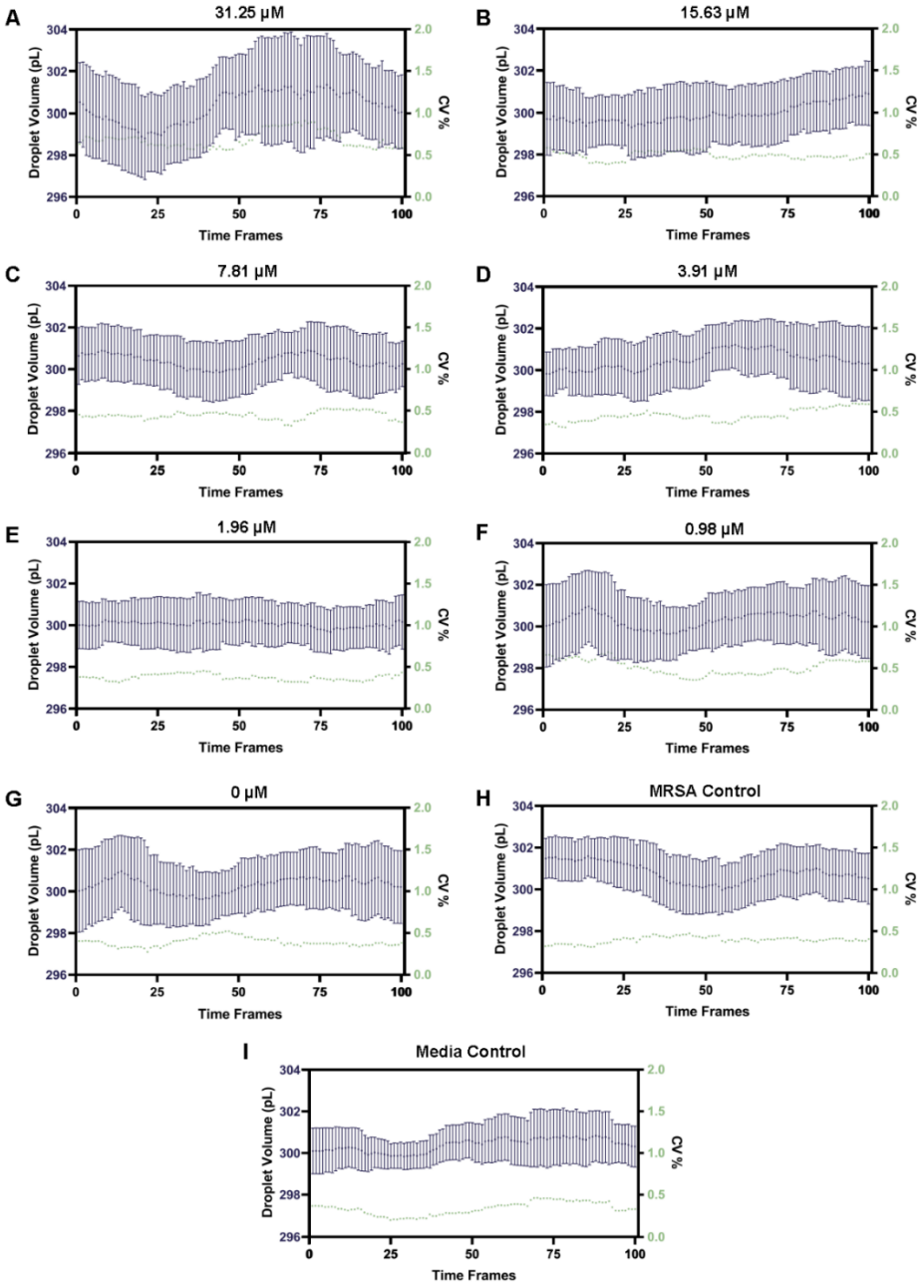

Figure 4.18. Monodispersity of 300 pL generated droplets encapsulated with MRSA and MD56 metal compound. Image-based feedback loop set at 300 pL. **(A)** 31.25 µM of MD56 encapsulated. Mean droplet volume 300.33 pL, SD 2.06 pL, CV 0.69%, FRR 0.90, and droplet generation speed 385/s. **(B)** 15.63 µM of MD56 encapsulated. Mean droplet volume 299.95 pL, SD 1.46 pL, CV 0.49%, FRR 0.90, and droplet generation speed 363/s. **(C)** 7.81 µM of MD56 encapsulated. Mean droplet volume 300.40 pL, SD 1.34 pL, CV 0.45%, FRR 0.90, and droplet generation speed 446/s. **(D)** 3.91 µM of MD56 encapsulated. Mean droplet volume 300.49 pL, SD 1.37 pL, CV 0.46%, FRR 0.90, and droplet generation speed 175/s. **(E)** 1.96 µM of MD56 encapsulated. Mean droplet volume 300.05 pL, SD 1.12 pL, CV 0.37%, FRR 0.94, and droplet generation speed 354/s. **(F)** 0.98 µM of MD56 encapsulated. Mean droplet volume 300.32 pL, SD 1.54 pL, CV 0.51%, FRR 0.90, and droplet generation speed 387/s. **(G)** 0 µM of MD56 encapsulated. Mean droplet volume 300.34 pL, SD 1.18 pL, CV 0.39%, FRR 0.89, and droplet generation speed 369/s. **(H)** MRSA only droplet control. Mean droplet volume 300.80 pL, SD 1.19 pL, CV 0.32%, FRR 0.88, and droplet generation speed 336/s. **(I)** Media only droplet control. Mean droplet volume 300.39 pL, SD 1.00 pL, CV 0.33%, FRR 0.88, and droplet generation speed 311/s. The average droplet volume (pL), standard deviation (SD), coefficient of variation (CV%) and flow rate ratio (FRR) of n=25 droplets are plotted for 100 saved frames. Each graph represents 1 of 3 repeats of 100 saved time frames.

Samples of encapsulated droplets were taken at 0 hours and 24 hours. Images of encapsulated droplets were taken at time point 0 hours and after 24 hours of incubation. Figure 4.19 presents the comparison of droplets before and after MRSA incubation for each sample. The control of media only does not appear to contain any bacterial cells and therefore, again, proves that contamination is not present in this assay.

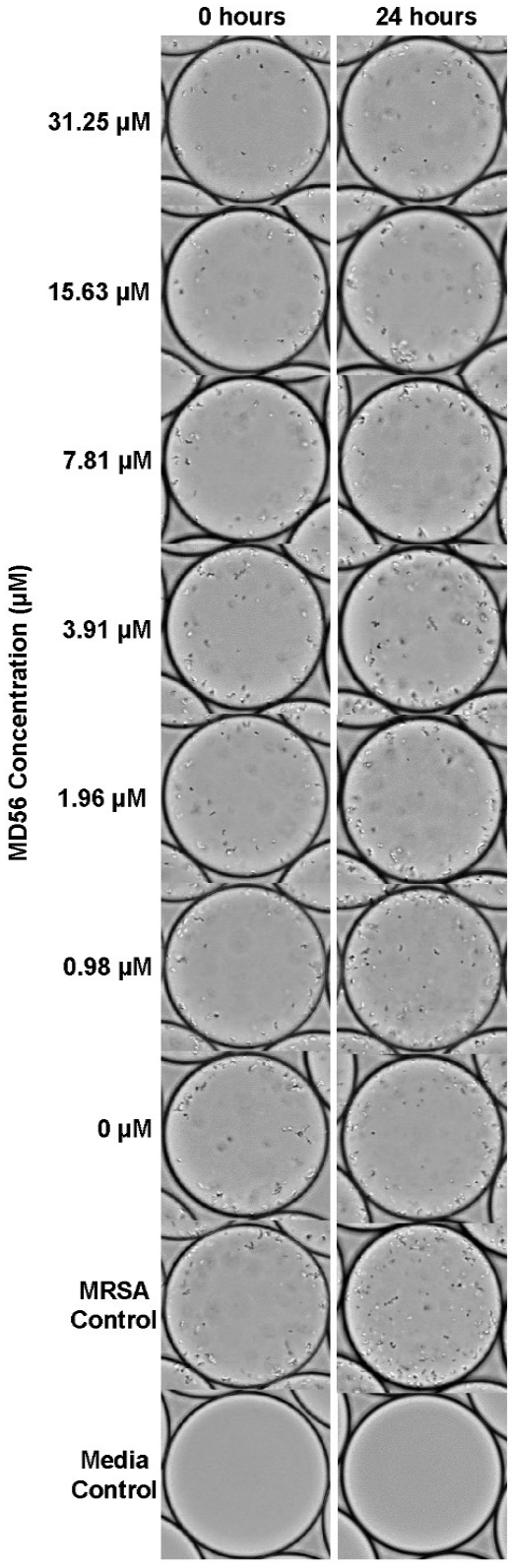

Figure 4.19. Image of MRSA proliferation inside 300pL droplets containing different MD56 concentrations.

To quantify this, CFU/ mL were counted as previously described in section 4.3.7 for both droplet samples and control samples (Figure 4.20). A change in log CFU/ mL was plotted for each MD56 concentration. The graph reveals a difference in the MIC between the droplet culture and the bulk culture. The MIC of the droplet culture is 31.25 µM as shown as the lowest concentration at which the bacteria has no increase in growth. It is worth noting, the control samples of MH media only did not display any CFU/ mL for the duration of the experiment, again indicating that this methodology of encapsulation prevent any contamination to the samples. The full results from the one-way ANOVA are presented in appendix 4.12.

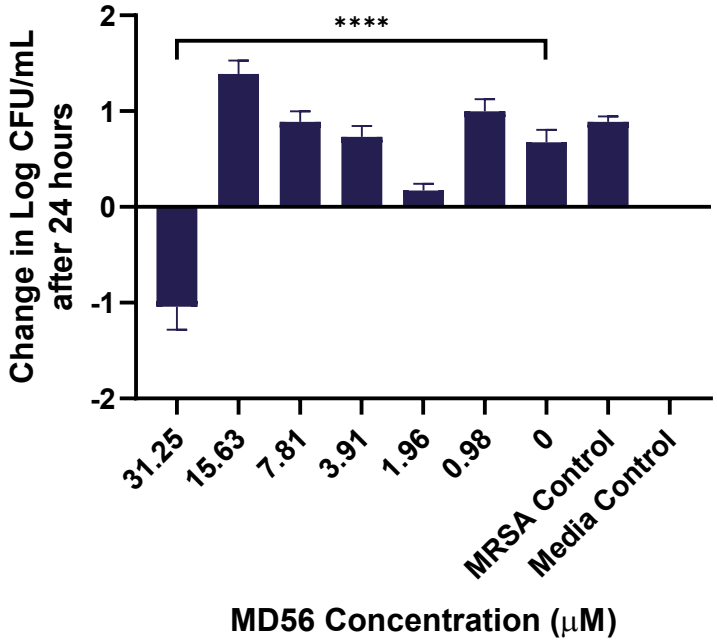

Figure 4.20. Change in MRSA Log CFU/mL after 24 hours of MD56 challenge in 300 pL droplet culture. The bar graph shows the change in log CFU/mL of MRSA treated with different MD56 concentrations in a droplet culture. Data represents n=3 technical replicates within one independent experiment. Each bar represents the mean change in CFU/ mL and error bars represent the standard deviation of 3 replicates. P values were determined by a one-way analysis of variance (ANOVA) with Dunnett's multiple comparison, comparing all treatments to 0 µM to analyse the impact of compound concentration on the growth of MRSA *P < 0.05, **P < 0.01, ***P < 0.001 and ****P < 0.0001.

On the other hand, Figure 4.21 demonstrates a different effect of MD56 on MRSA in a bulk culture from chapter 2. With an MIC as low as 1.95 µM, there was a significant difference between this concentration and 0 µM (P=0.0001). Concentrations below this, such as 0.98 µM and 0.49 µM did not show any differences in bacterial growth compared to the control (P= 0.6787 and P= 0.9997), respectively, meaning at these concentrations, MD56 has no effect on bacterial growth.

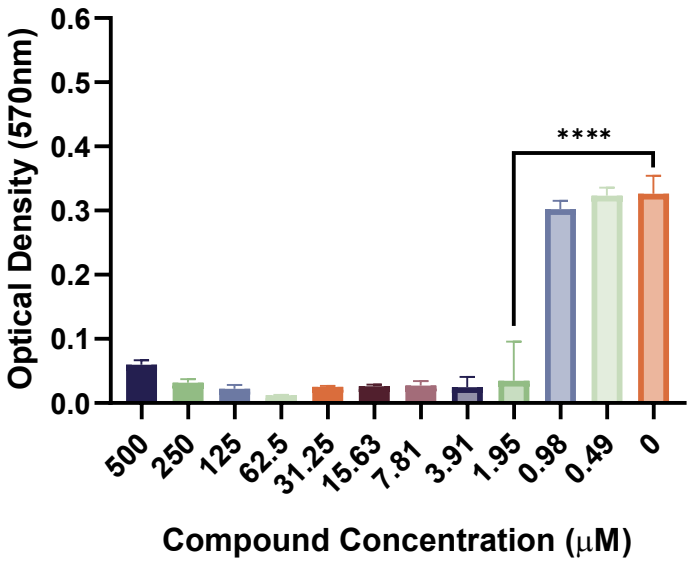

Figure 4.21. Optical density (570 nm) of MRSA after 24 hours of MD56 challenge in 100 µL bulk culture. The bar graph shows MRSA treated with different MD56 concentrations in a bulk culture. Data represents n=3 technical replicates within one independent experiment. Each bar represents the mean optical density (570 nm) and error bars represent the standard deviation of 3 replicates. P values were determined by a one-way analysis of variance (ANOVA) with Dunnett's multiple comparison, comparing all treatments to 0 µM to analyse the impact of compound concentration on the growth of MRSA *P < 0.05, **P < 0.01, ***P < 0.001 and ****P < 0.0001.

The radius of each droplet in each sample was monitored between the time points to ensure that droplets remain stable during the experiment and to investigate if increasing the MD56 concentration has any effect on droplet size. Figures in appendix 4.10 and appendix 4.11 illustrate the droplets monitored at 0 hours and 24 hours with a 10x and 20x objective. Figure 4.22 quantifies droplet stability of 300 pL droplets encapsulated with different starting MD56 concentrations. In this example, droplets remained stable after 24 hours for all concentrations tested.

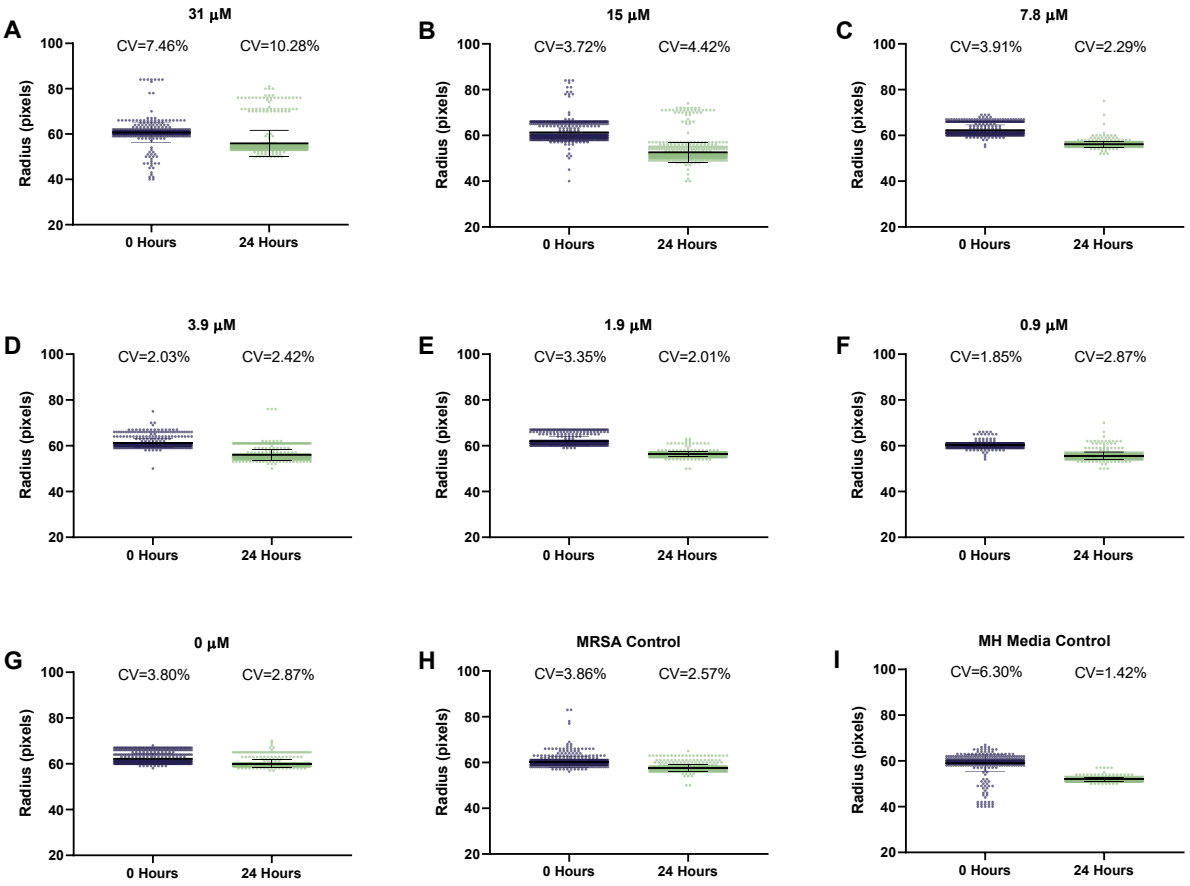

Figure 4.22. Droplet stability of 300 pL droplets encapsulated with different starting doxycycline CFU/mL concentrations. Each scatter plot illustrates the variance in droplet size at 0 and 24 hours of an emulsion incubated containing different MD56 concentrations and MRSA. **(A)** 31.5 µM. Mean = 61 pixels, SD= 5 pixels, CV= 7.46%, n= 563 droplets at 0 hours. Mean = 56 pixels, SD= 6 pixels, CV= 10.28%, n= 628 droplets at 24 hours. **(B)** 15.63 µM. Mean = 61 pixels, SD= 4 pixels, CV= 6.14%, n= 550 droplets at 0 hours. Mean = 53 pixels, SD= 4.42 pixels, CV= 8.41%, n= 814 droplets at 24 hours. **(C)** 7.8 µM. Mean = 62 pixels, SD= 2 pixels, CV= 3.91%, n= 627 droplets at 0 hours. Mean = 56 pixels, SD= 2 pixels, CV= 2.29%, n= 702 droplets at 24 hours. **(D)** 3.91 µM. Mean = 61 pixels, SD= 2 pixels, CV= 3.33%, n= 645 droplets at 0 hours. Mean = 56 pixels, SD= 2 pixels, CV= 4.32%, n= 752 droplets at 24 hours. **(E)** 1.96 µM. Mean= 62 pixels, SD= 2 pixels, CV= 3.35%, n= 639 droplets at 0 hours. Mean = 56 pixels, SD= 1 pixels, CV= 2.01%, n= 739 droplets at 24 hours. **(F)** 0.9 µM. Mean = 60 pixels, SD= 1 pixels, CV= 1.85%, n=649 droplets at 0 hours. Mean = 56 pixels, SD= 2 pixels, CV= 2.87%, n= 700 droplets at 24 hours. **(G)** 0 µM. Mean = 62 pixels, SD= 2 pixels, CV= 3.80%, n=614 droplets at 0 hours. Mean = 60 pixels, SD= 2 pixels, CV= 2.87%, n= 665 droplets at 24 hours. **(H)** MRSA only control. Mean = 60 pixels, SD= 2 pixels, CV= 3.86%, n=635 droplets at 0 hours. Mean = 58 pixels, SD= 1 pixels, CV= 2.57%, n= 677 droplets at 24 hours. **(I)** MH media control. Mean = 59 pixels, SD= 4 pixels, CV= 6.31%, n=635 droplets at 0 hours. Mean = 52 pixels, SD= 1 pixels, CV= 1.4%, n= 846 droplets at 24 hours. Data for each time point is n=3 from three representative images of different fields of view of the emulsion of one independent experiment. Each data point represents the radius (pixels) of an individual droplet in an image. Black line is the mean, and error bars show the standard deviation of droplet size.

4.4 Discussion

Summary

Encapsulating bacteria in picodroplets and designing a droplet-based AST could improve *in vitro* drug discovery in many ways, such as high-throughput screening, controlled microenvironments, enhanced sensitivity, and single-cell resolution. In the previous chapter, a platform was optimised using picodroplet technology to create droplets with identical picolitre volumes containing bacterial culture media. Results from chapter 3 concluded that mycobacteria culture media was unsuitable for maintaining identical bioreactor volumes. Thus, an important ESKAPE pathogen (MRSA) was chosen for encapsulation studies in this chapter due to its ability to be cultured in MH broth high with stable droplets.

This study successfully demonstrated the encapsulation of MRSA in monodisperse picodroplets using picodroplet technology. Key findings include: (1) successful generation of droplets with high monodispersity containing single or multiple MRSA cells, (2) maintenance of bacterial viability and proliferation within droplets, (3) observation of droplet shrinkage during bacterial growth, and (4) detection of differences in antibiotic susceptibility between the droplet and bulk cultures.

In this chapter, demonstrations show that MRSA bacteria can be captured in droplets at the single-cell or multi-cell range following Poisson statistic modelling. The picodroplet technology was able to generate MRSA containing droplets with high monodispersity and low variance in all experiments. Physically, the cell suspension did not block the inlet chip as presumed, allowing for a random distribution of bacteria entering the channels. The multiplication of bacteria in droplets can be observed through images, and their growth can be measured by counting CFU/mL at different time intervals. Droplets containing bacteria or antibiotics tend to decrease and have smaller sizes. The inhibitory effects of antibiotics to MRSA into droplets could be quantified. Additionally, the experimental design of each assay in this work resulted in no contamination, as demonstrated by no bacterial growth in any of the MH media only control samples.

Single-cell Encapsulation vs Inoculum Effect

To explore the behaviour of MRSA in droplets, bacteria were encapsulated at different starting concentrations and different droplet sizes. Our results demonstrated a clear inoculum effect in droplets, with higher initial bacterial concentrations leading to decreased proliferation rates. This effect was more pronounced in smaller droplets (60 pL) compared to larger ones (300 pL), likely due to faster depletion of nutrients and accumulation of waste products in the more confined space. These findings highlight the importance of considering droplet size and initial cell concentration when designing droplet-based assays for bacterial studies.

Droplet Shrinkage and Stability

The stability of droplets and droplet volume variations were monitored throughout this chapter to ensure that bacteria does not affect the stability of droplets. Results show discrepancy in droplet variation. Most experiments present a decrease in droplet radius after 6 hours of incubation, including the media control sample. However, for the multi-cell encapsulation in 300 pL experiment, only the bacteria containing droplets shrunk after 6 hours of incubation compared to the control. As mentioned in the literature review, droplet shrinkage when bacteria are encapsulated in droplets and incubated, have been observed (Geersens et al., 2022, Boitard et al., 2012, Schmitz et al., 2009, Joensson et al., 2011). These observations resulted in the postulation of why droplets decrease in volume when bacteria are encapsulated.

First, as droplets typically compose of an aqueous phase surrounding an immiscible oil phase, over time, water from the aqueous phase can evaporate, especially if the system is not perfectly sealed or if the oil phase has some permeability to water vapor. The temperature and humidity of the environment where the droplets are stored or incubated can affect the rate of evaporation. Higher temperatures or lower humidity levels can accelerate water loss from the droplets. This evaporation reduces the volume of the droplet, leading to shrinkage. Additionally, if there is an osmotic gradient between the droplet contents and the surrounding oil phase (or another external phase), water may move out of the droplet, further contributing to shrinkage.

Furthermore, nutrient consumption by growing bacteria generates an osmotic gradient, driving water transfer from occupied droplets to empty ones. There may be permeability to aqueous components through the surfactant bilayer. Our observation of droplet shrinkage aligns with previous studies (Boitard et al., 2012). The shrinkage appears to be correlated with bacterial growth, suggesting it could serve as a label-free indicator of metabolic activity. However, this phenomenon also introduces challenges for maintaining consistent microenvironments over time. Future assay designs may need to account for this dynamic change in droplet volume, perhaps by incorporating real-time size monitoring or developing methods to stabilize droplet volume during bacterial growth.

To mitigate droplet shrinkage due to evaporation, in the future, experiments should be in controlled environments with stable temperature and humidity and ensure that microfluidic devices are sealed to reduce exposure to ambient air. Adjust the osmolarity of the droplet contents to balance the osmotic pressure and reduce the driving force for water loss.

Nevertheless, it is crucial to note that optimising droplet shrinkage in droplet assays can provide advantages. For example, bacteria proliferate by utilising nutrients in the droplet, causing droplets to shrink. Therefore, droplet shrinkage may be advantageous in quantifying

bacterial proliferation as a label-free analysis technique. This would aid in rapid antimicrobial susceptibility testing.

Numerating Bacteria in Droplets

To quantify bacterial viability and proliferation in droplets, CFU/ mL was counted and analysed. To achieve this, the method adopted copied the same as (Liu et al., 2016), whereby samples of droplets at each time point were broken and the aqueous phase extracted for CFU plating. This approach provided quantitative analysis and could enumerate bacteria which were alive. However, this approach was time consuming and required a large emulsion volume of each sample and was therefore not suitable for a rapid AST. Possible further improvements in quantification include image/sorting/detection analysis of bacterial number and further detection sensitivity and resolution, as previously mentioned in the literature review.

Antibiotic Susceptibility in Droplets

To demonstrate the applicability of the picodroplet technology device in AST assay development, antimicrobial susceptibility of a front-line antibiotic as well as a novel investigative compound was encapsulated with MRSA and susceptibility was investigated.
The observed differences in MIC values between droplet and bulk assays for both doxycycline and MD56 highlight the unique microenvironment created within droplets. The consistently higher MICs in droplets (2-fold for doxycycline and 16-fold for MD56) suggest that bacteria may exhibit increased tolerance to antibiotics in these confined spaces. This could be due to several factors, including altered gene expression in response to confinement, reduced antibiotic penetration into bacterial clusters, or rapid local depletion of antibiotic concentrations. These findings underscore the importance of carefully interpreting droplet-based susceptibility results and suggest that droplet assays may provide insights into antibiotic efficacy under conditions more closely resembling *in vivo* microenvironments.

Various hypotheses explain the underlying causes of differences in MIC values. The first being that droplets hold different microenvironments to bacteria compared to bulk cultures. In droplet microfluidic assays, each droplet creates an isolated microenvironment for the bacterial cells. This isolation can lead to differences in nutrient availability, oxygen concentration, and waste-product accumulation compared to bulk cultures. Also, a phenomenon such as quorum sensing, where bacterial behaviour changes due to the density of the population, could affect antibiotic susceptibility, leading to different MIC values.

Similarly, the inoculum effect could be a reason for variations in MIC values. Inoculum effect was demonstrated in droplets (Postek et al., 2018). An issue was raised by Postek et al. (2018) which highlights an area of concern when merging conclusions from both assays. As the CLSI has stated that a standardised inoculum density of 5×10^5 CFU ml^{-1} is appropriate for BMD

assays (CLSI, 2015), this raises an issue with droplet-based AST. This value would equate to 1 CFU per 2000 pL droplet. However, in most droplet experiments, the droplet volume is required to be significantly smaller to reach single-cell encapsulation. In these diminutive compartments, the MIC is expected to increase (identical to the data presented in this chapter) due to a decrease in the number of antibiotic molecules per cell and therefore, the bacterial cells could survive higher concentrations of antibiotics.

Heterogeneity and stochastic effects are contenders for the explanation of different MICs. Droplet microfluidic assays can reveal heteroresistance, where subpopulations of bacteria within the same sample show different levels of resistance (Scheler et al., 2020). Bulk culture assays might mask these differences because the bulk MIC reflects the average response of the entire population. In addition, the modest volumes in droplet assays can lead to stochastic effects, where random variations in cell numbers or local conditions have a more pronounced impact on bacterial growth and antibiotic response, potentially leading to different MIC values.

However, the prospective reasoning is that the antibiotic molecules can pass through these droplet bilayers and into the oil phase or neighbouring droplets. This would change the final concentration of the antibiotic molecules in each droplet and therefore change the susceptibility concentration. Furthermore, it would have been interesting to look at an antibiotic that MRSA is resistant to as a control of inhibitory effects or to engineer a resistant strain to doxycycline and check if susceptibility is lost.

Conclusion and Future Work

In summary, the differences in bacterial growth and MIC values between the droplet microfluidic assays and the bulk culture assays arise from variations in microenvironmental conditions, bacterial interactions, antibiotic diffusion, detection sensitivity, and inoculum effects. These factors underscore the importance of considering the context and methodology when interpreting MIC results obtained from different assay formats.

Future work should direct towards further optimisation and validation steps to ensure the droplet-based AST meets gold-standard testing. Several key areas should be addressed:

1. Optimization of droplet size and composition to minimise shrinkage while maintaining single-cell encapsulation efficiency.
2. Development of real-time, label-free methods for monitoring bacterial growth within droplets, possibly leveraging the observed shrinkage effect.
3. Investigation of the mechanisms underlying the increased antibiotic tolerance in droplets, potentially through transcriptomic or proteomic analysis of encapsulated bacteria.

4. Exploration of multi-drug combinations in droplets to assess potential synergistic effects that may be masked in bulk assays.
5. Validation of droplet-based AST against a wider range of clinical isolates and comparison with standard clinical testing methods.
6. Integration of the optimized droplet-based AST into a fully automated, high-throughput screening platform for rapid antibiotic susceptibility testing in clinical settings.

First, since it was published that different bacterial species exhibit varying behaviours inside droplets (Du, Xu, Zhang, & Han, 2021), it is necessary to evaluate the growth rates and physiology of different bacterial species in droplets. Additionally, growth behaviour should be monitored when using different droplet volumes and different starting concentrations to find the optimal growth curve and assay duration. New PDMS chip geometries should allow for smaller droplet volumes to be generated. To achieve single-cell encapsulation, the smaller the droplet, the easier that is to achieve. Expanding the scale of the assay to facilitate parallel experiments running hundreds of experiments at once, including numerous antibiotics and dilution ranges, is required to achieve a high-throughput methodology.

The most important aspect of this assay for improvement is the downstream analysis of enumerating bacteria in the droplets and deciphering an MIC value. The best scenario is a label-free method, which is measured in real time with high sensitivity and specificity. Accurate measurement of bacteria or their physio/electrochemical properties in droplets can be achieved by employing the advanced imaging or sensing techniques discussed in section 4.1.4.

It would be beneficial if droplet analysis was an automated pipeline build into the droplet generating device. The final design of picodroplet technology should prioritise both end user friendliness and biosafety when working with pathogens. The bacteria cell suspension would frequently fall when connecting to an inlet channel, as there was no suitable holder. A 3D printed holder with correct size requirements would be suitable for moving forward.

The design of a new biocompatible surfactant is crucial for future work. It should ensure droplet stability during bacterial incubations and prevent small molecule drug leakage. These future tasks will require collaboration of multidisciplinary teams to improve the development of a droplet-based AST. After the final assay is optimised, a large-scale, side-by-side comparison in performing the droplet-based AST and current gold standard methods should be operated to evaluate the clinical significance of this methodology.

Chapter 5.

Limiting Small Molecule Leakage of Antibiotics from Picodroplets by Synthesising and Characterising Dendrimer Surfactants

5.1 Introduction

5.1.1 Small Molecule Drug Leakage from Droplets

Droplet-based biochemical assays depend on isolating reagents in individual droplets to prevent cross-contamination between them. The assumption in the design of AST assays in droplets is that the antibiotics remain isolated in individual droplets and cannot diffuse across the interface between a droplet and the continuous phase. That is, however, not the case as it has been reported that small molecules can leak from the droplet micelle layer (Ruszczak et al., 2023). Leakage is well characterised through three postulated mechanisms (illustrated in Figure 5.1). The first is that small molecules diffuse to the oil phase and transport from the oil to another droplet, followed by small micelles and or detached satellites, and transport between membranes of touching droplets (Ruszczak et al., 2023).

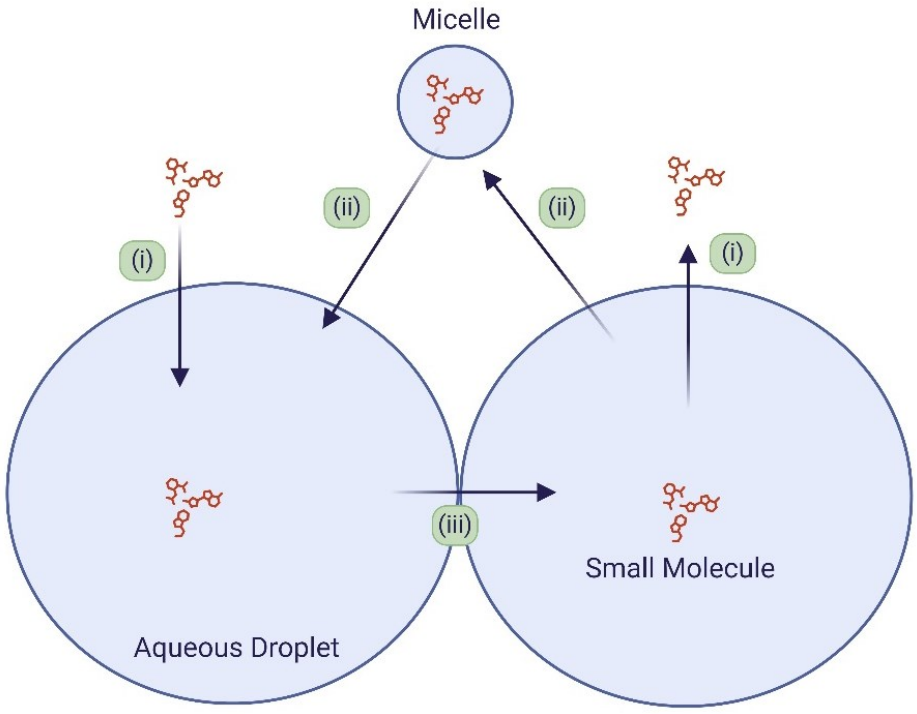

Figure 5.1. Three postulated mechanisms of small molecule drug leakage. (i) Small molecule diffusing into droplet. **(ii)** Small molecule budding off in micelle and fusing to another droplet. **(iii)** Small molecule diffusing between droplets. Image created on Biorender.com.

These mechanisms of small molecule leakage in droplet microfluidics have been extensively studied. Skhiri et al. (2012) provided a comprehensive analysis of molecular transport by surfactants in emulsions, demonstrating that the rate of exchange is strongly dependent on the hydrophobicity of the transported molecules. Their work showed that more hydrophobic molecules tend to have higher exchange rates, which has significant implications for the design of droplet-based assays (Skhiri et al., 2012). Building on this, Gruner et al. (2016) further elucidated the dynamics of molecular transport in emulsions, identifying key parameters that

influence leakage rates. They found that surfactant chemistry is crucial in controlling molecular retention, suggesting that custom-designed surfactants could mitigate leakage (Gruner et al., 2016). In addition, through testing a droplet-based system for quantifying nitrate in water, researchers found another mechanism by which crosstalk occurs is the conversion of an analyte to a gaseous intermediate, which afterwards diffuses between droplets. This non-surfactant driven mechanism of leakage could be corrected by a mathematical model (Nightingale et al., 2018).

These studies highlight the complex interplay between small molecule properties, surfactant characteristics, and leakage dynamics, underscoring the need for advanced surfactant designs to address this challenge. Ultimately, the limitations of leakage will enable antibiotics to move in and out of each droplet 'bioreactor', changing the final concentration in the assay and the virtue of droplet microfluidics as a miniaturised, high-throughput antibiotic susceptibility assay will dissolve.

To characterise and quantify small molecule drug leakage from droplets, methods using double emulsions (Etienne et al., 2018), fluorescent dyes (Gruner et al., 2016, Sandoz et al., 2014, Scheler et al., 2016, Skhiri et al., 2012), trapping droplet pairs (Bai et al., 2010), oil-based flow cytometry (Zinchenko et al., 2023) and analyte transfer by electrospray ionization mass spectrometry (ESI-MS) (Payne et al., 2023) has been performed.

One physiochemical property testified as a factor in drug leakage is the hydrophilicity of a molecule. A study demonstrated that highly hydrophilic dyes with LogD<-7 showed stable retention in droplets. When dyes with an increase in hydrophobicity were used, stable retention was achieved by changing the surfactant physical properties (Janiesch et al., 2015). Woronoff *et al.* also publicised that the exchange rate of small molecules between droplets depends on their hydrophobicity by showing a direct link between the retention of the fluorophores in an emulsion of droplets and the predicted partition coefficient of a dye (Woronoff et al., 2011). Predictive tools demonstrated high logP and logD values correlate with an increase in leakage and high polar surface areas and logS correlate with a decrease in leakage (Payne et al., 2023). This is a challenge for AST in droplets for mycobacteria, as the current treatment options are vastly hydrophobic in nature.

In addition to antibiotic retention in droplets, other biological assays use resazurin to quantify bacteria in droplets. Resazurin (Mw = 229.19 g/mol) is a fluorescent molecule with low fluorescent intensity. Resazurin is converted to highly fluorescent resorufin by cellular metabolism through an oxidation-reduction reaction and is therefore used as a viability marker. This cell viability assay has been applied to microbiology studies in droplet microfluidics when bacteria was encapsulated in droplets with resazurin. When the droplet becomes fluorescent,

the bacteria contained in the droplet is viable (Postek and Garstecki, 2022). The assay in droplets is suitable for the rapid detection of pathogens. However, this molecule is recognised for leaking out droplets within hours. Resazurin has therefore been used as a model to study small molecule drug leakage.

Various strategies have been explored to reduce small molecule leakage in droplet microfluidics. Sandoz et al. (2014) demonstrated that adding sugar additives to the aqueous phase could significantly improve signal fidelity in enzyme immunoassays by reducing fluorophore leakage. They found that sucrose and trehalose were particularly effective, improving fluorophore retention by up to 70%. However, they noted that this approach may not be suitable for all assays due to potential interference with biological processes. Taking a different approach, Scheler et al. (2016) proposed modifying the assay components themselves. They showed that replacing the commonly used fluorescent marker resorufin with its more hydrophobic variant, dodecylresorufin (C12R), significantly improved retention in microdroplet bacterial assays. This strategy of modifying assay components offers an alternative to changing surfactant properties but may be limited by the availability of suitable hydrophobic analogues for various assay molecules. We are unable to add sugar stabilisers into the droplets or change the reagents used. Consequently, changing the type and properties of the surfactant is best to optimise small molecule drug leakage.

5.1.2 Introduction, Structure, and Synthesis of Dendrimers

PAMAM (polyamidoamine) dendrimers are widely regarded as promising polymers that are used in numerous applications. Dendrimer-based surfactants could potentially decrease small molecule drug leakage from droplets due to their structure, function, and properties. PAMAM dendrimers were first discovered by Donald Tomalia and co-workers in the early 1980s (Abbasi et al., 2014). They are hyperbranched macromolecules which are symmetric and comprise tree-like arms and branches.

Dendrimers are characterised by a combination of functional groups which modify their physiochemical and biological properties (Abbasi et al., 2014). The organised structure of dendrimers gives them functions which are used in biomedical applications. Synthesised through a selection of chemical reactions (Abbasi et al., 2014), the molecules start with a central core, such as a central atom or group of atoms, from which other atoms branch out, known as 'dendrons'. The core of the dendrimer forms the foundation of the shape and size, as well as determines the direction of the branches that connect to functional groups at the periphery. As the structure grows outwards, the dendrimer grows from generation to generation, which is created by adding monomers to each functional group (Augustus et al., 2017). The increasing generations create the spherical structure of dendrimers which have diameters ranging from 1.1 nm for the 1st generation (G1) to 9 nm for G8 (Biricova and

Laznickova, 2009). The molecular weight of a dendrimer is uniform and does not differ between molecules (Patel et al., 2022).

Two possible mechanisms, divergent or convergent assembly, are involved in synthesising dendrimers (Tomalia et al., 2012). The divergent approach begins at the core and construction occurs outwards later by layer to create generations. This occurs due to two step wise reactions which is coupling of the monomer and transformation of the monomer end-group to create a new reactive surface for the coupling of a new monomer. This process is repeated for the desired generation (Augustus et al., 2017). The divergent approach produces high yield, which is advantageous for commercial scale production, however, shows low purity. The limitation of impurities arising from the divergent approach often stems from retro-Michael addition, intramolecular/intermolecular cyclization, or the absence of any side reactions involving repeating units (Augustus et al., 2017). Alternatively, the convergent approach starts from the exterior, the outermost arm of the final dendrimer and propagates in reverse to the divergent assembly (Tomalia et al., 2012). Only after coupling is completed is when activation of a single functional group at the centre of a dendric fragment occurs (Patel et al., 2022). The convergent route has advantages such as requiring fewer reactions from one generation to the next, resulting in fewer structural defects and greater purity. It also offers a more controlled process and reduces reagent consumption (Patel et al., 2022). In addition, the convergent method is the preferred method to produce asymmetric dendrimers with mixed structural elements (Patel et al., 2022). On the contrary, this approach is difficult to synthesise dendrimers with higher generations due to the high number of steps (Najafi et al., 2021).

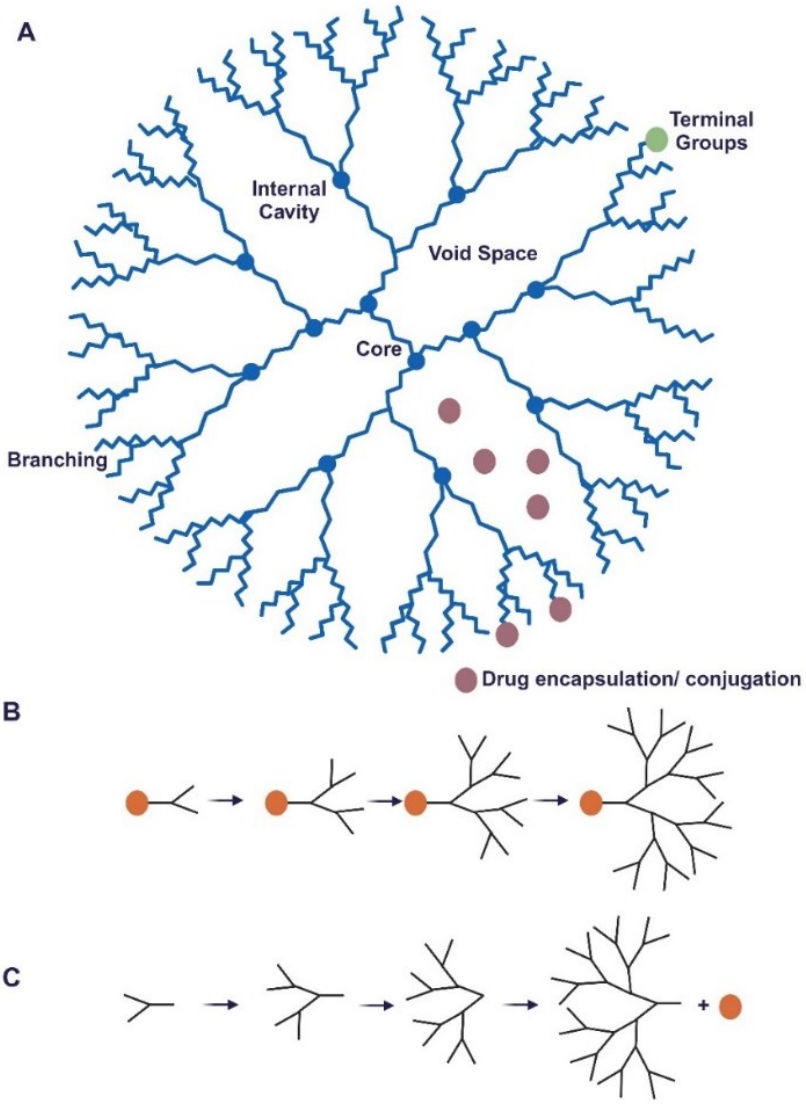

Figure 5.2. Schematic of dendrimer structure, drug interaction, and synthesis. (A) Structure of PAMAM dendrimer with core, internal cavities, generations, branching, functional groups, and drug encapsulation and conjugation. (B) Divergent synthesis. (C) Convergent synthesis. Image created on Biorender.com.

5.1.3 Characterisation of Dendrimers and Surfactants

The composition, shape, polydispersity, synthesis, conjugation, molecular weight, structural defects, and purity of dendrimers are screened by analytical techniques and other methods listed in the flow diagram in Figure 5.3. They include spectroscopy and spectrometry, scattering techniques, microscopy, size exclusion chromatography, electrical techniques, rheology, and physical properties (Biricova and Laznickova, 2009, Caminade et al., 2005, Kokare et al., 2021, Surya Prakash, 2013). In addition, to characterise surfactants as efficient droplet generating structures, the hydrophilic-lipophilic balance (HLB) is calculated from the weight percentage of the hydrophilic groups to the hydrophobic groups in a molecule (Ng and Rogers, 2019). Surfactants with a lower HLB balance will successfully generate water-in-oil droplets.

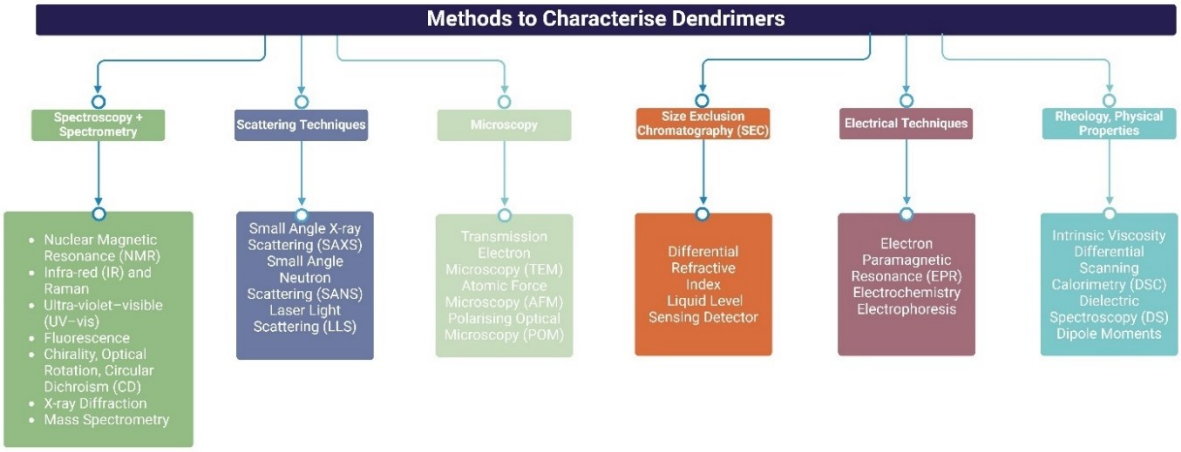

Figure 5.3. Methods to characterise dendrimers. Image created on Biorender.com.

5.1.4 Properties and Applications of Dendrimers

A dendrimer's properties are controlled by its end groups. The polymers have monodispersity, due to their controlled synthesis, rigorous purification process, and minimal size variation (Patel et al., 2022). Dendrimers hold sufficient properties including solubility, biocompatibility, biodegradability, distribution, covalent conjugation strategies, polyvalency, self-assembly, and electrostatic interactions. PAMAM dendrimers are highly soluble in aqueous solution (Biricova and Laznickova, 2009) and other molecules can either attach to the periphery or encapsulate in their interior voids (Abbasi et al., 2014)

Dendrimers are biocompatible if they contain the correct functional groups and are structured to a specific generation size. Dendrimers can be made more biocompatible by conjugating the dendrimer to biocompatibility units. Previous work showed the addition of polyethylene glycerol side chains to the dendrimer reduced liver uptake (Kim and Zimmerman, 1998). Since dendrimers are easily modified, it is typical to design the polymer with a strong degradation capability. In applications of medicine, it must degrade to prevent toxic effects. Biodegradability is shown by polyester dendrimers (Twibanire and Grindley, 2014). The distribution of dendrimers refers to how these highly branched macromolecules spread or localise within a given medium or environment.

Recently, there has been an extensive application of dendrimers in biomedicine. Many review articles have summarised their use and novel investigations (Labieniec-Watala and Watala, 2015, Abbasi et al., 2014, Najafi et al., 2021, Chauhan, Mahmoudi et al., 2021, Razmshoar et al., 2021). To summarise, dendrimers use in biomedicine include drug delivery, gene delivery, photodynamic therapy, catalysts, dendritic sensors, enhancing solubility, and anticancer drugs.

For example, camptothecin (CPT) has strong antitumor properties, however, the clinical application of the drug is hindered by poor bioavailability, low water solubility, instability, and

toxicity to normal cells. To overcome these limitations, CPT can be encapsulated in PAMAM dendrimers, allowing for sustained drug release. A study by Alibolandi et al. developed a CPT-loaded PEGylated PAMAM G5 dendrimer, further functionalized with AS1411 aptamers to enhance tumour targeting and improve cellular uptake (Alibolandi et al., 2017).

5.1.5 Drug-Dendrimer Interactions

A total of 40% of new chemical entities in the pharmaceutical industry are hydrophobic, which experience solubility issues (Patel et al., 2022). The use of dendrimers to enhance solubility has been studied. The interaction between drugs and dendrimers can form in one or two ways. The first method is by entrapment or encapsulation of drugs, whereby non-covalent forces, such as hydrogen bonds, hydrophobic interactions, and electrostatic interactions, encapsulate drugs in the structure of dendrimers. An increase in hydrophobic moieties are encapsulated as the structure of the dendrimer increases generation. The second is the interaction of a drug and the periphery of the dendrimer through covalent bond formation. Covalent conjugation of molecules can occur due to the terminal-functional groups of a dendrimer (Choudhary et al., 2017) According to Choudhary et al, the factors influencing drug solubilisation include; the concentration of dendrimer, temperature, pH, salts, the dendritic core properties, the nature of the solvent, the generation of the dendrimer, and the nature of the dendrimer surface.

5.1.6 Toxicity of Dendrimers

Despite the immense advanced applications of dendrimers to biomedicine, they have the potential to cause cytotoxicity. The toxicity of dendrimers to biological cells has been highlighted in various studies. Toxicity depends on dendrimer physiochemical properties such as their structure, size, and charge (Kheraldine et al., 2021). Dendrimers show more prominent toxicity if they are cationic, whereas toxicity is limited to anionic and neutral dendrimers (Janaszewska et al., 2019). The cytotoxicity ability of dendrimers is deemed to be generation dependent, with higher generation dendrimers having increased toxicity than lower generations (Espinar Buitrago and Muñoz Fernández, 2021, Chis et al., 2020). Jevprasesphant *et al.* demonstrated anionic or half generation dendrimers had significantly low toxicity to Caco-2 cells compared with cationic dendrimers (Jevprasesphant et al., 2003). Similarly, apoptosis was investigated in primary neuronal cultures challenged by G4 PAMAM dendrimers. Dendrimers modified with carbon chains showed cytotoxicity compared to dendrimers without terminal groups modified (Albertazzi et al., 2012).

It is presumed that cationic dendrimers with positively charged surfaces interact with negatively charged cell membranes, causing apoptosis, necrosis and/or autophagy resulting in cell lysis and death (Janaszewska et al., 2019, Kheraldine et al., 2021). This is presumably due to PAMAM dendrimers consuming highly branched structures and large molecular weights. In the

higher generations of cationic PAMAMs, the number of terminal amino groups increases, which leads to an increase in the positive charges present (Kheraldine et al., 2021).

From one perspective, dendrimers were studied for their antimicrobial properties (Staneva and Grabchev, 2021, Kumbhar et al., 2021). Dendrimers are believed to have the ability to penetrate and disrupt bacterial cell membranes, generate reactive oxygen species (ROS), interact with DNA, RNA, proteins, enzymes, efflux transporters, and inhibit biofilm formation (Kheraldine et al., 2021). As Gram-negative bacteria hold more hydrophilic cell membrane surfaces, they reduce the adhesion of hydrophobic dendrimers compared to the hydrophobic cell surface of Gram-positive bacteria (Staneva and Grabchev, 2021). As shown by Gonzalo et al. (2015), G4 PAMAM dendrimers significantly inhibit the growth of environmental microorganisms compared to G3 and G2. ROS formation was believed to be exclusive to OH-terminated PAMAM dendrimers and specifically linked to mitochondria (Gonzalo et al., 2015). Various approaches were taken to overcome toxicity, issues such as formulating surface engineered dendrimers or biocompatible dendrimers. In this case, where dendrimers are used for the applications of surfactants, the dendrimer must not have any antimicrobial properties.

5.1.7 Dendrimers for Micelles

Dendrimers are also hopeful contenders for reducing small molecule leakage across droplets due to their densely packed structures, which creates a size-exclusion effect that inhibits the diffusion of molecules through their barrier. More importantly, hydrogen bond formation is a mechanism which reduces the leakage of small molecules from the emulsions, enhancing their retention and stability. The functional groups on PAMAM dendrimers can act as hydrogen bond donors and acceptors. These groups can form hydrogen bonds with the polar groups of small molecules. This interaction "traps" small molecules within the dendrimer structure, effectively limiting their diffusion out of the droplets. The highly branched structure of PAMAM dendrimers creates many internal cavities and surface areas. Small molecules are encapsulated within these cavities through hydrogen bonding, as well as through other interactions like van der Waals forces and electrostatic interactions.

One promising example where PAMAM dendrimer-based surfactants were used to generate droplets and prevent small molecule leakage of droplets has been demonstrated. Chowdhury et al. (2019) reported the development of dendronized fluorosurfactants that showed improved stability and reduced inter-droplet transfer of small molecules compared to conventional surfactants. Their dendronized surfactants demonstrated a remarkable 100-fold decrease in inter-droplet transfer rates for a hydrophilic dye compared to a commonly used commercial surfactant. This significant improvement highlights the potential of dendrimer-based structures in addressing leakage issues in droplet microfluidics.

The unique properties of dendrimers that make them suitable for this application have been extensively reviewed by Tomalia and Khanna (2016) (Tomalia and Khanna, 2016). Their systematic framework for understanding dendrimer properties provides insights into why dendrimers are promising candidates for surfactant design, including their well-defined structure, high degree of branching, and numerous terminal groups that can be easily functionalized. These characteristics allow for precise control over the surfactant's interfacial properties, potentially enabling the design of surfactants that can effectively prevent small molecule leakage while maintaining droplet stability. In this chapter, PAMAM dendrimer-based surfactants are evaluated for their droplet generating potential and prevention of small molecule leakage.

5.1.8 Objectives and Aims of Chapter

The current commercial surfactants do not completely prevent inter-droplet transfer of small organic molecules encapsulated or produced inside picodroplets. To mitigate the undesirable leakage of small molecules from droplets, the aim is to synthesise a new dendrimer-based surfactant to enable drug-dendrimer interactions and characterise its efficiency as a droplet stabilising surfactant which prevents leakage of small molecules.
The aims of this chapter are as follows;

1. To synthesise and characterise PAMAM dendrimers at different generations and activate them for surfactant use.
2. To investigate the toxicity of synthesised dendrimers against *Mycobacterium abscessus*, *Staphylococcus aureus,* and *Pseudomonas aeruginosa.*
3. To test monodisperse and stable generation of dendrimer-based droplets using picodroplet technology.
4. To test resazurin small molecule leakage from dendrimer droplets and compare this to commercial surfactants.
5. To evaluate the efficiency of dendrimer surfactant to create monodisperse and stable droplets with mycobacterial culture media.

5.2 Methods

5.2.1 General Chemical, Reagent, and Media Preparation

All consumables and reagents were purchased from either Fisher Scientific, Melford, Biosynth, or Sigma-Aldrich, unless otherwise stated. Industrial partner Sphere Fluidics Ltd provided 5% Pico-Surf®, 3% FluoSurf™, and Novec™ 7500 reagents, and dry solvents. Any unlisted chemicals or reagents were of an analytical grade

Pico-Surf®

For studies using 5% Pico-Surf®, the reagent was used undiluted and stored at 4 °C.

Pico-Glide™

Pico-Glide™ was used undiluted and stored at 4 °C.

Phosphate Buffered Saline (PBS)

One tablet of PBS (Melford P32080-100T) was added to 100 mL of dH_2O to make a 1X solution. The PBS tablet was made of 137 mM sodium chloride, 2.7 mM potassium chloride, and 11.9 mM phosphate buffer. pH 7.4 at 25 °C.

Preparation of Resazurin Solution

1 mg of resazurin powder was dissolved into 10 mL of PBS solution. The mixture was filter-sterilised using a 0.22 µm sterile filter and stored at room temperature away from sunlight. The final concentration used was 100 µg/mL.

Preparation of 5% Dendrimer-Based Surfactants for Picodroplet Studies

AM50-06 and AM50-08 dendrimer surfactants were dissolved in Novec™ 7500 at 5% (w/v). The 5% oil solutions were made fresh and stored up to 48 hours at 4ºC.

Mueller-Hinton Broth

9.45 g of Mueller-Hinton broth was dissolved in 450 mL of dH_2O and then autoclaved (121 °C for 15 min).

Middlebrook 7H9 Broth

2.35 g of 7H9 broth base, 450 mL of dH_2O and 4 mL of 50% glycerol were added together before autoclaving (121 °C for 15 min). Once cooled, 1.25 mL of 20% filter sterile Tween80 is added along with 50 mL filter sterile ADC (albumin, dextrose, and catalase supplement).

ADC Supplement

5 g BSA (bovine serum albumin fraction v), 2 g dextrose, 0.85 g sodium chloride and 0.003 g catalase were added to 100 mL dH_2O. The components were dissolved before filter sterilising with a 0.22 µm sterile filter. The ADC supplement was stored at 4 °C.

Minimal Cholesterol Media

Minimal cholesterol media formation was adapted from (Gibson et al., 2021). Briefly, 2.61g of Middlebrook 7H9 media was dissolved in 500 mL of dH_2O. A magnetic stirrer bar was washed with ethanol and added. The mixture was autoclaved at 121 °C for 15 mins and then heated to 65 °C and placed on a hot magnetic stirrer plate. The cholesterol additive was added while the media was hot and stirring. The media was the left to cool and filtered through a filtration vacuum and stored for 2 weeks at 10 °C.

5.2.2 Synthesis of PAMAM Dendrimers

Synthesis of PAMAM Dendrimer with 4 Terminal OMe Groups (G0.5)

In a round bottom flask (500 mL), 11 mL of 60.1 g/mol of ethylene diamine (EDA) was added. 150 mL of methanol was added to dissolve the EDA using a magnetic stirrer bar at 200 rpm. Methyl acrylate (MA) was then added in an excess amount (75 mL, 0.83 mol, 86.09 g/mol) dropwise whilst the reaction was cooled to 0°C in an ice bath. The reaction was stirred overnight at room temperature. Next, the round bottom flask was placed on a rotary evaporator to eliminate any remaining unreacted MA and MeOH. The product was a yellow-coloured oil with a yield of 67.5g (100%). A sample was taken for NMR and IR analysis to ensure the purity of the product.

Synthesis of PAMAM Dendrimers with 4 Amine Terminal Groups (G1.0)

Some of the G0.5 product (30.11g) was transferred to a 500 mL round bottom flask. 150 mL of methanol was added to dissolve the product using a magnetic stirrer bar at 200 rpm. Excess EDA (100 mL) was added to the round bottom flask and left to stir on ice for 30 minutes. The reaction was then left stirring overnight with a sub-seal.

Purification of Full Generation PAMAM Dendrimers (G1.0)

Excess EDA of the G1.0 product was removed by rotary evaporator. The dendrimer was washed in 9:1 toluene: methanol. Methanol was then removed by a rotary evaporator. 150 mL of methanol was then added to the viscous solution to wash. Methanol was the removed by a rotary evaporator. This process was repeated until the peak of EDA (a singlet peak at 2.7) was no longer visible in the ^1H NMR spectrum.

5.2.3 Characterisation of PAMAM Dendrimers and Surfactants

Analytical Characterisation

^{1}H NMR spectrums were recorded using a Bruker 400MHz NMR instrument at the Babraham Research Campus, Cambridge. Chemical shifts of spectrums were estimated in ppm, the NMR spectra were examined using Topspin 3.0 NMR software. The infrared spectroscopy was recorded by a Nicolet™ iS20 FTIR Spectrometer instrument at Sphere Fluidics Ltd. Mass spectrometry equipment was used to determine the mass of compounds. Electrospray Ionisation Mass Spectrometry (ES-MS) was used for low molecular weight products (less than 1000 Da) and recorded using a Micromass Prospec spectrometer at the University of Sheffield. All analytical characterisation work were performed externally.

Hydrophilic-lipophilic Balance (HLB) Calculation

The HLB calculation was as follows;

$$\boldsymbol{HLB = 20 \times \left(\frac{Hydrophillic\ g/mol}{Hydrophobic\ g/mol\ + Hydrophillic\ g/mol}\right)}$$

PAMAM Dendrimer-Based Surfactant Toxicity Testing

The antimicrobial activity of Pico-Surf®, FluoSurf™, AM50-06, and AM50-08 against *Pseudomonas aeruginosa, Staphylococcus aureus,* NCTC *M. abscessus* (smooth)*, and* NCTC *M. abscessus* (rough) was assessed using optical density measurements. 10 mL of Mueller-Hinton broth or MiddleBrook 7H9 broth was inoculated with either the ESKAPE pathogens or mycobacteria species respectively from a frozen glycerol stock. Cultures were grown for 24 or 72 hours in an orbital incubator at 37 °C. Optical density (570 nm) was measured using a spectrophotometric plate reader (Biotek EL808) and the specific broth was used as the blank. Cultures were adjusted to 0.1 OD (570 nm) by re-suspending cells into 10 mL centrifuge tubes with broth. 96 well plates were designed with 5 µL of 5%, 2%, and 1% of each surfactant dissolved in Novec™ 7500 and 95 µL of each bacterial species in culture media. Each bacterial species was inoculated into wells at optical density (OD) 570 nm= 0.1. *P. aeruginosa* and *S. aureus* were incubated for 20 hours. The two mycobacterial species were incubated for 96 hours. Controls included Novec™ 7500 only, bacterial only, and media only. Novec™ 7500 only was to account for any potential inhibitory effects of the oil. Bacteria-only control was to establish standard growth patterns without test surfactants. Broth-only control was to confirm the sterility of the media and establish a baseline for optical density measurements. The final volume of each well was 100 µL and n=3 technical replicates on each plate. Optical density (570 nm) readings were taken at 20 and 96 hours using a spectrophotometric plate reader (Biotek EL808).

5.2.4 Picodroplet Generation Using Picodroplet Technology

PDMS Chip Fabrication

Microfluidic chips were made in-house at Aston University as described in section 3.2.10.

Set-up

Pico-Surf® (5%), FluoSurf™ (3%), AM50-06 (5%), and AM50-08 (5%) were used as the oil phase. PBS or 0.1mg/mL resazurin in PBS were used as the aqueous phase. The oil phase and aqueous phase (inlets) were delivered to a microchip with a 60 µm x 60 µm flow-focusing channel using silicon tubing with an OD (1 mm) and connected to a compressed air cylinder with regulators. LabView NXG 5 software was opened, ready to evaluate droplet formation.

Picodroplet Generation

After connecting all tubing to the picodroplet technology, the pressure is turned on and the initial inlet pressures are chosen and allowed to equilibrate before starting the data acquisition of measurements. A 60 x objective is focused on the channel where droplets that have been formed are flowing to the outlet. Droplet formation was recorded by a high-speed camera. Desired droplet volumes were imputed, and the feedback-loop initiated changes in the pressure of the inlets to adjust the droplet volumes. Droplets of sizes 300 pL were generated using the 60 µm x 60 µm flow-focusing channel PDMS chip. The average droplet volume (pL), standard deviation (SD), coefficient of variation (CV%), flow rate ratio (aq/oil), and generation speed (droplets/second) was calculated from 25 droplets by the pixel distance along the droplet image against the pixel difference of the background.

Picodroplet Collection and Incubation

Droplets were collected from the outlet by silicon tubing with an OD (1 mm) into a 1.5 mL centrifuge tube. Droplets of varying parameters, such as surfactant type were collected for incubation in the 37 ºC shaking incubator (180 rpm).

Picodroplet Imaging and Droplet Size Quantification

10 µL of each emulsion tested was added into a chamber slide (C-chip, Neubauer Improved, NanoEnTek) and imaged at different time points using an EVOS™ M5000 Imaging System with a 10x objective. Bright field images were taken. The 10x objective was used to assess droplet stability during incubation. Droplets were considered stable if they did not homogenise into separate phases, coalesce, flocculate, or invert phases. The droplet sizes of the emulsions at each time point were assessed using ImageJ with the Hough Circle Transform Plugin. Three representative images of three different fields of view of the emulsion were measured. The Hough Circle Transform Plugin allows for circular objects to be extracted from an image and each radius to be measured, leading to a dataset containing the position and radius of every

droplet detected on each image. Briefly, the perimeter of each droplet is found by Process > Find Edges. The threshold is then set, and a mask made by Image > Adjust > Threshold > Apply. Finally, the Hough Circle Transform Plugin was run by manually adjusting the minimum and maximum cutoff for the radii expected in the image. Measurements were exported as a results table. The measurements exported are: 1) the X and Y coordinates of the centre of each droplet, 2) the radius (in pixels) of each circle, 3) the Hough score for each circle, 4) the number of circles found within that frame, 5) the actual resolution that they transform, and 6) the frame in which the circle was found. The radius (in pixels) was plotted in GraphPad Prism 8 of each droplet on each image to assess and change in droplet size over time.

5.2.5 Assessment of Resazurin Leakage from Droplets

Droplet-to-oil Leakage

Bulk emulsions were generated by mixing surfactants (300 pL) and fluorescent dyes (100 pL) in 1.5 mL centrifuge tubes. Emulsions were made by vortexing the mixtures for 10 seconds. Surfactants tested were Pico-Surf, Fluro-Surf, AM50-06, or AM50-08. Aqueous phase fluorescent dye resazurin was made to a concentration of 100 µg/mL in PBS. Three repeats of each mixture were generated, as well as a surfactant control. Centrifuge tubes were wrapped in foil and incubated at 37^{o}C at 180 rpm. After 24 hours, 100 µL of the oil phase of each sample was added to a well of a 96 well plate. Absorbance readings (optical density 570 nm) were taken and imputed into the equation of the standard curve of each dye's concentration gradient to obtain the concentration of dye leaked into the oil phase from the bulk emulsion.

Droplet-to-droplet Leakage

Sample Preparation for Quantifying Droplet-to-Droplet Leakage

The picodroplet technology was used to generate two populations of 300 pL droplets for each surfactant tested. Surfactants included commercially available 5% Pico-Surf, commercially available 3% Fluro-Surf, 5% AM50-06 and 5% AM50-08. One droplet population contained PBS, and the other contained PBS + 0.1mg/mL resazurin. Monodispersity and the coefficient of variation were assessed using the data output from the droplet generating machine. Once droplet populations were collected in centrifuge tubes, the PBS, and PBS + resazurin population were mixed in a 1:1 v/v ratio into a separate centrifuge tube.

10 µL of each sample was added to a chamber slide and imaged using an EVOS M5000 imaging system with a 10x brightfield objective. Three fields of view of each emulsion were taken using the transmitted light and the Texas Red (585/624 nm) filter. Images were highlighted for overexposure and set to the same light, emission, and gain for each sample.

The three samples of PBS, PBS + resazurin and the mixed population were covered in foil and incubated at 37°C at 180 rpm. Time point images were taken at 0, 4, 8, and 24 hours.

Image Analysis of Fluorescent Intensity of Each Droplet

CellProfiler™ (version 4.2.4) imaging software was used to detect the mean fluorescent intensity of each droplet on each image. The pipeline created by (Bartkova et al., 2020), which is publicly available on GitHub (https://github.com/taltecmicrofluidics/CP-for-droplet-analysis), was imported and modified. Briefly, the fluorescent TIF images of the mixed populations at different time points were imported into the CP “images” module. Three images of the same sample were grouped to acquire 3 data repeats. Droplets were then identified as objects by the “IdentifyPrimaryObject” module. The threshold was set manually to find all the desired droplets and the typical diameter range for finding the droplets was 90-150 pixels. Droplets were excluded from the data set if they were outside the typical diameter range or touching the border of the image. Next, the pixel intensity units of the droplets detected were measured using the “MeasureObjectIntensity” module. Finally, the “ExportToSpreadsheet” module was used to export the data as a .csv file. The file was imported into GraphPad Prism 8 to analyse data of relative fluorescent intensity of each droplet. Each sample was plotted as a scatter graph over time and the number of droplets detected was noted.

5.2.6 Assessment of Monodispersity and Stability of AM50-06 using Mycobacterial Culture Media as the Aqueous Phase

The set-up, droplet generation, image analysis, and statistical calculations for assessing droplet monodispersity and stability were as described in (Section 5.2.4) with an exception that the aqueous phase was either PBS, 7H9 media , or cholesterol minimal media.

5.2.7 Statistical Analysis

Toxicity Broth Microdilution

All data collected were n=3 technical replicates. The broth microdilution assays were processed in Microsoft® Excel® for Microsoft 365 MSO (Version 2302 Build 16.0.16130.20806) 64-bit and then plotted and analysed using GraphPad Prism 8. Blank control values of broth only were deducted from bacteria containing wells. End point data was plotted in bar charts as the mean + SD. Data analysis was performed using GraphPad Prism 8 software. A two-way ANOVA was conducted to determine if there were any statistically significant differences between the means of the various treatment groups. Post-hoc analysis using a Tukey's comparisons tests was then performed to compare each treatment concentration against the untreated control (0 μM) and between surfactant concentrations. This allowed us to identify the concentration of surfactant at which a statistically significant

reduction in bacterial growth occurred. Statistical significance was defined as $P \leq 0.05$, with significance levels indicated as follows: **** $P \leq 0.0001$, *** $P \leq 0.001$, ** $P \leq 0.01$, * $P \leq 0.05$, ns $P > 0.05$.

Droplet Monodispersity and Size Distribution

Droplet monodispersity and size distribution were assessed using a function in Microsoft® Excel® for Microsoft 365 MSO (Version 2302 Build 16.0.16130.20806) 64-bit and then plotted and analysed using GraphPad Prism 8. The experimental results for assessing droplet monodispersity and size distribution of different variables are represented by average droplet volume (pL), standard deviation (SD), and coefficient of variation (CV%). For each experimental condition, approximately 2,500 droplets were analysed. To determine the size distribution and stability of collected and incubated droplets, the radius (in pixels) of each droplet identified on each image was plotted over the time course of the experiment. The coefficient of variation (CV%) was used to assess the change in the size variance of the droplets during incubation.

5.3 Results

5.3.1 General Synthesis of PAMAM Dendrimers

Motivated by the lack of commercially available surfactants suitable for microemulsion-based bioreactors which retain small molecules within them, this study describes the synthesis of a biocompatible fluorosurfactant for droplet generation with dendrimer-based structures. PAMAM dendrimer-based surfactants were selected as droplet stabilisers, hypothesising that these structures could hinder small molecule leakage from droplets. To test this, PAMAM dendrimers were synthesised by the divergent method. The smallest generation (G0.5) was formed first, followed by synthesis of the full dendrimer (G1.0). Two simple reactions; the 1,4 Michael addition and an amination reaction are employed to form full generation dendrimers. These steps can be repeated to increase the dendrimer in size. For this investigation, the dendrimers were synthesised up until the first generation. The mechanism of the 1,4 Michael addition step is shown in Figure 5.4. This step forms an ester-terminated PAMAM dendrimer. Methyl acrylate acts as the alpha-beta unsaturated carbonyl compound, which is used in this step. The carbonyl group exerts an electron-withdrawing influence on the alkene, creating a partially positive charge on the terminal carbon. This charge is eventually stabilised through resonance. As a result, the β carbon becomes electropositive, making it susceptible to nucleophilic attack by the EDA. Next, the second step is completed. The amidation reaction (mechanism illustrated in Figure 5.5) forms amine terminated PAMAM dendrimers. The positively charged carbonyl carbon, which is associated with the methoxy group, is attacked by the lone pair of nitrogen from EDA acting as a nucleophile. The resulting intermediate is then protonated by the second terminal amine. Subsequently, the methoxy group is transformed into a good leaving group, and the positive charge is neutralised through deprotonation, yielding the final product and an alcohol.

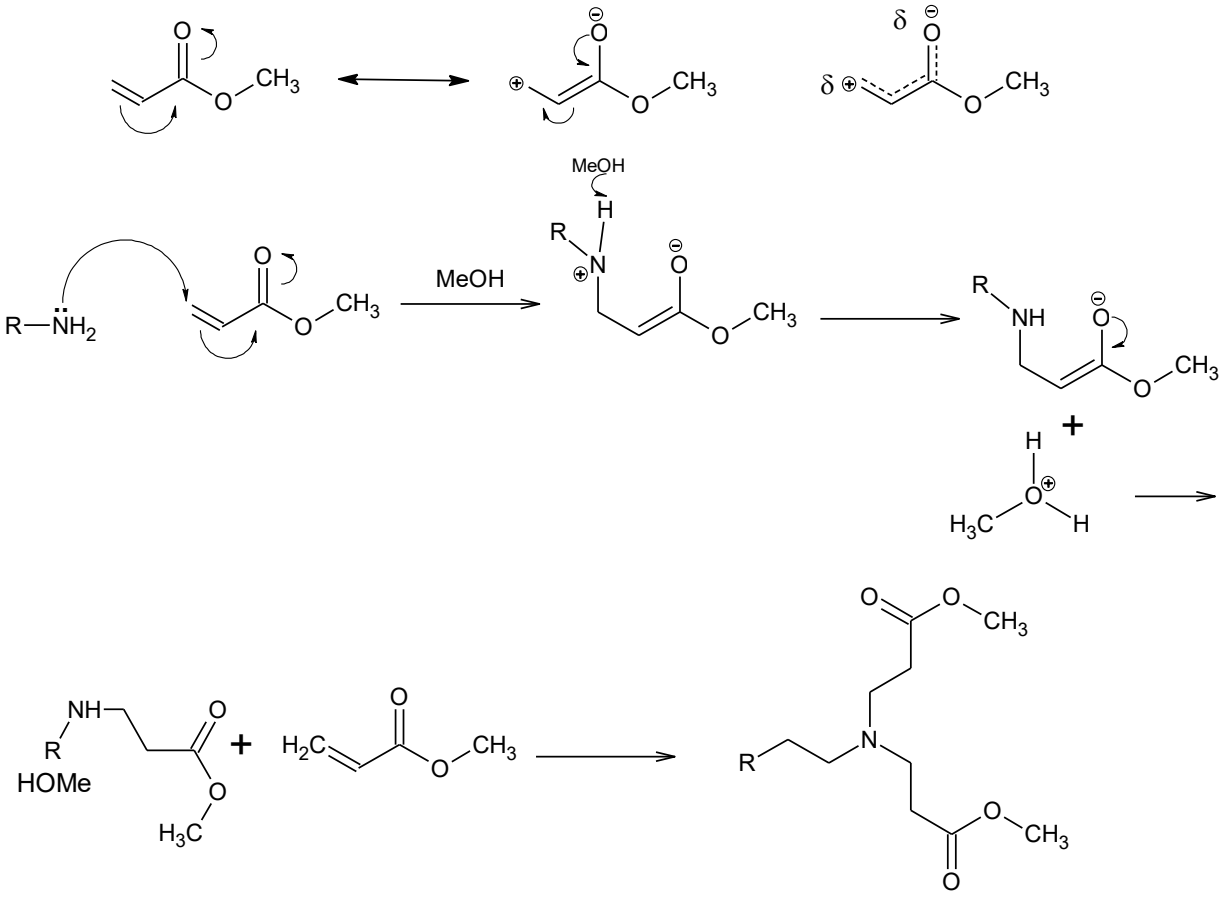

Figure 5.4. Mechanism of 1, 4 Michael addition step.

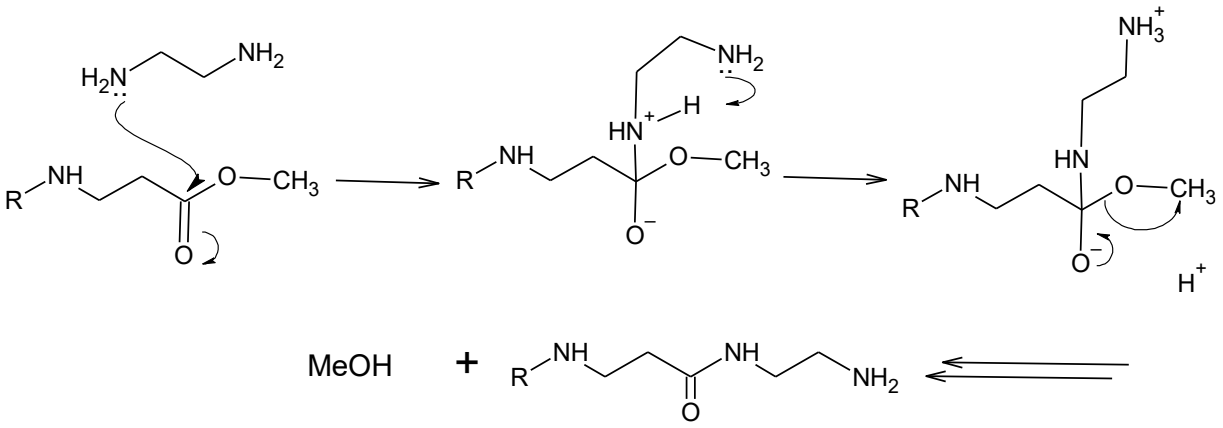

Figure 5.5. Mechanism of Amidation reaction step.

5.3.2 Synthesis and Purification of Half Generation (G0.5) PAMAM Dendrimers

Generation 0.5 half PAMAM dendrimers were first synthesised by adding methyl acrylate (MA) to ethylene diamine (EDA) in excess. The procedure is shown in Figure 5.6. Small amounts of the reaction solution were taken 24 hours after the reaction and analysed by ^{1}H NMR to check if MA was fully removed. Excess MA needed to be removed to avoid any side reactions during the next step. The reaction was placed on a rotary evaporator to remove MA until no visible peaks at 6.15 ppm and 6.37 ppm on the ^{1}H NMR analysis. At the end of the reaction, a viscous oil product was obtained.

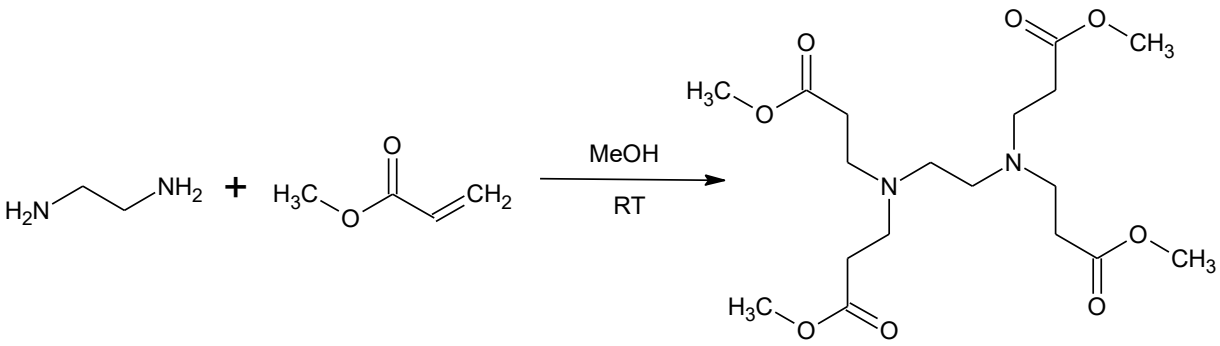

Figure 5.6. Synthesis of PAMAM dendrimer with 4 terminal OMe groups (G0.5)

5.3.3 Synthesis and Purification of Full Generation (G1.0) PAMAM Dendrimers

G1.0 full generation PAMAM dendrimers were next synthesised by adding EDA in excess to the product of G0.5 dendrimer, which was ester-terminated. Figure 5.7 illustrates the visualisation of the reaction. EDA was added dropwise at 0 °C and then stirred at room temperature. The completion of the reaction requires the excess EDA to attach to every ester group, resulting in homogeneous dendrimers and preventing unfavourable side reactions. This reaction took longer to complete than the synthesis of G0.5 reaction. After this amidation reaction was complete, the product was purified to remove the excess amount of reactants and prevent defects in further generation or surfactant synthesis. The reaction scheme in Figure 5.8 shows the side reactions caused by non-removal of EDA in dendrimer formation. The excess of EDA residues could lead to the production of smaller undesirable G0.5 dendrimers, as the unremovable of EDA can act as a new core and interact with additional MA. These smaller dendrimers are difficult to separate from G1.0 because of their similar structure. The molecular weight distribution of these dendrimers will therefore be broad as a result. In addition, cross-linking products or cyclisation compounds are also results of incomplete purification of EDA (Figure 5.8). Excess EDA was removed using a mixture of toluene and methanol at a 9:1 ratio. EDA binds to amide or amine groups, which is much harder to remove than MA. This is due to string hydrogen bonds between the dendrimer and the EDA. The excess EDA can be displaced by methanol, as it is a competitor for hydrogen bonds. The washing procedure was repeated and ^{1}H NMR analysis was obtained to ensure that the EDA peak (a singlet peak at 2.7) was no longer visible in the spectrum.

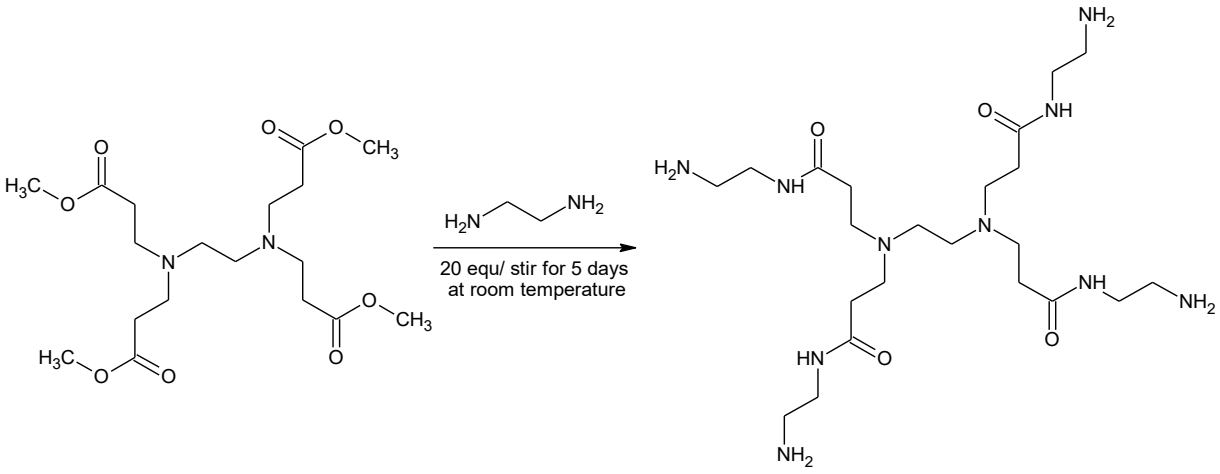

Figure 5.7. Synthesis of PAMAM dendrimer with 4 terminal amine groups (G1.0).

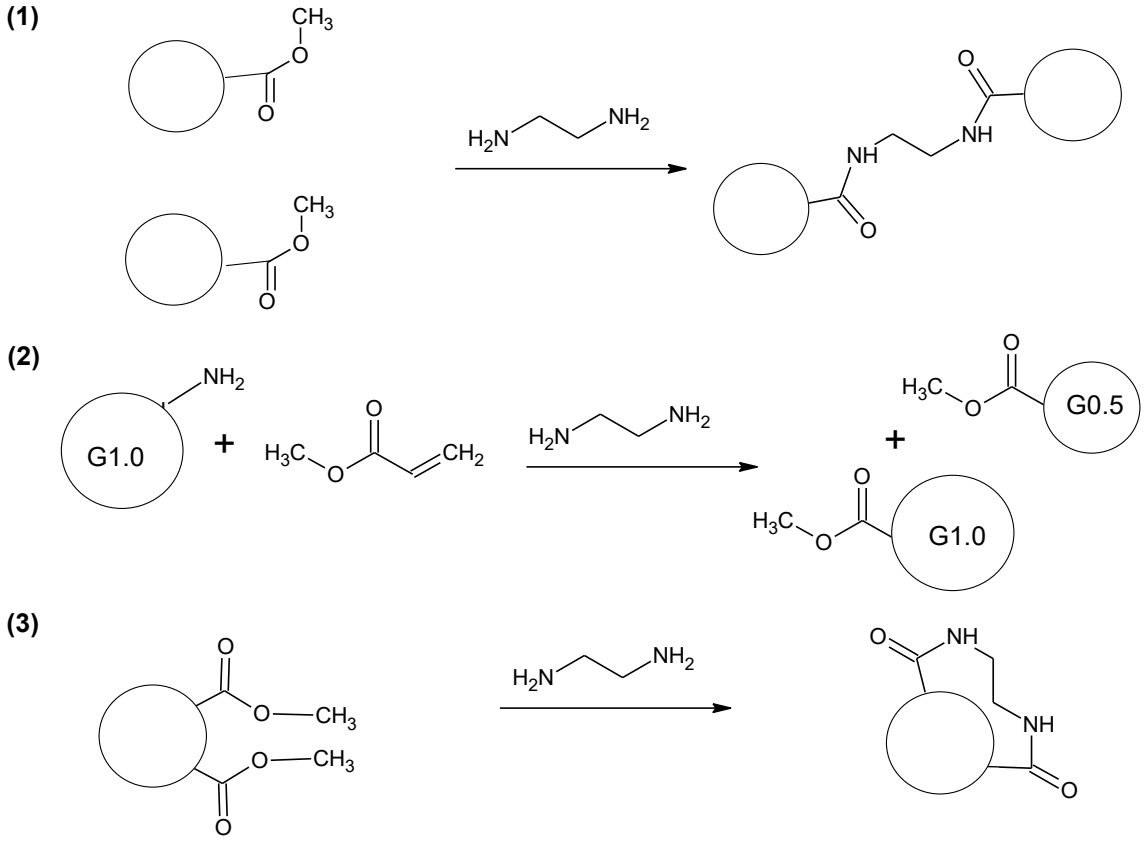

Figure 5.8. Purification of full generation dendrimers. Side reactions caused by non-removal of EDA in dendrimer (1) cross-linking resulted from Intermolecular reaction and (2) By-product (3) Cyclisation.

5.3.4 Characterisation of PAMAM Dendrimers

To characterise dendrimers, important tools such as ^{1}H NMR, infrared (IR) spectroscopy, and mass spectrometry were used to analyse if G0.5 and G1.0 were pure products. In a ^{1}H NMR spectrum of a G0.5 PAMAM dendrimer with 4 terminal OMe (methoxy) groups, it is expected to see peaks corresponding to the protons in the dendrimer structure such as the central core protons, branching protons, and terminal protons.

When determining the functional groups present in the products, IR spectroscopy was used to confirm the success of the reactions as they progress from half to full generation dendrimers. The G0.5 dendrimers have a peak present at 1734.50 cm^{-1} for the ester (ester C=O) groups (appendix 5.1). The G1.0 generation dendrimers have two peaks around 1633.65 and 1548.19 cm^{-1} for the amide carbonyl groups (appendix 5.2).

To examine if there was any presence of structural defects in the synthesised dendrimers, mass spectrometry was used to determine their precise molecular weights against their expected molecular weights based on their structural uniformity. To determine the mass of G0.5 and G1.0 dendrimers, electrospray ionisation mass spectrometry (ES-MS) was used. Appendix 5.3 and 5.4 shows the results of the ES-MS. Table 5.1 lists the expected and obtained molecular weights of G0.5 and G1.0 dendrimers. For G0.5 dendrimer, the obtained value (405.2 g/mol) showed similarities to the expected value (404 g/mol). Additionally, for G1.0 dendrimer, the obtained value (517.3 g/mol) was comparable to the expected value (516 g/mol). These dendrimers were sufficient to synthesise dendrimer-based surfactants based on the results confirming their purity.

Table 5.1. Molecular weight of PAMAM dendrimers. Each generation of PAMAM dendrimers (G0.5 and G1.0) listed with their molecular formula, number of terminal groups, expected molecular weight, and obtained molecular weight (g/mol) from mass spectrometry.

Dendrimer Generation	Molecular Formula	Terminal Groups	Expected Molecular Weight	Obtained Molecular Weight
G0.5	$C_{18}H_{22}N_20_8$	4	404 g/mol	405.2 g/mol
G1.0	$C_{22}H_{48}N_{10}O_4$	4	516 g/mol	517.3 g/mol

5.3.5 Dendrimer Coupling Reactions

After the full generation dendrimer was synthesised and checked for impurities, it was then coupled to Krytox™ to generate a droplet generating surfactant. Two different surfactant samples were generated; AM50-06 and AM50-08 with two different functional groups which are disclosed to Sphere Fluidics Ltd. The following experiments compare the two synthesised dendrimer-based surfactants.

5.3.6 Hydrophilic-lipophilic Balance (HLB) of Synthesised Dendrimers

To determine if a synthesised surfactant product is suitable for droplet generation, the hydrophilic-lipophilic balance (HLB) is calculated. The HLB is calculated from the weight percentage of the hydrophilic groups to the hydrophobic groups in a molecule (Ng and Rogers, 2019). This value ranges from 0-20 with values <6.0 being the correct balance of the

hydrophilic and lipophilic moieties for water-in-oil emulsions (Zheng et al., 2015). In contrast, a HLB value between 8-18 is more suitable for oil-in-water emulsions. Therefore, a low HLB number denotes a strong oil affinity, whereas a high HLB value signifies a high water solubility (Rahaman et al., 2023). The HLB calculation is defined as;

$$HLB = 20 \times \left(\frac{Hydrophillic\ g/mol}{Hydrophobic\ g/mol\ + Hydrophillic\ g/mol}\right)$$

Using this calculation from the known structures of the synthesised dendrimer-based surfactants, the HLB value of both AM50-06 and AM50-08 equates to 3. This implied that the surfactants synthesised would be efficient at generating water-in-oil droplets.

5.3.7 The Toxicity of Synthesised Dendrimer-based Surfactants against *Pseudomonas aeruginosa, Staphylococcus aureus,* and *Mycobacterium abscessus* species.

Once the characterisation of the dendrimers was established, investigations were achieved to test the toxicity of the synthesised dendrimer-based surfactants to ensure they do not have any antimicrobial properties when used to form bioreactors for droplet assay development. Two commercial surfactants, Pico-Surf® and FluoSurf™ were also studied as controls along with samples of AM50-06 and AM50-08. A Gram-negative, a Gram-positive, as well as mycobacteria species were tested to investigate if the dendrimers' structure specifically influenced different cell wall structures of bacteria. Optical density was measured as a marker of cell growth when bacteria were challenged with each surfactant. Surfactants were also diluted to 5%, 2%, and 1% concentrations except for FluoSurf™ which was tested in the dilution ranges of 3%, 2%, and 1% concentrations. Several controls were included in each assay to ensure validity and aid in result interpretation:

1. Novec™ 7500 oil-only control: To account for any potential inhibitory effects of the solvent.
2. Bacteria-only control: To establish standard growth patterns without test surfactants.
3. Broth-only control: To confirm the sterility of the media and establish a baseline for optical density measurements.
4. Positive controls: Commercially available biocompatible surfactants Pico-Surf® and FluoSurf™, was used at various concentrations to validate the assay's ability to detect non-toxic activity.

A two-way analysis of variance (ANOVA) with Tukey's multiple comparisons tests was used to analyse the effect of surfactant type and concentration on bacterial growth. Full results from the ANOVA tests can be presented in appendix 5.5-5.21.

Figure 5.10 provides the experimental data on each surfactant challenged to *P. aeruginosa.* The Gram-negative bacteria showed growth from 0-20 hours in all surfactant concentrations and types. The optical density significantly increased from 0 to 20 hours ($p < 0.001$) demonstrating Pico-Surf®' s biocompatibility. In addition, there was no significant difference between the growth of *P. aeruginosa* at 20 hours when challenged with either 5%, 2%, or 1% Pico-Surf® ($P > 0.05$) showing that changing the concentration of Pico-Surf® does not influence bacterial growth. In contrast to bacteria challenged with Novec™ 7500 oil only, the experiments where the surfactant dissolved in the oil had a significant increase in growth ($p < 0.001$). This suggests that the bacteria may be metabolising the surfactant. Both the commercial controls and the dendrimer-based surfactants show similar results of no toxicity (Figure 5.10 A-D). In accordance with the biocompatible surfactants available on the market,

the newly synthesised surfactants AM50-06 and AM50-08 upheld non-toxic performance to *P aeruginosa*.

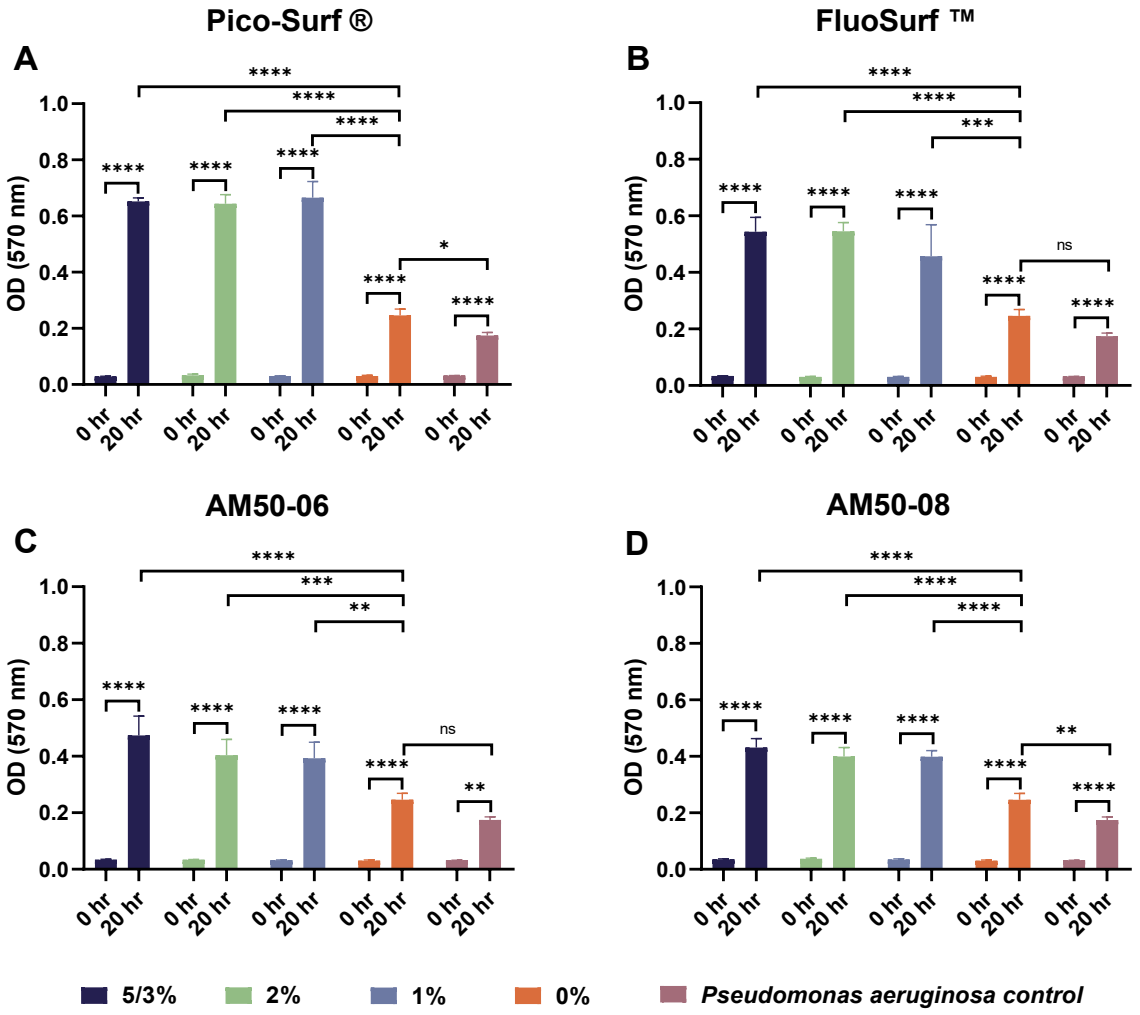

Figure 5.10. Toxicity of Pico-Surf®, FluoSurf™, AM50-06, and AM50-08 surfactant to *Pseudomonas aeruginosa* after 20 hours. (A) Bacterial growth at 0 and 20 hours with 5, 2, and 1% Pico-Surf®. **(B)** Bacterial growth at 0 and 20 hours with 3, 2, and 1% FluoSurf™. **(C)** Bacterial growth at 0 and 20 hours with 5, 2, and 1% AM50-06. **(D)** Bacterial growth at 0 and 20 hours with 5, 2, and 1% AM50-08. Optical density (570 nm) data represents n=3 technical replicates within one independent experiment. Mean values are shown and error bars represent standard deviation. P values were determined by a two-way analysis of variance (ANOVA) with Tukey's multiple comparisons tests to analyse the effect of surfactant type and time on bacterial growth. *P < 0.05, **P < 0.01, ***P < 0.001 and ****P < 0.0001.

Furthermore, when all four surfactants were tested for toxicity against *S. aureus* (a Gram-positive bacteria) promising results were also observed. Bacterial growth showed a significant difference between 0-20 hours for all surfactants, indicating the absence of toxicity to *S. aureus* in both commercial and synthesised dendrimers (Figure 5.11 (A-D)).

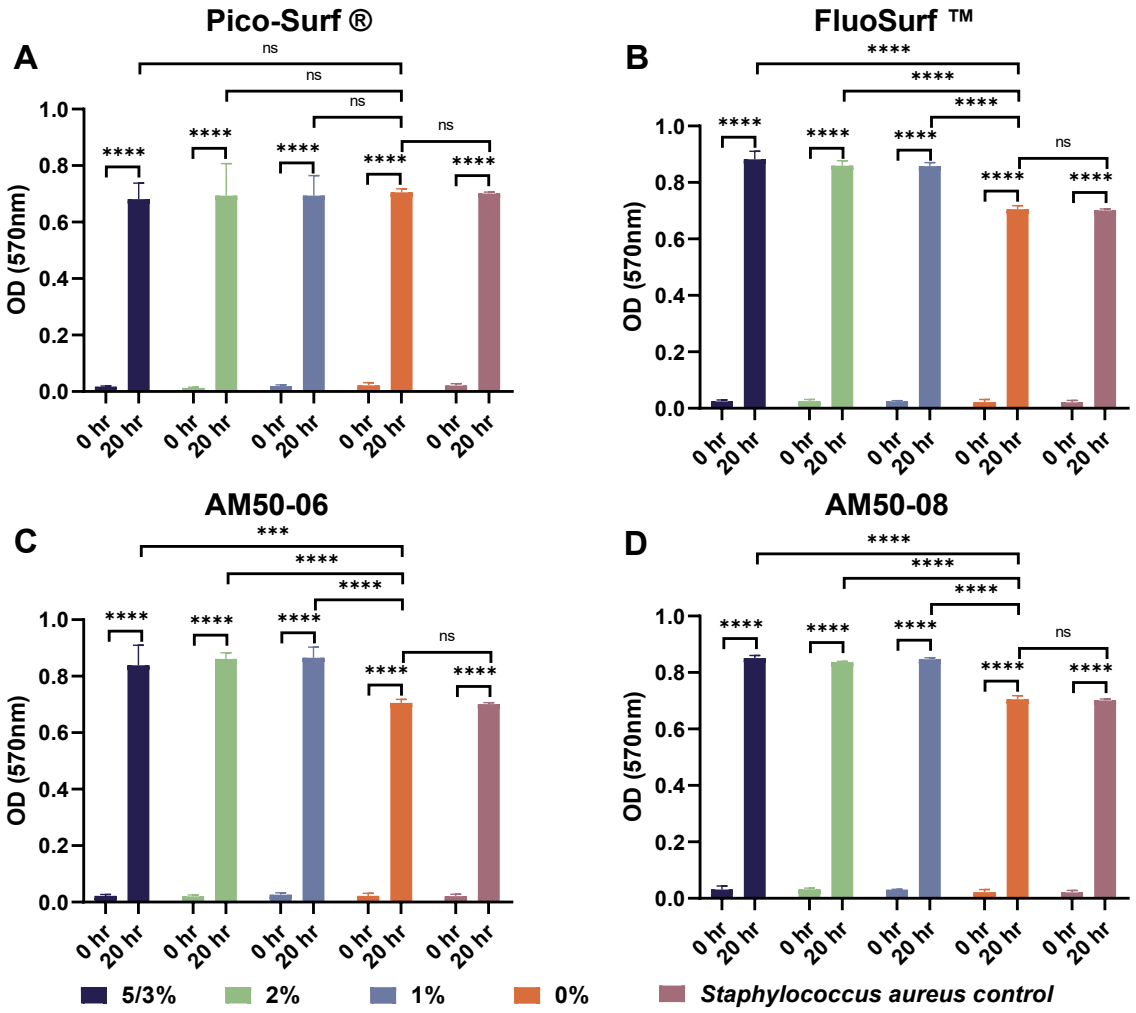

Figure 5.11. Toxicity of Pico-Surf®, FluoSurf™, AM50-06, and AM50-08 surfactant to *Staphylococcus aureus* after 20 hours. (A) Bacterial growth at 0 and 20 hours with 5, 2, and 1% Pico-Surf®. **(B)** Bacterial growth at 0 and 20 hours with 3, 2, and 1% FluoSurf™. **(C)** Bacterial growth at 0 and 20 hours with 5, 2, and 1% AM50-06. **(D)** Bacterial growth at 0 and 20 hours with 5, 2, and 1% AM50-08. Optical density (570 nm) data represents n=3 technical replicates within one independent experiment. Mean values are shown and error bars represent standard deviation. P values were determined by a two-way analysis of variance (ANOVA) with Tukey's multiple comparisons tests to analyse the effect of surfactant type and time on bacterial growth. *P < 0.05, **P < 0.01, ***P < 0.001 and ****P < 0.0001.

Next, mycobacterial species were tested as they have a difference in cell wall structure to Gram-positive and Gram-negative bacteria. *M. abscessus* has two morphotypes; smooth and rough. It is thought that by modulating the glycopeptidolipids (GPLs) on their cell wall, *M. abscessus* can transition from a smooth into a rough variant, which increases virulence and confers antibiotic resistance (Parmar and Tocheva, 2023). This difference in cell wall structure may interact differently with the dendrimer-based surfactants. Therefore, in addition to investigating Gram-positive and Gram-negative bacteria, a variant of the smooth morphotype and the rough morphotype of *M. abscessus* was tested. The results obtained from the analysis of each surfactant against NCTC *M. abscessus* Smooth variant after 96 hours are compared in Figure 5.12. The commercial surfactant Pico-Surf® showed no toxicity to the smooth variant,

as shown by the significant growth of 5%, 2%, and 1% experiments ($P < 0.0001$). In addition, there was no significant difference in the concentration of surfactant against bacterial growth (Figure 5.12 A). Surprisingly, the second commercial surfactant FluoSurf™, demonstrated that at 5% and 2% concentration had a toxic effect on the smooth variant. As the concentration of the surfactant was decreased to 1%, toxicity was eliminated by growth. Also, there was a significant difference in growth when challenged with oil, only explaining that the toxic effect is coming from the surfactant and not the oil (Figure 5.12 B). Likewise, the newly synthesised dendrimer surfactant AM50-06 showed that when increasing the strength of AM50-06 led to a reduction in bacterial growth (Figure 5.12 C). What is more interesting is that the other dendrimer-based surfactant AM50-08 displayed similar results to Pico-Surf® biocompatibility (Figure 15.12 D). There was a significant difference in bacterial growth after 96 hours for all surfactant concentrations. In accordance with the biocompatible surfactants available on the market, the newly synthesised surfactant AM50-06 mirrored FluoSurf™ surfactant with concentration dependent toxicity. In contrast, AM50-08 showcased similar non-toxic behaviour to the smooth variant of *M. abscessus*.

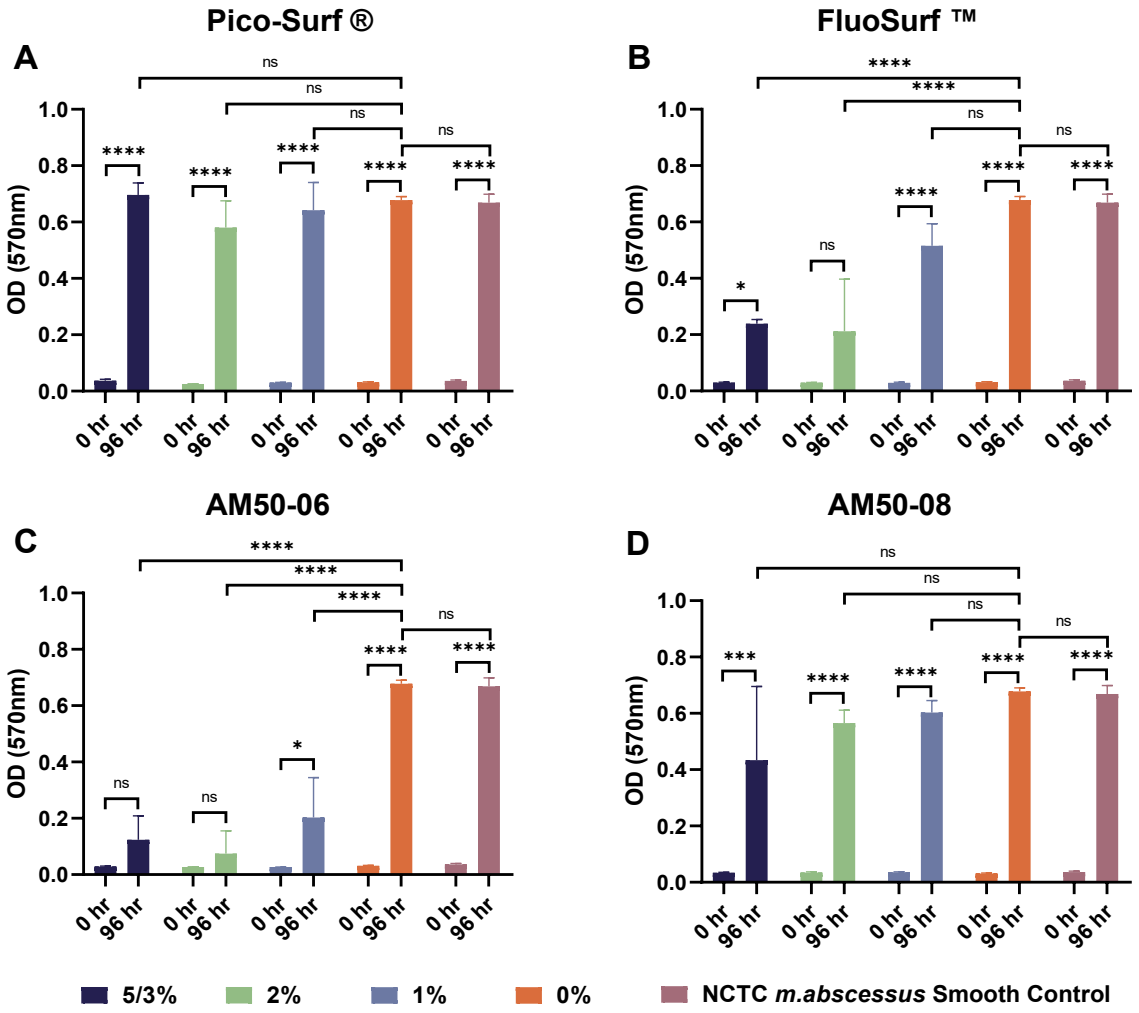

Figure 5.12. Toxicity of Pico-Surf®, FluoSurf™, AM50-06, and AM50-08 surfactant to *NCTC M. abscessus* Smooth variant at 96 hours. (A) Bacterial growth at 0 and 20 hours with 5, 2, and 1% Pico-Surf®. **(B)** Bacterial growth at 0 and 20 hours with 3, 2, and 1% FluoSurf™. **(C)** Bacterial growth at 0 and 20 hours with 5, 2, and 1% AM50-06. **(D)** Bacterial growth at 0 and 20 hours with 5, 2, and 1% AM50-08. Optical density (570 nm) data represents n=3 technical replicates within one independent experiment. Mean values are shown and error bars represent standard deviation. P values were determined by a two-way analysis of variance (ANOVA) with Tukey's multiple comparisons tests to analyse the effect of surfactant type and time on bacterial growth. *P < 0.05, **P < 0.01, ***P < 0.001 and ****P < 0.0001.

Interestingly, investigations of the toxicity of different structural surfactants against the NCTC *M. abscessus* rough variant showed toxicity to all surfactants (Figure 5.13). FluoSurf™ at a concentration of 1% was an exception where growth was witnessed. However, this had a significant difference to the oil control, suggesting that at 1%, the surfactant still inhibited growth. These toxicity findings suggest that all surfactants are non-toxic to Gram-positive and Gram-negative bacteria, however mycobacterial species with unique cell walls may have inhibited/toxic growth and therefor surface modification of the dendrimers are needed.

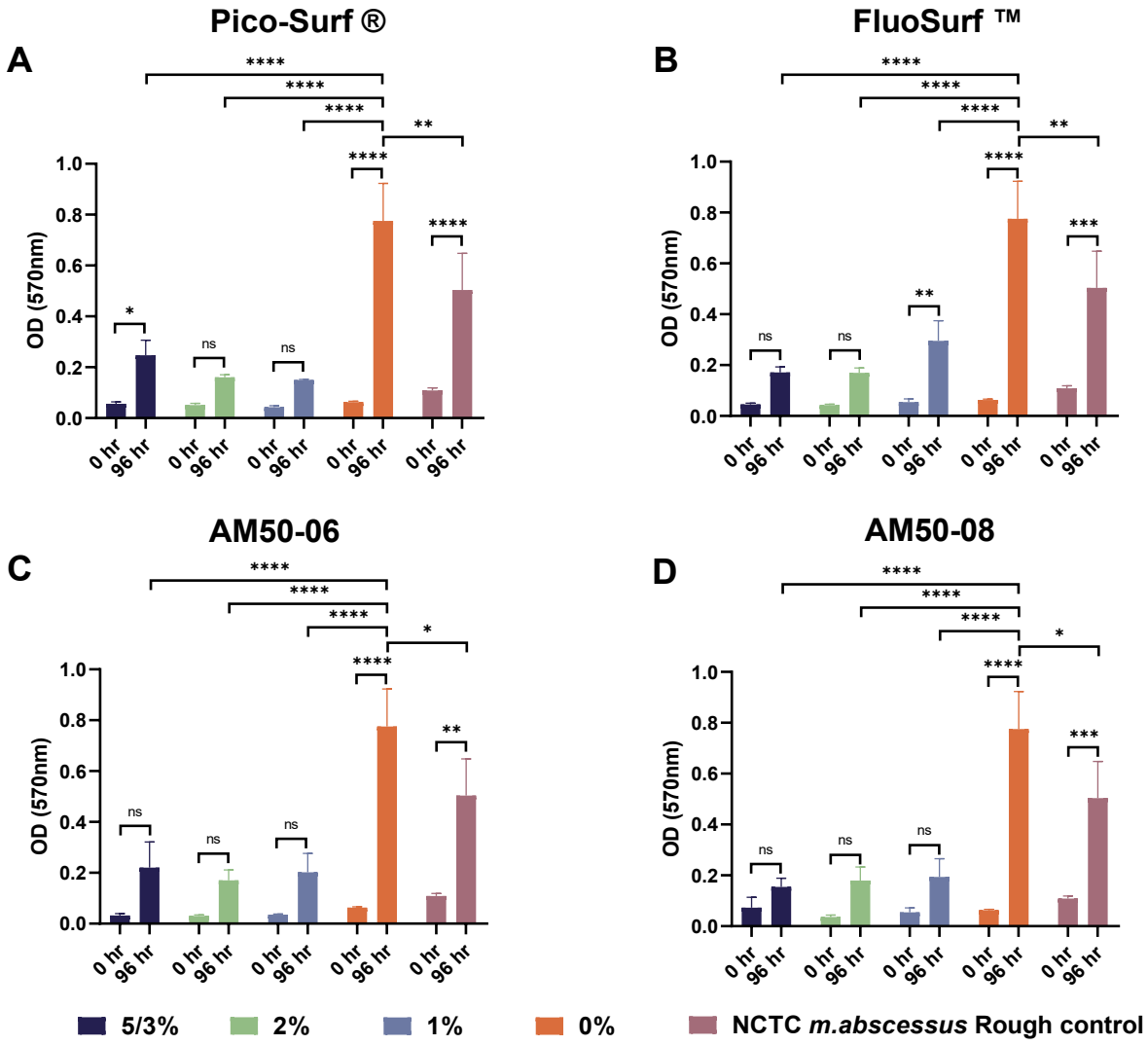

Figure 5.13. Toxicity of Pico-Surf®, FluoSurf™, AM50-06, and AM50-08 surfactant to *NCTC M.abscessus* rough variant at 96 hours. (A) Bacterial growth at 0 and 20 hours with 5, 2, and 1% Pico-Surf®. **(B)** Bacterial growth at 0 and 20 hours with 3, 2, and 1% FluoSurf™. **(C)** Bacterial growth at 0 and 20 hours with 5, 2, and 1% AM50-06. **(D)** Bacterial growth at 0 and 20 hours with 5, 2, and 1% AM50-08. Optical density (570 nm) data represents n=3 technical replicates within one independent experiment. Mean values are shown and error bars represent standard deviation. P values were determined by a two-way analysis of variance (ANOVA) with Tukey's multiple comparisons tests to analyse the effect of surfactant type and time on bacterial growth. *P < 0.05, **P < 0.01, ***P < 0.001 and ****P < 0.0001.

5.3.8 Assessing Small Molecule Leakage from Droplets into the Oil Phase of Newly Synthesised Dendrimer-Based Surfactants.

Once the dendrimer-based surfactants were synthesised and characterised, they were tested to give an insight if they prevented small molecule leakage from the aqueous phase of the droplet to the oil phase. The current study adopts resazurin as a marker of leakage. The two synthesised surfactants, AM50-06 and AM50-08, as well as two commercial surfactants Pico-Surf® and FluoSurf™ as controls, were tested using polydisperse bulk emulsions. Bulk emulsions were generated by vortexing 100 µg/ mL of resazurin in PBS and each surfactant.

The emulsions were stored in centrifuge tubes at room temperature for 24 hours and imaged at 0 hours and 24 hours as illustrated in Figure 5.14 A.

The image clearly shows that the oil phase colour changes in the Pico-Surf® sample in contrast to the other three surfactants, suggesting that brightly coloured resazurin has leaked from droplets containing Pico-Surf®. To quantify this, a standard curve of resazurin against optical density was plotted (Figure 5.14 B) to correlate the concentration of resazurin leaked into the oil phase of the emulsion. By taking an oil sample after 24 hours and monitoring the optical density, the linear regression of the standard curve was used to obtain the concentration of leakage of each surfactant. Figure 5.14 C shows that Pico-Surf® had a significant increase in resazurin concentration in the oil phase compared to the other surfactants, which indicates that the dendrimer-based surfactants prevent droplet-to-oil leakage compared to commercial Pico-Surf®. AM50-06 and AM50-08 reduced resazurin leakage into the oil phase by 85% and 78% respectively compared to Pico-Surf®, indicating their potential as superior surfactants for preventing antibiotic leakage in droplet-based AST.

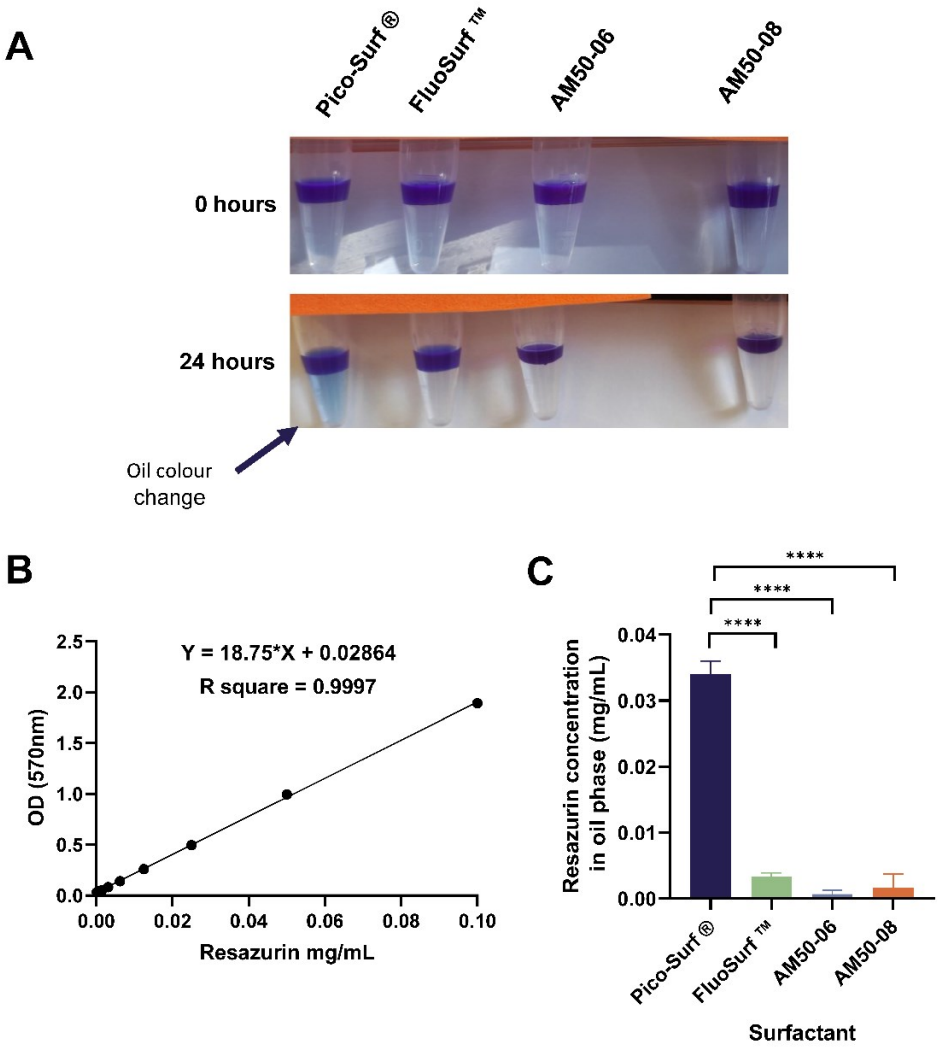

Figure 5.14. Assessment of resazurin leakage from polydisperse bulk emulsions into the oil phase. (A) Image of oil colour change of each surfactant after 24 hours. **(B)** Standard curve for resazurin (mg/ mL) versus optical density (570nm). **(C)** Resazurin concentration leaked into the oil phase of each surfactant tested after 24 hours (mg/ mL). Data represents n=3 technical replicates within one independent experiment. P values were determined by a one-way analysis of variance (ANOVA) with Tukey's multiple comparisons tests to analyse the effect of culture condition and time on bacterial growth. *P < 0.05, **P < 0.01, ***P < 0.001 and ****P < 0.0001.

5.3.9 Assessing Small Molecule Leakage from Droplets into Neighbouring Droplets of Newly Synthesised Dendrimer-Based Surfactants.

Next, resazurin leakage from droplets-to-droplets was assessed. To test the inter-droplet molecular transport, an assay needed to be developed to quantify the leakage and assess which surfactant prevents molecular transport in picolitre droplets. Similarly to the last experiment, resazurin (100 µg/ mL) was used as a marker of leakage. As resazurin fluoresces, a method which utilised fluorescent microscopy was chosen to visualise as well as quantify leakage. By using the picodroplet technology with the image-based closed-loop feedback, an assay was designed, developed, and validated, which Figure 5.15 illustrates. Briefly, if two populations of monodisperse droplets were generated - one consisting solely of PBS as the aqueous phase and another containing both PBS and resazurin - it was hypothesised that, as these emulsions were mixed and incubated in a 50:50 ratio, over time the 'empty' PBS droplets

would start to fluoresce due to leakage from the adjacent resazurin droplets. The surfactants which reduce the time of leakage could be determined by imaging the 'mixed' population of droplets and quantifying the mean fluorescent intensity of each droplet.

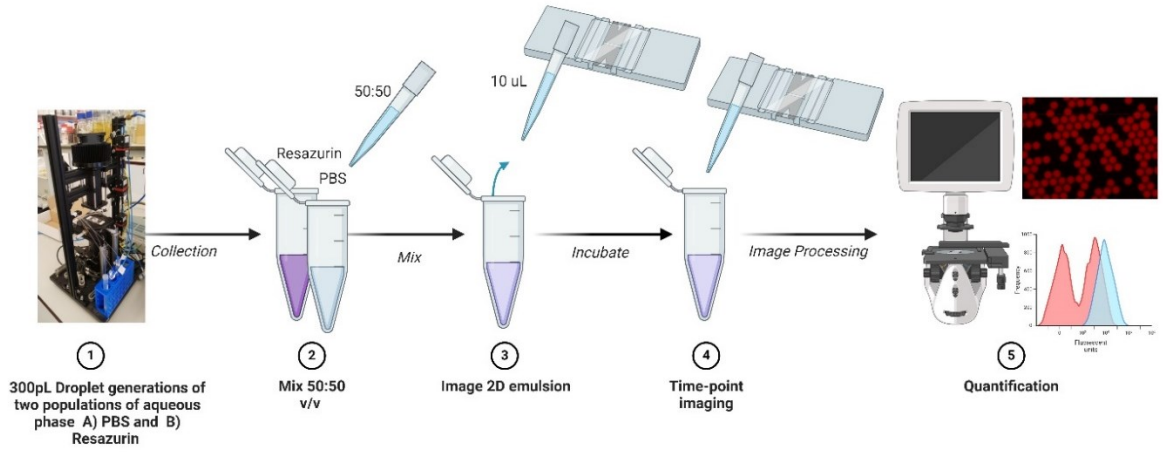

Figure 5.15. Schematic diagram of methodology to assess resazurin leakage from monodisperse droplets into other neighbouring droplets. Image created on Biorender.com.

Firstly, two populations of 300 pL droplets were generated and assessed for monodispersity to ensure that when the samples are mixed, both populations of droplets are identical in size for accurate results. To investigate if changing the aqueous phase from PBS only to PBS + resazurin effects 300 pL droplet generation, 300 pL was imputed into the feedback system and monodispersity was measured of different surfactant samples including Pico-Surf®, FluoSurf™, AM50-06, or AM50-08 surfactants. The volume of droplets generated with the eight samples can be shown in Figure 5.16.

Droplets encapsulated with PBS only and Pico-Surf® generated a mean droplet size of 299.98 pL, a SD of 0.84 pL, and a CV of 0.28% (Figure 5.16 A). Similarly, control of droplet generation was observed for PBS + resazurin with Pico-Surf®, (Figure 5.16 B), PBS only with FluoSurf™ (Figure 5.16 C), PBS + resazurin with FluoSurf™ (Figure 5.16 D), PBS only with AM50-06 (Figure E), PBS + resazurin with AM50-06 (Figure 5.16 F), PBS only with AM50-08 (Figure 5.16 G), and PBS + resazurin with AM50-08 (Figure 5.16 H). The mean values of droplet volumes were 0.57, 0.24, 0.28, 0.37, 0.26, 0.17, 0.21 pL in relation to the desired droplet size of 300 pL for Figures 5.16 (A-H). In addition, respectively to these samples, the average standard deviation for droplet generation were 0.97, 0.92, 1.18, 0.77, 1.22, 0.81, 1.07 pL. In all experiments generating droplets with the 60 µm x 60 µm flow-focusing channel, the coefficient of variations were below 0.41 %. When changing the aqueous phase and surfactant type, highly ultra-monodisperse droplets were successfully generated. This quality control ensured that the assay development was as accurate as possible when mixing the droplets.

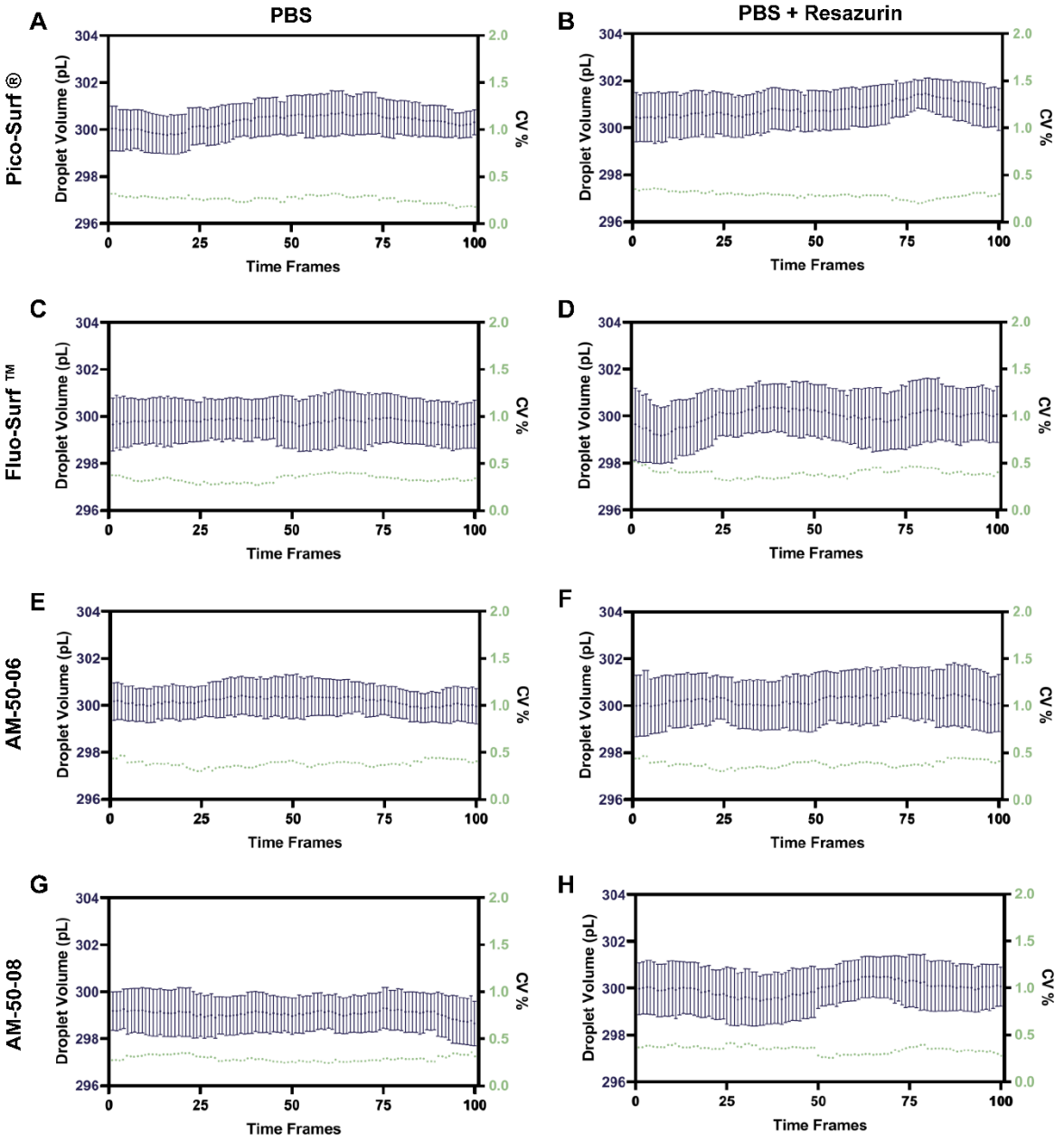

Figure 5.16. Monodispersity of 300 pL generated droplets encapsulated with either PBS or PBS + Resazurin and either Pico-Surf®, FluoSurf™, AM50-06, or AM50-08 surfactant. Image-based feedback loop set at 300 pL. **(A)** Mean droplet volume 299.98 pL, SD 0.83 pL, CV 0.28 %, FRR 0.91, and droplet generation speed 415/s. **(B)** Mean droplet volume 300.57 pL, SD 0.97 pL, CV 0.32%, FRR 0.93, and droplet generation speed 440/s. **(C)** Mean droplet volume 299.76 pL, SD 0.92 pL, CV 0.31 %, FRR 0.90, and droplet generation speed 412/s. **(D)** Mean droplet volume 300.28 pL, SD 1.18 pL, CV 0.39 %, FRR 0.89, and droplet generation speed 258/s. **(E)** Mean droplet volume 300.37 pL, SD 0.77 pL, CV 0.26%, FRR 0.93, and droplet generation speed 515/s. **(F)** Mean droplet volume 300.26 pL, SD 1.22 pL, CV 0.41%, FRR 0.84, and droplet generation speed 262.63/s. **(G)** Mean droplet volume 300.17 pL, SD 0.81 pL, CV 0.27%, FRR 0.86, and droplet generation speed 318/s. **(H)** Mean droplet volume 300.21 pL, SD 1.07 pL, CV 0.36%, FRR 0.86, and droplet generation speed 337/s. The average droplet volume (pL), standard deviation (SD), coefficient of variation (CV %) and flow rate ratio (FRR) of n=25 droplets are plotted for 100 saved frames. Each graph represents 1 of 3 repeats of 100 saved time frames.

After these 8 samples were generated, the PBS only population and PBS + resazurin population of each surfactant were mixed in a 50:50 ratio. At 0, 4, 8, and 24 hours, each sample of PBS only droplets, PBS + resazurin droplets, and mixed droplets were imaged to ensure they remained stable during the experiment. Figures 5.17-5.20 displays the droplet radius (in pixels) as well as the CV values for each sample and its controls. The data in Figure 5.17 depicts the stability of droplets during incubation generated with Pico-Surf® surfactant. All samples including (A) the PBS population, (B) the resazurin population, and (C) the mixed population remained monodisperse and stable for the duration of the experiment with CV values below 4%.

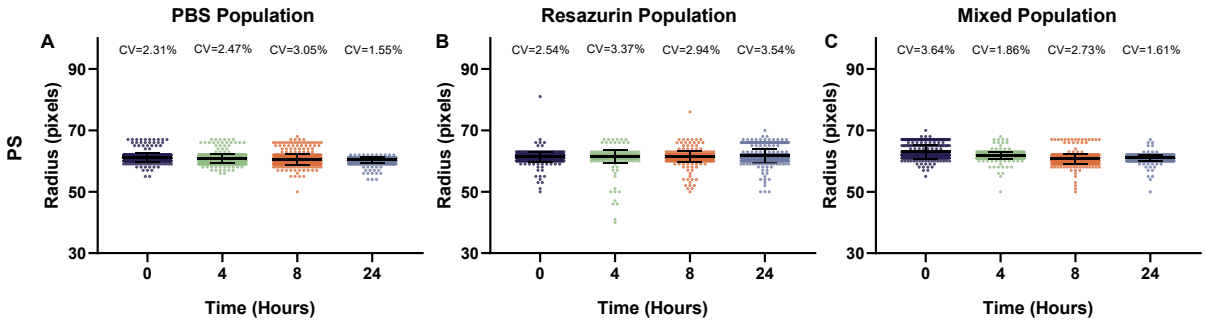

Figure 5.17. Droplet stability of 300 pL generated droplets with either PBS population, Resazurin population or a mixed population, and Pico-Surf® surfactant. Stability was measured for each sample of droplets for 24 hours. Each scatter plot illustrates the variance in droplet size over time of an emulsion with different aqueous phases. **(A)** Mean = 61 pixels, SD= 1 pixels, CV= 2.23%, n= 640 droplets at 0 hours. Mean = 61 pixels, SD= 1 pixels, CV= 2.47%, n= 638 droplets at 4 hours. Mean = 61 pixels, SD= 2 pixels, CV= 3.05%, n= 643 droplets at 8 hours. Mean = 60 pixels, SD= 1 pixels, CV= 1.55%, n= 658 droplets at 24 hours. **(B)** Mean = 61 pixels, SD= 2 pixels, CV= 2.54%, n= 632 droplets at 0 hours. Mean = 61 pixels, SD= 2 pixels, CV= 3.37%, n= 647 droplets at 4 hours. Mean = 61 pixels, SD= 2 pixels, CV= 2.94%, n= 621 droplets at 8 hours. Mean = 62 pixels, SD= 2 pixels, CV= 3.54%, n= 644 droplets at 24 hours. **(C)** Mean = 63 pixels, SD= 2 pixels, CV= 3.64%, n= 629 droplets at 0 hours. Mean = 62 pixels, SD= 1 pixels, CV= 1.86%, n= 620 droplets at 4 hours. Mean = 61 pixels, SD= 2 pixels, CV= 2.73%, n= 652 droplets at 8 hours. Mean = 61 pixels, SD= 1 pixels, CV= 1.61%, n= 636 droplets at 24 hours. Data for each time point is from three representative images of different fields of view of the emulsion. Each data point represents the radius (pixels) of an individual droplet in an image. Dotted line is the mean and error bars show the standard deviation of droplet size

The data in Figure 5.18 depicts the stability of droplets during incubation generated with FluoSurf™ surfactant. The PBS population (A) during incubation remained stable until 24 hours where variance was detected with a CV value of 15.32%. All other samples remained monodisperse and stable for the duration of the experiment with CV values below 5%. The unusual distribution of droplet integrity at 24 hours of the PBS population is likely due to the incubation condition such as an increase in evaporation and as this quality check was to ensure that the mixed population stays stable, this unlikely affects the results of this experiment.

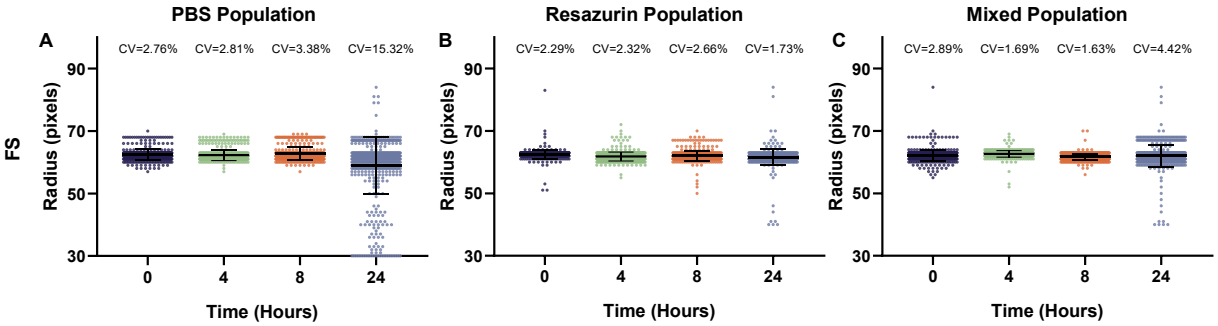

Figure 5.18. Droplet stability of 300 pL generated droplets with either PBS population, Resazurin population or a mixed population, and FluoSurf™ surfactant. Stability was measured for each sample of droplets for 24 hours. Each scatter plot illustrates the variance in droplet size over time of an emulsion with different aqueous phases. **(A)** Mean = 62 pixels, SD= 2 pixels, CV= 2.76%, n= 613 droplets at 0 hours. Mean = 62 pixels, SD= 2 pixels, CV= 2.81%, n= 597 droplets at 4 hours. Mean = 63 pixels, SD= 2 pixels, CV= 3.38%, n= 599 droplets at 8 hours. Mean = 59 pixels, SD= 9 pixels, CV= 15.32%, n= 696 droplets at 24 hours. **(B)** Mean = 63 pixels, SD= 1 pixels, CV= 2.29%, n= 598 droplets at 0 hours. Mean = 62 pixels, SD= 1 pixels, CV= 2.32%, n= 613 droplets at 4 hours. Mean = 62 pixels, SD= 2 pixels, CV= 2.66%, n= 597 droplets at 8 hours. Mean = 62 pixels, SD= 1 pixels, CV= 1.73%, n= 610 droplets at 24 hours. **(C)** Mean = 62 pixels, SD= 2 pixels, CV= 2.89%, n= 614 droplets at 0 hours. Mean = 63 pixels, SD= 1 pixels, CV= 2.89%, n= 604 droplets at 4 hours. Mean = 63 pixels, SD= 1 pixels, CV= 1.63%, n= 627 droplets at 8 hours. Mean = 62 pixels, SD= 3 pixels, CV= 4.42%, n= 625 droplets at 24 hours. Data for each time point is from three representative images of different fields of view of the emulsion. Each data point represents the radius (pixels) of an individual droplet in an image. Dotted line is the mean and error bars show the standard deviation of droplet size.

The data in Figure 5.19 depicts the stability of droplets during incubation generated with AM50-06 surfactant. All samples including (A) the PBS population, (B) the resazurin population, and (C) the mixed population remained monodisperse and stable for the duration of the experiment with CV values below 7%.

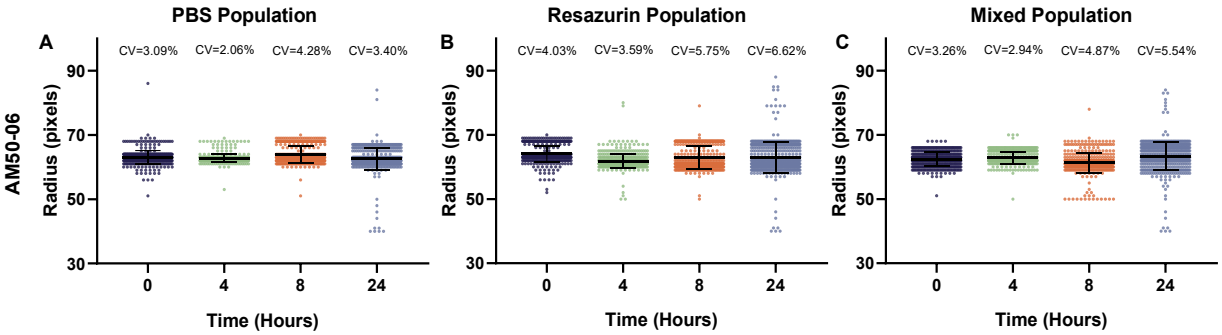

Figure 5.19. Droplet stability of 300 pL generated droplets with either PBS population, Resazurin population or a mixed population, and AM50-06 surfactant. Stability was measured for each sample of droplets for 24 hours. Each scatter plot illustrates the variance in droplet size over time of an emulsion with different aqueous phases. **(A)** Mean = 63 pixels, SD= 2 pixels, CV= 3.09%, n= 563 droplets at 0 hours. Mean = 63 pixels, SD= 1 pixels, CV= 2.06%, n= 519 droplets at 4 hours. Mean = 64 pixels, SD= 3 pixels, CV= 4.28%, n= 544 droplets at 8 hours. Mean = 63 pixels, SD= 2 pixels, CV= 3.40%, n= 557 droplets at 24 hours. **(B)** Mean = 62 pixels, SD= 3 pixels, CV= 4.03%, n= 538 droplets at 0 hours. Mean = 62 pixels, SD= 2 pixels, CV= 3.59%, n= 549 droplets at 4 hours. Mean = 63 pixels, SD= 4 pixels, CV= 5.75%, n= 608 droplets at 8 hours. Mean = 63 pixels, SD= 4 pixels, CV= 6.62%, n= 631 droplets at 24 hours. **(C)** Mean = 62 pixels, SD= 2 pixels, CV= 3.26%, n= 581 droplets at 0 hours. Mean = 63 pixels, SD= 2 pixels, CV= 2.94%, n= 588 droplets at 4 hours. Mean = 61 pixels, SD= 3 pixels, CV= 4.87%, n= 528 droplets at 8 hours. Mean = 63 pixels, SD= 4 pixels, CV= 5.54%, n= 582 droplets at 24 hours. Data for each time point is from three representative images of different fields of view of the emulsion. Each data point represents the radius (pixels) of an individual droplet in an image. Dotted line is the mean and error bars show the standard deviation of droplet size.

The data in Figure 5.20 depicts the stability of droplets during incubation generated with AM50-08 surfactant. All samples including (A) the PBS population, (B) the resazurin population, and (C) the mixed population remained monodisperse and stable for the duration of the experiment with CV values below 9%.

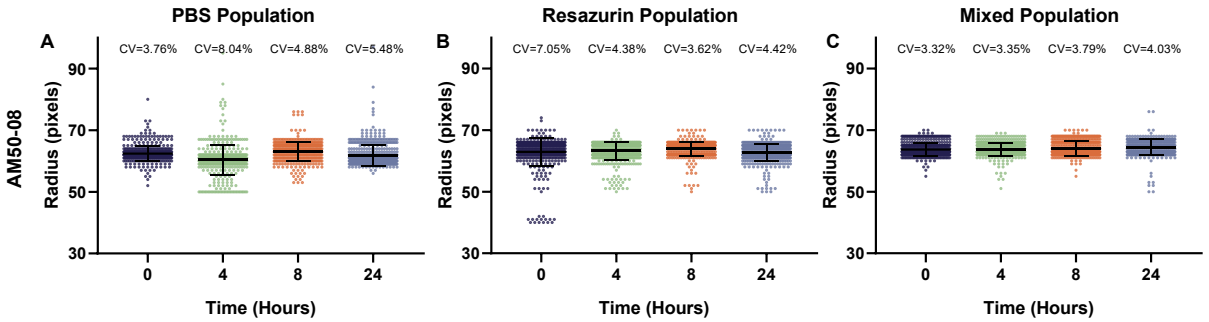

Figure 5.20. Droplet stability of 300 pL generated droplets with either PBS population, Resazurin population or a mixed population, and AM50-08 surfactant. Stability was measured for each sample of droplets for 24 hours. Each scatter plot illustrates the variance in droplet size over time of an emulsion with different aqueous phases. **(J)** Mean = 62 pixels, SD= 2 pixels, CV= 3.76%, n= 592 droplets at 0 hours. Mean = 60 pixels, SD= 5 pixels, CV= 8.04%, n= 513 droplets at 4 hours. Mean = 63 pixels, SD= 3 pixels, CV= 4.88%, n= 489 droplets at 8 hours. Mean = 62 pixels, SD= 3 pixels, CV= 5.48%, n= 603 droplets at 24 hours. **(K)** Mean = 63 pixels, SD= 4 pixels, CV= 7.05%, n= 619 droplets at 0 hours. Mean = 63 pixels, SD= 3 pixels, CV= 4.38%, n= 619 droplets at 4 hours. Mean = 64 pixels, SD= 3 pixels, CV= 3.62%, n= 628 droplets at 8 hours. Mean = 63 pixels, SD= 3 pixels, CV= 4.42%, n= 632 droplets at 24 hours. **(L)** Mean = 64 pixels, SD= 2 pixels, CV= 3.32%, n= 609 droplets at 0 hours. Mean = 64 pixels, SD= 2 pixels, CV= 3.35%, n= 599 droplets at 4 hours. Mean = 64 pixels, SD= 2 pixels, CV= 3.79%, n= 558 droplets at 8 hours. Mean = 64 pixels, SD= 3 pixels, CV= 4.03%, n= 559 droplets at 24 hours. Data for each time point is from three representative images of different fields of view of the emulsion. Each data point represents the radius (pixels) of an individual droplet in an image. Dotted line is the mean and error bars show the standard deviation of droplet size.

Fluorescent images were also taken at 0, 4, 8, and 24 hours to visualise resazurin leakage. As depicted in Figure 5.21, at 0 hours, each mixed population of resazurin and empty droplets for each surfactant tested had brightly coloured fluorescent droplets. After 4 hours, when fluorescent images were taken again, there was a notable difference. For droplets generated by Pico-Surf®, not only do the droplets containing fluorescent resazurin dimmer, but also the background ‘empty’ droplets have weakly fluoresced. By 24 hours, every droplet in the field of view is fluorescent. This trend is also visualised with FluoSurf™ and AM50-08. The dendrimer-based surfactant AM50-06 does not appear to show a second population of droplets fluoresce within four hours, however, by 24 hours the empty droplets are fluorescent, albeit at a lower fluorescence. This suggests that AM50-06 may increase the time it takes for resazurin to pass from one droplet to another.

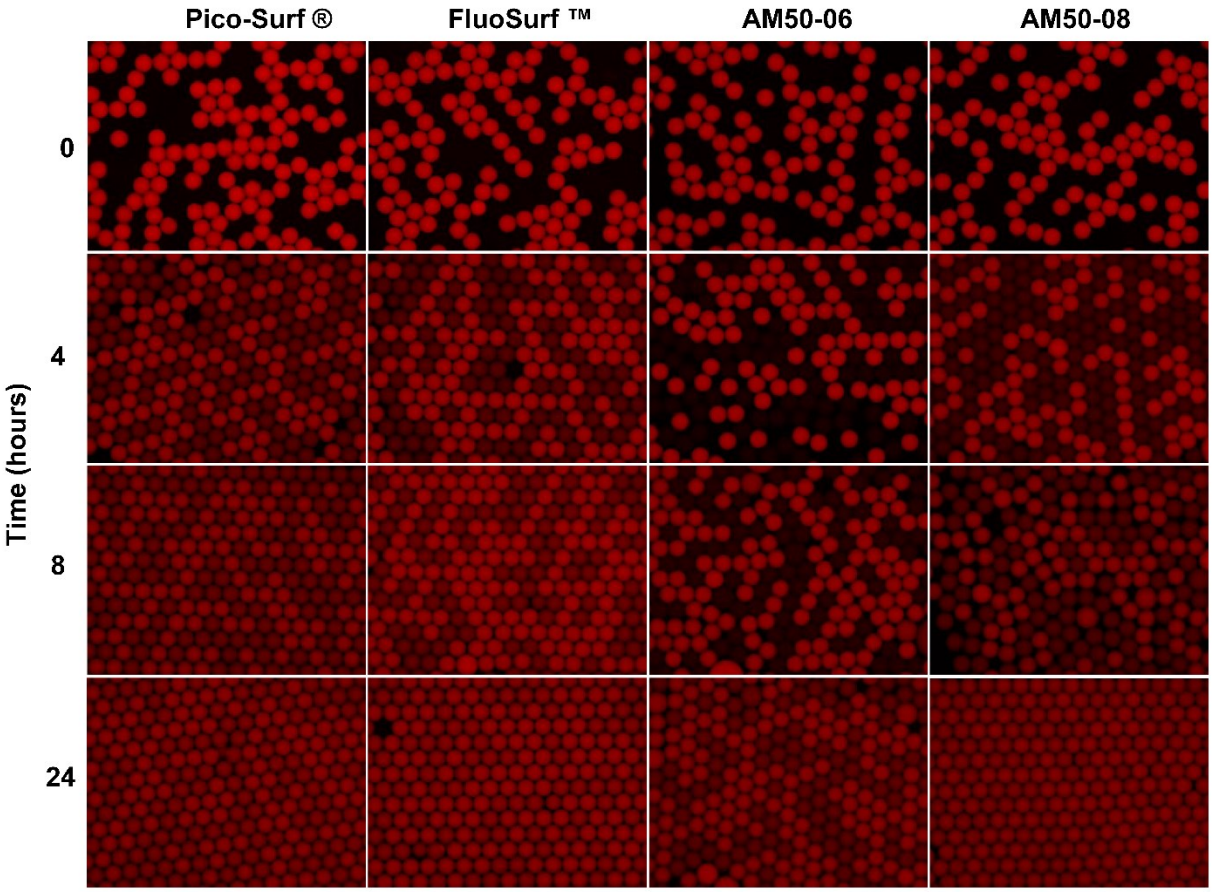

Figure 5.21. Fluorescent images over time of 300 pl droplets containing mixed droplets of PBS and PBS + Resazurin for each surfactant tested. From left to right are the different surfactant samples tested, Pico-Surf®, FluoSurf™, AM50-06, and AM50-08 surfactant. From top to bottom is images taken at time points 0, 4, 8, and 24 hours.

Quantitatively, these fluorescent images were processed in imaging software to obtain the mean fluorescent intensity of each individual droplet in a sample. A modified CellProfiler™ pipeline was used to identify the outlines of each droplet in an image and calculate the mean fluorescent intensity of that droplet. The scatter graphs in Figure 5.22 demonstrate the change in fluorescent intensity at 0, 4, 8, and 24 hours during incubation at 37 ºC in the shaking incubator. Droplets stabilised with Pico-Surf® were expected to immediately decrease in fluorescence as the resazurin concentration should move out of droplets and into empty droplets. This was the case as shown in Figure 5.22 A. At 4 hours, the population of droplets detected is split into two – one with the original fluorescence and one with the empty droplets starting to fluoresce. The image analysis software was able to detect the empty droplets as they started to fluoresce. The two populations are also confirmed by the increase in number of droplets identified (+271) and the increase in florescence variance, as calculated as CV (+17.19%). From 4 hours to 8, and 24, the trend stabilised and by 24 hours; the resazurin effusively leaked into bordering empty droplets and one population of droplet is identified as shown by a decrease in variation (CV= 9.75%). The FluoSurf™ and AM50-08 surfactants

exhibit a parallel trend to the commercial Pico-Surf®, with the empty droplets promptly fluorescing within four hours.

In contrast, the newly synthesised AM50-06 dendrimer-based surfactant increased the time it took for resazurin to leak in adjacent droplets. The difference is conveyed at 4 hours where the scatter column remains the one population with a low variance compared to the other surfactants (CV=3.56%). It is not until 8 hours that the empty droplets start to fluoresce, as shown by the two scatter populations, the decrease in mean fluorescent intensity of each individual droplet, and an increase in variance (CV= 42.87%). At 24 hours, the AM50-06 sample remains as two population, meaning that the once 'empty' droplets are not fully fluorescent, compared to the other surfactants.

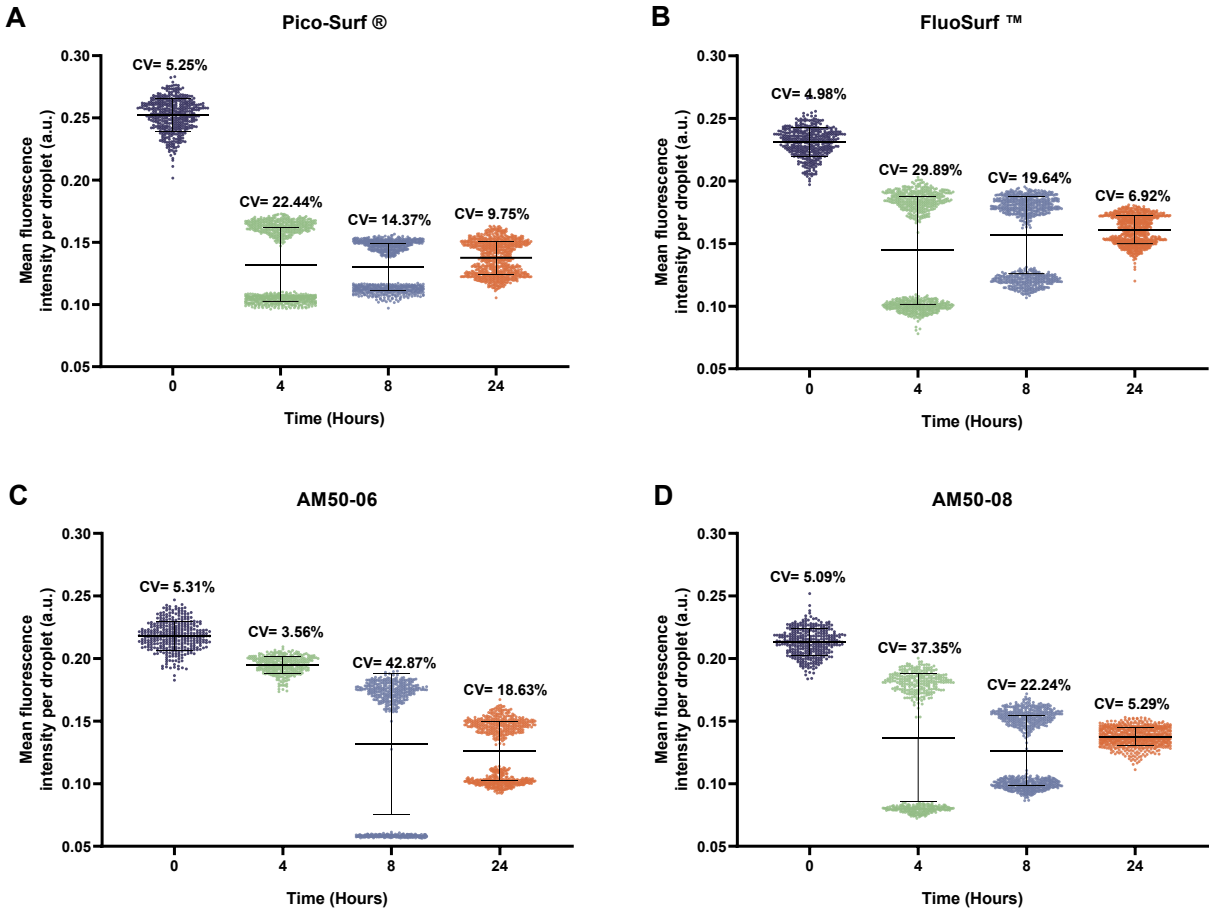

Figure 5.22. Mean fluorescent intensity of each droplet over time of 300 pl droplets containing mixed droplets of PBS and PBS + Resazurin for each surfactant tested. (A) Mean fluorescence intensity (a.u) of droplets generated with 5% Pico-Surf®. The number of droplets identified was 412, 683, 697, and 720 at 0, 4, 8, and 24 hours respectively. **(B)** Mean fluorescence intensity (a.u) of droplets generated with 3% FluoSurf™. The number of droplets identified was 384, 625, 675, and 698 at 0, 4, 8, and 24 hours, respectively. **(C)** Mean fluorescence intensity (a.u) of droplets generated with 5% AM50-06. The number of droplets identified was 338, 290, 484, and 598 at 0, 4, 8, and 24 hours, respectively. **(D)** Mean fluorescence intensity (a.u) of droplets generated with 5% AM50-08. The number of droplets identified was 335, 441, 618, 660 at 0, 4, 8, and 24 hours, respectively. Each data point represents the mean fluorescence intensity (a.u) of an individual droplet. Data for each time point is from four representative images of different fields of view of the emulsion. Solid line is the mean and error bars show the standard deviation of mean fluorescence intensity (a.u). Variance was assessed by coefficient of variation (CV%).

5.3.10 Monodispersity and Stability of Droplets Generated with 5% AM50-06 and Mycobacterial Culture Media.

To examine if monodisperse droplets can be produced with dendrimer-based surfactants and microbiology culture media, 300 pL droplets were generated with 5% of the lead candidate to reduce small molecule leakage - AM50-06 and either PBS as the control, Middlebrook 7H9 broth (7H9), and minimal cholesterol media (MCM) as the aqueous phase. The data were presented the same as all monodispersity investigations. As understood from the graphs in Figure 5.23, the capability to make monodisperse droplets with mycobacterial culture media were successful under these conditions. The mean values of droplet volumes for PBS, 7H9, and MCM aqueous phases were 0.32, 0.10, and 0.15 pL, respectively, within range to the desired droplet size of 300 pL. In all experiments generating droplets with 5% AM50-06 and bacterial culturing media, the standard deviations were below 1.12 pL and the coefficient of variations were below 0.37%. These results suggest that the structure of the dendrimer-based surfactant (AM50-06) is suitable for producing droplets of identical volume with mycobacterial culture media.

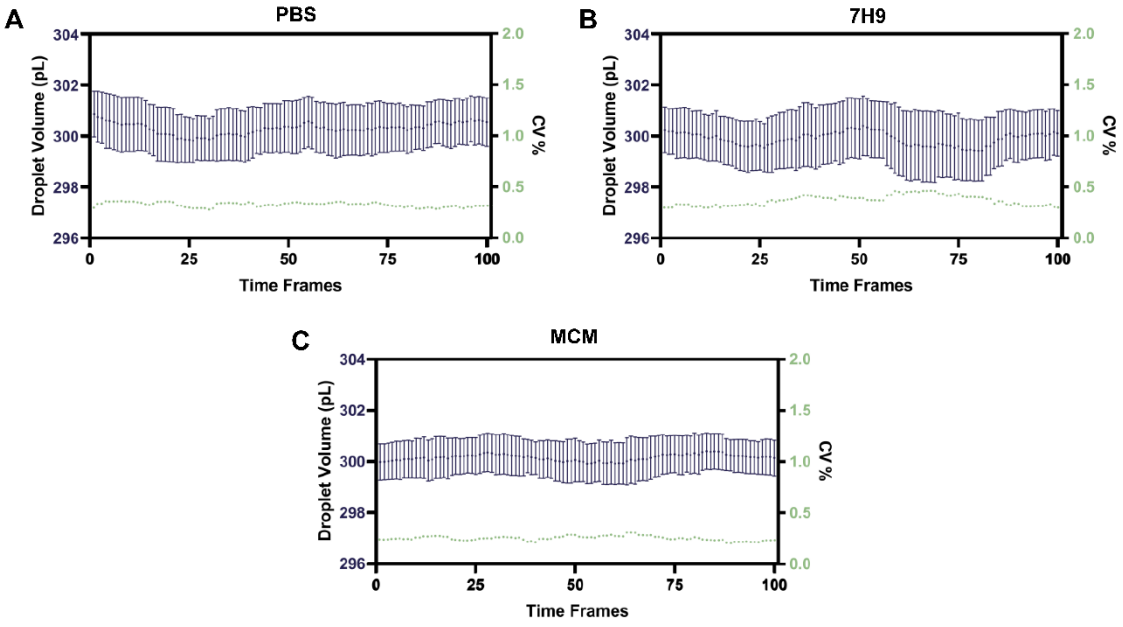

Figure 5.23. Droplet volume monodispersity of 300 pL droplets generated with 5% AM50-06 and mycobacteria culture media. (A) 300 pL droplets generated with PBS as the aqueous phase. Mean droplet volume 300.32 pL, SD 0.98 pL, CV 0.33%, FRR 0.95, and droplet generation speed 610/s. **(B)** 300 pL droplets generated with 7H9 media as the aqueous phase. Mean droplet volume 299.909 pL, SD 1.12 pL, CV 0.37%, FRR 0.95, and droplet generation speed 370/s. **(C)** 300 pL droplets generated with cholesterol media as the aqueous phase. Mean droplet volume 300.15 pL, SD 0.76 pL, CV 0.25%, FRR 1.04, and droplet generation speed 674/s. The average droplet volume (pL), standard deviation (SD) and coefficient of variation (CV %) of n=25 droplets are plotted for 100 saved frames. Each graph represents 1 of 3 repeats of 100 saved time frames.

After collecting these droplets in an emulsion and incubating them in culture conditions, the stability had unexpectedly improved compared to droplets stabilised with Pico-Surf® as explored in chapter 3. The images of the emulsions in each condition over time are illustrated in Figures 5.24-5.26. Figure 5.24 A shows the control aqueous phase PBS maintaining stability during 48 hours of incubation in each condition, quantified by variance values below 10%. In contrast, droplets generated with 7H9 media is different from PBS in several respects (Figure 5.25 B). Droplet stability was maintained in most conditions, with CV values below 10% indicating good monodispersity. However, incubation in static and anaerobic conditions led to increased CV values (13.85% and 12.67% at 48 hours, respectively), suggesting potential coalescence or Ostwald ripening under these conditions. This highlights the importance of considering incubation environment in droplet-based assays. Despite this, these results are an improvement from droplets created with 5% Pico-Surf® whereby droplets had coalesced within 24 hours with 7H9 media as shown in chapter 3. In addition, droplets generated with 5% AM50-06 and MCM media displayed excelled function as a droplet stabiliser with mycobacterial bioreactors (Figure 5.23 C), also improving on Pico-Surf® as a surfactant. Together, these results show promising utility for the lead candidate AM50-06 for producing droplet-based AST for bacterial species, including mycobacteria.

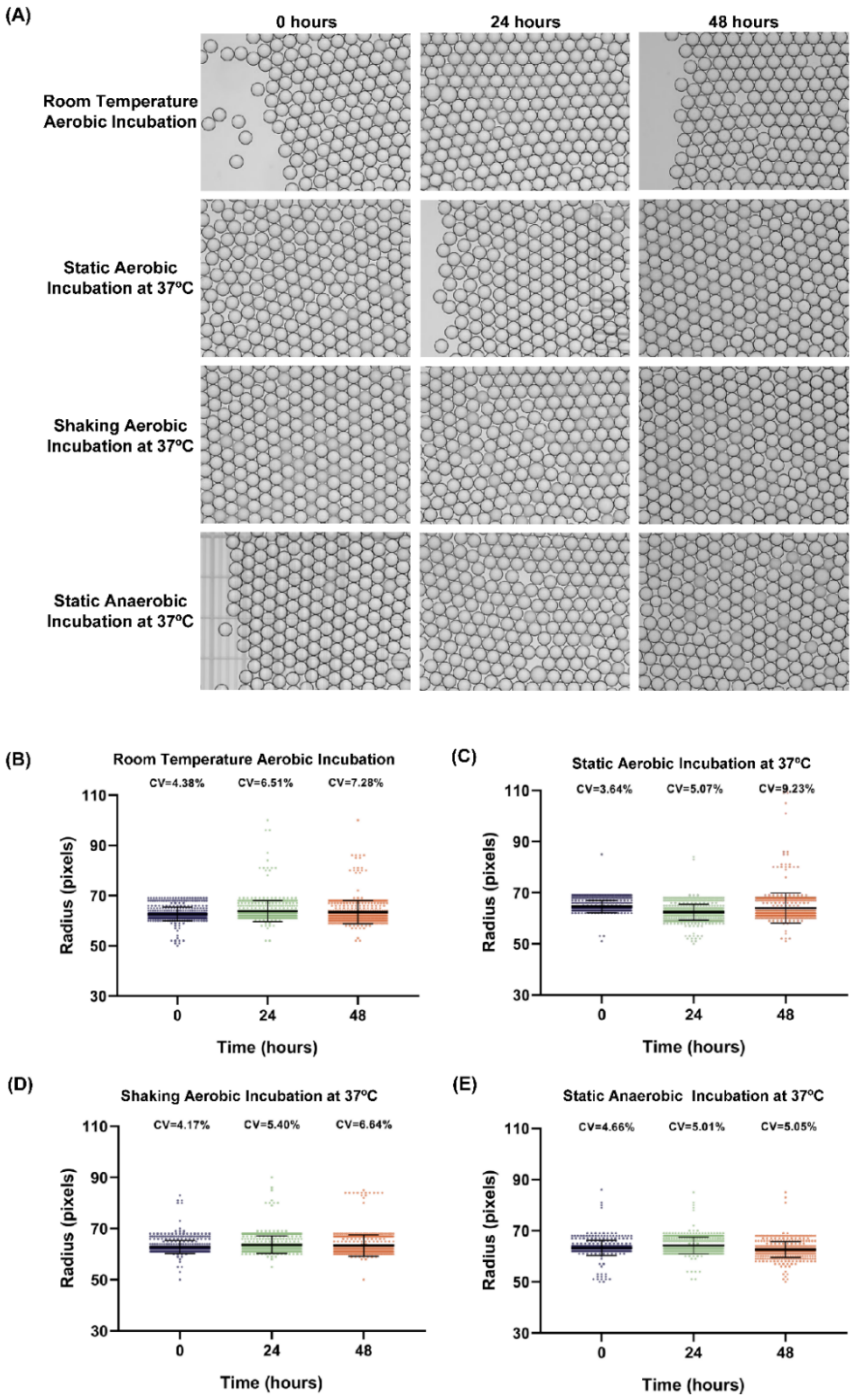

Figure 5.24. Droplet stability over 48 hours for droplets generated with 5% AM50-06 and PBS media. Each scatter plot illustrates the variance in droplet size over time of an emulsion in different incubation conditions. **(A)** Images of droplets in different incubation conditions at 0, 24, and 48 hours. **(B)** Droplets incubated at room temperature aerobically for 48 hours. Mean = 63 pixels, SD= 3 pixels, CV= 4.38%, n= 508 droplets at 0 hours. Mean = 64 pixels, SD= 4 pixels, CV= 6.51%, n= 568 droplets at 24 hours. Mean = 64 pixels, SD= 5 pixels, CV= 7.28%, n= 535 droplets at 48 hours. **(C)** Droplets incubated at 37ºC in the static incubator aerobically for 48 hours. Mean = 65 pixels, SD= 2 pixels, CV= 3.64%, n= 554 droplets at 0 hours. Mean = 62 pixels, SD= 3 pixels, CV= 5.07%, n= 612 droplets at 24 hours. Mean = 64 pixels, SD= 6 pixels, CV= 9.23%, n= 592 droplets at 48 hours. **(D)** Droplets incubated at 37ºC in the shaking incubator aerobically for 48 hours. Mean = 63 pixels, SD= 3 pixels, CV= 4.17%, n= 595 droplets at 0 hours. Mean = 64 pixels, SD= 3 pixels, CV= 5.40%, n= 581 droplets at 24 hours. Mean = 63 pixels, SD= 4 pixels, CV= 6.66%, n= 540 droplets at 48 hours. **(E)** Droplets incubated at 37ºC in the static incubator anaerobically for 48 hours. Mean = 63 pixels, SD= 3 pixels, CV= 4.66%, n= 537 droplets at 0 hours. Mean = 64 pixels, SD= 3 pixels, CV= 5.01%, n= 550 droplets at 24 hours. Mean = 63 pixels, SD= 3 pixels, CV= 5.05%, n= 509 droplets at 48 hours. Data for each time point is from three representative images of different fields of view of the emulsion. Each data point represents the radius (pixels) of an individual droplet in an image. Dotted line is the mean and error bars show the standard deviation of droplet size.

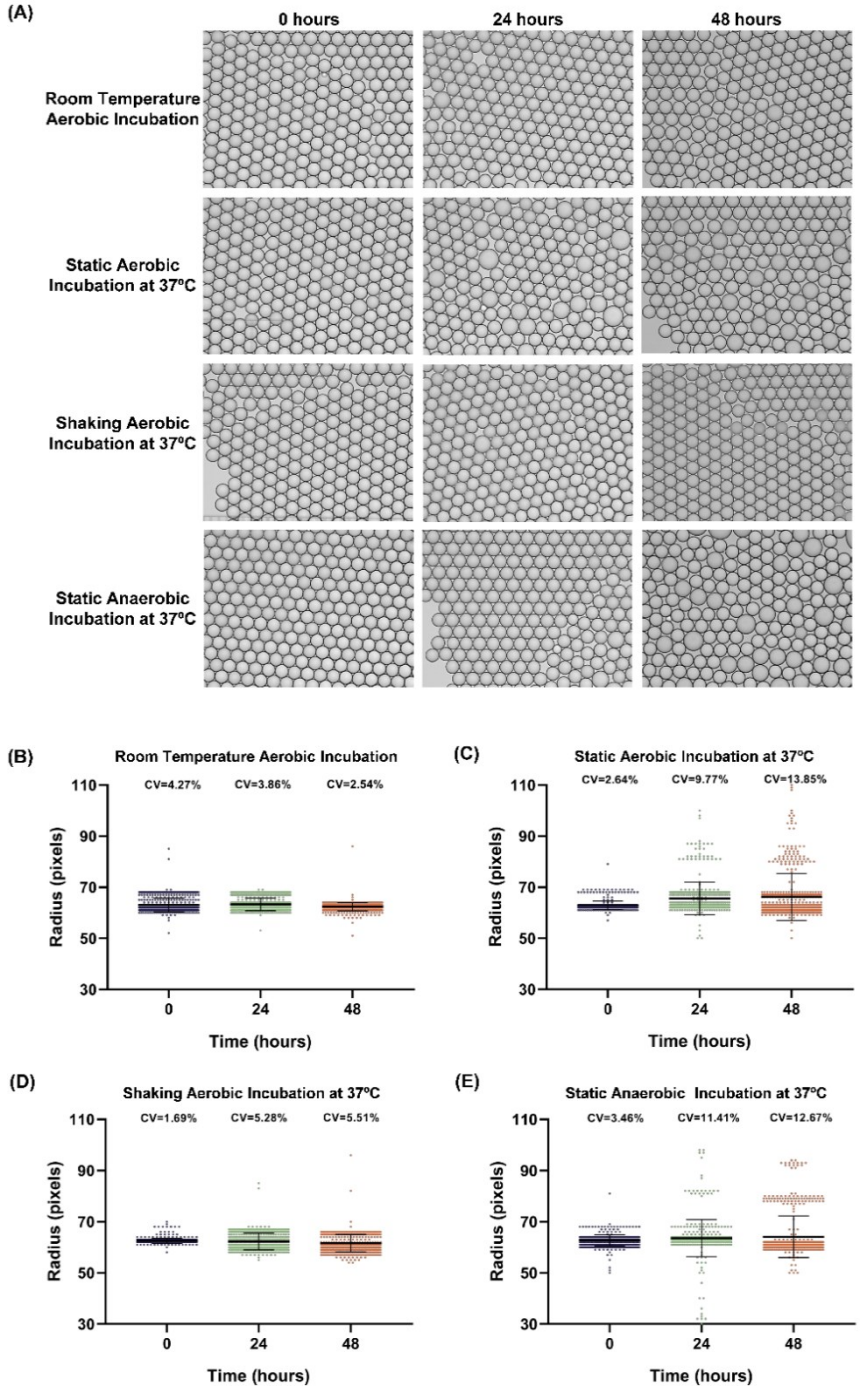

Figure 5.25. Droplet stability over 48 hours for droplets generated with 5% AM50-06 and 7H9 media. Each scatter plot illustrates the variance in droplet size over time of an emulsion in different incubation conditions. **(A)** Images of droplets in different incubation conditions at 0, 24, and 48 hours. **(B)** Droplets incubated at room temperature aerobically for 48 hours. Mean = 63 pixels, SD= 3 pixels, CV= 4.27%, n= 603 droplets at 0 hours. Mean = 63 pixels, SD= 2 pixels, CV= 3.86%, n= 639 droplets at 24 hours. Mean = 62 pixels, SD= 2 pixels, CV= 2.54%, n= 607 droplets at 48 hours. **(C)** Droplets incubated at 37ºC in the static incubator aerobically for 48 hours. Mean = 62 pixels, SD= 2 pixels, CV= 2.64%, n= 605 droplets at 0 hours. Mean = 66 pixels, SD= 6 pixels, CV= 9.77%, n= 432 droplets at 24 hours. Mean = 66 pixels, SD= 9 pixels, CV= 13.85%, n= 531 droplets at 48 hours. **(D)** Droplets incubated at 37ºC in the shaking incubator aerobically for 48 hours. Mean = 63 pixels, SD= 1 pixels, CV= 1.69%, n= 558 droplets at 0 hours. Mean = 62 pixels, SD= 3 pixels, CV= 5.28%, n= 674 droplets at 24 hours. Mean = 62 pixels, SD= 3 pixels, CV= 5.51%, n= 661 droplets at 48 hours. **(E)** Droplets incubated at 37ºC in the static incubator anaerobically for 48 hours. Mean = 62 pixels, SD= 2 pixels, CV= 3.46%, n= 620 droplets at 0 hours. Mean = 64 pixels, SD= 7 pixels, CV= 11.41%, n= 565 droplets at 24 hours. Mean = 64 pixels, SD= 8 pixels, CV= 12.67%, n= 510 droplets at 48 hours. Data for each time point is from three representative images of different fields of view of the emulsion. Each data point represents the radius (pixels) of an individual droplet in an image. Dotted line is the mean and error bars show the standard deviation of droplet size.

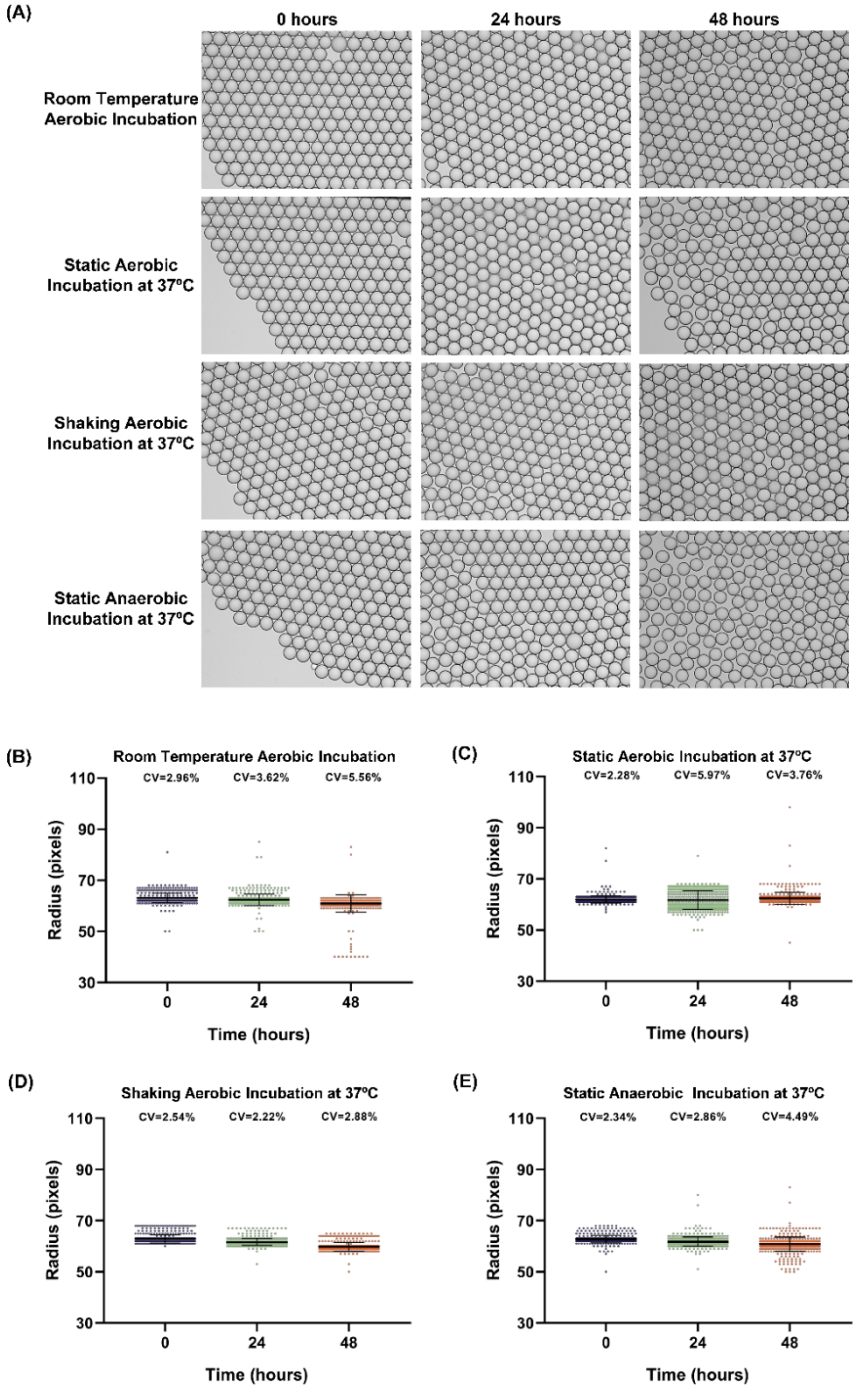

Figure 5.26. Droplet stability over 48 hours for droplets generated with 5% AM50-06 and MCM media. Each scatter plot illustrates the variance in droplet size over time of an emulsion in different incubation conditions. **(A)** Images of droplets in different incubation conditions at 0, 24, and 48 hours. **(B)** Droplets incubated at room temperature aerobically for 48 hours. Mean = 63 pixels, SD= 2 pixels, CV= 2.96%, n= 612 droplets at 0 hours. Mean = 62 pixels, SD= 2 pixels, CV= 3.62%, n= 610 droplets at 24 hours. Mean = 61 pixels, SD= 3 pixels, CV= 5.56%, n= 626 droplets at 48 hours. **(C)** Droplets incubated at 37ºC in the static incubator aerobically for 48 hours. Mean = 62 pixels, SD= 1 pixels, CV= 2.28%, n= 610 droplets at 0 hours. Mean = 62 pixels, SD= 4 pixels, CV= 5.97%, n= 710 droplets at 24 hours. Mean = 62 pixels, SD= 2 pixels, CV= 3.76%, n= 607 droplets at 48 hours. **(D)** Droplets incubated at 37ºC in the shaking incubator aerobically for 48 hours. Mean = 63 pixels, SD= 2 pixels, CV= 2.54%, n= 611 droplets at 0 hours. Mean = 62 pixels, SD= 1 pixels, CV= 2.22%, n= 628 droplets at 24 hours. Mean = 60 pixels, SD= 2 pixels, CV= 2.88%, n= 609 droplets at 48 hours. **(E)** Droplets incubated at 37ºC in the static incubator anaerobically for 48 hours. Mean = 63 pixels, SD= 1 pixels, CV= 2.34%, n= 555 droplets at 0 hours. Mean = 62 pixels, SD= 2 pixels, CV= 2.86%, n= 591 droplets at 24 hours. Mean = 61 pixels, SD= 3 pixels, CV= 4.49%, n= 625 droplets at 48 hours. Data for each time point is from three representative images of different fields of view of the emulsion. Each data point represents the radius (pixels) of an individual droplet in an image. Dotted line is the mean and error bars show the standard deviation of droplet size.

5. 4 Discussion

For a droplet-based AST, the concentration of antibiotic in each droplet bioreactor is required to maintain within the droplet. Unfortunately, small molecules can pass through the surfactant layer into the oil phase of the emulsion or into neighbouring droplets. In an AST assay, these inaccuracies in analytic concentrations will lead to non-reproducible results. A new novel droplet generating surfactant is essential for designing droplet-based AST and other drug discovery applications. An improved surfactant which is suitable for small molecule retention could specifically benefit AST assays. The concentration of the antibiotic inside the droplet would remain consistent over time, leading to more accurate and reproducible results, and giving better insight into bacterial response and drug efficacy. By reducing antibiotic leakage, higher-throughput testing will be enabled by minimising cross-contamination. Many droplets can be processed in parallel with confidence that each represents an independent assay. In addition, surfactants that retain a wider range of small molecules—whether hydrophilic or hydrophobic—expand the versatility of a droplet-based AST. This allows the assay to test not just standard antibiotics, but a broader array of drug candidates, including novel molecules with different physicochemical properties. The aim of this study was achieved through synthesising and characterising PAMAM demdrimers, coupling them to functional groups, testing their toxicity, and finally investigating their ability to prevent resazurin leakage from their droplets.

Previous research has highlighted the significance of PAMAM dendrimers in their capacity to encapsulate or attach to hydrophobic molecules. The hypothesis of this chapter was that a dendimer-based micell could encapsulate hydrophobic antibiotics in its structural cavities and prevent them from escaping each droplet. PAMAM dendrimers were synthesised using the divergent method to generate a full generation dendrimer (G.1). After purity was checked using characterisation techniques such as NRM, IR, and mass spectrometry, the dendrimer was coupled to two functional groups (disclosed by Sphere Fluidics Ltd) to create two new test compounds. These two test compounds (AM50-06 and AM50-08) were compared with commercial products Pico-Surf® and FluoSurf™ for toxicity, leakage into the oil phase, and leakage into neighbouring droplets.

When assessed for toxicity against different species of bacteria, AM50-06 and AM50-08 displayed variable results. A summary of the toxicity results is presented in the below table (Table 5.2). Both novel surfactants did not show any toxicity towards *P. aeruginosa* or *S. aureus*. AM50-06 showed toxicity for the smooth and rough variant of *M. abscessus*, however AM50-08 only showed toxicity to the rough variant of M. abscessus. The predominant toxicity to mycobacterial species may be due to their negatively charged cell wall and high lipid content. The cationic nature of the PAMAM dendrimer's terminal amine groups could potentially interact

more strongly with the mycobacterial cell wall, disrupting membrane integrity. As stated in the literature, negatively charged bacteria intereact with cationic dendrimers, causing apoptosis, necrosis and/or autophagy, resulting in cell lysis and death (Janaszewska et al., 2019, Kheraldine et al., 2021). As the end functional groups of each surfactant are unknown, correlating the charge of bacterial membrane to the charge of the dendrimer cannot be concluded. The methodology of measuring toxicity in this experiment may be a limitation to acquire accurate results. No conclusion can be drawn regarding cell viability due to the optical density measurement. Future studies should use CFU/ mL to quantify toxicity to bacteria to surfactants. In the case of mycobacteria, as the cells are extremely hydrophobic, they tend to clump together and this may cause inaccuracies in bacterial growth as speculated by the increased error bars. *M. abscessus* bacteria with rough morphologies are more hydrophobic and may be the reason for poorer toxicity results. In addition, the differences in toxicity between Gram-positive, Gram-negative, and acid-fast bacteria could be attributed to the differences in incubation time. As mycobacteria are slow growing, they were incubated for 96 hours and this could have caused an inhibitory effect compared to 24 hours. Future work should also include testing with a decrease in surfactant concentration.

Table 5.2. Summary of surfactant toxicity. Listed results which surfactant was toxic to *P. aeruginosa, S. aureus, M. abscessus* (smooth), and *M. abscessus* (rough).

	P. aeruginosa	***S. aureus***	***M. abscessus* (smooth)**	***M. abscessus* (rough)**
Pico-Surf®	Non-toxic	Non-toxic	Non-toxic	Toxic
FluoSurf™	Non-toxic	Non-toxic	Toxic	Toxic
AM50-06	Non-toxic	Non-toxic	Toxic	Toxic
AM50-08	Non-toxic	Non-toxic	Non-toxic	Toxic

The newly synthesised surfactants showed promising results at reducing resazurin leakage from droplets. Resazurin underwent a colour change as it was reduced into the oil phase, and this reduction could be quantified using a standard curve of resazurin and absorbance measurements. This was a rapid evaluation of leakage using a bulk emulsion. When developing these studies, the amount of resazurin leakage should be evaluated with an emulsion of monodisperse droplets generated by the picodroplet technology, as the literature states that bulk emulsions cause more small molecule leakage than monodisperse droplets.

Next, when assessing if AM50-06 or AM50-08 would reduce resazurin leakage from droplets into neighbouring droplets, compared to Pico-Surf®, an assay was developed and validated. The fluorescent image based technique was adapted from previous droplet image analysis pipelines. Not only was the effect of a dendrimer-based surfactant visually observed, but results were quantified by image analysis software CellProfiler™. Interestingly, AM50-06 proved to be efficient in minimising leakage to the oil-phase and between droplets, unlike Pico-Surf®. However, AM50-08 only prevented leakage into the oil phase (Table 5.3).To conclude,

AM50-06 is the lead surfactant for reducing the time of small molecule leakage compared with Pico-Surf®. The specific (undisclosed) structural features of AM50-06 may contribute to its superior performance in reducing inter-droplet leakage.

Table 5.3. Summary of both AM50-06 and AM50-08's ability to reduce resazurin leakage compared to Pico-Surf®.

	Reduced Leakage into the Oil Phase Compared to Pico-Surf®	Reduced Time of Leakage into Neighbouring Droplets Compared to Pico-Surf®
AM50-06	Yes	Yes
AM50-08	Yes	No

Our results with AM50-06 show improved small molecule retention compared to conventional surfactants, aligning with the findings of Chowdhury et al. (2019), who reported that dendronized fluorosurfactants reduced inter-droplet transfer of small molecules. Chowdhury et al. demonstrated high droplet stability in PCR thermal cycling and reduced inter-droplet transfer of a water-soluble fluorescent dye and doxycycline (Chowdhury et al., 2019). Our work extends these findings to PAMAM dendrimer-based surfactants, showing their potential for reducing leakage in droplet-based assays.

The improved retention of resazurin by AM50-06 can be understood in the context of the work by Gruner et al. (2016), who elucidated the dynamics of molecular transport in emulsions. They identified key parameters influencing leakage rates, including surfactant chemistry (Gruner et al., 2016). Our dendrimer-based surfactants likely create a more effective barrier at the oil-water interface, consistent with Gruner's findings on the importance of surfactant properties in controlling molecular retention.

Our approach of using fluorescence microscopy to quantify inter-droplet leakage builds upon the work of Etienne et al. (2018), who studied cross-talk between emulsion drops. While they focused on hydrophilic reagents, our study extends this to the fluorescent dye resazurin (Etienne et al., 2018). Furthermore, recent work by Zinchenko et al. (2023) using flow cytometry for leakage quantification offers a complementary high-throughput approach (Zinchenko et al., 2023). Future work could combine our dendrimer-based surfactants with their flow cytometry method to enable rapid screening of surfactant performance.

Notably, droplet stability showed improvement when assessed with AM50-06 and mycobacterial culture media under incubation conditions, as compared to the assessment conducted with Pico-Surf® in chapter 3. This positive outcome suggests that by making further

structural optimisations, AM50-06 could be utilised in microbiology drug discovery applications involving mycobacteria.

Our finding that AM50-06 improves droplet stability in mycobacterial culture media advances the work of Skhiri et al. (2012), who studied the dynamics of molecular transport by surfactants in emulsions. Skhiri et al. demonstrated that the exchange rate of small molecules between droplets depends on their hydrophobicity. Our dendrimer-based surfactant appears to effectively reduce this exchange in complex biological media, representing a significant advance for droplet-based bacterial assays.

Additional characterisation methods of the droplet-based surfactants could be included in the future roadmap of optimising an improved surfactant. For instance, interfacial tension and surface tension measurements could be used such as the pendant drop method and the critical micelle concentration. Other techniques such as rhelogy or microscopy could demonstrate the surfactants viscosity and size, shape, and distribution respectively. Zeta potential measurements could also be used to provide information about the surface charge of the droplets, which is influenced by the surfactant used. This helps in understanding the stability of the emulsion, as a higher absolute zeta potential typically indicates better electrostatic stabilisation. These methods would provide different pieces of information about droplet-based surfactants, contributing to a comprehensive understanding of their properties and behaviors in various applications.

To further optimise the reducing effects of dendrimer-based surfactants, further generations should be synthesised such as (G1-G4) as this increase in structure complexity will increase further internal cavities and binding sites to capture hydrophobic drugs (Choudhary et al., 2017). However, a fine balance needs to be met when increasing the dendrimers generations as to not induce toxicity as when dendrimer generations increase, toxicity increases (Gonzalo et al., 2015).

A limitation of this study was that resazurin was the only small molecule tested for leakage. Other fluorescent dyes, such as propidium iodide, methylene blue, ethidium bromide, congo red, and crystal violet, could be additional models for leakage as they would present different chemical structures and possible different binding mechanisms to dendrimers. This would provide better understanding of how different physiochemical properise of small molecules could contribute in inducing inter-droplet leakage. As these dyes are colourful, the rapid assessment of leaking into the oil phase will be suitable. However, a specific fluorescent microscope with the varying spectrum of wavelengths from these dyes would be needed to assess droplet-droplet leakage.

Alternatively, a more specific test using hydrophobic fluorescent antimicrobials, such as rifampicin, would create a chemically relevant assay. As leakage is dependant on how hydrophobic a moleule is (Skhiri et al., 2012), it would be suitable to test hydrophobic antibitics which are clinically relevant. For instance, the logP of rifampicin is approximately 3.7-4.0, and thus would currently be imposbe to demonstrate a suseptibility test which was accurate in droplets. By testing current front line drugs in this assay, the validation of a surfactant for a droplet-based AST will become more robust.

As this approch for measuring crosstalk was done by flurescence microscoply, only a small range or analytes can be assessed which fluoresce. A label-free approach wherby crosstalk can be measured could be demonstrated by mass spectrometry in the futue. A study showing utility of droplet microfluidics coupled to electrospray ionization mass spectrometry has been demonstrated to measure leakage of a broad range of analytes (Payne et al., 2023). Leakage is quantified by the amount of analyte loss from the analyte droplets and gain of analytes into the “empty” droplets. By using this approach in the future, a range of clinically relevaant antibiotics such as non-fluresent ones could be studies for their suitability in a droplet-based AST.

Surfactants that reduce small molecule leakage can have significant positive impacts across a wide range of fields. A new surfactant could enhance drug encapsulation and controlled release in drug delivery systems. Industries which would benefit from this novel surfactant are pharmaceuticals, cosmetic, food and beverage, biomedical, and environmetal. A novels surfanctant which has improve on small molecule retention could facilitate more controlled and sustained release of drugs, enhancing therapeutic efficacy of drug delivery and reducing side effects. In cosmetics, preventing leakage of active ingredients, such as vitamins, peptides, or other small molecules, ensures that these ingredients remain effective until application, enhancing the product's efficacy. An example of an improved surfactant in the food and beverage industry is to aid the emulsification of oils and fats which can lead to more stable food products. While surfactants with cabibilities to reduce small molecule leakage can offer numerous benefits, their use must be carefully evaluated for toxicity and environmental impact.

Chapter 6.

General Discussion

6.1 General Discussion and Conclusions

Antimicrobial resistance (AMR) is an increasing problem in human health. One of the major efforts to reduce AMR is to innovate new technologies to advance the antimicrobial drug discovery process. The focus of recent scientific research in creating innovative technologies for reducing the burden of AMR has been improving the issues associated with antibiotic susceptibility testing (AST) for drug discovery purposes. One of the strategies used to overcome challenges such as low-throughput, cell heterogeneity, lengthy culturing times, and poor clinical translation is to apply droplet fluidics. Droplet fluidics allows for parallel experiments, reduces costs for reagents and consumables, encapsulates bacteria at the single-cell level, enables real-time monitoring, facilitates advanced data processing, and creates controlled microenvironments. Designing a droplet-based AST is a complex matter involving multidisciplinary efforts. The aims of this thesis were to test a novel metal-based compound with the traditional AST method, and then to optimise aspects in the design and validation of a droplet platform for AST as a whole. Several droplet-based AST were previously designed but do not address factors such as stabilising droplets with various bacterial culture medias, optimising the starting concentration of bacteria and droplet size for defining assay endpoints, and preventing antibiotic leakage from each droplet. In this study, physical, chemical, and biological techniques were used to address these challenges.

6.1.1 Chapter 2

In chapter 2, a set of metal-based novel compounds were investigated for their antimicrobial activity against a range of Gram-negative, Gram-positive, and acid-fast bacteria. These compounds were repurposed from failed anti-cancer compounds. In recent years, the exploration of metal-based compounds has become increasingly attractive due to their chemical variability. Investigations comprised two different standard antibiotic susceptibility tests; broth microdilution and resazurin reduction assays. The metal compounds tested were ruthenium, copper, or osmium-based structures. The lead compounds which showed broad spectrum activity were MD7 and MD56, which are both ruthenium-based complexes. Li, Collins, and Keene (2015) found that ruthenium complexes are effective antimicrobial agents, which align with previous observations.(Li et al., 2015). Unlike other studies, this investigation tested metal-based compounds against a panel of highly resistant pathogens including, “ESKAPE” pathogens and mycobacterial species, demonstrating a broad spectrum activity which encouragingly promotes them for future clinical use. In addition, this study compared results from two different standard AST; broth microdilution and resazurin reduction assay, which yielded variable results, demonstrating the poor utility of using standard AST into clinical translation in the drug discovery process.

6.1.2 Chapter 3

Chapter 3 utilised and tested Sphere Fluidics picodroplet technology to create droplets of desired volumes with low variance using an image-based closed-loop feedback mechanism. The picodroplet outperformed other droplet generating devices. Droplets were generated with high monodispersity and stability (CV<10%). Examination of droplet robustness using microbiology culturing media was never tested in previous literature. The study concluded that the droplet stabilising surfactant PicoSurf® was not suitable for generating droplets with mycobacterial species, which was likely due to the extra additives in the media compared to PBS. Poor droplet stability will have an impact on cell-based assays, and a new surfactant is required to address this issue.

6.1.3 Chapter 4

To evaluate and validate the picodroplet technologies performance of the encapsulation of bacteria in monodisperse picodroplets, in chapter 4, droplets were generated containing MRSA and monitored for droplet monodispersity and stability, bacteria viability, proliferation, and bacteria antibiotic susceptibility. This study successfully demonstrated the encapsulation of MRSA in monodisperse picodroplets using picodroplet technology. Key findings include: (1) successful generation of droplets with high monodispersity containing single or multiple MRSA cells, (2) maintenance of bacterial viability and proliferation within droplets, (3) observation of droplet shrinkage during bacterial growth, and (4) detection of differences in antibiotic susceptibility between the droplet and bulk cultures. These finding highlight the importance of considering the context and methodology when interpreting MIC results obtained from different assay formats.

6.1.4 Chapter 5

Finaly, in chapter 5, a dendrimer-based micelle was synthesised with the hypothesis that it could encapsulate hydrophobic antibiotics in its structural cavities and prevent them from escaping each droplet. Previous research has highlighted the significance of PAMAM dendrimers in their capacity to encapsulate or attach to hydrophobic molecules (Choudhary et al., 2017). This current investigation found that the newly synthesised surfactant AM50-06 proved to be efficient in minimising leakage to the oil-phase and between droplets in an emulsion. In addition, validation of AM50-06 as a surfactant for generating droplets was displayed by testing its toxicity against Gram-positive, Gram-negative, and acid fast bacteria, as well as its ability to form monodisperse and stable droplet with mycobacterial culture media during incubation conditions. The dendrimer showed no toxicity towards a Gram-positive and a Gram-negative bacterium, however, did reduce cell growth of mycobacterial species. Additionally, droplet stability showed improvement when assessed with AM50-06 and mycobacterial culture media under incubation conditions, as compared to the assessment conducted with PicoSurf® in chapter 3. This positive outcome suggests that by making further

structural optimisations, AM50-06 could be utilised in microbiology drug discovery applications by generating highly monodisperse and stable droplets and reducing antibiotic leakage from droplets.

6.2 Future Work

In the immediate future, there are several experimental studies that would be fascinating for further exploring and expanding this work. First, the mechanism of action, the frequency of resistance, and additional cytotoxicity testing should be performed on the lead metal-based compounds before moving onto *in vivo* studies. This will develop their potential as lead candidates in the antimicrobial drug discovery pipeline.

Next, collaborative efforts should further enhance the picodroplet technology for end-user applications, including biosafety concerns and compacting the equipment into a fully automated bench-top device. Droplet monodispersity and stability studies using the picodroplet technology should be performed with additional controls of mycobacterial media to determine the cause of destabilisation. Moreover, longer incubation times should be observed to apply a droplet-based assay to slow-growing microorganisms.

The results from this thesis promotes utility of establishing droplet-based assays using picodroplet technology. Moving forward, efforts should concentrate on the downstream analysis of bacteria in droplets and how to accurately quantify antibiotic susceptibility with high sensitivity and specificity. If the downstream analysis of endpoint data is automated, that would be advantageous. Electrophysiology of bacterial cell walls as a biomarker of susceptibility are an exciting advancement and an alternative approach to phenotypic evaluation. Recently, studies have shown an approach for rapid detection of proliferative bacteria at the single-cell level by monitoring membrane-potential dynamics in bacterial cell walls (Stratford et al., 2019). In addition, nanomotion technology to quantify bacterial vibrations due to their metabolic activity has been employed as it does not reply on assessing bacterial growth curves (Sturm et al., 2024). Combining these techniques with droplet microfluidics could enable rapid AST at the single cell level and aid in the development of minimising the time to result.

Finally, optimising the structure of the lead surfactant AM50-06 would be a fruitful area to explore in the future. By further synthesising the generations of the PAMAM dendrimer using the divergent method, and thus increasing hydrophobic drug encapsulation/coagulation, an improved product could minimise small molecule leakage. However, with additional generations, the biocompatibility is disrupted due to an increase in toxicity. Therefore, careful considerations are required to find a balance between higher structural generations and toxicity.

In the future, the newly designed surfactant which prevents antibiotic drug leakage could generate droplets encapsulating mycobacteria and creating a 3D microenvironment for modelling infection conditions *in vitro*. The non-replicating persistent state of *M. tuberculosis* could be experimentally modelled in droplets by modifying the droplet environment, including nutrient deprivation and hypoxia. Eventually, the complexity of this new *in vitro* assay could be developed to include co-encapsulation of immune cells to establish the TB granuloma (as illustrated in Figure 6.1). The enhanced physiological relevance could yield precise clinical outcomes of antibiotic impact on tuberculosis infection.

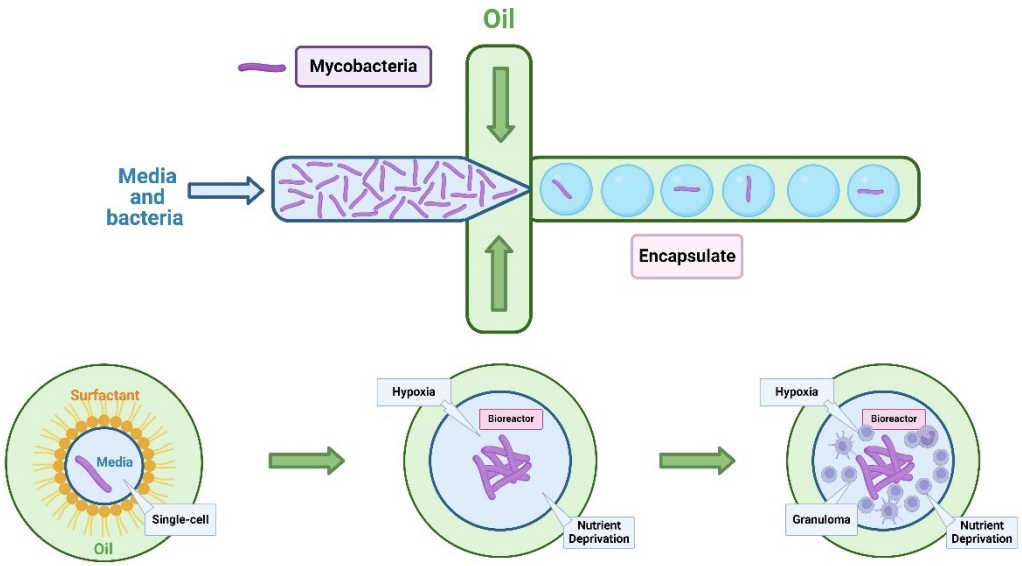

Figure 6.1. Schematic of proposed *in vitro* antibiotic susceptibility testing of non-replicating persistent tuberculosis in picolitre droplets. Individual mycobacterial cells are encapsulated at the single-cell level and the droplet microenvironment is manipulated to induce persistence. Additionally, co-encapsulation of additional immune cells could promote granuloma formation in the droplet bioreactor. Green is the oil phase and blue is the aqueous phase. Image created on Biorender.com.

Expanding on this idea, when combating encapsulated bacteria with antibiotics, there are two conceivable ways to enhance antibiotic incorporation into the assay. These are a dual aqueous system or a pico-injection system. In a dual aqueous phase system, droplets are generated by introducing two immiscible aqueous solutions into a microfluidic device. These phases typically comprise one with bacteria and culture media, and the other containing antibiotic. The phases of the thesis mix at the junction where droplets are generated. Pico-injection is a technique used to inject minimal (picolitre-scale) volumes of liquid into preformed droplets as they flow through a microfluidic channel. This allows for the precise addition of reagents, cells, or other components to the droplets after they have been generated. In the case of developing an AST for non-replicating persistent *M. tuberculosis*, the bacteria are required to induce into a non-replicative state before antibiotic challenge. There, the pico-injection method would be more suitable for this model. Nevertheless, both methods of antibiotic addition into droplet would require development of the current picodroplet technology.

6.3 The Impact of a Droplet-Based AST

A droplet-based AST has the potential to drastically impact various aspects of clinical microbiology, healthcare, and public health. The potential commercialisation of an automated droplet-based AST adoption could lead to more effective management of bacterial infections, ultimately benefiting both individual patients and public health at large. As well as picodroplet technology implementation at the basic research level to address innovation in antimicrobial drug discovery, the technology could be applied clinically. Unlike phenotypic antibiotic susceptibility tests, the technology could enable healthcare industries to make quicker and more accurate treatment decisions by reducing decision-making time and providing precise answers. Accurate and timely susceptibility results decrease reliance on broad-spectrum antibiotics, thereby reducing the occurrence of adverse drug reactions. Droplet-based AST can result in faster recovery times and shorter hospital stays, ultimately lowering healthcare costs. The application of a Droplet-based AST would ultimately contribute to a precision medicine-based healthcare system whereby the right patient receives the right antibiotic at the right time.

Furthermore, droplet-based AST can have a significant impact on wastewater management, particularly in the context of monitoring and mitigating the spread of antibiotic resistance in the environment. A literature review by Singh et al. emphasises that advanced technologies, including nanotechnologies, will have a future role in wastewater management (Singh et al., 2023). A prior review article highlighted future trends and prospects for the development of droplet microfluidics in wastewater-based epidemiology (Ou et al., 2021). In addition, a key study demonstrating potential of a droplet-based assay in wastewater management showed the detection of E.coli in droplets from drinking water contaminated with faeces. The process of bacterial detection in drinking water was reduces to 8 hours, compared to 2-4 days of the traditional culturing techniques (Golberg et al., 2014). By incorporating droplet-based AST, a robust approach is introduced in this field which enables surveillance of AMR in wastewater, assessment of wastewater treatment efficacy, support for regulatory compliance and policy development, and protection of public health. Wastewater often contains antibiotic-resistant bacteria due to the discharge of human and animal waste. Droplet-based AST can swiftly and accurately identify antibiotic resistance in these bacterial populations, providing crucial data on the prevalence of resistance in wastewater. The high-throughput and rapid nature of droplet-based AST allows for real-time or near-real-time monitoring of antibiotic resistance trends in wastewater treatment plants. This can help identify emerging resistance patterns and hotspots. Policymakers can utilise the generated data to understand the current status of antibiotic resistance in wastewater and develop regulations and guidelines to curb its environmental transmission.

Another interesting field of application of a droplet-based AST is the ability to impact biosafety and defence against pathogens, particularly in the context of bioterrorism, public health

preparedness, and the safe handling of dangerous microorganisms. The technology has the potential to impact these areas through (1) swift identification and response to biological threats, (2) enhancing public health readiness, and (3) aiding in bio surveillance and intelligence. A review article highlights the application of microfluidics for detection of biological warfare agents (Mondal et al., 2020). In the event of a bioterrorism attack or accidental release of a pathogen, droplet-based AST allows for the rapid determination of the antibiotic susceptibility profile of the pathogen. This enables authorities to identify effective treatments and promptly implement them, reducing the potential impact of the biological threat. The ability to rapidly determine the antibiotic susceptibility of pathogens during a public health emergency is crucial for effective response. Critical data obtained from droplet-based AST can guide public health decisions, including the stockpiling of effective antibiotics and the allocation of medical resources.

In conclusion, the optimisation work in this thesis contributing to the development of a droplet-based AST will impact various aspects of clinical microbiology, healthcare, and public health in the content of AMR. The studies shown in this thesis represent an expansion of our understanding of droplet fluidic dynamics and bacterial behaviour within droplets. This knowledge will be beneficial in informing future work on developing a fully automated droplet-based AST platform.

Chapter 7.

References

ABATE, A. R., ROMANOWSKY, M. B., AGRESTI, J. J. & WEITZ, D. A. 2009. Valve-based flow focusing for drop formation. *Applied Physics Letters,* 94**,** 023503.

ABBASI, E., AVAL, S. F., AKBARZADEH, A., MILANI, M., NASRABADI, H. T., JOO, S. W., HANIFEHPOUR, Y., NEJATI-KOSHKI, K. & PASHAEI-ASL, R. 2014. Dendrimers: synthesis, applications, and properties.

ABDEL-WAHAB, A. A., ATAYA, S. & SILBERSCHMIDT, V. V. 2017. Temperature-dependent mechanical behaviour of PMMA: Experimental analysis and modelling. *Polymer Testing,* 58**,** 86-95.

ABOU-HASSAN, A., SANDRE, O. & CABUIL, V. 2010. Microfluidics in Inorganic Chemistry. *Angewandte Chemie International Edition,* 49**,** 6268-6286.

AHMED, S. K., HUSSEIN, S., QURBANI, K., IBRAHIM, R. H., FAREEQ, A., MAHMOOD, K. A. & MOHAMED, M. G. 2024. Antimicrobial resistance: Impacts, challenges, and future prospects. *Journal of Medicine, Surgery, and Public Health,* 2**,** 100081.

ALBERTAZZI, L., MICKLER, F. M., PAVAN, G. M., SALOMONE, F., BARDI, G., PANNIELLO, M., AMIR, E., KANG, T., KILLOPS, K. L., BRÄUCHLE, C., AMIR, R. J. & HAWKER, C. J. 2012. Enhanced bioactivity of internally functionalized cationic dendrimers with PEG cores. *Biomacromolecules,* 13**,** 4089-97.

ALIBOLANDI, M., TAGHDISI, S. M., RAMEZANI, P., HOSSEINI SHAMILI, F., FARZAD, S. A., ABNOUS, K. & RAMEZANI, M. 2017. Smart AS1411-aptamer conjugated pegylated PAMAM dendrimer for the superior delivery of camptothecin to colon adenocarcinoma in vitro and in vivo. *Int J Pharm,* 519**,** 352-364.

ALTAF, M., MILLER CH FAU - BELLOWS, D. S., BELLOWS DS FAU - O'TOOLE, R. & O'TOOLE, R. 2010. Evaluation of the Mycobacterium smegmatis and BCG models for the discovery of Mycobacterium tuberculosis inhibitors.

AN, Q., LI, C., CHEN, Y., DENG, Y., YANG, T. & LUO, Y. 2020. Repurposed drug candidates for antituberculosis therapy. *European Journal of Medicinal Chemistry,* 192**,** 112175.

ANNA, S. L., BONTOUX, N. & STONE, H. A. 2003. Formation of dispersions using “flow focusing” in microchannels. *Applied Physics Letters,* 82**,** 364-366.

ANTIMICROBIAL RESISTANCE COLLABORATORS 2022. Global burden of bacterial antimicrobial resistance in 2019: a systematic analysis. *Lancet,* 399**,** 629-655.

ANTON, N. & VANDAMME, T. F. 2011. Nano-emulsions and micro-emulsions: clarifications of the critical differences. *Pharm Res,* 28**,** 978-85.

ARDRÉ, M., DOULCIER, G., BRENNER, N. & RAINEY, P. B. 2022. A leader cell triggers end of lag phase in populations of Pseudomonas fluorescens. *microLife,* 3**,** uqac022.

ARMSTRONG DEREK, T., EISEMANN, E. & PARRISH, N. 2023. A Brief Update on Mycobacterial Taxonomy, 2020 to 2022. *Journal of Clinical Microbiology,* 61**,** e00331-22.

ASHAOLU, T. J. 2021. Nanoemulsions for health, food, and cosmetics: a review. *Environmental Chemistry Letters,* 19**,** 3381-3395.

ASTETE, C. E. & SABLIOV, C. M. 2006. Synthesis and characterization of PLGA nanoparticles. *Journal of Biomaterials Science, Polymer Edition,* 17**,** 247-289.

AUGUSTSSON, P., MAGNUSSON, C., NORDIN, M., LILJA, H. & LAURELL, T. 2012. Microfluidic, label-free enrichment of prostate cancer cells in blood based on acoustophoresis. *Anal Chem,* 84**,** 7954-62.

AUGUSTUS, E. N., ALLEN, E. T., NIMIBOFA, A. & DONBEBE, W. A Review of Synthesis, Characterization and Applications of Functionalized Dendrimers. 2017.

BAI, Y., HE, X., LIU, D., PATIL, S. N., BRATTON, D., HUEBNER, A., HOLLFELDER, F., ABELL, C. & HUCK, W. T. S. 2010. A double droplet trap system for studying mass transport across a droplet-droplet interface. *Lab on a Chip,* 10**,** 1281-1285.

BAI, Y., PATIL, S. N., BOWDEN, S. D., POULTER, S., PAN, J., SALMOND, G. P., WELCH, M., HUCK, W. T. & ABELL, C. 2013. Intra-species bacterial quorum sensing studied at single cell level in a double droplet trapping system. *Int J Mol Sci,* 14**,** 10570-81.

BAKER, E. J., MOLLOY, A. & COX, J. A. G. 2023. Drug Repurposing for the Treatment of Mycobacterium abscessus Infections. *Infectious Microbes & Diseases,* 5.

BARET, J.-C. 2012. Surfactants in droplet-based microfluidics. *Lab on a Chip,* 12**,** 422-433.

BARET, J. C., MILLER, O. J., TALY, V., RYCKELYNCK, M., EL-HARRAK, A., FRENZ, L., RICK, C., SAMUELS, M. L., HUTCHISON, J. B., AGRESTI, J. J., LINK, D. R., WEITZ, D. A. & GRIFFITHS, A. D. 2009. Fluorescence-activated droplet sorting (FADS): efficient microfluidic cell sorting based on enzymatic activity. *Lab Chip,* 9**,** 1850-8.

BAROUD, C. N., GALLAIRE, F. & DANGLA, R. 2010. Dynamics of microfluidic droplets. *Lab on a Chip,* 10**,** 2032-2045.

BARTKOVA, S., VENDELIN, M., SANKA, I., PATA, P. & SCHELER, O. 2020. Droplet image analysis with user-friendly freeware CellProfiler. *Analytical Methods,* 12**,** 2287-2294.

BASOVA, E. Y. & FORET, F. 2015. Droplet microfluidics in (bio)chemical analysis. *Analyst,* 140**,** 22-38.

BATT, S. M., MINNIKIN, D. E. & BESRA, G. S. 2020. The thick waxy coat of mycobacteria, a protective layer against antibiotics and the host's immune system. *The Biochemical journal,* 477**,** 1983-2006.

BATYRSHINA, Y. R. & SCHWARTZ, Y. S. 2019. Modeling of Mycobacterium tuberculosis dormancy in bacterial cultures. *Tuberculosis,* 117**,** 7-17.

BAYOT, M. L., MIRZA, T. M. & SHARMA, S. 2024. Acid Fast Bacteria. StatPearls Publishing.

BECKER, H. & GÄRTNER, C. 2000. Polymer microfabrication methods for microfluidic analytical applications. *ELECTROPHORESIS,* 21**,** 12-26.

BECKER, H. & GÄRTNER, C. 2008. Polymer microfabrication technologies for microfluidic systems. *Analytical and Bioanalytical Chemistry,* 390**,** 89-111.

BEEBE, D. J., GLENNYS A. MENSING, A. & WALKER, G. M. 2002. Physics and Applications of Microfluidics in Biology. *Annual Review of Biomedical Engineering,* 4**,** 261-286.

BERA, B., KHAZAL, R. & SCHROËN, K. 2021. Coalescence dynamics in oil-in-water emulsions at elevated temperatures. *Scientific Reports,* 11**,** 10990.

BETANCOURT-GALINDO, R., REYES-RODRÍGUEZ, P. Y., PUENTE-URBINA, B. A., ÁVILA-ORTA, C. A., RODRÍGUEZ-FERNÁNDEZ, O. S., CADENAS-PLIEGO, G., LIRA-SALDIVAR, R. H. & GARCÍA-CERDA, L. A. J. J. O. N. 2014. Synthesis of copper nanoparticles by thermal decomposition and their antimicrobial properties. 2014**,** 10.

BIBETTE, J., MORSE, D. C., WITTEN, T. A. & WEITZ, D. A. 1992. Stability criteria for emulsions. *Phys Rev Lett,* 69**,** 2439-2442.

BIRICOVA, V. & LAZNICKOVA, A. 2009. Dendrimers: Analytical characterization and applications. *Bioorganic Chemistry,* 37**,** 185-192.

BOEDICKER, J. Q., LI, L., KLINE, T. R. & ISMAGILOV, R. F. 2008. Detecting bacteria and determining their susceptibility to antibiotics by stochastic confinement in nanoliter droplets using plug-based microfluidics. *Lab on a Chip,* 8**,** 1265-1272.

BOEDICKER, J. Q., VINCENT, M. E. & ISMAGILOV, R. F. 2009. Microfluidic confinement of single cells of bacteria in small volumes initiates high-density behavior of quorum sensing and growth and reveals its variability. *Angew Chem Int Ed Engl,* 48**,** 5908-11.

BOEHME, C. C., NABETA, P., HILLEMANN, D., NICOL, M. P., SHENAI, S., KRAPP, F., ALLEN, J., TAHIRLI, R., BLAKEMORE, R., RUSTOMJEE, R., MILOVIC, A., JONES, M., O'BRIEN, S. M., PERSING, D. H., RUESCH-GERDES, S., GOTUZZO, E., RODRIGUES, C., ALLAND, D. & PERKINS, M. D. 2010. Rapid molecular detection of tuberculosis and rifampin resistance. *N Engl J Med,* 363**,** 1005-15.

BOITARD, L., COTTINET, D., KLEINSCHMITT, C., BREMOND, N., BAUDRY, J., YVERT, G. & BIBETTE, J. 2012. Monitoring single-cell bioenergetics via the coarsening of emulsion droplets. *Proc Natl Acad Sci U S A,* 109**,** 7181-6.

BOROS, E., DYSON, P. J. & GASSER, G. 2020. Classification of Metal-Based Drugs according to Their Mechanisms of Action. *Chem,* 6**,** 41-60.

BROOK, I. 1989. Inoculum effect. *Rev Infect Dis,* 11**,** 361-8.

BROSCH, R., GORDON, S. V., GARNIER, T., EIGLMEIER, K., FRIGUI, W., VALENTI, P., DOS SANTOS, S., DUTHOY, S., LACROIX, C., GARCIA-PELAYO, C., INWALD, J. K., GOLBY, P., GARCIA, J. N., HEWINSON, R. G., BEHR, M. A., QUAIL, M. A., CHURCHER, C., BARRELL, B. G., PARKHILL, J. & COLE, S. T. 2007. Genome plasticity of BCG and impact on vaccine efficacy. *Proc Natl Acad Sci U S A,* 104**,** 5596-601.

BRÜSSOW, H. 2024. The antibiotic resistance crisis and the development of new antibiotics. *Microbial Biotechnology,* 17**,** e14510.

BURKI, T. K. 2018. The global cost of tuberculosis. *Lancet Respir Med,* 6**,** 13.
BUTLER, M. S., HENDERSON, I. R., CAPON, R. J. & BLASKOVICH, M. A. T. 2023. Antibiotics in the clinical pipeline as of December 2022. *The Journal of Antibiotics,* 76**,** 431-473.
BYRNES, S. A., PHILLIPS, E. A., HUYNH, T., WEIGL, B. H. & NICHOLS, K. P. 2018. Polydisperse emulsion digital assay to enhance time to detection and extend dynamic range in bacterial cultures enabled by a statistical framework. *Analyst,* 143**,** 2828-2836.
CABANE, B. & HÉNON, S. 2007. Liquides : solutions, dispersions, émulsions, gels.
CAMINADE, A.-M., LAURENT, R. & MAJORAL, J.-P. 2005. Characterization of dendrimers. *Advanced Drug Delivery Reviews,* 57**,** 2130-2146.
CANTWELL, C., MCGRATH, J. S., SMITH, C. A. & WHYTE, G. 2024. Image-Based Feedback of Multi-Component Microdroplets for Ultra-Monodispersed Library Preparation. *Micromachines* [Online], 15.
CARNES, E. C., LOPEZ, D. M., DONEGAN, N. P., CHEUNG, A., GRESHAM, H., TIMMINS, G. S. & BRINKER, C. J. 2010. Confinement-induced quorum sensing of individual Staphylococcus aureus bacteria. *Nat Chem Biol,* 6**,** 41-5.
CASCIOFERRO, S., CARBONE, D., PARRINO, B., PECORARO, C., GIOVANNETTI, E., CIRRINCIONE, G. & DIANA, P. 2021. Therapeutic Strategies To Counteract Antibiotic Resistance in MRSA Biofilm-Associated Infections. 16**,** 65-80.
CHANG, C. B., WILKING, J. N., KIM, S. H., SHUM, H. C. & WEITZ, D. A. 2015. Monodisperse Emulsion Drop Microenvironments for Bacterial Biofilm Growth. *Small,* 11**,** 3954-61.
CHAUHAN, A. A.-O. Dendrimers for Drug Delivery. LID - 10.3390/molecules23040938 [doi] LID - 938.
CHIRCOV, C. & GRUMEZESCU, A. M. 2019. Chapter 6 - Nanoemulsion preparation, characterization, and application in the field of biomedicine. *In:* GRUMEZESCU, A. M. (ed.) *Nanoarchitectonics in Biomedicine.* William Andrew Publishing.
CHIS, A. A., DOBREA, C., MORGOVAN, C., ARSENIU, A. M., RUS, L. L., BUTUCA, A., JUNCAN, A. M., TOTAN, M., VONICA-TINCU, A. L., CORMOS, G., MUNTEAN, A. C., MURESAN, M. L., GLIGOR, F. G. & FRUM, A. 2020. Applications and Limitations of Dendrimers in Biomedicine. 25**,** 3982.
CHOI, J., YOO, J., KIM, K. J., KIM, E. G., PARK, K. O., KIM, H., KIM, H., JUNG, H., KIM, T., CHOI, M., KIM, H. C., RYOO, S., JUNG, Y. G. & KWON, S. 2016. Rapid drug susceptibility test of Mycobacterium tuberculosis using microscopic time-lapse imaging in an agarose matrix. *Appl Microbiol Biotechnol,* 100**,** 2355-65.
CHOPRA, I. & ROBERTS, M. 2001. Tetracycline Antibiotics: Mode of Action, Applications, Molecular Biology, and Epidemiology of Bacterial Resistance. *Microbiology and Molecular Biology Reviews,* 65**,** 232-260.
CHOUDHARY, S., GUPTA, L., RANI, S., DAVE, K. & GUPTA, U. 2017. Impact of Dendrimers on Solubility of Hydrophobic Drug Molecules. *Front Pharmacol,* 8**,** 261.
CHOWDHURY, M. S., ZHENG, W., KUMARI, S., HEYMAN, J., ZHANG, X., DEY, P., WEITZ, D. A. & HAAG, R. 2019. Dendronized fluorosurfactant for highly stable water-in-fluorinated oil emulsions with minimal inter-droplet transfer of small molecules. *Nature Communications,* 10**,** 4546.
CLSI 2015. Methods for Dilution Antimicrobial Susceptibility Tests for Bacteria That Grow Aerobically. *In:* P.A, W. (ed.).
COLE, M. C. & KENIS, P. J. A. 2009. Multiplexed electrical sensor arrays in microfluidic networks. *Sensors and Actuators B: Chemical,* 136**,** 350-358.
COLLINS, D. J., ALAN, T., HELMERSON, K. & NEILD, A. 2013. Surface acoustic waves for on-demand production of picoliter droplets and particle encapsulation. *Lab on a Chip,* 13**,** 3225-3231.
COLLINS, D. J., NEILD, A., DEMELLO, A., LIU, A.-Q. & AI, Y. 2015. The Poisson distribution and beyond: methods for microfluidic droplet production and single cell encapsulation. *Lab on a Chip,* 15**,** 3439-3459.
COURTOIS, F., OLGUIN, L. F., WHYTE, G., THEBERGE, A. B., HUCK, W. T. S., HOLLFELDER, F. & ABELL, C. 2009. Controlling the Retention of Small Molecules in Emulsion Microdroplets for Use in Cell-Based Assays. *Analytical Chemistry,* 81**,** 3008-3016.
CRAMER, C., FISCHER, P. & WINDHAB, E. J. 2004. Drop formation in a co-flowing ambient fluid. *Chemical Engineering Science,* 59**,** 3045-3058.

CRAWFORD, D. F., SMITH, C. A. & WHYTE, G. 2017. Image-based closed-loop feedback for highly mono-dispersed microdroplet production. *Sci Rep,* 7**,** 10545.
CUI, J. Q., CUI, B., LIU, F. X., LIN, Y. & YAO, S. 2022. A multiplexable microfluidic injector for versatile encoding of droplets. *Sensors and Actuators B: Chemical,* 371**,** 132573.
DAI, B. & LEAL, L. G. 2008. The mechanism of surfactant effects on drop coalescence. *Physics of Fluids,* 20**,** 040802.
DALECKI, A. G., HAEILI, M., SHAH, S., SPEER, A., NIEDERWEIS, M., KUTSCH, O. & WOLSCHENDORF, F. 2015. Disulfiram and Copper Ions Kill Mycobacterium tuberculosis in a Synergistic Manner. *Antimicrob Agents Chemother,* 59**,** 4835-44.
DARBY, E. M., TRAMPARI, E., SIASAT, P., GAYA, M. S., ALAV, I., WEBBER, M. A. & BLAIR, J. M. A. 2023. Molecular mechanisms of antibiotic resistance revisited. *Nature Reviews Microbiology,* 21**,** 280-295.
DE OLIVEIRA, D. M. P., FORDE, B. M., KIDD, T. J., HARRIS, P. N. A., SCHEMBRI, M. A., BEATSON, S. A., PATERSON, D. L. & WALKER, M. J. 2020. Antimicrobial Resistance in ESKAPE Pathogens. *Clin Microbiol Rev,* 33.
DERESINSKI, S. 2009. Vancomycin Heteroresistance and Methicillin-Resistant Staphylococcus aureus. *The Journal of Infectious Diseases,* 199**,** 605-609.
DESAI, A. N. & HURTADO, R. M. 2018. Infections and outbreaks of nontuberculous mycobacteria in hospital settings. *Curr Treat Options Infect Dis,* 10**,** 169-181.
DIAZ-TANG, G., MENESES, E. M., PATEL, K., MIRKIN, S., GARCÍA-DIÉGUEZ, L., PAJON, C., BARRAZA, I., PATEL, V., GHALI, H., TRACEY, A. P., BLANAR, C. A., LOPATKIN, A. J. & SMITH, R. P. 2022. Growth productivity as a determinant of the inoculum effect for bactericidal antibiotics. 8**,** eadd0924.
DIJAMENTIUK, A., MANGAVEL, C., ELFASSY, A., MICHAUX, F., BURGAIN, J., RONDAGS, E., DELAUNAY, S., FERRIGNO, S., REVOL-JUNELLES, A.-M. & BORGES, F. 2023. Invert emulsions alleviate biotic interactions in bacterial mixed culture. *Microbial Cell Factories,* 22**,** 16.
DING, C., LIU, Y., GUO, Y., GUO, X., KANG, Q., YAN, X. & HE, Z. 2023. Precise digital bacteria enumeration and antibiotic susceptibility testing via a portable vibrating capillary-based droplet platform. *Sensors and Actuators B: Chemical,* 380**,** 133254.
DORMAN, S. E., NAHID, P., KURBATOVA, E. V., PHILLIPS, P. P. J., BRYANT, K., DOOLEY, K. E., ENGLE, M., GOLDBERG, S. V., PHAN, H. T. T., HAKIM, J., JOHNSON, J. L., LOURENS, M., MARTINSON, N. A., MUZANYI, G., NARUNSKY, K., NERETTE, S., NGUYEN, N. V., PHAM, T. H., PIERRE, S., PURFIELD, A. E., SAMANEKA, W., SAVIC, R. M., SANNE, I., SCOTT, N. A., SHENJE, J., SIZEMORE, E., VERNON, A., WAJA, Z., WEINER, M., SWINDELLS, S. & CHAISSON, R. E. 2021. Four-Month Rifapentine Regimens with or without Moxifloxacin for Tuberculosis. *New England Journal of Medicine,* 384**,** 1705-1718.
DOROBANTU, L. S., YEUNG, A. K. C., FOGHT, J. M. & GRAY, M. R. 2004. Stabilization of Oil-Water Emulsions by Hydrophobic Bacteria. 70**,** 6333-6336.
DOUGLAS, E. J. A., ALKHZEM, A. H., WONFOR, T., LI, S., WOODMAN, T. J., BLAGBROUGH, I. S. & LAABEI, M. 2022. Antibacterial activity of novel linear polyamines against Staphylococcus aureus. *Front Microbiol,* 13**,** 948343.
DREYFUS, R., TABELING, P. & WILLAIME, H. 2003. Ordered and disordered patterns in two-phase flows in microchannels. *Phys Rev Lett,* 90**,** 144505.
DULBERGER, C. L., RUBIN, E. J. & BOUTTE, C. C. 2020. The mycobacterial cell envelope — a moving target. *Nature Reviews Microbiology,* 18**,** 47-59.
DWYER, F. P., GYARFAS, E. C., ROGERS, W. P. & KOCH, J. H. 1952. Biological Activity of Complex Ions. *Nature,* 170**,** 190-191.
ELWARD, A. M., MCANDREWS, J. M. & YOUNG, V. L. 2009. Methicillin-Sensitive and Methicillin-Resistant Staphylococcus aureus: Preventing Surgical Site Infections Following Plastic Surgery. *Aesthetic Surgery Journal,* 29**,** 232-244.
END-TB 2016. Expand New Drug Markets for TB. *END-TB 2021***,** 1-30.
ERNST, J. D. 2012. The immunological life cycle of tuberculosis. *Nature Reviews Immunology,* 12**,** 581-591.

ESPINAR BUITRAGO, M. D. L. S. & MUÑOZ FERNÁNDEZ, M. Á. 2021. Chapter 10 - Dendrimers and their applications in biomedicine: Dendrimer-drug interaction, a new therapeutic alternative. *In:* KESHARWANI, P. (ed.) *Dendrimer-Based Nanotherapeutics.* Academic Press.

ETIENNE, G., VIAN, A., BIOČANIN, M., DEPLANCKE, B. & AMSTAD, E. 2018. Cross-talk between emulsion drops: how are hydrophilic reagents transported across oil phases? *Lab on a Chip,* 18**,** 3903-3912.

EUN, Y. J., UTADA, A. S., COPELAND, M. F., TAKEUCHI, S. & WEIBEL, D. B. 2011. Encapsulating bacteria in agarose microparticles using microfluidics for high-throughput cell analysis and isolation. *ACS Chem Biol,* 6**,** 260-6.

FAIT, A., SILVA, S. F., ABRAHAMSSON JÅ, H. & INGMER, H. 2024. Staphylococcus aureus response and adaptation to vancomycin. *Adv Microb Physiol,* 85**,** 201-258.

FAÚNDEZ, G., TRONCOSO, M., NAVARRETE, P. & FIGUEROA, G. 2004. Antimicrobial activity of copper surfaces against suspensions of Salmonella enterica and Campylobacter jejuni. *BMC Microbiol,* 4**,** 19.

FAUSTINO, V., CATARINO, S. O., LIMA, R. & MINAS, G. 2016. Biomedical microfluidic devices by using low-cost fabrication techniques: A review. *Journal of Biomechanics,* 49**,** 2280-2292.

FENG, X., LIU, B. F., LI, J. & LIU, X. 2015. Advances in coupling microfluidic chips to mass spectrometry. *Mass Spectrom Rev,* 34**,** 535-57.

FIROOZMAND, H. & ROUSSEAU, D. 2016. Microbial cells as colloidal particles: Pickering oil-in-water emulsions stabilized by bacteria and yeast. *Food Research International,* 81**,** 66-73.

FREI, A., VERDEROSA, A. D., ELLIOTT, A. G., ZUEGG, J. & BLASKOVICH, M. A. T. 2023. Metals to combat antimicrobial resistance. *Nature Reviews Chemistry,* 7**,** 202-224.

FU, H., ZENG, W., LI, S. & YUAN, S. 2017. Electrical-detection droplet microfluidic closed-loop control system for precise droplet production. *Sensors and Actuators A: Physical,* 267**,** 142-149.

GAJIC, I., KABIC, J., KEKIC, D., JOVICEVIC, M., MILENKOVIC, M., MITIC CULAFIC, D., TRUDIC, A., RANIN, L. & OPAVSKI, N. 2022. Antimicrobial Susceptibility Testing: A Comprehensive Review of Currently Used Methods. *Antibiotics,* 11**,** 427.

GARTI, N. & ASERIN, A. 2013. Double Emulsions. *In:* TADROS, T. (ed.) *Encyclopedia of Colloid and Interface Science.* Berlin, Heidelberg: Springer Berlin Heidelberg.

GASSER, G., OTT, I. & METZLER-NOLTE, N. 2011. Organometallic Anticancer Compounds. *Journal of Medicinal Chemistry,* 54**,** 3-25.

GEERSENS, É., VUILLEUMIER, S. & RYCKELYNCK, M. 2022. Growth-Associated Droplet Shrinkage for Bacterial Quantification, Growth Monitoring, and Separation by Ultrahigh-Throughput Microfluidics. *ACS Omega,* 7**,** 12039-12047.

GEISLINGER, T. M. & FRANKE, T. 2013. Sorting of circulating tumor cells (MV3-melanoma) and red blood cells using non-inertial lift. *Biomicrofluidics,* 7**,** 044120.

GENCTURK, E., MUTLU, S. & ULGEN, K. O. 2017. Advances in microfluidic devices made from thermoplastics used in cell biology and analyses. *Biomicrofluidics,* 11**,** 051502.

GETAHUN, H., MATTEELLI, A., CHAISSON, R. E. & RAVIGLIONE, M. 2015. Latent Mycobacterium tuberculosis infection. *N Engl J Med,* 372**,** 2127-35.

GIBSON, S. E. R., HARRISON, J. & COX, J. A. G. 2018. Modelling a Silent Epidemic: A Review of the In Vitro Models of Latent Tuberculosis. *Pathogens (Basel, Switzerland),* 7**,** 88.

GIBSON, S. E. R., HARRISON, J. & COX, J. A. G. 2021. Drug Susceptibility Screening Using In Vitro Models of Hypoxic Non-Replicating Persistent Mycobacteria. *In:* PARISH, T. & KUMAR, A. (eds.) *Mycobacteria Protocols.* New York, NY: Springer US.

GOLBERG, A., LINSHIZ, G., KRAVETS, I., STAWSKI, N., HILLSON, N. J., YARMUSH, M. L., MARKS, R. S. & KONRY, T. 2014. Cloud-Enabled Microscopy and Droplet Microfluidic Platform for Specific Detection of Escherichia coli in Water. *PLOS ONE,* 9**,** e86341.

GONG, M. M. & SINTON, D. 2017. Turning the Page: Advancing Paper-Based Microfluidics for Broad Diagnostic Application. *Chem Rev,* 117**,** 8447-8480.

GONZALO, S., RODEA-PALOMARES, I., LEGANÉS, F., GARCÍA-CALVO, E., ROSAL, R. & FERNÁNDEZ-PIÑAS, F. 2015. First evidences of PAMAM dendrimer internalization in microorganisms of environmental relevance: A linkage with toxicity and oxidative stress. *Nanotoxicology,* 9**,** 706-718.

GOSS, C. H., KANEKO, Y., KHUU, L., ANDERSON, G. D., RAVISHANKAR, S., AITKEN, M. L., LECHTZIN, N., ZHOU, G., CZYZ, D. M., MCLEAN, K., OLAKANMI, O., SHUMAN, H. A., TERESI, M., WILHELM, E., CALDWELL, E., SALIPANTE, S. J., HORNICK, D. B., SIEHNEL, R. J., BECKER, L., BRITIGAN, B. E. & SINGH, P. K. 2018. Gallium disrupts bacterial iron metabolism and has therapeutic effects in mice and humans with lung infections. *Sci Transl Med,* 10.

GRUNER, P., RIECHERS, B., SEMIN, B., LIM, J., JOHNSTON, A., SHORT, K. & BARET, J.-C. 2016. Controlling molecular transport in minimal emulsions. *Nature Communications,* 7**,** 10392.

GRZELAK, E. M., CHOULES, M. P., GAO, W., CAI, G., WAN, B., WANG, Y., MCALPINE, J. B., CHENG, J., JIN, Y., LEE, H., SUH, J.-W., PAULI, G. F., FRANZBLAU, S. G., JAKI, B. U. & CHO, S. 2019. Strategies in anti-Mycobacterium tuberculosis drug discovery based on phenotypic screening. *The Journal of Antibiotics,* 72**,** 719-728.

GUMBO, T., CIRRINCIONE, K. & SRIVASTAVA, S. 2020. Repurposing drugs for treatment of Mycobacterium abscessus: a view to a kill. *J Antimicrob Chemother,* 75**,** 1212-1217.

GUO, M. T., ROTEM, A., HEYMAN, J. A. & WEITZ, D. A. 2012. Droplet microfluidics for high-throughput biological assays. *Lab Chip,* 12**,** 2146-55.

GYIMAH, N., JÕEMAA, R., PÄRNAMETS, K., SCHELER, O., RANG, T. & PARDY, T. PID Controller Tuning Optimization Using Genetic Algorithm for Droplet Size Control in Microfluidics. 2022 18th Biennial Baltic Electronics Conference (BEC), 4-6 Oct. 2022 2022a. 1-6.

GYIMAH, N., SCHELER, O., RANG, T. & PARDY, T. Digital twin for controlled generation of water-in-oil microdroplets with required size. 2022 23rd International Conference on Thermal, Mechanical and Multi-Physics Simulation and Experiments in Microelectronics and Microsystems (EuroSimE), 25-27 April 2022 2022b. 1-7.

HAEBERLE, S., ZENGERLE, R. & DUCRÉE, J. 2007. Centrifugal generation and manipulation of droplet emulsions. *Microfluidics and Nanofluidics,* 3**,** 65-75.

HALAWA, E. M., FADEL, M., AL-RABIA, M. W., BEHAIRY, A., NOUH, N. A., ABDO, M., OLGA, R., FERICEAN, L., ATWA, A. M., EL-NABLAWAY, M. & ABDEEN, A. 2023. Antibiotic action and resistance: updated review of mechanisms, spread, influencing factors, and alternative approaches for combating resistance. *Front Pharmacol,* 14**,** 1305294.

HARMON, J. B., GRAY, H. K., YOUNG, C. C. & SCHWAB, K. J. 2020. Microfluidic droplet application for bacterial surveillance in fresh-cut produce wash waters. *PLoS One,* 15**,** e0233239.

HE, Z., WU, H., YAN, X. & LIU, W. 2022. Recent advances in droplet microfluidics for microbiology. *Chinese Chemical Letters,* 33**,** 1729-1742.

HENGOJU, S., TOVAR, M., MAN, D. K. W., BUCHHEIM, S. & ROSENBAUM, M. A. 2020. Droplet Microfluidics for Microbial Biotechnology. Berlin, Heidelberg: Springer Berlin Heidelberg.

HOLTZE, C., WEISSE, S. A. & VRANCEANU, M. 2017. Commercial Value and Challenges of Drop-Based Microfluidic Screening Platforms–An Opinion. LID - 193.

HORKA, M., SUN, S., RUSZCZAK, A., GARSTECKI, P. & MAYR, T. 2016. Lifetime of Phosphorescence from Nanoparticles Yields Accurate Measurement of Concentration of Oxygen in Microdroplets, Allowing One To Monitor the Metabolism of Bacteria. *Analytical Chemistry,* 88**,** 12006-12012.

HOSSAIN, T. J. 2024. Methods for screening and evaluation of antimicrobial activity: A review of protocols, advantages, and limitations. *Eur J Microbiol Immunol (Bp)*.

HOU, R. C. W., LIN, M. Y., WANG, M. M. C. & TZEN, J. T. C. 2003. Increase of Viability of Entrapped Cells of Lactobacillus delbrueckii ssp. bulgaricus in Artificial Sesame Oil Emulsions. *Journal of Dairy Science,* 86**,** 424-428.

HOUBEN, R. M. G. J. & DODD, P. J. 2016. The Global Burden of Latent Tuberculosis Infection: A Re-estimation Using Mathematical Modelling. *PLoS medicine,* 13**,** e1002152-e1002152.

HU, Y.-T., TING, Y., HU, J.-Y. & HSIEH, S.-C. 2017. Techniques and methods to study functional characteristics of emulsion systems. *Journal of Food and Drug Analysis,* 25**,** 16-26.

HUANG, H.-K., CHENG, H.-W., LIAO, C.-C., LIN, S.-J., CHEN, Y.-Z., WANG, J.-K., WANG, Y.-L. & HUANG, N.-T. 2020. Bacteria encapsulation and rapid antibiotic susceptibility test using a microfluidic microwell device integrating surface-enhanced Raman scattering. *Lab on a Chip,* 20**,** 2520-2528.

HUANG, S., SRIMANI, J. K., LEE, A. J., ZHANG, Y., LOPATKIN, A. J., LEONG, K. W. & YOU, L. 2015. Dynamic control and quantification of bacterial population dynamics in droplets. *Biomaterials,* 61**,** 239-245.

HUDSON, M. A. & LOCKLESS STEVE, W. 2022. Elucidating the Mechanisms of Action of Antimicrobial Agents. *mBio,* 13**,** e02240-21.

ISLER, B., DOI, Y., BONOMO ROBERT, A. & PATERSON DAVID, L. 2018. New Treatment Options against Carbapenem-Resistant Acinetobacter baumannii Infections. *Antimicrobial Agents and Chemotherapy,* 63**,** 10.1128/aac.01110-18.

ISRAELACHVILI, J. 1994. The science and applications of emulsions — an overview. *Colloids and Surfaces A: Physicochemical and Engineering Aspects,* 91**,** 1-8.

ITALIA, V., GIAKOUMAKI, A. N., BONFADINI, S., BHARADWAJ, V., LE PHU, T., EATON, S. M., RAMPONI, R., BERGAMINI, G., LANZANI, G. & CRIANTE, L. 2019. Laser-Inscribed Glass Microfluidic Device for Non-Mixing Flow of Miscible Solvents. *Micromachines,* 10**,** 23.

JAHN, I. J., ŽUKOVSKAJA, O., ZHENG, X. S., WEBER, K., BOCKLITZ, T. W., CIALLA-MAY, D. & POPP, J. 2017. Surface-enhanced Raman spectroscopy and microfluidic platforms: challenges, solutions and potential applications. *Analyst,* 142**,** 1022-1047.

JANASZEWSKA, A., LAZNIEWSKA, J., TRZEPIŃSKI, P., MARCINKOWSKA, M. & KLAJNERT-MACULEWICZ, B. 2019. Cytotoxicity of Dendrimers. 9**,** 330.

JANIESCH, J.-W., WEISS, M., KANNENBERG, G., HANNABUSS, J., SURREY, T., PLATZMAN, I. & SPATZ, J. P. 2015. Key Factors for Stable Retention of Fluorophores and Labeled Biomolecules in Droplet-Based Microfluidics. *Analytical Chemistry,* 87**,** 2063-2067.

JEE, B. 2020. Understanding the early host immune response against Mycobacterium tuberculosis. *Central-European journal of immunology,* 45**,** 99-103.

JEONG, Y., JANG, H., KANG, J., NAM, J., SHIN, K., KWON, S. & CHOI, J. 2021. Color-Coded Droplets and Microscopic Image Analysis for Multiplexed Antibiotic Susceptibility Testing. *Biosensors* [Online], 11.

JEVPRASESPHANT, R., PENNY, J., ATTWOOD, D., MCKEOWN, N. B. & D'EMANUELE, A. 2003. Engineering of Dendrimer Surfaces to Enhance Transepithelial Transport and Reduce Cytotoxicity. *Pharmaceutical Research,* 20**,** 1543-1550.

JIN, S. H., JEONG, H.-H., LEE, B., LEE, S. S. & LEE, C.-S. 2015. A programmable microfluidic static droplet array for droplet generation, transportation, fusion, storage, and retrieval. *Lab on a Chip,* 15**,** 3677-3686.

JIN, Z., NIE, M., HU, R., ZHAO, T., XU, J., CHEN, D., YUN, J., MA, L. Z. & DU, W. 2018. Dynamic Sessile-Droplet Habitats for Controllable Cultivation of Bacterial Biofilm. 14**,** 1800658.

JÕEMAA, R., GYIMAH, N., ASHRAF, K., PÄRNAMETS, K., ZAFT, A., SCHELER, O., RANG, T. & PARDY, T. 2023. CogniFlow-Drop: Integrated Modular System for Automated Generation of Droplets in Microfluidic Applications. *IEEE Access,* 11**,** 104905-104929.

JOENSSON, H. N., UHLÉN, M. & SVAHN, H. A. 2011. Droplet size based separation by deterministic lateral displacement—separating droplets by cell-induced shrinking. *Lab on a Chip,* 11**,** 1305-1310.

JOHANSEN, M. D., HERRMANN, J.-L. & KREMER, L. 2020. Non-tuberculous mycobacteria and the rise of Mycobacterium abscessus. *Nature Reviews Microbiology,* 18**,** 392-407.

JONAS, O. B., IRWIN, A., BERTHE, F. C. J., LE GALL, F. G. & MARQUEZ, P. V. 2017. Drug-resistant infections : a threat to our economic future (Vol. 2) : final report (English). *In:* GROUP, W. B. (ed.). HNP/Agriculture Global Antimicrobial Resistance Initiative Washington, D.C.

JONG, B. E., WU, T. S., CHEN, N. Y., YANG, C. H., SHU, C. C., WANG, L. S., WU, T. L., LU, J. J., CHIU, C. H., LAI, H. C. & CHUNG, W. H. 2022. Impact on Macrolide Resistance of Genetic Diversity of Mycobacterium abscessus Species. *Microbiol Spectr,* 10**,** e0274922.

JOSEPHIDES, D., DAVOLI, S., WHITLEY, W., RUIS, R., SALTER, R., GOKKAYA, S., VALLET, M., MATTHEWS, D., BENAZZI, G., SHVETS, E., GESELLCHEN, F., GEERE, D., LIU, X., LI, X., MACKWORTH, B., YOUNG, W., OWEN, Z., SMITH, C., STARKIE, D., WHITE, J., SWEENEY, B., HINCHLIFFE, M., TICKLE, S., LIGHTWOOD, D. J., REHAK, M., CRAIG, F. F. & HOLMES, D. 2020. Cyto-Mine: An Integrated, Picodroplet System for High-Throughput Single-Cell Analysis, Sorting, Dispensing,

and Monoclonality Assurance. *SLAS TECHNOLOGY: Translating Life Sciences Innovation,* 25**,** 177-189.
JOSHI, S., SHALLAL, A. & ZERVOS, M. 2021. Vancomycin-Resistant Enterococci: Epidemiology, Infection Prevention, and Control. *Infect Dis Clin North Am,* 35**,** 953-968.
JUNG, Y. G., KIM, H., LEE, S., KIM, S., JO, E., KIM, E. G., CHOI, J., KIM, H. J., YOO, J., LEE, H. J., KIM, H., JUNG, H., RYOO, S. & KWON, S. 2018. A rapid culture system uninfluenced by an inoculum effect increases reliability and convenience for drug susceptibility testing of Mycobacterium tuberculosis. *Sci Rep,* 8**,** 8651.
KALANTARIFARD, A., ALIZADEH-HAGHIGHI, E. & ELBUKEN, C. 2022. A microfluidic droplet system for ultra-monodisperse droplet generation: A universal approach. *Chemical Engineering Science,* 261**,** 117947.
KALANTARIFARD, A., ALIZADEH HAGHIGHI, E. & ELBUKEN, C. 2018. Damping hydrodynamic fluctuations in microfluidic systems. *Chemical Engineering Science,* 178**,** 238-247.
KAM, J. Y., HORTLE, E., KROGMAN, E., WARNER, S. E., WRIGHT, K., LUO, K., CHENG, T., MANUNEEDHI CHOLAN, P., KIKUCHI, K., TRICCAS, J. A., BRITTON, W. J., JOHANSEN, M. D., KREMER, L. & OEHLERS, S. H. 2022. Rough and smooth variants of Mycobacterium abscessus are differentially controlled by host immunity during chronic infection of adult zebrafish. *Nat Commun,* 13**,** 952.
KAMINSKI, T. S., SCHELER, O. & GARSTECKI, P. 2016. Droplet microfluidics for microbiology: techniques, applications and challenges. *Lab on a Chip,* 16**,** 2168-2187.
KANG, W., SARKAR, S., LIN, Z. S., MCKENNEY, S. & KONRY, T. 2019. Ultrafast Parallelized Microfluidic Platform for Antimicrobial Susceptibility Testing of Gram Positive and Negative Bacteria. *Analytical Chemistry,* 91**,** 6242-6249.
KAO, Y.-T., KAMINSKI, T. S., POSTEK, W., GUZOWSKI, J., MAKUCH, K., RUSZCZAK, A., VON STETTEN, F., ZENGERLE, R. & GARSTECKI, P. 2020. Gravity-driven microfluidic assay for digital enumeration of bacteria and for antibiotic susceptibility testing. *Lab on a Chip,* 20**,** 54-63.
KARGES, J., KUANG, S., MASCHIETTO, F., BLACQUE, O., CIOFINI, I., CHAO, H. & GASSER, G. 2020. Rationally designed ruthenium complexes for 1- and 2-photon photodynamic therapy. *Nature Communications,* 11**,** 3262.
KAWAGUCHI, H. 2000. Functional polymer microspheres. *Progress in Polymer Science,* 25**,** 1171-1210.
KEAYS, M. C., O'BRIEN, M., HUSSAIN, A., KIELY, P. A. & DALTON, T. 2016. Rapid identification of antibiotic resistance using droplet microfluidics. *Bioengineered,* 7**,** 79-87.
KEMPA, E. E., SMITH, C. A., LI, X., BELLINA, B., RICHARDSON, K. A.-O., PRINGLE, S., GALMAN, J. A.-O., TURNER, N. A.-O. & BARRAN, P. A.-O. X. Coupling Droplet Microfluidics with Mass Spectrometry for Ultrahigh-Throughput Analysis of Complex Mixtures up to and above 30 Hz.
KHERALDINE, H., RACHID, O., HABIB, A. M., AL MOUSTAFA, A.-E., BENTER, I. F. & AKHTAR, S. 2021. Emerging innate biological properties of nano-drug delivery systems: A focus on PAMAM dendrimers and their clinical potential. *Advanced Drug Delivery Reviews,* 178**,** 113908.
KIM, J., CHO, H. & HAN, K.-H. 2021. Disposable capacitive electrical droplet measurement (DisC-EDM) based on a film-chip technique. *Sensors and Actuators B: Chemical,* 344**,** 130192.
KIM, S. B., YOON, S. Y., SUNG, H. J. & KIM, S. S. 2008a. Cross-Type Optical Particle Separation in a Microchannel. *Analytical Chemistry,* 80**,** 2628-2630.
KIM, S. J. 2005. Drug-susceptibility testing in tuberculosis: methods and reliability of results. *Eur Respir J,* 25**,** 564-9.
KIM, U., QIAN, J., KENRICK, S. A., DAUGHERTY, P. S. & SOH, H. T. 2008b. Multitarget dielectrophoresis activated cell sorter. *Analytical chemistry,* 80**,** 8656-8661.
KIM, Y. & ZIMMERMAN, S. C. 1998. Applications of dendrimers in bio-organic chemistry. *Current Opinion in Chemical Biology,* 2**,** 733-742.
KOH, W.-G. & PISHKO, M. V. 2006. Fabrication of cell-containing hydrogel microstructures inside microfluidic devices that can be used as cell-based biosensors. *Analytical and Bioanalytical Chemistry,* 385**,** 1389-1397.
KOKARE, C. R., KHOT, S. V., GORAIN, B. & KESHARWANI, P. 2021. Chapter 8 - Characterization of dendrimers. *In:* KESHARWANI, P. (ed.) *Dendrimer-Based Nanotherapeutics.* Academic Press.

KOWALSKA-KROCHMAL, B. & DUDEK-WICHER, R. 2021. The Minimum Inhibitory Concentration of Antibiotics: Methods, Interpretation, Clinical Relevance. *Pathogens,* 10.

KUMAR, A., ALAM, A., GROVER, S., PANDEY, S., TRIPATHI, D., KUMARI, M., RANI, M., SINGH, A., AKHTER, Y., EHTESHAM, N. Z. & HASNAIN, S. E. 2019. Peptidyl-prolyl isomerase-B is involved in Mycobacterium tuberculosis biofilm formation and a generic target for drug repurposing-based intervention. *npj Biofilms and Microbiomes,* 5**,** 3.

KUMBHAR, S. A., GORAIN, B., CHOUDHURY, H. & KESHARWANI, P. 2021. Chapter 9 - Safety and toxicity issues of dendrimers. *In:* KESHARWANI, P. (ed.) *Dendrimer-Based Nanotherapeutics.* Academic Press.

LABIENIEC-WATALA, M. & WATALA, C. 2015. PAMAM Dendrimers: Destined for Success or Doomed to Fail? Plain and Modified PAMAM Dendrimers in the Context of Biomedical Applications. *Journal of Pharmaceutical Sciences,* 104**,** 2-14.

LEE, A., XIE, Y. L., BARRY, C. E. & CHEN, R. Y. 2020. Current and future treatments for tuberculosis. *Bmj,* 368**,** m216.

LEE, A. S., DE LENCASTRE, H., GARAU, J., KLUYTMANS, J., MALHOTRA-KUMAR, S., PESCHEL, A. & HARBARTH, S. 2018. Methicillin-resistant Staphylococcus aureus. *Nature Reviews Disease Primers,* 4**,** 18033.

LEE, C.-Y., LIN, Y.-H. & LEE, G.-B. 2009. A droplet-based microfluidic system capable of droplet formation and manipulation. *Microfluidics and Nanofluidics,* 6**,** 599-610.

LEE, S. H. 2016. Tuberculosis Infection and Latent Tuberculosis. *Tuberculosis and respiratory diseases,* 79**,** 201-206.

LEI, W., DECKERS, A., LUCHENA, C., POPOVA, A., REISCHL, M., JUNG, N., BRÄSE, S., SCHWARTZ, T., KRIMMELBEIN, I. K., TIETZE, L. F. & LEVKIN, P. A. 2022. Droplet Microarray as a Powerful Platform for Seeking New Antibiotics Against Multidrug-Resistant Bacteria. 6**,** 2200166.

LI, F., COLLINS, J. G. & KEENE, F. R. 2015. Ruthenium complexes as antimicrobial agents. *Chemical Society Reviews,* 44**,** 2529-2542.

LI, H. & STECKL, A. J. 2019. Paper Microfluidics for Point-of-Care Blood-Based Analysis and Diagnostics. *Anal Chem,* 91**,** 352-371.

LI, J., MCCLEMENTS, D. J. & MCLANDSBOROUGH, L. A. 2001. Interaction between Emulsion Droplets and Escherichia coli Cells. 66**,** 570-657.

LI, Y., CHERUKURY, H., LABANIEH, L., ZHAO, W. & KANG, D.-K. 2020. Rapid Detection of β-Lactamase-Producing Bacteria Using the Integrated Comprehensive Droplet Digital Detection (IC 3D) System. *Sensors (Basel, Switzerland),* 20**,** 4667.

LI, Y., KUMAR, S., ZHANG, L., WU, H. & WU, H. 2023. Characteristics of antibiotic resistance mechanisms and genes of Klebsiella pneumoniae. *Open Med (Wars),* 18**,** 20230707.

LINK, D. R., GRASLAND-MONGRAIN, E., DURI, A., SARRAZIN, F., CHENG, Z. D., CRISTOBAL, G., MARQUEZ, M. & WEITZ, D. A. 2006. Electric control of droplets in microfluidic devices. *Angewandte Chemie-International Edition,* 45**,** 2556-2560.

LIU, W.-W. & ZHU, Y. 2020. "Development and application of analytical detection techniques for droplet-based microfluidics"-A review. *Analytica Chimica Acta,* 1113**,** 66-84.

LIU, X., PAINTER, R. E., ENESA, K., HOLMES, D., WHYTE, G., GARLISI, C. G., MONSMA, F. J., REHAK, M., CRAIG, F. F. & SMITH, C. A. 2016. High-throughput screening of antibiotic-resistant bacteria in picodroplets. *Lab on a Chip,* 16**,** 1636-1643.

LOIZOU, K., WONG, V.-L. & HEWAKANDAMBY, B. 2018. Examining the Effect of Flow Rate Ratio on Droplet Generation and Regime Transition in a Microfluidic T-Junction at Constant Capillary Numbers. 3**,** 54.

LOKENSGARD, E. 2016. *Industrial Plastics: Theory and Applications*, Cengage Learning.

LOPEMAN, R. C., HARRISON, J., DESAI, M. & COX, J. A. G. 2019. Mycobacterium abscessus: Environmental Bacterium Turned Clinical Nightmare. *Microorganisms,* 7.

LÓPEZ-ROA, P., ESTEBAN, J. & MUÑOZ-EGEA, M. C. 2022. Updated Review on the Mechanisms of Pathogenicity in Mycobacterium abscessus, a Rapidly Growing Emerging Pathogen. *Microorganisms,* 11.

LU, X., SAMUELSON, D. R., XU, Y., ZHANG, H., WANG, S., RASCO, B. A., XU, J. & KONKEL, M. E. 2013. Detecting and Tracking Nosocomial Methicillin-Resistant Staphylococcus aureus Using a Microfluidic SERS Biosensor. *Analytical Chemistry,* 85**,** 2320-2327.

LUO, J., LI, J., YANG, H., YU, J. & WEI, H. 2017. Accurate Detection of Methicillin-Resistant Staphylococcus aureus in Mixtures by Use of Single-Bacterium Duplex Droplet Digital PCR. 55**,** 2946-2955.

LY, M. H., NAÏTALI-BOUCHEZ, M., MEYLHEUC, T., BELLON-FONTAINE, M.-N., LE, T. M., BELIN, J.-M. & WACHÉ, Y. 2006. Importance of bacterial surface properties to control the stability of emulsions. *International Journal of Food Microbiology,* 112**,** 26-34.

LYU, F., XU, M., CHENG, Y., XIE, J., RAO, J. & TANG, S. K. 2015. Quantitative detection of cells expressing BlaC using droplet-based microfluidics for use in the diagnosis of tuberculosis. *Biomicrofluidics,* 9**,** 044120.

MA, S.-Y., CHIANG, Y.-C., HSU, C.-H., CHEN, J.-J., HSU, C.-C., CHAO, A.-C. & LIN, Y.-S. 2019. Peanut Detection Using Droplet Microfluidic Polymerase Chain Reaction Device. 2019**,** 4712084.

MAHMOUDI, A., SADI, K. S. & MALAEKEH-NIKOUEI, B. 2021. Chapter 13 - Surface engineered dendrimers as novel option for enhanced pharmaceutical and biomedical potential. *In:* KESHARWANI, P. (ed.) *Dendrimer-Based Nanotherapeutics.* Academic Press.

MAI-PROCHNOW, A., CLAUSON, M., HONG, J. & MURPHY, A. B. 2016. Gram positive and Gram negative bacteria differ in their sensitivity to cold plasma. *Scientific Reports,* 6**,** 38610.

MAO, L. & MIAO, S. 2015. Structuring Food Emulsions to Improve Nutrient Delivery During Digestion. *Food Engineering Reviews,* 7**,** 439-451.

MARKETSANDMARKETS. 2023. *Microfluidics Market - Global Forecast to 2028* [Online]. Available: https://www.marketsandmarkets.com/Market-Reports/microfluidics-market-1305.html [Accessed 10 August 2024].

MARTIN, C. J., CAREY, A. F. & FORTUNE, S. M. 2016. A bug's life in the granuloma. *Seminars in Immunopathology,* 38**,** 213-220.

MARTINEZ-DUARTE, R. 2012. Microfabrication technologies in dielectrophoresis applications--a review. *Electrophoresis,* 33**,** 3110-3132.

MATA, A., FLEISCHMAN, A. J. & ROY, S. 2005. Characterization of Polydimethylsiloxane (PDMS) Properties for Biomedical Micro/Nanosystems. *Biomedical Microdevices,* 7**,** 281-293.

MCCLEMENTS, D. J. 2007. Critical Review of Techniques and Methodologies for Characterization of Emulsion Stability. *Critical Reviews in Food Science and Nutrition,* 47**,** 611-649.

MCDONALD, J. C., DUFFY, D. C., ANDERSON, J. R., CHIU, D. T., WU, H., SCHUELLER, O. J. & WHITESIDES, G. M. 2000. Fabrication of microfluidic systems in poly(dimethylsiloxane). *Electrophoresis,* 21**,** 27-40.

MEEHAN, C. J., GOIG, G. A., KOHL, T. A., VERBOVEN, L., DIPPENAAR, A., EZEWUDO, M., FARHAT, M. R., GUTHRIE, J. L., LAUKENS, K., MIOTTO, P., OFORI-ANYINAM, B., DREYER, V., SUPPLY, P., SURESH, A., UTPATEL, C., VAN SOOLINGEN, D., ZHOU, Y., ASHTON, P. M., BRITES, D., CABIBBE, A. M., DE JONG, B. C., DE VOS, M., MENARDO, F., GAGNEUX, S., GAO, Q., HEUPINK, T. H., LIU, Q., LOISEAU, C., RIGOUTS, L., RODWELL, T. C., TAGLIANI, E., WALKER, T. M., WARREN, R. M., ZHAO, Y., ZIGNOL, M., SCHITO, M., GARDY, J., CIRILLO, D. M., NIEMANN, S., COMAS, I. & VAN RIE, A. 2019. Whole genome sequencing of Mycobacterium tuberculosis: current standards and open issues. *Nature Reviews Microbiology,* 17**,** 533-545.

MEHTAR, S., WIID, I. & TODOROV, S. D. 2008. The antimicrobial activity of copper and copper alloys against nosocomial pathogens and Mycobacterium tuberculosis isolated from healthcare facilities in the Western Cape: an in-vitro study. *J Hosp Infect,* 68**,** 45-51.

MICHELS, H. T., NOYCE, J. O. & KEEVIL, C. W. 2009. Effects of temperature and humidity on the efficacy of methicillin-resistant Staphylococcus aureus challenged antimicrobial materials containing silver and copper. *Lett Appl Microbiol,* 49**,** 191-5.

MILLER, E., ROTEA, M. & ROTHSTEIN, J. P. 2010. Microfluidic device incorporating closed loop feedback control for uniform and tunable production of micro-droplets. *Lab on a Chip,* 10**,** 1293-1301.

MILLER, M. B. & BASSLER, B. L. 2001. Quorum Sensing in Bacteria. 55**,** 165-199.

MILLER, W. R. & ARIAS, C. A. 2024. ESKAPE pathogens: antimicrobial resistance, epidemiology, clinical impact and therapeutics. *Nature Reviews Microbiology*.
MILTENYI, S., MÜLLER, W., WEICHEL, W. & RADBRUCH, A. 1990. High gradient magnetic cell separation with MACS. *Cytometry,* 11**,** 231-8.
MIROWSKI, E., MORELAND, J., ZHANG, A., RUSSEK, S. E. & DONAHUE, M. J. 2005. Manipulation and sorting of magnetic particles by a magnetic force microscope on a microfluidic magnetic trap platform. *Applied Physics Letters,* 86**,** 243901.
MOHD ISA, N. S., EL KADRI, H., VIGOLO, D. & GKATZIONIS, K. 2022. The Effect of Bacteria on the Stability of Microfluidic-Generated Water-in-Oil Droplet. 13**,** 2067.
MOISEEVA, E. V., FLETCHER, A. A. & HARNETT, C. K. 2011. Thin-film electrode based droplet detection for microfluidic systems. *Sensors and Actuators B: Chemical,* 155**,** 408-414.
MONDAL, B., BHAVANASHRI, N., MOUNIKA, S. P., TUTEJA, D., TANDI, K. & SONIYA, H. 2020. Chapter 6 - Microfluidics application for detection of biological warfare agents. *In:* FLORA, S. J. S. & PACHAURI, V. (eds.) *Handbook on Biological Warfare Preparedness.* Academic Press.
MÜLLER, R. H., MÄDER, K. & GOHLA, S. 2000. Solid lipid nanoparticles (SLN) for controlled drug delivery - a review of the state of the art. *Eur J Pharm Biopharm,* 50**,** 161-77.
MURRAY, C. J. L., IKUTA, K. S., SHARARA, F., SWETSCHINSKI, L., ROBLES AGUILAR, G., GRAY, A., HAN, C., BISIGNANO, C., RAO, P., WOOL, E., JOHNSON, S. C., BROWNE, A. J., CHIPETA, M. G., FELL, F., HACKETT, S., HAINES-WOODHOUSE, G., KASHEF HAMADANI, B. H., KUMARAN, E. A. P., MCMANIGAL, B., ACHALAPONG, S., AGARWAL, R., AKECH, S., ALBERTSON, S., AMUASI, J., ANDREWS, J., ARAVKIN, A., ASHLEY, E., BABIN, F.-X., BAILEY, F., BAKER, S., BASNYAT, B., BEKKER, A., BENDER, R., BERKLEY, J. A., BETHOU, A., BIELICKI, J., BOONKASIDECHA, S., BUKOSIA, J., CARVALHEIRO, C., CASTAÑEDA-ORJUELA, C., CHANSAMOUTH, V., CHAURASIA, S., CHIURCHIÙ, S., CHOWDHURY, F., CLOTAIRE DONATIEN, R., COOK, A. J., COOPER, B., CRESSEY, T. R., CRIOLLO-MORA, E., CUNNINGHAM, M., DARBOE, S., DAY, N. P. J., DE LUCA, M., DOKOVA, K., DRAMOWSKI, A., DUNACHIE, S. J., DUONG BICH, T., ECKMANNS, T., EIBACH, D., EMAMI, A., FEASEY, N., FISHER-PEARSON, N., FORREST, K., GARCIA, C., GARRETT, D., GASTMEIER, P., GIREF, A. Z., GREER, R. C., GUPTA, V., HALLER, S., HASELBECK, A., HAY, S. I., HOLM, M., HOPKINS, S., HSIA, Y., IREGBU, K. C., JACOBS, J., JAROVSKY, D., JAVANMARDI, F., JENNEY, A. W. J., KHORANA, M., KHUSUWAN, S., KISSOON, N., KOBEISSI, E., KOSTYANEV, T., KRAPP, F., KRUMKAMP, R., KUMAR, A., KYU, H. H., LIM, C., LIM, K., LIMMATHUROTSAKUL, D., LOFTUS, M. J., LUNN, M., MA, J., MANOHARAN, A., MARKS, F., MAY, J., MAYXAY, M., MTURI, N., et al. 2022. Global burden of bacterial antimicrobial resistance in 2019: a systematic analysis. *The Lancet,* 399**,** 629-655.
MURSHED, S. M. S., TAN, S. H., NGUYEN, N. T., WONG, T. N. & YOBAS, L. 2009. Microdroplet formation of water and nanofluids in heat-induced microfluidic T-junction. *Microfluidics and Nanofluidics,* 6**,** 253-259.
NAJAFI, F., SALAMI-KALAJAHI, M. & ROGHANI-MAMAQANI, H. 2021. A review on synthesis and applications of dendrimers. *Journal of the Iranian Chemical Society,* 18**,** 503-517.
NG, N. & ROGERS, M. A. 2019. Surfactants. *In:* MELTON, L., SHAHIDI, F. & VARELIS, P. (eds.) *Encyclopedia of Food Chemistry.* Oxford: Academic Press.
NGE, P. N., ROGERS, C. I. & WOOLLEY, A. T. 2013. Advances in Microfluidic Materials, Functions, Integration, and Applications. *Chemical Reviews,* 113**,** 2550-2583.
NGUYEN, N.-T., LASSEMONO, S. & CHOLLET, F. A. 2006. Optical detection for droplet size control in microfluidic droplet-based analysis systems. *Sensors and Actuators B: Chemical,* 117**,** 431-436.
NIELSEN, J. B., HANSON, R. L., ALMUGHAMSI, H. M., PANG, C., FISH, T. R. & WOOLLEY, A. T. 2020. Microfluidics: Innovations in Materials and Their Fabrication and Functionalization. *Anal Chem,* 92**,** 150-168.
NIGHTINGALE, A. M., HASSAN, S.-U., EVANS, G. W. H., COLEMAN, S. M. & NIU, X. 2018. Nitrate measurement in droplet flow: gas-mediated crosstalk and correction. *Lab on a Chip,* 18**,** 1903-1913.
NIU, X., ZHANG, M., PENG, S., WEN, W. & SHENG, P. 2007. Real-time detection, control, and sorting of microfluidic droplets. *Biomicrofluidics,* 1**,** 44101.

NOLAN, V. C., RAFOLS, L., HARRISON, J., SOLDEVILA-BARREDA, J. J., CROSATTI, M., GARTON, N. J., WEGRZYN, M., TIMMS, D. L., SEATON, C. C., SENDRON, H., AZMANOVA, M., BARRY, N. P. E., PITTO-BARRY, A. & COX, J. A. G. 2022. Indole-containing arene-ruthenium complexes with broad spectrum activity against antibiotic-resistant bacteria. *Curr Res Microb Sci,* 3**,** 100099.

NOTARO, A., JAKUBASZEK, M., ROTTHOWE, N., MASCHIETTO, F., VINCK, R., FELDER, P. S., GOUD, B., THARAUD, M., CIOFINI, I., BEDIOUI, F., WINTER, R. F. & GASSER, G. 2020. Increasing the Cytotoxicity of Ru(II) Polypyridyl Complexes by Tuning the Electronic Structure of Dioxo Ligands. *Journal of the American Chemical Society,* 142**,** 6066-6084.

NOVOTNÝ, J. & FORET, F. 2017a. Fluid manipulation on the micro-scale: Basics of fluid behavior in microfluidics. *J Sep Sci,* 40**,** 383-394.

NOVOTNÝ, J. & FORET, F. 2017b. Fluid manipulation on the micro-scale: Basics of fluid behavior in microfluidics. *Journal of separation science,* 40**,** 383-394.

O'RORKE, R. D., WOOD, C. D., WÄLTI, C., EVANS, S. D., DAVIES, A. G. & CUNNINGHAM, J. E. 2012. Acousto-microfluidics: Transporting microbubble and microparticle arrays in acoustic traps using surface acoustic waves. *Journal of Applied Physics,* 111**,** 094911.

OEDIT, A., VULTO, P., RAMAUTAR, R., LINDENBURG, P. W. & HANKEMEIER, T. 2015. Lab-on-a-Chip hyphenation with mass spectrometry: strategies for bioanalytical applications. *Curr Opin Biotechnol,* 31**,** 79-85.

OKAFOR, C. N., REWANE, A. & MOMODU, II 2024. Bacillus Calmette Guerin. *StatPearls.* Treasure Island (FL) ineligible companies. Disclosure: Ayesan Rewane declares no relevant financial relationships with ineligible companies. Disclosure: Ifeanyi Momodu declares no relevant financial relationships with ineligible companies.: StatPearls Publishing

ORTSEIFEN, V., VIEFHUES, M., WOBBE, L. & GRÜNBERGER, A. 2020. Microfluidics for Biotechnology: Bridging Gaps to Foster Microfluidic Applications. 8.

OTA, Y., SAITO, K., TAKAGI, T., MATSUKURA, S., MORITA, M., TSUNEDA, S. & NODA, N. 2019. Fluorescent nucleic acid probe in droplets for bacterial sorting (FNAP-sort) as a high-throughput screening method for environmental bacteria with various growth rates. *PLoS One,* 14**,** e0214533.

OU, Y., CAO, S., ZHANG, J., DONG, W., YANG, Z. & YU, Z. 2021. Droplet microfluidics on analysis of pathogenic microbes for wastewater-based epidemiology. *TrAC Trends in Analytical Chemistry,* 143**,** 116333.

PAI, M., NICOL, M. P. & BOEHME, C. C. 2016. Tuberculosis Diagnostics: State of the Art and Future Directions. *Microbiol Spectr,* 4.

PANG, Z., RAUDONIS, R., GLICK, B. R., LIN, T.-J. & CHENG, Z. 2019. Antibiotic resistance in Pseudomonas aeruginosa: mechanisms and alternative therapeutic strategies. *Biotechnology Advances,* 37**,** 177-192.

PARISH, T. 2020. In vitro drug discovery models for Mycobacterium tuberculosis relevant for host infection. *Expert Opinion on Drug Discovery,* 15**,** 349-358.

PARISH, T. & STOKER, N. G. 1999. Mycobacteria: Bugs and bugbears (Two steps forward and one step back). *Molecular Biotechnology,* 13**,** 191-200.

PARK, S.-Y., WU, T.-H., CHEN, Y., TEITELL, M. A. & CHIOU, P.-Y. 2011. High-speed droplet generation on demand driven by pulse laser-induced cavitation. *Lab on a Chip,* 11**,** 1010-1012.

PARMAR, S. & TOCHEVA, E. I. 2023. The cell envelope of Mycobacterium abscessus and its role in pathogenesis. *PLoS Pathog,* 19**,** e1011318.

PATEL, P., PATEL, V. & PATEL, P. M. 2022. Synthetic strategy of dendrimers: A review. *Journal of the Indian Chemical Society,* 99**,** 100514.

PAYNE, E. M., HOLLAND-MORITZ, D. A., SUN, S. & KENNEDY, R. T. 2020. High-throughput screening by droplet microfluidics: perspective into key challenges and future prospects. *Lab on a Chip,* 20**,** 2247-2262.

PAYNE, E. M., TARAJI, M., MURRAY, B. E., HOLLAND-MORITZ, D. A., MOORE, J. C., HADDAD, P. R. & KENNEDY, R. T. 2023. Evaluation of Analyte Transfer between Microfluidic Droplets by Mass Spectrometry. *Analytical Chemistry,* 95**,** 4662-4670.

PIETERS, J. 2001. Entry and survival of pathogenic mycobacteria in macrophages. *Microbes Infect,* 3**,** 249-55.
PIRUSKA, A., NIKCEVIC, I., LEE, S. H., AHN, C., HEINEMAN, W. R., LIMBACH, P. A. & SELISKAR, C. J. 2005. The autofluorescence of plastic materials and chips measured under laser irradiation. *Lab Chip,* 5**,** 1348-54.
POSTEK, W., GARGULINSKI, P., SCHELER, O., KAMINSKI, T. S. & GARSTECKI, P. 2018. Microfluidic screening of antibiotic susceptibility at a single-cell level shows the inoculum effect of cefotaxime on E. coli. *Lab on a Chip,* 18**,** 3668-3677.
POSTEK, W. & GARSTECKI, P. 2022. Droplet Microfluidics for High-Throughput Analysis of Antibiotic Susceptibility in Bacterial Cells and Populations. *Accounts of Chemical Research,* 55**,** 605-615.
PRESTINACI, F., PEZZOTTI, P. & PANTOSTI, A. 2015. Antimicrobial resistance: a global multifaceted phenomenon. *Pathog Glob Health,* 109**,** 309-18.
PREVENTION, C. F. D. C. A. 2006. Emergence of Mycobacterium tuberculosis with extensive resistance to second-line drugs--worldwide, 2000-2004. *MMWR Morb Mortal Wkly Rep,* 55**,** 301-5.
RAFFI, M., MEHRWAN, S., BHATTI, T. M., AKHTER, J. I., HAMEED, A., YAWAR, W. & UL HASAN, M. M. 2010. Investigations into the antibacterial behavior of copper nanoparticles against Escherichia coli. *Annals of Microbiology,* 60**,** 75-80.
RAHAMAN, S. M., BHATTARAI, A., KUMAR, D., SINGH, B. & SAHA, B. 2023. Chapter 11 - Application of biosurfactants as emulsifiers in the processing of food products with diverse utilization in the baked goods. *In:* INAMUDDIN & ADETUNJI, C. O. (eds.) *Applications of Next Generation Biosurfactants in the Food Sector.* Academic Press.
RAMAKRISHNAN, L. 2012. Revisiting the role of the granuloma in tuberculosis. *Nature Reviews Immunology,* 12**,** 352-366.
RAZMSHOAR, P., SHAKOORJAVAN, S. & AKBARI, S. 2021. Chapter 12 - Surface-engineered dendrimers in targeting and delivery of drugs. *In:* KESHARWANI, P. (ed.) *Dendrimer-Based Nanotherapeutics.* Academic Press.
RENWICK, M. J., SIMPKIN, V. & MOSSIALOS, E. 2016. European Observatory Health Policy Series. *Targeting innovation in antibiotic drug discovery and development: The need for a One Health – One Europe – One World Framework.* Copenhagen (Denmark): European Observatory on Health Systems and Policies

REYGAERT, W. C. 2018. An overview of the antimicrobial resistance mechanisms of bacteria. *AIMS Microbiol,* 4**,** 482-501.
RHOADES, E. R., FRANK, A. A. & ORME, I. M. 1997. Progression of chronic pulmonary tuberculosis in mice aerogenically infected with virulent Mycobacterium tuberculosis. *Tubercle and Lung Disease,* 78**,** 57-66.
ROBERT DE SAINT VINCENT, M., CASSAGNÈRE, S., PLANTARD, J. & DELVILLE, J.-P. 2012. Real-time droplet caliper for digital microfluidics. *Microfluidics and Nanofluidics,* 13**,** 261-271.
ROSENBERG, B., VAN CAMP, L. & KRIGAS, T. 1965. Inhibition of Cell Division in Escherichia coli by Electrolysis Products from a Platinum Electrode. *Nature,* 205**,** 698-699.
RÜGER, K., HAMPEL, A., BILLIG, S., RÜCKER, N., SUERBAUM, S. & BANGE, F. C. 2014. Characterization of rough and smooth morphotypes of Mycobacterium abscessus isolates from clinical specimens. *J Clin Microbiol,* 52**,** 244-50.
RUSSELL, D. G., CARDONA, P.-J., KIM, M.-J., ALLAIN, S. & ALTARE, F. 2009. Foamy macrophages and the progression of the human tuberculosis granuloma. *Nature Immunology,* 10**,** 943-948.
RUSZCZAK, A., JANKOWSKI, P., VASANTHAM, S. K., SCHELER, O. & GARSTECKI, P. 2023. Physicochemical Properties Predict Retention of Antibiotics in Water-in-Oil Droplets. *Analytical Chemistry,* 95**,** 1574-1581.
SAIKIA, S. & CHETIA, P. 2024. Antibiotics: From Mechanism of Action to Resistance and Beyond. *Indian Journal of Microbiology*.
SALAH, I., PARKIN, I. P. & ALLAN, E. 2021. Copper as an antimicrobial agent: recent advances. *RSC Advances,* 11**,** 18179-18186.

SANDOZ, P. A., CHUNG, A. J., WEAVER, W. M. & DI CARLO, D. 2014. Sugar Additives Improve Signal Fidelity for Implementing Two-Phase Resorufin-Based Enzyme Immunoassays. *Langmuir,* 30**,** 6637-6643.

SANKA, I., BARTKOVA, S., PATA, P., ERNITS, M., MEINBERG, M. M., AGU, N., ARUOJA, V., SMOLANDER, O.-P. & SCHELER, O. 2023. User-friendly analysis of droplet array images. *Analytica Chimica Acta,* 1272**,** 341397.

SANKA, I., BARTKOVA, S., PATA, P., SMOLANDER, O.-P. & SCHELER, O. 2021. Investigation of Different Free Image Analysis Software for High-Throughput Droplet Detection. *ACS Omega,* 6**,** 22625-22634.

SARTIPZADEH, O., NAGHIB, S. M., SEYFOORI, A., RAHMANIAN, M. & FATEMINIA, F. S. 2020. Controllable size and form of droplets in microfluidic-assisted devices: Effects of channel geometry and fluid velocity on droplet size. *Materials Science and Engineering: C,* 109**,** 110606.

SCANLON, T. C., DOSTAL, S. M. & GRISWOLD, K. E. 2014a. A high-throughput screen for antibiotic drug discovery. *Biotechnology and bioengineering,* 111**,** 232-243.

SCANLON, T. C., DOSTAL, S. M. & GRISWOLD, K. E. 2014b. A high-throughput screen for antibiotic drug discovery. *Biotechnol Bioeng,* 111**,** 232-43.

SCHELER, O., KAMINSKI, T. S., RUSZCZAK, A. & GARSTECKI, P. 2016. Dodecylresorufin (C12R) Outperforms Resorufin in Microdroplet Bacterial Assays. *ACS Applied Materials & Interfaces,* 8**,** 11318-11325.

SCHELER, O., MAKUCH, K., DEBSKI, P. R., HORKA, M., RUSZCZAK, A., PACOCHA, N., SOZAŃSKI, K., SMOLANDER, O.-P., POSTEK, W. & GARSTECKI, P. 2020. Droplet-based digital antibiotic susceptibility screen reveals single-cell clonal heteroresistance in an isogenic bacterial population. *Scientific Reports,* 10**,** 3282.

SCHMID, L. & FRANKE, T. 2013. SAW-controlled drop size for flow focusing. *Lab on a Chip,* 13**,** 1691-1694.

SCHMITZ, C. H. J., ROWAT, A. C., KÖSTER, S. & WEITZ, D. A. 2009. Dropspots: a picoliter array in a microfluidic device. *Lab on a Chip,* 9**,** 44-49.

SCHÖN, T., WERNGREN, J., MACHADO, D., BORRONI, E., WIJKANDER, M., LINA, G., MOUTON, J., MATUSCHEK, E., KAHLMETER, G., GISKE, C., SANTIN, M., CIRILLO, D. M., VIVEIROS, M. & CAMBAU, E. 2020. Antimicrobial susceptibility testing of Mycobacterium tuberculosis complex isolates - the EUCAST broth microdilution reference method for MIC determination. *Clin Microbiol Infect,* 26**,** 1488-1492.

SCHULZ, M., CALABRESE, S., HAUSLADEN, F., WURM, H., DROSSART, D., STOCK, K., SOBIERAJ, A. M., EICHENSEHER, F., LOESSNER, M. J., SCHMELCHER, M., GERHARDTS, A., GOETZ, U., HANDEL, M., SERR, A., HAECKER, G., LI, J., SPECHT, M., KOCH, P., MEYER, M., TEPPER, P., ROTHER, R., JEHLE, M., WADLE, S., ZENGERLE, R., VON STETTEN, F., PAUST, N. & BORST, N. 2020. Point-of-care testing system for digital single cell detection of MRSA directly from nasal swabs. *Lab on a Chip,* 20**,** 2549-2561.

SCHUMACHER, A., VRANKEN, T., MALHOTRA, A., ARTS, J. J. C. & HABIBOVIC, P. 2018. In vitro antimicrobial susceptibility testing methods: agar dilution to 3D tissue-engineered models. *European Journal of Clinical Microbiology & Infectious Diseases,* 37**,** 187-208.

SEO, M., NIE, Z., XU, S., MOK, M., LEWIS, P. C., GRAHAM, R. & KUMACHEVA, E. 2005. Continuous Microfluidic Reactors for Polymer Particles. *Langmuir,* 21**,** 11614-11622.

SESEN, M., ALAN, T. & NEILD, A. 2017. Droplet control technologies for microfluidic high throughput screening (μHTS). *Lab on a Chip,* 17**,** 2372-2394.

SHANG, L., CHENG, Y. & ZHAO, Y. 2017. Emerging Droplet Microfluidics. *Chemical Reviews,* 117**,** 7964-8040.

SHER, M., ZHUANG, R., DEMIRCI, U. & ASGHAR, W. 2017. Paper-based analytical devices for clinical diagnosis: recent advances in the fabrication techniques and sensing mechanisms. *Expert review of molecular diagnostics,* 17**,** 351-366.

SHIM, J.-U., CRISTOBAL, G., LINK, D. R., THORSEN, T. & FRADEN, S. 2007. Using Microfluidics to Decouple Nucleation and Growth of Protein Crystals. *Crystal Growth & Design,* 7**,** 2192-2194.

SIDDIQUI, A. H. & KOIRALA, J. 2024. Methicillin-Resistant Staphylococcus aureus. *StatPearls.* Treasure Island (FL) ineligible companies. Disclosure: Janak Koirala declares no relevant financial relationships with ineligible companies.: StatPearls Publishing

SINGH, A. K. & GUPTA, U. D. 2018. Animal models of tuberculosis: Lesson learnt. *The Indian journal of medical research,* 147**,** 456-463.

SINGH, B. J., CHAKRABORTY, A. & SEHGAL, R. 2023. A systematic review of industrial wastewater management: Evaluating challenges and enablers. *Journal of Environmental Management,* 348**,** 119230.

SINGHAL, R. & MYNEEDU, V. P. 2015. Microscopy as a diagnostic tool in pulmonary tuberculosis. *International Journal of Mycobacteriology,* 4**,** 1-6.

SKHIRI, Y., GRUNER, P., SEMIN, B., BROSSEAU, Q., PEKIN, D., MAZUTIS, L., GOUST, V., KLEINSCHMIDT, F., EL HARRAK, A., HUTCHISON, J. B., MAYOT, E., BARTOLO, J.-F., GRIFFITHS, A. D., TALY, V. & BARET, J.-C. 2012. Dynamics of molecular transport by surfactants in emulsions. *Soft Matter,* 8**,** 10618-10627.

SMITH, C. A., LI, X., MIZE, T. H., SHARPE, T. D., GRAZIANI, E. I., ABELL, C. & HUCK, W. T. 2013. Sensitive, high throughput detection of proteins in individual, surfactant-stabilized picoliter droplets using nanoelectrospray ionization mass spectrometry. *Anal Chem,* 85**,** 3812-6.

SMITH KENNETH, P. & KIRBY JAMES, E. 2018. The Inoculum Effect in the Era of Multidrug Resistance: Minor Differences in Inoculum Have Dramatic Effect on MIC Determination. *Antimicrobial Agents and Chemotherapy,* 62**,** 10.1128/aac.00433-18.

SMITH, W. P. J., WUCHER, B. R., NADELL, C. D. & FOSTER, K. R. 2023. Bacterial defences: mechanisms, evolution and antimicrobial resistance. *Nature Reviews Microbiology,* 21**,** 519-534.

SMITTEN, K. L., SCATTERGOOD, P. A., KIKER, C., THOMAS, J. A. & ELLIOTT, P. I. P. 2020. Triazole-based osmium(ii) complexes displaying red/near-IR luminescence: antimicrobial activity and super-resolution imaging. *Chemical Science,* 11**,** 8928-8935.

SONGOK, J. & TOIVAKKA, M. 2016. Enhancing Capillary-Driven Flow for Paper-Based Microfluidic Channels. *ACS Applied Materials & Interfaces,* 8**,** 30523-30530.

SQUIRES, T. M. & QUAKE, S. R. 2005. Microfluidics: Fluid physics at the nanoliter scale. *Reviews of Modern Physics,* 77**,** 977-1026.

STANEVA, D. & GRABCHEV, I. 2021. Chapter 20 - Dendrimer as antimicrobial agents. *In:* KESHARWANI, P. (ed.) *Dendrimer-Based Nanotherapeutics.* Academic Press.

STEINBACHER, J. L. & MCQUADE, D. T. 2006. Polymer chemistry in flow: New polymers, beads, capsules, and fibers. *Journal of Polymer Science Part A: Polymer Chemistry,* 44**,** 6505-6533.

STOLNIK, S., ILLUM, L. & DAVIS, S. S. 1995. Long circulating microparticulate drug carriers. *Advanced Drug Delivery Reviews,* 16**,** 195-214.

STOLOVICKI, E., ZIBLAT, R. & WEITZ, D. A. 2018. Throughput enhancement of parallel step emulsifier devices by shear-free and efficient nozzle clearance. *Lab on a Chip,* 18**,** 132-138.

STRATFORD, J. P., EDWARDS, C. L. A., GHANSHYAM, M. J., MALYSHEV, D., DELISE, M. A., HAYASHI, Y. & ASALLY, M. 2019. Electrically induced bacterial membrane-potential dynamics correspond to cellular proliferation capacity. 116**,** 9552-9557.

STURM, A., JÓŹWIAK, G., VERGE, M. P., MUNCH, L., CATHOMEN, G., VOCAT, A., LURASCHI-EGGEMANN, A., ORLANDO, C., FROMM, K., DELARZE, E., ŚWIĄTKOWSKI, M., WIELGOSZEWSKI, G., TOTU, R. M., GARCÍA-CASTILLO, M., DELFINO, A., TAGINI, F., KASAS, S., LASS-FLÖRL, C., GSTIR, R., CANTÓN, R., GREUB, G. & CICHOCKA, D. 2024. Accurate and rapid antibiotic susceptibility testing using a machine learning-assisted nanomotion technology platform. *Nature Communications,* 15**,** 2037.

SUEA-NGAM, A., HOWES, P. D., SRISA-ART, M. & DEMELLO, A. J. 2019. Droplet microfluidics: from proof-of-concept to real-world utility? *Chemical Communications,* 55**,** 9895-9903.

SUGIURA, S., NAKAJIMA, M., TONG, J., NABETANI, H. & SEKI, M. 2000. Preparation of Monodispersed Solid Lipid Microspheres Using a Microchannel Emulsification Technique. *Journal of Colloid and Interface Science,* 227**,** 95-103.

SURYA PRAKASH, G. 2013. Synthesis and Analytical Characterization of Ester and Amine Terminated PAMAM Dendrimers. *Global Journal of Medical Research,* 13**,** 7-15.

TABELING, P. 2005. *Introduction to microfluidics*, OUP Oxford.
TABELING, P. & CHEN, S. 2005. *Introduction to Microfluidics*, OUP Oxford.
TAN, S.-H., NGUYEN, N.-T., YOBAS, L. & KANG, T. G. 2010. Formation and manipulation of ferrofluid droplets at a microfluidicT-junction. *Journal of Micromechanics and Microengineering,* 20**,** 045004.
TAYLOR, T. A. & UNAKAL, C. G. 2024. Staphylococcus aureus Infection. *StatPearls.* Treasure Island (FL) ineligible companies. Disclosure: Chandrashekhar Unakal declares no relevant financial relationships with ineligible companies.: StatPearls Publishing

TECHNOLOGY, I. O. E. A. 2017. paper-based capillary action. *Electronics Letters,* 53**,** 1339-1339.
TENJE, M., FORNELL, A., OHLIN, M. & NILSSON, J. 2018. Particle Manipulation Methods in Droplet Microfluidics. *Analytical Chemistry,* 90**,** 1434-1443.
TEREKHOV, S. S., SMIRNOV, I. V., MALAKHOVA, M. V., SAMOILOV, A. E., MANOLOV, A. I., NAZAROV, A. S., DANILOV, D. V., DUBILEY, S. A., OSTERMAN, I. A., RUBTSOVA, M. P., KOSTRYUKOVA, E. S., ZIGANSHIN, R. H., KORNIENKO, M. A., VANYUSHKINA, A. A., BUKATO, O. N., ILINA, E. N., VLASOV, V. V., SEVERINOV, K. V., GABIBOV, A. G. & ALTMAN, S. 2018. Ultrahigh-throughput functional profiling of microbiota communities. *Proc Natl Acad Sci U S A,* 115**,** 9551-9556.
THE LANCET 2024. Antimicrobial resistance: an agenda for all. *The Lancet,* 403**,** 2349.
THEBERGE, A. B., COURTOIS, F., SCHAERLI, Y., FISCHLECHNER, M., ABELL, C., HOLLFELDER, F. & HUCK, W. T. S. 2010. Microdroplets in Microfluidics: An Evolving Platform for Discoveries in Chemistry and Biology. *Angewandte Chemie International Edition,* 49**,** 5846-5868.
THEURETZBACHER, U., BARALDI, E., CIABUSCHI, F. & CALLEGARI, S. 2023. Challenges and shortcomings of antibacterial discovery projects. *Clin Microbiol Infect,* 29**,** 610-615.
TOMALIA, D. A., CHRISTENSEN, J. B. & BOAS, U. 2012. Synthetic methodologies. *In:* TOMALIA, D. A., CHRISTENSEN, J. B. & BOAS, U. (eds.) *Dendrimers, Dendrons, and Dendritic Polymers: Discovery, Applications, and the Future.* Cambridge: Cambridge University Press.
TOMALIA, D. A. & KHANNA, S. N. 2016. A Systematic Framework and Nanoperiodic Concept for Unifying Nanoscience: Hard/Soft Nanoelements, Superatoms, Meta-Atoms, New Emerging Properties, Periodic Property Patterns, and Predictive Mendeleev-like Nanoperiodic Tables. *Chemical Reviews,* 116**,** 2705-2774.
TONIOLO, C., RUTSCHMANN, O. & MCKINNEY, J. D. 2021. Do chance encounters between heterogeneous cells shape the outcome of tuberculosis infections? *Current Opinion in Microbiology,* 59**,** 72-78.
TOVAR, M., MAHLER, L., BUCHHEIM, S., ROTH, M. & ROSENBAUM, M. A. 2020. Monitoring and external control of pH in microfluidic droplets during microbial culturing. *Microbial Cell Factories,* 19**,** 16.
TRAN, T. M., KIM, S. C., MODAVI, C. & ABATE, A. R. 2022. Robotic automation of droplet microfluidics. *Biomicrofluidics,* 16**,** 014102.
TRAN, T. M., LAN, F., THOMPSON, C. S. & ABATE, A. R. 2013. From tubes to drops: droplet-based microfluidics for ultrahigh-throughput biology. *Journal of Physics D: Applied Physics,* 46**,** 114004.
TWIBANIRE, J. D. A. K. & GRINDLEY, T. B. 2014. Polyester Dendrimers: Smart Carriers for Drug Delivery. *Polymers* [Online], 6.
UMBANHOWAR, P. B., PRASAD, V. & WEITZ, D. A. 2000. Monodisperse emulsion generation via drop break off in a coflowing stream. *Langmuir,* 16**,** 347-351.
UTADA, A. S., CHU, L. Y., FERNANDEZ-NIEVES, A., LINK, D. R., HOLTZE, C. & WEITZ, D. A. 2007. Dripping, Jetting, Drops, and Wetting: The Magic of Microfluidics. *MRS Bulletin,* 32**,** 702-708.
VAITHIYANATHAN, M., SAFA, N. & MELVIN, A. T. 2019. FluoroCellTrack: An algorithm for automated analysis of high-throughput droplet microfluidic data. *PLOS ONE,* 14**,** e0215337.
VAN DER ARK, K. C. H., NUGROHO, A. D. W., BERTON-CARABIN, C., WANG, C., BELZER, C., DE VOS, W. M. & SCHROEN, K. 2017. Encapsulation of the therapeutic microbe Akkermansia muciniphila in a double emulsion enhances survival in simulated gastric conditions. *Food Research International,* 102**,** 372-379.

VAN ELBURG, B., COLLADO-LARA, G., BRUGGERT, G.-W., SEGERS, T., VERSLUIS, M. & LAJOINIE, G. 2021. Feedback-controlled microbubble generator producing one million monodisperse bubbles per second. *Review of Scientific Instruments,* 92.

VAN WIJK, J., HEUNIS, T., HARMZEN, E., DICKS, L. M. T., MEULDIJK, J. & KLUMPERMAN, B. 2014. Compartmentalization of bacteria in microcapsules. *Chemical Communications,* 50**,** 15427-15430.

VESTERGAARD, M., FREES, D. & INGMER, H. 2019. Antibiotic Resistance and the MRSA Problem. *Microbiology Spectrum,* 7**,** 10.1128/microbiolspec.gpp3-0057-2018.

VICTORIA, L., GUPTA, A., GÓMEZ, J. L. & ROBLEDO, J. 2021. Mycobacterium abscessus complex: A Review of Recent Developments in an Emerging Pathogen. *Front Cell Infect Microbiol,* 11**,** 659997.

VINCK, R., GANDIOSO, A., BURCKEL, P., SAUBAMÉA, B., CARIOU, K. & GASSER, G. 2022. Red-Absorbing Ru(II) Polypyridyl Complexes with Biotin Targeting Spontaneously Assemble into Nanoparticles in Biological Media. *Inorg Chem,* 61**,** 13576-13585.

VISCA, P., PISA, F. & IMPERI, F. 2019. The antimetabolite 3-bromopyruvate selectively inhibits Staphylococcus aureus. *Int J Antimicrob Agents,* 53**,** 449-455.

VITKO, N. P. & RICHARDSON, A. R. 2013. Laboratory maintenance of methicillin-resistant Staphylococcus aureus (MRSA). *Curr Protoc Microbiol,* Chapter 9**,** Unit 9C.2.

VOLPATTI, L. R. & YETISEN, A. K. 2014. Commercialization of microfluidic devices. *Trends in Biotechnology,* 32**,** 347-350.

VYAWAHARE, S., GRIFFITHS, A. D. & MERTEN, C. A. 2010. Miniaturization and parallelization of biological and chemical assays in microfluidic devices. *Chemistry & biology,* 17**,** 1052-1065.

WALZL, G., MCNERNEY, R., DU PLESSIS, N., BATES, M., MCHUGH, T. D., CHEGOU, N. N. & ZUMLA, A. 2018. Tuberculosis: advances and challenges in development of new diagnostics and biomarkers. *Lancet Infect Dis,* 18**,** e199-e210.

WANG, J., DU, L., HAN, Y., ZHANG, D. & JING, D. 2023. Advancing in situ single-cell microbiological analysis through a microwell droplet array with a gradual open sidewall. *Lab on a Chip,* 23**,** 5165-5172.

WANG, M. M., TU, E., RAYMOND, D. E., YANG, J. M., ZHANG, H., HAGEN, N., DEES, B., MERCER, E. M., FORSTER, A. H., KARIV, I., MARCHAND, P. J. & BUTLER, W. F. 2005. Microfluidic sorting of mammalian cells by optical force switching. *Nature Biotechnology,* 23**,** 83-87.

WANG, Y., ZHOU, X., YANG, Z., XU, T., FU, H., FONG, C.-C., SUN, J., CHIN, Y. R., ZHANG, L., GUAN, X. & YANG, M. 2024. An integrated and multi-functional droplet-based microfluidic platform for digital DNA amplification. *Biosensors and Bioelectronics,* 246**,** 115831.

WEI, Y., PALACIOS ARAYA, D. & PALMER, K. L. 2024. Enterococcus faecium: evolution, adaptation, pathogenesis and emerging therapeutics. *Nature Reviews Microbiology*.

WEIBEL, D. B., DILUZIO, W. R. & WHITESIDES, G. M. 2007. Microfabrication meets microbiology. *Nature Reviews Microbiology,* 5**,** 209-218.

WHITE, A. R., JALALI, M. & SHENG, J. 2019. A new ecology-on-a-chip microfluidic platform to study interactions of microbes with a rising oil droplet. *Sci Rep,* 9**,** 13737.

WHITESIDES, G. M. 2006. The origins and the future of microfluidics. *Nature,* 442**,** 368-373.

WHO 2015. The END-TB Strategy. *WHO 2012***,** 1-20.

WHO 2017. Antibacterial agents in clinical development: an analysis of the antibacterial clinical development pipeline, including tuberculosis. *In:* ORGANIZATION, G. W. H. (ed.).

WHO 2020. Global Tuberculosis Report 2020.

WHO 2024a. 2023 Antibacterial agents in clinical and preclinical development. Geneva: World Health Organization.

WHO 2024b. WHO bacterial priority pathogens list, 2024: bacterial pathogens of public health importance to guide research, development and strategies to prevent and control antimicrobial resistance.

WONG, F., ZHENG, E. J., VALERI, J. A., DONGHIA, N. M., ANAHTAR, M. N., OMORI, S., LI, A., CUBILLOS-RUIZ, A., KRISHNAN, A., JIN, W., MANSON, A. L., FRIEDRICHS, J., HELBIG, R., HAJIAN, B., FIEJTEK, D. K., WAGNER, F. F., SOUTTER, H. H., EARL, A. M., STOKES, J. M., RENNER, L. D. &

COLLINS, J. J. 2024. Discovery of a structural class of antibiotics with explainable deep learning. *Nature,* 626**,** 177-185.
WONGKONGKATEP, P., MANOPWISEDJAROEN, K., TIPOSOTH, P., ARCHAKUNAKORN, S., PONGTHARANGKUL, T., SUPHANTHARIKA, M., HONDA, K., HAMACHI, I. & WONGKONGKATEP, J. 2012. Bacteria Interface Pickering Emulsions Stabilized by Self-assembled Bacteria–Chitosan Network. *Langmuir,* 28**,** 5729-5736.
WORONOFF, G., EL HARRAK, A., MAYOT, E., SCHICKE, O., MILLER, O. J., SOUMILLION, P., GRIFFITHS, A. D. & RYCKELYNCK, M. 2011. New Generation of Amino Coumarin Methyl Sulfonate-Based Fluorogenic Substrates for Amidase Assays in Droplet-Based Microfluidic Applications. *Analytical Chemistry,* 83**,** 2852-2857.
WRIGHT, W. W. 1989. Plastics materials (5th edition) J. A. Brydson, Butterworths, London, 1989. pp. 864, price £57.50. ISBN 0-408-00721-4. *British Polymer Journal,* 21**,** 525-525.
WU, Z., CHEN, X., WU, Z., ZHANG, Q. & GAO, Q. 2019. Experimental study of fabricating a four-layers Cantor fractal microfluidic chip by CO2 laser system. *Microsystem Technologies,* 25**,** 1251-1256.
XIA, Y., SI, J. & LI, Z. 2016. Fabrication techniques for microfluidic paper-based analytical devices and their applications for biological testing: A review. *Biosens Bioelectron,* 77**,** 774-89.
XIA, Y. & WHITESIDES, G. M. 1998. Soft Lithography. 37**,** 550-575.
XIE, Y., DIXON, A. J., RICKEL, J. M. R., KLIBANOV, A. L. & HOSSACK, J. A. 2020. Closed-loop feedback control of microbubble diameter from a flow-focusing microfluidic device. *Biomicrofluidics,* 14.
XU, J. & ATTINGER, D. 2008. Drop on demand in a microfluidic chip. *Journal of Micromechanics and Microengineering,* 18**,** 065020.
YALCIN, S. E., SHARMA, A., QIAN, S., JOO, S. W. & BAYSAL, O. 2010. Manipulating particles in microfluidics by floating electrodes. *ELECTROPHORESIS,* 31**,** 3711-3718.
YANG, Y., NOVIANA, E., NGUYEN, M. P., GEISS, B. J., DANDY, D. S. & HENRY, C. S. 2017. Paper-Based Microfluidic Devices: Emerging Themes and Applications. *Anal Chem,* 89**,** 71-91.
YI, Q., CAI, D., XIAO, M., NIE, M., CUI, Q., CHENG, J., LI, C., FENG, J., URBAN, G., XU, Y. C., LAN, Y. & DU, W. 2019. Direct antimicrobial susceptibility testing of bloodstream infection on SlipChip. *Biosens Bioelectron,* 135**,** 200-207.
YOW, H. N. & ROUTH, A. F. 2006. Formation of liquid core–polymer shell microcapsules. *Soft Matter,* 2**,** 940-949.
YUNUS, N. A. M., NILI, H. & GREEN, N. G. 2013. Continuous separation of colloidal particles using dielectrophoresis. *ELECTROPHORESIS,* 34**,** 969-978.
ZANG, E., BRANDES, S., TOVAR, M., MARTIN, K., MECH, F., HORBERT, P., HENKEL, T., FIGGE, M. T. & ROTH, M. 2013. Real-time image processing for label-free enrichment of Actinobacteria cultivated in picolitre droplets. *Lab on a Chip,* 13**,** 3707-3713.
ZENG, S., LI, B., SU, X. O., QIN, J. & LIN, B. 2009. Microvalve-actuated precise control of individual droplets in microfluidic devices. *Lab on a Chip,* 9**,** 1340-1343.
ZENG, W., LI, S. & WANG, Z. Characterization of syringe-pump-driven versus pressure-driven microfluidic flows. 2015 International Conference on Fluid Power and Mechatronics (FPM), 5-7 Aug. 2015 2015a. 711-715.
ZENG, W., LI, S. & WANG, Z. 2015b. Closed-loop feedback control of droplet formation in a T-junction microdroplet generator. *Sensors and Actuators A: Physical,* 233**,** 542-547.
ZENG, W., YANG, S., LIU, Y., YANG, T., TONG, Z., SHAN, X. & FU, H. 2022. Precise monodisperse droplet generation by pressure-driven microfluidic flows. *Chemical Engineering Science,* 248**,** 117206.
ZHANG, C., KHOSHMANESH, K., MITCHELL, A. & KALANTAR-ZADEH, K. 2010. Dielectrophoresis for manipulation of micro/nano particles in microfluidic systems. *Anal Bioanal Chem,* 396**,** 401-20.
ZHANG, Y., HO, Y. P., CHIU, Y. L., CHAN, H. F., CHLEBINA, B., SCHUHMANN, T., YOU, L. & LEONG, K. W. 2013. A programmable microenvironment for cellular studies via microfluidics-generated double emulsions. *Biomaterials,* 34**,** 4564-72.
ZHANG, Z., ZHOU, L., XIE, N., NICE, E. C., ZHANG, T., CUI, Y. & HUANG, C. 2020. Overcoming cancer therapeutic bottleneck by drug repurposing. *Signal Transduct Target Ther,* 5**,** 113.

ZHAO, A., SUN, J. & LIU, Y. 2023. Understanding bacterial biofilms: From definition to treatment strategies. 13.

ZHAO, C.-X. & MIDDELBERG, A. P. J. 2011. Two-phase microfluidic flows. *Chemical Engineering Science,* 66**,** 1394-1411.

ZHENG, B., GERDTS, C. J. & ISMAGILOV, R. F. 2005. Using nanoliter plugs in microfluidics to facilitate and understand protein crystallization. *Curr Opin Struct Biol,* 15**,** 548-55.

ZHENG, Y., ZHENG, M., MA, Z., XIN, B., GUO, R. & XU, X. 2015. 8 - Sugar Fatty Acid Esters. *In:* AHMAD, M. U. & XU, X. (eds.) *Polar Lipids.* Elsevier.

ZHU, P. & WANG, L. 2017. Passive and active droplet generation with microfluidics: a review. *Lab on a Chip,* 17**,** 34-75.

ZHU, Y. & FANG, Q. 2013. Analytical detection techniques for droplet microfluidics—A review. *Analytica Chimica Acta,* 787**,** 24-35.

ZIAIE, B., BALDI, A., LEI, M., GU, Y. & SIEGEL, R. A. 2004. Hard and soft micromachining for BioMEMS: review of techniques and examples of applications in microfluidics and drug delivery. *Advanced Drug Delivery Reviews,* 56**,** 145-172.

ZINCHENKO, A., DEVENISH, S. R. A. & HOLLFELDER, F. 2023. Rapid quantitative assessment of small molecule leakage from microdroplets by flow cytometry and improvement of fluorophore retention in biochemical assays. 2023.04.23.538007.

Chapter 8.

Appendix

Appendix 4.1. 2-way ANOVA results of encapsulated MRSA (CFU/mL) in 60 pL droplets at a starting inoculum of $2.42x10^7$. Multiple comparisons test was conducted between the 60 pL droplet culture and the 60 pL droplet control culture.

Tukey's multiple comparisons test	Significant?	Summary	Adjusted P Value
0:60 pL Droplet Culture vs. 0:60 pL Droplet Control	Yes	****	<0.0001
0:60 pL Droplet Culture vs. 2:60 pL Droplet Culture	No	ns	0.9811
0:60 pL Droplet Culture vs. 2:60 pL Droplet Control	Yes	****	<0.0001
0:60 pL Droplet Culture vs. 4:60 pL Droplet Culture	Yes	****	<0.0001
0:60 pL Droplet Culture vs. 4:60 pL Droplet Control	Yes	****	<0.0001
0:60 pL Droplet Culture vs. 6:60 pL Droplet Culture	Yes	***	0.0009
0:60 pL Droplet Culture vs. 6:60 pL Droplet Control	Yes	****	<0.0001
0:60 pL Droplet Control vs. 2:60 pL Droplet Culture	Yes	****	<0.0001
0:60 pL Droplet Control vs. 2:60 pL Droplet Control	No	ns	>0.9999
0:60 pL Droplet Control vs. 4:60 pL Droplet Culture	Yes	****	<0.0001
0:60 pL Droplet Control vs. 4:60 pL Droplet Control	No	ns	>0.9999
0:60 pL Droplet Control vs. 6:60 pL Droplet Culture	Yes	****	<0.0001
0:60 pL Droplet Control vs. 6:60 pL Droplet Control	No	ns	>0.9999
2:60 pL Droplet Culture vs. 2:60 pL Droplet Control	Yes	****	<0.0001
2:60 pL Droplet Culture vs. 4:60 pL Droplet Culture	Yes	****	<0.0001
2:60 pL Droplet Culture vs. 4:60 pL Droplet Control	Yes	****	<0.0001
2:60 pL Droplet Culture vs. 6:60 pL Droplet Culture	Yes	**	0.0051
2:60 pL Droplet Culture vs. 6:60 pL Droplet Control	Yes	****	<0.0001
2:60 pL Droplet Control vs. 4:60 pL Droplet Culture	Yes	****	<0.0001
2:60 pL Droplet Control vs. 4:60 pL Droplet Control	No	ns	>0.9999
2:60 pL Droplet Control vs. 6:60 pL Droplet Culture	Yes	****	<0.0001
2:60 pL Droplet Control vs. 6:60 pL Droplet Control	No	ns	>0.9999
4:60 pL Droplet Culture vs. 4:60 pL Droplet Control	Yes	****	<0.0001
4:60 pL Droplet Culture vs. 6:60 pL Droplet Culture	No	ns	0.0559
4:60 pL Droplet Culture vs. 6:60 pL Droplet Control	Yes	****	<0.0001
4:60 pL Droplet Control vs. 6:60 pL Droplet Culture	Yes	****	<0.0001
4:60 pL Droplet Control vs. 6:60 pL Droplet Control	No	ns	>0.9999
6:60 pL Droplet Culture vs. 6:60 pL Droplet Control	Yes	****	<0.0001

Appendix 4.2. 2-way ANOVA results of encapsulated MRSA (CFU/mL) in 300 pL droplets at a stating inoculum of $2.42x10^7$. Multiple comparisons test was conducted between the 300 pL droplet culture and the 300 pL droplet control culture.

Tukey's multiple comparisons test	Significant?	Summary	Adjusted P Value
0:300 pL Droplet Culture vs. 0:300 pL Droplet Control	Yes	****	<0.0001
0:300 pL Droplet Culture vs. 2:300 pL Droplet Culture	Yes	****	<0.0001
0:300 pL Droplet Culture vs. 2:300 pL Droplet Control	Yes	****	<0.0001
0:300 pL Droplet Culture vs. 4:300 pL Droplet Culture	Yes	****	<0.0001
0:300 pL Droplet Culture vs. 4:300 pL Droplet Control	Yes	****	<0.0001
0:300 pL Droplet Culture vs. 6:300 pL Droplet Culture	Yes	****	<0.0001
0:300 pL Droplet Culture vs. 6:300 pL Droplet Control	Yes	****	<0.0001
0:300 pL Droplet Control vs. 2:300 pL Droplet Culture	Yes	****	<0.0001
0:300 pL Droplet Control vs. 2:300 pL Droplet Control	No	ns	>0.9999
0:300 pL Droplet Control vs. 4:300 pL Droplet Culture	Yes	****	<0.0001
0:300 pL Droplet Control vs. 4:300 pL Droplet Control	No	ns	>0.9999
0:300 pL Droplet Control vs. 6:300 pL Droplet Culture	Yes	****	<0.0001
0:300 pL Droplet Control vs. 6:300 pL Droplet Control	No	ns	>0.9999
2:300 pL Droplet Culture vs. 2:300 pL Droplet Control	Yes	****	<0.0001
2:300 pL Droplet Culture vs. 4:300 pL Droplet Culture	No	ns	0.9668
2:300 pL Droplet Culture vs. 4:300 pL Droplet Control	Yes	****	<0.0001
2:300 pL Droplet Culture vs. 6:300 pL Droplet Culture	Yes	****	<0.0001
2:300 pL Droplet Culture vs. 6:300 pL Droplet Control	Yes	****	<0.0001
2:300 pL Droplet Control vs. 4:300 pL Droplet Culture	Yes	****	<0.0001
2:300 pL Droplet Control vs. 4:300 pL Droplet Control	No	ns	>0.9999
2:300 pL Droplet Control vs. 6:300 pL Droplet Culture	Yes	****	<0.0001
2:300 pL Droplet Control vs. 6:300 pL Droplet Control	No	ns	>0.9999
4:300 pL Droplet Culture vs. 4:300 pL Droplet Control	Yes	****	<0.0001
4:300 pL Droplet Culture vs. 6:300 pL Droplet Culture	Yes	****	<0.0001
4:300 pL Droplet Culture vs. 6:300 pL Droplet Control	Yes	****	<0.0001
4:300 pL Droplet Control vs. 6:300 pL Droplet Culture	Yes	****	<0.0001
4:300 pL Droplet Control vs. 6:300 pL Droplet Control	No	ns	>0.9999
6:300 pL Droplet Culture vs. 6:300 pL Droplet Control	Yes	****	<0.0001

Appendix 4.3. 2-way ANOVA results of encapsulated MRSA (CFU/mL) in 300 pL droplets at a stating inoculum of $5.82x10^8$. Multiple comparisons test was conducted between the 300 pL droplet culture and the 300 pL droplet control culture.

Tukey's multiple comparisons test	Significant?	Summary	Adjusted P Value
0:300 pL Droplet Culture vs. 0:300 pL Droplet Control	Yes	****	<0.0001
0:300 pL Droplet Culture vs. 2:300 pL Droplet Culture	No	ns	0.2327
0:300 pL Droplet Culture vs. 2:300 pL Droplet Control	Yes	****	<0.0001
0:300 pL Droplet Culture vs. 4:300 pL Droplet Culture	Yes	****	<0.0001
0:300 pL Droplet Culture vs. 4:300 pL Droplet Control	Yes	****	<0.0001
0:300 pL Droplet Culture vs. 6:300 pL Droplet Culture	Yes	**	0.0083
0:300 pL Droplet Culture vs. 6:300 pL Droplet Control	Yes	****	<0.0001
0:300 pL Droplet Control vs. 2:300 pL Droplet Culture	Yes	****	<0.0001
0:300 pL Droplet Control vs. 2:300 pL Droplet Control	No	ns	>0.9999
0:300 pL Droplet Control vs. 4:300 pL Droplet Culture	Yes	****	<0.0001
0:300 pL Droplet Control vs. 4:300 pL Droplet Control	No	ns	>0.9999
0:300 pL Droplet Control vs. 6:300 pL Droplet Culture	Yes	****	<0.0001
0:300 pL Droplet Control vs. 6:300 pL Droplet Control	No	ns	>0.9999
2:300 pL Droplet Culture vs. 2:300 pL Droplet Control	Yes	****	<0.0001
2:300 pL Droplet Culture vs. 4:300 pL Droplet Culture	Yes	****	<0.0001
2:300 pL Droplet Culture vs. 4:300 pL Droplet Control	Yes	****	<0.0001
2:300 pL Droplet Culture vs. 6:300 pL Droplet Culture	No	ns	0.6205
2:300 pL Droplet Culture vs. 6:300 pL Droplet Control	Yes	****	<0.0001
2:300 pL Droplet Control vs. 4:300 pL Droplet Culture	Yes	****	<0.0001
2:300 pL Droplet Control vs. 4:300 pL Droplet Control	No	ns	>0.9999
2:300 pL Droplet Control vs. 6:300 pL Droplet Culture	Yes	****	<0.0001
2:300 pL Droplet Control vs. 6:300 pL Droplet Control	No	ns	>0.9999
4:300 pL Droplet Culture vs. 4:300 pL Droplet Control	Yes	****	<0.0001
4:300 pL Droplet Culture vs. 6:300 pL Droplet Culture	Yes	**	0.0013
4:300 pL Droplet Culture vs. 6:300 pL Droplet Control	Yes	****	<0.0001
4:300 pL Droplet Control vs. 6:300 pL Droplet Culture	Yes	****	<0.0001
4:300 pL Droplet Control vs. 6:300 pL Droplet Control	No	ns	>0.9999
6:300 pL Droplet Culture vs. 6:300 pL Droplet Control	Yes	****	<0.0001

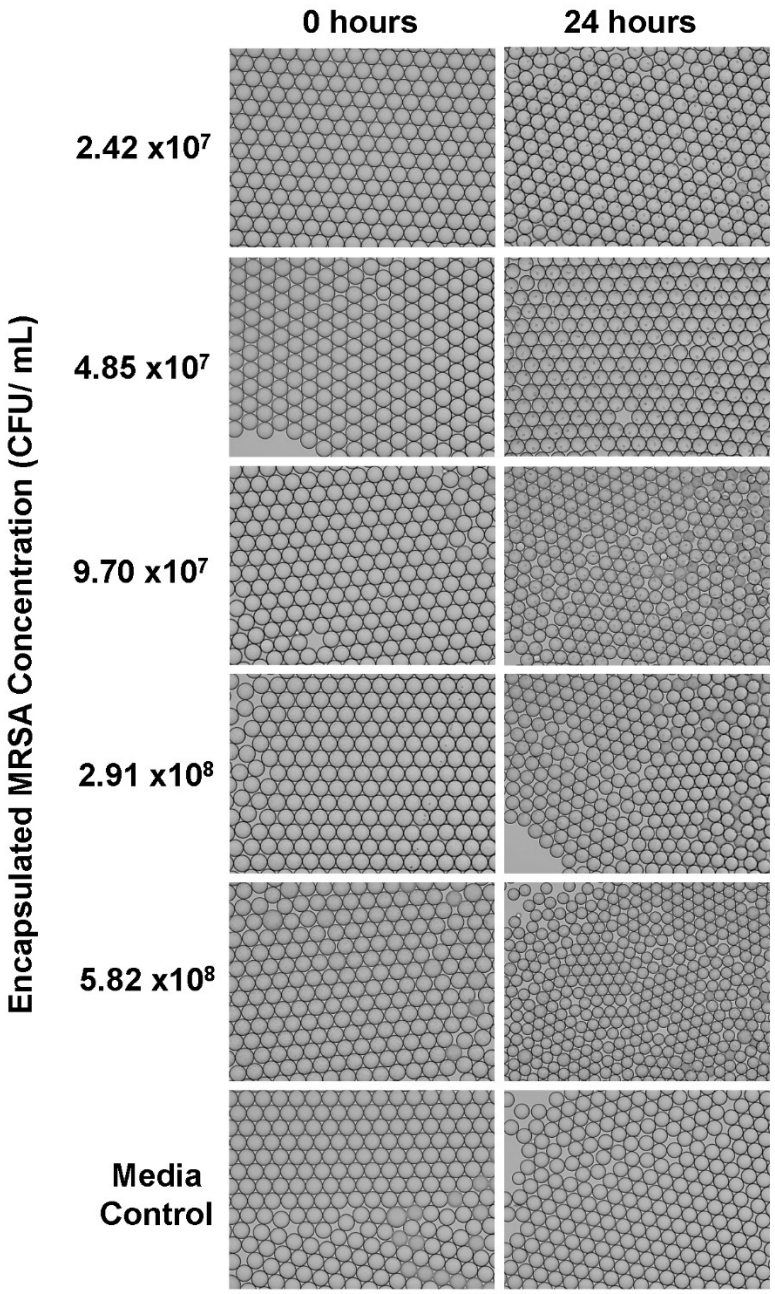

Figure 4.4. Image of MRSA proliferation inside 300pL droplets containing different starting encapsulated MRSA concentration (CFU/ mL) concentrations. x10 objective.

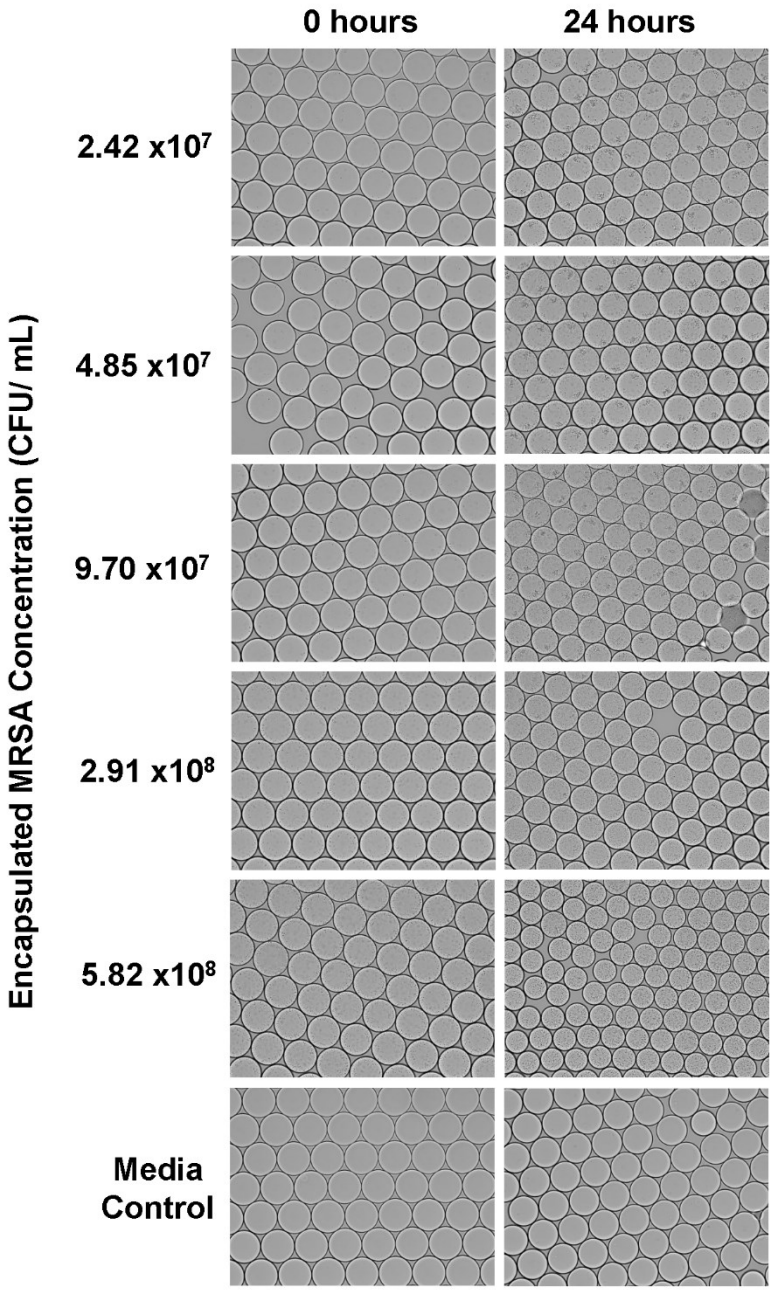

Figure 4.5. Image of MRSA proliferation inside 300pL droplets containing different starting encapsulated MRSA concentration (CFU/ mL) concentrations. x20 objective.

Appendix 4.6. 2-way ANOVA results of Change in MRSA Log CFU/mL after 24 hours of 300 pL droplets encapsulated with different starting CFU/mL concentration compared to 3 mL bulk culture. Multiple comparisons test was conducted between the 300 pL droplet culture and the 3 mL bulk control culture.

Tukey's multiple comparisons test	Significant?	Summary	Adjusted P Value
2.42 x107:300 pL Droplet Culture vs. 2.42 x107:3 mL Bulk Culture	Yes	**	0.01
2.42 x107:300 pL Droplet Culture vs. 4.85 x107:300 pL Droplet Culture	Yes	***	0.0002
2.42 x107:300 pL Droplet Culture vs. 4.85 x107:3 mL Bulk Culture	No	ns	>0.9999
2.42 x107:300 pL Droplet Culture vs. 9.70 x107:300 pL Droplet Culture	Yes	****	<0.0001
2.42 x107:300 pL Droplet Culture vs. 9.70 x107:3 mL Bulk Culture	Yes	****	<0.0001
2.42 x107:300 pL Droplet Culture vs. 2.91 x108:300 pL Droplet Culture	Yes	****	<0.0001
2.42 x107:300 pL Droplet Culture vs. 2.91 x108:3 mL Bulk Culture	Yes	****	<0.0001
2.42 x107:300 pL Droplet Culture vs. 5.82 x108:300 pL Droplet Culture	Yes	****	<0.0001
2.42 x107:300 pL Droplet Culture vs. 5.82 x108:3 mL Bulk Culture	Yes	****	<0.0001
2.42 x107:300 pL Droplet Culture vs. Media Control:300 pL Droplet Culture	Yes	****	<0.0001
2.42 x107:300 pL Droplet Culture vs. Media Control:3 mL Bulk Culture	Yes	****	<0.0001
2.42 x107:3 mL Bulk Culture vs. 4.85 x107:300 pL Droplet Culture	Yes	****	<0.0001
2.42 x107:3 mL Bulk Culture vs. 4.85 x107:3 mL Bulk Culture	No	ns	0.0631
2.42 x107:3 mL Bulk Culture vs. 9.70 x107:300 pL Droplet Culture	Yes	****	<0.0001
2.42 x107:3 mL Bulk Culture vs. 9.70 x107:3 mL Bulk Culture	Yes	****	<0.0001
2.42 x107:3 mL Bulk Culture vs. 2.91 x108:300 pL Droplet Culture	Yes	****	<0.0001
2.42 x107:3 mL Bulk Culture vs. 2.91 x108:3 mL Bulk Culture	Yes	****	<0.0001
2.42 x107:3 mL Bulk Culture vs. 5.82 x108:300 pL Droplet Culture	Yes	****	<0.0001
2.42 x107:3 mL Bulk Culture vs. 5.82 x108:3 mL Bulk Culture	Yes	****	<0.0001
2.42 x107:3 mL Bulk Culture vs. Media Control:300 pL Droplet Culture	Yes	****	<0.0001
2.42 x107:3 mL Bulk Culture vs. Media Control:3 mL Bulk Culture	Yes	****	<0.0001
4.85 x107:300 pL Droplet Culture vs. 4.85 x107:3 mL Bulk Culture	Yes	****	<0.0001
4.85 x107:300 pL Droplet Culture vs. 9.70 x107:300 pL Droplet Culture	Yes	*	0.0246
4.85 x107:300 pL Droplet Culture vs. 9.70 x107:3 mL Bulk Culture	No	ns	>0.9999
4.85 x107:300 pL Droplet Culture vs. 2.91 x108:300 pL Droplet Culture	No	ns	0.067
4.85 x107:300 pL Droplet Culture vs. 2.91 x108:3 mL Bulk Culture	Yes	****	<0.0001
4.85 x107:300 pL Droplet Culture vs. 5.82 x108:300 pL Droplet Culture	Yes	***	0.0003
4.85 x107:300 pL Droplet Culture vs. 5.82 x108:3 mL Bulk Culture	Yes	****	<0.0001
4.85 x107:300 pL Droplet Culture vs. Media Control:300 pL Droplet Culture	Yes	****	<0.0001
4.85 x107:300 pL Droplet Culture vs. Media Control:3 mL Bulk Culture	Yes	****	<0.0001
4.85 x107:3 mL Bulk Culture vs. 9.70 x107:300 pL Droplet Culture	Yes	****	<0.0001
4.85 x107:3 mL Bulk Culture vs. 9.70 x107:3 mL Bulk Culture	Yes	****	<0.0001

4.85 x107:3 mL Bulk Culture vs. 2.91 x108:300 pL Droplet Culture	Yes	****	<0.0001
4.85 x107:3 mL Bulk Culture vs. 2.91 x108:3 mL Bulk Culture	Yes	****	<0.0001
4.85 x107:3 mL Bulk Culture vs. 5.82 x108:300 pL Droplet Culture	Yes	****	<0.0001
4.85 x107:3 mL Bulk Culture vs. 5.82 x108:3 mL Bulk Culture	Yes	****	<0.0001
4.85 x107:3 mL Bulk Culture vs. Media Control:300 pL Droplet Culture	Yes	****	<0.0001
4.85 x107:3 mL Bulk Culture vs. Media Control:3 mL Bulk Culture	Yes	****	<0.0001
9.70 x107:300 pL Droplet Culture vs. 9.70 x107:3 mL Bulk Culture	No	ns	0.1178
9.70 x107:300 pL Droplet Culture vs. 2.91 x108:300 pL Droplet Culture	No	ns	>0.9999
9.70 x107:300 pL Droplet Culture vs. 2.91 x108:3 mL Bulk Culture	Yes	**	0.0019
9.70 x107:300 pL Droplet Culture vs. 5.82 x108:300 pL Droplet Culture	No	ns	0.9862
9.70 x107:300 pL Droplet Culture vs. 5.82 x108:3 mL Bulk Culture	Yes	****	<0.0001
9.70 x107:300 pL Droplet Culture vs. Media Control:300 pL Droplet Culture	Yes	****	<0.0001
9.70 x107:300 pL Droplet Culture vs. Media Control:3 mL Bulk Culture	Yes	****	<0.0001
9.70 x107:3 mL Bulk Culture vs. 2.91 x108:300 pL Droplet Culture	No	ns	0.2551
9.70 x107:3 mL Bulk Culture vs. 2.91 x108:3 mL Bulk Culture	Yes	****	<0.0001
9.70 x107:3 mL Bulk Culture vs. 5.82 x108:300 pL Droplet Culture	Yes	**	0.0028
9.70 x107:3 mL Bulk Culture vs. 5.82 x108:3 mL Bulk Culture	Yes	****	<0.0001
9.70 x107:3 mL Bulk Culture vs. Media Control:300 pL Droplet Culture	Yes	****	<0.0001
9.70 x107:3 mL Bulk Culture vs. Media Control:3 mL Bulk Culture	Yes	****	<0.0001
2.91 x108:300 pL Droplet Culture vs. 2.91 x108:3 mL Bulk Culture	Yes	***	0.0005
2.91 x108:300 pL Droplet Culture vs. 5.82 x108:300 pL Droplet Culture	No	ns	0.9164
2.91 x108:300 pL Droplet Culture vs. 5.82 x108:3 mL Bulk Culture	Yes	****	<0.0001
2.91 x108:300 pL Droplet Culture vs. Media Control:300 pL Droplet Culture	Yes	****	<0.0001
2.91 x108:300 pL Droplet Culture vs. Media Control:3 mL Bulk Culture	Yes	****	<0.0001
2.91 x108:3 mL Bulk Culture vs. 5.82 x108:300 pL Droplet Culture	No	ns	0.0876
2.91 x108:3 mL Bulk Culture vs. 5.82 x108:3 mL Bulk Culture	No	ns	0.9979
2.91 x108:3 mL Bulk Culture vs. Media Control:300 pL Droplet Culture	Yes	****	<0.0001
2.91 x108:3 mL Bulk Culture vs. Media Control:3 mL Bulk Culture	Yes	****	<0.0001
5.82 x108:300 pL Droplet Culture vs. 5.82 x108:3 mL Bulk Culture	Yes	**	0.0044
5.82 x108:300 pL Droplet Culture vs. Media Control:300 pL Droplet Culture	Yes	****	<0.0001
5.82 x108:300 pL Droplet Culture vs. Media Control:3 mL Bulk Culture	Yes	****	<0.0001
5.82 x108:3 mL Bulk Culture vs. Media Control:300 pL Droplet Culture	Yes	****	<0.0001
5.82 x108:3 mL Bulk Culture vs. Media Control:3 mL Bulk Culture	Yes	****	<0.0001
Media Control:300 pL Droplet Culture vs. Media Control:3 mL Bulk Culture	No	ns	>0.9999

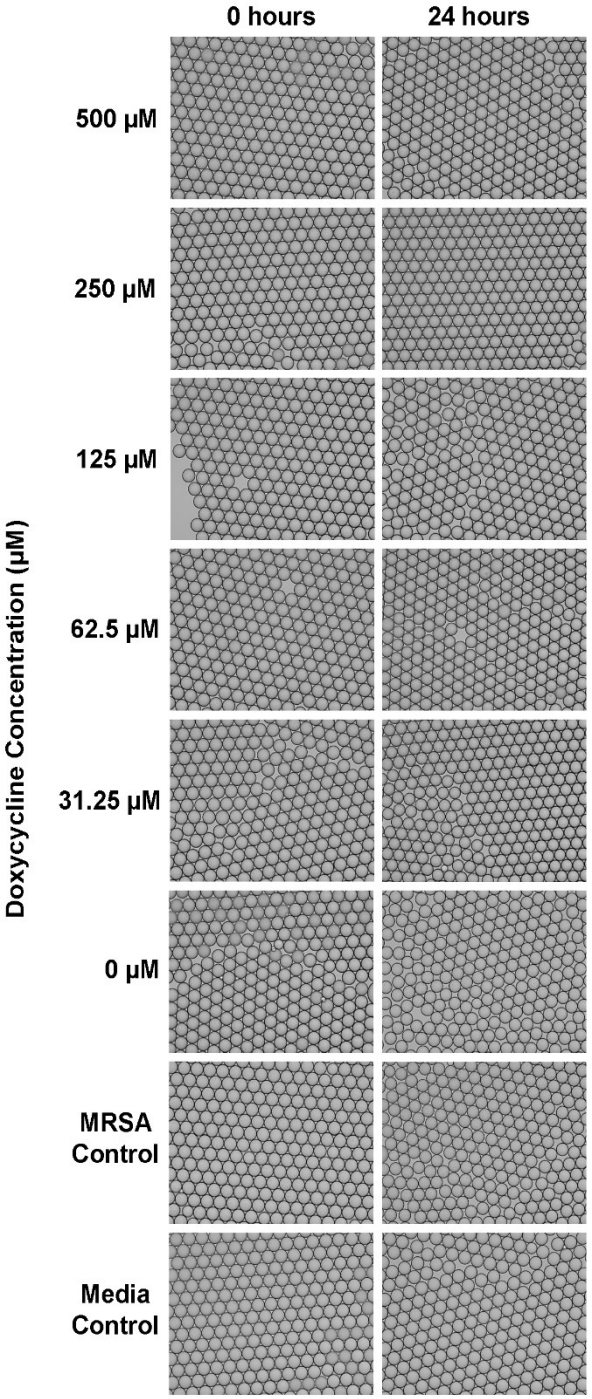

Figure 4.7. Image of MRSA proliferation inside 300pL droplets containing different doxycycline concentrations. x10 objective.

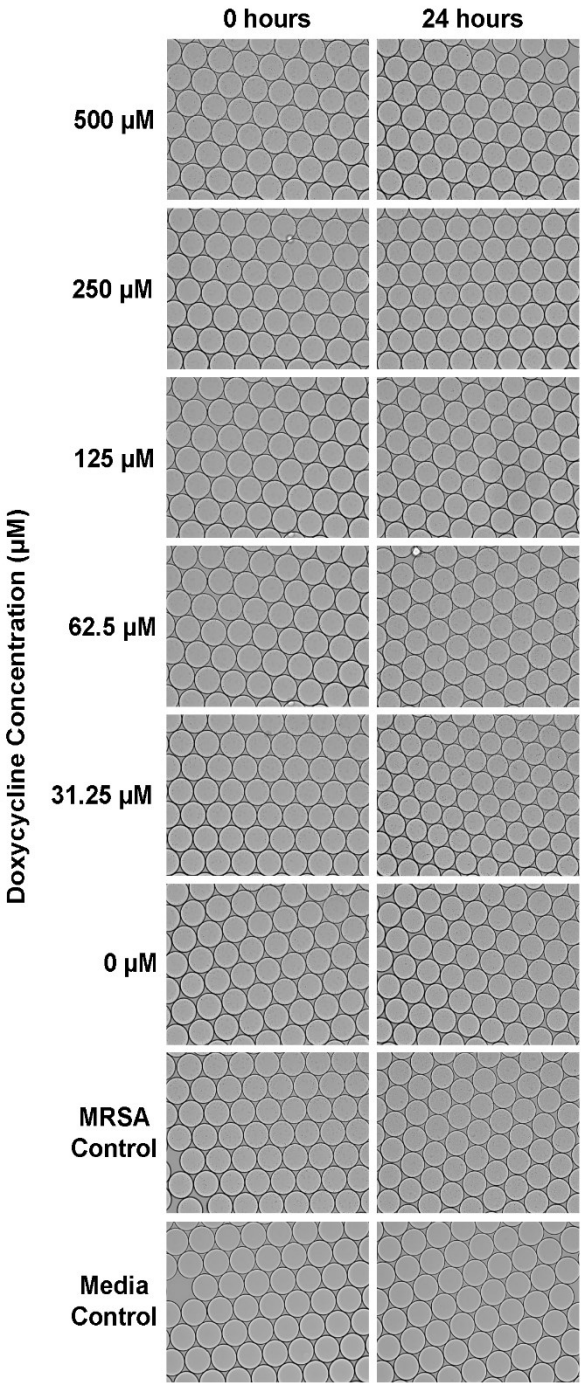

Figure 4.8. Image of MRSA proliferation inside 300pL droplets containing different doxycycline concentrations. x20 objective.

Appendix 4.9. 2-way ANOVA results of MRSA proliferation inside 300pL droplets containing different MD56 concentrations compared to 3 mL bulk culture. Multiple comparisons test was conducted between the 300 pL droplet culture and the 3 mL bulk control culture

Tukey's multiple comparisons test	Significant?	Summary	Adjusted P Value
500:300 pL Droplet Culture vs. 500:3 mL Bulk Culture	No	ns	>0.9999
500:300 pL Droplet Culture vs. 250:300 pL Droplet Culture	Yes	****	<0.0001
500:300 pL Droplet Culture vs. 250:3 mL Bulk Culture	No	ns	0.9725
500:300 pL Droplet Culture vs. 125:300 pL Droplet Culture	Yes	****	<0.0001
500:300 pL Droplet Culture vs. 125:3 mL Bulk Culture	Yes	****	<0.0001
500:300 pL Droplet Culture vs. 62.5:300 pL Droplet Culture	Yes	****	<0.0001
500:300 pL Droplet Culture vs. 62.5:3 mL Bulk Culture	Yes	****	<0.0001
500:300 pL Droplet Culture vs. 31.25:300 pL Droplet Culture	Yes	****	<0.0001
500:300 pL Droplet Culture vs. 31.25:3 mL Bulk Culture	Yes	****	<0.0001
500:300 pL Droplet Culture vs. 0:300 pL Droplet Culture	Yes	****	<0.0001
500:300 pL Droplet Culture vs. 0:3 mL Bulk Culture	Yes	****	<0.0001
500:300 pL Droplet Culture vs. MRSA Control:300 pL Droplet Culture	Yes	****	<0.0001
500:300 pL Droplet Culture vs. MRSA Control:3 mL Bulk Culture	Yes	****	<0.0001
500:300 pL Droplet Culture vs. Media Control:300 pL Droplet Culture	Yes	****	<0.0001
500:300 pL Droplet Culture vs. Media Control:3 mL Bulk Culture	Yes	****	<0.0001
500:3 mL Bulk Culture vs. 250:300 pL Droplet Culture	Yes	****	<0.0001
500:3 mL Bulk Culture vs. 250:3 mL Bulk Culture	No	ns	0.9995
500:3 mL Bulk Culture vs. 125:300 pL Droplet Culture	Yes	****	<0.0001
500:3 mL Bulk Culture vs. 125:3 mL Bulk Culture	Yes	****	<0.0001
500:3 mL Bulk Culture vs. 62.5:300 pL Droplet Culture	Yes	****	<0.0001
500:3 mL Bulk Culture vs. 62.5:3 mL Bulk Culture	Yes	****	<0.0001
500:3 mL Bulk Culture vs. 31.25:300 pL Droplet Culture	Yes	****	<0.0001
500:3 mL Bulk Culture vs. 31.25:3 mL Bulk Culture	Yes	****	<0.0001
500:3 mL Bulk Culture vs. 0:300 pL Droplet Culture	Yes	****	<0.0001
500:3 mL Bulk Culture vs. 0:3 mL Bulk Culture	Yes	****	<0.0001
500:3 mL Bulk Culture vs. MRSA Control:300 pL Droplet Culture	Yes	****	<0.0001
500:3 mL Bulk Culture vs. MRSA Control:3 mL Bulk Culture	Yes	****	<0.0001
500:3 mL Bulk Culture vs. Media Control:300 pL Droplet Culture	Yes	****	<0.0001
500:3 mL Bulk Culture vs. Media Control:3 mL Bulk Culture	Yes	****	<0.0001
250:300 pL Droplet Culture vs. 250:3 mL Bulk Culture	Yes	**	0.0041
250:300 pL Droplet Culture vs. 125:300 pL Droplet Culture	Yes	****	<0.0001
250:300 pL Droplet Culture vs. 125:3 mL Bulk Culture	Yes	***	0.0001
250:300 pL Droplet Culture vs. 62.5:300 pL Droplet Culture	Yes	****	<0.0001
250:300 pL Droplet Culture vs. 62.5:3 mL Bulk Culture	Yes	****	<0.0001
250:300 pL Droplet Culture vs. 31.25:300 pL Droplet Culture	Yes	****	<0.0001
250:300 pL Droplet Culture vs. 31.25:3 mL Bulk Culture	Yes	****	<0.0001
250:300 pL Droplet Culture vs. 0:300 pL Droplet Culture	Yes	****	<0.0001
250:300 pL Droplet Culture vs. 0:3 mL Bulk Culture	Yes	****	<0.0001

250:300 pL Droplet Culture vs. MRSA Control:300 pL Droplet Culture	Yes	****	<0.0001
250:300 pL Droplet Culture vs. MRSA Control:3 mL Bulk Culture	Yes	****	<0.0001
250:300 pL Droplet Culture vs. Media Control:300 pL Droplet Culture	Yes	****	<0.0001
250:300 pL Droplet Culture vs. Media Control:3 mL Bulk Culture	Yes	****	<0.0001
250:3 mL Bulk Culture vs. 125:300 pL Droplet Culture	Yes	****	<0.0001
250:3 mL Bulk Culture vs. 125:3 mL Bulk Culture	Yes	****	<0.0001
250:3 mL Bulk Culture vs. 62.5:300 pL Droplet Culture	Yes	****	<0.0001
250:3 mL Bulk Culture vs. 62.5:3 mL Bulk Culture	Yes	****	<0.0001
250:3 mL Bulk Culture vs. 31.25:300 pL Droplet Culture	Yes	****	<0.0001
250:3 mL Bulk Culture vs. 31.25:3 mL Bulk Culture	Yes	****	<0.0001
250:3 mL Bulk Culture vs. 0:300 pL Droplet Culture	Yes	****	<0.0001
250:3 mL Bulk Culture vs. 0:3 mL Bulk Culture	Yes	****	<0.0001
250:3 mL Bulk Culture vs. MRSA Control:300 pL Droplet Culture	Yes	****	<0.0001
250:3 mL Bulk Culture vs. MRSA Control:3 mL Bulk Culture	Yes	****	<0.0001
250:3 mL Bulk Culture vs. Media Control:300 pL Droplet Culture	Yes	****	<0.0001
250:3 mL Bulk Culture vs. Media Control:3 mL Bulk Culture	Yes	****	<0.0001
125:300 pL Droplet Culture vs. 125:3 mL Bulk Culture	No	ns	0.6821
125:300 pL Droplet Culture vs. 62.5:300 pL Droplet Culture	No	ns	0.9999
125:300 pL Droplet Culture vs. 62.5:3 mL Bulk Culture	No	ns	0.9651
125:300 pL Droplet Culture vs. 31.25:300 pL Droplet Culture	No	ns	0.9925
125:300 pL Droplet Culture vs. 31.25:3 mL Bulk Culture	No	ns	>0.9999
125:300 pL Droplet Culture vs. 0:300 pL Droplet Culture	No	ns	>0.9999
125:300 pL Droplet Culture vs. 0:3 mL Bulk Culture	No	ns	>0.9999
125:300 pL Droplet Culture vs. MRSA Control:300 pL Droplet Culture	No	ns	>0.9999
125:300 pL Droplet Culture vs. MRSA Control:3 mL Bulk Culture	No	ns	>0.9999
125:300 pL Droplet Culture vs. Media Control:300 pL Droplet Culture	No	ns	0.7683
125:300 pL Droplet Culture vs. Media Control:3 mL Bulk Culture	No	ns	0.7683
125:3 mL Bulk Culture vs. 62.5:300 pL Droplet Culture	No	ns	0.1239
125:3 mL Bulk Culture vs. 62.5:3 mL Bulk Culture	No	ns	>0.9999
125:3 mL Bulk Culture vs. 31.25:300 pL Droplet Culture	Yes	*	0.0389
125:3 mL Bulk Culture vs. 31.25:3 mL Bulk Culture	No	ns	0.9923
125:3 mL Bulk Culture vs. 0:300 pL Droplet Culture	No	ns	0.4083
125:3 mL Bulk Culture vs. 0:3 mL Bulk Culture	No	ns	0.9768
125:3 mL Bulk Culture vs. MRSA Control:300 pL Droplet Culture	No	ns	0.8549
125:3 mL Bulk Culture vs. MRSA Control:3 mL Bulk Culture	No	ns	0.9577
125:3 mL Bulk Culture vs. Media Control:300 pL Droplet Culture	No	ns	>0.9999
125:3 mL Bulk Culture vs. Media Control:3 mL Bulk Culture	No	ns	>0.9999
62.5:300 pL Droplet Culture vs. 62.5:3 mL Bulk Culture	No	ns	0.4441
62.5:300 pL Droplet Culture vs. 31.25:300 pL Droplet Culture	No	ns	>0.9999
62.5:300 pL Droplet Culture vs. 31.25:3 mL Bulk Culture	No	ns	0.9117

62.5:300 pL Droplet Culture vs. 0:300 pL Droplet Culture	No	ns	>0.9999
62.5:300 pL Droplet Culture vs. 0:3 mL Bulk Culture	No	ns	0.959
62.5:300 pL Droplet Culture vs. MRSA Control:300 pL Droplet Culture	No	ns	0.9974
62.5:300 pL Droplet Culture vs. MRSA Control:3 mL Bulk Culture	No	ns	0.9776
62.5:300 pL Droplet Culture vs. Media Control:300 pL Droplet Culture	No	ns	0.17
62.5:300 pL Droplet Culture vs. Media Control:3 mL Bulk Culture	No	ns	0.17
62.5:3 mL Bulk Culture vs. 31.25:300 pL Droplet Culture	No	ns	0.2
62.5:3 mL Bulk Culture vs. 31.25:3 mL Bulk Culture	No	ns	>0.9999
62.5:3 mL Bulk Culture vs. 0:300 pL Droplet Culture	No	ns	0.8296
62.5:3 mL Bulk Culture vs. 0:3 mL Bulk Culture	No	ns	>0.9999
62.5:3 mL Bulk Culture vs. MRSA Control:300 pL Droplet Culture	No	ns	0.9945
62.5:3 mL Bulk Culture vs. MRSA Control:3 mL Bulk Culture	No	ns	0.9997
62.5:3 mL Bulk Culture vs. Media Control:300 pL Droplet Culture	No	ns	>0.9999
62.5:3 mL Bulk Culture vs. Media Control:3 mL Bulk Culture	No	ns	>0.9999
31.25:300 pL Droplet Culture vs. 31.25:3 mL Bulk Culture	No	ns	0.6843
31.25:300 pL Droplet Culture vs. 0:300 pL Droplet Culture	No	ns	0.9998
31.25:300 pL Droplet Culture vs. 0:3 mL Bulk Culture	No	ns	0.7928
31.25:300 pL Droplet Culture vs. MRSA Control:300 pL Droplet Culture	No	ns	0.9565
31.25:300 pL Droplet Culture vs. MRSA Control:3 mL Bulk Culture	No	ns	0.8522
31.25:300 pL Droplet Culture vs. Media Control:300 pL Droplet Culture	No	ns	0.0572
31.25:300 pL Droplet Culture vs. Media Control:3 mL Bulk Culture	No	ns	0.0572
31.25:3 mL Bulk Culture vs. 0:300 pL Droplet Culture	No	ns	0.9972
31.25:3 mL Bulk Culture vs. 0:3 mL Bulk Culture	No	ns	>0.9999
31.25:3 mL Bulk Culture vs. MRSA Control:300 pL Droplet Culture	No	ns	>0.9999
31.25:3 mL Bulk Culture vs. MRSA Control:3 mL Bulk Culture	No	ns	>0.9999
31.25:3 mL Bulk Culture vs. Media Control:300 pL Droplet Culture	No	ns	0.9973
31.25:3 mL Bulk Culture vs. Media Control:3 mL Bulk Culture	No	ns	0.9973
0:300 pL Droplet Culture vs. 0:3 mL Bulk Culture	No	ns	0.9995
0:300 pL Droplet Culture vs. MRSA Control:300 pL Droplet Culture	No	ns	>0.9999
0:300 pL Droplet Culture vs. MRSA Control:3 mL Bulk Culture	No	ns	0.9999
0:300 pL Droplet Culture vs. Media Control:300 pL Droplet Culture	No	ns	0.5001
0:300 pL Droplet Culture vs. Media Control:3 mL Bulk Culture	No	ns	0.5001
0:3 mL Bulk Culture vs. MRSA Control:300 pL Droplet Culture	No	ns	>0.9999
0:3 mL Bulk Culture vs. MRSA Control:3 mL Bulk Culture	No	ns	>0.9999
0:3 mL Bulk Culture vs. Media Control:300 pL Droplet Culture	No	ns	0.9899
0:3 mL Bulk Culture vs. Media Control:3 mL Bulk Culture	No	ns	0.9899
MRSA Control:300 pL Droplet Culture vs. MRSA Control:3 mL Bulk Culture	No	ns	>0.9999

MRSA Control:300 pL Droplet Culture vs. Media Control:300 pL Droplet Culture	No	ns	0.9104
MRSA Control:300 pL Droplet Culture vs. Media Control:3 mL Bulk Culture	No	ns	0.9104
MRSA Control:3 mL Bulk Culture vs. Media Control:300 pL Droplet Culture	No	ns	0.9795
MRSA Control:3 mL Bulk Culture vs. Media Control:3 mL Bulk Culture	No	ns	0.9795
Media Control:300 pL Droplet Culture vs. Media Control:3 mL Bulk Culture	No	ns	>0.9999

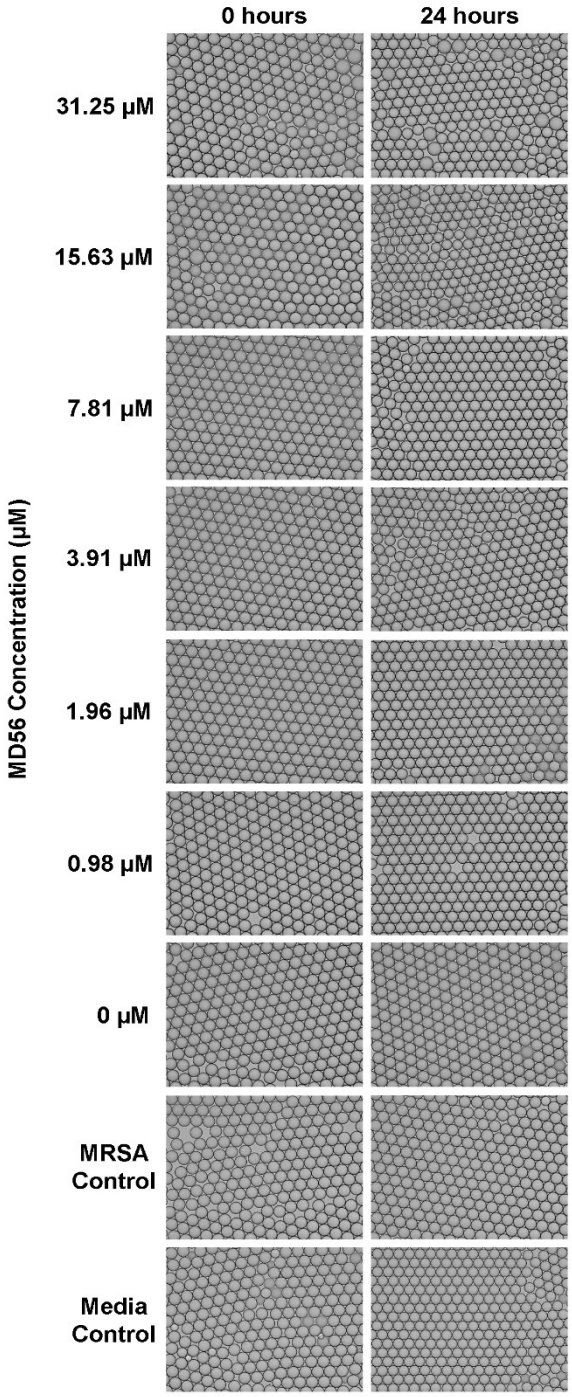

Figure 4.10. Image of MRSA proliferation inside 300pL droplets containing different MD56 concentrations. x10 objective.

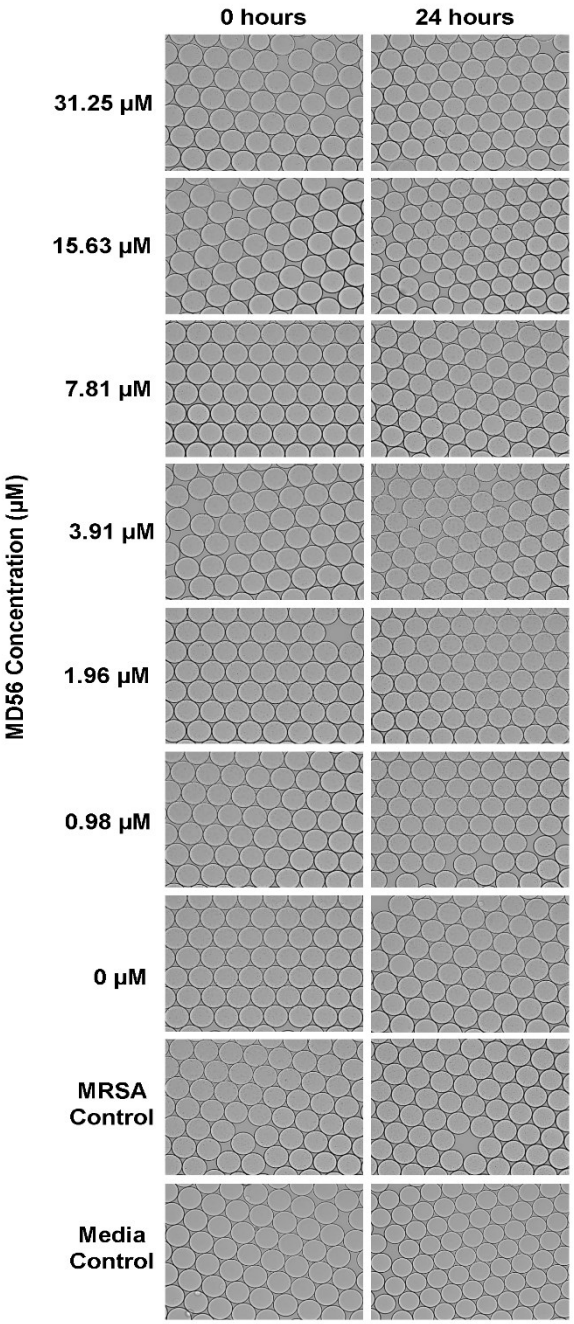

Appendix 4.11. Image of MRSA proliferation inside 300pL droplets containing different MD56 concentrations. x20 objective.

Appendix 4.12. One-way ANOVA results of MRSA proliferation inside 300pL droplets containing different MD56 concentrations. Multiple comparisons test was conducted between the 300 pL droplet culture and the 3 mL bulk control culture.

Dunnett's multiple comparisons test	Significant?	Summary	Adjusted P Value
500 vs. 250	No	ns	0.6516
500 vs. 125	No	ns	0.2279
500 vs. 62.5	Yes	*	0.0432
500 vs. 31.25	No	ns	0.3408
500 vs. 15.63	No	ns	0.3699
500 vs. 7.81	No	ns	0.4317
500 vs. 3.91	No	ns	0.3268
500 vs. 1.95	No	ns	0.5314
500 vs. 0.98	Yes	****	<0.0001
500 vs. 0.49	Yes	****	<0.0001
500 vs. 0.24	Yes	****	<0.0001
500 vs. 0.12	Yes	****	<0.0001
500 vs. 0	Yes	****	<0.0001
500 vs. MRSA Control	Yes	****	<0.0001
250 vs. 125	No	ns	>0.9999
250 vs. 62.5	No	ns	0.9609
250 vs. 31.25	No	ns	>0.9999
250 vs. 15.63	No	ns	>0.9999
250 vs. 7.81	No	ns	>0.9999
250 vs. 3.91	No	ns	>0.9999
250 vs. 1.95	Yes	**	0.0049
250 vs. 0.98	Yes	****	<0.0001
250 vs. 0.49	Yes	****	<0.0001
250 vs. 0.24	Yes	****	<0.0001
250 vs. 0.12	Yes	****	<0.0001
250 vs. 0	Yes	****	<0.0001
250 vs. MRSA Control	Yes	****	<0.0001
125 vs. 62.5	No	ns	>0.9999
125 vs. 31.25	No	ns	>0.9999
125 vs. 15.63	No	ns	>0.9999
125 vs. 7.81	No	ns	>0.9999
125 vs. 3.91	No	ns	>0.9999
125 vs. 1.95	Yes	***	0.0007
125 vs. 0.98	Yes	****	<0.0001
125 vs. 0.49	Yes	****	<0.0001
125 vs. 0.24	Yes	****	<0.0001
125 vs. 0.12	Yes	****	<0.0001
125 vs. 0	Yes	****	<0.0001
125 vs. MRSA Control	Yes	****	<0.0001
62.5 vs. 31.25	No	ns	0.999
62.5 vs. 15.63	No	ns	0.9983
62.5 vs. 7.81	No	ns	0.9957
62.5 vs. 3.91	No	ns	0.9992
62.5 vs. 1.95	Yes	****	<0.0001

62.5 vs. 0.98	Yes	****	<0.0001
62.5 vs. 0.49	Yes	****	<0.0001
62.5 vs. 0.24	Yes	****	<0.0001
62.5 vs. 0.12	Yes	****	<0.0001
62.5 vs. 0	Yes	****	<0.0001
62.5 vs. MRSA Control	Yes	****	<0.0001
31.25 vs. 15.63	No	ns	>0.9999
31.25 vs. 7.81	No	ns	>0.9999
31.25 vs. 3.91	No	ns	>0.9999
31.25 vs. 1.95	Yes	**	0.0013
31.25 vs. 0.98	Yes	****	<0.0001
31.25 vs. 0.49	Yes	****	<0.0001
31.25 vs. 0.24	Yes	****	<0.0001
31.25 vs. 0.12	Yes	****	<0.0001
31.25 vs. 0	Yes	****	<0.0001
31.25 vs. MRSA Control	Yes	****	<0.0001
15.63 vs. 7.81	No	ns	>0.9999
15.63 vs. 3.91	No	ns	>0.9999
15.63 vs. 1.95	Yes	**	0.0015
15.63 vs. 0.98	Yes	****	<0.0001
15.63 vs. 0.49	Yes	****	<0.0001
15.63 vs. 0.24	Yes	****	<0.0001
15.63 vs. 0.12	Yes	****	<0.0001
15.63 vs. 0	Yes	****	<0.0001
15.63 vs. MRSA Control	Yes	****	<0.0001
7.81 vs. 3.91	No	ns	>0.9999
7.81 vs. 1.95	Yes	**	0.002
7.81 vs. 0.98	Yes	****	<0.0001
7.81 vs. 0.49	Yes	****	<0.0001
7.81 vs. 0.24	Yes	****	<0.0001
7.81 vs. 0.12	Yes	****	<0.0001
7.81 vs. 0	Yes	****	<0.0001
7.81 vs. MRSA Control	Yes	****	<0.0001
3.91 vs. 1.95	Yes	**	0.0012
3.91 vs. 0.98	Yes	****	<0.0001
3.91 vs. 0.49	Yes	****	<0.0001
3.91 vs. 0.24	Yes	****	<0.0001
3.91 vs. 0.12	Yes	****	<0.0001
3.91 vs. 0	Yes	****	<0.0001
3.91 vs. MRSA Control	Yes	****	<0.0001
1.95 vs. 0.98	Yes	****	<0.0001
1.95 vs. 0.49	Yes	****	<0.0001
1.95 vs. 0.24	Yes	****	<0.0001
1.95 vs. 0.12	Yes	****	<0.0001
1.95 vs. 0	Yes	****	<0.0001
1.95 vs. MRSA Control	Yes	****	<0.0001
0.98 vs. 0.49	No	ns	0.9204
0.98 vs. 0.24	No	ns	0.9025

0.98 vs. 0.12	No	ns	0.9431
0.98 vs. 0	No	ns	0.8351
0.98 vs. MRSA Control	Yes	****	<0.0001
0.49 vs. 0.24	No	ns	>0.9999
0.49 vs. 0.12	No	ns	>0.9999
0.49 vs. 0	No	ns	>0.9999
0.49 vs. MRSA Control	Yes	****	<0.0001
0.24 vs. 0.12	No	ns	>0.9999
0.24 vs. 0	No	ns	>0.9999
0.24 vs. MRSA Control	Yes	****	<0.0001
0.12 vs. 0	No	ns	>0.9999
0.12 vs. MRSA Control	Yes	****	<0.0001
0 vs. MRSA Control	Yes	****	<0.0001

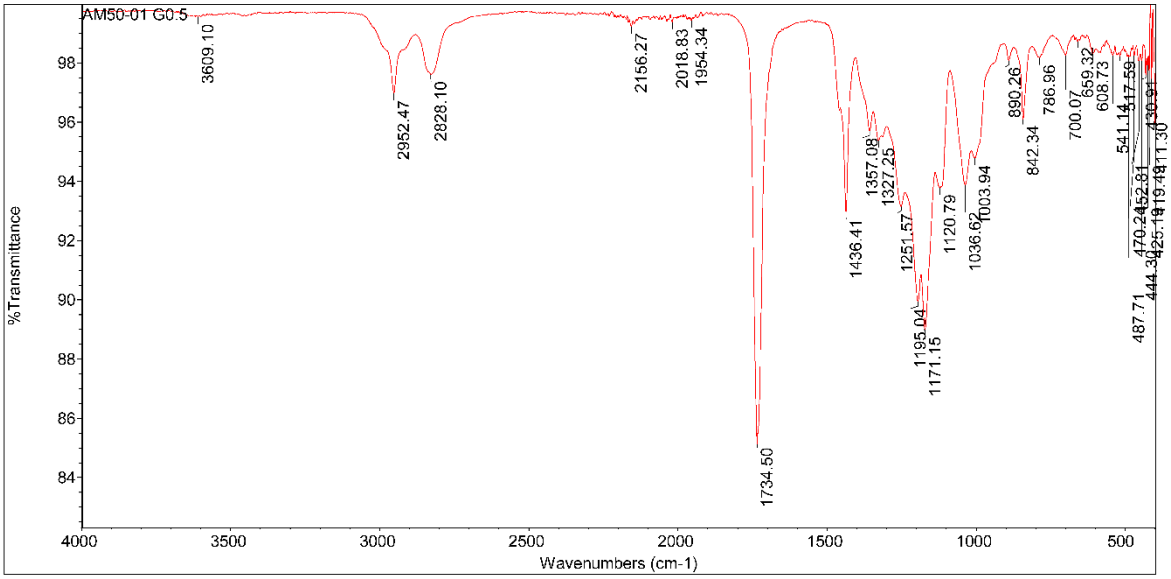

Appendix 5.1. IR Spectra for G0.5 PAMAM dendrimer with 4 terminal OMe groups.

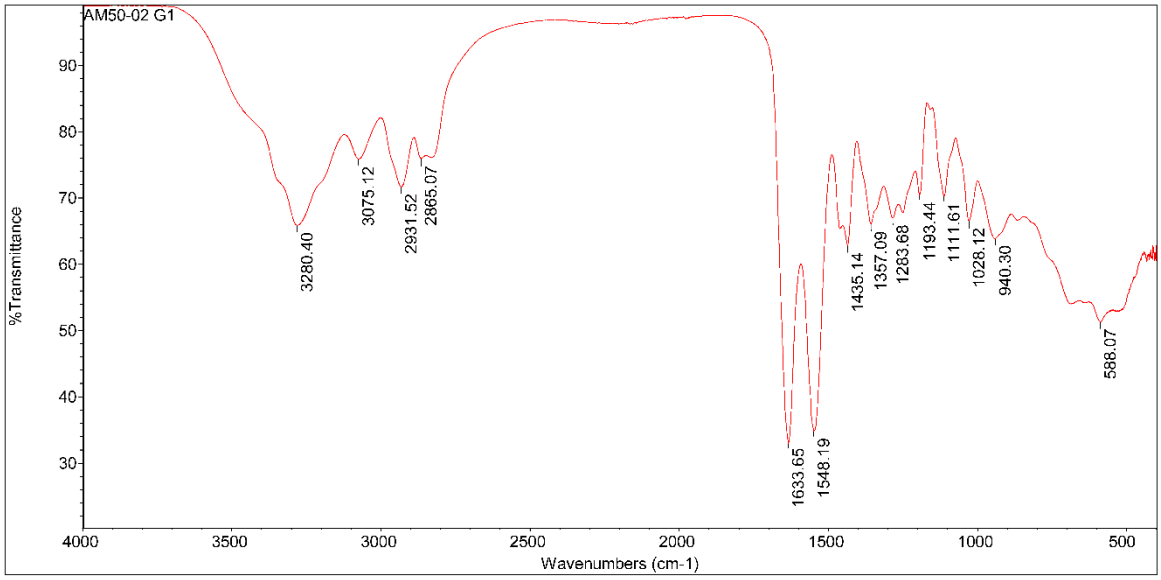

Appendix 5.2. IR Spectra for G1.0 PAMAM dendrimer with 4 terminal amine groups.

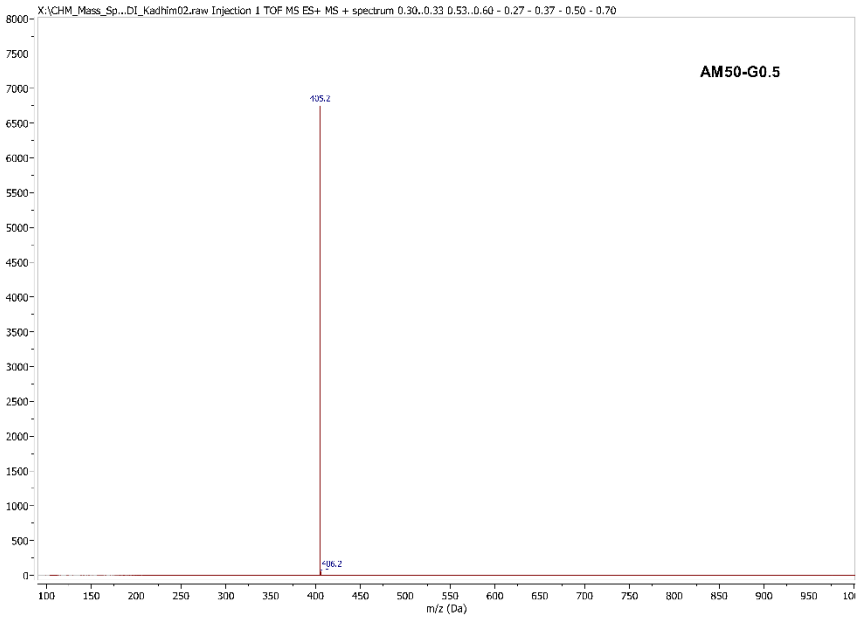

Appendix 5.3. Mass spectrometry of G0.5 PAMAM dendrimer with 4 terminal OMe groups.

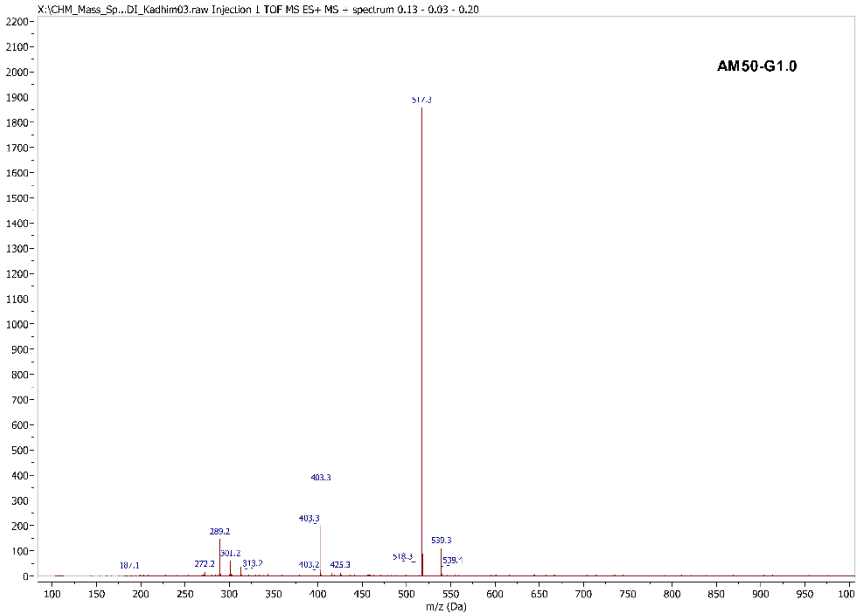

Appendix 5.4. Mass spectrometry of G1.0 PAMAM dendrimer with 4 terminal amine groups.

Appendix 5.5. 2- Way ANOVA of toxicity of PicoSurf® to *Pseudomonas aeruginosa* after 20 hours.

Tukey's multiple comparisons test	Significant?	Summary	Adjusted P Value
0 hr:5% vs. 0 hr:2%	No	ns	>0.9999
0 hr:5% vs. 0 hr:1%	No	ns	>0.9999
0 hr:5% vs. 0 hr:0%	No	ns	>0.9999
0 hr:5% vs. 0 hr:Pseudomonas aeruginosa Only	No	ns	>0.9999
0 hr:5% vs. 20 hr:5%	Yes	****	<0.0001
0 hr:5% vs. 20 hr:2%	Yes	****	<0.0001
0 hr:5% vs. 20 hr:1%	Yes	****	<0.0001
0 hr:5% vs. 20 hr:0%	Yes	****	<0.0001
0 hr:5% vs. 20 hr:Pseudomonas aeruginosa Only	Yes	****	<0.0001
0 hr:2% vs. 0 hr:1%	No	ns	>0.9999
0 hr:2% vs. 0 hr:0%	No	ns	>0.9999
0 hr:2% vs. 0 hr:Pseudomonas aeruginosa Only	No	ns	>0.9999
0 hr:2% vs. 20 hr:5%	Yes	****	<0.0001
0 hr:2% vs. 20 hr:2%	Yes	****	<0.0001
0 hr:2% vs. 20 hr:1%	Yes	****	<0.0001
0 hr:2% vs. 20 hr:0%	Yes	****	<0.0001
0 hr:2% vs. 20 hr:Pseudomonas aeruginosa Only	Yes	****	<0.0001
0 hr:1% vs. 0 hr:0%	No	ns	>0.9999
0 hr:1% vs. 0 hr:Pseudomonas aeruginosa Only	No	ns	>0.9999
0 hr:1% vs. 20 hr:5%	Yes	****	<0.0001
0 hr:1% vs. 20 hr:2%	Yes	****	<0.0001
0 hr:1% vs. 20 hr:1%	Yes	****	<0.0001
0 hr:1% vs. 20 hr:0%	Yes	****	<0.0001
0 hr:1% vs. 20 hr:Pseudomonas aeruginosa Only	Yes	****	<0.0001
0 hr:0% vs. 0 hr:Pseudomonas aeruginosa Only	No	ns	>0.9999
0 hr:0% vs. 20 hr:5%	Yes	****	<0.0001
0 hr:0% vs. 20 hr:2%	Yes	****	<0.0001
0 hr:0% vs. 20 hr:1%	Yes	****	<0.0001
0 hr:0% vs. 20 hr:0%	Yes	****	<0.0001
0 hr:0% vs. 20 hr:Pseudomonas aeruginosa Only	Yes	****	<0.0001
0 hr:Pseudomonas aeruginosa Only vs. 20 hr:5%	Yes	****	<0.0001
0 hr:Pseudomonas aeruginosa Only vs. 20 hr:2%	Yes	****	<0.0001
0 hr:Pseudomonas aeruginosa Only vs. 20 hr:1%	Yes	****	<0.0001
0 hr:Pseudomonas aeruginosa Only vs. 20 hr:0%	Yes	****	<0.0001
0 hr:Pseudomonas aeruginosa Only vs. 20 hr:Pseudomonas aeruginosa Only	Yes	****	<0.0001
20 hr:5% vs. 20 hr:2%	No	ns	>0.9999
20 hr:5% vs. 20 hr:1%	No	ns	0.9993
20 hr:5% vs. 20 hr:0%	Yes	****	<0.0001
20 hr:5% vs. 20 hr:Pseudomonas aeruginosa Only	Yes	****	<0.0001
20 hr:2% vs. 20 hr:1%	No	ns	0.969
20 hr:2% vs. 20 hr:0%	Yes	****	<0.0001
20 hr:2% vs. 20 hr:Pseudomonas aeruginosa Only	Yes	****	<0.0001
20 hr:1% vs. 20 hr:0%	Yes	****	<0.0001
20 hr:1% vs. 20 hr:Pseudomonas aeruginosa Only	Yes	****	<0.0001
20 hr:0% vs. 20 hr:Pseudomonas aeruginosa Only	Yes	*	0.0252

Appendix 5.6. 2- Way ANOVA of toxicity of FluoSurf™ to *Pseudomonas aeruginosa* after 20 hours.

Tukey's multiple comparisons test	Significant?	Summary	Adjusted P Value
0 hr:3% vs. 0 hr:2%	No	ns	>0.9999
0 hr:3% vs. 0 hr:1%	No	ns	>0.9999
0 hr:3% vs. 0 hr:0%	No	ns	>0.9999
0 hr:3% vs. 0 hr:Pseudomonas aeruginosa Only	No	ns	>0.9999
0 hr:3% vs. 20 hr:3%	Yes	****	<0.0001
0 hr:3% vs. 20 hr:2%	Yes	****	<0.0001
0 hr:3% vs. 20 hr:1%	Yes	****	<0.0001
0 hr:3% vs. 20 hr:0%	Yes	***	0.0001
0 hr:3% vs. 20 hr:Pseudomonas aeruginosa Only	Yes	*	0.0115
0 hr:2% vs. 0 hr:1%	No	ns	>0.9999
0 hr:2% vs. 0 hr:0%	No	ns	>0.9999
0 hr:2% vs. 0 hr:Pseudomonas aeruginosa Only	No	ns	>0.9999
0 hr:2% vs. 20 hr:3%	Yes	****	<0.0001
0 hr:2% vs. 20 hr:2%	Yes	****	<0.0001
0 hr:2% vs. 20 hr:1%	Yes	****	<0.0001
0 hr:2% vs. 20 hr:0%	Yes	****	<0.0001
0 hr:2% vs. 20 hr:Pseudomonas aeruginosa Only	Yes	**	0.0094
0 hr:1% vs. 0 hr:0%	No	ns	>0.9999
0 hr:1% vs. 0 hr:Pseudomonas aeruginosa Only	No	ns	>0.9999
0 hr:1% vs. 20 hr:3%	Yes	****	<0.0001
0 hr:1% vs. 20 hr:2%	Yes	****	<0.0001
0 hr:1% vs. 20 hr:1%	Yes	****	<0.0001
0 hr:1% vs. 20 hr:0%	Yes	****	<0.0001
0 hr:1% vs. 20 hr:Pseudomonas aeruginosa Only	Yes	**	0.0094
0 hr:0% vs. 0 hr:Pseudomonas aeruginosa Only	No	ns	>0.9999
0 hr:0% vs. 20 hr:3%	Yes	****	<0.0001
0 hr:0% vs. 20 hr:2%	Yes	****	<0.0001
0 hr:0% vs. 20 hr:1%	Yes	****	<0.0001
0 hr:0% vs. 20 hr:0%	Yes	****	<0.0001
0 hr:0% vs. 20 hr:Pseudomonas aeruginosa Only	Yes	**	0.0093
0 hr:Pseudomonas aeruginosa Only vs. 20 hr:3%	Yes	****	<0.0001
0 hr:Pseudomonas aeruginosa Only vs. 20 hr:2%	Yes	****	<0.0001
0 hr:Pseudomonas aeruginosa Only vs. 20 hr:1%	Yes	****	<0.0001
0 hr:Pseudomonas aeruginosa Only vs. 20 hr:0%	Yes	****	<0.0001
0 hr:Pseudomonas aeruginosa Only vs. 20 hr:Pseudomonas aeruginosa Only	Yes	*	0.0102
20 hr:3% vs. 20 hr:2%	No	ns	>0.9999
20 hr:3% vs. 20 hr:1%	No	ns	0.2789
20 hr:3% vs. 20 hr:0%	Yes	****	<0.0001
20 hr:3% vs. 20 hr:Pseudomonas aeruginosa Only	Yes	****	<0.0001
20 hr:2% vs. 20 hr:1%	No	ns	0.2619
20 hr:2% vs. 20 hr:0%	Yes	****	<0.0001
20 hr:2% vs. 20 hr:Pseudomonas aeruginosa Only	Yes	****	<0.0001
20 hr:1% vs. 20 hr:0%	Yes	***	0.0001
20 hr:1% vs. 20 hr:Pseudomonas aeruginosa Only	Yes	****	<0.0001
20 hr:0% vs. 20 hr:Pseudomonas aeruginosa Only	No	ns	0.5167

Appendix 5.7. 2- Way ANOVA of toxicity of AM50-06 to *Pseudomonas aeruginosa* after 20 hours.

Tukey's multiple comparisons test	Significant?	Summary	Adjusted P Value
0 hr:5% vs. 0 hr:2%	No	ns	>0.9999
0 hr:5% vs. 0 hr:1%	No	ns	>0.9999
0 hr:5% vs. 0 hr:0%	No	ns	>0.9999
0 hr:5% vs. 0 hr:Pseudomonas aeruginosa Only	No	ns	>0.9999
0 hr:5% vs. 20 hr:5%	Yes	****	<0.0001
0 hr:5% vs. 20 hr:2%	Yes	****	<0.0001
0 hr:5% vs. 20 hr:1%	Yes	****	<0.0001
0 hr:5% vs. 20 hr:0%	Yes	****	<0.0001
0 hr:5% vs. 20 hr:Pseudomonas aeruginosa Only	Yes	**	0.0019
0 hr:2% vs. 0 hr:1%	No	ns	>0.9999
0 hr:2% vs. 0 hr:0%	No	ns	>0.9999
0 hr:2% vs. 0 hr:Pseudomonas aeruginosa Only	No	ns	>0.9999
0 hr:2% vs. 20 hr:5%	Yes	****	<0.0001
0 hr:2% vs. 20 hr:2%	Yes	****	<0.0001
0 hr:2% vs. 20 hr:1%	Yes	****	<0.0001
0 hr:2% vs. 20 hr:0%	Yes	****	<0.0001
0 hr:2% vs. 20 hr:Pseudomonas aeruginosa Only	Yes	**	0.0018
0 hr:1% vs. 0 hr:0%	No	ns	>0.9999
0 hr:1% vs. 0 hr:Pseudomonas aeruginosa Only	No	ns	>0.9999
0 hr:1% vs. 20 hr:5%	Yes	****	<0.0001
0 hr:1% vs. 20 hr:2%	Yes	****	<0.0001
0 hr:1% vs. 20 hr:1%	Yes	****	<0.0001
0 hr:1% vs. 20 hr:0%	Yes	****	<0.0001
0 hr:1% vs. 20 hr:Pseudomonas aeruginosa Only	Yes	**	0.0016
0 hr:0% vs. 0 hr:Pseudomonas aeruginosa Only	No	ns	>0.9999
0 hr:0% vs. 20 hr:5%	Yes	****	<0.0001
0 hr:0% vs. 20 hr:2%	Yes	****	<0.0001
0 hr:0% vs. 20 hr:1%	Yes	****	<0.0001
0 hr:0% vs. 20 hr:0%	Yes	****	<0.0001
0 hr:0% vs. 20 hr:Pseudomonas aeruginosa Only	Yes	**	0.0014
0 hr:Pseudomonas aeruginosa Only vs. 20 hr:5%	Yes	****	<0.0001
0 hr:Pseudomonas aeruginosa Only vs. 20 hr:2%	Yes	****	<0.0001
0 hr:Pseudomonas aeruginosa Only vs. 20 hr:1%	Yes	****	<0.0001
0 hr:Pseudomonas aeruginosa Only vs. 20 hr:0%	Yes	****	<0.0001
0 hr:Pseudomonas aeruginosa Only vs. 20 hr:Pseudomonas aeruginosa Only	Yes	**	0.0016
20 hr:5% vs. 20 hr:2%	No	ns	0.3292
20 hr:5% vs. 20 hr:1%	No	ns	0.1702
20 hr:5% vs. 20 hr:0%	Yes	****	<0.0001
20 hr:5% vs. 20 hr:Pseudomonas aeruginosa Only	Yes	****	<0.0001
20 hr:2% vs. 20 hr:1%	No	ns	>0.9999
20 hr:2% vs. 20 hr:0%	Yes	***	0.0005
20 hr:2% vs. 20 hr:Pseudomonas aeruginosa Only	Yes	****	<0.0001
20 hr:1% vs. 20 hr:0%	Yes	**	0.0013
20 hr:1% vs. 20 hr:Pseudomonas aeruginosa Only	Yes	****	<0.0001
20 hr:0% vs. 20 hr:Pseudomonas aeruginosa Only	No	ns	0.2901

Appendix 5.8. 2- Way ANOVA of toxicity of AM50-08 to *Pseudomonas aeruginosa* after 20 hours.

Tukey's multiple comparisons test	Significant?	Summary	Adjusted P Value
0 hr:5% vs. 0 hr:2%	No	ns	>0.9999
0 hr:5% vs. 0 hr:1%	No	ns	>0.9999
0 hr:5% vs. 0 hr:0%	No	ns	>0.9999
0 hr:5% vs. 0 hr:Pseudomonas aeruginosa Only	No	ns	>0.9999
0 hr:5% vs. 20 hr:5%	Yes	****	<0.0001
0 hr:5% vs. 20 hr:2%	Yes	****	<0.0001
0 hr:5% vs. 20 hr:1%	Yes	****	<0.0001
0 hr:5% vs. 20 hr:0%	Yes	****	<0.0001
0 hr:5% vs. 20 hr:Pseudomonas aeruginosa Only	Yes	****	<0.0001
0 hr:2% vs. 0 hr:1%	No	ns	>0.9999
0 hr:2% vs. 0 hr:0%	No	ns	>0.9999
0 hr:2% vs. 0 hr:Pseudomonas aeruginosa Only	No	ns	>0.9999
0 hr:2% vs. 20 hr:5%	Yes	****	<0.0001
0 hr:2% vs. 20 hr:2%	Yes	****	<0.0001
0 hr:2% vs. 20 hr:1%	Yes	****	<0.0001
0 hr:2% vs. 20 hr:0%	Yes	****	<0.0001
0 hr:2% vs. 20 hr:Pseudomonas aeruginosa Only	Yes	****	<0.0001
0 hr:1% vs. 0 hr:0%	No	ns	>0.9999
0 hr:1% vs. 0 hr:Pseudomonas aeruginosa Only	No	ns	>0.9999
0 hr:1% vs. 20 hr:5%	Yes	****	<0.0001
0 hr:1% vs. 20 hr:2%	Yes	****	<0.0001
0 hr:1% vs. 20 hr:1%	Yes	****	<0.0001
0 hr:1% vs. 20 hr:0%	Yes	****	<0.0001
0 hr:1% vs. 20 hr:Pseudomonas aeruginosa Only	Yes	****	<0.0001
0 hr:0% vs. 0 hr:Pseudomonas aeruginosa Only	No	ns	>0.9999
0 hr:0% vs. 20 hr:5%	Yes	****	<0.0001
0 hr:0% vs. 20 hr:2%	Yes	****	<0.0001
0 hr:0% vs. 20 hr:1%	Yes	****	<0.0001
0 hr:0% vs. 20 hr:0%	Yes	****	<0.0001
0 hr:0% vs. 20 hr:Pseudomonas aeruginosa Only	Yes	****	<0.0001
0 hr:Pseudomonas aeruginosa Only vs. 20 hr:5%	Yes	****	<0.0001
0 hr:Pseudomonas aeruginosa Only vs. 20 hr:2%	Yes	****	<0.0001
0 hr:Pseudomonas aeruginosa Only vs. 20 hr:1%	Yes	****	<0.0001
0 hr:Pseudomonas aeruginosa Only vs. 20 hr:0%	Yes	****	<0.0001
0 hr:Pseudomonas aeruginosa Only vs. 20 hr:Pseudomonas aeruginosa Only	Yes	****	<0.0001
20 hr:5% vs. 20 hr:2%	No	ns	0.5049
20 hr:5% vs. 20 hr:1%	No	ns	0.4507
20 hr:5% vs. 20 hr:0%	Yes	****	<0.0001
20 hr:5% vs. 20 hr:Pseudomonas aeruginosa Only	Yes	****	<0.0001
20 hr:2% vs. 20 hr:1%	No	ns	>0.9999
20 hr:2% vs. 20 hr:0%	Yes	****	<0.0001
20 hr:2% vs. 20 hr:Pseudomonas aeruginosa Only	Yes	****	<0.0001
20 hr:1% vs. 20 hr:0%	Yes	****	<0.0001
20 hr:1% vs. 20 hr:Pseudomonas aeruginosa Only	Yes	****	<0.0001
20 hr:0% vs. 20 hr:Pseudomonas aeruginosa Only	Yes	**	0.0024

Appendix 5.9. 2- Way ANOVA of toxicity of Pico-Surf® to *Staphylococcus aureus* after 20 hours.

Tukey's multiple comparisons test	Significant?	Summary	Adjusted P Value
0 hr:5% vs. 0 hr:2%	No	ns	>0.9999
0 hr:5% vs. 0 hr:1%	No	ns	>0.9999
0 hr:5% vs. 0 hr:0%	No	ns	>0.9999
0 hr:5% vs. 0 hr:Staphylococcus aureus Only	No	ns	>0.9999
0 hr:5% vs. 20 hr:5%	Yes	****	<0.0001
0 hr:5% vs. 20 hr:2%	Yes	****	<0.0001
0 hr:5% vs. 20 hr:1%	Yes	****	<0.0001
0 hr:5% vs. 20 hr:0%	Yes	****	<0.0001
0 hr:5% vs. 20 hr:Staphylococcus aureus Only	Yes	****	<0.0001
0 hr:2% vs. 0 hr:1%	No	ns	>0.9999
0 hr:2% vs. 0 hr:0%	No	ns	>0.9999
0 hr:2% vs. 0 hr:Staphylococcus aureus Only	No	ns	>0.9999
0 hr:2% vs. 20 hr:5%	Yes	****	<0.0001
0 hr:2% vs. 20 hr:2%	Yes	****	<0.0001
0 hr:2% vs. 20 hr:1%	Yes	****	<0.0001
0 hr:2% vs. 20 hr:0%	Yes	****	<0.0001
0 hr:2% vs. 20 hr:Staphylococcus aureus Only	Yes	****	<0.0001
0 hr:1% vs. 0 hr:0%	No	ns	>0.9999
0 hr:1% vs. 0 hr:Staphylococcus aureus Only	No	ns	>0.9999
0 hr:1% vs. 20 hr:5%	Yes	****	<0.0001
0 hr:1% vs. 20 hr:2%	Yes	****	<0.0001
0 hr:1% vs. 20 hr:1%	Yes	****	<0.0001
0 hr:1% vs. 20 hr:0%	Yes	****	<0.0001
0 hr:1% vs. 20 hr:Staphylococcus aureus Only	Yes	****	<0.0001
0 hr:0% vs. 0 hr:Staphylococcus aureus Only	No	ns	>0.9999
0 hr:0% vs. 20 hr:5%	Yes	****	<0.0001
0 hr:0% vs. 20 hr:2%	Yes	****	<0.0001
0 hr:0% vs. 20 hr:1%	Yes	****	<0.0001
0 hr:0% vs. 20 hr:0%	Yes	****	<0.0001
0 hr:0% vs. 20 hr:Staphylococcus aureus Only	Yes	****	<0.0001
0 hr:Staphylococcus aureus Only vs. 20 hr:5%	Yes	****	<0.0001
0 hr:Staphylococcus aureus Only vs. 20 hr:2%	Yes	****	<0.0001
0 hr:Staphylococcus aureus Only vs. 20 hr:1%	Yes	****	<0.0001
0 hr:Staphylococcus aureus Only vs. 20 hr:0%	Yes	****	<0.0001
0 hr:Staphylococcus aureus Only vs. 20 hr:Staphylococcus aureus Only	Yes	****	<0.0001
20 hr:5% vs. 20 hr:2%	No	ns	>0.9999
20 hr:5% vs. 20 hr:1%	No	ns	>0.9999
20 hr:5% vs. 20 hr:0%	No	ns	0.9997
20 hr:5% vs. 20 hr:Staphylococcus aureus Only	No	ns	>0.9999
20 hr:2% vs. 20 hr:1%	No	ns	>0.9999
20 hr:2% vs. 20 hr:0%	No	ns	>0.9999
20 hr:2% vs. 20 hr:Staphylococcus aureus Only	No	ns	>0.9999
20 hr:1% vs. 20 hr:0%	No	ns	>0.9999
20 hr:1% vs. 20 hr:Staphylococcus aureus Only	No	ns	>0.9999
20 hr:0% vs. 20 hr:Staphylococcus aureus Only	No	ns	>0.9999

Appendix 5.10. 2- Way ANOVA of toxicity of FluoSurf™ to *Staphylococcus aureus* after 20 hours.

Tukey's multiple comparisons test	Significant?	Summary	Adjusted P Value
0 hr:3% vs. 0 hr:2%	No	ns	>0.9999
0 hr:3% vs. 0 hr:1%	No	ns	>0.9999
0 hr:3% vs. 0 hr:0%	No	ns	>0.9999
0 hr:3% vs. 0 hr:Staphylococcus aureus Only	No	ns	>0.9999
0 hr:3% vs. 20 hr:3%	Yes	****	<0.0001
0 hr:3% vs. 20 hr:2%	Yes	****	<0.0001
0 hr:3% vs. 20 hr:1%	Yes	****	<0.0001
0 hr:3% vs. 20 hr:0%	Yes	****	<0.0001
0 hr:3% vs. 20 hr:Staphylococcus aureus Only	Yes	****	<0.0001
0 hr:2% vs. 0 hr:1%	No	ns	>0.9999
0 hr:2% vs. 0 hr:0%	No	ns	>0.9999
0 hr:2% vs. 0 hr:Staphylococcus aureus Only	No	ns	>0.9999
0 hr:2% vs. 20 hr:3%	Yes	****	<0.0001
0 hr:2% vs. 20 hr:2%	Yes	****	<0.0001
0 hr:2% vs. 20 hr:1%	Yes	****	<0.0001
0 hr:2% vs. 20 hr:0%	Yes	****	<0.0001
0 hr:2% vs. 20 hr:Staphylococcus aureus Only	Yes	****	<0.0001
0 hr:1% vs. 0 hr:0%	No	ns	>0.9999
0 hr:1% vs. 0 hr:Staphylococcus aureus Only	No	ns	>0.9999
0 hr:1% vs. 20 hr:3%	Yes	****	<0.0001
0 hr:1% vs. 20 hr:2%	Yes	****	<0.0001
0 hr:1% vs. 20 hr:1%	Yes	****	<0.0001
0 hr:1% vs. 20 hr:0%	Yes	****	<0.0001
0 hr:1% vs. 20 hr:Staphylococcus aureus Only	Yes	****	<0.0001
0 hr:0% vs. 0 hr:Staphylococcus aureus Only	No	ns	>0.9999
0 hr:0% vs. 20 hr:3%	Yes	****	<0.0001
0 hr:0% vs. 20 hr:2%	Yes	****	<0.0001
0 hr:0% vs. 20 hr:1%	Yes	****	<0.0001
0 hr:0% vs. 20 hr:0%	Yes	****	<0.0001
0 hr:0% vs. 20 hr:Staphylococcus aureus Only	Yes	****	<0.0001
0 hr:Staphylococcus aureus Only vs. 20 hr:3%	Yes	****	<0.0001
0 hr:Staphylococcus aureus Only vs. 20 hr:2%	Yes	****	<0.0001
0 hr:Staphylococcus aureus Only vs. 20 hr:1%	Yes	****	<0.0001
0 hr:Staphylococcus aureus Only vs. 20 hr:0%	Yes	****	<0.0001
0 hr:Staphylococcus aureus Only vs. 20 hr:Staphylococcus aureus Only	Yes	****	<0.0001
20 hr:3% vs. 20 hr:2%	No	ns	0.5051
20 hr:3% vs. 20 hr:1%	No	ns	0.4131
20 hr:3% vs. 20 hr:0%	Yes	****	<0.0001
20 hr:3% vs. 20 hr:Staphylococcus aureus Only	Yes	****	<0.0001
20 hr:2% vs. 20 hr:1%	No	ns	>0.9999
20 hr:2% vs. 20 hr:0%	Yes	****	<0.0001
20 hr:2% vs. 20 hr:Staphylococcus aureus Only	Yes	****	<0.0001
20 hr:1% vs. 20 hr:0%	Yes	****	<0.0001
20 hr:1% vs. 20 hr:Staphylococcus aureus Only	Yes	****	<0.0001
20 hr:0% vs. 20 hr:Staphylococcus aureus Only	No	ns	>0.9999

Appendix 5.11. 2- Way ANOVA of toxicity of AM50-06 to *Staphylococcus aureus* after 20 hours.

Tukey's multiple comparisons test	Significant?	Summary	Adjusted P Value
0 hr:5% vs. 0 hr:2%	No	ns	>0.9999
0 hr:5% vs. 0 hr:1%	No	ns	>0.9999
0 hr:5% vs. 0 hr:0%	No	ns	>0.9999
0 hr:5% vs. 0 hr:Staphylococcus aureus Only	No	ns	>0.9999
0 hr:5% vs. 20 hr:5%	Yes	****	<0.0001
0 hr:5% vs. 20 hr:2%	Yes	****	<0.0001
0 hr:5% vs. 20 hr:1%	Yes	****	<0.0001
0 hr:5% vs. 20 hr:0%	Yes	****	<0.0001
0 hr:5% vs. 20 hr:Staphylococcus aureus Only	Yes	****	<0.0001
0 hr:2% vs. 0 hr:1%	No	ns	>0.9999
0 hr:2% vs. 0 hr:0%	No	ns	>0.9999
0 hr:2% vs. 0 hr:Staphylococcus aureus Only	No	ns	>0.9999
0 hr:2% vs. 20 hr:5%	Yes	****	<0.0001
0 hr:2% vs. 20 hr:2%	Yes	****	<0.0001
0 hr:2% vs. 20 hr:1%	Yes	****	<0.0001
0 hr:2% vs. 20 hr:0%	Yes	****	<0.0001
0 hr:2% vs. 20 hr:Staphylococcus aureus Only	Yes	****	<0.0001
0 hr:1% vs. 0 hr:0%	No	ns	>0.9999
0 hr:1% vs. 0 hr:Staphylococcus aureus Only	No	ns	>0.9999
0 hr:1% vs. 20 hr:5%	Yes	****	<0.0001
0 hr:1% vs. 20 hr:2%	Yes	****	<0.0001
0 hr:1% vs. 20 hr:1%	Yes	****	<0.0001
0 hr:1% vs. 20 hr:0%	Yes	****	<0.0001
0 hr:1% vs. 20 hr:Staphylococcus aureus Only	Yes	****	<0.0001
0 hr:0% vs. 0 hr:Staphylococcus aureus Only	No	ns	>0.9999
0 hr:0% vs. 20 hr:5%	Yes	****	<0.0001
0 hr:0% vs. 20 hr:2%	Yes	****	<0.0001
0 hr:0% vs. 20 hr:1%	Yes	****	<0.0001
0 hr:0% vs. 20 hr:0%	Yes	****	<0.0001
0 hr:0% vs. 20 hr:Staphylococcus aureus Only	Yes	****	<0.0001
0 hr:Staphylococcus aureus Only vs. 20 hr:5%	Yes	****	<0.0001
0 hr:Staphylococcus aureus Only vs. 20 hr:2%	Yes	****	<0.0001
0 hr:Staphylococcus aureus Only vs. 20 hr:1%	Yes	****	<0.0001
0 hr:Staphylococcus aureus Only vs. 20 hr:0%	Yes	****	<0.0001
0 hr:Staphylococcus aureus Only vs. 20 hr:Staphylococcus aureus Only	Yes	****	<0.0001
20 hr:5% vs. 20 hr:2%	No	ns	0.9856
20 hr:5% vs. 20 hr:1%	No	ns	0.9574
20 hr:5% vs. 20 hr:0%	Yes	***	0.0002
20 hr:5% vs. 20 hr:Staphylococcus aureus Only	Yes	***	0.0002
20 hr:2% vs. 20 hr:1%	No	ns	>0.9999
20 hr:2% vs. 20 hr:0%	Yes	****	<0.0001
20 hr:2% vs. 20 hr:Staphylococcus aureus Only	Yes	****	<0.0001
20 hr:1% vs. 20 hr:0%	Yes	****	<0.0001
20 hr:1% vs. 20 hr:Staphylococcus aureus Only	Yes	****	<0.0001
20 hr:0% vs. 20 hr:Staphylococcus aureus Only	No	ns	>0.9999

Appendix 5.12. 2- Way ANOVA of toxicity of AM50-08 to *Staphylococcus aureus* after 20 hours.

Tukey's multiple comparisons test	Significant?	Summary	Adjusted P Value
0 hr:5% vs. 0 hr:2%	No	ns	>0.9999
0 hr:5% vs. 0 hr:1%	No	ns	>0.9999
0 hr:5% vs. 0 hr:0%	No	ns	0.8983
0 hr:5% vs. 0 hr:Staphylococcus aureus Only	No	ns	0.8568
0 hr:5% vs. 20 hr:5%	Yes	****	<0.0001
0 hr:5% vs. 20 hr:2%	Yes	****	<0.0001
0 hr:5% vs. 20 hr:1%	Yes	****	<0.0001
0 hr:5% vs. 20 hr:0%	Yes	****	<0.0001
0 hr:5% vs. 20 hr:Staphylococcus aureus Only	Yes	****	<0.0001
0 hr:2% vs. 0 hr:1%	No	ns	>0.9999
0 hr:2% vs. 0 hr:0%	No	ns	0.8568
0 hr:2% vs. 0 hr:Staphylococcus aureus Only	No	ns	0.8079
0 hr:2% vs. 20 hr:5%	Yes	****	<0.0001
0 hr:2% vs. 20 hr:2%	Yes	****	<0.0001
0 hr:2% vs. 20 hr:1%	Yes	****	<0.0001
0 hr:2% vs. 20 hr:0%	Yes	****	<0.0001
0 hr:2% vs. 20 hr:Staphylococcus aureus Only	Yes	****	<0.0001
0 hr:1% vs. 0 hr:0%	No	ns	0.9316
0 hr:1% vs. 0 hr:Staphylococcus aureus Only	No	ns	0.8983
0 hr:1% vs. 20 hr:5%	Yes	****	<0.0001
0 hr:1% vs. 20 hr:2%	Yes	****	<0.0001
0 hr:1% vs. 20 hr:1%	Yes	****	<0.0001
0 hr:1% vs. 20 hr:0%	Yes	****	<0.0001
0 hr:1% vs. 20 hr:Staphylococcus aureus Only	Yes	****	<0.0001
0 hr:0% vs. 0 hr:Staphylococcus aureus Only	No	ns	>0.9999
0 hr:0% vs. 20 hr:5%	Yes	****	<0.0001
0 hr:0% vs. 20 hr:2%	Yes	****	<0.0001
0 hr:0% vs. 20 hr:1%	Yes	****	<0.0001
0 hr:0% vs. 20 hr:0%	Yes	****	<0.0001
0 hr:0% vs. 20 hr:Staphylococcus aureus Only	Yes	****	<0.0001
0 hr:Staphylococcus aureus Only vs. 20 hr:5%	Yes	****	<0.0001
0 hr:Staphylococcus aureus Only vs. 20 hr:2%	Yes	****	<0.0001
0 hr:Staphylococcus aureus Only vs. 20 hr:1%	Yes	****	<0.0001
0 hr:Staphylococcus aureus Only vs. 20 hr:0%	Yes	****	<0.0001
0 hr:Staphylococcus aureus Only vs. 20 hr:Staphylococcus aureus Only	Yes	****	<0.0001
20 hr:5% vs. 20 hr:2%	No	ns	0.5267
20 hr:5% vs. 20 hr:1%	No	ns	0.9997
20 hr:5% vs. 20 hr:0%	Yes	****	<0.0001
20 hr:5% vs. 20 hr:Staphylococcus aureus Only	Yes	****	<0.0001
20 hr:2% vs. 20 hr:1%	No	ns	0.8733
20 hr:2% vs. 20 hr:0%	Yes	****	<0.0001
20 hr:2% vs. 20 hr:Staphylococcus aureus Only	Yes	****	<0.0001
20 hr:1% vs. 20 hr:0%	Yes	****	<0.0001
20 hr:1% vs. 20 hr:Staphylococcus aureus Only	Yes	****	<0.0001
20 hr:0% vs. 20 hr:Staphylococcus aureus Only	No	ns	0.9997

Appendix 5.13. 2- Way ANOVA of toxicity of PicoSurf® to *NCTC m.abscessus* Smooth variant after 96 hours.

Tukey's multiple comparisons test	Significant?	Summary	Adjusted P Value
0 hr:5% vs. 0 hr:2%	No	ns	>0.9999
0 hr:5% vs. 0 hr:1%	No	ns	>0.9999
0 hr:5% vs. 0 hr:0%	No	ns	>0.9999
0 hr:5% vs. 0 hr:*Mycobacterium Abscessus* Only	No	ns	>0.9999
0 hr:5% vs. 96 hr:5%	Yes	****	<0.0001
0 hr:5% vs. 96 hr:2%	Yes	****	<0.0001
0 hr:5% vs. 96 hr:1%	Yes	****	<0.0001
0 hr:5% vs. 96 hr:0%	Yes	****	<0.0001
0 hr:5% vs. 96 hr:*Mycobacterium Abscessus* Only	Yes	****	<0.0001
0 hr:2% vs. 0 hr:1%	No	ns	>0.9999
0 hr:2% vs. 0 hr:0%	No	ns	>0.9999
0 hr:2% vs. 0 hr:*Mycobacterium Abscessus* Only	No	ns	>0.9999
0 hr:2% vs. 96 hr:5%	Yes	****	<0.0001
0 hr:2% vs. 96 hr:2%	Yes	****	<0.0001
0 hr:2% vs. 96 hr:1%	Yes	****	<0.0001
0 hr:2% vs. 96 hr:0%	Yes	****	<0.0001
0 hr:2% vs. 96 hr:*Mycobacterium Abscessus* Only	Yes	****	<0.0001
0 hr:1% vs. 0 hr:0%	No	ns	>0.9999
0 hr:1% vs. 0 hr:*Mycobacterium Abscessus* Only	No	ns	>0.9999
0 hr:1% vs. 96 hr:5%	Yes	****	<0.0001
0 hr:1% vs. 96 hr:2%	Yes	****	<0.0001
0 hr:1% vs. 96 hr:1%	Yes	****	<0.0001
0 hr:1% vs. 96 hr:0%	Yes	****	<0.0001
0 hr:1% vs. 96 hr:*Mycobacterium Abscessus* Only	Yes	****	<0.0001
0 hr:0% vs. 0 hr:*Mycobacterium Abscessus* Only	No	ns	>0.9999
0 hr:0% vs. 96 hr:5%	Yes	****	<0.0001
0 hr:0% vs. 96 hr:2%	Yes	****	<0.0001
0 hr:0% vs. 96 hr:1%	Yes	****	<0.0001
0 hr:0% vs. 96 hr:0%	Yes	****	<0.0001
0 hr:0% vs. 96 hr:*Mycobacterium Abscessus* Only	Yes	****	<0.0001
0 hr:*Mycobacterium Abscessus* Only vs. 96 hr:5%	Yes	****	<0.0001
0 hr:*Mycobacterium Abscessus* Only vs. 96 hr:2%	Yes	****	<0.0001
0 hr:*Mycobacterium Abscessus* Only vs. 96 hr:1%	Yes	****	<0.0001
0 hr:*Mycobacterium Abscessus* Only vs. 96 hr:0%	Yes	****	<0.0001
0 hr:*Mycobacterium Abscessus* Only vs. 96 hr:*Mycobacterium Abscessus* Only	Yes	****	<0.0001
96 hr:5% vs. 96 hr:2%	No	ns	0.0703
96 hr:5% vs. 96 hr:1%	No	ns	0.9077
96 hr:5% vs. 96 hr:0%	No	ns	0.9999
96 hr:5% vs. 96 hr:*Mycobacterium Abscessus* Only	No	ns	0.9976
96 hr:2% vs. 96 hr:1%	No	ns	0.8253
96 hr:2% vs. 96 hr:0%	No	ns	0.1893
96 hr:2% vs. 96 hr:*Mycobacterium Abscessus* Only	No	ns	0.2892
96 hr:1% vs. 96 hr:0%	No	ns	0.9931
96 hr:1% vs. 96 hr:*Mycobacterium Abscessus* Only	No	ns	0.9992
96 hr:0% vs. 96 hr:*Mycobacterium Abscessus* Only	No	ns	>0.9999

Appendix 5.14. 2- Way ANOVA of toxicity of FluoSurf™ to *NCTC m.abscessus* Smooth variant after 96 hours.

Tukey's multiple comparisons test	Significant?	Summary	Adjusted P Value
0 hr:3% vs. 0 hr:2%	No	ns	>0.9999
0 hr:3% vs. 0 hr:1%	No	ns	>0.9999
0 hr:3% vs. 0 hr:0%	No	ns	>0.9999
0 hr:3% vs. 0 hr:*Mycobacterium Abscessus* Only	No	ns	>0.9999
0 hr:3% vs. 96 hr:3%	Yes	*	0.0203
0 hr:3% vs. 96 hr:2%	No	ns	0.0586
0 hr:3% vs. 96 hr:1%	Yes	****	<0.0001
0 hr:3% vs. 96 hr:0%	Yes	****	<0.0001
0 hr:3% vs. 96 hr:*Mycobacterium Abscessus* Only	Yes	****	<0.0001
0 hr:2% vs. 0 hr:1%	No	ns	>0.9999
0 hr:2% vs. 0 hr:0%	No	ns	>0.9999
0 hr:2% vs. 0 hr:*Mycobacterium Abscessus* Only	No	ns	>0.9999
0 hr:2% vs. 96 hr:3%	Yes	*	0.0206
0 hr:2% vs. 96 hr:2%	No	ns	0.0593
0 hr:2% vs. 96 hr:1%	Yes	****	<0.0001
0 hr:2% vs. 96 hr:0%	Yes	****	<0.0001
0 hr:2% vs. 96 hr:*Mycobacterium Abscessus* Only	Yes	****	<0.0001
0 hr:1% vs. 0 hr:0%	No	ns	>0.9999
0 hr:1% vs. 0 hr:*Mycobacterium Abscessus* Only	No	ns	>0.9999
0 hr:1% vs. 96 hr:3%	Yes	*	0.02
0 hr:1% vs. 96 hr:2%	No	ns	0.0578
0 hr:1% vs. 96 hr:1%	Yes	****	<0.0001
0 hr:1% vs. 96 hr:0%	Yes	****	<0.0001
0 hr:1% vs. 96 hr:*Mycobacterium Abscessus* Only	Yes	****	<0.0001
0 hr:0% vs. 0 hr:*Mycobacterium Abscessus* Only	No	ns	>0.9999
0 hr:0% vs. 96 hr:3%	Yes	*	0.0219
0 hr:0% vs. 96 hr:2%	No	ns	0.063
0 hr:0% vs. 96 hr:1%	Yes	****	<0.0001
0 hr:0% vs. 96 hr:0%	Yes	****	<0.0001
0 hr:0% vs. 96 hr:*Mycobacterium Abscessus* Only	Yes	****	<0.0001
0 hr:*Mycobacterium Abscessus* Only vs. 96 hr:3%	Yes	*	0.0271
0 hr:*Mycobacterium Abscessus* Only vs. 96 hr:2%	No	ns	0.0769
0 hr:*Mycobacterium Abscessus* Only vs. 96 hr:1%	Yes	****	<0.0001
0 hr:*Mycobacterium Abscessus* Only vs. 96 hr:0%	Yes	****	<0.0001
0 hr:*Mycobacterium Abscessus* Only vs. 96 hr:*Mycobacterium Abscessus* Only	Yes	****	<0.0001
96 hr:3% vs. 96 hr:2%	No	ns	>0.9999
96 hr:3% vs. 96 hr:1%	Yes	**	0.0013
96 hr:3% vs. 96 hr:0%	Yes	****	<0.0001
96 hr:3% vs. 96 hr:*Mycobacterium Abscessus* Only	Yes	****	<0.0001
96 hr:2% vs. 96 hr:1%	Yes	***	0.0004
96 hr:2% vs. 96 hr:0%	Yes	****	<0.0001
96 hr:2% vs. 96 hr:*Mycobacterium Abscessus* Only	Yes	****	<0.0001
96 hr:1% vs. 96 hr:0%	No	ns	0.1215
96 hr:1% vs. 96 hr:*Mycobacterium Abscessus* Only	No	ns	0.1654
96 hr:0% vs. 96 hr:*Mycobacterium Abscessus* Only	No	ns	>0.9999

Appendix 5.16. 2- Way ANOVA of toxicity of AM50-06 to *NCTC m.abscessus* Smooth variant after 96 hours.

Tukey's multiple comparisons test	Significant?	Summary	Adjusted P Value
0 hr:5% vs. 0 hr:2%	No	ns	>0.9999
0 hr:5% vs. 0 hr:1%	No	ns	>0.9999
0 hr:5% vs. 0 hr:0%	No	ns	>0.9999
0 hr:5% vs. 0 hr:*Mycobacterium Abscessus* Only	No	ns	>0.9999
0 hr:5% vs. 96 hr:5%	No	ns	0.6361
0 hr:5% vs. 96 hr:2%	No	ns	0.9926
0 hr:5% vs. 96 hr:1%	Yes	*	0.045
0 hr:5% vs. 96 hr:0%	Yes	****	<0.0001
0 hr:5% vs. 96 hr:*Mycobacterium Abscessus* Only	Yes	****	<0.0001
0 hr:2% vs. 0 hr:1%	No	ns	>0.9999
0 hr:2% vs. 0 hr:0%	No	ns	>0.9999
0 hr:2% vs. 0 hr:*Mycobacterium Abscessus* Only	No	ns	>0.9999
0 hr:2% vs. 96 hr:5%	No	ns	0.615
0 hr:2% vs. 96 hr:2%	No	ns	0.9905
0 hr:2% vs. 96 hr:1%	Yes	*	0.0419
0 hr:2% vs. 96 hr:0%	Yes	****	<0.0001
0 hr:2% vs. 96 hr:*Mycobacterium Abscessus* Only	Yes	****	<0.0001
0 hr:1% vs. 0 hr:0%	No	ns	>0.9999
0 hr:1% vs. 0 hr:*Mycobacterium Abscessus* Only	No	ns	>0.9999
0 hr:1% vs. 96 hr:5%	No	ns	0.6108
0 hr:1% vs. 96 hr:2%	No	ns	0.99
0 hr:1% vs. 96 hr:1%	Yes	*	0.0413
0 hr:1% vs. 96 hr:0%	Yes	****	<0.0001
0 hr:1% vs. 96 hr:*Mycobacterium Abscessus* Only	Yes	****	<0.0001
0 hr:0% vs. 0 hr:*Mycobacterium Abscessus* Only	No	ns	>0.9999
0 hr:0% vs. 96 hr:5%	No	ns	0.6684
0 hr:0% vs. 96 hr:2%	No	ns	0.9951
0 hr:0% vs. 96 hr:1%	No	ns	0.0502
0 hr:0% vs. 96 hr:0%	Yes	****	<0.0001
0 hr:0% vs. 96 hr:*Mycobacterium Abscessus* Only	Yes	****	<0.0001
0 hr:*Mycobacterium Abscessus* Only vs. 96 hr:5%	No	ns	0.7331
0 hr:*Mycobacterium Abscessus* Only vs. 96 hr:2%	No	ns	0.9982
0 hr:*Mycobacterium Abscessus* Only vs. 96 hr:1%	No	ns	0.0626
0 hr:*Mycobacterium Abscessus* Only vs. 96 hr:0%	Yes	****	<0.0001
0 hr:*Mycobacterium Abscessus* Only vs. 96 hr:*Mycobacterium Abscessus* Only	Yes	****	<0.0001
96 hr:5% vs. 96 hr:2%	No	ns	0.9879
96 hr:5% vs. 96 hr:1%	No	ns	0.815
96 hr:5% vs. 96 hr:0%	Yes	****	<0.0001
96 hr:5% vs. 96 hr:*Mycobacterium Abscessus* Only	Yes	****	<0.0001
96 hr:2% vs. 96 hr:1%	No	ns	0.258
96 hr:2% vs. 96 hr:0%	Yes	****	<0.0001
96 hr:2% vs. 96 hr:*Mycobacterium Abscessus* Only	Yes	****	<0.0001
96 hr:1% vs. 96 hr:0%	Yes	****	<0.0001
96 hr:1% vs. 96 hr:*Mycobacterium Abscessus* Only	Yes	****	<0.0001
96 hr:0% vs. 96 hr:*Mycobacterium Abscessus* Only	No	ns	>0.9999

Appendix 5.17. 2- Way ANOVA of toxicity of AM50-08 to *NCTC m.abscessus* Smooth variant after 96 hours.

Tukey's multiple comparisons test	Significant?	Summary	Adjusted P Value
0 hr:5% vs. 0 hr:2%	No	ns	>0.9999
0 hr:5% vs. 0 hr:1%	No	ns	>0.9999
0 hr:5% vs. 0 hr:0%	No	ns	>0.9999
0 hr:5% vs. 0 hr:*Mycobacterium Abscessus* Only	No	ns	>0.9999
0 hr:5% vs. 96 hr:5%	Yes	***	0.0005
0 hr:5% vs. 96 hr:2%	Yes	****	<0.0001
0 hr:5% vs. 96 hr:1%	Yes	****	<0.0001
0 hr:5% vs. 96 hr:0%	Yes	****	<0.0001
0 hr:5% vs. 96 hr:*Mycobacterium Abscessus* Only	Yes	****	<0.0001
0 hr:2% vs. 0 hr:1%	No	ns	>0.9999
0 hr:2% vs. 0 hr:0%	No	ns	>0.9999
0 hr:2% vs. 0 hr:*Mycobacterium Abscessus* Only	No	ns	>0.9999
0 hr:2% vs. 96 hr:5%	Yes	***	0.0005
0 hr:2% vs. 96 hr:2%	Yes	****	<0.0001
0 hr:2% vs. 96 hr:1%	Yes	****	<0.0001
0 hr:2% vs. 96 hr:0%	Yes	****	<0.0001
0 hr:2% vs. 96 hr:*Mycobacterium Abscessus* Only	Yes	****	<0.0001
0 hr:1% vs. 0 hr:0%	No	ns	>0.9999
0 hr:1% vs. 0 hr:*Mycobacterium Abscessus* Only	No	ns	>0.9999
0 hr:1% vs. 96 hr:5%	Yes	***	0.0005
0 hr:1% vs. 96 hr:2%	Yes	****	<0.0001
0 hr:1% vs. 96 hr:1%	Yes	****	<0.0001
0 hr:1% vs. 96 hr:0%	Yes	****	<0.0001
0 hr:1% vs. 96 hr:*Mycobacterium Abscessus* Only	Yes	****	<0.0001
0 hr:0% vs. 0 hr:*Mycobacterium Abscessus* Only	No	ns	>0.9999
0 hr:0% vs. 96 hr:5%	Yes	***	0.0004
0 hr:0% vs. 96 hr:2%	Yes	****	<0.0001
0 hr:0% vs. 96 hr:1%	Yes	****	<0.0001
0 hr:0% vs. 96 hr:0%	Yes	****	<0.0001
0 hr:0% vs. 96 hr:*Mycobacterium Abscessus* Only	Yes	****	<0.0001
0 hr:*Mycobacterium Abscessus* Only vs. 96 hr:5%	Yes	***	0.0005
0 hr:*Mycobacterium Abscessus* Only vs. 96 hr:2%	Yes	****	<0.0001
0 hr:*Mycobacterium Abscessus* Only vs. 96 hr:1%	Yes	****	<0.0001
0 hr:*Mycobacterium Abscessus* Only vs. 96 hr:0%	Yes	****	<0.0001
0 hr:*Mycobacterium Abscessus* Only vs. 96 hr:*Mycobacterium Abscessus* Only	Yes	****	<0.0001
96 hr:5% vs. 96 hr:2%	No	ns	0.684
96 hr:5% vs. 96 hr:1%	No	ns	0.3664
96 hr:5% vs. 96 hr:0%	No	ns	0.0559
96 hr:5% vs. 96 hr:*Mycobacterium Abscessus* Only	No	ns	0.0721
96 hr:2% vs. 96 hr:1%	No	ns	0.9999
96 hr:2% vs. 96 hr:0%	No	ns	0.8283
96 hr:2% vs. 96 hr:*Mycobacterium Abscessus* Only	No	ns	0.8839
96 hr:1% vs. 96 hr:0%	No	ns	0.9825
96 hr:1% vs. 96 hr:*Mycobacterium Abscessus* Only	No	ns	0.9927
96 hr:0% vs. 96 hr:*Mycobacterium Abscessus* Only	No	ns	>0.9999

Appendix 5.18. 2- Way ANOVA of toxicity of Pico-Surf® to *NCTC M.abscessus* rough variant after 96 hours

Tukey's multiple comparisons test	Significant?	Summary	Adjusted P Value
0 hr:5% vs. 0 hr:2%	No	ns	>0.9999
0 hr:5% vs. 0 hr:1%	No	ns	>0.9999
0 hr:5% vs. 0 hr:0%	No	ns	>0.9999
0 hr:5% vs. 0 hr:*Mycobacterium Abscessus* Only	No	ns	0.985
0 hr:5% vs. 96 hr:5%	Yes	*	0.0177
0 hr:5% vs. 96 hr:2%	No	ns	0.443
0 hr:5% vs. 96 hr:1%	No	ns	0.5817
0 hr:5% vs. 96 hr:0%	Yes	****	<0.0001
0 hr:5% vs. 96 hr:*Mycobacterium Abscessus* Only	Yes	****	<0.0001
0 hr:2% vs. 0 hr:1%	No	ns	>0.9999
0 hr:2% vs. 0 hr:0%	No	ns	>0.9999
0 hr:2% vs. 0 hr:*Mycobacterium Abscessus* Only	No	ns	0.9732
0 hr:2% vs. 96 hr:5%	Yes	*	0.0143
0 hr:2% vs. 96 hr:2%	No	ns	0.3851
0 hr:2% vs. 96 hr:1%	No	ns	0.5173
0 hr:2% vs. 96 hr:0%	Yes	****	<0.0001
0 hr:2% vs. 96 hr:*Mycobacterium Abscessus* Only	Yes	****	<0.0001
0 hr:1% vs. 0 hr:0%	No	ns	>0.9999
0 hr:1% vs. 0 hr:*Mycobacterium Abscessus* Only	No	ns	0.9408
0 hr:1% vs. 96 hr:5%	Yes	*	0.0101
0 hr:1% vs. 96 hr:2%	No	ns	0.299
0 hr:1% vs. 96 hr:1%	No	ns	0.4155
0 hr:1% vs. 96 hr:0%	Yes	****	<0.0001
0 hr:1% vs. 96 hr:*Mycobacterium Abscessus* Only	Yes	****	<0.0001
0 hr:0% vs. 0 hr:*Mycobacterium Abscessus* Only	No	ns	0.9966
0 hr:0% vs. 96 hr:5%	No	ns	0.0512
0 hr:0% vs. 96 hr:2%	No	ns	0.6537
0 hr:0% vs. 96 hr:1%	No	ns	0.7752
0 hr:0% vs. 96 hr:0%	Yes	****	<0.0001
0 hr:0% vs. 96 hr:*Mycobacterium Abscessus* Only	Yes	****	<0.0001
0 hr:*Mycobacterium Abscessus* Only vs. 96 hr:5%	No	ns	0.2454
0 hr:*Mycobacterium Abscessus* Only vs. 96 hr:2%	No	ns	0.9868
0 hr:*Mycobacterium Abscessus* Only vs. 96 hr:1%	No	ns	0.9976
0 hr:*Mycobacterium Abscessus* Only vs. 96 hr:0%	Yes	****	<0.0001
0 hr:*Mycobacterium Abscessus* Only vs. 96 hr:*Mycobacterium Abscessus* Only	Yes	****	<0.0001
96 hr:5% vs. 96 hr:2%	No	ns	0.6683
96 hr:5% vs. 96 hr:1%	No	ns	0.5258
96 hr:5% vs. 96 hr:0%	Yes	****	<0.0001
96 hr:5% vs. 96 hr:*Mycobacterium Abscessus* Only	Yes	**	0.0035
96 hr:2% vs. 96 hr:1%	No	ns	>0.9999
96 hr:2% vs. 96 hr:0%	Yes	****	<0.0001
96 hr:2% vs. 96 hr:*Mycobacterium Abscessus* Only	Yes	***	0.0002
96 hr:1% vs. 96 hr:0%	Yes	****	<0.0001
96 hr:1% vs. 96 hr:*Mycobacterium Abscessus* Only	Yes	***	0.0001
96 hr:0% vs. 96 hr:*Mycobacterium Abscessus* Only	Yes	**	0.0049

Appendix 5.19. 2- Way ANOVA of toxicity of FluoSurf™ to *NCTC M.abscessus* rough variant after 96 hours.

Tukey's multiple comparisons test	Significant?	Summary	Adjusted P Value
0 hr:3% vs. 0 hr:2%	No	ns	>0.9999
0 hr:3% vs. 0 hr:1%	No	ns	>0.9999
0 hr:3% vs. 0 hr:0%	No	ns	>0.9999
0 hr:3% vs. 0 hr:*Mycobacterium Abscessus* Only	No	ns	0.9684
0 hr:3% vs. 96 hr:3%	No	ns	0.3001
0 hr:3% vs. 96 hr:2%	No	ns	0.3183
0 hr:3% vs. 96 hr:1%	Yes	**	0.0029
0 hr:3% vs. 96 hr:0%	Yes	****	<0.0001
0 hr:3% vs. 96 hr:*Mycobacterium Abscessus* Only	Yes	****	<0.0001
0 hr:2% vs. 0 hr:1%	No	ns	>0.9999
0 hr:2% vs. 0 hr:0%	No	ns	>0.9999
0 hr:2% vs. 0 hr:*Mycobacterium Abscessus* Only	No	ns	0.9584
0 hr:2% vs. 96 hr:3%	No	ns	0.2743
0 hr:2% vs. 96 hr:2%	No	ns	0.2913
0 hr:2% vs. 96 hr:1%	Yes	**	0.0026
0 hr:2% vs. 96 hr:0%	Yes	****	<0.0001
0 hr:2% vs. 96 hr:*Mycobacterium Abscessus* Only	Yes	****	<0.0001
0 hr:1% vs. 0 hr:0%	No	ns	>0.9999
0 hr:1% vs. 0 hr:*Mycobacterium Abscessus* Only	No	ns	0.9876
0 hr:1% vs. 96 hr:3%	No	ns	0.3839
0 hr:1% vs. 96 hr:2%	No	ns	0.405
0 hr:1% vs. 96 hr:1%	Yes	**	0.0041
0 hr:1% vs. 96 hr:0%	Yes	****	<0.0001
0 hr:1% vs. 96 hr:*Mycobacterium Abscessus* Only	Yes	****	<0.0001
0 hr:0% vs. 0 hr:*Mycobacterium Abscessus* Only	No	ns	0.998
0 hr:0% vs. 96 hr:3%	No	ns	0.6114
0 hr:0% vs. 96 hr:2%	No	ns	0.6332
0 hr:0% vs. 96 hr:1%	Yes	*	0.0149
0 hr:0% vs. 96 hr:0%	Yes	****	<0.0001
0 hr:0% vs. 96 hr:*Mycobacterium Abscessus* Only	Yes	****	<0.0001
0 hr:*Mycobacterium Abscessus* Only vs. 96 hr:3%	No	ns	0.9713
0 hr:*Mycobacterium Abscessus* Only vs. 96 hr:2%	No	ns	0.9766
0 hr:*Mycobacterium Abscessus* Only vs. 96 hr:1%	No	ns	0.0739
0 hr:*Mycobacterium Abscessus* Only vs. 96 hr:0%	Yes	****	<0.0001
0 hr:*Mycobacterium Abscessus* Only vs. 96 hr:*Mycobacterium Abscessus* Only	Yes	***	0.0002
96 hr:3% vs. 96 hr:2%	No	ns	>0.9999
96 hr:3% vs. 96 hr:1%	No	ns	0.3121
96 hr:3% vs. 96 hr:0%	Yes	****	<0.0001
96 hr:3% vs. 96 hr:*Mycobacterium Abscessus* Only	Yes	***	0.0005
96 hr:2% vs. 96 hr:1%	No	ns	0.2942
96 hr:2% vs. 96 hr:0%	Yes	****	<0.0001
96 hr:2% vs. 96 hr:*Mycobacterium Abscessus* Only	Yes	***	0.0004
96 hr:1% vs. 96 hr:0%	Yes	****	<0.0001
96 hr:1% vs. 96 hr:*Mycobacterium Abscessus* Only	Yes	*	0.0355
96 hr:0% vs. 96 hr:*Mycobacterium Abscessus* Only	Yes	**	0.0089

Appendix 5.20. 2- Way ANOVA of toxicity of AM50-06 to *NCTC M.abscessus* rough variant after 96 hours.

Tukey's multiple comparisons test	Significant?	Summary	Adjusted P Value
0 hr:5% vs. 0 hr:2%	No	ns	>0.9999
0 hr:5% vs. 0 hr:1%	No	ns	>0.9999
0 hr:5% vs. 0 hr:0%	No	ns	>0.9999
0 hr:5% vs. 0 hr:*Mycobacterium Abscessus* Only	No	ns	0.9592
0 hr:5% vs. 96 hr:5%	No	ns	0.0898
0 hr:5% vs. 96 hr:2%	No	ns	0.3659
0 hr:5% vs. 96 hr:1%	No	ns	0.1567
0 hr:5% vs. 96 hr:0%	Yes	****	<0.0001
0 hr:5% vs. 96 hr:*Mycobacterium Abscessus* Only	Yes	****	<0.0001
0 hr:2% vs. 0 hr:1%	No	ns	>0.9999
0 hr:2% vs. 0 hr:0%	No	ns	>0.9999
0 hr:2% vs. 0 hr:*Mycobacterium Abscessus* Only	No	ns	0.9549
0 hr:2% vs. 96 hr:5%	No	ns	0.0861
0 hr:2% vs. 96 hr:2%	No	ns	0.3545
0 hr:2% vs. 96 hr:1%	No	ns	0.1507
0 hr:2% vs. 96 hr:0%	Yes	****	<0.0001
0 hr:2% vs. 96 hr:*Mycobacterium Abscessus* Only	Yes	****	<0.0001
0 hr:1% vs. 0 hr:0%	No	ns	>0.9999
0 hr:1% vs. 0 hr:*Mycobacterium Abscessus* Only	No	ns	0.9695
0 hr:1% vs. 96 hr:5%	No	ns	0.1007
0 hr:1% vs. 96 hr:2%	No	ns	0.3986
0 hr:1% vs. 96 hr:1%	No	ns	0.1744
0 hr:1% vs. 96 hr:0%	Yes	****	<0.0001
0 hr:1% vs. 96 hr:*Mycobacterium Abscessus* Only	Yes	****	<0.0001
0 hr:0% vs. 0 hr:*Mycobacterium Abscessus* Only	No	ns	0.9994
0 hr:0% vs. 96 hr:5%	No	ns	0.3418
0 hr:0% vs. 96 hr:2%	No	ns	0.7811
0 hr:0% vs. 96 hr:1%	No	ns	0.4938
0 hr:0% vs. 96 hr:0%	Yes	****	<0.0001
0 hr:0% vs. 96 hr:*Mycobacterium Abscessus* Only	Yes	***	0.0003
0 hr:*Mycobacterium Abscessus* Only vs. 96 hr:5%	No	ns	0.7518
0 hr:*Mycobacterium Abscessus* Only vs. 96 hr:2%	No	ns	0.9904
0 hr:*Mycobacterium Abscessus* Only vs. 96 hr:1%	No	ns	0.8871
0 hr:*Mycobacterium Abscessus* Only vs. 96 hr:0%	Yes	****	<0.0001
0 hr:*Mycobacterium Abscessus* Only vs. 96 hr:*Mycobacterium Abscessus* Only	Yes	**	0.001
96 hr:5% vs. 96 hr:2%	No	ns	0.995
96 hr:5% vs. 96 hr:1%	No	ns	>0.9999
96 hr:5% vs. 96 hr:0%	Yes	****	<0.0001
96 hr:5% vs. 96 hr:*Mycobacterium Abscessus* Only	Yes	*	0.0103
96 hr:2% vs. 96 hr:1%	No	ns	0.9999
96 hr:2% vs. 96 hr:0%	Yes	****	<0.0001
96 hr:2% vs. 96 hr:*Mycobacterium Abscessus* Only	Yes	**	0.0023
96 hr:1% vs. 96 hr:0%	Yes	****	<0.0001
96 hr:1% vs. 96 hr:*Mycobacterium Abscessus* Only	Yes	**	0.0059
96 hr:0% vs. 96 hr:*Mycobacterium Abscessus* Only	Yes	*	0.0304

Appendix 5.21. 2- Way ANOVA of toxicity of AM50-08 to *NCTC m.abscessus* rough variant after 96 hours

Tukey's multiple comparisons test	Significant?	Summary	Adjusted P Value
0 hr:5% vs. 0 hr:2%	No	ns	0.999
0 hr:5% vs. 0 hr:1%	No	ns	>0.9999
0 hr:5% vs. 0 hr:0%	No	ns	>0.9999
0 hr:5% vs. 0 hr:*Mycobacterium Abscessus* Only	No	ns	0.9997
0 hr:5% vs. 96 hr:5%	No	ns	0.8468
0 hr:5% vs. 96 hr:2%	No	ns	0.5802
0 hr:5% vs. 96 hr:1%	No	ns	0.43
0 hr:5% vs. 96 hr:0%	Yes	****	<0.0001
0 hr:5% vs. 96 hr:*Mycobacterium Abscessus* Only	Yes	****	<0.0001
0 hr:2% vs. 0 hr:1%	No	ns	>0.9999
0 hr:2% vs. 0 hr:0%	No	ns	>0.9999
0 hr:2% vs. 0 hr:*Mycobacterium Abscessus* Only	No	ns	0.9504
0 hr:2% vs. 96 hr:5%	No	ns	0.4509
0 hr:2% vs. 96 hr:2%	No	ns	0.2283
0 hr:2% vs. 96 hr:1%	No	ns	0.1493
0 hr:2% vs. 96 hr:0%	Yes	****	<0.0001
0 hr:2% vs. 96 hr:*Mycobacterium Abscessus* Only	Yes	****	<0.0001
0 hr:1% vs. 0 hr:0%	No	ns	>0.9999
0 hr:1% vs. 0 hr:*Mycobacterium Abscessus* Only	No	ns	0.9924
0 hr:1% vs. 96 hr:5%	No	ns	0.6599
0 hr:1% vs. 96 hr:2%	No	ns	0.3831
0 hr:1% vs. 96 hr:1%	No	ns	0.2643
0 hr:1% vs. 96 hr:0%	Yes	****	<0.0001
0 hr:1% vs. 96 hr:*Mycobacterium Abscessus* Only	Yes	****	<0.0001
0 hr:0% vs. 0 hr:*Mycobacterium Abscessus* Only	No	ns	0.9988
0 hr:0% vs. 96 hr:5%	No	ns	0.8399
0 hr:0% vs. 96 hr:2%	No	ns	0.6015
0 hr:0% vs. 96 hr:1%	No	ns	0.4649
0 hr:0% vs. 96 hr:0%	Yes	****	<0.0001
0 hr:0% vs. 96 hr:*Mycobacterium Abscessus* Only	Yes	***	0.0001
0 hr:*Mycobacterium Abscessus* Only vs. 96 hr:5%	No	ns	0.998
0 hr:*Mycobacterium Abscessus* Only vs. 96 hr:2%	No	ns	0.9589
0 hr:*Mycobacterium Abscessus* Only vs. 96 hr:1%	No	ns	0.8928
0 hr:*Mycobacterium Abscessus* Only vs. 96 hr:0%	Yes	****	<0.0001
0 hr:*Mycobacterium Abscessus* Only vs. 96 hr:*Mycobacterium Abscessus* Only	Yes	***	0.0004
96 hr:5% vs. 96 hr:2%	No	ns	>0.9999
96 hr:5% vs. 96 hr:1%	No	ns	0.9985
96 hr:5% vs. 96 hr:0%	Yes	****	<0.0001
96 hr:5% vs. 96 hr:*Mycobacterium Abscessus* Only	Yes	***	0.0006
96 hr:2% vs. 96 hr:1%	No	ns	>0.9999
96 hr:2% vs. 96 hr:0%	Yes	****	<0.0001
96 hr:2% vs. 96 hr:*Mycobacterium Abscessus* Only	Yes	**	0.0013
96 hr:1% vs. 96 hr:0%	Yes	****	<0.0001
96 hr:1% vs. 96 hr:*Mycobacterium Abscessus* Only	Yes	**	0.002
96 hr:0% vs. 96 hr:*Mycobacterium Abscessus* Only	Yes	*	0.0154